MID-CRETACEOUS pCO_2, CARBON-CYCLING AND THE RISE OF THE FLOWERING PLANTS

CORINNE ALEXANDRA FAY

DEPARTMENT OF EARTH SCIENCES, UCL

THESIS SUBMITTED FOR THE AWARD OF DOCTOR OF PHILOSOPHY

JULY 2014

Declaration

I, Corinne Alexandra Fay, confirm that the work presented in this thesis is my own. Where information has been derived from other sources, I confirm that this has been indicated in the thesis.

Abstract

The mid-Cretaceous (Aptian–Cenomanian) climate was characterised by steadily increasing temperatures likely driven by high atmospheric CO_2. The climate system was dynamic: throughout this interval there were several dramatic carbon cycle perturbations (of 1–2 Myrs duration) due to initiation of marine anoxia (OAEs) resulting in burial of organic carbon. However, pCO_2 values and trends are generally poorly constrained for much of this time interval.

During the mid-Cretaceous, angiosperms (flowering plants) underwent a rapid poleward diversification and radiation; by the Cenomanian they comprised around 70% of floras. However, hypotheses detailing the competitive replacement of incumbent floras by advantageous angiosperm adaptations do not fully explain the timing and nature of early angiosperm evolution.

This thesis provides a record of Albian–Cenomanian carbon cycling and explores the role of climate change and pCO_2 decline (CO_2 starvation hypothesis) as forcing factors on angiosperm radiation. This is achieved using fossil material from the Nuussuaq Peninsula, West Greenland. Carbon isotope stratigraphy constrains the stratigraphic age (Middle Albian-Cenomanian) and identifies two intervals of carbon cycle disturbance. Macerated leaf cuticle and palynological studies reveal detailed floral assemblages (in which angiosperms, including Eudicots, were poorly represented but present throughout) and unprecedented ecological information. New pCO_2 estimates for the Middle Albian are generated from stomatal density measurements, which, integrated with other similar datasets, suggest average pCO_2 in the Aptian-Early Cenomanian of 575 ppm with a decline of ~150 ppm in the Middle Albian. The subsequent rise in pCO_2 through to the Late Albian coincides with a 30 % increase in angiosperm abundance and increased global temperatures; strongly suggesting the role of climate on angiosperm radiation. However, comparisons of vein density, stomatal conductance, stomatal density and pore length between fossil and extant angiosperms reveals angiosperms already possessed advantageous adaptations expected from a low pCO_2 climate by the mid-Albian.

Acknowledgements

I would like to take the opportunity to express my sincere gratitude to several people and organisations without whom this research would not have been possible.

I am deeply indebted to my supervisors Dr Stuart Robinson, Professor Jenny McElwain and Professor Paul Bown for all your guidance, support and encouragement.

Contributions from various funding sources were gratefully received, and without which there would be no research. These funding sources include: three and a half years of funding from NERC, the UCL Graduate Research Fund for supporting a training trip to Dublin, the Palaeontological Association for providing a travel grant to a conference, and the Royal Society and National Geographic for funding in part the Greenland 2009 field season and subsequent research costs.

Without the effort and dedication of the field team, I would have had no material to work on, and I hope the new data in my thesis make your efforts worthwhile; many thanks: Stuart Robinson, Jenny McElwain, Stephen Hesselbo, Richard Barclay, Ken Amor, Gunver Pedersen and Ingrid Hesselbo.

Special thanks to Jim Davy, the man at the heart of UCL and responsible for the success of many PhD students; without all your assistance in the HF lab for long hours in tedious conditions I would not have generated the data for my research. I will always be extremely thankful for the epifluorescence microscope you constructed from the depths of the laboratory stores to call my own for a while.

I must thank Jenny McElwain's research group at UCD, for being so welcoming and patient in teaching me palaeobotanical techniques; in particular, Richard Barclay, for your ongoing assistance with all things botanical. Collaboration with Maurits Horikx and Ulrich Heimhofer in Hannover, Germany, regarding the pollen data in this thesis, was a pleasure and I wish Maurits all the best for his PhD success.

To all friends old and new at UCL, I greatly appreciate sharing the PhD experience, in particular Cherry, Amy and Marianne for always brightening up my day when I return from working in darkness on the epifluorescence scope. A special mention must be given to Nicky Young who has always buckled up next to me in the front seat of life's rollercoaster since our undergrad days in Oxford – you know how much you are appreciated.

Finally, at the very core of us all, I would not be where I am today without all the support and care of my family, who never stopped encouraging and reminding me the world is much bigger than a train ride to London and life in a lab. Adam – you already know how much I appreciate your unfaltering support; it has been an incredible eleven years and the sun is still rising.

Table of Contents

Equations, Tables and Figures List

1. Introduction

1.1 Research aims

This major aim of this thesis is to investigate the relationship between carbon cycling, variations in the partial pressure of atmospheric CO_2 (pCO_2) and the rapid diversification and radiation of the flowering plants (angiosperms) during the mid-Cretaceous (Albian–Cenomanian), so that competing hypotheses regarding the roles of climate and pCO_2 on angiosperm diversification may be tested. A second aim is to improve knowledge of Cretaceous carbon cycling through comparison of new, detailed reconstructions of pCO_2 with pre-existing Cretaceous data. Finally, the thesis aims to improve our understanding of the stratigraphy and palaeoenvironments of the Cretaceous Nuussuaq Group (West Greenland), and to use palaeoenvironmental and palaeoecological information from the floral assemblage contained within those sediments to provide new insights into mid-Cretaceous climate variability.

1.2 Scientific rationale

The Cretaceous period (145.5–66.0 Ma; Ogg *et al*., 2012) is widely cited as an example of greenhouse climate: a warm world with no significant polar ice and, as such, is regarded by some as our best available means to understand Earth surface processes and feedbacks in the wake of future climate change (e.g. Hay, 2010; Hay and Flögel, 2012). Antarctic mean annual temperature estimates for the mid-Cretaceous are on the order of 14–27 °C (Francis and Poole, 2002), whilst sea surface temperatures over the same interval are estimated as high as 30–35 °C (Forster *et al*., 2007; Jenkyns *et al*., 2012). Benthic estimates from the $\delta^{18}O$ of foraminifera reveal significantly warmer temperatures than present day, around 10–14 °C (Huber *et al*., 2002).

High global temperatures throughout the Cretaceous were primarily driven by high concentrations of atmospheric greenhouse gases, predominantly CO_2. However, current estimates of pCO_2 through the Cretaceous, based on biogeochemical modelling and proxies, are highly variable, with a range on the order of 1400 ppm for a single time interval (Passalia, 2009) and many of the approaches to estimate pCO_2 lack the temporal resolution to reveal short-term (<1 Myrs) variations. This uncertainty over absolute pCO_2 values has implications for our understanding of Cretaceous climate sensitivity (e.g. Royer *et al*., 2012).

The source of high CO_2 was likely tectonic; break-up of the supercontinent Pangaea, during the Jurassic and Cretaceous, resulted in the generation of new Mid-Ocean Ridge spreading centres, which released large amounts of mantle-derived CO_2 into the atmosphere (Caldeira and Rampino, 1991; Larson, 1991; Scotese, 1991). The mantle instability associated with the tectonic break-up also led to the emplacement of Large Igneous Provinces (LIPs; Bryan and Ernst, 2008) which also contributed additional large amounts of CO_2, perhaps over geologically brief (few Myrs) intervals.

The marine sedimentary record of the Cretaceous is punctuated by the occurrence of organic-rich black shale, deposited during times of widespread (basin-wide to global) anoxia, during so-called 'Oceanic Anoxic Events' (OAEs; Schlanger and Jenkyns, 1976). OAEs may reflect changes in climate, ocean circulation and/or surface productivity, and have been linked to tectonic changes and LIP emplacement via carbon cycle feedbacks (e.g. Erbacher *et al.,* 1996, 2011; Jenkyns, 1999, 2003). The large-scale burial of organic carbon during OAEs represents significant disturbance of the carbon cycle, and the frequency of such events through the Cretaceous reveals how dynamic carbon cycling and climate likely were (e.g. Föllmi *et al.*, 2012).

The Cretaceous was also a time of biotic innovation, particularly for terrestrial plants. The apparently abrupt appearance of the angiosperms in the fossil record was described by Darwin as an "abominable mystery" (Coiffard *et al*., 2012). The exact origin and age of the base of the angiosperm phylogenetic tree is still debated throughout the palaeobotanical community, although the general consensus supports an Early Cretaceous or older age (e.g. Taylor *et al.*, 2009; Friis *et al.*, 2011). Pollen and plant fossil records indicate significant diversification and radiation of the angiosperms occurred in the mid-Cretaceous, commencing around 5 Myr earlier (110 Ma) at lower palaeolatitudes (Lupia *et al.*, 1999). Most mechanisms proposed for angiosperm diversification during the mid-Cretaceous focus on a disturbed ecological niche of early angiosperms, whereby the floral population was frequently reset by catastrophic environmental events such as flood or fire (Wing and Boucher, 1998; Herman, 2002; Feild *et al*., 2009). The majority of research suggests a wet or ever-moist aspect to the disturbed habitat, but the habit of early angiosperms: herbaceous (no persistent woody stem above ground; Hickey and Doyle, 1977; Taylor and Hickey, 1992) versus woody understory (woody-stemmed plants of shrub-size, not reaching the forest canopy; Feild *et al*., 2004; Coiffard *et al*., 2007), has yet to be fully established. Mechanisms of early angiosperm diversification and radiation, based on a wet, disturbed

palaeoenvironmental niche, explore the significance of physical-trait acquisition which may have out-competed the incumbent flora. For example, flexible flower-based reproduction combined with faster growth rates, high leaf vein density and drought-tolerant features may have been advantageous in disturbed palaeoenvironments (Regal, 1977; Retallack and Dilcher, 1981; Stebbins, 1981; Bond, 1989; Midgley and Bond, 1991; Eriksson *et al.*, 2000; Bond and Scott, 2010; Brodribb and Feild, 2010; Feild *et al*., 2011a, b). However, if the angiosperms emerged in the Early Cretaceous as fossil evidence suggests, the ideas on radiation mechanisms do not fully explain why it took on the order of 30 Myrs to obtain a dominant ecological foothold. In addition, disturbed environments like those affected by flood and fire were likely a common occurrence throughout the Cretaceous (Scott, 2009). The role of global climate changes during the Cretaceous on the angiosperm diversification and radiation should be considered, but has yet to be fully explored. Both Feild *et al*. (2004) and Coiffard and Gomez (2012) suggested that the angiosperm radiation to higher palaeolatitudes was probably prevented by seasonally cold high-latitude climates with a possibility of frost. They hypothesise that only when global temperatures increased sufficiently during the mid-Cretaceous were the angiosperms able to shift poleward with the warm, frost-free climate belt.

Changing atmospheric pCO_2 over short events, such as OAEs may have imposed selective forcing on the floral community, particularly through CO_2 starvation (Teslenko, 1967; Robinson, 1994; McElwain *et al*., 2005a). This thesis aims to reconstruct atmospheric pCO_2 over an OAE; contributing new data to pre-existing compilations of pCO_2 (e.g. Passalia, 2009) to refine the present understanding of pCO_2 levels throughout the Cretaceous, and to produce a record of pCO_2 which can be reconciled with measured changes in floral composition, in particular the dominance of the angiosperms. This integrated approach will permit exploration into the extent which pCO_2 variation may have influenced angiosperm radiation and diversification in the mid-Cretaceous through CO_2 starvation. Direct comparison of changes in pCO_2, floral composition and palaeoenvironmental and ecological interpretations from a single stratigraphic record may distinguish between the influences of pCO_2 (CO_2 starvation) from the role of global climate change (shifting climate belts; Coiffard and Gomez, 2012) on angiosperm radiation. To achieve this, a fossil flora-rich, terrestrial lithology section from West Greenland was sampled in 2009 through the interval of angiosperm diversification (Albian–Cenomanian) from which the following approach was adopted:

1. Carbon isotope stratigraphy of fossil wood and bulk sediment organic matter is measured to assess carbon cycle dynamics and for stratigraphic correlation to published carbon isotope stratigraphy in order to refine stratigraphic age constraints.
2. Relative angiosperm abundance measurements constrain the timing of angiosperm radiation through the interval. Examination of floral composition reveals palaeoecological and palaeoenvironmental information.
3. Stomatal frequency measurements of macerated fossil leaf cuticle provide pCO_2 estimates through the interval.

1.3 Thesis structure

In order to address the research aims, the thesis follows the format:

Chapter 1: Introduction

After setting out the research aims and scientific rationale supporting this research, aspects of dynamic Cretaceous Earth systems are discussed, including: carbon cycling, the prevalence of marine anoxia and the current state of pCO_2 reconstructions for the Cretaceous. The patterns of angiosperm diversification and radiation through the Cretaceous are described and accompanied by an account of proposed mechanisms of the angiosperm rise to dominance. Gaps in our present understanding of the relationship between angiosperm radiation and climate change are identified, from which the hypothesis and research themes of the present study are distilled. The information in this chapter provides the climatic and environmental context into which the new data are interpreted.

Chapter 2: Approach and geological setting

This chapter outlines the approaches relevant to this thesis and introduces the geological setting of the field area. First, the use of carbon isotope stratigraphy to identify carbon cycle disturbances in terrestrial carbon reservoirs is detailed. Second, an overview of atmospheric pCO_2 proxies and models, including a discussion of their relative merits is provided. Third, there is a discussion of other types of information that can be derived from macerated cuticle records: including floral abundance, palaeoclimate information and assessments of stomatal conductance from stomatal measurements. Finally, an account of the fieldwork in West Greenland is given; justifying the site selection, providing a record of

the samples collected and a description of the stratigraphic sections in the form of a graphic log with depositional environment interpretation. Biostratigraphic age estimates from previous studies are discussed and new data, analysed by colleagues in Hannover, are integrated to provide a preliminary age-model.

Chapter 3: Carbon isotope stratigraphy

This chapter presents stratigraphic records of % total organic carbon (% TOC), % total inorganic carbon (% TIC), and carbon isotope ($\delta^{13}C$ ‰VPDB) data from fossil wood and bulk organic matter. The carbon isotope stratigraphy of the section is interpreted, exploring the influence of fossil wood preservation and relationships between TOC and isotope ratios. The isotope data are correlated to marine carbon isotope records in order to provide additional age constraints for the section and to identify intervals of global carbon cycle disturbance.

Chapter 4: Extraction and morphotyping of fossil leaf cuticle

The method of macerating cuticle from sediment is provided in this chapter, in addition to an outline of the benefits of studying cuticle by epifluorescence microscopy over other established techniques. An overview of the cuticle fragment sorting process and construction of the character matrix is followed by a justification of cuticle features used in the character matrix and to categorise morphotypes. The morphotypes are described and identified based on comparison to previously published descriptions and macrofossil leaf samples collected from the field area.

Chapter 5: Floral and palaeoclimate reconstruction

The records of floral change represented by the distribution of morphotypes from the macerated cuticle record are compared to the pollen record derived by colleagues in Hannover, and to previous macrofossil studies completed in the area (Boyd, 1998a-c, 2000, 2004). These changes are compared to: the overall global pollen record, the North American pollen and macrofossil record, and through the introduction of landscape ecology, compared to floral changes in the European record. The floral assemblage is interpreted in terms of plant ecology and habit, providing palaeoclimatic information which is supported by the ecological implications of unique fossil epiphylls (living on the leaf surface) and saprotrophs (decomposition of leaf litter) in addition to other leaf cuticle features which serve multiple ecological uses (e.g. papillose stomata).

Chapter 6: Stomatal measurements and pCO_2

Using morphotypes with sufficient abundance and preservation (as identified in Chapters 4 and 5), the stomatal density and index data are measured, providing the basis of the calibration for pCO_2 reconstruction using the nearest living equivalent (NLE) stomatal ratio and transfer function method. The NLEs are described with a justification of their selection, in addition to an explanation of the calibration processes. The new pCO_2 estimates are compared to other published mid-Cretaceous estimates of pCO_2 derived from the stomatal proxy method. The suitability of previous NLE selections is considered and the compilation of pCO_2 estimates recalibrated accordingly. Measurements of stomatal sizes permits the maximum theoretical stomatal conductance to be calculated, providing insights into the role of transpirational changes linked to pCO_2 variations, in addition to revealing the different strategies of angiosperms and gymnosperms which may have played a key part in the success of the former.

Chapter 7: Synthesis

An integrated interpretation of changes based upon the data presented in the previous chapters is considered in the context of the Cretaceous climate system as outlined in Chapter 1. Through this discussion the research themes are addressed and potential future work is proposed.

1.4 Cretaceous climate

1.4.1 Earth surface temperatures through the Cretaceous

The Cretaceous world is widely regarded as an example of greenhouse climate, with a wide range of evidence supporting warm global temperatures (Figure 1.1). The TEX_{86} palaeothermometer based on the composition of membrane lipids of Crenarchaeota (Wuchter *et al.*, 2004) has facilitated estimates of sea surface temperature (hereafter SST) at a variety of palaeolatitudes, ranging from 26–30 °C for the Early Cretaceous at 60 °S palaeolatitude (Jenkyns *et al.*, 2012; Figure 1.1), to as high as 35 °C in the equatorial Atlantic by the mid-Cretaceous (Forster *et al.*, 2007; Figure 1.1).

Cretaceous ocean temperatures derived from oxygen isotope ratios of planktonic and benthic foraminifera reveal SSTs of around 26–30 °C in the mid- Cretaceous for the tropical north Atlantic (Norris and Wilson, 1998 Figure 1.1) and intermediate–deep water temperatures of around 15°C (e.g. Huber *et al.*, 2002; Bice *et al.*, 2003). The SSTs from

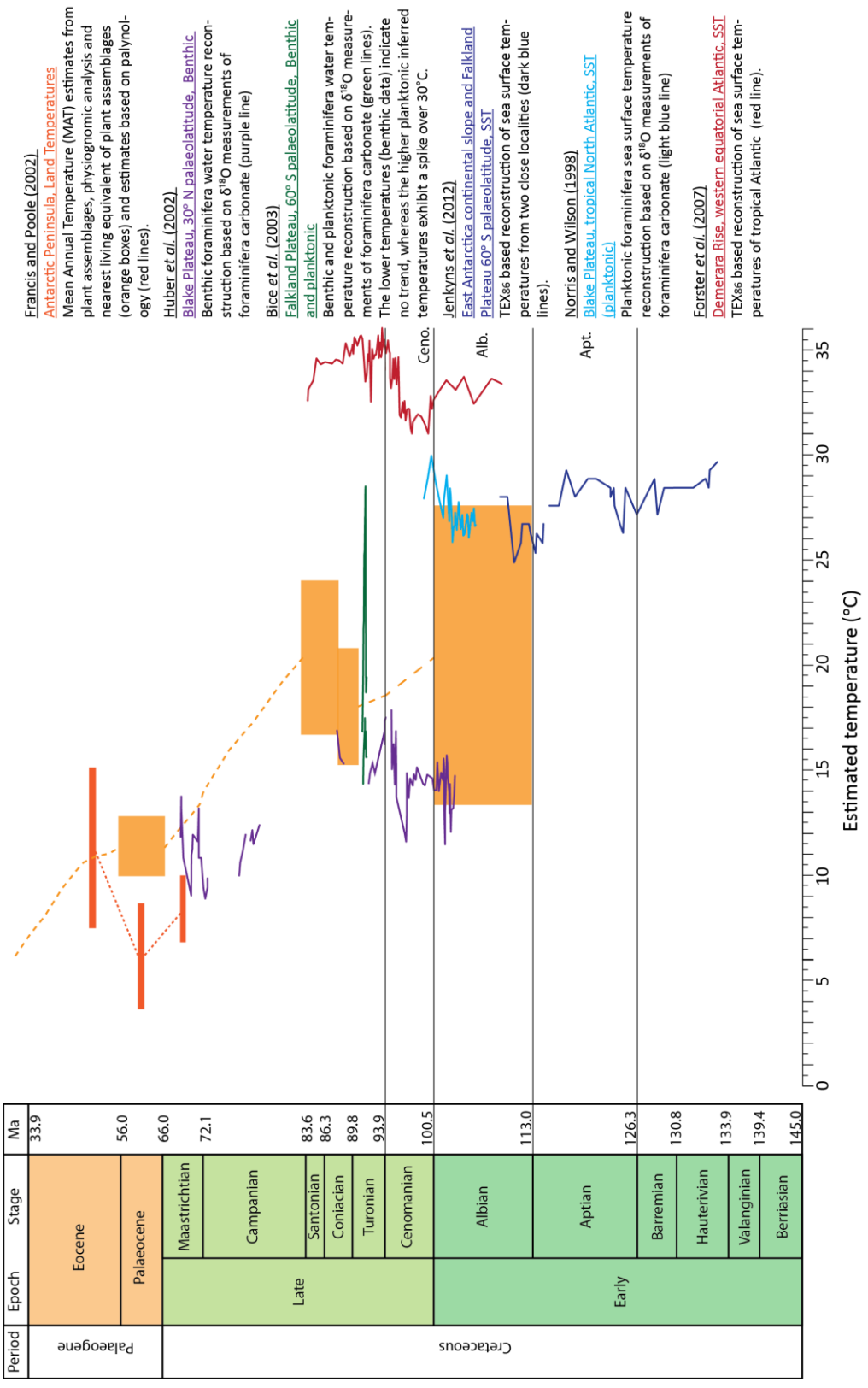

Figure 1.1: Summary of proxy-based palaeotemperature estimates through the Cretaceous (timescale adapted from Ogg et al., 2012), covering: terrestrial MAT estimates from fossil assemblages, TEX_{86} SST estimates for the Equatorial Atlantic and the Southern Ocean, and oxygen isotope based estimates from marine carbonate of planktonic and benthic foraminifera.

foraminifera and TEX_{86} agree well with each other and suggest reduced latitudinal gradients compared to modern (e.g. Huber *et al.*, 2002); the bottom-water temperatures are strikingly different to the modern (1–4˚C). Land-based mean annual temperature (hereafter MAT) estimates based on plant assemblage composition, leaf physiognomic interpretation and extrapolation of nearest living equivalents of floral assemblages (Francis and Poole, 2002 for summary) indicate high Antarctic MAT of 13–27 °C during the mid-Cretaceous (orange boxes in Figure 1.1). Temperatures increased from the Aptian through the Albian to a maximum in the Cenomanian (Figure 1.1; Clarke and Jenkyns, 1999; Friedrich *et al.*, 2012). This increase in temperature through the Albian is supported by the compilation by Frakes (1999) which suggests an increase in marine temperatures of around 5 °C during the Albian and MAT estimates of 13 °C for Arctic palaeolatitudes and 17–20 °C for mid-latitudes (Spicer *et al.*, 2002).

1.4.2 Cretaceous carbon cycling

According to climate models (e.g. Barron and Washington, 1985), the Cretaceous greenhouse climate could only be sustained through elevated atmospheric CO_2 concentrations likely controlled by long-term changes in the carbon cycle. Such changes reflect the response of the Earth ocean-atmosphere system to processes occurring on geological timescales, in contrast to the short-term carbon cycle which incorporates relatively rapid processes such as the production (through photosynthesis) and respiration of organic matter.

The long-term carbon cycle (Figure 1.2; Berner, 2003) demonstrates the balance between the four main carbon reservoirs: the mantle, land (with organic and inorganic carbon in rocks), ocean (carbonate carbon and organic carbon reservoirs) and the atmosphere. Between these reservoirs a series of biogeochemical processes exchange carbon from one reservoir to the next; for example, photosynthetic life utilises atmospheric CO_2 or CO_2 dissolved in seawater to form organic matter, a proportion of which is buried as organic carbon in sediments. This sediment may subsequently be weathered, releasing CO_2 back into the atmosphere. Alternatively, at destructive margins the sediment may be subducted into the mantle, delivering the carbon to the mantle reservoir.

In a case of an increase in atmospheric CO_2 concentration, the greenhouse effect would increase global temperatures and cause an acceleration of the hydrological cycle (e.g. Barron *et al.*, 1989; Suarez *et al.*, 2011), which would increase silicate weathering rates.

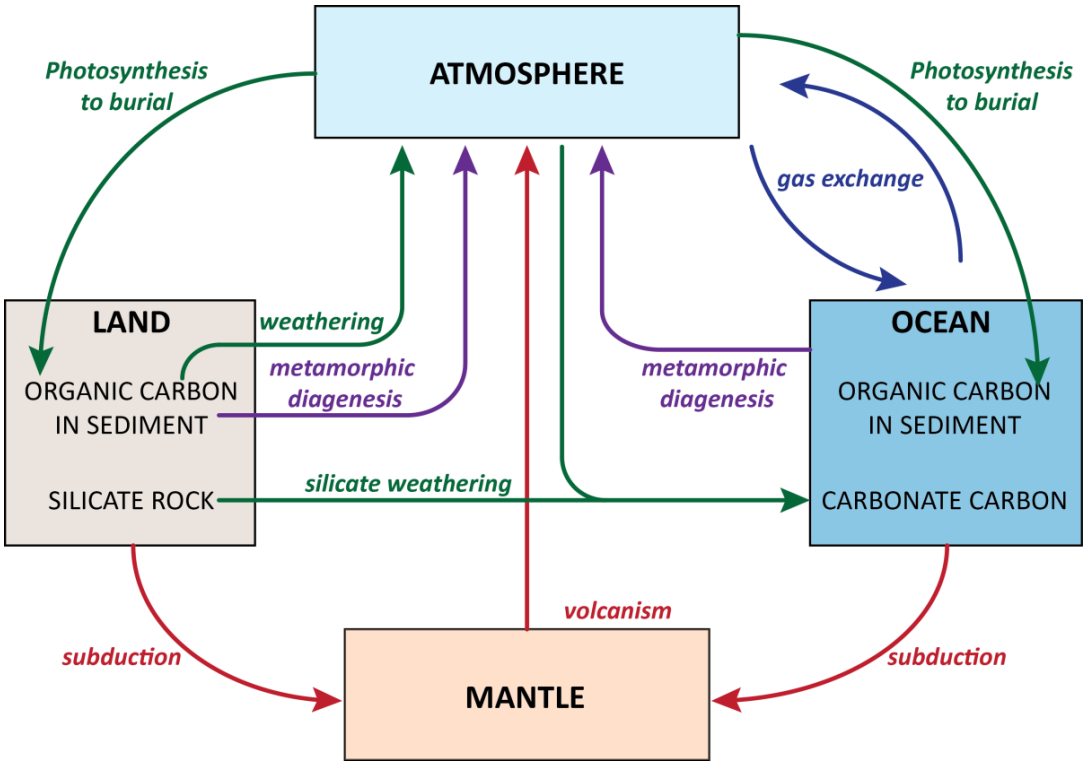

Figure 1.2: The long-term carbon cycle modified from Berner (2003) showing carbon reservoirs (boxes) and summary processes between reservoirs (arrow).

Silicate weathering is an important carbon sink (Figure 1.2), drawing atmospheric carbon into rivers leading to production of carbonate in the oceans (Equation 1.1).

Equation 1.1: Equation of silicate weathering.

$$2CO_2 + 3H_2O + CaAl_2Si_2O_8 \rightarrow Ca^{2+} + 2HCO_3^- + Al_2Si_2O_5OH_4$$

Additionally, as the amount of carbon dioxide in the atmosphere increases, the atmosphere-ocean coupling causes an increase in CO_2 dissolved in the ocean. This causes an increase in marine acidity, which is buffered by dissolution of marine carbonate through movements of the carbonate compensation depth (Zeebe, 2012).

1.4.3 Tectonic events in the Cretaceous as a long-term CO_2 driver

High atmospheric CO_2 most likely originated from mantle degassing associated with tectonic activity through the Cretaceous, including supercontinent break-up and Large Igneous Province (hereafter: LIP) emplacement.

1.4.3.1 Plate tectonic changes

During the Middle Jurassic to end Cretaceous global palaeogeography evolved from a single super continent, Pangaea, to a more dispersed configuration (Figure 1.3) and, consequently, led to an increase in the length and volume of oceanic spreading centres.

The amount of CO_2 produced by mantle degassing at spreading centres can increase due to an increase in the length of the spreading ridge or an increase in spreading rates (Larson, 1991). Therefore, it is likely the break-up of Pangaea resulted in an increased supply of CO_2 to the atmosphere. In addition to the creation of spreading ridges associated with the tectonic reconfiguration in the latter stages of the Mesozoic, it has been proposed that the rate of sea floor spreading may have increased from the middle to late Aptian (Larson, 1991). This is evidenced by a sharp decrease in marine strontium isotope ratios $^{87}Sr/^{86}Sr$ (Figure 1.4), which was interpreted as increase in ^{86}Sr sourced from increased hydrothermal activity associated with an increase in spreading rate (Jones and Jenkyns, 2001). This additional contribution of CO_2 and that associated with the ongoing plate tectonic changes through the Early Cretaceous likely contributed to the increase in temperatures from the Aptian (Figure 1.1).

1.4.3.2 Large Igneous Province (LIP) emplacement

An increase in ocean crust production rates may have been driven by a mantle super plume leading to the emplacement of several LIPs through the Cretaceous (Larson, 1991; Figure 1.4) including:

1. Ontong-Java Plateau - an oceanic plateau mostly emplaced between 126–119 Ma based on osmium isotope data from Tejada *et al.* (2009), with some renewed activity around 96–84 Ma.
2. The Kerguelen Plateau - an oceanic plateau mostly emplaced between 119–109 Ma (Courtillot and Renne, 2003).
3. The Caribbean Plateau - an oceanic plateau emplaced between 90–89 Ma (Courtillot and Renne, 2003).

Estimates of the amount of CO_2 that could have degassed from the volumes of basalt extruded over a few Myr are on the order of 1000–4200 ppm corresponding to an estimated warming of 2.8–7.7 °C (Caldeira and Rampino, 1991).

Figure 1.3 (next page): Mollewide projection palaeogeographic reconstructions by Ron Blakey (http://cpgeosystems.com) for:

A = 150 Ma, Late Jurassic; B = 120 Ma, Early Cretaceous; C = 105 Ma, mid-Cretaceous; D = Late Cretaceous; E = 65 Ma, K-T boundary.

Light blue indicates shallow oceanic waters; dark blue indicates deeper water and land is represented by shades of green and brown.

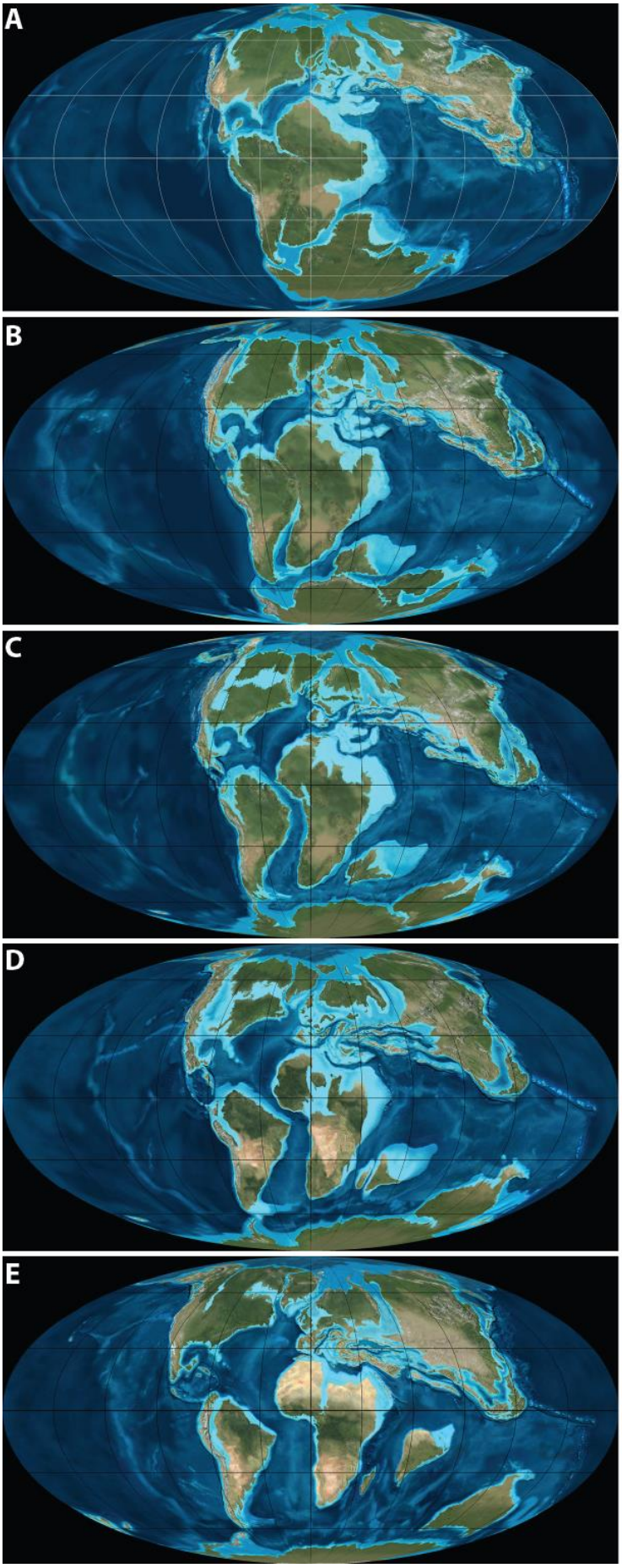

150 Ma
Late Jurassic

120 Ma
Early Cretaceous

105 Ma
mid-Cretaceous

90 Ma
Late Cretaceous

65 Ma
K-T boundary

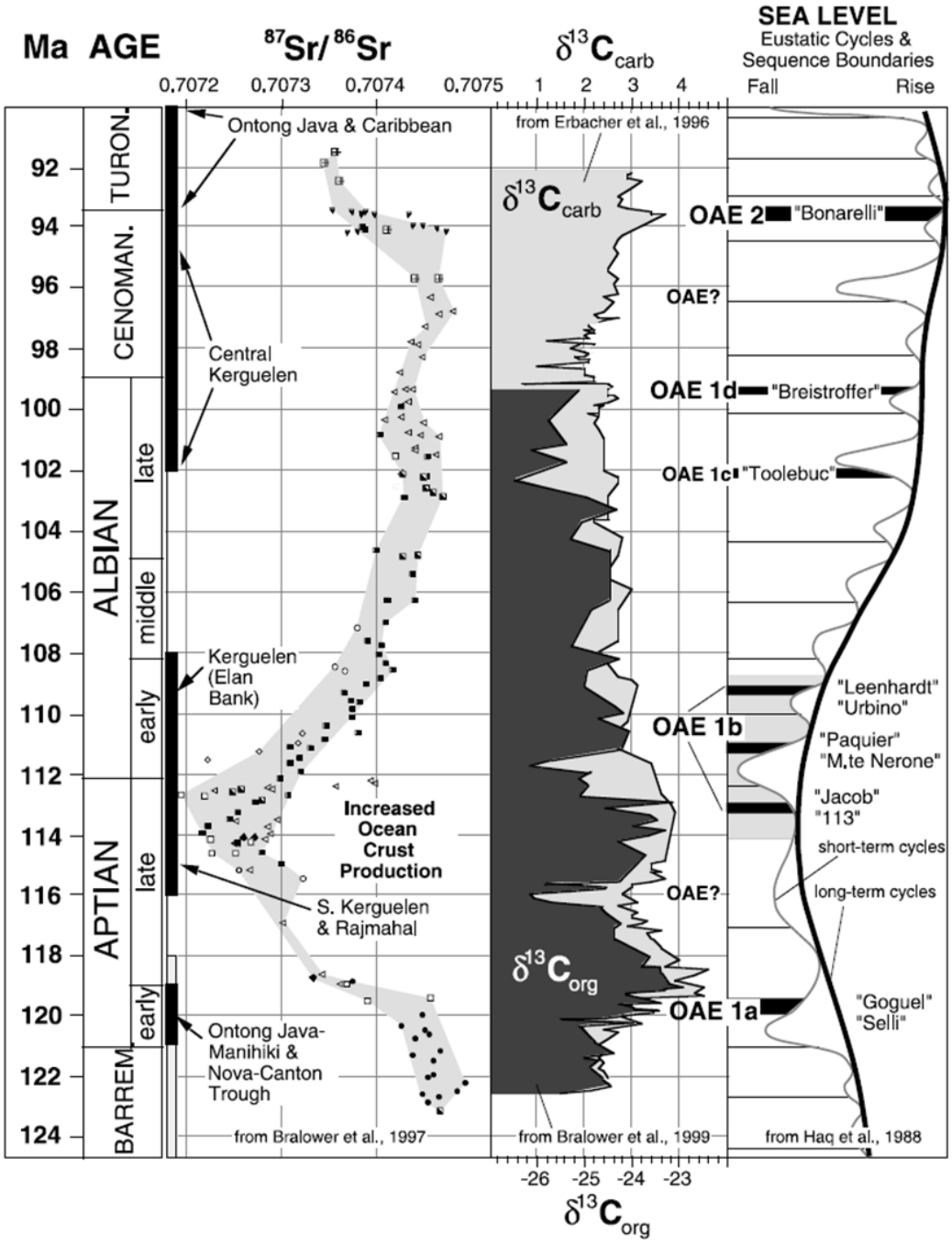

Figure 1.4: Summary diagram for the mid-Cretaceous from Leckie et al. (2002), showing from left to right (with references from Leckie et al.): the age, period of oceanic plateau emplacement, strontium isotope ratios of marine carbonate, organic carbon and carbonate carbon isotope ratios, and eustatic sea level changes with short-term cycles superimposed on the long-term trend. Also indicated are the occurrences of known Oceanic Anoxic Events (OAEs) through this interval (Section 1.4.4).

Therefore, LIP emplacement contributed to the atmospheric carbon reservoir in addition to longer-term mantle degassing through spreading ridges. These tectonic-driven shifts in the global carbon budget were the most likely cause of high atmospheric CO_2 through the Cretaceous.

1.4.4 Oceanic Anoxic Events (OAEs) and short-term changes in pCO_2

Organic-rich black shale deposits of basin-wide distribution occurred several times in the Cretaceous geological record (Föllmi, 2012). These deposits represent durations of marine anoxia on the order of 1 Myr, defined as Oceanic Anoxic Events (hereafter OAEs) by Schlanger and Jenkyns (1976). Respiration of organic matter in the ocean consumes dissolved oxygen, and in cases where surface productivity increases, or ocean circulation stagnates, the oxygen minimum zone can be rendered completely anoxic. Anaerobic bacterial decomposition of organic matter is less efficient than aerobic decomposition, resulting in excess carbon burial in black shales on the order of 1–25 % organic carbon

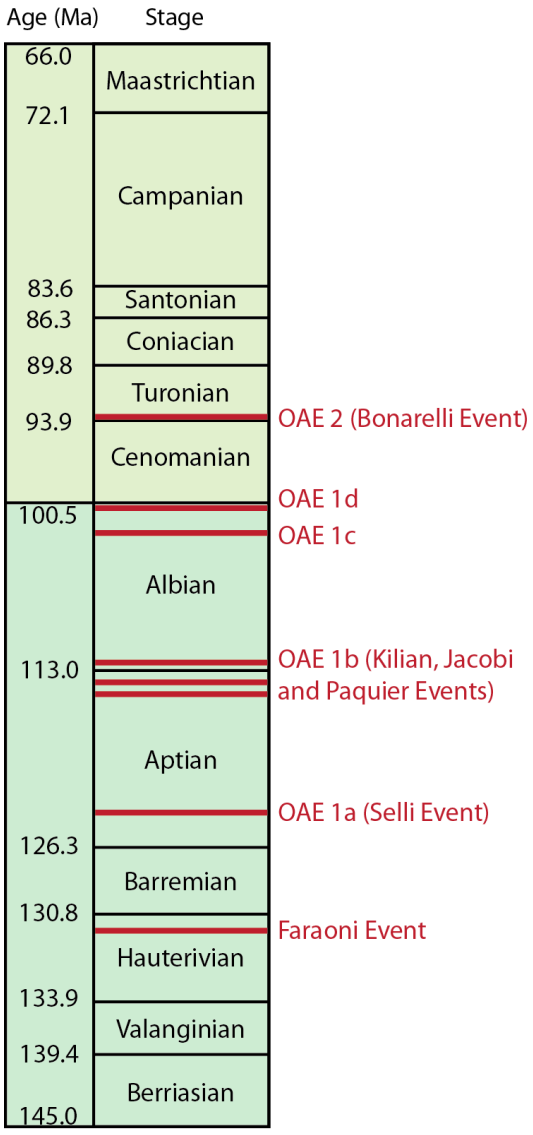

Figure 1.5: Simple Cretaceous timescale adapted from GTS2012 (Ogg et al., 2012) with known OAEs in red.

(Demaison and Moore, 1980). The balance of productivity, sea-level and ocean circulation controlled the mode by which anoxia was achieved during any given event (Thurow *et al*., 1992; Erbacher *et al.*, 1996, 2001; Leckie *et al*., 2002; Jenkyns, 2003; Herrle *et al*., 2003).

The repetition of OAEs through the Cretaceous (Figure 1.5) reveals how frequently an anoxic mode could be induced in the oceans and raises key questions about the sensitivity of carbon cycling through the Cretaceous. Many studies have embarked to address these questions by examining the palaeoclimatic parameters surrounding these events (Figure 1.4; Leckie *et al.* 2002; Föllmi, 2012).

Proposed trigger mechanisms for Cretaceous OAEs vary for each event, but many have been linked to increased surface productivity driven by rapidly increased atmospheric CO_2 from mantle-derived sources accelerating the hydrological cycle and/or enhanced marine vertical mixing delivering more nutrients to surface waters (Tarduno *et al*., 1991; Erba, 1994; Larson, 1991; Larson and Erba, 1999; Weissert and Erba, 2004). In some cases iron micronutrient fertilisation associated with LIP emplacement may also have had a role in sustaining productivity (e.g. Larson and Erba, 1999). A comprehensive review of OAE generation in the Cretaceous by Jenkyns (1999, 2003) also incorporated many of the climate feedbacks associated with these events (Figure 1.6).

For some events, methane may have been released through destabilisation of methane hydrates (Jahrens *et al*., 2001; Weissert and Erba, 2004; van Breugel *et al.*, 2007; Wagner *et al*., 2007; Méhay *et al*., 2009). Methane is a more potent greenhouse gas than CO_2, and oxidises in approximately 10 yrs to CO_2, (Dickens *et al*., 1995) thereby further enhancing greenhouse warming as a driver for the environmental changes that led to marine anoxia (Figure 1.6).

OAEs were terminated through negative feedbacks in the Earth System. The enhanced preservation of organic matter during an OAE removed carbon from the carbon cycle, which would have ordinarily been respired releasing CO_2 back into the ocean. As a result, marine carbon burial in black shale acts as a major carbon sink, drawing down atmospheric CO_2 reducing global temperatures (Figure 1.6, Kump and Arthur, 1999). Additionally, accelerated hydrological cycling may have increased silicate weathering (providing sufficient exposure) providing an additional down draw of atmospheric CO_2, although the burial of organic carbon is most likely the main self-limiting factor of OAEs. With declining

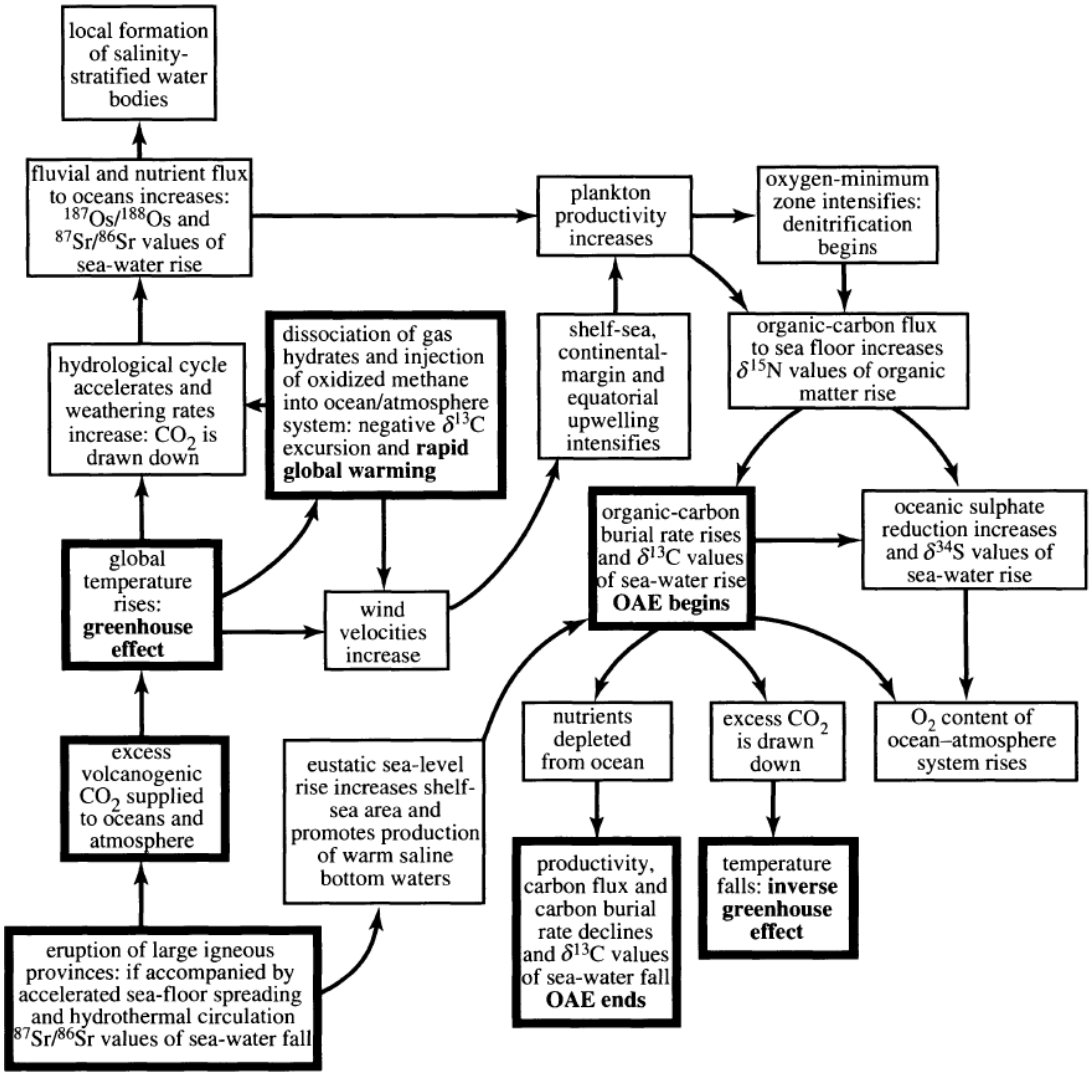

Figure 1.6: Possible relationships between OAEs, greenhouse gas emission and geochemical responses flow chart, from Jenkyns (2003).

global temperatures, the hydrological cycle intensity would have decreased, reducing continental run off, which in turn, decreased nutrient flux and marine productivity.

Despite the differing circumstances triggering each event, OAEs in the Cretaceous were a physical manifestation of disturbance to the carbon cycle and reveal how dynamic Cretaceous carbon cycling and, consequently, climate were.

1.4.5 Cretaceous pCO_2 estimates

Despite the ideas discussed regarding long- and short-term changes in CO_2 during the Cretaceous related to OAEs and tectonics, quantitative estimates and detailed records of atmospheric pCO_2 are still relatively few in number. Passalia (2009) compiled a summary of the available data and models for the Early Cretaceous (Figure 1.7), revealing little consensus on the typical values of pCO_2 in the Cretaceous, nor clear agreement in relative

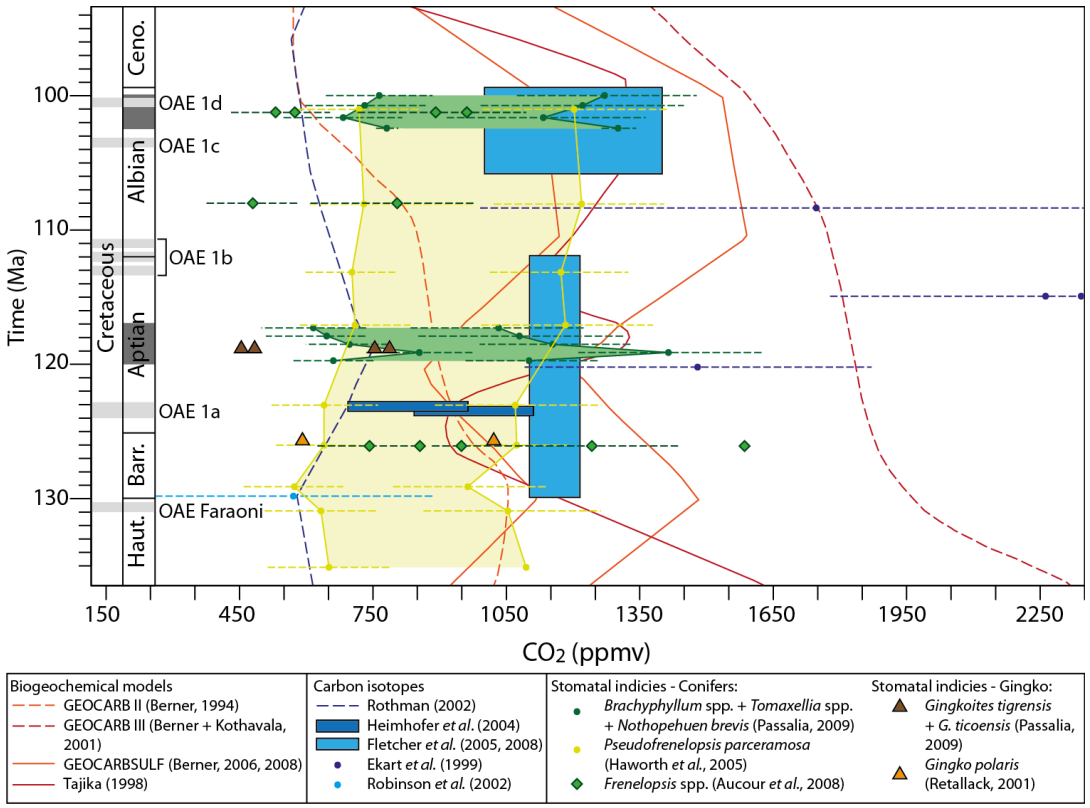

Figure 1.7: pCO_2 reconstructions through the Early Cretaceous summarised by Passalia (2009, references therein) based on: stomatal index measurements of plants (green, brown and yellow/orange), various carbon isotope based reconstructions including pedogenic carbonates (blue), and different biogeochemical models (red continuous and dashed lines).

trends. The various approaches that have been adopted to reconstruct Cretaceous atmospheric CO_2 concentrations are reviewed in Section 2.3.

Some of the discord between reconstructed trends in pCO_2 may reflect differences in stratigraphic resolution of the methods applied; for example, the biogeochemical models have a resolution on the order of 10 Myrs, whereas proxy-based data resolution is generally higher and possesses the capacity to reconstruct short duration pCO_2 changes. The stomatal density-based pCO_2 reconstruction by Haworth *et al.* (2005; Figure 1.7) spans a long interval but has a temporal resolution on the order of 4–8 Myrs, and produces fairly consistent estimates of pCO_2 through the mid-Cretaceous. However, pCO_2 estimates derived from the stomatal density of a similar (within the Cheirolepidiaceae family) by Passalia (2009) covers a shorter time interval, but with a temporal resolution on the order of 1 Myr, revealing an increase and decline in pCO_2 on the order of 200 ppm in the mid-Aptian during the interval defined as OAE1b, and a decrease close to 100 ppm during OAE1d close to the Albian–Cenomanian boundary (Figure 1.7).

High-resolution studies from proxies (such as Passalia, 2009) are the best means of assessing relative changes in pCO_2 during intervals of carbon cycle disturbance and have been successfully applied in other cases. For example, Barclay *et al.* (2010) used stomatal density data from fossil Lauraceae through the Cenomanian–Turonian boundary to reconstruct pCO_2 during OAE2, revealing an increase in pCO_2 at the onset of the OAE, followed by a subsequent 26 % decrease interpreted as carbon sequestration due to black shale deposition.

The great variability in pCO_2 estimates for the Cretaceous and the few high-resolution studies reveal a large gap in the scientific community's ability to quantify pCO_2 levels in the Cretaceous or to test the hypothesised effects of disturbances to the carbon cycle. The studies of Barclay *et al*. (2010) and Passalia (2009) span OAEs but there is scope for more work to be done to understand variability within and between OAEs. Improving estimates of pCO_2 values through the Cretaceous has important implications for understanding Cretaceous climate sensitivity to pCO_2 (Bice *et al.*, 2006; Royer *et al.*, 2012).

1.5 Angiosperms in the Cretaceous

1.5.1 Angiosperm origins

Darwin referred to the abrupt appearance of the angiosperms in the geological record as an abominable mystery (Coiffard *et al*., 2007) but in order to truly appreciate when the angiosperms diverged from the seed plants, an appreciation of what features comprise an angiosperm is required. Most early work used the presence of a flower-like structure as the key feature separating angiosperms from other plant types, whereby the so-called "ABC model" of angiosperm flower identification was used (Figure 1.8; Friis *et al.*, 2011).

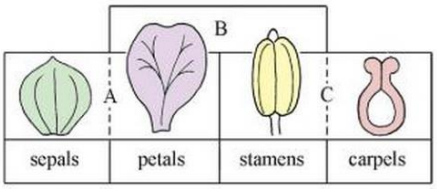

Figure 1.8: The so-called "ABC model" for flower organ identification from Friis et al. (2011).

The unique stamen with two pairs of pollen sacs is uniform across angiosperm flowers, having likely developed from the microsporangiate structures of seed plants (Crane, 1985; Doyle and Donoghue, 1993; Friis *et al.*, 2006). Additionally, the enclosed ovary (by the carpel) and ovules with a double-layered seed coat distinguish angiosperms from the other seed plants (Magallón, 2009; Willis and McElwain, 2014). The reproductive cycle of angiosperms also differs from the gymnosperms, involving double fertilisation (dual sperm

release to fertilise the egg to form the zygote and the storage tissues in the seed; Willis and McElwain, 2014).

Angiosperm lineages are divided into two major groups (replacing the monocotyledon and dicotyledon division) comprising: the ANITA group of basal angiosperms (Amborellales, Nymphaeales, Illiciaceae, Trimeniaceae and Austrobaileyales; Qiu *et al.*, 1999) and the core angiosperm lineages which contain most of the living angiosperms (Chloranthales, Magnoliids, Monocots, Ceratophyllales and Eudicots; Willis and McElwain, 2014). Attempts to assess the timing and order of angiosperm feature acquisition (e.g. the stamen, carpel and other organs comprising the flower; Figure 1.8) led to different theories on flower origins, in particular highlighting the likely relationship of angiosperms to similar fossil plant types (Taylor *et al.*, 2009; Friis *et al.,* 2011; Willis and McElwain, 2014). As a result, historically many plant groups have been cited as the ancestor of angiosperms at some point, including: Caytoniales, Czekanowskiaes, Glossopteridales, Bennettitales, Pentoxylales and Gigantopteridales (Taylor *et al.*, 2009). Modern molecular phylogeny indicates that the Caytoniales are most likely the closest sister taxa to angiosperms, indicating that the ancestral seed plant to angiosperms is extinct (Hilton and Bateman, 2006; Willis and McElwain, 2014). Similar interpretations based on the function of female structures of basal angiosperms and *Caytonia* supports the molecular phylogeny interpretation (Doyle, 2012 and references therein).

A number of problematic fossils (e.g. *Sanmiguelia, Fercula, Problematospermum*) indicate potentially a pre-Cretaceous age for the origin of angiosperm or angiosperm-like plants (Taylor *et al.*, 2009). Acknowledging this, assigning an age to the origin of angiosperms becomes impossible. Instead, the age of the angiosperms must be considered both in terms of the time of origin (which remains unknown) and the time of initial diversification (Figure 1.9; Friis *et al.*, 2011 and references therein). Everything from this diversification point (where all plant characteristics can be definitively assigned to the angiosperm group) onwards is called the crown group, and everything prior is considered a stem lineage (including the enigmatic Jurassic and Triassic fossils).

The earliest unequivocal angiosperms of the crown group are Early Cretaceous in age (McElwain *et al.* 2005; Willis and McElwain, 2014), based on unambiguous monoaperturate pollen of Valanginian and Hauterivian age (Hughes, 1994; Brenner, 1996) in addition to fossil flowers (Friis *et al.*, 1999, 2006; Willis and McElwain, 2014) and fruits (Dilcher, 1989; Friis *et al.,* 2010; Willis and McElwain, 2014) of Barremian–Aptian age.

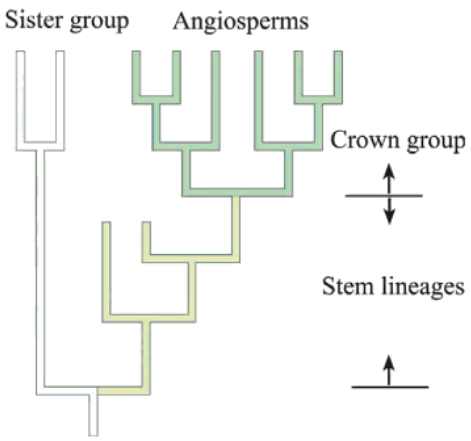

Figure 1.9: From Friis et al. (2011) originally adapted from Doyle and Donoghue (1993), showing the two age points that can be assigned to the angiosperms: the point of origin (the separation of the group from sister groups) and the age of diversification, the point from which the crown group contain all angiosperm characteristics.

1.5.2 Patterns of angiosperm diversification

Several studies compiling floral macrofossil and pollen records for angiosperms and other plant groups (including cycadophytes, pteridophytes and conifers) from North America reveal a significant increase in the dominance of angiosperms from 0 % to 70 % relative abundance in flora across 115–90 Ma (e.g. Lidgard and Crane; 1988, 1990). The relative abundance of conifers within the floras remained similar over this interval; although Lidgard and Crane noted that there were significant systematic changes within this group through the Cretaceous, including the decline of the Cheirolepidiaceae. Cycadophytes and pteridophytes showed a decrease in the make-up of each flora by the Late Cretaceous.

Comparison of the palynofloral response to that reflected in the macrofossil leaf specimens (Figure 1.10) reveals an apparent difference in the observed rate of the radiation and rise to floral dominance of angiosperms (Lidgard and Crane, 1990): whilst the macrofossil leaf data indicated angiosperms comprised 70 % of species by the Cenomanian, a more gradual trend is reflected in the pollen record, where the percentage composition does not reach 50 % until the late Campanian (Figure 1.10). Differences in patterns of diversity and abundance between sporomorph (pollen and spores) and macrofossil data sets have been identified at other times in the fossil record (e.g. during the Triassic-Jurassic boundary, Mander *et al.*, 2010) and is likely in part due to taphonomic differences between the two fossil types (i.e. dispersal range and preservation of sporomorphs related to depositional environment and the possibility of under-representation of reproductively specialised plants; Mander *et al.*, 2010).

Lupia *et al.* (1999) produced a new palynological-based diversity and relative abundance dataset for North America, selecting only published data with good age and palaeolatitude

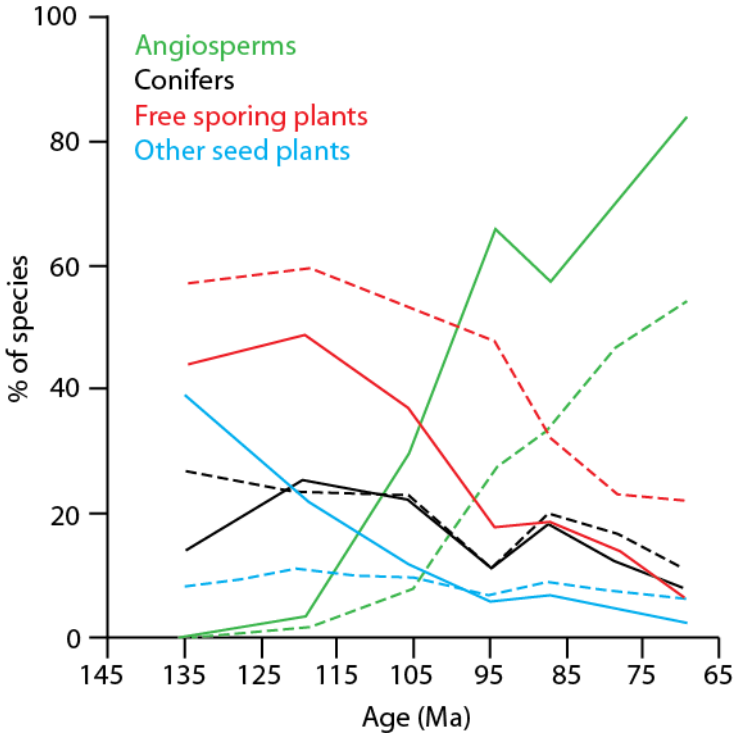

Figure 1.10: Redrawn from Lidgard and Crane (1990), showing in-flora abundance as a percentage contribution of species with time for plant groups (as labelled) for macrofossils (solid lines) and palynology (dashed line).

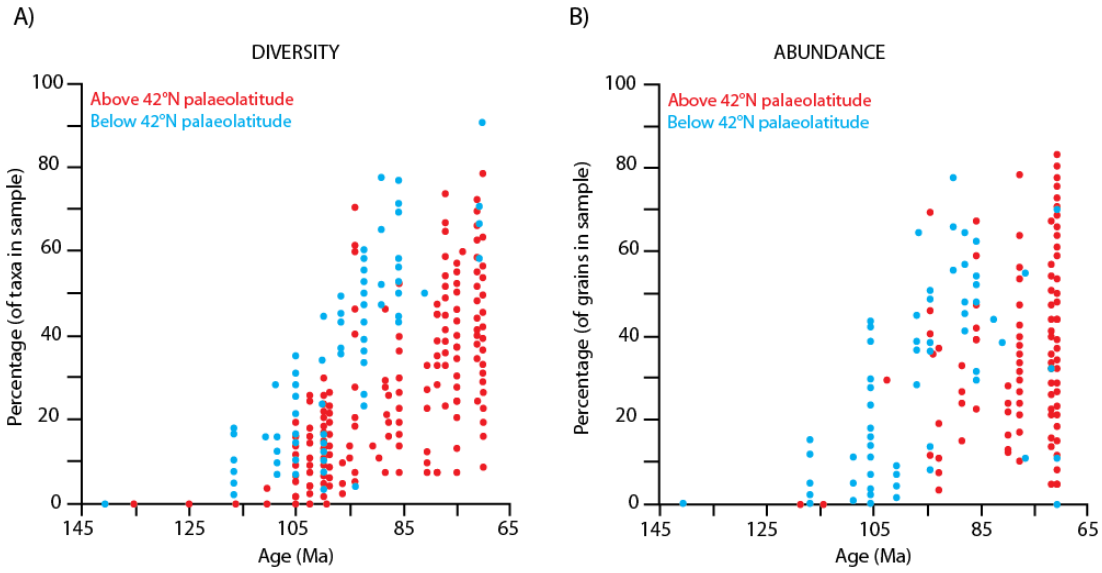

Figure 1.11: Redrawn from Lupia et al. (1999) showing in-flora diversity (A) and abundance (B) for angiosperm samples above 42°N palaeolatitude (red) and samples below 42°N palaeolatitude (blue).

constraints in order to cover a range of palaeolatitudes through the Cretaceous (Figure 1.11). Below 42 °N palaeolatitude the angiosperms diversified more rapidly and reached higher levels of in-flora diversity (67 % versus 42 %) by the end of the Cretaceous compared to higher palaeolatitudes (Figure 1.11A). A similar pattern was observed in the in-flora abundance data, whereby below 42 °N palaeolatitude an earlier and more rapid increase in angiosperm abundance was recorded, compared to higher latitudes (Figure 1.11B). The apparent poleward migration of angiosperms has been observed in similar studies to Lupia *et al.* (1999) elsewhere across Pangaea, including Australia (Nagalingum *et al.*, 2002) and Europe (Heimhofer *et al.* 2005, 2007; Coiffard *et al.*, 2006, 2007, 2012). The latter studies suggest the radiation of the angiosperms at mid-palaeolatitudes occurred during the early Albian. Even the ages of angiosperm pollen first occurrence for individual sections reveal a coarse poleward migratory trend (Figure 1.12; Hickey and Doyle, 1977; Doyle, 2012), whereby monosulcate pollen from basal angiosperms (monocots) appeared before tricolpate pollen from higher angiosperms (eudicots).

Subsequent individual studies of angiosperm pollen occurrences support the summary by Hickey and Doyle: the oldest angiosperm pollen in South America dates from the Aptian (Romero and Archangelsky, 1986), in Antarctica the oldest angiosperm material dates from around the early Albian (Truswell, 1990), and in Alaska the oldest angiosperm megafossils

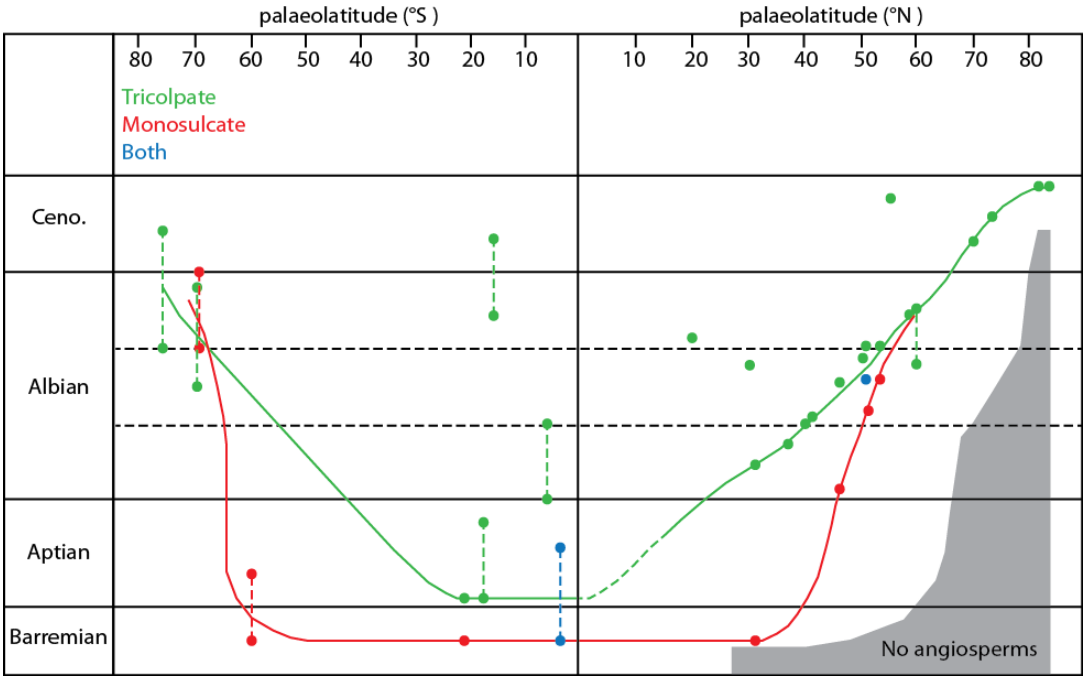

Figure 1.12: From Hickey and Doyle (1977), a summary of the first occurrences of Tricolpate and Monosulcate angiosperm pollen with palaeolatitude and time through the mid-Cretaceous, with site localities labelled in the figure and referenced within Hickey and Doyle (1977).

date from the late Albian (Scott and Smiley, 1979). Studies from West Greenland (approximately 55–60 °N palaeolatitude, Smith *et al.* 1994) identify Tricolpate pollen from the Atane Formation near Skansen, but unfortunately the age of this Formation at that locality is poorly constrained (Koppelhus and Pedersen, 1993).

1.5.3 Mechanisms of angiosperm radiation

Ideas on the cause of angiosperm diversification and radiation focus on the physical characteristics of angiosperms that may have provided a competitive advantage over the incumbent flora in certain habitats. A review by Feild *et al*. (2009) proposes a xerophobic (drought avoidance) early history of angiosperms based on a synthesis of phylogenetic, ecophysiological and geological evidence. Occupying an ever-moist topical niche permitted low risk experimentation of leaf structure, for example the adaptation of reticulate venation. This leaf structure allowed angiosperms to make broad light-catching leaves that maximised photosynthetic rates. Feild *et al.* suggest that any apparently xeric (dry tolerant) angiosperm fossils likely inhabited a wet microsite and that the angiosperms used the ever-wet disturbed niche as a foothold for the first 10–15 Myrs of evolution, with low diversity levels. The experiments in form later provided the plants with the ability to cope in drier environments. Additionally, there is increasing evidence that apparently xeromorphic features serve multiple functions. For example, leaf surface features thought to reduce transpirational water loss in dry environments could also prevent oversaturation of the leaf surface in very wet environments (Haworth and McElwain, 2008).

The habit (form) of early angiosperms is also generally unknown, with two schools of thought considering early angiosperms as either:

1. *Herbaceous* – weedy plants with high reproduction and growth rates, which inhabited close-to-channel riparian, nutrient-rich palaeoenvironments (Hickey and Doyle, 1977; Taylor and Hickey, 1992), or;
2. *Woody understory* – part of the 'dark and disturbed' hypothesis where angiosperms originated in the shady, disturbed (frequently decimated) banks of rivers, not as trees but shrub-size plants (Feild *et al*., 2004; Coiffard *et al.,* 2007).

Despite no consensus on early angiosperm habit, in general most literature agrees that angiosperms occupied disturbed palaeoenvironments through their beneficial fast growth rates. 'Disturbed environments' can be considered as an umbrella term for many different palaeoenvironments including coastal lowlands (Herman, 2002), near river channels (in herbaceous or woody understory form – Hickey and Doyle, 1977; Taylor and Hickey, 1992;

Feild *et al.*, 2004; Coiffard *et al.*, 2007), or even entirely aquatic (Sun *et al.*, 2008). However, the generally poor age constraints of terrestrial deposits makes attribution of the earliest specific palaeoenvironment for the crown group of angiosperms problematic. Depending on the inferred "first" palaeohabitat, a number of radiation and diversification mechanisms concerning advantageous angiosperm traits have been postulated, in addition to the experimentation in form in ever-wet niches later becoming advantageous in drier environments (Feild *et al.*, 2009).

Fossil evidence indicating the co-radiation of anthophilic (flower-visiting) insects with angiosperms in the mid-to-Late Cretaceous is one such proposed mechanism favouring the spread of angiosperms (Grimaldi, 1999). The anthophile insects were present in the Cretaceous and some as early as the Jurassic (leading to speculation on the role of pre-Cretaceous obscure angiosperms and possible Bennettitalean flower-like bracts in the development of these insects; Grimaldi, 1999 and references therein). However, the anthophile insects also underwent a diversification in the mid-to-Late Cretaceous, suggesting a possible relationship between the success of the angiosperms and this insect group; if insect pollination was more efficient than wind pollination over greater areas, the angiosperms could have gained an advantage this way (Regal, 1977).

However, the role of insect pollinators was probably more important in the later stages of angiosperm diversification through the Cenozoic (Stebbins, 1981; Midgley and Bond, 1991) based on the subsequent changes in diversity and abundance of this group through this interval (Grimaldi, 1999). Additionally, the initial phase of angiosperm diversification occurred prior to the apparent radiation of anthophilic insects (Grimaldi, 1999).

An alternative mechanism of angiosperm radiation considers Bond's slow seedling hypothesis (Bond, 1989; Midgley and Bond, 1991), whereby gymnosperm seedlings, in particular conifers, were slow to grow in areas of regeneration compared to angiosperms. Stebbins (1981) outlined the importance of the difference in reproduction between angiosperms and gymnosperms (angiosperms have double fertilisation, a closed carpel providing protection, and features reducing the time between pollination and fertilisation), which made angiosperms more flexible in their reproduction. Flexible angiosperm reproduction is supported by the observed range of fossil seed sizes which were interpreted to be adapted to the openness of vegetation (larger seeds associated with closed forest vegetation; Eriksson *et al.*, 2000).

Angiosperms maximised leaf photosynthetic capacity from low values in the Early Cretaceous, to high values by the mid-Cretaceous (Brodribb and Feild, 2010; Feild *et al.* 2011a) evidenced by a surge in leaf vein density in two phases (Figure 1.13). The first phase at the Albian–Cenomanian boundary was coincident with evidence for the first appearance of large angiosperm trees revealing a significant change in angiosperm hydraulic capacity, but fossil evidence suggests the trees were still restricted to floodplain zones (Feild *et al*., 2011b). The second surge in increased photosynthetic rates occurred at the Maastrichtian–Paleocene boundary when angiosperms began to dominate a wider variety of palaeoenvironments. However, a lack of data for the Turonian may exaggerate this trend and in reality photosynthetic rates may have increased more gradually (Brodribb and Feild, 2010). Regarding the dark and disturbed hypothesis (early angiosperms occupied the shady understory of disturbed environments like fluvial channels), higher leaf vein density and large broad leaves maximised photosynthetic capacities of plants in otherwise shady positions (Feild *et al.,* 2004, 2009).

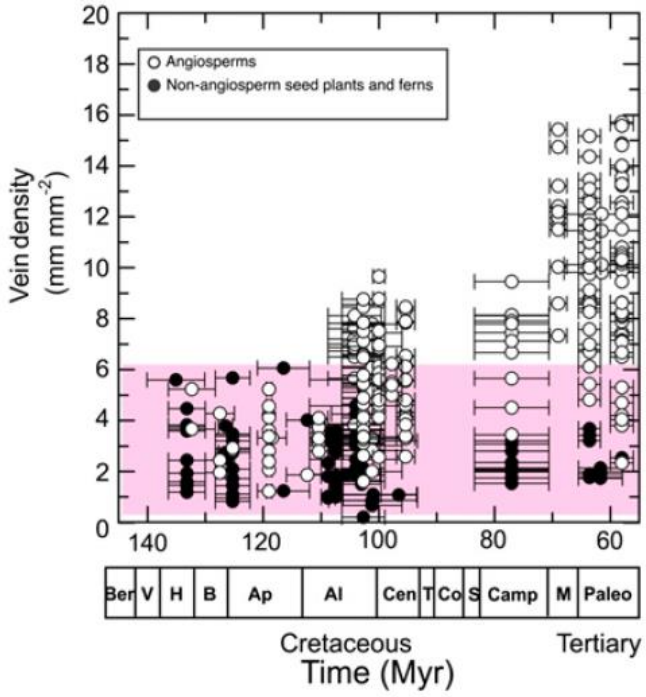

Figure 1.13: From Feild et al. (2011b) showing two phases of increase in angiosperm leaf vein density (open circles): the first during the Albian–Cenomanian, the second from the Maastrichtian–Palaeocene. Closed circles = seed plants and ferns. Pink area = modern and fossil range of non-angiosperms.

1.5.4 The role of palaeoclimate on radiation mechanisms

Becker (2000) critiques Bond's slow seedling hypothesis referring to the inability to separate the generality of angiosperms having more efficient reproductive systems and higher growth rates from the effects that changes of palaeoclimate had on the radiation and diversification mechanisms. As previously suggested, angiosperms were suited to disturbed habitats, based on the physical characteristics of angiosperm reproduction rate and flexibility (Stebbins, 1981; Midgley and Bond, 1991; Eriksson *et al.*, 2000; Brodribb and

Feild, 2010; Feild *et al.* 2011a, b). In areas of regeneration angiosperms had the competitive advantage, because, despite the fact that the gymnosperms were stress-tolerant, they are not considered to be active colonisers (Regal, 1977; Retallack and Dilcher, 1981). Ongoing disturbances over a given area may eventually lead to a transition in floral dominance, towards angiosperms.

Bond and Scott (2010) propose that the angiosperms were facilitated by a self-propelled fire regime, whereby the accumulation of a flammable mass was accelerated by the high productivity of early angiosperms, and as a result angiosperm forests were not fully established until the Eocene when the frequency of fires reduced. This implicates the role of palaeoclimatic zones (seasonally dry) and high oxygen conditions (predicted from models Bond and Scott, 2010 and references therein) favouring the spread of forest fires (evidenced in the geological record by charcoal, with a maximum concentration in the Early-mid Cretaceous (Scott *et al.*, 2014 and references therein).

However, of all the proposed mechanisms, none fully explain why it took the angiosperms on the order of 30 Myr to flourish beyond the restricted ecological niche of disturbed palaeoenvironments. This has led to studies exploring the role of global palaeoclimate changes promoting a modification of the floral balance. Coiffard and Gomez (2012) examine changes in floral composition with respect to palaeolatitudinal climate belt changes reconstructed by Chumakov *et al.* (1995) based on the compilation of geological and fossil evidence (Figure 1.14A-C).

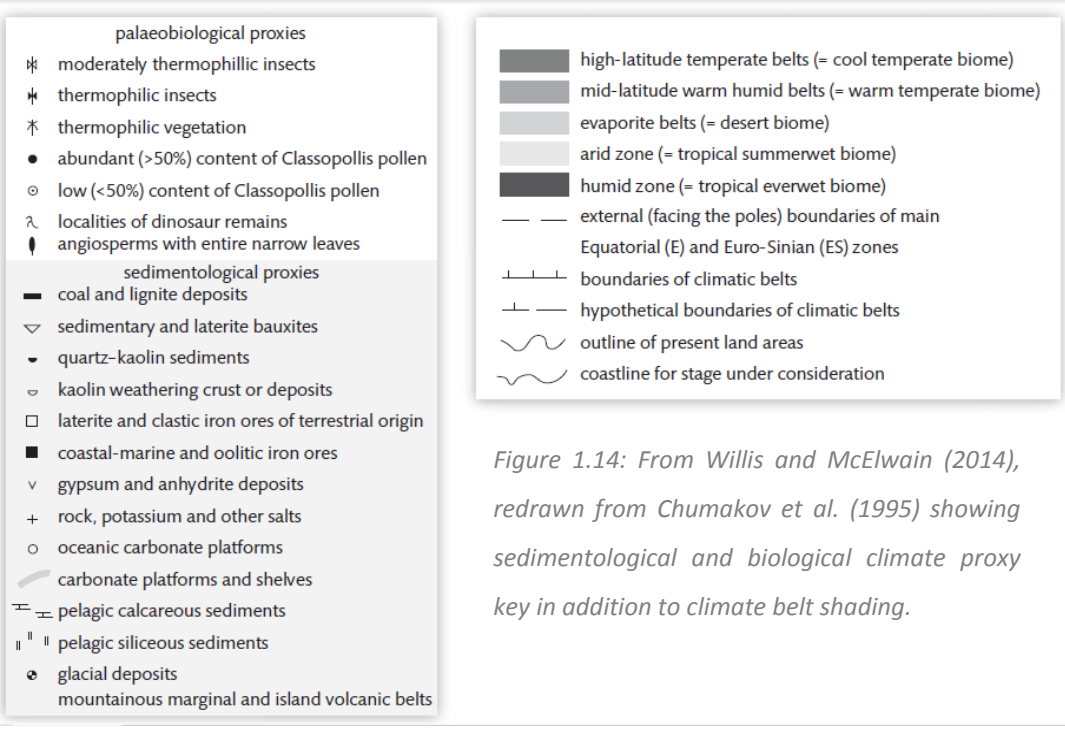

Figure 1.14: From Willis and McElwain (2014), redrawn from Chumakov et al. (1995) showing sedimentological and biological climate proxy key in addition to climate belt shading.

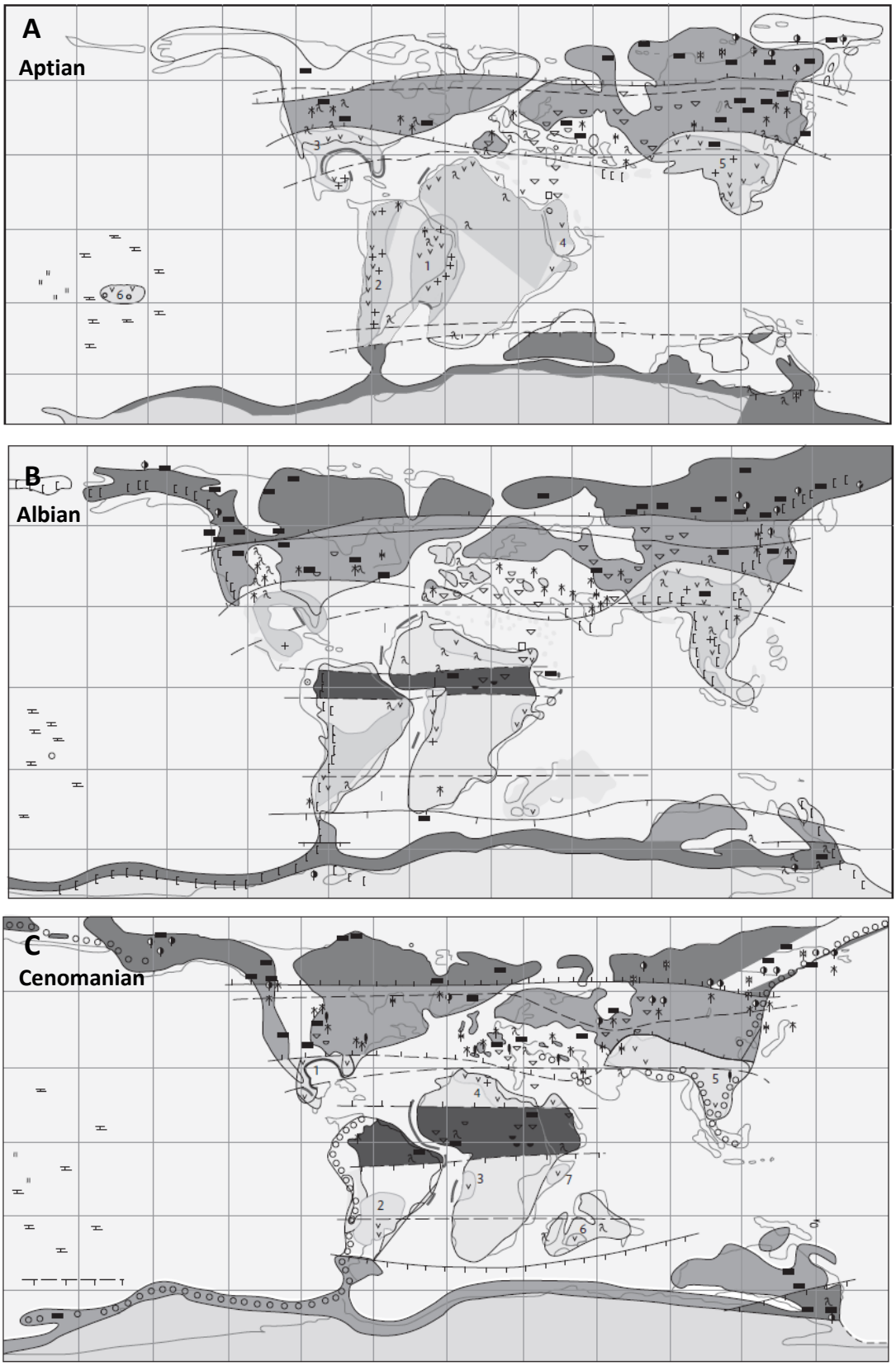

Figure 1.14 (continued): From Willis and McElwain (2014), redrawn from Chumakov et al. (1995) climate belt reconstruction using sedimentological and fossil evidence (key on previous page) for A: Aptian, B: Albian, C: Cenomanian, showing climate zones (shading).

In the early Cretaceous, low latitudes (30 °S–30°N) were dominated by arid and evaporitic climate zones, which were at least seasonally dry (Chumakov *et al.*, 1995; Figure 1.14A); the angiosperm fossil record was sparse but predominantly represented by aquatic and floodplain understory floras (Coiffard *et al.*, 2006, 2007, 2008; Coiffard and Gomez, 2012).

By the Albian, a low latitude humid belt evidenced by bauxites and coals (Figure 1.14 B) persisted and expanded through to the end Cretaceous (Figure 1.14B, C; Chumakov *et al.*, 1995), and floral assemblages from this belt were angiosperm dominant by the Cenomanian (Coiffard *et al.*, 2006, 2007, 2008; Coiffard and Gomez, 2012). In addition, the climate belt reconstructions indicate extensive forests close to the polar region in a high-latitude (60–90 °N) temperate belt, with the mid-latitude (30–60 °N) warm humid belt expanding into the arid zone through the Albian and Cenomanian (Figure 1.14 B, C). During this interval the ecological range of angiosperms is proposed to have expanded rapidly by the Cenomanian, where, at high latitudes, shrub and small riparian angiosperm trees became more common, although forests remained dominated by conifers until the end of the Cretaceous (Coiffard *et al.,* 2007; Coiffard and Gomez, 2012). The increase in global warmth into the Albian allowed the northward movement of megathermal forests to mid-latitudes (Figure 1.14) but may have invoked competition due to the physical barrier of the Tethys Sea (Maslin *et al.*, 2005; Coiffard and Gomez, 2012), allowing the new angiosperm habit adaptations to increase species radiation. The subsequent warming into the Cenomanian continued the spread of angiosperms (in particular the Eudicots) into high latitudes (Coiffard and Gomez, 2012). The role of seasonal temperatures may also explain why the radiation occurred from the palaeoequatorial regions when the mid-latitudes were interpreted to be wetter (Figure 1.14), since the potential for frost initially inhibited growth of angiosperms at higher latitudes, until the shift in climate belts (Feild *et al*., 2004).

1.5.5 The role of pCO_2 on angiosperm radiation

Shifting climate zones may not be the only potential global forcing factor on floral populations though the Cretaceous; changes in pCO_2 have also been suggested (Moor, 1983; Robinson, 1994; McElwain *et al*., 2005) but have yet to be fully tested. Although it has been suggested there may have been transient periods of C4 photosynthetic pathway development in the Cretaceous (Kuypers *et al.*, 1999; Cowling, 2001; Osborne and Sack, 2012) the dominant photosynthetic pathway in the Cretaceous was the C3 pathway, which involves CO_2 fixation by the enzyme Rubisco into a 6-carbon molecule which decays almost immediately into two 3-carbon molecules. The enzyme will uptake oxygen if the available CO_2 concentration is low or if oxygen (the product of photosynthesis) has built up in the

tissue due to water stress or high temperatures causing the stomatal pores to remain closed. Uptake of oxygen results in photorespiration which has a high energy demand, doesn't contribute to sugar making in the rest of the Calvin (C3) cycle, and can lead to a net loss in CO_2 (Pallardy, 2008).

1.5.5.1 Essentials of the CO_2 starvation hypothesis

Robinson (1994) used the generalised hypothesis of stomatal regulation of Cowan (1977) and Cowan and Farquhar (1977) as a starting point for the CO_2 starvation hypothesis, whereby plants seek to optimise stomatal behaviour in order to maximise photosynthetic gain, balanced against water use efficiency. The Cowan-Farquhar hypothesis expresses this in mathematical form; where the optimal stomatal conductance a plant attains is restricted to a curve along which marginal returns for stomatal opening are proportional to the costs of such opening. Robinson suggested this relationship represents an equilibrium plants would follow providing the evolutionary forcing pressures were significant enough to warrant such a change and if there was sufficient time for natural selection. However, Robinson proposes that these two conditions are not uniformly met in practise, resulting in variation of plant stomatal regulation based on genetic and environmental factors. The three main factors influencing the efficiency of stomatal control examined by Robinson were CO_2 concentration, light intensity and moisture availability.

Modern plants maintain a CO_2 gradient between the atmosphere and intracellular CO_2 concentration of approximately 30 % through stomatal regulation to balance photosynthetic effects, resulting in an assimilation cost of 27 % compared to no gradient between intracellular and atmospheric CO_2 (von Caemmerer and Evans, 1991; Robinson, 1994; McElwain *et al.,* 2005). Robinson presents modelled results on the achievable CO_2 gradient of a plant if it maintains a 27 % assimilation cost despite changing atmospheric CO_2 concentrations (Figure 1.15). The results indicated that in a high CO_2 world like the Cretaceous (several times pre-industrial levels), a plant could easily support CO_2 gradients of 50-65 % and as a result the plant could maximise water use efficiency by: occluding

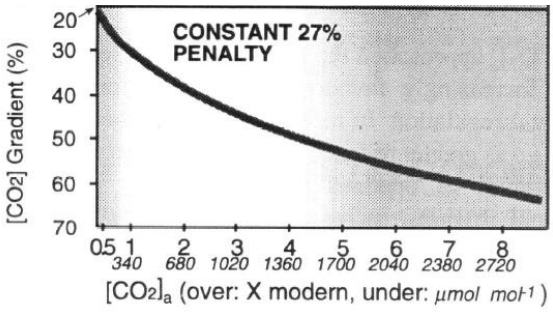

Figure 1.15: From Robinson (1994) showing the maximum CO_2 gradient possible when 27 % assimilation penalty is maintained. Large CO_2 gradients are possible at higher atmospheric CO_2 concentrations.

excess stomatal pores, decreasing the density of stomata across the leaf surface, or by controlling the pores to only partially open (McElwain *et al*., 2005).

The threshold at which a decrease in CO_2 becomes difficult for the plant to fix carbon is called the ecological CO_2 compensation point (ECCP), marking the point where water-loss endurance becomes paramount as the plant opens pores wider for longer, and may also increase the number of stomata on the leaf surface in order to maintain a reasonable CO_2 gradient (Robinson, 1994; McElwain *et al*., 2005). Rubisco is CO_2 saturated for modern plants at around 900 ppm (three times pre-industrial levels). However, Cretaceous flora were likely adapted to higher CO_2 conditions; and there is evidence that modern flora have adjusted stomatal responses as a result of extensive pCO_2 variations due to recent glacial cycles and through having never been exposed to pCO_2 of >350 ppmV (Pagani *et al*., 1999; Pearson and Palmer, 2000; Royer *et al*., 2001). As a result, the atmospheric pCO_2 corresponding to the ECCP for Cretaceous flora is unknown. However, if atmospheric pCO_2 did fall below this unknown threshold in the Cretaceous, physiological drought would have been imposed on the floral population. Therefore CO_2 starvation would have favoured plants possessing characteristics capable to cope with physiological drought, or could more rapidly adapt to such conditions (Robinson, 1994; McElwain *et al*., 2005).

1.5.5.2 Angiosperm adaptations advantageous in reduced pCO_2 environments

As discussed previously, early angiosperms likely experimented with form in a low-stress ever-moist ecological niche, resulting in adaptations beneficial to enduring physiological drought (Haworth and McElwain, 2008; Feild *et al*., 2009). McElwain *et al*. (2005) argue that features evolved by plants which improve water-use efficiency would have been beneficial if CO_2 levels declined beyond the ECCP threshold. Such advantageous traits have been identified in early angiosperm plant fossils, including:

1. *Higher hydraulic conductive capacity* – from the evolution of vessels in angiosperms from gymnosperm tracheids (McElwain *et al*., 2005a). The vessels had a higher conductive capacity and so could support higher rates of photosynthetic activity (Brodribb and Feild, 2010). However, due to the structure of the angiosperm vessel which has a perforated end wall between one vessel element and the next, air embolisms (where air is drawn through this perforate wall) could occur at times of water-stress, or freeze-thaw cycles (McElwain *et al.,* 2005 and references therein). This complements the suggestion that angiosperms radiated from the

palaeoequator rather than the wetter mid-latitudes due to the possibility of seasonal frost (Feild *et al*., 2004).

2. *Increased efficiency of stomatal controls.* The duration of opening and closing stomata for angiosperms may have been faster than most gymnosperms (McElwain *et al.,* 2005), and the xerophyllous nature of gymnosperm leaves including thick cuticle and lignification inhibited the rate of stomatal opening and closing (Robinson, 1994). In addition, angiosperms may have had higher maximum stomatal conductance than other floral groups, which in the event of decreasing CO_2, would have allowed angiosperms to maintain an ideal CO_2 gradient for longer when combined with greater stomatal control (McElwain *et al*., 2005).
3. *High speciation rates* – early angiosperm high speciation and growth rates would have been better suited to enduring CO_2 starvation (Robinson, 1994). Genetic analysis suggests angiosperms evolved rapidly (up to ten times the average for other photosynthetic organism; Runnegar, 1991, Robinson, 1994).
4. *Reticulate venation* – arose in the plant record independently in different plant groups through time (McElwain *et al*., 2005 and references therein). However, the support provided by this leaf venation pattern, combined with xylem vessels permitted large angiosperm leaves, and removed the need to support leaf integrity with lignin. The effect of decreasing lignin may have increased stomatal control in angiosperms.

Ultimately, McElwain *et al*. (2005) propose that a combination of these features led to angiosperms being more successful during CO_2 starvation, since they could maximise water use efficiency whilst maintaining CO_2 gradients for longer than other plant groups. If early angiosperms occupied an ever-wet to occasionally dry palaeoenvironment, water stress imposed by CO_2 starvation would also be reduced, further enhancing the angiosperm's relative success (Robinson, 1994).

1.5.5.3 Early indications on the validity of the CO_2 starvation hypothesis

McElwain *et al.* (2005) plotted diversity data for angiosperms, gymnosperms and pteridophytes against estimated atmospheric pCO_2 from biogeochemical models (Figure 1.16A-C). The observed trends indicate an increase in angiosperm diversity with decreased CO_2 alongside a small decline in gymnosperm diversity and a larger decline in pteridophytes diversity.

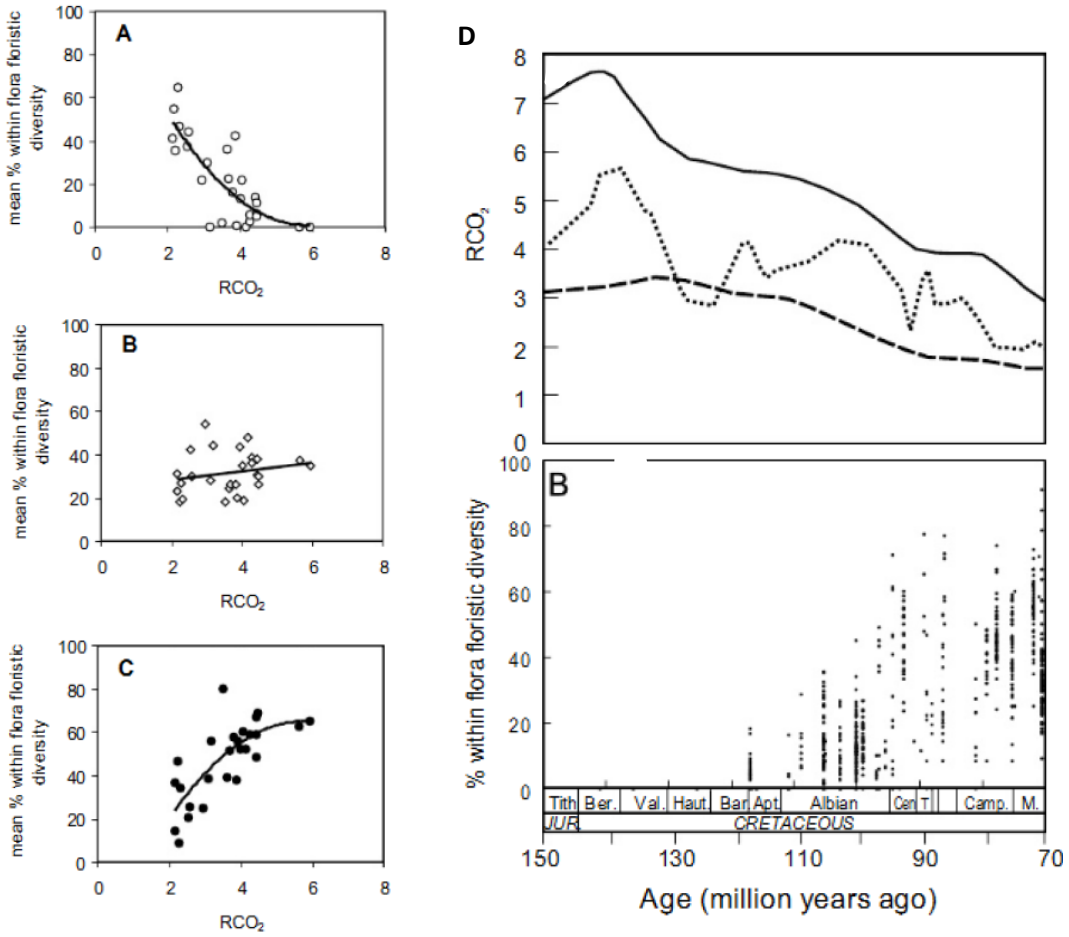

Figure 1.16: From McElwain et al. (2005)

A-C: Mean percentage in-flora diversity against estimated CO_2 (RCO_2 = ratio to pre-industrial values) for the flora age for A = angiosperms, B = gymnosperms, C = pteridophytes

D: Percent in-flora diversity with age of angiosperms (bottom) presented with three different model based estimates of CO_2 (references within McElwain et al.).

When both diversity and CO_2 are considered simultaneously though time (Figure 1.16D, McElwain *et al.*, 2005), CO_2 was apparently declining prior to the angiosperm diversification, suggesting the ECCP value was passed at a certain threshold of CO_2 triggering the radiation. However, the geochemical models of atmospheric CO_2 reconstructions are based on considerable number of assumptions and have a low temporal resolution (Section 2.3.1) such that short-term (on the order of < a few Myr) carbon cycle perturbations are beyond the resolution of geochemical modelling.

Robinson's (1994) hypothesis relies on plants adjusting stomatal behaviours providing natural selection has time to do so. In addition to the possibility of a general decline in atmospheric CO_2 passing the ECCP through the Cretaceous (Late Cretaceous), which would be confirmed by the absolute pCO_2 value estimates from this thesis, the role of relatively rapid CO_2 decline on plants with less water-use efficient adaptations could also be explored

(McElwain *et al.*, 2005). Such rapid declines in pCO_2 have been identified through the Cretaceous during OAEs as a result of carbon sequestration in black shales (Barclay *et al.*, 2010) and the frequency of these episodes particularly through the Early Cretaceous (Figure 1.5) and around the time of angiosperm diversification in the mid-Cretaceous provides an opportunity to explore the influence of CO_2 starvation on floral communities.

1.6 Research themes

The present study aims to address some of the gaps in the current understanding of mid-Cretaceous carbon cycling and climate, in particular the lack of constraint on Cretaceous pCO_2 estimates, the sparse coverage of high-resolution reconstructions during intervals of carbon cycle disturbance of short duration (< few Myr), and the poor age-constraints on angiosperm occurrences (pollen and macrofossils) for the Greenland area. Palaeoenvironmental and palaeoclimatic inferences derived from changes in floral composition and botanical features (e.g. measurements of stomata) may also contribute to the current understanding of the distribution and temporal evolution of palaeoclimatic zones in the Cretaceous.

By focussing on the Albian–Cenomanian time interval, the present study aims to better understand and explore the relative importance of global climate and changes in pCO_2 as forcing factors on the diversification and radiation of the angiosperms.

In order to address these research goals, a four-step approach is adopted to obtain the required palaeoenvironmental and palaeoclimatic information:

1. Identification of a flora-rich section spanning part of the angiosperm diversification and radiation (Albian-Cenomanian)
2. Understanding carbon cycling through the interval using carbon isotope stratigraphy.
3. Reconstruction of pCO_2 through the interval using stomatal density and index data.
4. Derivation of additional palaeoclimatic information from study of plant fossil features and sedimentology.

The research goals will be addressed by coupling the data collected in the present study to previously published regional floral diversity and abundance, and through interpretation in the context of Cretaceous palaeoclimates as outlined in this chapter.

2: Approach and geological setting

2.1 Introduction

In order to address the research themes outlined in Chapter 1, information must be gathered on changes in carbon cycling through the Albian–Cenomanian (including pCO_2) and floral compositional changes through the same time interval. To avoid uncertainties with stratigraphic correlation between disparate areas or environments, ideally all datasets should come from the same stratigraphic section. This constrains the choice of section to one containing a high concentration of plant fossils, which are most commonly found in terrestrial sedimentary successions. As a result, selection of a terrestrial depositional environment also predetermines the methods applied to assess carbon cycling and changes in atmospheric pCO_2 through the interval.

Carbon isotope stratigraphies through terrestrial sediments can be generated by using fossil wood and bulk sedimentary organic matter. Such records can be compared with carbon isotope profiles from other carbon reservoirs (e.g. marine carbonates) to assess whether carbon isotope excursions occur across terrestrial and marine carbon reservoirs and thus represent expressions of global carbon cycling events (e.g. Gröcke *et al.,* 1999; 2006; Robinson and Hesselbo, 2004). In addition, correlation of a terrestrial carbon isotope stratigraphy to a well-dated marine stratigraphy provides a means of refining age estimates of terrestrial sediments, which tend to be less reliably dated than marine sediments. Atmospheric pCO_2 estimates in plant-rich terrestrial sediments can be derived from the stomatal density and index measured from fossil leaf cuticle (e.g. McElwain 1998; Rundgren and Beerling, 1999) and thus it is possible to constrain carbon cycle and palaeobotanical changes within the same stratigraphic section.

The field area selected for this study is the north coast of the Nuussuaq Peninsula, West Greenland, which has a high quality fossil plant record recognised by many workers from as far back as Heer (1874a, b, 1880, 1882, 1883a, b) to more recent studies by Boyd (1998 a, b, c, 2000, 2004). The selected sections were sampled in a 2009 field season led by Stuart Robinson. This chapter reviews the approaches used to address the research goals and provides an overview of the geological setting of the Cretaceous sediments, including a discussion of the lithostratigraphy and chronostratigraphy of the key stratigraphic sections sampled in the 2009 field season.

2.2 Carbon isotope stratigraphy

2.2.1 Carbon isotope fractionation

Carbon in the natural environment is present in two stable forms: ^{13}C and ^{12}C, whereby the proton number in the atomic nucleus remains the same (6) but the neutron numbers differ, such that ^{13}C has 7 neutrons in the nucleus versus 6 in ^{12}C. By having different atomic masses, slight physical and chemical differences arise in the behaviour of molecules containing the different isotopes (Mook, 2000).

The delta notation ($\delta^{13}C$) expresses the relative ratios of ^{13}C to ^{12}C of a material as a per mil (‰) deviation from an accepted standard value which is assigned a value of zero (Equation 2.1). Positive values indicate a relative enrichment of ^{13}C in a material compared to the standard, and negative values indicate the material is ^{12}C richer than the standard. $\delta^{13}C$ values were originally calibrated to the isotopic ratio of a Cretaceous belemnite carbonate sample from the PeeDee Formation in the USA. The material subsequently ran out, but a new reference was calibrated on the basis of the fossil material by a laboratory in Vienna, providing a means of normalising data back to the original PDB (PeeDee Belemnite) standard, such that all data published can be directly compared in the context of the Vienna PDB (VPDB).

$$\delta^{13}C = \left(\frac{\left(\frac{^{13}C}{^{12}C}\right)_{sample} - \left(\frac{^{13}C}{^{12}C}\right)_{standard}}{\left(\frac{^{13}C}{^{12}C}\right)_{standard}} \right) \times 10^{3}$$

Equation 2.1: Delta notation for carbon isotope ratios between ^{12}C and ^{13}C.

The processes transporting carbon between carbon reservoirs in the carbon cycle (Figure 1.2) represent a series of physical and chemical reactions that can result in fractionation of the stable carbon isotopes due to the greater mobility and chemical favourability of ^{12}C (Mook, 2000), giving each carbon reservoir a particular $\delta^{13}C$ range (Figure 2.1; Kump and Arthur, 1999).

In the oceans, there is no significant fractionation effect associated with precipitation of inorganic carbonate resulting in $\delta^{13}C$ values reflecting the ambient marine dissolved inorganic carbon (DIC) $\delta^{13}C$ at the point of formation. This is not the case for all biologically-mediated carbonate precipitation as some species exhibit specific biological fractionations that can result in some difference in $\delta^{13}C$ on the order of ± 1–2 ‰ from the ambient marine DIC $\delta^{13}C$ values (Armstrong and Brasier, 2004).

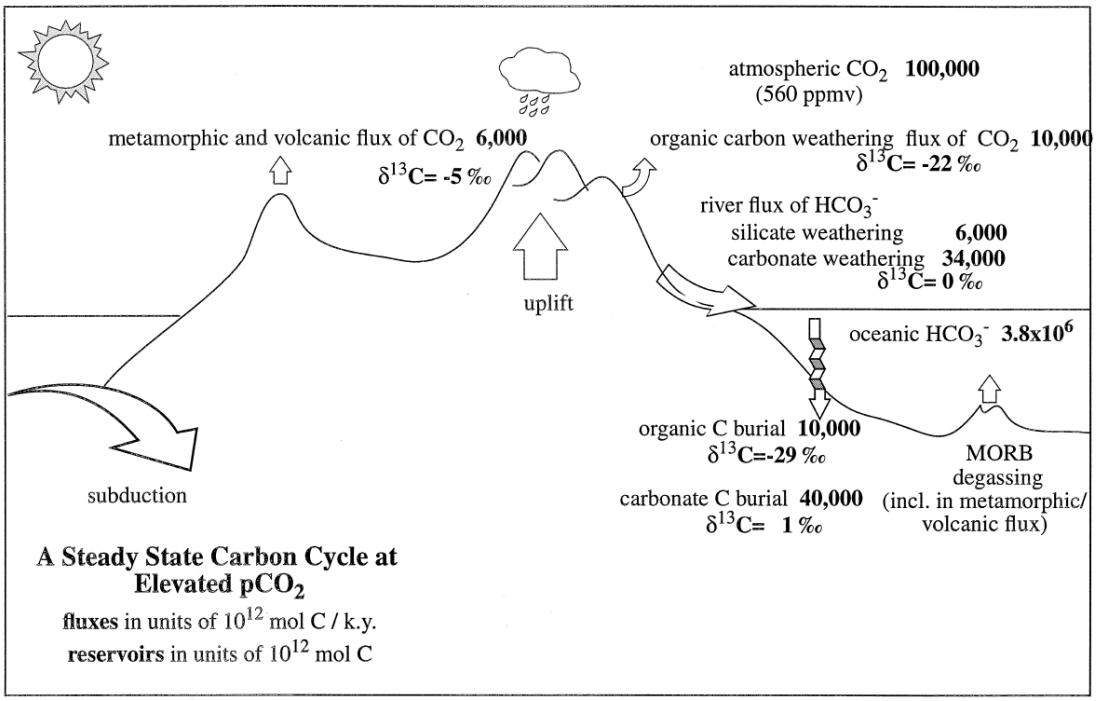

Figure 2.1: The long-term carbon cycle showing carbon fluxes and reservoir content (bold type) and general $\delta^{13}C$ values for a steady state, from Kump and Arthur (1999).

The biological pump is primarily responsible for the distribution of carbon isotopes in both the long- and short-term carbon cycles. Without the strong preference of ^{12}C by photosynthetic life on Earth resulting in a non-equilibrium isotopic fractionation effect, the various carbon species in the ocean and atmosphere would resemble the mantle-derived carbon source of around -5 ‰ because the mantle continually degasses through geological time (Armstrong and Brasier, 2004). Instead, marine organic carbon possess significantly more negative $\delta^{13}C$ values (Figure 2.1) and as a result the ocean DIC is driven to more positive $\delta^{13}C$ values (around 0 ‰) compared to the mantle source as a result of the ^{12}C deficiency.

2.2.2 Carbon isotope stratigraphy

Over time the $\delta^{13}C$ value of a given carbon reservoir can evolve depending on changes in the rates of addition and removal of carbon from the reservoir. Carbon isotope stratigraphy measures the changes in $\delta^{13}C$ of a given reservoir through time in order to interpret changes in the balance of carbon-cycle sources and sinks. However, the material on which $\delta^{13}C$ is measured must be considered carefully as additional factors control and influence $\delta^{13}C$ that may be unrelated to carbon cycling. Figure 2.1 gives generalised $\delta^{13}C$ values for carbon sources and sinks but these values can vary in geological materials, depending on biological 'vital effects', environmental effects and diagenesis. In this chapter, these issues are explored with respect to fossil wood and bulk terrestrial organic matter.

2.2.2.1 $\delta^{13}C$ variation in fossil wood

All means of photosynthesis results in ^{12}C enrichment in organic matter, but the amount of fractionation is controlled by the photosynthetic pathway. Plants which use the C3 photosynthetic pathway record $\delta^{13}C$ values ranging -20 ‰ to -37 ‰ (Kohn, 2010). The largest discrimination of carbon isotopes during C3 photosynthesis occur at the diffusion of atmospheric CO_2 through the leaf epidermis via stomatal pores, and at the fixation site of carbon (Figure 2.2; Farquhar *et al.*, 1989; Tieszen, 1991).

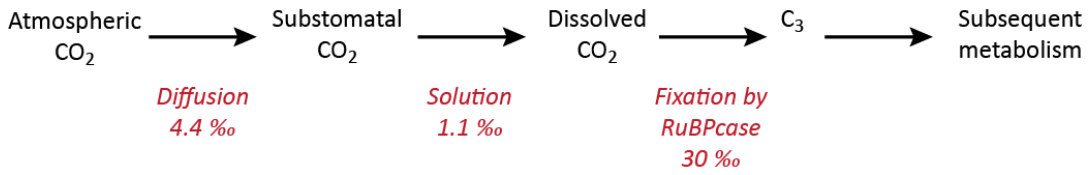

Figure 2.2: Redrawn from Tiezsen (1991) showing the photosynthetic pathway for C3 plants with processes in red indicating where fractionation could occur, along with theoretical values of carbon isotope discrimination at each step (Farquhar et al., 1989).

Plants which utilise the C4 photosynthetic pathway have $\delta^{13}C$ values ranging between -8 ‰ and -16 ‰ (Vogel, 1993) as the result of the different processes that lead to carbon fixation (O'Leary, 1981). The difference in the average $\delta^{13}C$ values of C3 photosynthetic pathway compared to C4 is one of the main methods used to identify the occurrence of C4 plants in the geological record, indicating their presence as early as the Oligocene (Urban *et al.*, 2010). It is possible that the C4 photosynthetic pathway may have evolved several times in the geological past as transient floras (Osborne and Sack, 2012) but, if so, C4 plants must have comprised a low proportion of flora, and the characteristic isotopic $\delta^{13}C$ signal may have been swamped by the dominance of C3 pathway plants (Spicer, 1991; Bocherens *et al.*, 1994 and references therein).

Changes in pCO_2 (partial pressure) may have some effect on the $\delta^{13}C$ value of higher plant matter since higher pCO_2 increases the availability of $^{12}CO_2$, further enriching the plant with ^{12}C (Gröcke *et al.*, 1999). The relationship was tested by plant growth chamber data by Schubert and Jahren (2012) by controlling all other environmental factors, and agreed with the theoretical hyperbolic relationship between pCO_2 and plant $\delta^{13}C$. However, compilations of $\delta^{13}C$ values of modern higher plants from studies where pCO_2 and $\delta^{13}C_{atm}$ values were recorded, reveals the majority of variation in plant $\delta^{13}C$ can be explained by a change in the $\delta^{13}C$ ratio of the atmosphere rather than the pCO_2 (Arens *et al.*, 2000; Gröcke, 2002).

Changes in the atmospheric carbon reservoir are not the only factor influencing the $\delta^{13}C$ of plant material; considerable variation has been recorded from isotopic analyses of different parts of an individual plant, ranging 5–6 ‰ (Leavitt and Long, 1986; Gröcke, 2002; McCarroll and Loader, 2004) raising the issue of several additional factors influencing the $\delta^{13}C$ of fossil plant material. As indicated in Figure 2.2 (Tiezsen, 1991) carbon fixation is not the end product of carbon processing in a plant, and compounds created by further metabolism also fractionate carbon isotopes (Figure 2.3; Gröcke, 2002; McCarroll and Loader, 2004). Based on the preservation potential of the carbon-bearing components of higher plant organic matter, experimental evidence for C3 plants suggests $\delta^{13}C$ values of fossil coal and charcoal should average around -29 ‰ due to preferential carbohydrate loss during diagenesis (Spiker and Hatcher, 1987; Gröcke, 2002 and references therein). However most studies of pre-Oligocene plant fossil wood yield values around -24 ‰ to -25 ‰ (e.g. Gröcke *et al.*, 1999; Gröcke, 2002), revealing a 3 ‰ $\delta^{13}C$ enrichment from expected values during charcoalification and coalification. The exact cause has yet to be clarified, with experimental tests producing variable results depending on heating regime employed (Colombo, 1968; Jones and Chaloner, 1991; Gröcke, 2002 for review).

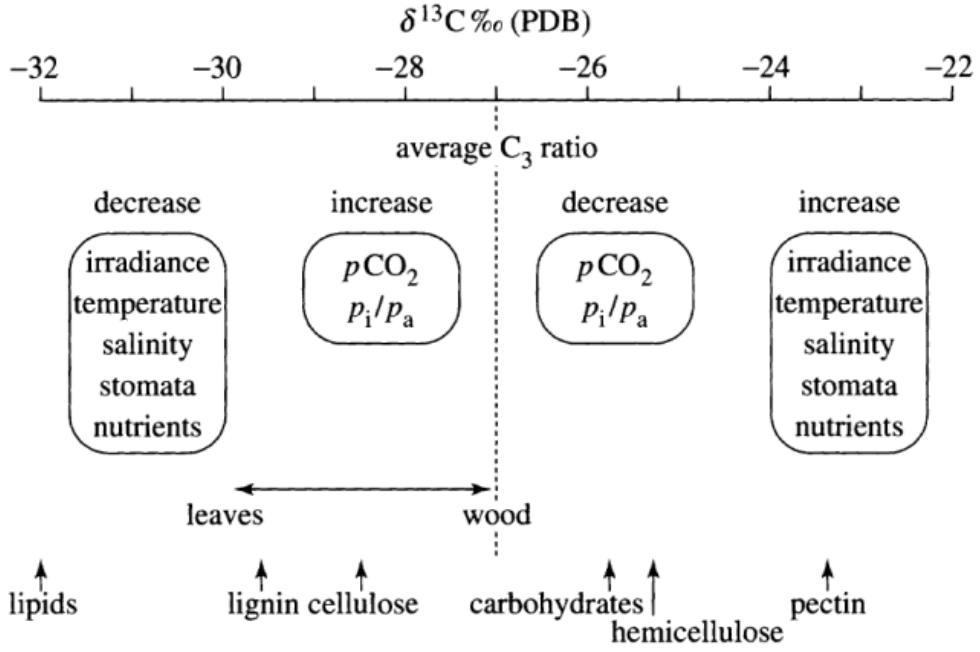

Figure 2.3: From Gröcke (2002), showing the difference in carbon isotope ratios from the average C3 plant ratio for different components of wood tissue, in addition to the difference between wood and leaves (shown by arrows). The factors in boxes refer to environmental influences showing the effect of an increase or decrease of the factor on the isotope ratio deviation from the average value.

Other factors controlling the $\delta^{13}C$ of higher plant matter include the age and size of the tree, which affects the hydraulic conductance of a plant (McCarroll and Loader, 2004; McDowell *et al.,* 2011). The habit (herbaceous, understory, canopy former) and size of the tree may also influence the amount of recycled respired CO_2 encountered, which also is reflected in the $\delta^{13}C$ of higher plant matter (McDowell *et al.,* 2011). Outside the canopy other environmental factors influence the discrimination of carbon isotopes, primarily through water-stress; although where water is plentiful, carbon isotope discrimination is driven by the photosynthetic rate, which is controlled mainly by temperature, irradiance and nutrient availability (Figure 2.3; Gröcke, 2002; McCarroll and Loader, 2004). The plant type analysed may also be important: a study by Schouten *et al*. (2007) across the Palaeocene–Eocene boundary negative carbon isotope event revealed the magnitude of the plant isotopic anomaly in the angiosperms was twice that of conifers, differing by 3 ‰, possibly reflecting differences in water-use efficiency.

2.2.2.2 $\delta^{13}C$ variation of bulk organic matter

Fossil wood carbon isotope stratigraphies can be supplemented with bulk organic matter to fill sampling gaps and confirm trends (e.g. Gröcke *et al*., 2006). In the case of fluvially dominated environments it can be assumed that the bulk organic matter represents a mixture of carbon sources, predominantly phytoclasts (wood and plant debris), with a likely smaller pollen and spore component. In addition, since a sediment sample comprises many small pieces of such debris, some of the extreme variation of values that might be measured from individual wood fragments is smoothed out.

However, taphonomic influences on the composition of the bulk organic matter may vary sufficiently to change the relative proportion of organic components through the section, which can be reflected in measured $\delta^{13}C$ values. This is most likely with a significant change in depositional environment, for example the transition from fluvio-deltaic to lacustrine or even marine incursions, leading to contributions to the bulk $\delta^{13}C$ value from higher plant, phytoplankton and/or algal organic matter (e.g. Hesselbo *et al.,* 2003). This issue can be accounted for if carbon isotope stratigraphy of both bulk organic matter and fossil wood are measured.

2.2.2.3 Correlation of wood and terrestrial sediment organic matter $\delta^{13}C$ value to marine records

Despite the variability inherent in the $\delta^{13}C$ of higher plants, many authors have shown that over long intervals of geological time, global scale carbon cycle disturbances can be

identified in $\delta^{13}C$ of terrestrial organic matter, allowing correlation of terrestrial, marginal and marine carbon isotope records (e.g. Gröcke *et al*., 1999, 2006; Hesselbo *et al*., 2000, 2002, 2003, 2007; Wilson and Norris, 2002; Herrle *et al*., 2002, 2003, 2004; Tsikos *et al*., 2004; Robinson and Hesselbo, 2004; Reichelt, 2005; Bornemann *et al*., 2005; Sageman *et al*., 2006; Barclay *et al*., 2010; Gale *et al*., 2011).

The identification of synchronous shifts in $\delta^{13}C$ values in different geological materials and reservoirs can be used to stratigraphically correlate geographically separated areas. This is particularly useful in the case of terrestrial sediments which often have poor age constraints compared to marine sediments with well-defined biostratigraphies. In terrestrial palaeoenvironments ideally all independently derived correlation ties (e.g. magnetostratigraphy, palynology) should be used to provide additional constraints on carbon isotope correlation (e.g. Robinson and Hesselbo, 2004).

In addition to improving age controls for terrestrial deposits, the correlation of a terrestrially-derived $\delta^{13}C$ record to a marine record can confirm the occurrence of a globally significant carbon-cycle event. This is because the atmospheric carbon reservoir is many times smaller than the marine reservoir (Figure 2.1) and extremely well mixed; as such, $\delta^{13}C$ changes in the atmospheric reservoir are indicative of changes in the global average $\delta^{13}C$ of marine DIC, rather than a consequence of local effects. The abundance of successful studies correlating fossil wood $\delta^{13}C$ records to marine carbonate and organic matter $\delta^{13}C$ records, suggests that the $\delta^{13}C$ of atmospheric CO_2 has the greatest control on $\delta^{13}C_{wood}$ over geological timescales. For many studies in the Mesozoic, it has been suggested that the other factors that influence plant $\delta^{13}C$ (e.g. environmental stresses, plant type and reworking) generally result in varying amounts of noise around a longer-term signal (e.g. Gröcke *et al*., 1999; Hesselbo *et al*., 2000, 2002, 2003 Robinson and Hesselbo, 2004). Comparison of $\delta^{13}C_{org}$ values provides a cross-check on $\delta^{13}C_{wood}$ curves and may reveal spurious values in the fossil wood datasets (e.g. C. Fay, unpublished Master's thesis). Conversely, changes in terrestrial $\delta^{13}C_{org}$ may also deviate from the wood isotope stratigraphy on account of changes in organic matter source associated with changes in lithology and depositional environment (e.g. Hesselbo *et al.*, 2003), so clearly care must be taken when interpreting $\delta^{13}C$ from a sequence containing multiple depositional environments.

2.3 Methods of pCO_2 reconstruction

The demand for fossil plant-rich terrestrial lithologies limits the choice of CO_2 palaeobarometer to the stomatal density and index of fossil leaves (Section 2.3.3) but knowledge of other proxy approaches and geochemical models is important for data comparison. In particular, understanding the benefits and shortcomings of the proxy methods and the geochemical models may help reveal some of the discord in the current understanding of Cretaceous pCO_2 as outlined in Chapter 1.

2.3.1 Geochemical modelling

Geochemical models of atmospheric pCO_2 attempt to quantify rates and define rate laws for processes transferring carbon between carbon reservoirs in the long-term carbon cycle (Figure 1.2) by assuming a quasi-steady state in carbon exchange persists over long time intervals. The GEOCARB model (Berner, 1991) assumes the rate of carbon release into the surface, ocean and atmosphere through organic carbon and carbonate weathering, and volcanic, metamorphic and diagenetic processes on organic carbon and carbonates, equals the rate of carbon burial (organic carbon and carbonate). Carbon isotope fractionation associated with the processes is considered to be a balanced distribution (Berner, 1991; Royer *et al*., 2001 for review).

The simplifications required to make a working model of a complex cycle through time, in addition to uncertainties associated with estimate of model parameters, result in significant uncertainty in the resulting "best-estimate" of atmospheric pCO_2 (Royer *et al*., 2001). Modifications and revisions to the original GEOCARB model to accommodate new data and refined mass balance calculations result in significant variations in the "best-estimate" of Cretaceous pCO_2 (Figure 2.4; GEOCARB II, Berner, 1994; GEOCARB III, Berner and Kothavala, 2001; Tajika, 1998, 1999; GEOCARBSULF, Berner, 2006, 2008).

Despite these revisions, the uncertainty in pCO_2 estimates based on biogeochemical models remains large. In addition, the temporal resolution of geochemical models is limited by the resolution of input data, which for most models is on the order of 10 Myrs (Royer *et al*., 2001). As a result, short-lived carbon cycling events cannot be resolved by such reconstructions. However, these models are useful for considering long-term changes in carbon cycling in terms of the driving processes between carbon reservoirs.

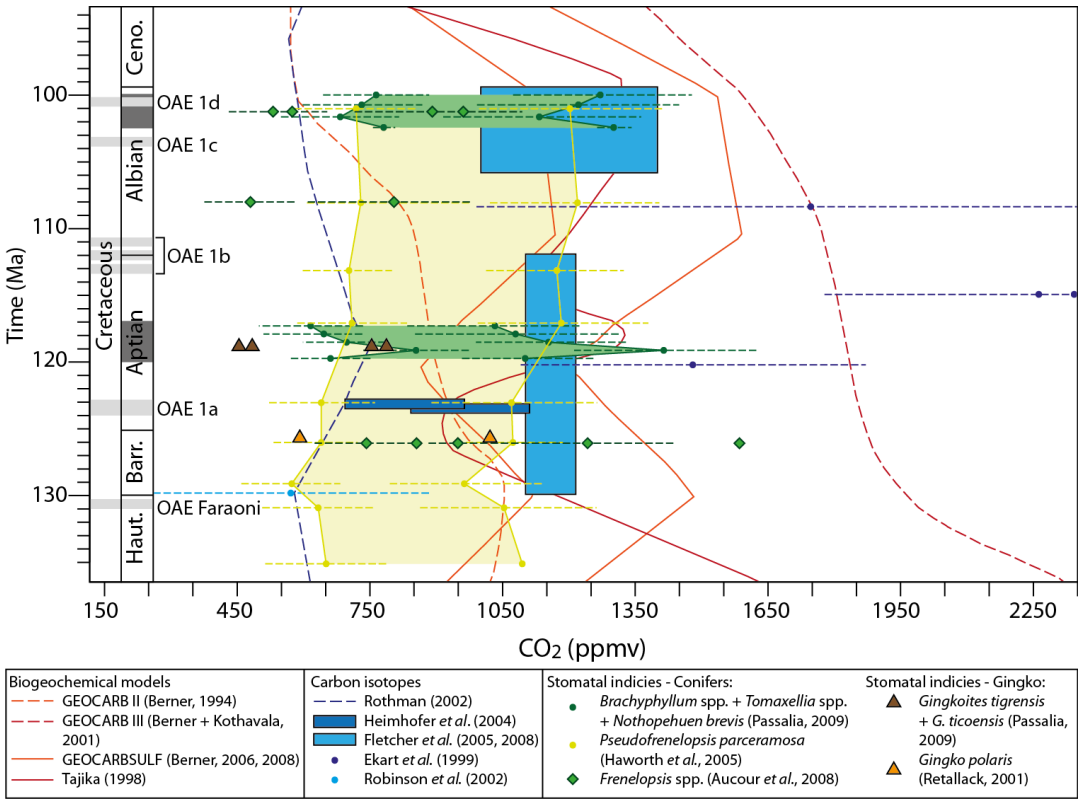

Figure 2.4: pCO_2 reconstructions through the Early Cretaceous summarised by Passalia (2009, references therein) based on stomatal index measurements of plants (green, brown and yellow/orange), various carbon isotope based reconstructions including pedogenic carbonates (blue), and different biogeochemical models (red continuous and dashed lines).

2.3.2 Proxy-based approaches

There are a number of pCO_2 proxies applied to the geological record, some of which have not been applied to the Cretaceous, primarily due to preservational restrictions (e.g. boron-isotopes in planktonic foraminifera, described in Royer *et al.*, 2001) and, as such, the following discussion focuses on techniques that have been used in the Cretaceous.

2.3.2.1 $\delta^{13}C$ of phytoplankton

In a similar way to higher plants, autotrophs fractionate carbon isotopes at two main points in the photosynthetic pathway: where CO_2 diffuses through the boundary layer into the organism and during carbon fixation, such that phytoplankton $\delta^{13}C$ is a function of the ratio of internal to ambient CO_2. The concentration of CO_2 in the water, $[CO_{2\,(aq)}]$, controls this ratio in the case of phytoplankton. Using alkenones (biomarkers from calcareous nannoplankton) these relationships have been extensively exploited to reconstruct Cenozoic pCO_2 (e.g. Pagani *et al.*, 1999). For the Cretaceous alkenones are extremely rare.

Consequently, attempts have been made to relate the difference between $\delta^{13}C$ of other biomarkers or bulk marine organic matter and carbonate to pCO_2 (e.g. Freeman and Hayes, 1992; Heimhofer *et al*., 2004). However, the [$CO_{2\ (aq)}$] obtained may not reflect the true global value due to upwelling or stagnant waters and productivity-driven local conditions (Royer *et al*., 2001 and references therein), which may prove problematic for reconstructions using this method during Cretaceous OAEs when ocean dynamics were variable.

2.3.2.2 $\delta^{13}C$ of pedogenic carbonates

Pedogenic carbonates form in regions typically receiving less than 800 mm of precipitation annually, in well-aerated soils (Royer, 1999; Royer *et al*., 2001; Robinson *et al*., 2002). The pedogenic carbonates form 10^2–10^3 times slower than soil respiration, hence this carbon flux dominates the carbon source in pedogenic carbonates (Cerling, 1991; Ekart *et al*., 1999; Royer *et al*., 2001). By modelling the diffusion-production relationship for well-aerated soils, and assuming that pedogenic carbonates form in equilibrium with soil CO_2, the relationship between the $\delta^{13}C_{carb}$ value and pCO_2 can be obtained (Cerling, 1991; Ekart *et al*., 1999). The fractionation is most sensitive to soil temperature estimates: 20 °C versus 30 °C soil temperature can result in a pCO_2 estimate varying by 700 to 1500 ppmv (Royer *et al*., 2001 and references therein). The proxy is difficult to use over intervals of rapid carbon isotopic change, like OAEs, unless the age is well-constrained (problematic for terrestrial stratigraphies) because the model requires an estimate of atmospheric $\delta^{13}C$ derived from marine chemostratigraphy by assuming constant fractionation factor and ocean-atmosphere equilibrium (Royer *et al*., 2001).

2.3.2.3 $\delta^{13}C$ of bryophytes

Bryophytes are non-vascular plants (liverworts, mosses and hornworts) which do not possess stomatal pores for gas exchange, but instead uptake CO_2 for photosynthesis through passive diffusion into cells (Fletcher *et al*., 2005). The CO_2 uptake and the resulting $\delta^{13}C$ of the organic material is controlled by the kinetics of Rubisco and the diffusion of CO_2 into the cells, which are controlled by the concentration of CO_2 much like phytoplankton (Fletcher *et al*., 2005, 2008; Section 2.3.2.1). The sensitivity of the bryophyte $\delta^{13}C$ to pCO_2 was explored for several extant species by Fletcher *et al*. (2005) revealing minor sensitivities of $\delta^{13}C$ (in liverworts only) to growth temperature, substrate type and water availability, providing a relationship between pCO_2 and $\delta^{13}C$ of this plant type for palaeo-CO_2 reconstruction using fossil material (e.g. Fletcher *et al*., 2005, 2008). However, fossil

bryophytes are rare, and are predominantly found in terrestrial lithologies which often are poorly age constrained.

2.3.3 Stomatal density and index

To achieve the objectives of this thesis, the stomatal density and index of fossil leaves provides the best suited approach for reconstructing atmospheric pCO_2. Stomatal density (Equation 2.2) quantifies the number of stomatal pores per mm^2 of leaf surface. The underlying principle of the relationship between plant stomatal density and pCO_2 is based on the observation first made by Salisbury (1927), that plants regulate the number of stomata on the leaf surface over long time intervals in response to changes in the partial pressure of CO_2 (pCO_2). The role of pCO_2 specifically, and not the mole fraction of CO_2 was identified by Woodward and Bazzaz (1988). This regulation of the plant ratio of internal pCO_2 to external ambient pCO_2 is the main factor controlling stomatal initiation, whereby in times of pCO_2 decline, the stomatal density increases to maintain carbon fixation rates through photosynthesis (Woodward, 1987; Woodward and Bazzaz, 1988; Royer *et al*., 2001 for review). The stomatal pore, however, is also responsible for a large fraction of plant water loss through transpiration, and, as a result, the water-use efficiency (carbon gain per unit of water loss) of the plant decreases as the stomatal density increases. During times of high pCO_2 as stomatal density decreases, the plant improves water-use efficiency, indicating that stomatal control represents a trade-off between carbon gain and water loss. On short timescales (minutes to days), plants additionally regulate water use efficiency by using the guard cells to control the aperture of the stomatal pore and also by changing the leaf angle relative to the sun.

$$Stomatal\ density\ (mm^{-2}) = \frac{number\ of\ stomata}{area\ in\ mm^2}$$

Equation 2.2: Stomatal density calculation (Salisbury, 1927).

However, a number of environmental factors influence the apparent stomatal density (e.g. water-stress, temperatures and irradiance) in addition to the species studied (Salisbury, 1927; Beerling and Woodward, 1996; Beerling, 1999, Royer *et al*., 2001). Salisbury (1927) realised that the area of epidermal cells were likely decreasing in response to the environmental conditions, causing an apparent increase in stomatal density. In order to account for this, he defined the stomatal index: whilst the stomatal density is the number of stomatal pores over a given area, the stomatal index is the number of stomata with reference to the number of every cell (epidermal and stomatal) across a given area (Equation 2.3).

$$Stomatal\ index\ (\%) = \frac{stomatal\ density}{epidermal\ cells\ density\ +\ stomatal\ density} \times 100$$

Equation 2.3: Stomatal index calculation (Salisbury, 1927).

Tests of different environmental factors on measured stomatal density and index reveals the stomatal index successfully accounts for environmental factors that influence leaf area, whilst having no effect on the stomatal initiation factor of changing pCO_2, making this method well suited to examining palaeo-pCO_2. In addition to using stomatal index, it is recommended that large datasets should be collected to negate bias from sun-shade leaf variation (McElwain, 1998) and that pCO_2 reconstructions should be limited to a single plant type per calibration (e.g. Retallack, 2001; Haworth *et al*., 2005; Aucour *et al*., 2008; Passalia, 2009; Barclay *et al*., 2010).

The stomatal index values obtained for a given plant type through a section provide a means of assessing the relative changes in pCO_2, but, to produce quantitative pCO_2 estimates, the data must be calibrated using either transfer functions or the stomatal ratio approach. The transfer function method uses historical or experimental datasets of plant stomatal index response to pCO_2 in order to create a calibration set that can be used to back calculate the fossil values. This method works well for extant plant groups, (e.g. the Holocene pCO_2 reconstruction of Rundgren and Beerling, 1999) but is less applicable to ancient periods in Earth history. This is because many modern plants have persisted through 2 million years of rapid and repeated changes in pCO_2 associated with glacial-interglacial climate variability. Short-timescale growth chamber experiments show that these plants have evolved a sensitivity ceiling in stomatal initiation response to elevated CO_2 (Royer *et al*., 2001). Thus, many present-day plants show little to no response at the high pCO_2 levels likely in the pre-Quaternary, prohibiting the use of these plants as training sets for the transfer function for a high CO_2 world (Haworth *et al*., 2005, 2010).

The stomatal ratio method is more appropriate than the transfer function approach for use on pre-Cenozoic fossil material, particularly for plant groups that are extinct (McElwain *et al.*, 1998; Royer *et al.,* 2001; Haworth *et al*., 2005). A nearest living equivalent (hereafter NLE) forms the reference to pCO_2, and is selected based on morphological and ecological traits which are comparable to that interpreted from the fossil plant. When dealing with fossil material, information on the ecology of a plant can be assessed by facies and palaeoenvironmental analysis, with particular attention being paid to the palaeohydrological setting, as this is important in selecting an NLE. It may be that more than one species represents a suitable NLE in which case average stomatal index across

recent NLE species can be used to create a generalised NLE stomatal index tie-point to modern pCO_2 (e.g. Haworth *et al*., 2005; Passalia, 2009).

To calculate pCO_2 the stomatal index of the NLE is compared to that of the fossil, defining the stomatal ratio (SR; Chaloner and McElwain, 1997). The first calibration to pCO_2 by Chaloner and McElwain (1997) using the stomatal ratios (SR) of four plants (*Sawdonia ornata* and *Aglaophyton major* - Devonian; *Swillingtonia denticulata* – Carboniferous; *Lebachia frondosa* – Permian) was achieved by comparing the SR values to the GEOCARB model output (Berner, 1994; Figure 2.5). Through this comparison, 1SR unit equated to $2RCO_2$ units (where RCO_2 is the ratio of past pCO_2 to pre-industrial levels of 300 ppm), forming the "Carboniferous standardisation".

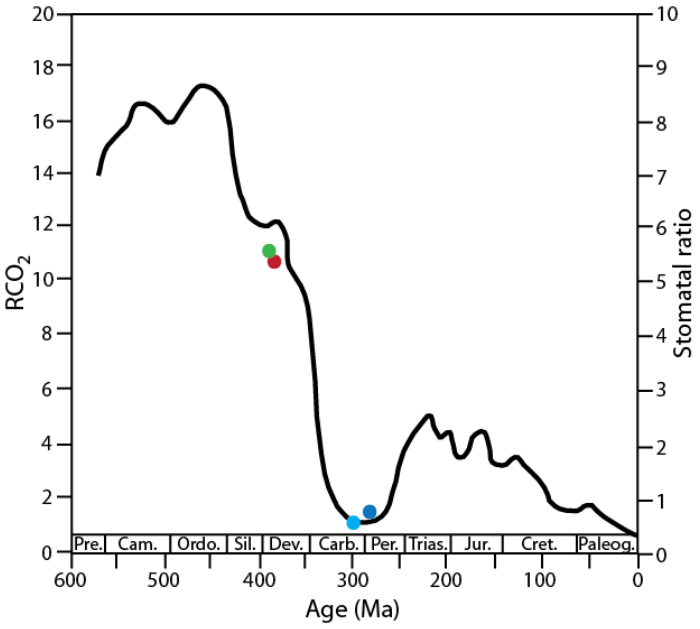

Figure 2.5: Redrawn from Chaloner and McElwain (1997) showing four Palaeozoic plant SR (A. major – green; S. ornata – red; S. dentata – light blue; L. frondosa – dark blue) against the GEOCARB reconstruction of RCO_2 from Berner (1994), revealing 1 SR unit = $2RCO_2$ units.

The "Recent standardisation" was developed by McElwain (1998) by assuming Recent material collected in an atmosphere around pre-industrial levels (300 ppm) would present the relationship: 1 SR unit equates to $1RCO_2$ unit. Thus, these two standardisations provide an upper and lower limit for pCO_2 reconstructions whereby the true pCO_2 value for Mesozoic plants would lie somewhere between the two (McElwain, 1998).

Since this method relies on biogeochemical models, the pCO_2 estimates obtained by this method are semi-quantitative (Royer *et al.,* 2001). However, the relationship is based on an observed coherence in the stomatal ratio of plants to the geochemical model over a coarse temporal resolution, and as such, represents two individual and separate information sources producing a similar trend, which would indicate a linear relationship between the two is likely (McElwain, 1998). In addition, using the GEOCARB II model to calibrate

stomatal index data to pCO_2 does not preclude the identification of rapid pCO_2 changes, rather, it allows high-resolution studies to be superimposed on the long-term carboncycle balance.

2.3.3.3 Other considerations

Other factors which need to be considered when interpreting pCO_2 estimates include the palaeoaltitude of the fossil material, since stomatal initiation is sensitive to pCO_2 (not molar concentration of CO_2) and the assumption that overall atmospheric pressure has not varied through time is untested. Therefore pCO_2 estimates from plants from altitude cannot be assumed to yield equal atmospheric CO_2 concentrations (Rundgren and Beerling, 1999). This is not a problem if palaeoelevation is known, but that is not always the case, although some inferences might be made given the geological palaeoclimatic and palaeo-floral context.

The pCO_2 may also vary due to canopy scale effects, depending on where the leaf was situated in the plant; in the canopy core respired CO_2 can cause increased pCO_2 (Salisbury, 1927; Royer *et al*., 2001). The influence becomes more important when large scale forests are considered, for example the present-day Amazon rainforest has canopy pCO_2 values 30 % higher than ambient (Grace *et al*., 1995; Royer *et al*., 2001). This canopy effect could be present in Cretaceous pCO_2 reconstructions and would most likely be manifested as noise in the stomatal index data and subsequent pCO_2 reconstruction. In a similar approach to dealing with sun and shade leaf morphologies, this effect is best managed by the collection of large datasets, in addition to comparing the stomatal index and pCO_2 reconstructions of different plant species. Where similar trends are tracked by multiple plant species, more certain pCO_2 trends can be inferred.

Poor age constraint of terrestrial stratigraphies may impair the placement of a pCO_2 reconstruction derived from stomatal index if there is no carbon isotope stratigraphy to correlate to a well-dated marine section. However, in combination with carbon isotope correlations to a marine record, high temporal resolution pCO_2 estimates can successfully be generated over relatively short time intervals including episodes of carbon cycle disturbance (e.g. the Triassic–Jurassic boundary: McElwain *et al.,* 1999; Bonis *et al.*, 2010; and Cenomanian–Turonian OAE2: Barclay *et al*., 2010).

2.4 Floral analysis

2.4.1 Floral group abundance

Assessing floral composition change through an interval of geological time can be achieved by studying macrofossils. However, such fossils are often rare and confined to a limited number of horizons. An alternative approach is to use fossil leaf cuticle fragments that are disseminated in the sediment. Fossil leaf cuticle is a wax-like substance which covers all exposed surfaces of a plant, including the leaf, where it retains an impression of the surface cellular detail (epidermal cells and stomatal pores). The cuticle can be retrieved from the host sediment by acidification which leaves behind only acid-resistant organic debris (cuticle, wood fragments, and pollen and spores).

Fossil leaf cuticle has been demonstrated to have sufficiently different genetically defined characters (genotypic) to distinguish between plant groups (Figure 2.6), even to genus and species level depending on preservation (Boyd, 1998 a-c; Barclay *et al*., 2007). The Cuticle Database, developed by Barclay *et al.* (2007), is an online resource of cuticle images for the purpose of identifying fossil material. The user identifies the material by following an identification key flowchart with example images to compare the sample material to at each flowchart query point.

Since fossil leaf cuticle preserves epidermal cell and stomatal complex detail, macerated cuticle and cuticle preserved on macrofossil specimens can be used to measure stomatal density and index for pCO_2 reconstruction (subject to the issues discussed in Section 2.3). However, whilst macrofossil identification is relatively straightforward, the smaller and more fragmentary nature of disseminated cuticle can be more problematic to identify. In these cases the concept of morphotypes is employed (Barclay *et al*., 2007; Barclay, 2010), whereby a morphotype represents cuticle pieces sharing the same characteristics, and, by extension, are assumed to represent the same plant type. A few pieces representing the holomorphotype possess all the cuticle traits required to identify that particular morphotype, and serve as the reference for comparison of cuticle pieces that may not have all traits but possess sufficient to distinguish them from other floral types. As a result, cuticle fractions that may have been deemed too small for stomatal density measurements, or because stomata were not preserved, can be sorted into plant groups using the morphotyping method with the application of a logical and decisive character assessment like that of Barclay *et al.* (2007). Thus, a compilation of cuticle-based relative abundance data of plant groups provides an additional record that can be compared to macrofossil

	Major Characters	Genotype	Phenotype
CUTICLE	Papillae type and position	X	X
	Secretory structures (glands, glandular hairs)	X	
	Stomatal complex type	X	
	Stomatal distribution (rows, dispersed, sunken)	X	
	Stomatal position (amphistomatous, hypostomatous)	X	X
	Striations (intercellular, intracellular, epicuticular wax)	X	X
	Trichomes (type, complexity, location)	X	
	Trichome bases plus surrounding cell arrangement and number	X	
	Cell walls (degree of crenulation)		X
	Hydathodes (position, size, number)		X
	Papilla number and size		X
	Stomatal density		X
	Stomatal index		X
	Trichome density		X
LEAF	Palisade parenchyma (structure)		X
	Palisade to mesophyll parenchyma ratio		X

Figure 2.6: Summary of genotypic (genetic) controlled cuticle characters, compared with phenotypic (environmentally) controlled characters, from Barclay et al. (2007).

data in order to understand floral changes through a stratigraphic section and how changes relate to carbon cycling and palaeoclimate.

2.4.2 Additional palaeoclimate information

As summarised by Barclay *et al*. (2007) some features of leaf cuticle depend on the palaeoenvironmental conditions rather than genetics (Figure 2.6), and can thus potentially, be used to derive palaeoclimate information. For example, purported xeromorphic leaf cuticle adaptations include thick cuticle, sunken stomata and stomatal furrows, trichome (hair), and both epidermal and stomatal papillae (Watson and Alvin, 1996; Haworth and McElwain, 2008). These features reduce water vapour loss by increasing the resistance of the boundary layer of still air around the leaf surface which inhibits water vapour transpiration, increasing the boundary layer stability and increases the path length of water vapour loss (Haworth and McElwain, 2008).

However, these features are not solely restricted to plants which inhabited water-stressed environments based on facies analysis (e.g. the Wealden Flora of Southern England; Watson and Alvin, 1996), and therefore should not be used to infer aridity without consideration of the depositional environment. Instead, cuticle features may have served multiple functions in the palaeoenvironment, and interpretation alongside the sedimentology can be used to support palaeoclimatic reconstructions (Haworth and McElwain, 2008).

Other palaeoclimatic indicators can be revealed by evidence of epiphytic communities in the phyllosphere (organisms living passively on the leaf surface). If true epiphylls (not

parasitic) these organisms draw water solely from free water on the leaf surface, indicating likely humid conditions prevailed, potentially with high mean annual rainfall (Andrew and Harris, 2000; Taylor *et al.*, 2009). Modern epiphylls are found in great abundance in tropical rainforests, where plants possess leaf-form adaptations such as drip tips to regulate the amount of water on the leaf surface (Lücking and Bernecker-Lücking, 2005). Identification of leaf tips which may aid water shedding may also indicate high annual rainfall.

2.4.3 Stomatal conductance (g_{wmax})

Stomatal conductance is the main plant control on transpirational water losses, whereby reduced stomatal conductance results in less water loss, although environmental factors such as irradiance, atmospheric humidity and air movement also play an important role in water loss (Beerling and Woodward, 2001). The transpirational feedback of vegetation on the hydrological cycle has yet to be fully explored in the geological record and, in particular, differences between angiosperm and gymnosperm floras. An assessment of the maximum theoretical stomatal conductance to water vapour (g_{wmax}) can be measured from stomatal density and stomatal size (Franks and Beerling, 2009; Equation 2.4).

$$g_{wmax} = \frac{\frac{d}{v} \times D \times a_{max}}{\left(l + \frac{\pi}{2}\sqrt{\frac{a_{max}}{\pi}}\right)}$$

Equation 2.4: Stomatal conductance to water vapour from Franks and Beerling (2009).

Where:
d = diffusivity of water vapour in air (m^2s^{-1})
v = molar volume of air (m^3mol^{-1})
D = stomatal density (m^{-2})
a_{max} = maximum open area of stomatal pore (m^2)
l = pore depth (m)

The stomatal conductance increases with an increase in stomatal density (D) and/or an increase in stomatal size (a_{max}). Growth experiments of plants in elevated pCO_2 revealed an increase in growth and photosynthesis, but a decrease in stomatal conductance (Ainsworth and Long, 2005 and references therein). In such short timescale experiments the decrease in stomatal conductance was mainly reflected in a decreased in stomatal size (Beerling and Woodward, 2001). However, leaf measurements of stomatal conductance on fossil material (Figure 2.7; Franks and Beerling, 2009 and references therein) and historical herbarium material (Lammertsa *et al.*, 2011) indicated at elevated pCO_2, stomatal conductance decreased as a result of the stomatal density decreasing, and that the stomatal size increased. This difference in results likely reflects the difference in timescales

between growth chamber studies and the centennial-to-geological timescales involved with historical and fossil-based measurements.

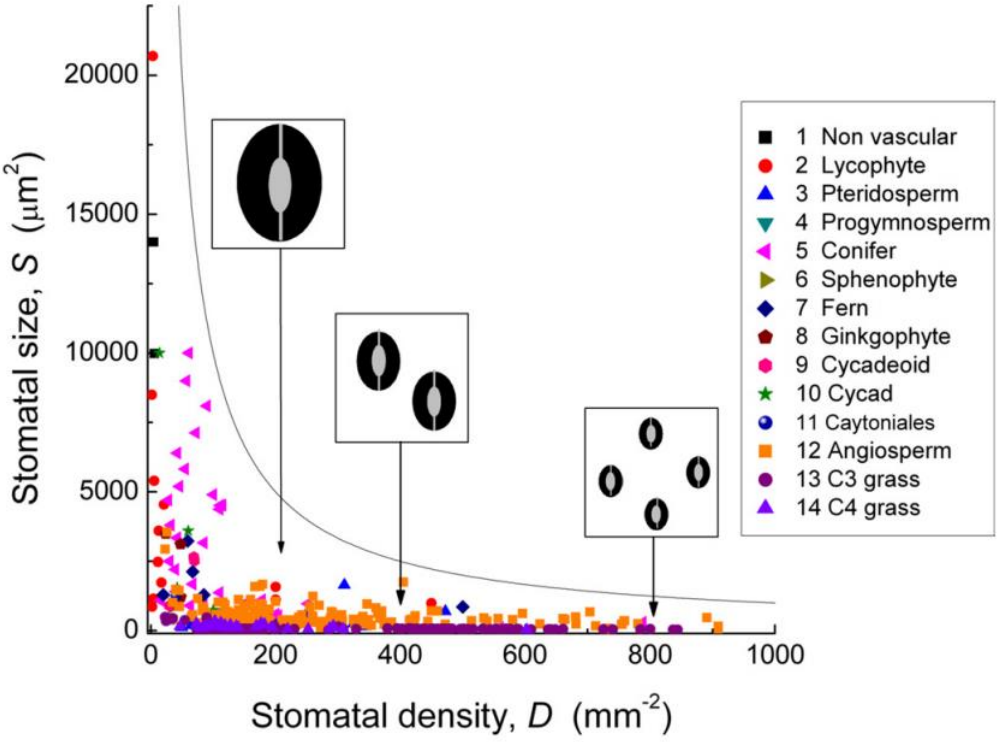

Figure 2.7: From Franks and Beerling (2009), showing the relationship between stomatal density and stomatal size for fossil plants types as indicated in the key through the Phanerozoic.

Whilst the Franks and Beerling (2009) relationship between stomatal density and stomatal size on stomatal packing on the leaf surface holds true for most fossil material, whereby many small stomata are utilised during low pCO_2 intervals, and fewer, larger pores in elevated pCO_2 (Figure 2.7); data from the Triassic–Jurassic boundary by Steinthorsdottir *et al*. (2012) indicated that this is not prerequisite. Across the Triassic–Jurassic boundary, pCO_2 doubled as the result of Central Atlantic Magmatic Province (CAMP) volcanism and proposed methane release resulting in an exceptionally high pCO_2 world (Steinthorsdottir *et al*., 2012 and references therein). Over this interval, Steinthorsdottir *et al*. measured a 50–60 % decrease in stomatal density of Ginkgoales and Bennettitales plant species, as expected from the well-established relationship of pCO_2 and stomatal density (Salisbury, 1927; Section 2.3.3). However, through the same interval the stomatal length also declined from around 19 µm to 14 µm in the Ginkgoales species (Figure 2.9).

If decreased stomatal conductance is interpreted as a decrease in plant transpiration, the impact on the hydrological cycle may have been increased run-off, since plants were taking up less water with root systems (Betts *et al*., 2007; Steinthorsdottir *et al*., 2012). There are, therefore, implications for palaeohydrology and nutrification, which have yet to be

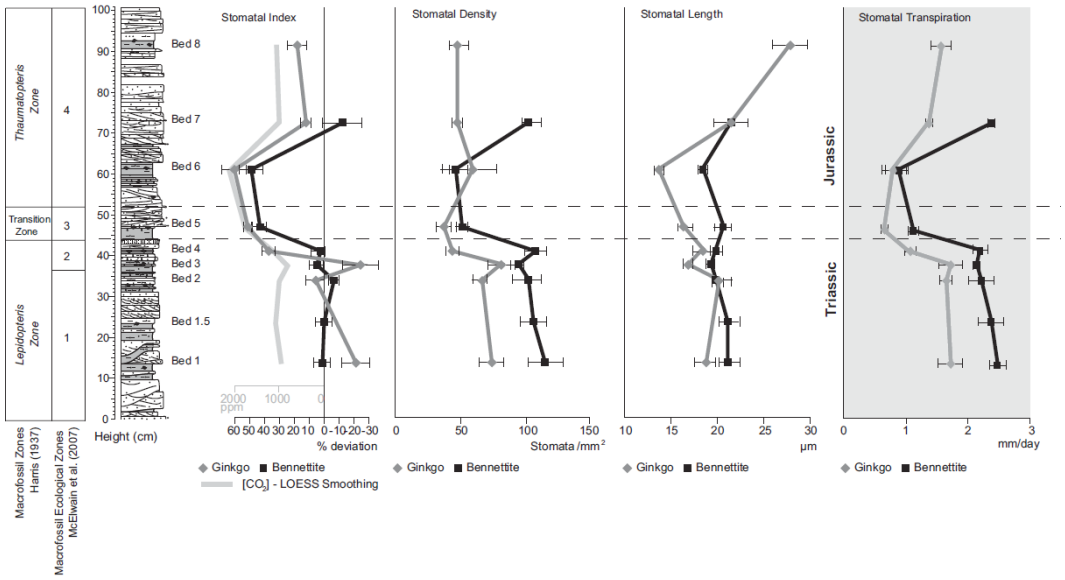

Figure 2.8: From Steinthorsdottir et al. (2012), summary of results collected over Triassic–Jurassic boundary, showing a significant decrease in stomatal index and density, in addition to a decline in stomatal length, resulting in decreased modelled stomatal (grey box) for Ginkgo and Bennittite plants.

explored in the Cretaceous. In addition, the influence of stomatal conductance on the Cretaceous hydrological cycle may provide important palaeoclimatic information to assist in distinguishing between the role of Cretaceous climate belt shift from the role of changes in pCO_2 on the radiation and diversification of flowering plants, particularly when combined with a record of cuticle feature-based palaeoclimatic indications. Such a fully integrated assessment of all ecological and palaeoclimatic information derived from plant-form, stomatal measurements and the sedimentology in which the fossils were found, would provide new insights into our current understanding of Cretaceous climate.

2.5 Field Area: Nuussuaq Peninsula, West Greenland

2.5.1 Location and geological history of selected area

To achieve the research goals, this thesis uses materials collected from the Albian–Cenomanian strata on the north coast of the Nuussuaq Peninsula, West Greenland (Figure 2.9). Uncovering the geological history of the West Greenland has primarily been the result of hydrocarbon exploration. Offshore seismic lines and wells drilled in the 1970s to 1990s were followed by more extensive onshore searches (Chalmers and Pulvertaft, 2001; Dam *et al.*, 2009 and references therein for review), revealing the Late Mesozoic and Palaeocene sediments were deposited in a complex of faulted basins. Driven by the hydrocarbon potential, onshore investigations in the early 1990s focussed on the Nuussuaq Basin, which

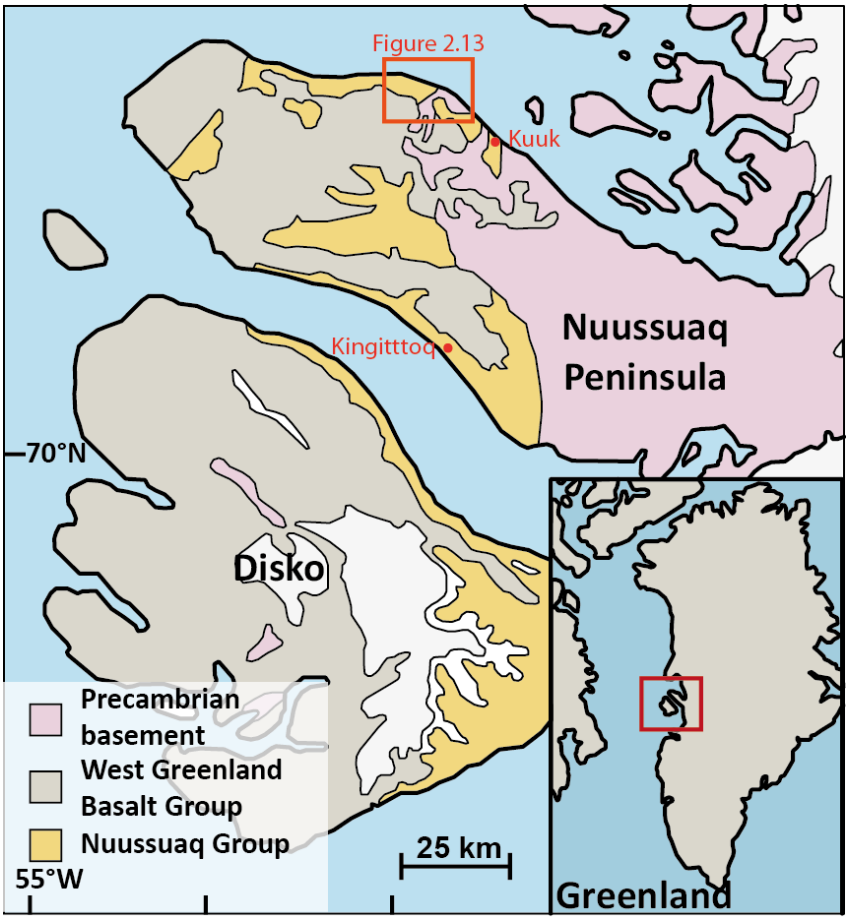

Figure 2.9: Location of the Nuussuaq Peninsula in West Greenland (inset). Distribution of the Nuussuaq Group with respect to pre-Cambrian basement and Palaeogene volcanics. Locations mentioned in text identified. North coast geology highlighted by box presented in more detail in Figure 2.13. Adapted from Dam et al. (2009).

outcrops on the Nuussuaq Peninsula, Disko Island and Svartenhuk Halvø to the north (Figure 2.9). From 1990 onwards extensive studies have established and mapped the onshore geology, covering the lithology, biostratigraphy, geochemistry and structural aspects (Dam *et al*., 2009 and references therein).

However, knowledge of the excellent floral assemblages preserved in the Cretaceous–Paleogene deposits of the Nuussuaq Basin was known long before the first hydrocarbon exploration. One of the earliest workers to describe and collect fossil plant specimens from several expeditions was Heer (1874a, b, 1880, 1882, 1883 a, b). By the end of his extensive investigation, Heer had 600 plant species and had established distinctive Cretaceous floras based on differential floral assemblages, separated spatially and temporally (Dam *et al*., 2009). Since then, major floral studies have been conducted by Seward (Seward, 1926, Seward and Conway, 1935, 1939) and Boyd (1998a, b, c, 2000). The latter represents a detailed study of the Early Cretaceous flora including descriptions of angiosperms,

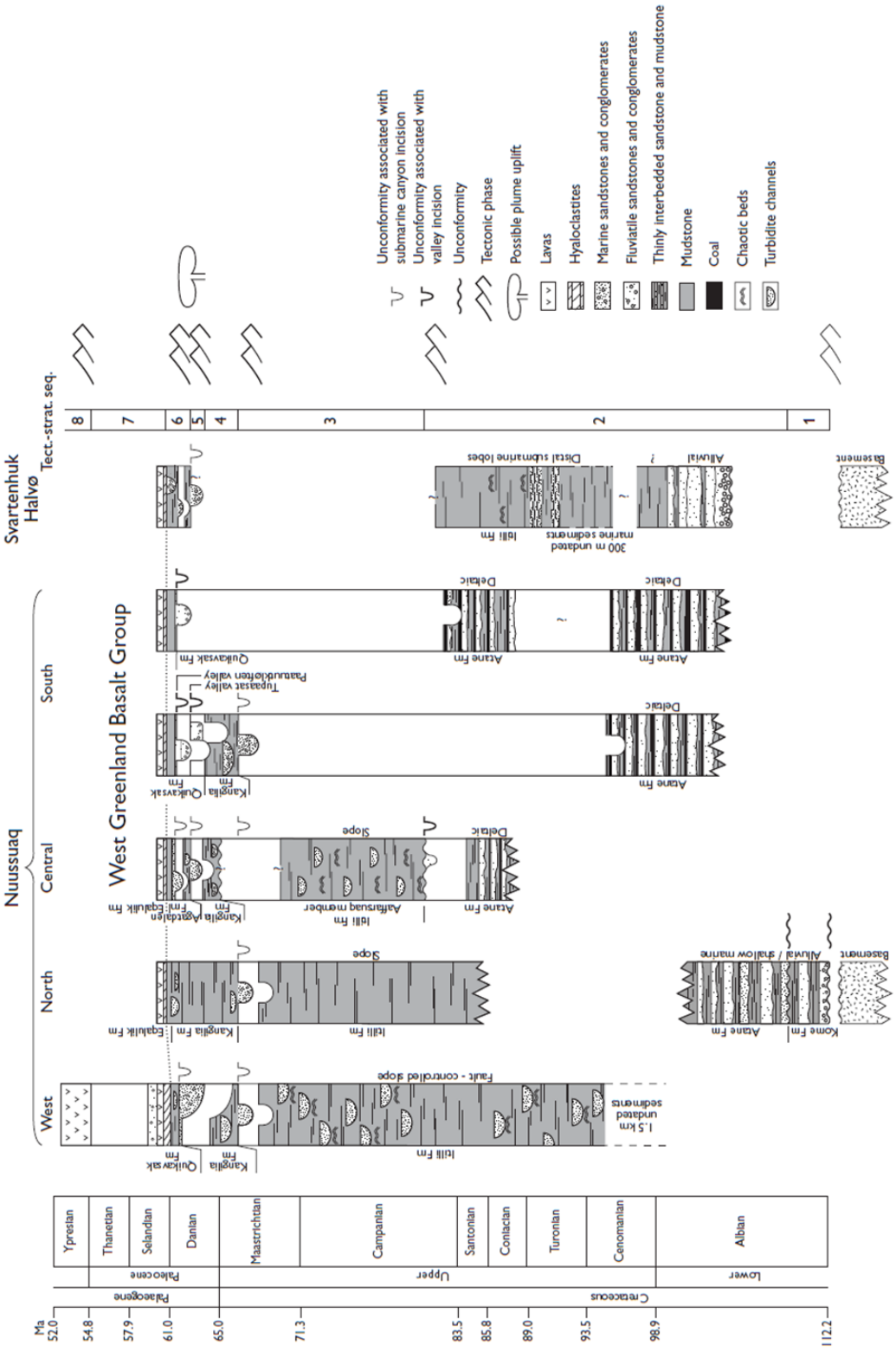

Figure 2.10: Division of Late Cretaceous deposits of West Greenland into tectonostratigraphic sequences (TSS) 1-8, from Dam and Nøhr-Hansen (2001). Includes generalised stratigraphic logs across the Nuussuaq Peninsula and Svarten-Halvø which indicate that on the north coast of the Nuussuaq Peninsula, the Albian deposits are the Kome to Atane Formations, which occur during TSS 1 and 2.

Bennettitales and other floral forms from florules (high yield floral horizons) along the north coast of the Nuussuaq Peninsula. The work of Boyd was influential in forming the basis of the field sampling strategy.

The sedimentary basins of Baffin Bay have a complicated history from a series of rifting episodes responsible for the eventual opening of the Labrador Sea. Dam and Nøhr-Hansen (2001) divided the Cretaceous–Palaeogene sediments of Nuussuaq and Svarten-Halvø into eight tectonostratigraphic sequences (TSS), which contain lithologies defined by tectonic processes (Figure 2.10). They grouped the sequences into two major phases of regional rifting: TSS 1–2, where Early Cretaceous rifting was followed by Cenomanian–Early Campanian thermal subsidence, and TSS 3–8 Late Cretaceous-Early Palaeocene rifting associated with the opening of the Labrador Sea.

This thesis utilises sediments deposited through the interval defined by TSS1–2, specifically focussing on the components of the Nuussuaq Group that outcrop on the north coast of the Nuussuaq Peninsula, including (in stratigraphic order) the Kome Formation, the Slibestensfjeldet Formation and the Ravn Kløft and Kingittoq Members of the Atane Formation (Figure 2.11).

The present study uses the most up-to-date Nuussuaq Group definitions developed by Dam *et al*. (2009) to avoid confusion with similar terminology of previous studies (Figure 2.12). TSS 1 includes the Kome Formation and the Slibestensfjeldet Formation. Both are syn-rift

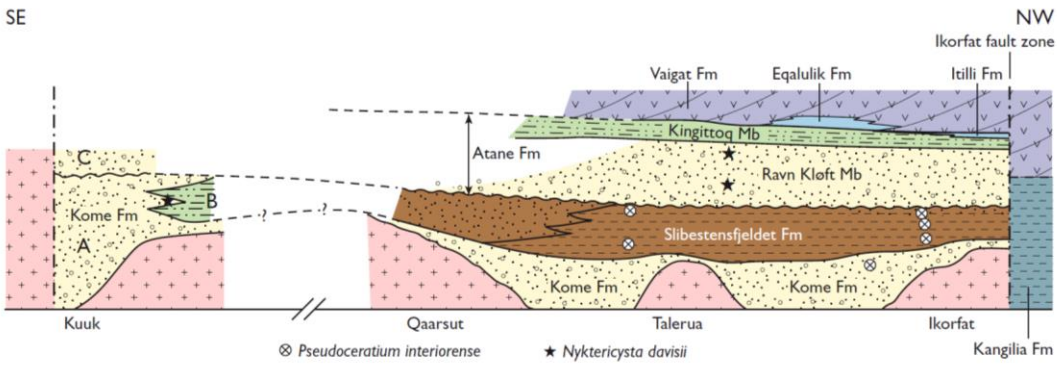

Figure 2.11: Summarised cross-section along the north coast of the Nuussuaq Peninsula between Kuuk and Ikorfat from Dam et al. (2009), showing the relationships between the constituents of the Nuussuaq Group. The eroded pre-Cambrian basement is overlain by the Kome Formation, followed by the localised deep lake deposits of the Slibestensfjeldet Formation, whose extension beyond Ikorfat is unknown due to the Ikorfat fault zone. The Ravn Kløft and Kingittoq Members of the Atane Formation are overlain by volcanics.

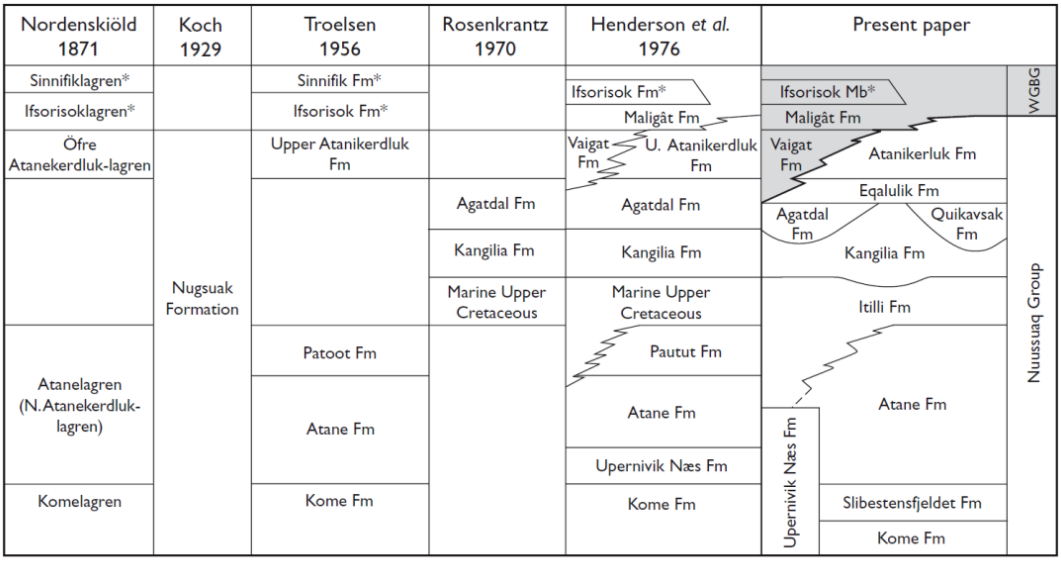

Figure 2.12: Redefinition of the Nuussuaq Group by Dam et al. (2009) compared to previous studies (referenced within Dam et al.). The present study will use the Nuussuaq Group Formation and Member classifications of Dam et al. labelled "Present paper" in the figure.

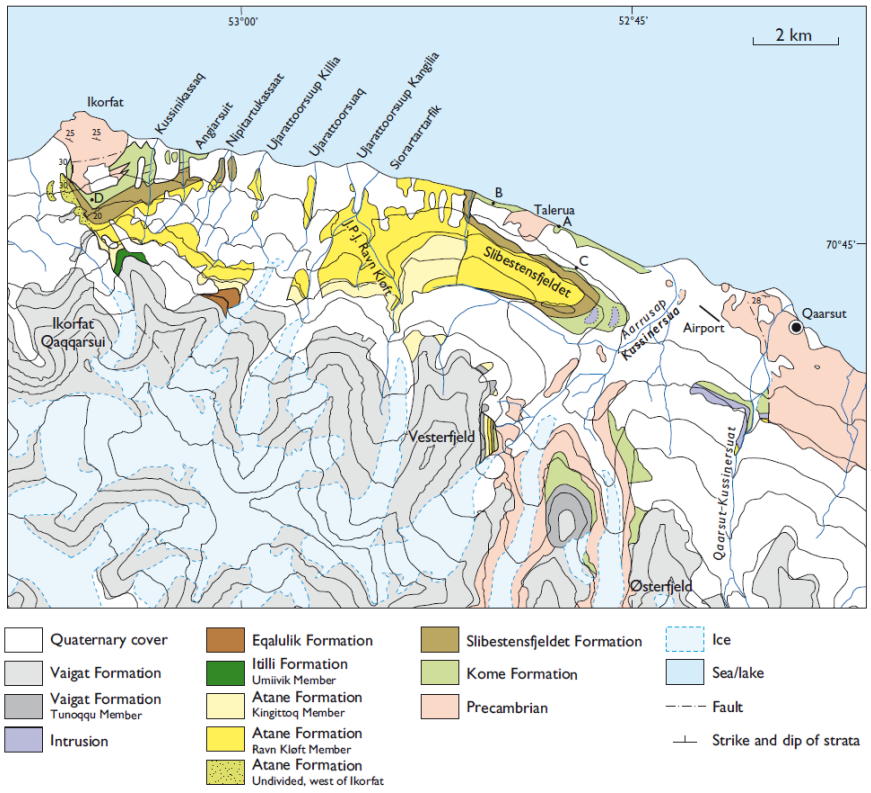

Figure 2.13: Geological map along the north coast of the Nuussuaq Peninsula from Ikorfat to Qaarsut taken from Dam et al. (2009). Shows distribution of the Nuussuaq Group: including the Kome Formation, Slibestensfjeldet Formation and the Ravn Kløft and Kingittoq Members of the Atane Formation.

deposits of Albian age based on fossil assemblage estimates. The sedimentology along the north coast of the Nuussuaq Peninsula records erosion and infilling of Pre-Cambrian basement topography, followed by sedimentation from short transportation rivers with interdistributary lakes and organic-rich floodplain mudstones (Kome Formation). The Slibestensfjeldet Formation (Figure 2.13) represents a large lake, deepest at the eastern end around Kussinikassaq with evidence of occasional brackish incursions.

TSS2 denotes a period of thermal subsidence basally defined by a major flooding surface. The resulting sedimentation in the north and west of the Nuussuaq area are offshore and deep marine sediments of the Itilli Formation. To the south and east of the Nuussuaq area, the Atane and Upernivik Næs Formations were deposited, which are characterised by sediments of fluvio-deltaic and shallow marine origins respectively (Dam *et al*., 2009). The transition between the deep marine and shallow marine/fluvio-deltaic sedimentation was controlled by the Kuugannguaq-Qunnilik Fault situated west of the field area.

The Atane Formation can be studied on the Nuussuaq Peninsula, but the base of the section is rarely exposed, and the lowermost portion of the Formation is only visible in the south and central region of the peninsular and East Disko. The Atane Formation has been newly subdivided by Dam *et al*. (2009) into four members, of which on the north coast of the Nuussuaq Peninsula, the Ravn Kløft Member (Albian–Cenomanian) and Kingittoq Member (Albian–Lower Turonian) are exposed (Figure 2.13). The Ravn Kløft Member is fluvially dominated at the base, leading into interbedded deltaic and estuarine deposits, and is topped by fluvial sediments with a range of fluvial styles and interdistributary swamps, floodplains and sub-aerial deposition (Figure i, Appendix A; Figure 2.16).

2.5.2 Selected field sites

The field season ran from 24th July 2009 – 18th August 2009, with a field team comprising: Stuart Robinson, Jennifer McElwain, Stephen Hesselbo, Gunver Pedersen, Richard Barclay, Ken Amor and Ingrid Hesselbo. The area around the Nuussuaq Peninsula was selected based on the work of Boyd (1998a-c; 2000; 2004) who had extensively documented floral specimens along the coast (Figure 2.14B), indicating that the stratigraphic and palaeontological objectives could be fulfilled there. The field season started close to the Ikorfat promontory at Camp 1 (Figure 2.14A) with logging and sampling of the LK, KK and ANE sections, representing the oldest Cretaceous stratigraphy in the area. At camp 2 (Figure 2.14A) the RKE and RKW sections were measured and sampled both of which are stratigraphically younger than the sections sampled at Camp 1. Many of Boyd's florule

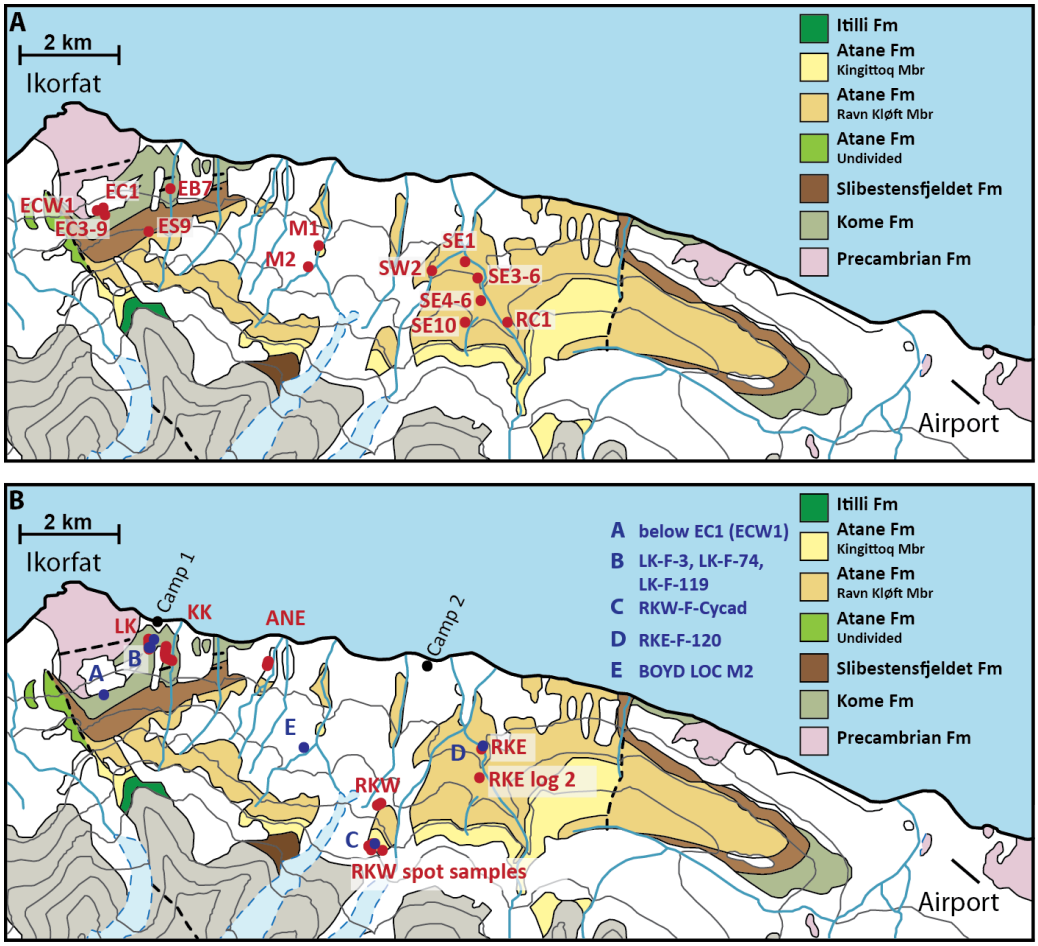

Figure 2.14: Geological map of the field area redrawn from Dam et al. (2009) showing rock formations as described in Dam et al.:

A = Field localities visited by Boyd (1998) where fossil flora samples were collected

B = Field localities of the 2009 field season led by Stuart Robinson, with stratigraphic sections labelled in red, and fossil sample keys for samples collected at Boyd's locations shown in dark blue.

horizons were not located in areas conducive to detailed stratigraphic work, but many of their equivalent horizons were identified in the measured sections; where possible Boyd's florule horizons were resampled.

2.5.3 Field data

At sites LK, KK, ANE, RKE, RKElog2 and RKW (Figure 2.14) standard graphic logs were produced and samples were located precisely against the measured section. The samples collected were: 'Bulk sediment' samples - approximately 500 g samples of the lithology were collected at a resolution between 0.2–1.0 m and split between two sample bags labelled A and B to create two sample sets for use in the present study (samples were labelled according to the section followed by B for 'bulk' and finally the sample number,

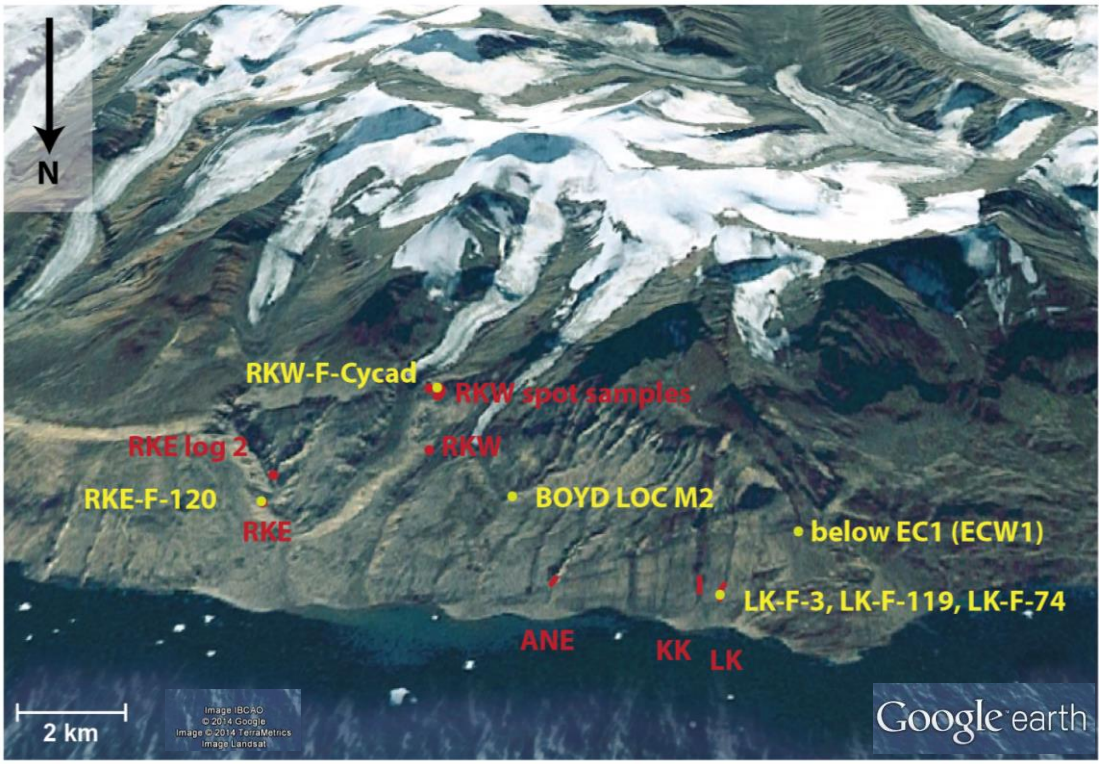

Figure 2.15: Google Earth™ view of the field area looking south showing stratigraphic sections in red, and the location of fossil leaf samples collected based on Boyd's localities labelled in yellow, with the sample reference key for the respective samples collected at that site.

e.g. LK-B-10); fossil wood samples - collected wherever they were found in the section of a reasonable size (generally greater than 1 cm^3 in volume; labelled with a W instead of a B representing 'wood' e.g. LK-W-39); lithology samples – only 1–2 samples collected per section as supplementary samples of key or unusual lithologies (labelled L for lithology, e.g. LK-L-1).

From the field notes, I drew a neat graphic log for each section including the sample list in order to provide a record of the material available for the present study (Figure ii, Appendix A). In Figures 2.14 and 2.15, the locality 'RKW Spot samples' indicates the location where grab samples were collected from the Kingittoq Member but not recorded against a graphic log, due to poor exposure. Instead, these samples were recorded with an elevation above sea level derived from map and GPS based measurements, and were tied to the RKW graphic log by calculating the height above the top of the logged section (Table 2.1).

At the fossil flora collection sites notes of the approximate volume of material quarried, the site fossil yield, the number of fossil specimens and preliminary identification were made (Appendix A), but full systematic methods for fossil collection were not employed in the field study.

	Sample	Elevation (m above sea level)	Height from top of RKW section (m)
Kingittoq Member	RKW-B-748m	**748**	**2.2**
	RKW-B-760m	**760**	**14.2**
	RKW-B-780m	**780**	**34.2**
	RKW-B-797m	**797**	**51.2**
	RKW-B-799m	**799**	**53.2**
	RKW-B-818m	**818**	**72.2**
	RKW-B-831m	**831**	**85.2**
	RKW-B-833m	**833**	**87.2**

Table 2.1: List of grab samples collected at locality RKW Spot samples (Figure 2.14) recorded as an elevation above sea level, and tied to the graphic log by calculated height from the top of the section.

2.5.4 Composite section overview with interpretation

A summary stratigraphic log based on the field information is presented in Figure 2.16 with the field workers' interpretation of the height of formation boundaries based on the definitions of Dam *et al.* (2009), in addition to the associated interpreted palaeoenvironment. The LK section was interpreted to represent part of the middle and upper portion of the Kome Formation, with alternating sandstone and siltstone bearing abundant fossil wood pieces, plant beds and coaly layers representing fan deltas with interdistributary bays and over bank deposits. The LK and KK sections share a small stratigraphic overlap (Figure 2.17), permitting the continuation of the composite log between these two sections. The transition between the Kome Formation to the Slibestensfjeldet Formation was interpreted to lie close to the boundary between the two sections, where the KK section thick unit of fairly uniform siltstone with limited abundance of fossil wood represents the large and deep lake that formed through a rising of the water table (Dam *et al*., 2009).

There is a stratigraphic gap of 40–50 m between the KK and ANE sections (Figure 2.17); the ANE section was interpreted as part of the lake infill process, where the top of the

Figure 2.16 (next page): Summary graphic log of composite section (key to symbols: Appendix A, Figure ii) showing span of individual sections and approximate stratigraphic gaps between. The field workers interpretation of the span of formations defined by Dam et al. (2009) is presented alongside an interpretation of the palaeoenvironment of each formation (from Dam et al. and references therein). The available fossil biostratigraphic constraints on formation age are presented with references within Dam et al. (2009).

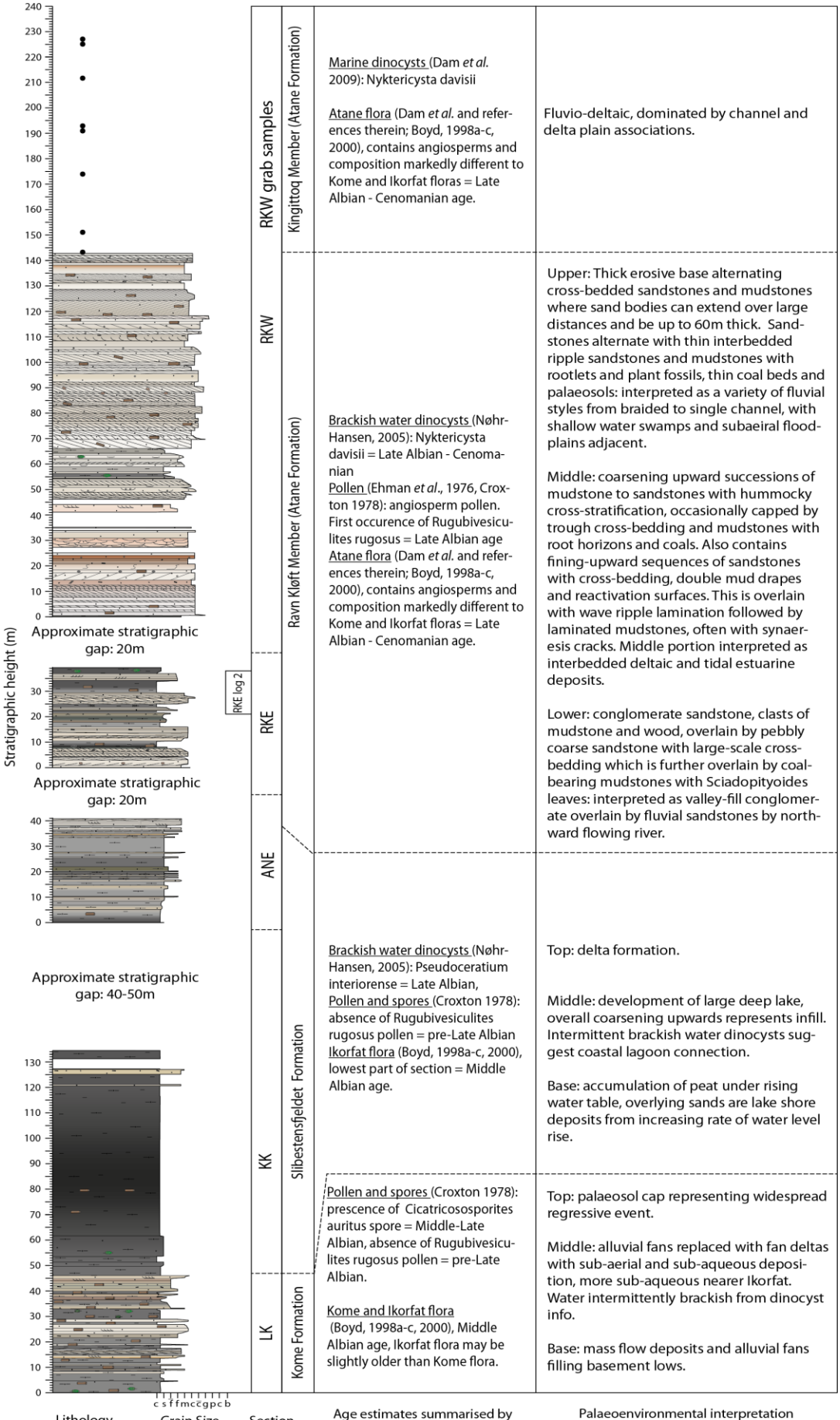
Stratigraphic height (m)
Approximate stratigraphic gap: 20m
Approximate stratigraphic gap: 20m
Approximate stratigraphic gap: 40-50m
RKE log 2
RKW grab samples
RKW
RKE
ANE
KK
LK
Kingittoq Member (Atane Formation)
Ravn Kløft Member (Atane Formation)
Slibestensfjeldet Formation
Kome Formation
Marine dinocysts (Dam et al. 2009): Nyktericysta davisii
Atane flora (Dam et al. and references therein; Boyd, 1998a-c, 2000), contains angiosperms and composition markedly different to Kome and Ikorfat floras = Late Albian - Cenomanian age.
Fluvio-deltaic, dominated by channel and delta plain associations.
Brackish water dinocysts (Nøhr-Hansen, 2005): Nyktericysta davisii = Late Albian - Cenomanian
Pollen (Ehman et al., 1976, Croxton 1978): angiosperm pollen. First occurence of Rugubivesiculites rugosus = Late Albian age
Atane flora (Dam et al. and references therein; Boyd, 1998a-c, 2000), contains angiosperms and composition markedly different to Kome and Ikorfat floras = Late Albian - Cenomanian age.
Upper: Thick erosive base alternating cross-bedded sandstones and mudstones where sand bodies can extend over large distances and be up to 60m thick. Sandstones alternate with thin interbedded ripple sandstones and mudstones with rootlets and plant fossils, thin coal beds and palaeosols: interpreted as a variety of fluvial styles from braided to single channel, with shallow water swamps and subaeiral floodplains adjacent.
Middle: coarsening upward successions of mudstone to sandstones with hummocky cross-stratification, occasionally capped by trough cross-bedding and mudstones with root horizons and coals. Also contains fining-upward sequences of sandstones with cross-bedding, double mud drapes and reactivation surfaces. This is overlain with wave ripple lamination followed by laminated mudstones, often with synaeresis cracks. Middle portion interpreted as interbedded deltaic and tidal estuarine deposits.
Lower: conglomerate sandstone, clasts of mudstone and wood, overlain by pebbly coarse sandstone with large-scale cross-bedding which is further overlain by coal-bearing mudstones with Sciadopityoides leaves: interpreted as valley-fill conglomerate overlain by fluvial sandstones by northward flowing river.
Brackish water dinocysts (Nøhr-Hansen, 2005): Pseudoceratium interiorense = Late Albian,
Pollen and spores (Croxton 1978): absence of Rugubivesiculites rugosus pollen = pre-Late Albian
Ikorfat flora (Boyd, 1998a-c, 2000), lowest part of section = Middle Albian age.
Top: delta formation.
Middle: development of large deep lake, overall coarsening upwards represents infill. Intermittent brackish water dinocysts suggest coastal lagoon connection.
Base: accumulation of peat under rising water table, overlying sands are lake shore deposits from increasing rate of water level rise.
Pollen and spores (Croxton 1978): prescence of Cicatricososporites auritus spore = Middle-Late Albian, absence of Rugubivesiculites rugosus pollen = pre-Late Albian.
Kome and Ikorfat flora (Boyd, 1998a-c, 2000), Middle Albian age, Ikorfat flora may be slightly older than Kome flora.
Top: palaeosol cap representing widespread regressive event.
Middle: alluvial fans replaced with fan deltas with sub-aerial and sub-aqueous deposition, more sub-aqueous nearer Ikorfat. Water intermittently brackish from dinocyst info.
Base: mass flow deposits and alluvial fans filling basement lows.
c s f f m c c g p c b
Lithology
Grain Size
Section
Age estimates summarised by Dam et al. (2009)
Palaeoenvironmental interpretation from Dam et al., (2009)

measured section is close to the base of the Atane Formation. A stratigraphic gap of around 20 m between the ANE and RKE section was estimated in the field, and the RKE section was interpreted as the lower to middle portion of the Ravn Kløft Member, comprising sandstone layers alternating with siltstone and coal beds, and similar leaf mats as the LK section. The initially coarse sandstones at the base of the RKE section were interpreted as fluvial sands from the lower Ravn Kløft Member. The remainder of the RKE section likely passes into deltaic deposits from the middle portion of the Ravn Kløft Member. There is another gap of around 20 m between the RKE and RKW section, and the RKW section was interpreted as a continuation of the Ravn Kløft Member, where the thick sandstone beds with a variety of bedding types, represent an extensive fluvial system with changing fluvial styles, from braided to single channels. The presence of many fossil wood pieces and the occasional siltstone and carbonaceous layer indicates the likely presence of adjacent floodplain and swampy depositional environments (Dam *et al.*, 2009). The top of the section and the grab samples listed in Table 2.1 were interpreted as representative of the Kingittoq Member of the Atane Formation which was summarised by Dam *et al*. (2009) as deltaic cycles, although no graphic log was recorded for this Member due to inaccessibility of the available exposures.

2.5.5 Age constraints

Samples from the present study were supplied to Maurits Horikx and Ulrich Heimhofer at the Institute for Geology at Leibniz Universität Hannover, Germany, who chemically macerated the samples in order to separate the pollen and spore fraction of organic debris within the sediment. Angiosperm pollen was found in the lowest stratigraphic sample collected in the Kome Formation (Table 2.2), although the abundance was low.

Most pollen grains were found in the lacustrine Slibestensfjeldet formation, which may be expected based on taphonomy. The presence of angiosperm pollen, in particular the Eudicot affinity pollen (Striatopollis, Tricolpites) was interpreted by Horikx and Heimhofer to indicate that the age at the base of the section must be no older than Middle Albian.

When these new data are combined with the age constraints from palynology and the macrofloral record (Figure 2.16) a tentative age-model can be suggested for the composite section (Figure 2.17). The unpublished data from Horikx and Heimhofer agrees with previous palynological data estimates of a Middle Albian age for the logged portion of the Kome Formation; with the other macrofloral and palynological studies supporting a pre-

Late Albian age for the Slibestensfjeldet Formation and Late Albian to Cenomanian age for the Atane Formation (Figures 2.16 and 2.17).

Sample	Stratigraphic Height (m)	Pollen species
LK-B-4	0.00	1 retimonocolpites
LK-B-24	9.91	2 clavatipollenites; 1 retimonocolpites
LK-B-81	33.00	barren
LK-B-119	40.95	1 tricolpites; 1 striatopollis; 18 clavatipollenites; 1 cf. clavatipollenites/retimonocolpites; 1 cf. clavatipollenites/astropollis
KK-B-137	47.72	1 phimopollenites (?)
KK-B-156	55.32	6 dichastopollenites; 3 clavatipollenites; 2 cf. clavatipollenites/retimonocolpites; 1 tricolpites; 1 striatopollis; 2 retimonocolpites; 1 phimopollenites (?)
KK-B-414	132.09	5 clavatipollenites; 1 cf. clavatipollenites/astropollis
ANE-B-470	166.05	barren
ANE-B-477	173.96	1 tricolpites; 8 clavatipollenites; 1 cf. clavatipollenites/retimonocolpites; 1 cf. clavatipollenites/astropollis
RKE-B-9	187.00	2 clavatipollenites
RKE-B-30	197.75	barren
RKE-B-44	203.54	barren
RKE-B-117	216.60	1 tricolpites
RKW-B-55	264.00	clavatipollenites
LK-B-1	?	barren
RKE-B-50	?	barren

Table 2.2: Summary of angiosperm pollen types identified by Maurits Horikx based on material from the present study (identified by sample name and stratigraphic height).

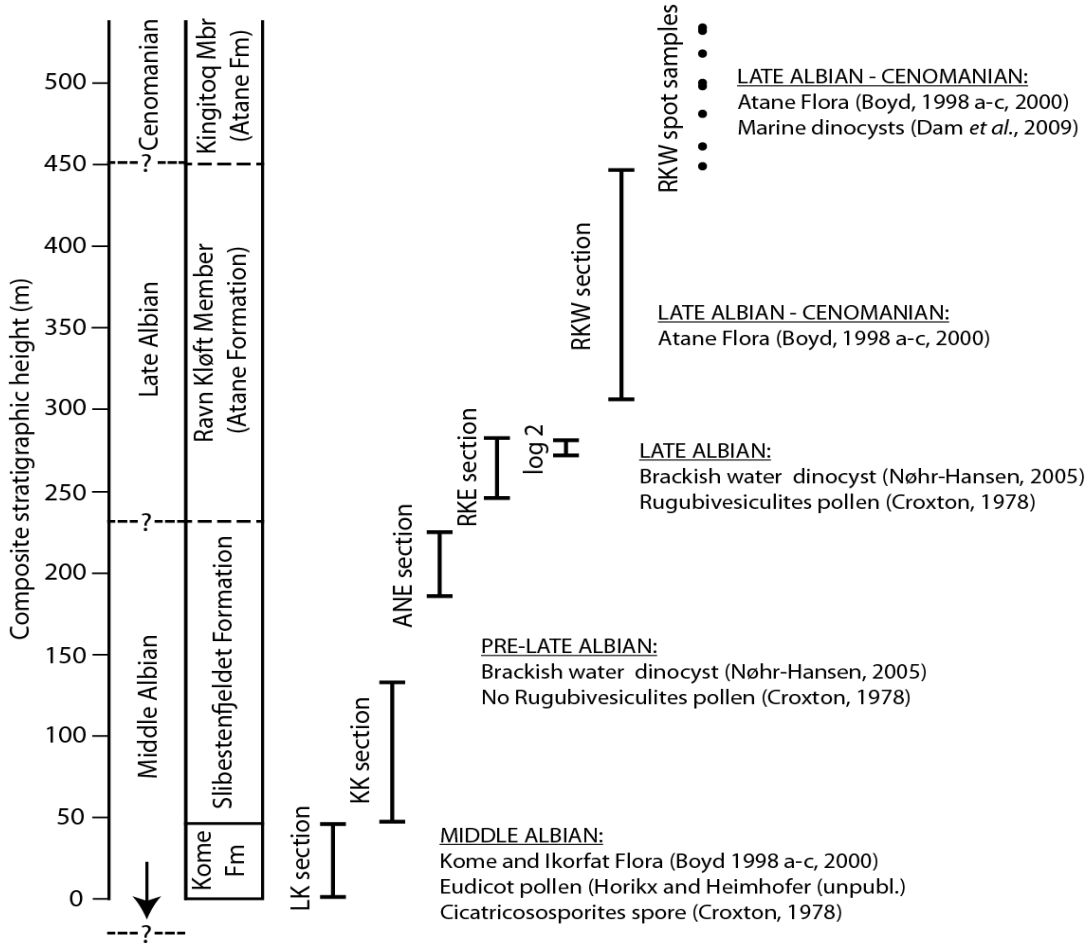

Figure 2.17: Working age constraints for the interval studied based on palynological and floral estimates. The stratigraphic range of each section is shown with stratigraphic gaps.

3. Carbon isotope stratigraphy

3.1 Introduction

This chapter presents geochemical data from bulk sediment and fossil wood samples, used to produce a carbon isotope stratigraphy for West Greenland that is correlated with other Aptian-to-Cenomanian marine and terrestrially-derived carbon isotope records. The correlation of isotope events not only identifies intervals of carbon cycle disturbance but also refines the age model for this composite section.

3.2 Methods

3.2.1 Total Carbon (TC) and Total Organic Carbon (TOC)

The total organic carbon content (TOC) of sediment samples was required to estimate the amount of sample needed for isotope ratio mass spectrometry. However, TOC and TIC (total inorganic carbon) contents are also useful for palaeoenvironmental interpretations in conjunction with sedimentology.

3.2.1.1. Powdering of samples

Bulk sediment samples were cleaned with deionised water and a stiff brush. A blunt scalpel was used to scrape away weathering products to ensure a fresh sample was analysed. The samples were dried in labelled watch glasses in an oven at 60 °C overnight. Samples were powdered using a TEMA mill, requiring a minimum of 10 cm^3 of sample for operation. The TEMA mill was cleaned after every sample by brushing out the mill pot and interior rings whilst dry, cleaning with water and dried on paper towels before cleaning with acetone to remove any residual organic debris and to aid drying.

3.2.1.2 Preparations for analysis

Analyses were conducted on a Flash EA 1112 series elemental analyser using Eager 300 software. Each sample was analysed twice, once to determine Total Carbon content (TC) and again, after decarbonation, to determine Total Organic Carbon (TOC). The difference between the two values provides the Total Inorganic Carbon (TIC) content, which was assumed to be entirely associated with stoichiometric calcium carbonate.

For TC analysis, approximately 10–30 mg of sample was weighed depending on the expected carbon content estimated from sample colour. For samples known to have very

high carbon content (e.g. coals), it was necessary to weigh less than 10 mg. Samples and standards were weighed into 5 mm diameter tin capsules, pinched shut and folded to remove air from the capsule before compressing into a rounded cube; samples were stored in a sample tray in a desiccator.

TOC runs required additional preparation to remove carbonate before analysis. Samples were weighed into 10 mm silver capsules and placed on a hot plate at 50 °C. A pipette was used to deliver 100 µl of 10 % HCl to each sample. The samples were left for an hour before adding another 100 µl of acid, with the process repeated until the reaction was complete, at which point the samples were left to dry completely. Once dry, the silver capsules were double-wrapped in 10 mm diameter tin capsules by wrapping the tin over the silver capsules before compressing into a rounded cube. This was found to be the best way of preventing sample loss due to brittle, fractured silver capsules.

The calibration standard was an in-house material: MD2517bog, with a measured carbon content of 4.591 ± 0.059 % and nitrogen content of: 0.511 ± 0.033 %. As close to 10, 20 and 30 mg of standard were weighed for the first three analyses respectively in each run in order to produce the calibration curve. Two additional analyses of standard material weighing between 10–30 mg were analysed as unknowns in each run in order to monitor variability within a run and between runs.

3.2.1.3 Data collection and analysis

The Flash EA combusted the sample in an O_2-rich atmosphere, producing CO_2, N_2O, and NO_x; a column of copper reduced the nitrogen species to N_2. N_2 and CO_2 were separated by a Gas Chromatography (GC) coil before being analysed separately at the detector. Eager 300 software analysed the chromatogram data to calculate % carbon and % nitrogen for each analysis using a calibration curve generated from the known carbon and nitrogen content of the standard material. The standard analyses treated as unknowns provided a means of assessing the reliability of the run: if poor run performance was indicated all samples in that run were reanalysed after appropriate action was taken to rectify the issue with the Flash EA. The average 'unknown' standard carbon percentage calculated for all runs (from which data is included in this thesis) falls within the error of the known carbon content value, with a standard deviation of ± 0.12 % (Table 3.1).

Standard MD2517bog	Expected value	Average value	Standard deviation	No. analyses
	4.591 ± 0.059 ‰	4.642 ‰	±0.12 ‰	52

Table 3.1: Summary of Flash EA performance based on reproducibility of the in-run standard MD2517bog.

3.2.2 Organic carbon isotope ratios of fossil wood and bulk sediment

3.2.2.1 Sample preparation

Large pieces of fossil wood were cleaned with deionised water and a brush to remove any sediment adhered to the surface. The pieces were rinsed over a 180 µm sieve to retain any wood fragments which split on contact with water due to the coalified nature of the pieces. Smaller pieces of fossil wood were picked from the dry sediment spread across a piece of clean paper with a damp, fine brush. The collected fragments were rinsed under deionised water in a 180 µm sieve with gentle agitation to remove any adhered sediment. Samples were dried in a labelled watch glass in an oven at 60 °C overnight. Water in fractures occasionally ruptured the fossil wood during the drying process, so samples were kept far apart in the oven to prevent showering of material onto neighbouring samples. Once dried, the samples were visually inspected and described. The samples were powdered in an agate pestle and mortar which was cleaned with water and acetone between samples. The samples were stored in clean, labelled sample bags. Bulk sediment samples for isotopic analyses were taken as aliquots from the powder produced for TC/TOC analyses.

3.2.2.2 Carbonate removal from fossil wood and bulk sediment samples

1 cm^3 of powdered sample was added to a labelled centrifuge tube, topped up with 10 % hydrochloric acid to 11 ml and left for two hours with the lid slightly unscrewed to vent gas released from the reaction of acid with any carbonate phases present. The acid was added slowly to gauge the intensity of the reaction with carbonate, but these samples were carbonate-poor, as evidenced from the TC/TOC data. Since there was no immediate reaction upon acid addition for most samples, the tubes were agitated to ensure thorough mixing of acid and sediment.

Samples were centrifuged at 2000 rpm for 10 minutes, and the waste acid decanted off to be neutralised with sodium bicarbonate for disposal. Samples were replenished with acid and the process repeated until the reaction with HCl was complete.

The acid was observed to turn lurid yellow after some time mixed with the sample. This was most pronounced in the sediment samples, but also in the fossil wood. The cause of the colouration was suspected to most likely be due to iron ions in solution. However, the possibility that the colouration was due to an organic leach was of concern, as this could influence the carbon isotope ratios measured. Neutralisation of the yellow-coloured acid resulted in a brown precipitate in a colourless solution, indicating the yellow colouration was most likely ferric (III) chloride produced by reaction of HCl with iron in the sediment; upon neutralisation the iron precipitated into the hydrated form FeO(OH). Iron oxide as a weathering product was the most likely source of iron as it was observed as rust-coloured staining on some samples prior to preparation. Since it was possible some iron may have originated as pyrite or siderite in the sample, the HCl was replaced for each sample until the acid remained colourless to pale straw.

Once the reactions with HCl were complete, the samples were rinsed by replacement of the acid with deionised water, agitated to mix the sediment and water, then centrifuged for 10 minutes before the supernate was decanted. The process was repeated until the pH of the water was neutral as indicated by pH paper. Since the acid concentrated at the sediment-solution interface after being centrifuged, the pH of the last few drops of decanted supernate was tested. The number of rinses varied between samples, and ranged from 5 to >10 repetitions. Once rinsed, the samples were dried with open tops in an oven at 60 °C. The samples were powdered in an agate pestle and mortar after drying to remix the sample.

3.2.2.3 IRMS – standard and sample preparation

For calibration of carbon isotope data to VPDB, a suite of standards were analysed covering a wide range of $\delta^{13}C$ values, which were each repeated four times through a run to monitor drift and reproducibility. Table 3.2 outlines the standard material type (calibration purposes or performance monitor), alongside the amount required for an isotope analysis assuming no gas dilution is applied by the mass spectrometer system. The standard weights were calculated based on the carbon content derived from stoichiometry to provide 4–5 V of signal on the mass-44 detector of the mass spectrometer.

Standard	Type	Material	Supplier	Weight required ± 10 (µg)	Known $\delta^{13}C$ ‰ VPDB value
ANU[1]	Calibration	Sucrose	NIST/IAEA	100µl (150µg)	-10.449±0.033
USGS40[1]	Calibration	L-glutamic acid	NIST/IAEA	100µl (140µg)	-26.389±0.042
IAEA-CH3	Calibration	Cellulose	IAEA	160	-24.724±0.041
USGS24	Calibration	Graphite	NIST/IAEA	70	-16.049±0.035
WF[2]	Calibration	Wheat flour	OAE Labs	150	-26.430±0.080
CF[2]	Monitoring	Corn flour	OAE labs	150	-10.99±0.060
GRAP	Monitoring	Graphite	BDH	70	Still in determination

Table 3.2: Standards used, showing material purpose, type, the weight required for mass spectrometry analysis assuming no gas dilution, and the internationally accepted $\delta^{13}C$ values with respect to VPDB.

[1]*Solution standards: 100 µl of stock standard solution was delivered to each capsule providing dried weight indicated in brackets.*

[2]*Not internationally calibrated*

Samples and powder standards were weighed on a microbalance into 5 mm diameter tin capsules, which were pinched shut and folded flat to remove air, before rolling and compressing into a rounded cube and placed in position in the sample tray. The sample tray was stored in a desiccator until the run was analysed. The amount of decarbonated powdered sample required was estimated from the TOC results to ensure around 70 µg of carbon was delivered to the mass spectrometer (Equation 3.1).

$$Amount\ to\ weigh\ (mg) = \frac{Amount\ of\ carbon\ (mg)\ required\ by\ mass\ spec.}{Estimated\ percentage\ of\ organic\ carbon\ in\ sample} \times 100$$

Equation 3.1: Amount of material required for isotope analysis.

The calibration standards ANU and USGS40, however, were made from a stock solution whereby a pre-determined amount of powder sample (designed to give an appropriate peak height on the mass spectrometer) was dissolved into deionised water, from which 100 µl of solution was delivered into a tin capsule by a pipette before being dried overnight in an oven at 60 °C. Two in-house monitoring standards, GRAP and CF (Table 3.2) were analysed as unknowns twice in each run. A long-term record of the variability of these two standards is kept by the laboratory to monitor reproducibility and to determine the carbon isotope ratio of GRAP. The carbon isotope ratio of CF is known but is not internationally calibrated.

3.2.2.4 EA-IRMS configuration

The mass spectrometer system consists of a Flash EA 1112 series elemental analyser connected to a Conflo IV continuous flow interface (CFI) which delivers the prepared sample gas to a Delta V Advantage IRMS (Isotope Ratio Mass Spectrometer). The $\delta^{13}C$ of every analysis was compared to a reference gas and calibrated to ‰ VPDB using the calibration standard suite. The Flash EA operated in a similar manner as the machine used for TC and TOC determination: whereby the sample was combusted and the resulting gas mixture passed into the reactor columns by a helium carrier gas.

3.2.2.5 Data calibration

The graphical output of every analysis was examined to ensure the mass-44 peak height was around 4000–6000 mV, and to check for large nitrogen peaks before the CO_2 peak, which would indicate air was trapped in the capsule during folding. Failed analyses were discarded from the data set and the sample reanalysed in another run. In the case that a calibration standard analysis was clearly erroneous due to excess N_2, the result was discarded and not used in the calibration, highlighting the importance of multiple standard analyses of each standard per run.

Once satisfied that the calibration standard data were reliable, by assessment of the standard deviation and analysis of peak shapes, the average measured isotope ratio value of each standard was plotted against the known value (Table 3.2) in a calibration plot (Figure 3.1). The gradient of the calibration line and the associated r^2 value should be close to 1 in an acceptable run. The r^2 value of the calibration lines of all runs analysed in this thesis were never below 0.99935. The equation of the calibration line was applied to the measured $\delta^{13}C$ values for samples and monitoring standards to provide $\delta^{13}C$ values with respect to VPDB.

3.2.2.6 Data checks –monitoring standards

Two monitoring standards were analysed twice each in every run: CF (corn flour) which has an accepted value of -10.99 ‰ and GRAP (graphite), which is an in-house standard with an isotope ratio still in determination but provided an average value of -25.39 ‰ over the duration of analysis in this thesis (Table 3.3). The CF monitoring standard possesses a greater standard deviation than GRAP (Table 3.3) but both standard deviations are similar to the calibration standards (which were never above 0.2 ‰, with most around 0.1 ‰).

Monitoring Standard	CF	GRAP
Expected $\delta^{13}C$ value (‰VPDB)	-10.99	n/a
Average calibrated $\delta^{13}C$ (‰ VPDB)	-11.04	-25.39
Standard Deviation (1 σ, ‰)	±0.25	±0.12
Number of analyses	36	38

Table 3.3: Summary of mass spectrometer performance based on monitoring standards: comparison of average calibrated $\delta^{13}C$ (‰ VPDB) to accepted value (for CF only), associated standard deviation of calibrated $\delta^{13}C$ values.

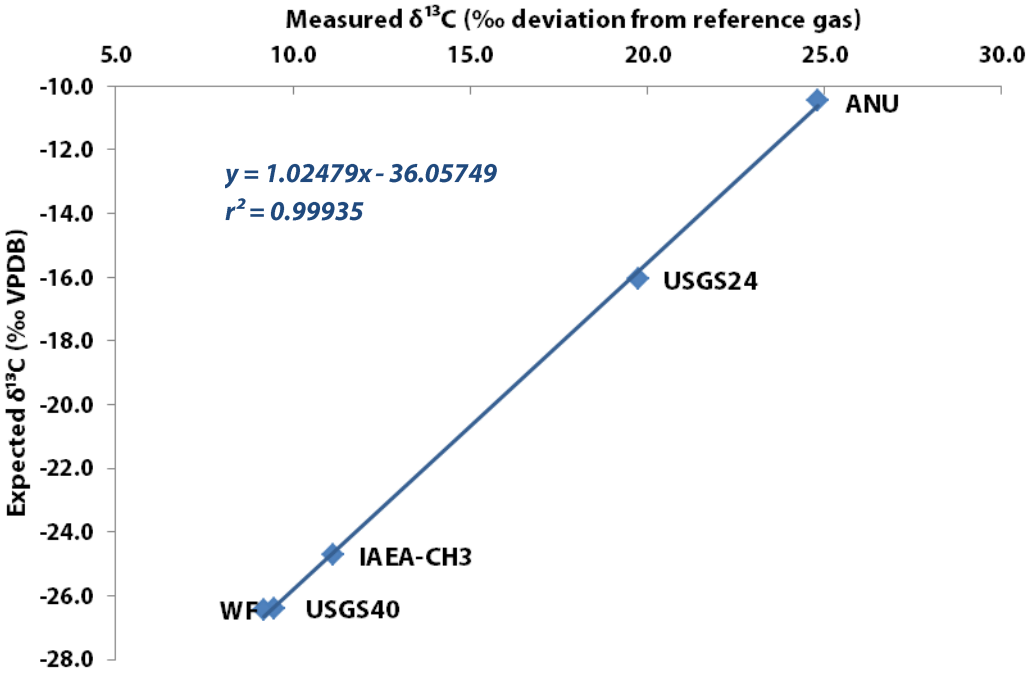

Figure 3.1: Calibration plot example from run 20110317_CAF3 (fossil wood), showing the measured (with respect to reference CO_2 gas) isotope ratio against the known isotope ratio (with respect to VPDB). The calibration line drawn between these data points provides the calibration equation for all other analyses within the run.

Examination of $\delta^{13}C$ values of the two monitoring standards against relative run order for all 19 runs analysed for this study (Figure 3.2 and 3.3) indicates there is no consistent trend in behaviour through time between the two standards. There is a suggestion of a slight drift of 0.2–0.3 ‰ in the GRAP data (Figure 3.2) towards the end of the run series, which falls outside the ± 1σ error presented around the average $\delta^{13}C$ value but this drift is not observed in the CF data (Figure 3.3).

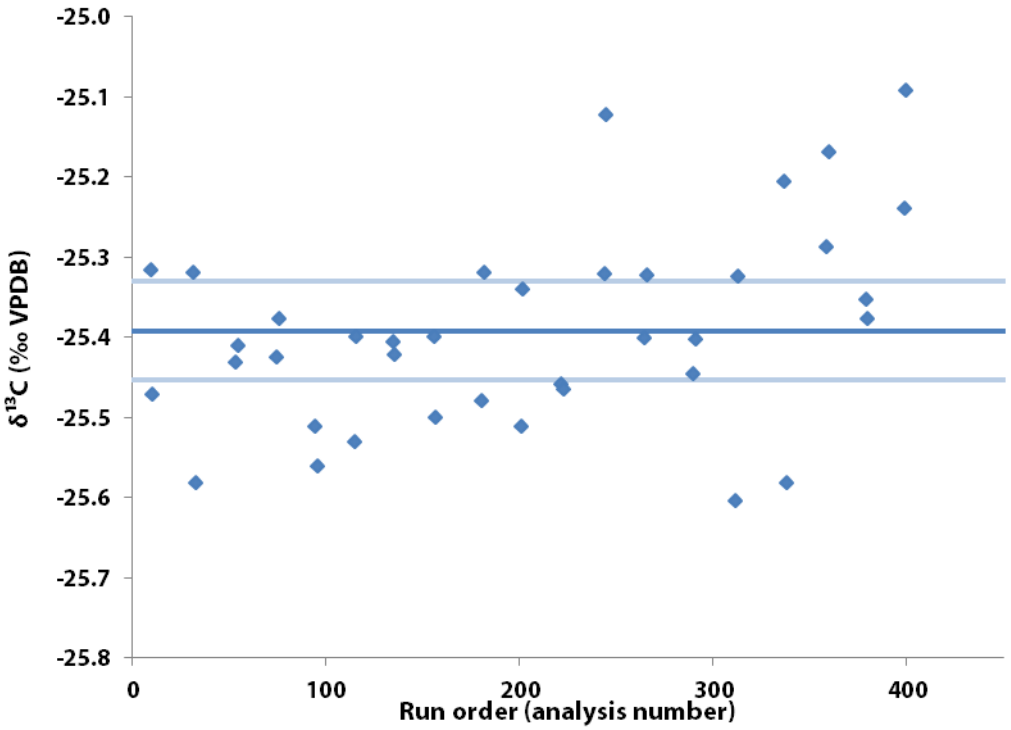

Figure 3.2: $\delta^{13}C$ values of GRAP in chronological order with overall average value (dark blue line) with ± 1σ error (light blue lines).

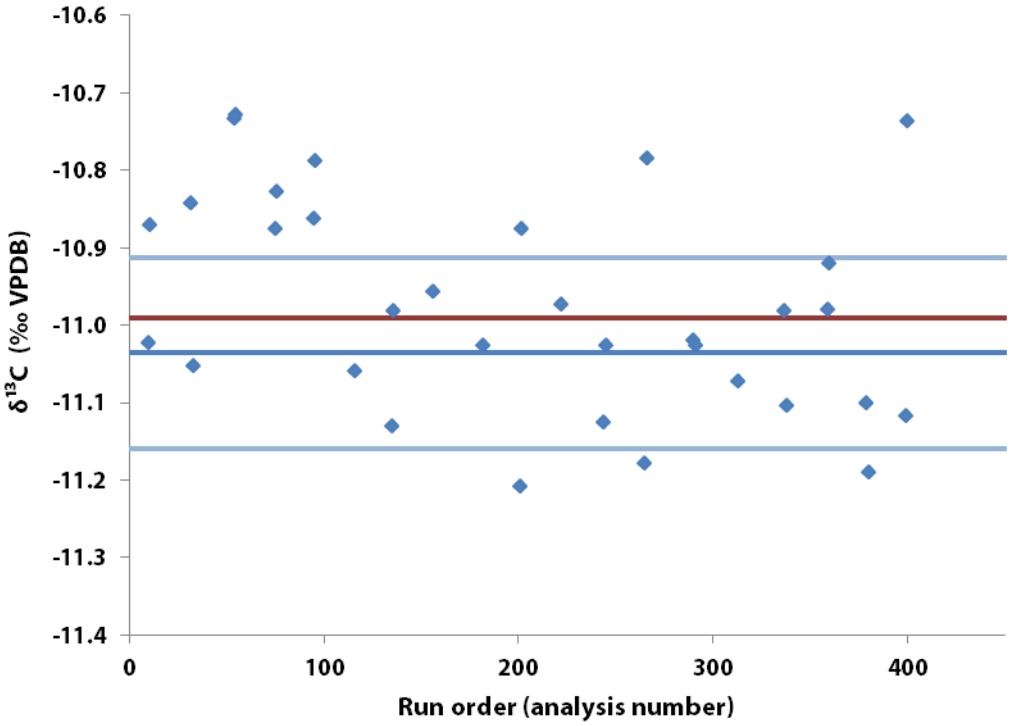

Figure 3.3: $\delta^{13}C$ values of CF in chronological order with overall average value (dark blue line) with ± 1σ error (light blue lines), compared to the accepted $\delta^{13}C$ value (red line).

3.3 Results

3.3.1 TC, TOC and TIC data

3.3.1.1 Sample repeats

In addition to the standard unknowns, two samples (LK-B-53 and LK-B-84) were analysed every run as an additional long-term variability monitor (Table 3.4). The standard deviation of TC runs is better than TOC runs for both sample repeats, which likely reflects the influence of the additional sample preparation of acidification and drying required for TOC runs. The standard deviations of the sample repeats are comparable to the standard, suggesting the TC and TOC data are reliable and that the error for TC, TOC and TIC values is approximately ± 0.1–0.2 %.

	Standard MD2517bog	LK-B-53 Total Carbon	LK-B-53 Organic Carbon	LK-B-84 Total Carbon	LK-B-84 Organic Carbon
Expected Value	4.591 ± 0.059 %				
Average Carbon (%)	4.642	4.032	4.015	2.594	2.616
Standard Deviation (1σ, ‰)	±0.12	±0.08	±0.18	±0.09	±0.10
Number	48	15	15	14	17

Table 3.4: Summary of Flash EA performance based on reproducibility of the in-run standard MD2517bog and two sample repeats, LK-B-53 and LK-B-84.

3.3.1.2 LK section (Kome Fm – Slibestensfjeldet Fm)

The resolution of samples analysed through the LK section is on the order of one sample every 0.1–0.3 m. The TOC content varies from 0.14 % to 71.81 %, with an average value of 10.25 % ± 17.59 (1σ). The variation revealed by such a large standard deviation is clearly observed in the TOC data presented against stratigraphic height (Figure 3.4), where there are several 'spikes' of high TOC content. As a result, in contrast to the mean, the median TOC value for this section is 3.4 %. The horizons of high TOC content occur through the section, generally coinciding with coal and coaly horizons, or horizons with large amounts of wood or carbonaceous material. In general, more sandy horizons possess lower TOC content.

TIC content varies from 0.00 % to 9.52 % with an average value of 0.50 % ± 1.18 (1σ). However, examination of TIC against stratigraphic height (Figure 3.4) reveals there are only two horizons with >3 % TIC, and so in contrast to the mean, the median TIC content is 0.13

%. The higher TIC horizons appear to coincide with sandy layers where the organic carbon content is higher than the general background values of 0–10 % TOC.

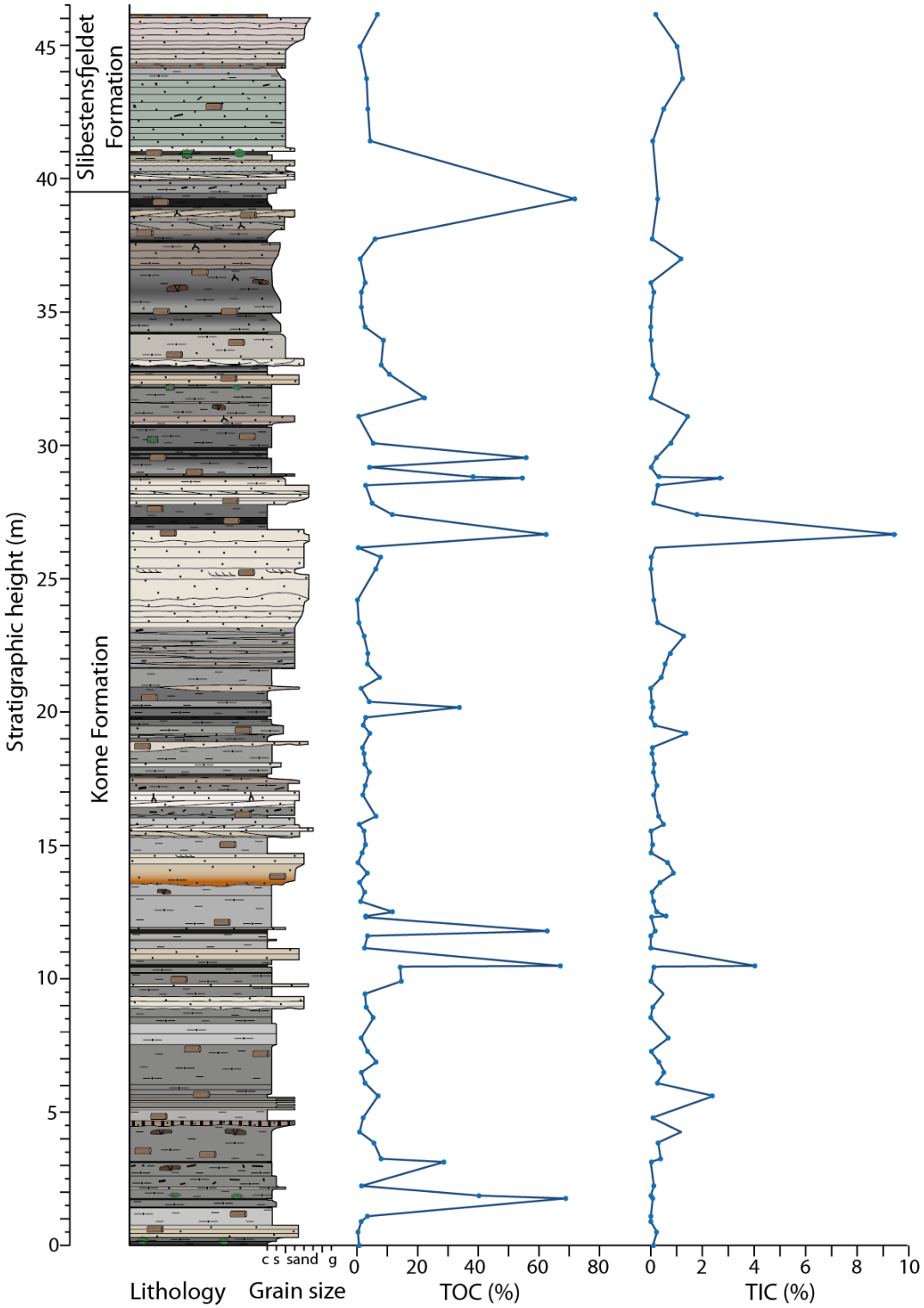

Figure 3.4: LK section stratigraphic log with total organic carbon (TOC) and total inorganic carbon (TIC) content. Key to graphic log in Appendix A, Figure ii.

3.3.1.3 KK section (Slibestensfjeldet Fm)

The resolution of samples analysed in the KK section is on the order of one sample every 1.5–2.0m. The TOC content varies from 1.33 % to 13.51 %, with an average value of 5.14 % ± 1.93 (1σ). There is only one analysed horizon with TOC content >10 % but the median TOC content is similar to the mean, at 5.47 %. The high TOC content horizon occurs in a sandstone layer (Figure 3.5).

The TIC content varies from 0 % to 5.19 %, with an average value of 0.84 % ± 1.18 (1σ). There are only three horizons analysed with a TIC content of >3 %, one of which occurs in the same sand horizon as the high TOC content data point (Figure 3.5). There is greater variability in TOC and carbonate content in the lower 30 m of the section.

3.3.1.4 ANE section (Slibestensfjeldet Fm – Ravn Kløft Mbr)

The resolution of samples analysed in the ANE section is on the order of one sample every 1.5–2.0 m. The TOC content varies from 0.28 % to 25.62 %, with an average of 3.32 % ± 5.33 (1σ). Examination of the TOC data with respect to stratigraphic height (Figure 3.6) reveals only one analysed horizon has a TOC content >5 %, and as a result the median TOC value is 2.33 %. When the horizon of high TOC is excluded from the standard deviation calculation, the standard deviation falls to 0.95, indicating a much lower variation in TOC through the section.

The TIC content is invariable, ranging from 0 % to 1.27 %, with an average value of 0.24 % ± 0.30 (1σ). Only one horizon has a TIC content of >1 % carbonate, but this does not occur at the same horizon as the maximum TOC content of the section.

3.3.1.5 RKE section (Ravn Kløft Mbr)

The samples from the main section (RKE in Figure 2.14, 2.15) were analysed at a resolution of one sample every 0.2–1.0 m (Figure 3.7). The parallel section (RKE log 2 in Figure 2.14, 2.15) was not sampled across the full span of the section (Figure 3.8) but the resolution across the sampled interval is approximately one sample every metre. The TOC content of both sections ranges from 0.28 % to 58.54 %, with an average value of 7.62 % ± 11.00 (1σ). The median value is 4.26 % which differs slightly from the mean because only one horizon in the parallel section (Figure 3.8) and seven samples in the main RKE section (Figure 3.7) have >20 % TOC. The high TOC content horizons occur in coaly mudstone lithology.

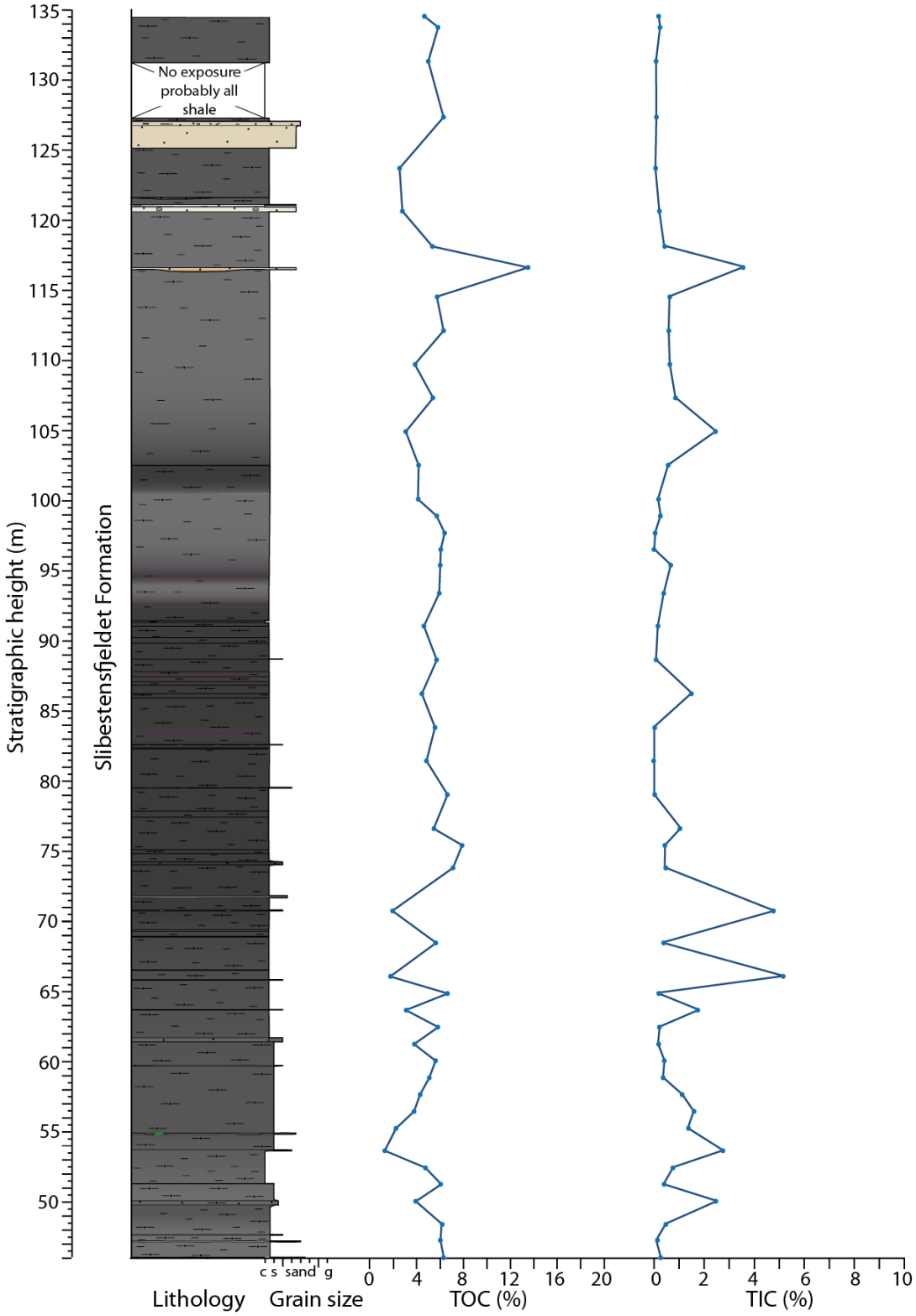

Figure 3.5: KK section stratigraphic log with total organic carbon (TOC) and total inorganic carbon (TIC) content. Key to graphic log in Appendix A, Figure ii.

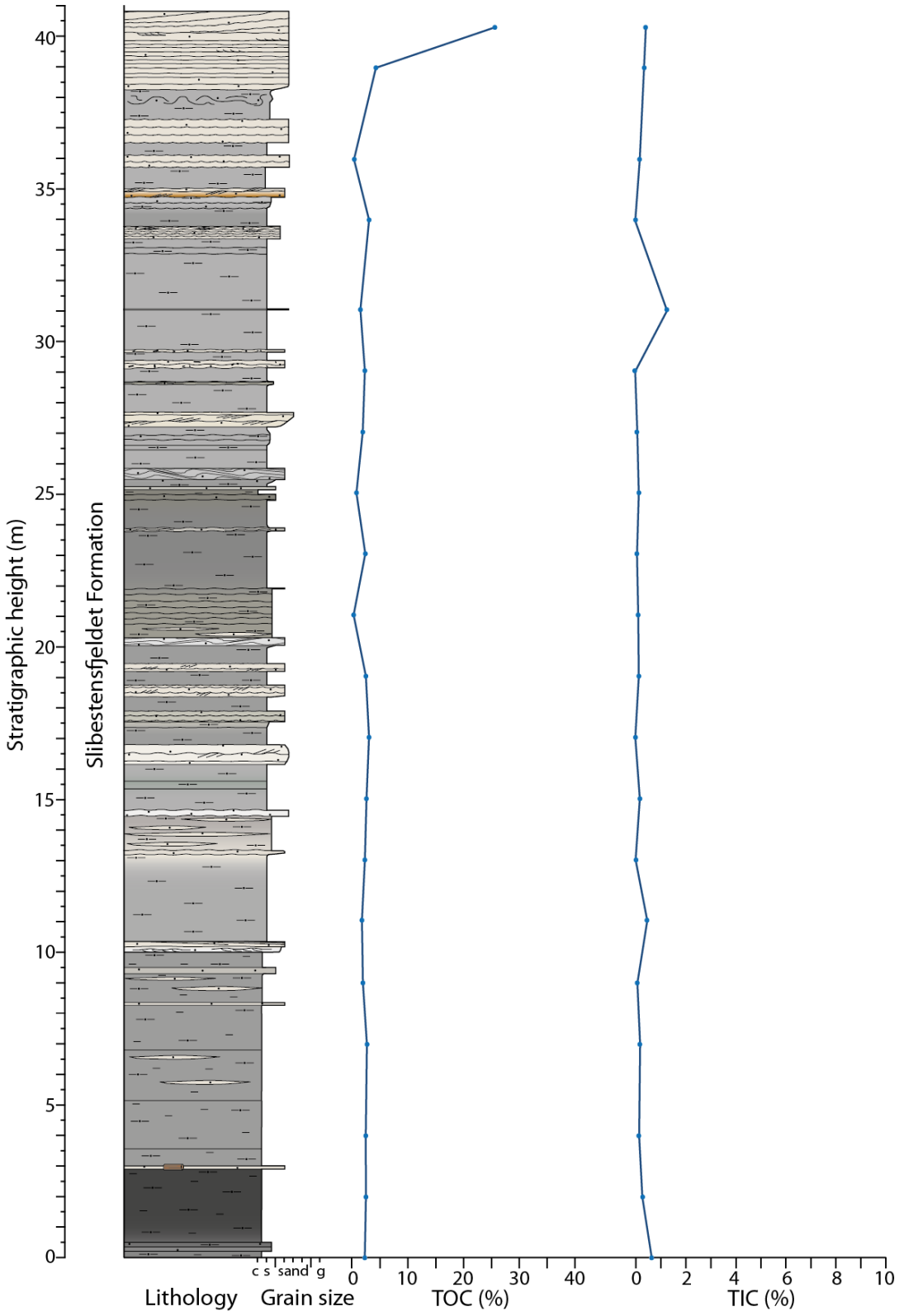

Figure 3.6: ANE section stratigraphic log with total organic carbon (TOC) and total inorganic carbon (TIC) content. Key to graphic log in Appendix A, Figure ii.

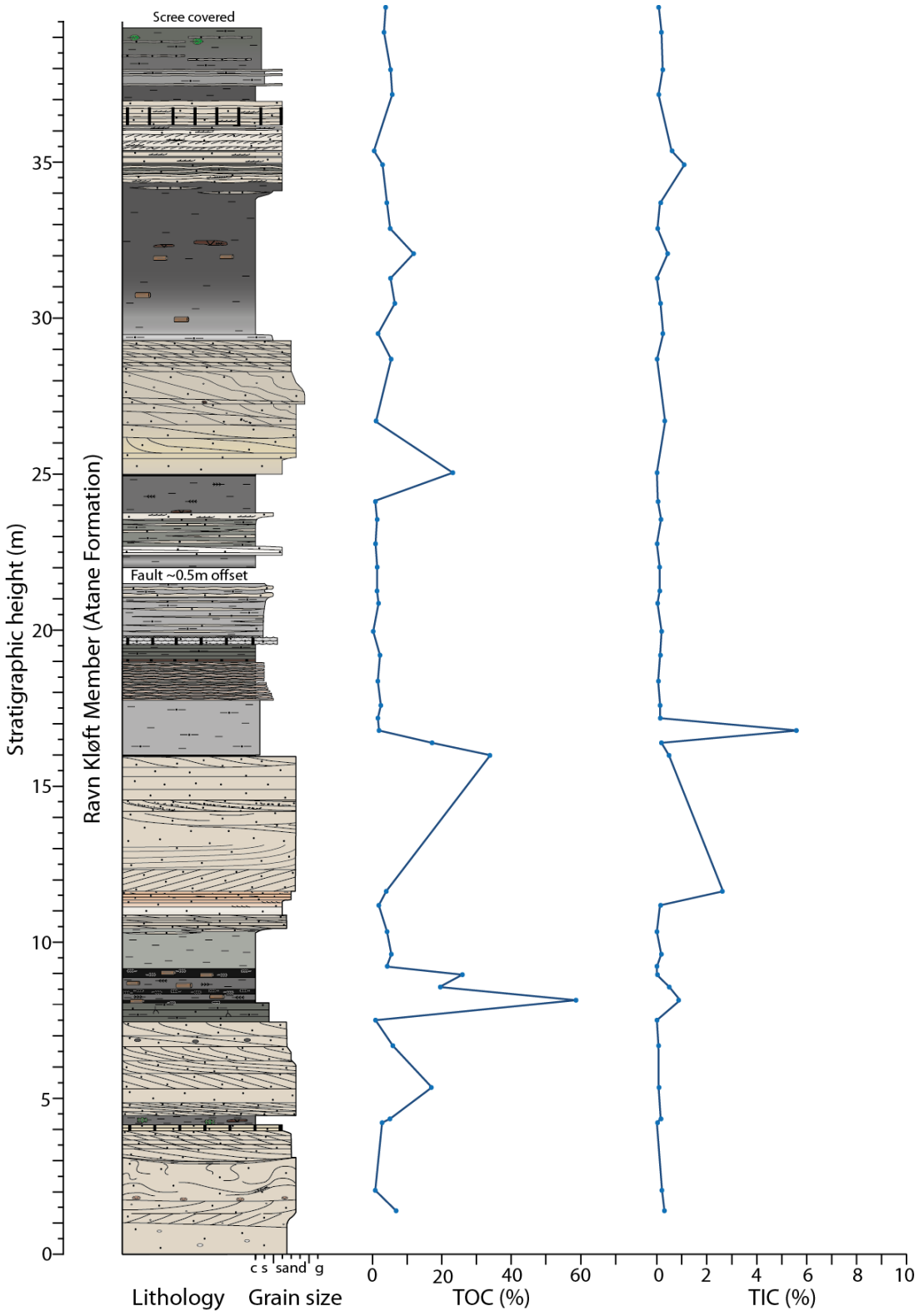

Figure 3.7: RKE main section stratigraphic log with total organic carbon (TOC) total inorganic carbon (TIC) content. Key to graphic log in Appendix A, Figure ii.

The TIC content across both sections ranges from 0 % to 5.64 %, with an average value of 0.34 % ± 0.86 (1σ), indicating low variability through the sections, which is clear from the data presented against stratigraphic height (Figures 3.7 and 3.8). No samples in the parallel section have >1 % TIC, but in the main RKE section, two horizons contained >2 % TIC, and the median values of both the sections is 0.13 %.

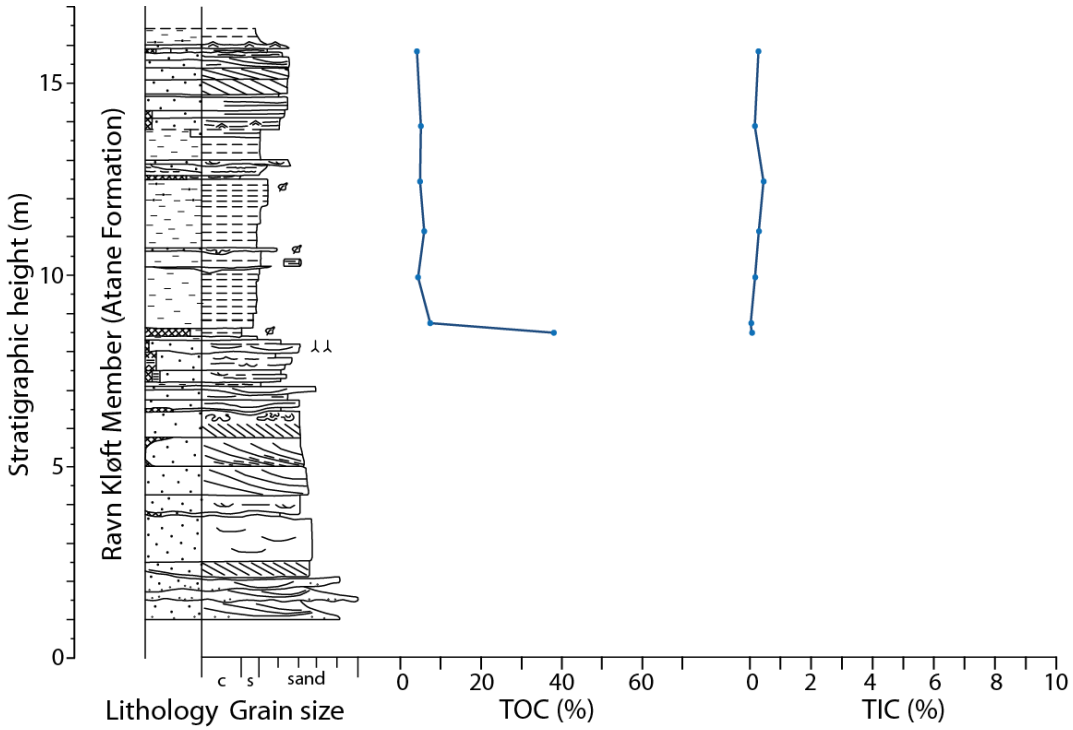

Figure 3.8: RKE parallel section stratigraphic log with total organic carbon (TOC) and total inorganic carbon (TIC) content. Key to graphic log in Appendix A, Figure ii.

3.3.1.6 RKW section (Ravn Kløft Mbr – Kingittoq Mbr)

There were only six bulk sediment samples collected in the Ravn Kløft Member from the RKW section, and only seven grab samples collected from the Kingittoq Member, due, respectively, to the predominance of clean, coarse sand and poor exposure (graphic logs, Appendix A).

The range in TOC content across both sampled intervals is 0.29 % to 15.44 %, with an average value of 3.55 % ± 3.82 (1σ). Only one horizon has a TOC value of >5 %, and so the median value of the sampled material was 2.78 % (Figure i, Appendix B).

The TIC content ranges between 0.01 % and 1.76 %, with an average value of 0.57 % ± 0.52 (1σ). There is very little variation in TIC content through the section, and the median value of 0.48 % is close to the mean value (Figure i, Appendix B).

3.3.2 Carbon isotope data - sample repeats and uncertainty estimate

In addition to monitoring standards CF and GRAP, three fossil wood (LK-W-9, RKE-W-5 and RKW-W-36) and two bulk sediment samples (LK-B-53 and LK-B-84: the same as the TC/TOC repeats) were selected as repeats to be analysed every run. These sample repeats were intended to serve a similar purpose to the monitoring standards, but had the added benefit of being the same sample material type as the rest of the samples analysed, and therefore the influence of combustion effects and sample size analysed on $\delta^{13}C$ could be explored.

There was no observed trend in the $\delta^{13}C_{org}$ (organic carbon of bulk sediment) with relative time (run order) for the two bulk sediment sample repeats (Figure 3.9).

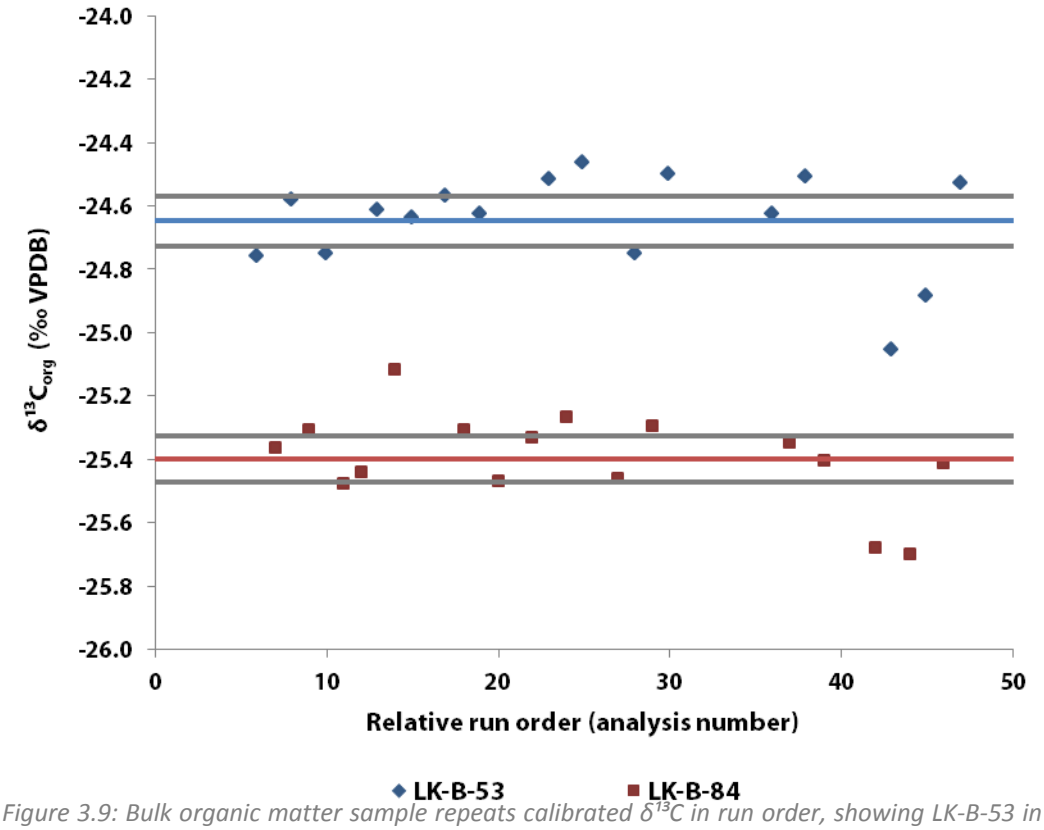

Figure 3.9: Bulk organic matter sample repeats calibrated $\delta^{13}C$ in run order, showing LK-B-53 in blue and LK-B-84 in red, with average and 1 σ error for both samples indicated by horizontal lines through the data.

In addition, for select samples, a range of sample weights were analysed in order to understand the response of $\delta^{13}C_{org}$ and $\delta^{13}C_{wood}$ values to analyses with mass-44 peak amplitudes outside the ideal range of 4000–6000 mV (Figure 3.10). Samples LK-W-9 and RKW-W-36 had less range in measured peak amplitude and presented no significant relationship between peak amplitude and $\delta^{13}C_{wood}$ (r^2 values close to 0; Figure 3.10). The other three sample repeats (RKE-W-5, LK-B-53, LK-B-84) present a positive relationship between $\delta^{13}C_{(wood\ or\ org)}$ and peak amplitude, with r^2 values ranging 0.48–0.65. The range of

$\delta^{13}C_{(wood\ or\ org)}$ values for these three samples is on the order of 0.44–0.58 ‰, with standard deviations up to 0.26 (Table 3.5).

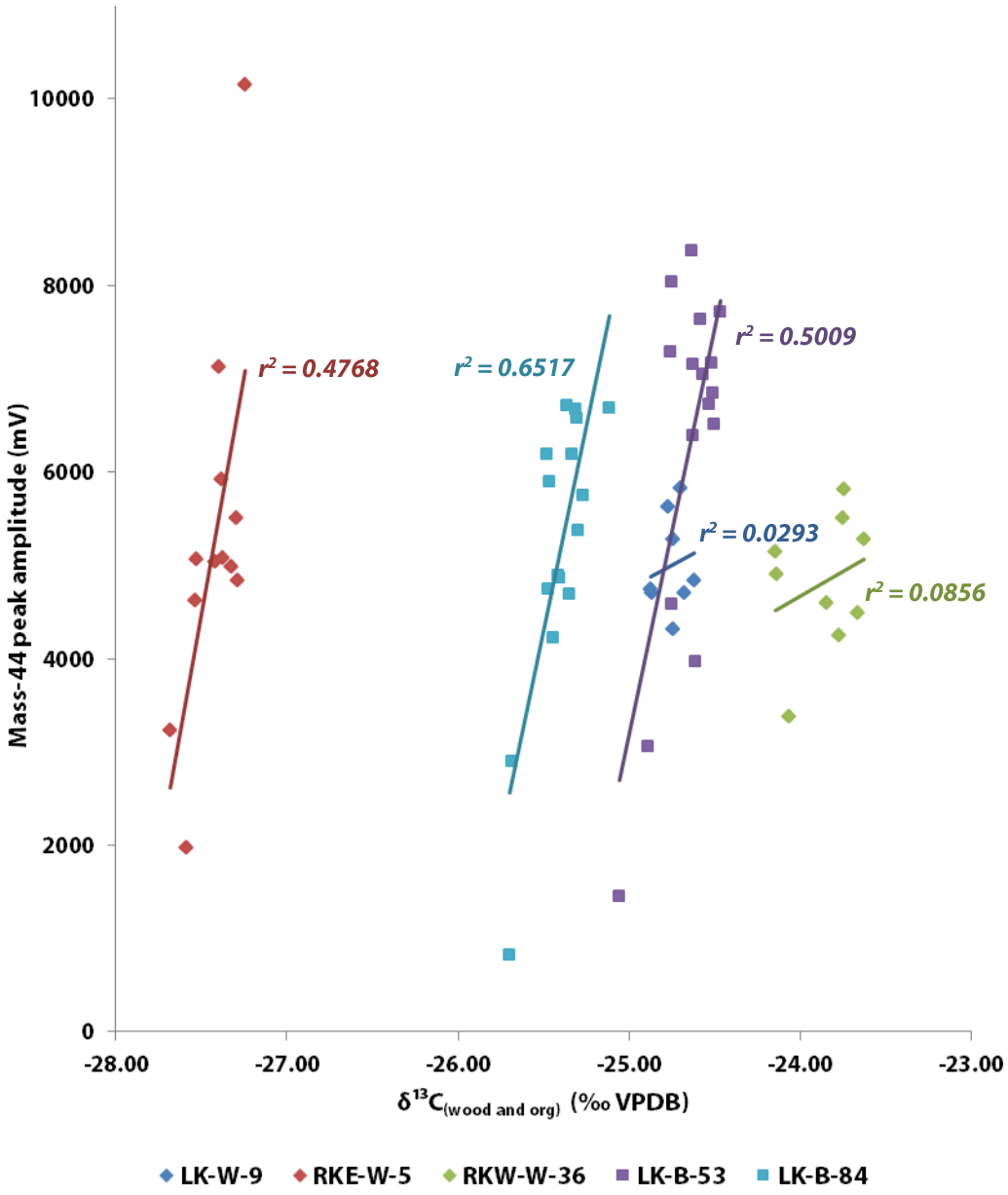

Figure 3.10: Fossil wood and bulk sediment sample repeats showing the result of variable amounts of sample weighed deliberately outside the optimal range of mass spectrometer operation (peak amplitudes of 4000-6000 mV). Trend lines for each sample set are presented with r^2 values.

However, if only the data from the optimal mass-44 peak amplitude range of 4000–6000 mV are considered (Table 3.5), the standard deviation decreases to around 0.10 with a corresponding range in $\delta^{13}C_{(wood\ and\ org)}$ on the order of 0.25–0.36 ‰. An exception was RKW-W-36 with a higher standard deviation of 0.20 and range in $\delta^{13}C_{(wood)}$ of 0.52 ‰.

These repeat analyses indicate that there was a combustion effect on $\delta^{13}C$, such that low sample weights resulted in an isotopically lighter $\delta^{13}C_{(wood\ and\ org)}$, on the order of 0.5 ‰ (Figure 3.10, Table 3.5), which adds error to the data. However, if a sample had a mass-44 signal outside of the ideal range, then it was reanalysed to minimize this effect. The sample weight tests indicate that the standard deviations of unknowns are comparable to those of the monitoring standards, CF and GRAP.

Sample	All mass-44 peak amplitude data				4000-6000 mV peak amplitude only			
	Average $\delta^{13}C$ (‰VPDB)	Std. Dev.	Range in $\delta^{13}C$ (‰VPDB)	No. of analyses	Average $\delta^{13}C$ (‰ VPDB)	Std. Dev.	Range in $\delta^{13}C$ (‰VPDB)	No. of analyses
LK-B-53	-24.66	0.21	0.55	16	-24.59	0.09	0.29	12
LK-B-84	-25.47	0.26	0.58	16	-25.34	0.1	0.36	12
LK-W-9	no weight experiment performed				-24.75	0.09	0.26	8
RKE-W-5	-27.42	0.13	0.44	12	-27.39	0.1	0.25	8
RKW-W-36	-23.86	0.2	0.52	9	-23.84	0.2	0.52	8

Table 3.5: Summary of sample repeat performance in terms of average carbon isotope ratio and standard deviation and range of all sample weights compared to those only supplying optimal carbon amounts to the mass spectrometer.

3.3.3 Carbon isotope data – bulk organic matter

3.3.3.1 LK Section (Kome Fm – Slibestensfjeldet Fm)

The $\delta^{13}C_{org}$ values through the LK section range from -23.77 ‰ to -26.70 ‰ (a variation of 2.93 ‰), with an average $\delta^{13}C_{org}$ of -24.98 ‰ ±0.57 (1σ). Examination of $\delta^{13}C_{org}$ against stratigraphic height indicates two patterns of variation (Figure 3.11): there is noise from one sample to the next on the order of 0.5–1.0 ‰, which creates an apparent noise envelope through the section. However, there are also trends through the section of greater magnitude than this noise envelope; including an increase to more positive $\delta^{13}C_{org}$ in the first 12 m of the section, from around -25.5 ‰ to -23.8 ‰ (Figure 3.11), followed by an overall decrease to around -26.0 ‰ (at approximately 25 m stratigraphic height).

Subsequent $\delta^{13}C_{org}$ values increase to -24.3 ‰ at around 43 m height near the top of the LK section.

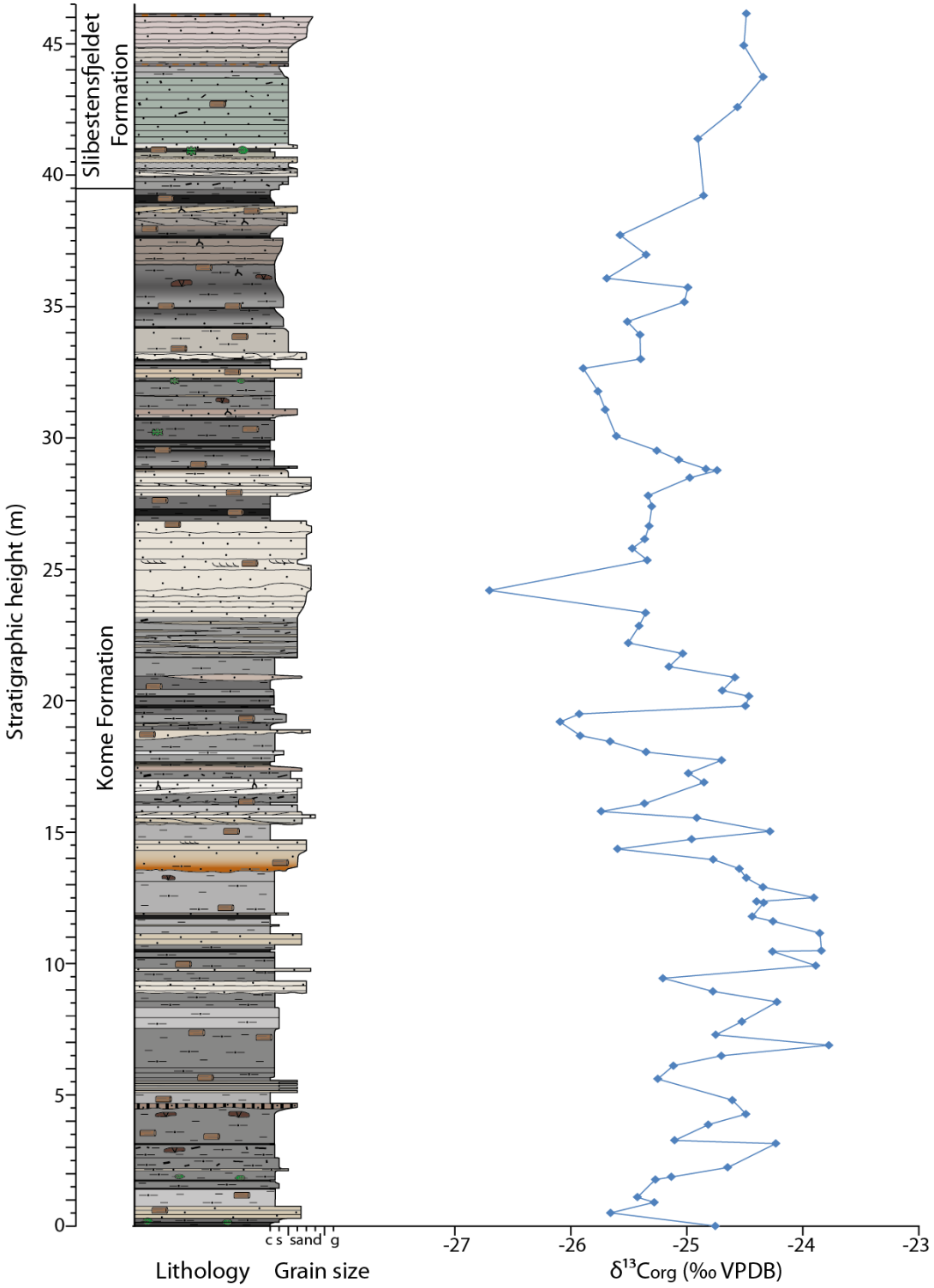

Figure 3.11: LK section stratigraphic log with bulk organic matter carbon isotope ratios. Key to graphic log in Appendix A, Figure ii.

3.3.3.2 KK Section (Slibestensfjeldet Fm)

The $\delta^{13}C_{org}$ values through the KK section range from -25.86 ‰ to -24.56 ‰ (variation of 1.3 ‰), with an average value of -25.14 ‰ ± 0.32 (1σ) (Figure 3.12). There are no apparent excursions through the section, with a small increase to more positive values on the order of 1.0 ‰ in the first 6 m of the section. There is a subsequent decrease of approximately 1.5 ‰ by 57 m stratigraphic height. At around 124 m stratigraphic height there is an increase in $\delta^{13}C_{org}$ from around -25.8 ‰ to around -24.5 ‰ at the top of the logged section. There are no major excursions or trends in the interval between these two small excursions at the top and bottom of the section and the noise throughout the interval is small, on the order of 0.25 ‰.

3.3.3.3 ANE Section (Slibestensfjeldet Fm)

The $\delta^{13}C_{org}$ values through the ANE section vary from -25.97 ‰ to -25.26 ‰ (a range of 0.71 ‰), with an average value of -25.50 ‰ ±0.18 (1σ). The low variation can be observed in $\delta^{13}C_{org}$ values against stratigraphic height (Figure 3.13), where there is a general increase in values from about 21 m height to the top of the section on the order of 0.5 ‰. However, the top portion of the section also presents more noise on the order of 0.25 ‰ compared to very little in the first 20 m of the section.

3.3.3.4 RKE Section (Ravn Kløft Mbr)

The $\delta^{13}C_{org}$ values through both RKE sections vary from -26.78 ‰ to -24.11 ‰ (a range of 2.67 ‰), with an average value of -25.01 ‰ ± 0.54 (1σ). The variability can be observed in $\delta^{13}C_{org}$ against stratigraphic height for both sections comprising the RKE dataset (Figure 3.14) where there is noise in $\delta^{13}C_{org}$ from one horizon to the next, on the order of 0.5 ‰.

However, there are also trends of greater magnitude than the noise envelope, for example at 4.3 m stratigraphic height in the main section (Figure 3.14 – blue data) there is a negative excursion of around -26.8 ‰. At around 30 m height in the main section there is another negative excursion of around -26.0 ‰. Between these two intervals there is a general increase in $\delta^{13}C_{org}$ values from around -25.5 ‰ at about 8 m height in the main section, to about -24.5 ‰ at 37 m height.

$\delta^{13}C_{org}$ of the secondary section at the RKE locality have been plotted alongside the main section data according to the field notes on correlation (Figure 3.14 – green data) and are generally isotopically heavier than the main section by 0.5–1.0 ‰. A similar shift to the primary section, from more negative values of around -25.0 ‰ between 8–11 m height to

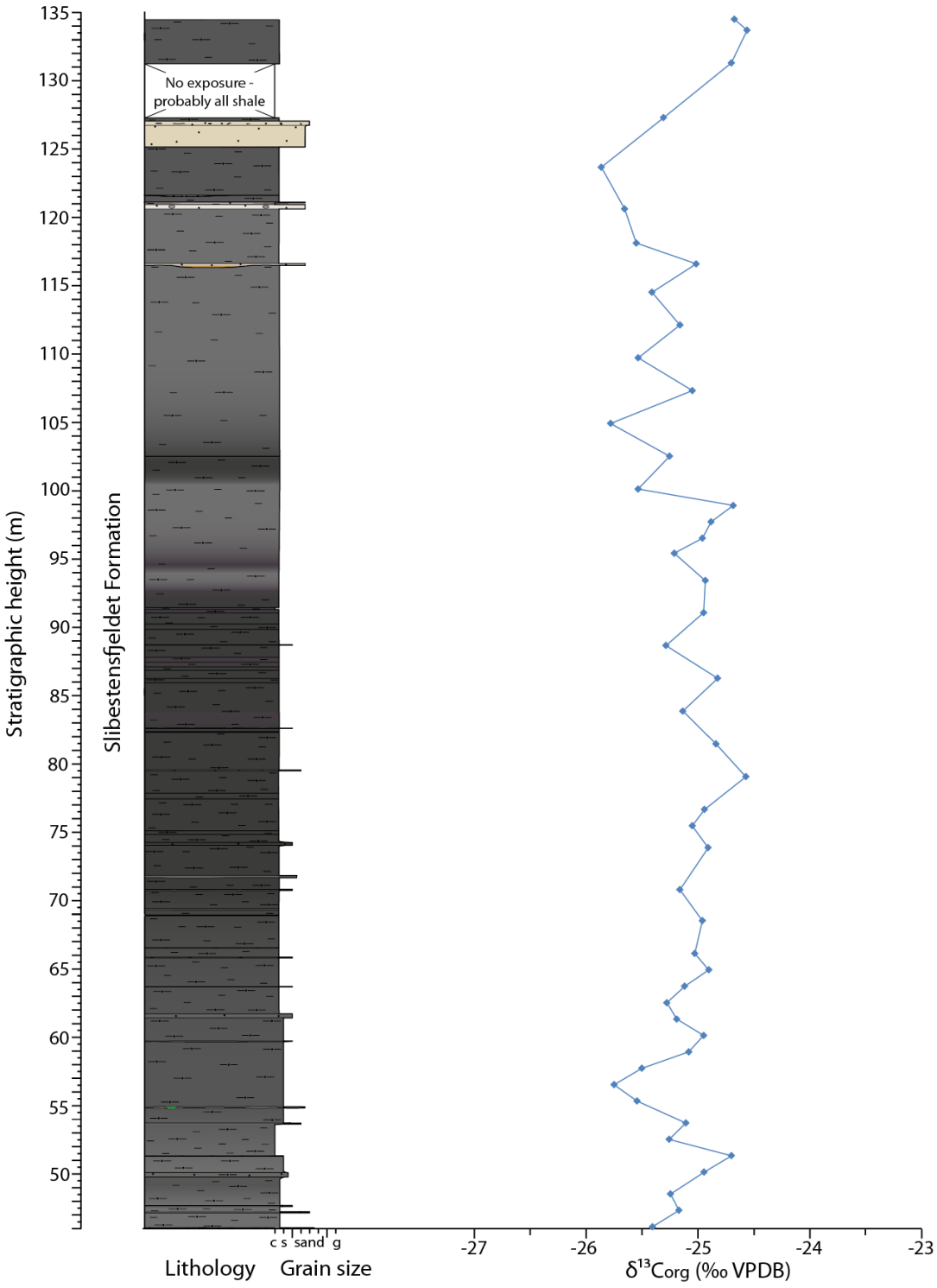

Figure 3.12: KK section stratigraphic log with bulk organic matter carbon isotope ratios. Key to graphic log in Appendix A, Figure ii.

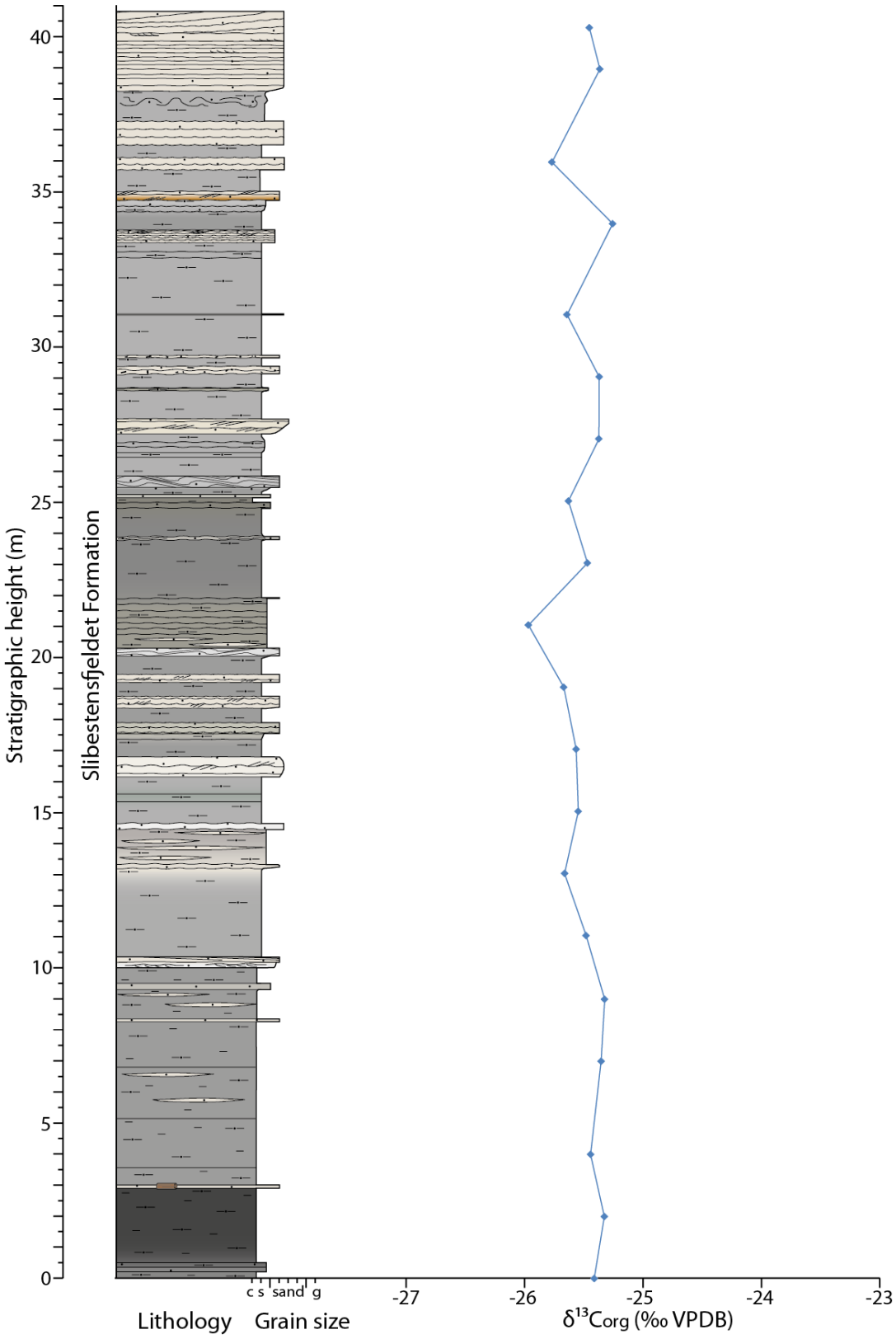

Figure 3.13: ANE section stratigraphic log with bulk organic matter carbon isotope ratios. Key to graphic log in Appendix A, Figure ii.

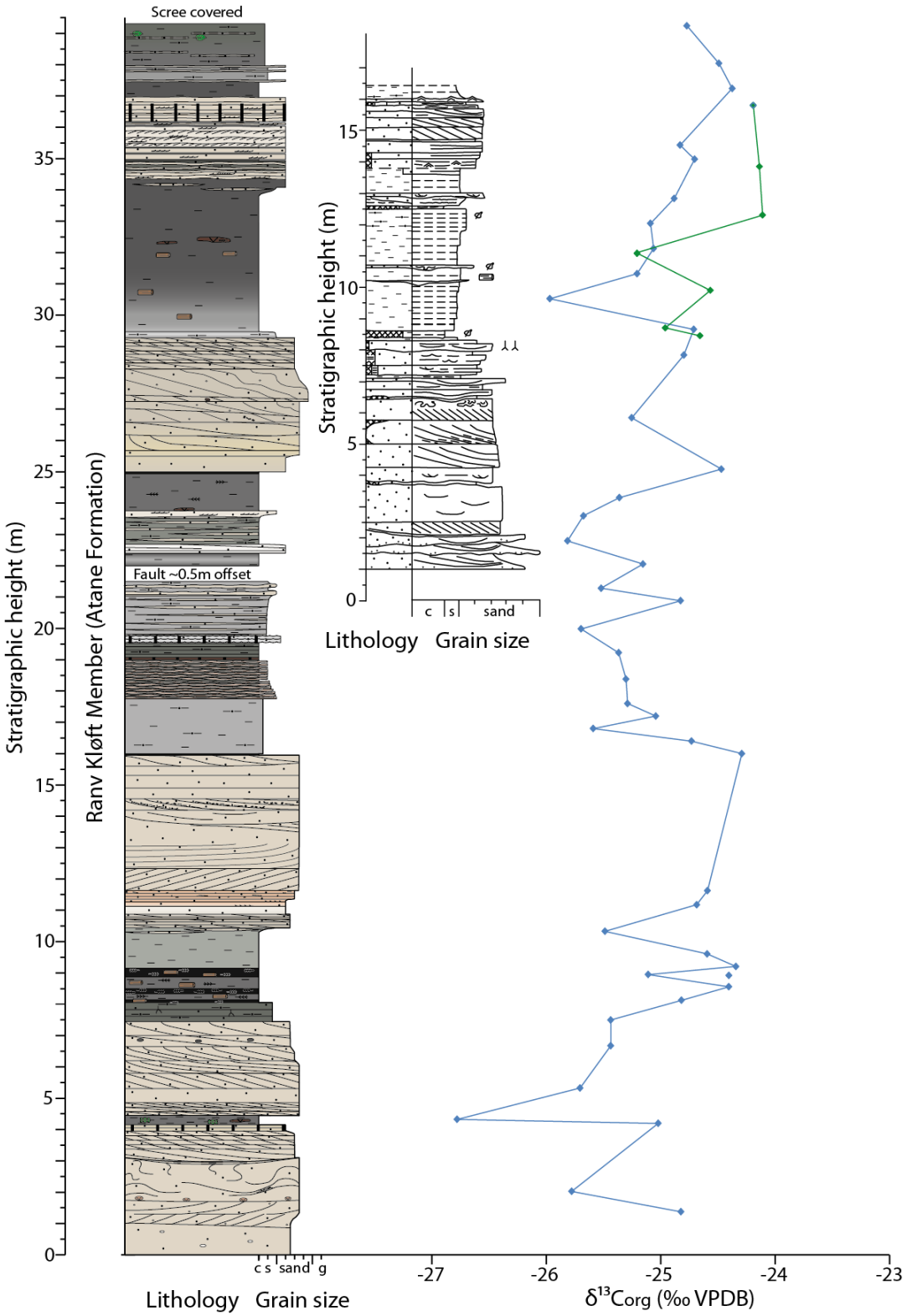

Figure 3.14: RKE section stratigraphic logs with bulk organic matter carbon isotope ratios of the main section (blue) and secondary section (green). Key to graphic log in Appendix A, Figure ii.

more positive values closer to -24.0 ‰ at 12–16m height, is observed in the secondary section.

3.3.3.5 RKW Section (Ravn Kløft Mbr – Kingitoq Mbr)

As previously mentioned, there are few bulk sediment samples for the RKW section (both logged section and grab samples). The $\delta^{13}C_{org}$ ranges from -25.99 ‰ to -24.45 ‰ (range of 1.55 ‰), with an average value of -24.49 ‰ ± 0.44 (1σ) (Figure ii, Appendix B). There are insufficient data points for the RKW section to reveal any significant trends in isotope ratios, but values are close to -25.0 ‰ at 40–60 m height in the logged portion of the section. The $\delta^{13}C_{org}$ values measured from 140–190 m are isotopically heavier, at around -24.75 ‰, followed by an apparent decrease in $\delta^{13}C_{org}$ to close to -25.75 ‰ until 216 m height. The top-most samples collected at 223–225 m stratigraphic height in the RKW section suggest $\delta^{13}C_{org}$ returns to values close to those lower in the section, around -24.75 ‰.

3.3.4 Carbon isotope data – fossil wood

3.3.4.1 Fossil wood preservation classification

Previous studies have examined the role of fossil wood preservation on $\delta^{13}C_{wood}$ but no systematic offset with different styles of preservation has yet been observed (e.g. Gröcke, 2002; Hesselbo *et al.*, 2002; Robinson and Hesselbo, 2004; Pearce *et al.*, 2005). Nonetheless, before the fossil wood samples were powdered, a description of each piece was made (Table 3.6). This provided the basis to group the fossil wood samples into classes based on similar preservational characteristics in order to investigate any influence on carbon isotope discrimination.

Character	Information recorded
Surface lustre	vitreous, silky, dull
Habit	cubic , blocky, fibrous, flat
Shape	rounded, angular
Hardness (streak)	hard, soft, not possible
Number of pieces	number and whether likely from a single piece of wood
Weathering products	note of iron staining present/absent
Sediment present	note of sediment adhered to sample or grains mixed in with very small multiple wood pieces.

Table 3.6: Summary of descriptions made of fossil wood pieces before powdering sample.

Class 1

These samples were black in colour, possessed a vitreous lustre and found to be hard and brittle when the streak was tested. These samples had no (or only minor) oxidation staining or adhered sediment, and were mainly composed of many small pieces (mm-scale) with a blocky or cubic habit. It was thought that these samples may represent multiple original wood fragments; although it was also possible one originally whole wood piece could have broken into many pieces. These samples were the most coalified, evidenced by the vitreous lustre, brittle nature and cubic fracture.

Class 2

Class 2 contains samples similar to class 1, except the pieces were larger in size and taken to represent an individual original piece of fossil wood. Some pieces had fine-grained (clay) sediment coating which could not be removed from the exterior of the sample, but the interior was vitreous and brittle and exhibited blocky/cubic fracture habit.

Class 3

Like classes 1 and 2, these samples were also coalified fossil wood, but differed in that they showed considerable oxidation staining on surfaces that had not been removed by washing. There was little adhered sediment on surfaces, and generally these samples were cm-scale pieces and often identified as an originally individual wood fragment. The majority had the same cubic habit and were hard and brittle as classes 1 and 2, with a vitreous lustre.

Class 4

Class 4 contains coalified fossil wood with some sediment content. This varied from a fine grained coating on surfaces to fossil wood interlayered with sediment. The concern with sediment contamination was two-fold. First, it may affect the $\delta^{13}C_{wood}$ analysis due to an inaccurate sample weight being used. Second, the sediment could contain carbon from a non-wood source, which would lead to contamination of the $\delta^{13}C_{wood}$ value measured. Coarse quartz-dominated sediment was easily removed and so did not present a contamination issue.

Class 5

Class 5 samples were possibly less coalified than the first four classes, since the lustre was silky, suggesting some of the original wood structure was preserved, but they still had a blocky habit and were hard. In addition, all samples in this class had some sediment present, which may have reduced the apparent lustre. The samples in class 5 likely represent part of the preservational spectrum between coal and charcoal on account of the lustre compared to habit. The amount of iron oxidation present in these samples was variable.

Class 6

Class 6 contains charcoalified samples, identified by a dull-to-silky lustre, a softer streak and fibrous to blocky habit. The fibrous habit suggested some of the original wood structure was preserved, as expected in charcoalified wood. None of these samples had iron oxidation staining, but there was a mixture of sediment amounts present: many samples had grains present, which were removed before analysis, but some also had minor amounts of fine-grain cover on surfaces.

Class 7

Class 7 contains samples that were not definitively fossil wood samples. They had a dull lustre and were irregular or plate-like in habit. Often the samples were wrapped around grains, suggesting they were once soft and easily deformed. They were, on the whole, small pieces, with no iron oxidation staining and had soft streaks. It is possible that these samples were the remains of organic matter from the terrestrial realm associated with wood and other plant matter.

Summary of classification

Of the 94 pieces collected in the LK section, just over 80 % of samples occur in classes 1–4 (Table 3.7). There is a more even spread across preservation types in the RKW section: 35 % of samples collected classified as coalified wood (classes 1–4), 28 % of samples are in the charcoalified wood group (classes 5 and 6) and the remaining 37 % in the more ambiguous class 7. The RKE section has the fewest number of fossil wood pieces collected (18), of which 77 % are coalified wood, and the remaining samples fell in class 7.

Section	Wood Class							
	1	2	3	4	5	6	7	Total
LK	34	17	21	6	4	7	4	94
RKE	6	1	7	0	0	0	4	18
RKW	14	4	1	1	1	15	21	57

Table 3.7: Number of fossil wood pieces grouped into wood classes for each section.

3.3.4.2 LK section (Kome Fm – Slibestensfjeldet Fm)

The $\delta^{13}C_{wood}$ measured in the LK section range from -27.39 ‰ to -21.56 ‰ (a variation of 5.83 ‰), with an average value of -25.25 ‰ ± 1.05 (1σ). $\delta^{13}C_{wood}$ increases from the base of the section from -25.25 ‰, to the most positive values of the entire section of around -21.5 ‰ at approximately 14 m height (Figure 3.15). There is a subsequent decrease in $\delta^{13}C_{wood}$ values from this point to values approaching -27.0 ‰ at around 20 m height. Across these general trends and throughout the remainder of the section, there is considerable noise from one sample to the next on the order of 1.5 ‰. No particular trends other than this apparent noise can be observed in the top 20–25 m of section.

3.3.4.3 RKE section (Ravn Kløft Mbr)

There were insufficient fossil wood pieces collected through the main RKE section to reveal any significant trends; however, $\delta^{13}C_{wood}$ varied from -27.41 ‰ to -23.74 ‰ (a range of 3.67 ‰) with an average value of -25.17 ‰ ± 0.98 (1σ) (Figure 3.16). At around 9 m height in the section the most negative $\delta^{13}C_{wood}$ is recorded (-27.41 ‰) with samples 1 m above and below yielding values close to -25.0 ‰, with the exception of a sample around 8.5 m height with a $\delta^{13}C_{wood}$ value close to -26.25 ‰. There is a large amount of variation in the four remaining data horizons around 30–35 m height, ranging from around -26.0 ‰ to -24.0 ‰. There is insufficient data for trend resolution and may partially reflect noise in the data as exhibited in the rest of the carbon isotope stratigraphy.

3.3.4.4 RKW section (Ravn Kløft Mbr – Kingitoq Mbr)

Measured $\delta^{13}C_{wood}$ in the RKW section varied from -25.77 ‰ to -22.21 ‰ (a range of 3.56 ‰) with an average value of -24.39 ‰ ± 0.84 (1σ). Examination of $\delta^{13}C_{wood}$ against the logged stratigraphy (Figure 3.17) reveals that noise is a dominant feature of the chemostratigraphy, with variation from one sample to the next on the order of 1.0–1.5 ‰. As a result of the noise envelope, there are no significant excursions identified in the

section, but there may be an overall positive trend in $\delta^{13}C_{wood}$ from close to -25.7 ‰ at around 18 m height, to values nearer -23.0 ‰ around 115 m height.

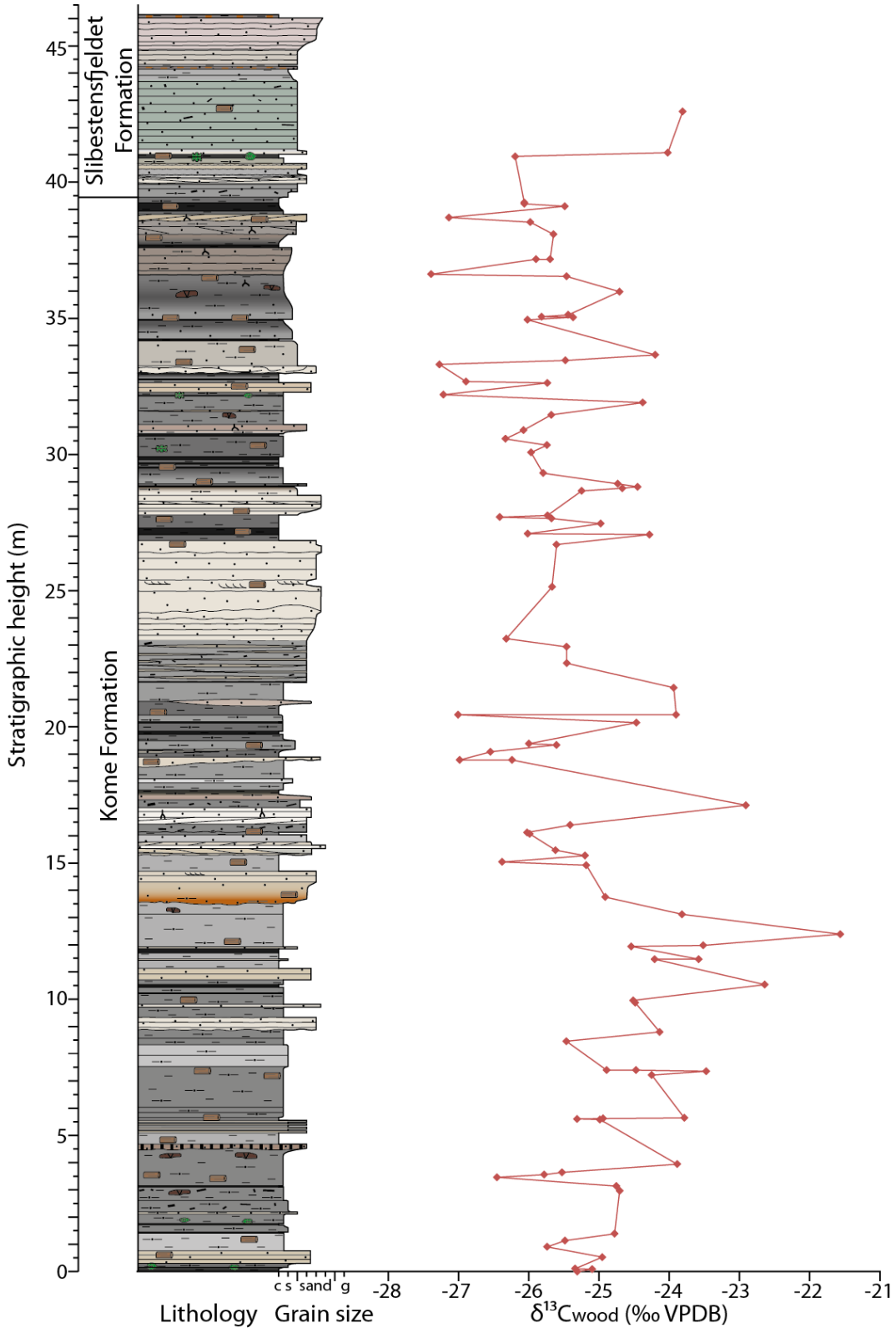

Figure 3.15: LK section stratigraphic log with fossil wood carbon isotope ratios. Key to graphic log in Appendix A, Figure ii.

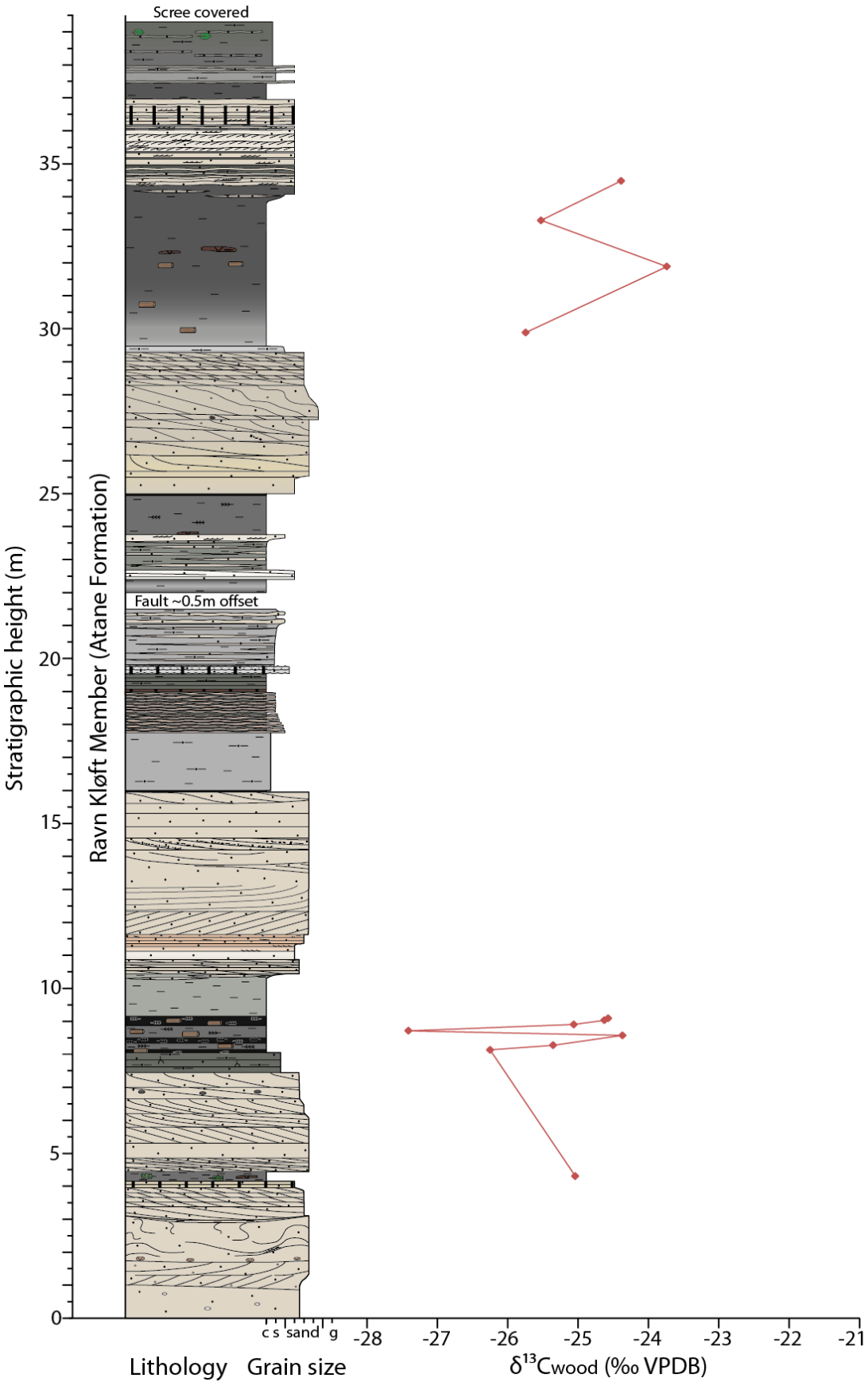

Figure 3.16: RKE main section stratigraphic log with fossil wood carbon isotope ratios. Key to graphic log in Appendix A, Figure ii.

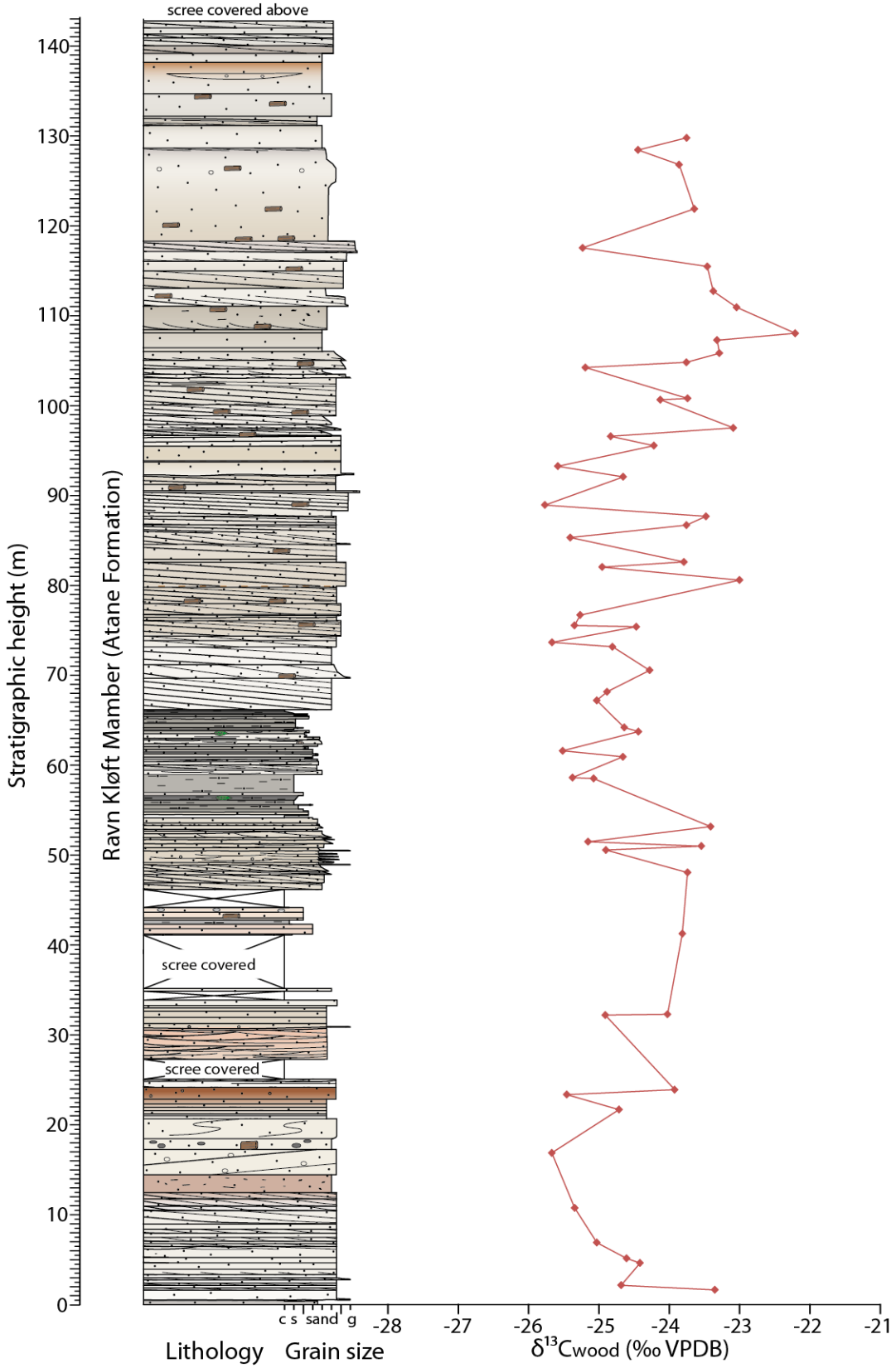

Figure 3.17: RKW logged section stratigraphic log with fossil wood carbon isotope ratios. Key to graphic log in Appendix A, Figure ii.

3.4 Discussion

3.4.1 Does depositional setting influence bulk sediment $\delta^{13}C$?

In order to interpret the bulk sediment isotopic data as a (semi-) reliable tracer of global carbon cycling, it is necessary to first consider whether other factors may have influenced the record. The most notable of these might be organic matter source related to depositional environment. A frequency histogram of TOC from each Formation is shown in Figure 3.18.

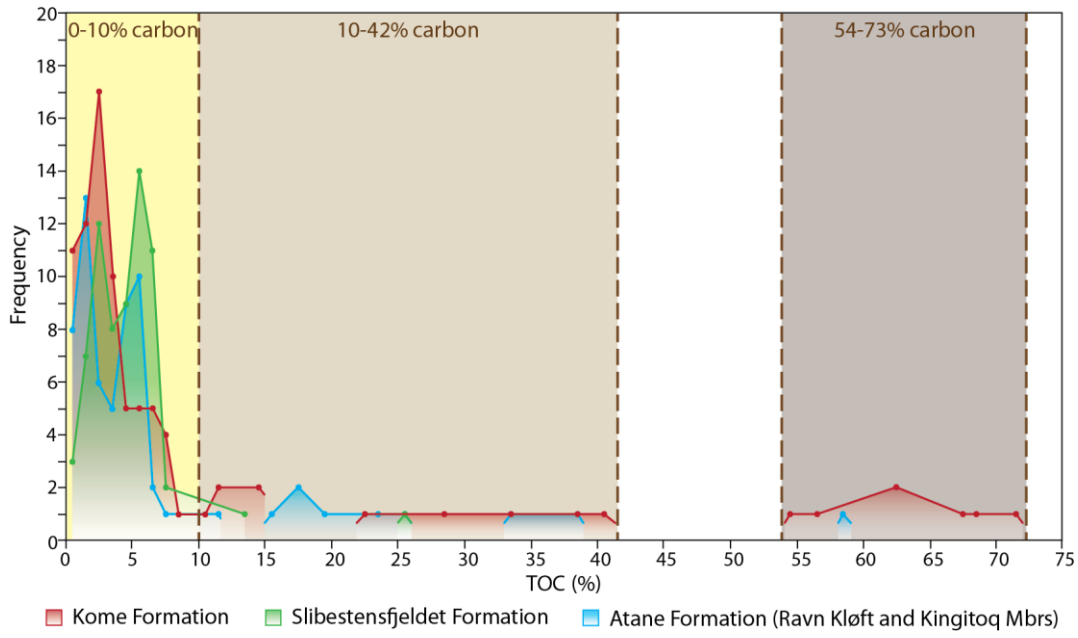

Figure 3.18: Frequency histograms of organic carbon content, colour-coded for each section. Brown dashed lines and shading indicate grouping of data based on histogram distributions. Bin size = 1%. The total number of samples varied between sections, with the most samples (87) analysed in the Kome Formation (LK section). More comparable sample numbers were analysed for the Slibestensfjeldet Formation (KK and ANE sections) and Atane Formation (RKE and RKW sections), with 68 and 63 samples respectively.

In all Formations, most samples contain 0–10 % TOC, with a substantial tail towards high values of <42% A very high TOC group is identified in the Kome Formation histogram, and by one data point in the Atane Formation, with TOC contents of 54–73 %. The lithology for horizons in this TOC range are either coal or leaf-mat deposits, as expected for similar fluvio-deltaic depositional environments identified in both the Kome and Atane Formation (Dam *et al*., 2009; Section 2.5) The relationship of TOC and lithology is less clear for the rest of the data. For the Kome and Atane formations, horizons with up to 40 % TOC are predominantly lithologies proximal to coal horizons, coaly mudstones or silt-rich shale and mudstones containing fossil wood fragments or leaf fossils. However, in the

Slibestensfjeldet Formation the lithology of the horizons within the 10–42 % TOC range may reflect episodes of greater fluvial input (flooding) washing in a greater proportion of phytoclasts, which were redeposited downslope. By comparison, sandstones in the Kome and Atane Formations have the lowest TOC content, mostly comprising a 1–4 % TOC sub-peak within the 0–10 % range. In the Kome Formation the lithologies falling within the 5–9 % organic carbon range are generally sandy siltstones with fossil wood present. In general the Kome and Atane Formations appear to have the most similar TOC distribution, which is expected since the depositional environments are similar (Dam *et al.*, 2009; Section 2.5). Overall, with the exception of coal and leaf-mat horizons, it is difficult to identify a clear relationship between horizon TOC and likely carbon origin, since the range in depositional environments encountered in the composite section result in similar amounts of TOC in a horizon, predominantly in the 0–10 % organic carbon range.

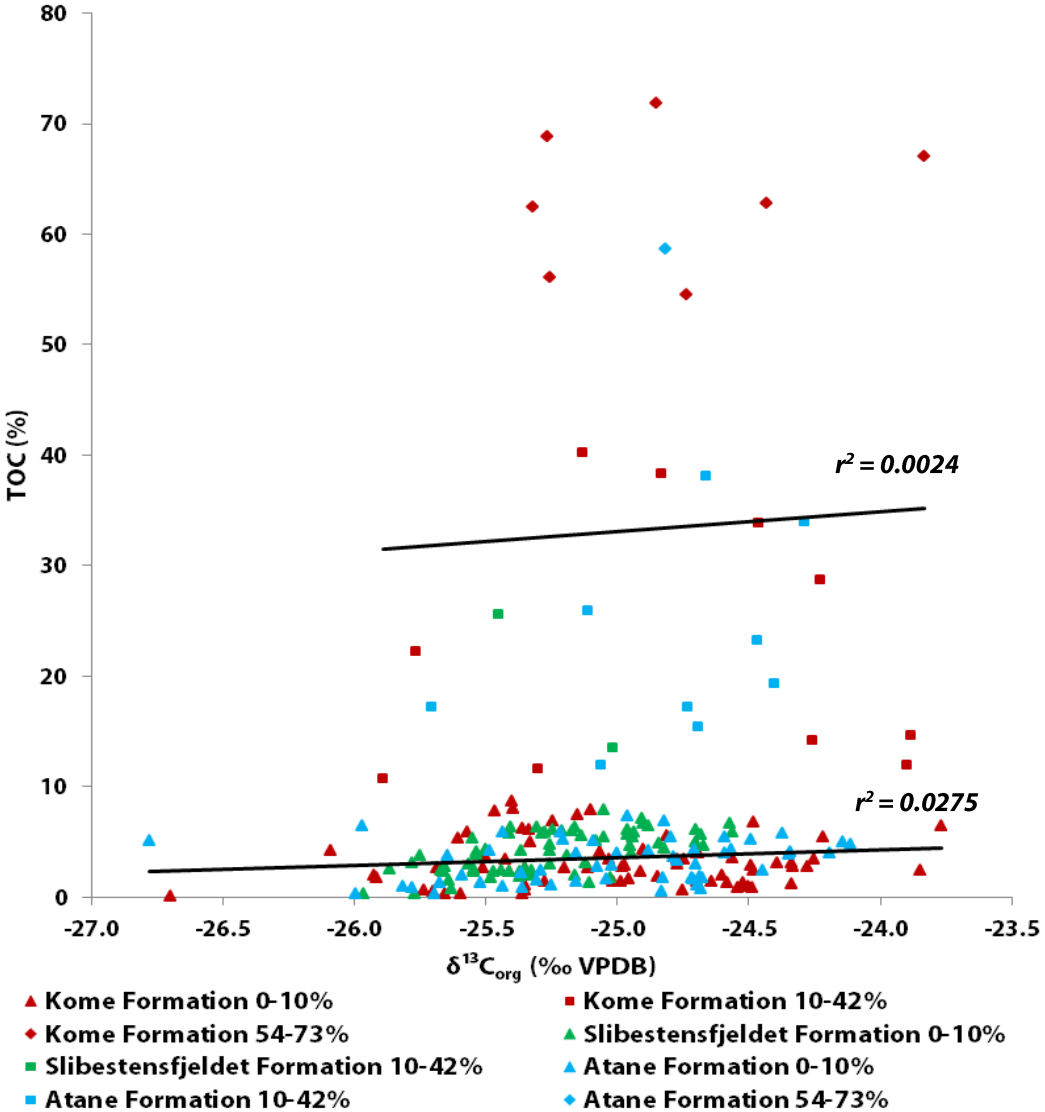

Figure 3.19: TOC versus $\delta^{13}C_{org}$ of bulk sediment samples by Formation and TOC content grouping as defined in Figure 3.18.

Examination of $\delta^{13}C_{org}$ against TOC content could reveal relationships between carbon origin and isotopic variation through the stratigraphy if the carbon sources differ in isotopic signature. When all the data is considered as a whole, no significant relationship between $\delta^{13}C_{org}$ and TOC content is identified, with an r^2 value of 0.035 for a linear trend line. For all Formations, there is no significant relationship observed between %TOC and $\delta^{13}C_{org}$ for high TOC content (>10 % TOC; Figure 3.19).

Closer examination of the lower TOC content group (<10 %) reveals there is no relationship between TOC and $\delta^{13}C_{org}$ for the Kome and Atane Formations (Figure 3.20). Based on the lithology of these Formations, the organic matter sources are most likely detrital fossil wood and plant matter (including coal layers), reflecting the fluvio-deltaic associated depositional environments (Section 2.5; Dam *et al.*, 2009).

However, a positive correlation between TOC and $\delta^{13}C_{org}$ is observed in the <10 % TOC content data from the Slibestensfjeldet Formation, with an r^2 value of 0.3938 (Figure 3.20). The highest organic carbon content group from the Kome and Atane Formations (red and blue diamonds, Figure 3.19) most likely represent fossil wood and plant matter (coals), and have $\delta^{13}C_{org}$ values around -24.0 ‰ to -25.5 ‰, averaging close to -25.0 ‰. The <10 % TOC data from the Slibestensfjeldet Formation have $\delta^{13}C_{org}$ values ranging -24.5 ‰ to -26.0 ‰ with an average value 0.5 ‰ lighter than plant material from the Kome and Atane Formation. Average $\delta^{13}C_{org}$ of modern lake organisms are typically -26.0 ± 3 ‰ for benthic algae, and -32.0 ± 3 ‰ for planktonic algae (France, 1995; Wang *et al*., 2013). If such values were applied to the $\delta^{13}C_{org}$ of the Slibestensfjeldet Formation, this could account for the more negative $\delta^{13}C_{org}$ values compared to higher plant matter from the Kome and Atane Formations and the positive relationship between TOC and $\delta^{13}C_{org}$ of the Slibestensfjeldet Formation, therefore, reflects differences in carbon sourcing between the lacustrine and fluvio-deltaic depositional settings. However, determining $\delta^{13}C_{org}$ of carbon source end-members for a lacustrine deposit is complex; the relative proportions and changes in size of carbon sources through time need to be quantified and may vary due to changing vegetation catchment, lake productivity, water turbulence, lake size and water depth (Wang *et al*., 2013). Many studies of Cenozoic-to-Recent lacustrine deposits utilise an integrated multiproxy approach: combining carbon-to-nitrogen ratios (C/N), TOC content, $\delta^{15}N_{org}$ (nitrogen isotope ratios of organic matter) and the separation of pelagic phytoplankton and benthic microalgae $\delta^{13}C_{org}$ profiles (e.g. Talbot and Johannessen, 1992;

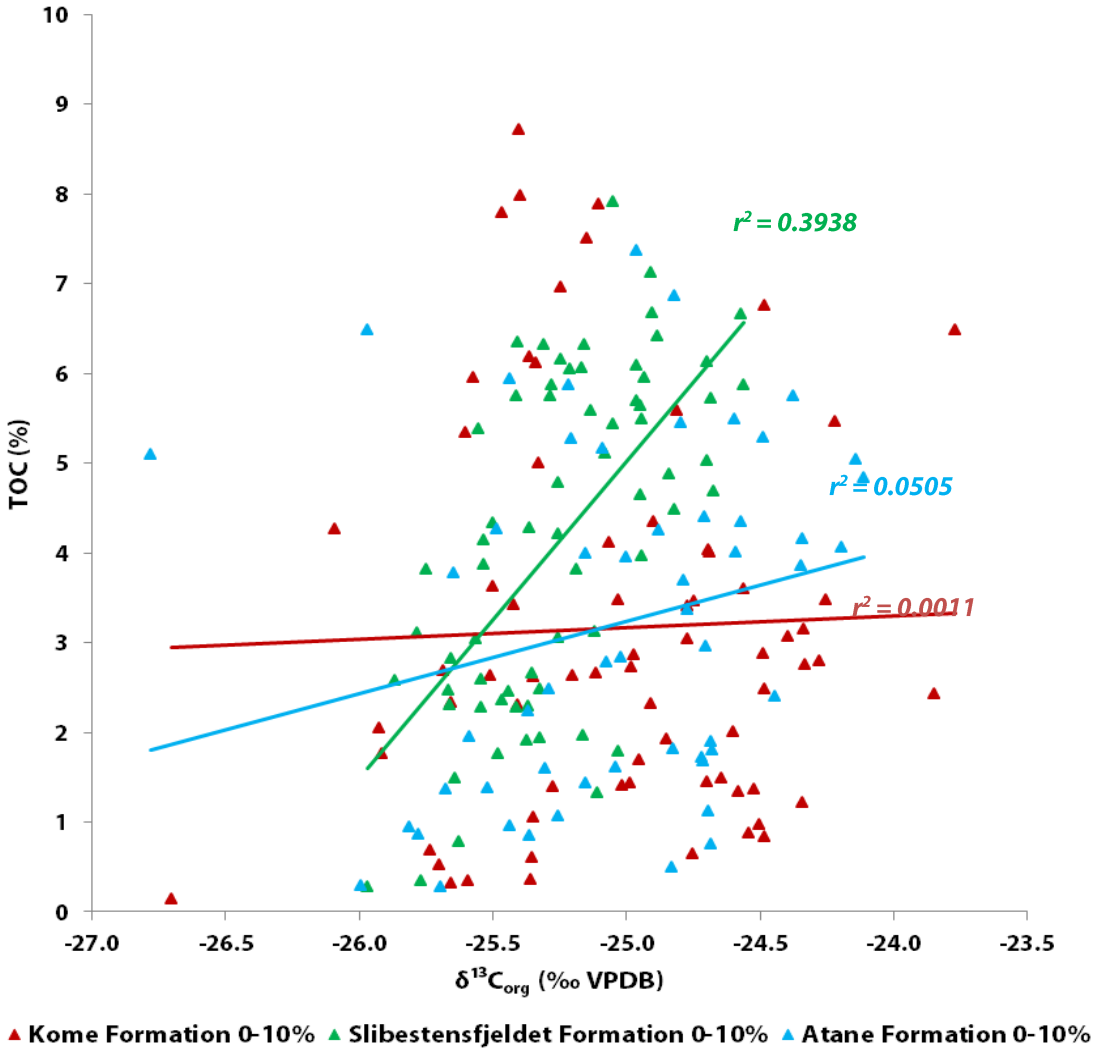

Figure 3.20: TOC versus $\delta^{13}C_{org}$ of bulk sediment samples by Formation for TOC <10 %.

Meyers and Ishiwatari, 1993; Meyers, 1994; Thornton and McManus, 1994; Meyers and Lallier-vergés, 1999; Lücke *et al.*, 2003; Wang *et al.*, 2013). However, for older sediments, including the Cretaceous Slibestensfjeldet Formation, the preservation of nitrogen is typically insufficient for analysis due to diagenesis (Rau *et al.* 1987). The nitrogen contents measured as part of the TC and TOC data collection process were low and are considered unreliable. In spite of the apparent positive relationship, the resulting variation in $\delta^{13}C_{org}$ is small, on the order of 1 ‰ and so is unlikely to represent a significant difference in organic matter source, but may reflect small-scale variation of lacustrine carbon sources through time (Wang *et al.*, 2013).

3.4.2 Fossil wood preservation

3.4.2.1 Fossil wood classification and $\delta^{13}C_{wood}$

Before interpreting the fossil wood isotope data, consideration is given to whether preservation has introduced any bias. $\delta^{13}C_{wood}$ for the LK and RKW sections are plotted

against stratigraphic height (there were insufficient samples from RKE to be useful in this context) and colour-coded to represent wood class (Figures 3.21 and 3.22 respectively). The seven wood classes are grouped into three collections: classes 1–4 (squares in Figures 3.21 and 3.22) representing the various preservational forms of coalified wood; classes 5 and 6 (triangles in Figures 3.21 and 3.22) represent varying degrees of charcoalified wood preservation; and class 7 data kept separate as material that was likely to be fossil wood but with some other terrestrial organic matter also possibly present.

The LK section (Figure 3.21) is predominantly coal (classes 1–4) and there is no strong relationship observed between fossil wood class and $\delta^{13}C_{wood}$. Charcoal and coal preservation produce similar $\delta^{13}C_{wood}$ values. In this section, class 7 $\delta^{13}C_{wood}$ values also lie within the isotope range of the coal and charcoal data around it. Since the entire section is dominated by coal pieces there is no observed relationship of fossil wood preservation to lithology.

The RKW section (Figure 3.22) contains many samples from class 7, and has more charcoal samples than the LK section. The coal samples are mainly class 1, with only one oxidised sample (class 3) and only one possibly sediment contaminated sample (class 4). No strong relationship between wood preservation and $\delta^{13}C_{wood}$ is observed in the RKW section, with all three preservational types (coal, charcoal and class 7) falling within the same isotopic range. Most charcoal and class 7 samples occur between 75–100 m stratigraphic height in fluvial sands, but coals also occur within the overlying 30 m above of fluvial sands.

When the isotope data is grouped by preservational type in box plots for each section (Figure 3.23), it is observed that the RKW section $\delta^{13}C_{wood}$ values (Figure 3.23B) are on the order of +0.5–1.0 ‰ more positive than the LK section (Figure 3.23A). There is no significant or consistent relationship between the $\delta^{13}C_{wood}$ of coalified fossil wood compared to charcoalified fossil wood across both sections (Figure 3.23). In both sections, the average $\delta^{13}C_{wood}$ of class 7 is more negative than both coalified and charcoalified fossil wood, although all classes are statistically indistinguishable. Thus, preservational type does not influence $\delta^{13}C_{wood}$ values outside the stratigraphic variability observed in both sections. The slightly more negative $\delta^{13}C_{wood}$ observed in class 7 data for both sections may indicate that some of the samples analysed may not be purely fossil wood as suggested from the descriptions of the material.

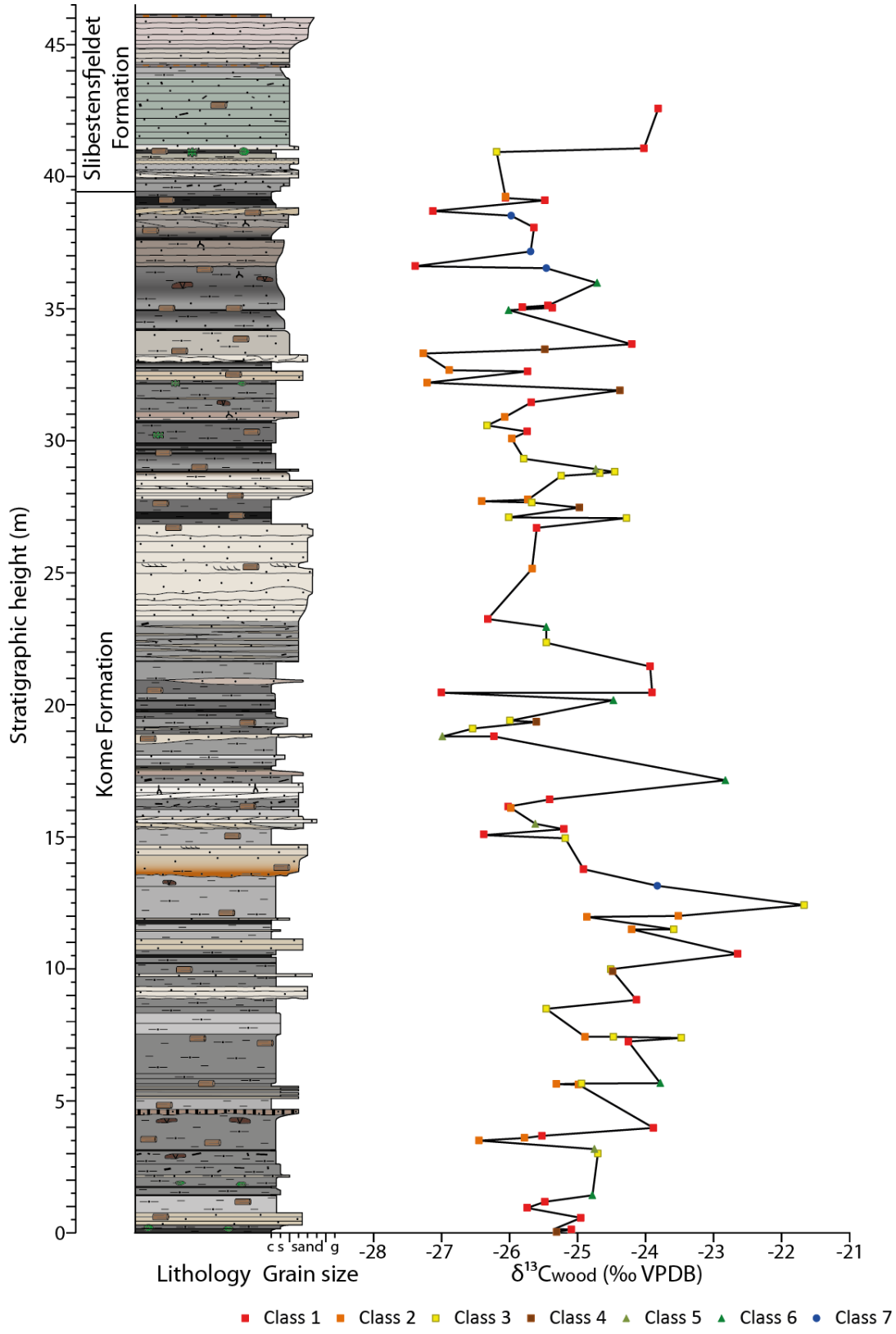

Figure 3.21: LK section $\delta^{13}C_{wood}$ against stratigraphic log, colour-coded by wood class. Key to graphic log in Appendix A, Figure ii.

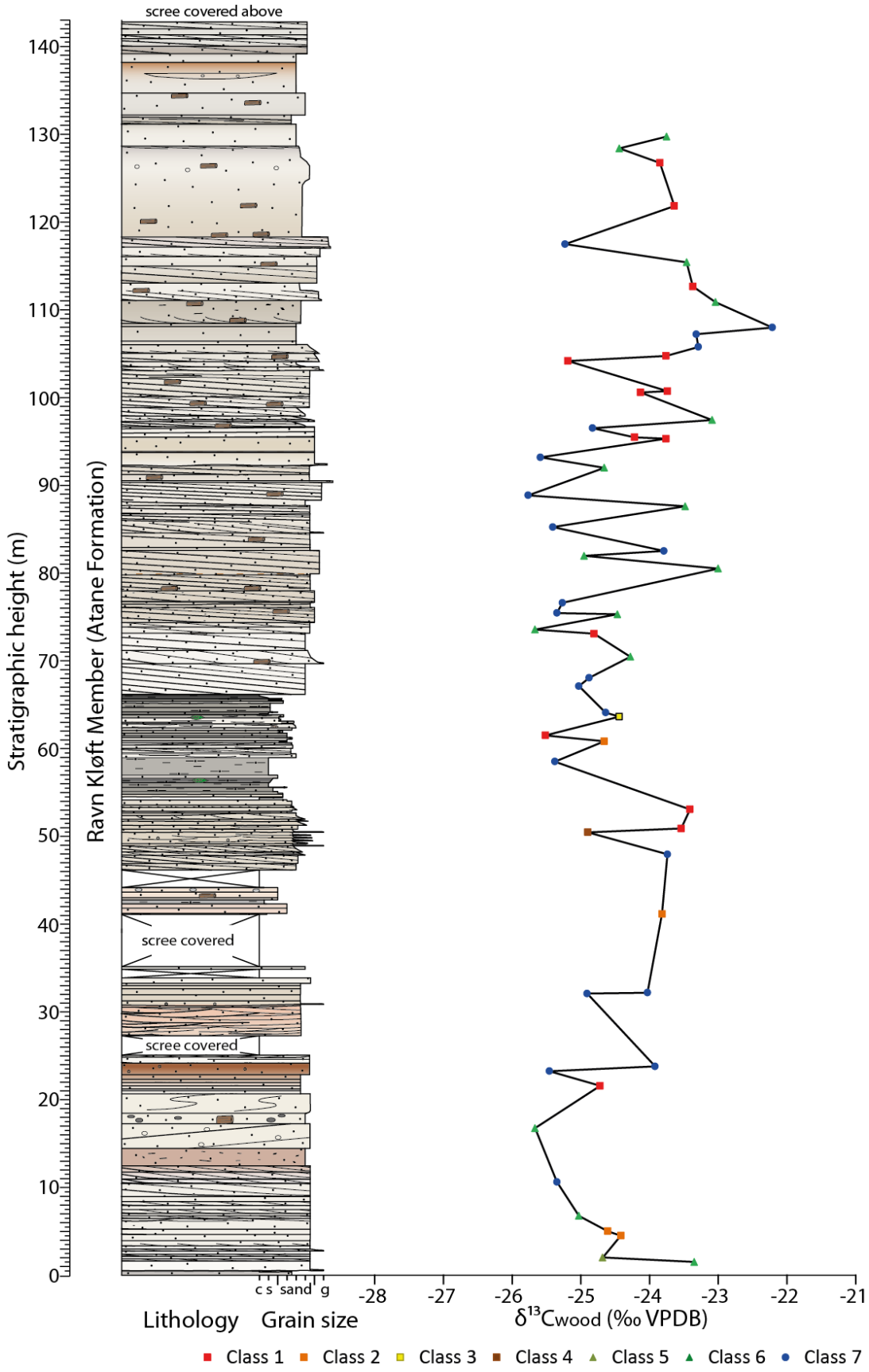

Figure 3.22: RKW section $\delta^{13}C_{wood}$ against stratigraphic log, colour-coded by wood class. Key to graphic log in Appendix A, Figure ii.

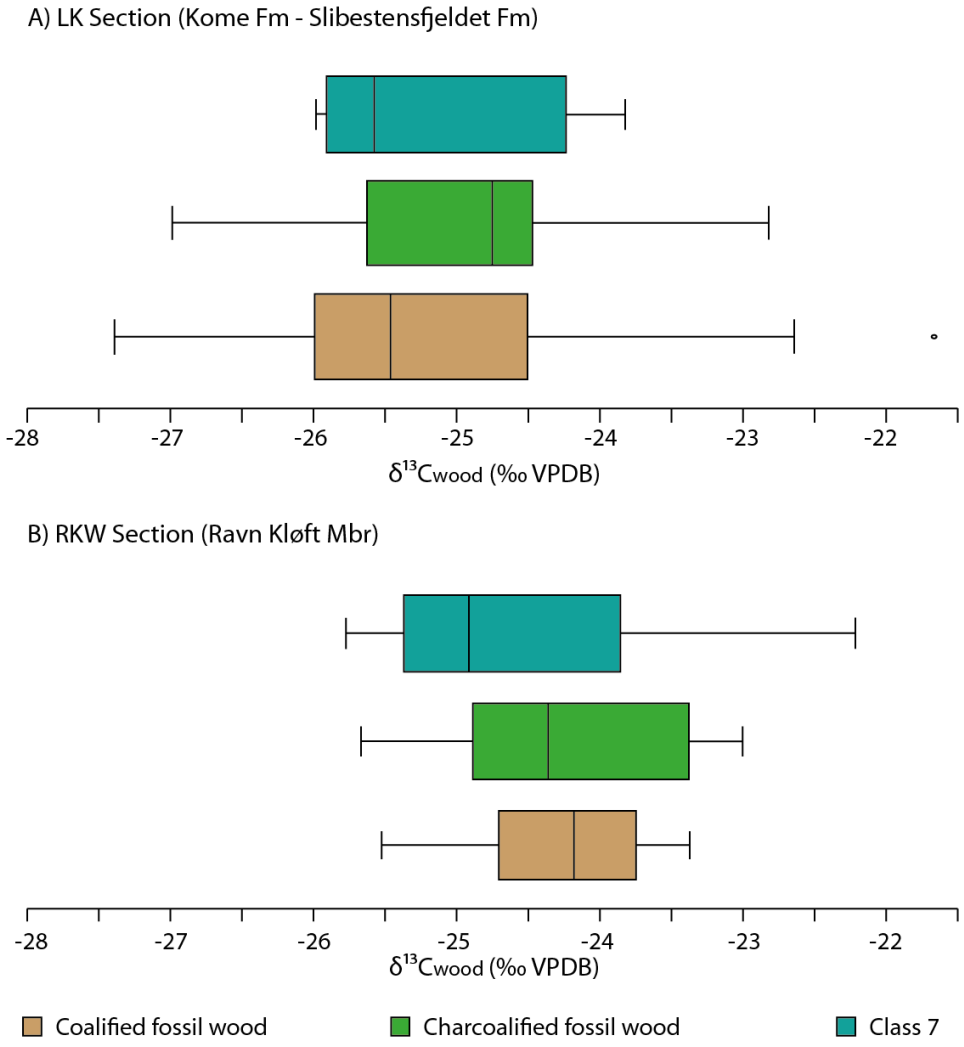

Figure 3.23: $\delta^{13}C_{wood}$ box plots grouped by preservational type for (A) LK and (B) RKW sections. Box plots drawn in PAST software, whereby box edges = 25th and 75th percentile, the central line in the box represents the median and the whiskers represent 2nd and 98th percentile. Outliers are indicated by a point outside of the box plot.

3.4.2.2 Carbon content of decarbonated wood samples

A comparison of the carbon content of fossil wood with $\delta^{13}C_{wood}$ may assist in determining the suitability of different preservational types for isotope stratigraphy. An approximation (as it is based on decarbonated sample weights) of the carbon content of fossil wood samples was made by the following approach. Approximately linear relationships for each standard material can be defined between the mass-44 peak and standard weight (Figure 3.24). The carbon contents of the standards are estimated through stoichiometry (Table 3.8), allowing these linear relationships to be viewed as carbon content contours which were interpolated between the different standards (Figure 3.24).

Standard	Material	Formula	Estimated carbon content (%)
USGS24	Graphite	C	100
GRAP	Graphite	C	100
ANU	Sucrose	$C_{12}H_{22}O_{11}$	42.1
USGS40	L-glutamic acid	$C_5H_9NO_4$	40.8
IAEA-CH3	Cellulose	$C_6H_{10}O_5$	44.4

Table 3.8: Summary of carbon content of calibration standards and monitoring standards based on stoichiometry.

The carbon contours have a large error reflected by the cloud of data points surrounding the 100 % carbon contour, and by the approximate 42 % contour from the ANU and USGS40 data. The average value for IAEA-CH3 falls close to the 42 % contour despite having an estimated 44.4% carbon content, suggesting an error in this approach of at least several percent. The contours do not intersect the origin most likely due to a non-linear effect in the mass spectrometer at low analysis weights and peak amplitudes < 1000 mV.

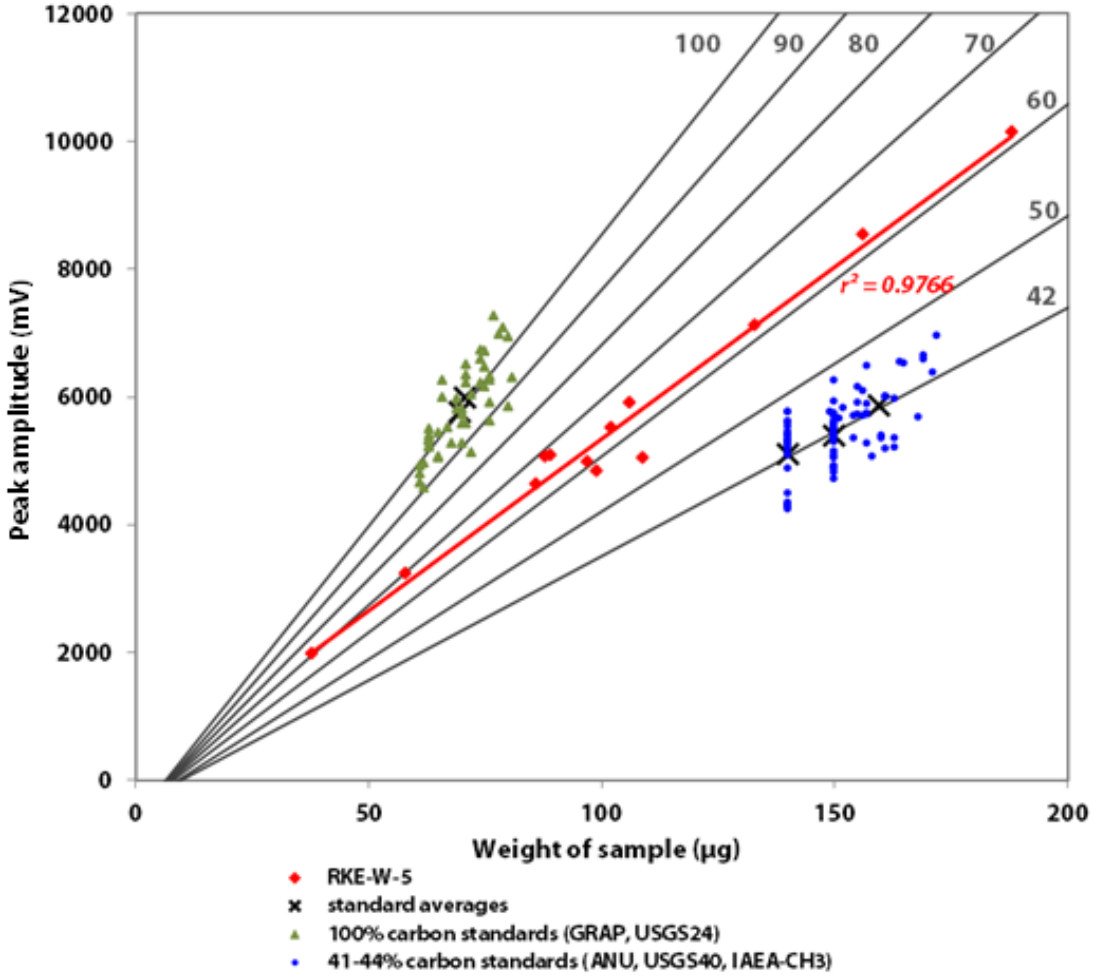

Figure 3.24: Standard mass-44 peak amplitudes against amount of material weighed. Approximate carbon content contours positions using known carbon content of graphite (GRAP, USGS24) and other standards (ANU, USGS40, IAEA-CH3).

The sample repeat RKE-W-5, for which $\delta^{13}C_{wood}$ was analysed for a range of sample weights, presents a strong linear trend with an r^2 value of 0.9766 (red data, Figure 3.24) supporting the approach. However, the gradient transects the contours slightly, reflecting the uncertainty in the carbon contours derived from the standards. As such, the carbon content of samples derived using this method are strictly considered as approximate relative estimates of organic carbon content in decarbonated samples due to this uncertainty.

Most of the fossil wood samples contain approximately 50–80 % carbon based on this approach (Figure 3.25), with some samples falling below the approximate 42 % carbon content contour between the 80–100 µg sample weight range. Even when these samples were reanalysed with larger samples weights (ranging from 200–825 µg) they still fall below the approximate 42 % contour. These samples are mostly class 7 (blue circles) with two fossil wood samples from class 6 (dark green triangles) and likely contain the least amount of carbon out of all the fossil wood samples analysed.

When the average data point for each wood class is considered (large colour-code symbols, Figure 3.25), classes 1–5 fall close to one another. Due to the low carbon content of two of the class 6 samples, the average value plots far from the rest of the data. Similarly, the average value of the class 7 samples is less than 42 % due to multiple low carbon content samples. However, if the class 6 and 7 samples with a peak amplitude of <2500 mV are excluded from the average calculations, the average values plot close to class 1–5 averages, i.e. between 60–70% carbon. The low estimated carbon contents (<42 %) of some class 7 samples supports the observation that these samples are likely not purely fossil wood. However, clearly all wood classes have variable carbon contents ranging from 42–80 % which is not related to preservational type.

The $\delta^{13}C_{wood}$ values for all wood pieces falling below the approximate 50 % carbon content contour (Figure 3.25) have been highlighted in the carbon isotope profile of both the LK and RKW sections (Figure 3.26). Comparison of $\delta^{13}C_{wood}$ against stratigraphic height (Figure 3.26) reveals no consistent difference in $\delta^{13}C_{wood}$ of samples with approximately <50 % carbon content compared to those with >50 % carbon content. This suggests that neither carbon content nor preservational style is leading to a systematic bias in the $\delta^{13}C$ stratigraphy.

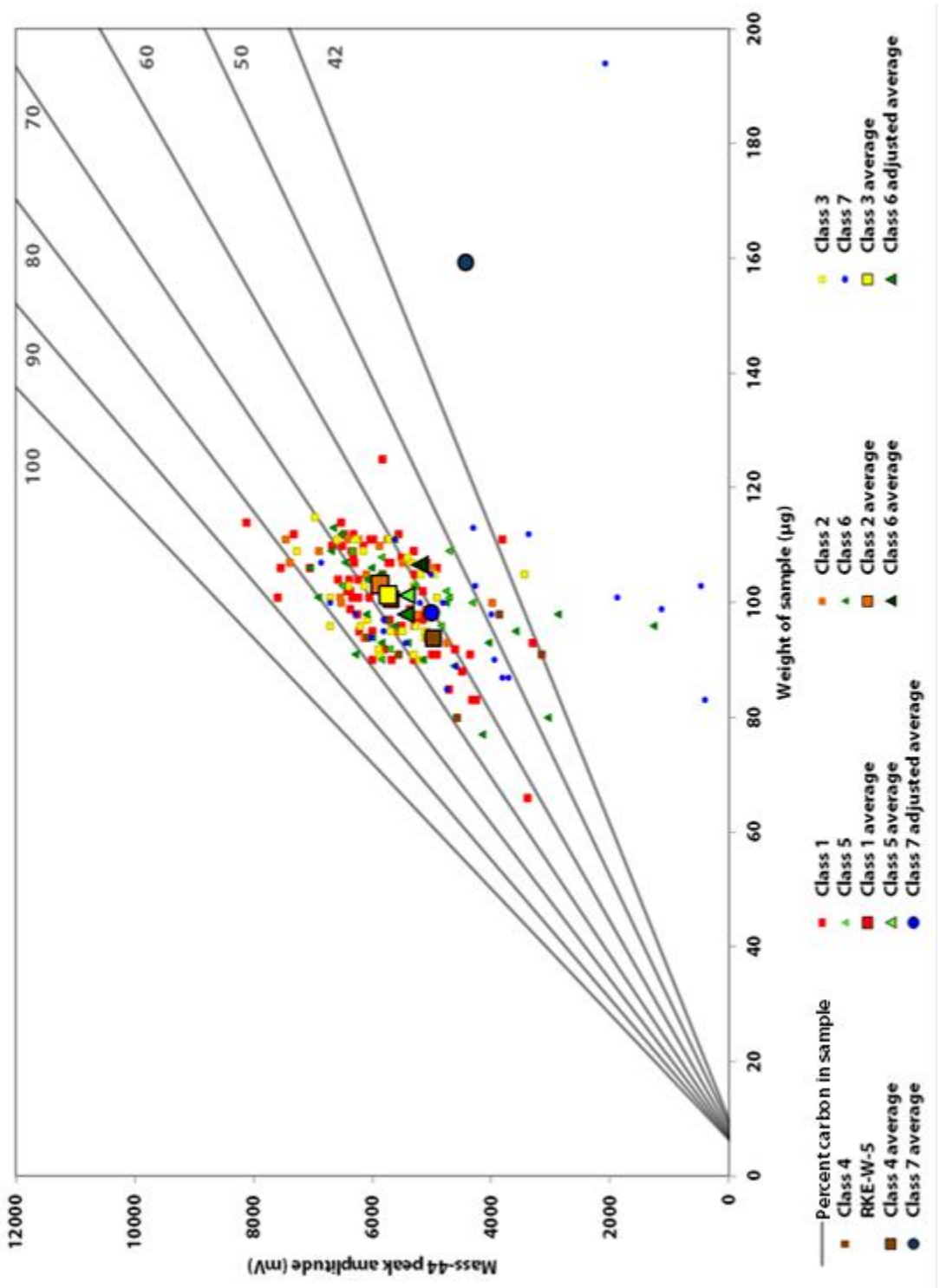

Figure 3.25: Standard and wood sample mass-44 peak amplitudes against amount of material weighed, showing wood sample data colour-coded by wood class, with average values as larger symbols. Approximate carbon content contours positions using known carbon content of graphite (GRAP, USGS24) and other standards (ANU, USGS40, IAEA-CH3).

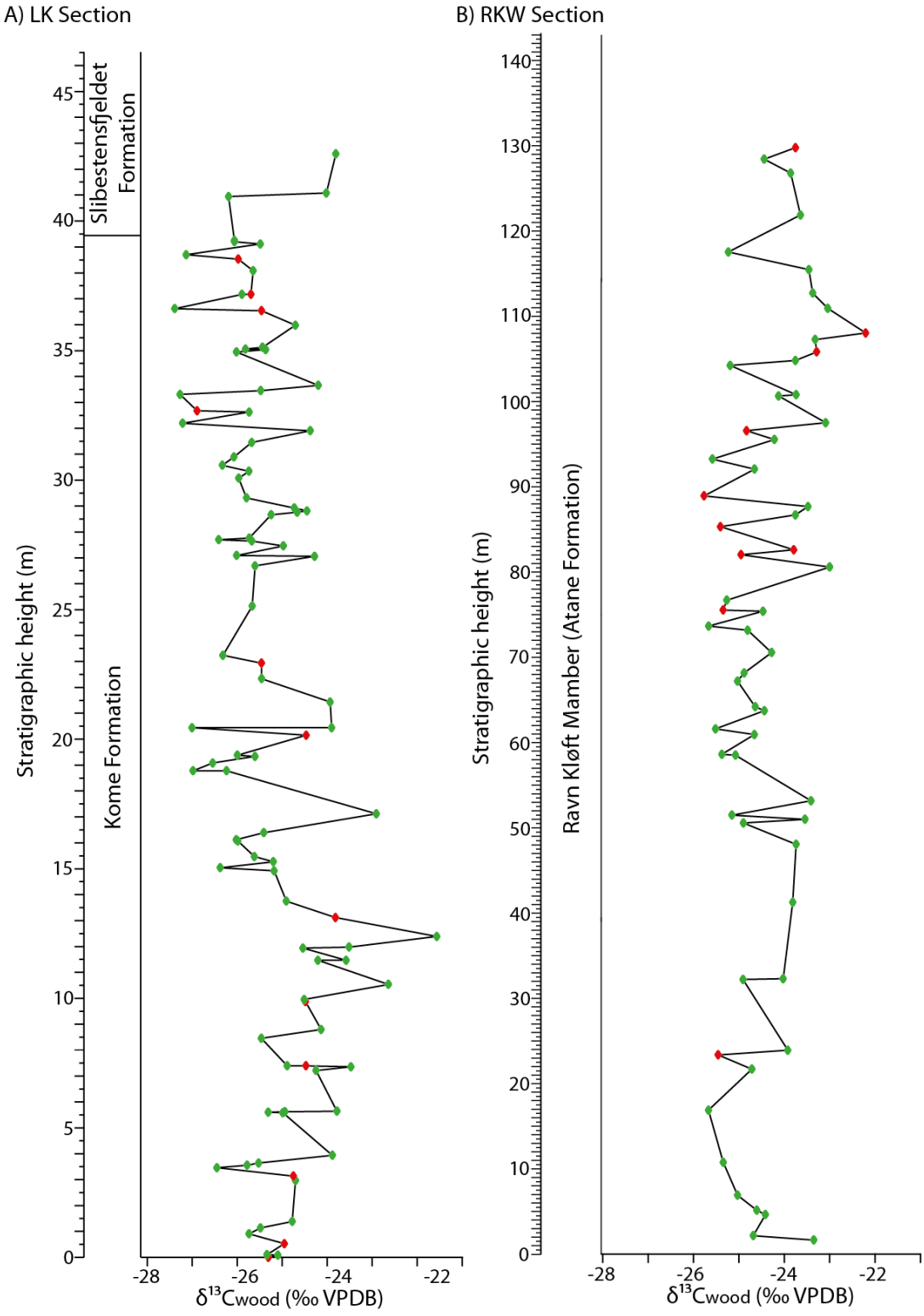

Figure 3.26: $\delta^{13}C_{wood}$ against stratigraphic height, colour-coded by carbon content of approximately <50 % (red) and >50 % (green) for (A) LK Section and (B) RKW Section.

3.4.3 Summary of organic carbon sources

The range of $\delta^{13}C_{wood}$ and $\delta^{13}C_{org}$ values (-21 ‰ to -28 ‰) is consistent with plant matter utilising a C3 photosynthetic pathway, with no evidence of C4 pathways. Therefore, the palaeobotanical and isotopic evidence presented in this thesis strongly supports a C3 dominated ecosystem in West Greenland during the Albian–Cenomanian. Based on the data presented in this thesis, $\delta^{13}C_{wood}$ does not appear to be affected by either preservational style or organic carbon content of the fossil wood. This supports previous studies of Mesozoic isotope stratigraphy concerning fossil wood preservation (Hesselbo *et al*., 2000; Gröcke, 2002; Robinson and Hesselbo, 2004; Pearce *et al*., 2005) where no systematic offset in $\delta^{13}C_{wood}$ with fossil wood preservation was observed. Thus, the isotope stratigraphy generated in this thesis is comparable to previous studies and likely faithfully follows global atmospheric carbon reservoir trends (Section 3.5).

3.4.4 Stratigraphic trends in $\delta^{13}C_{wood}$ and $\delta^{13}C_{org}$

The $\delta^{13}C_{org}$ and $\delta^{13}C_{wood}$ data show consistent stratigraphic trends across both datasets (Figure 3.27). In the Kome Formation, a small positive shift is observed in both the $\delta^{13}C_{org}$ and $\delta^{13}C_{wood}$ data (Figure 3.27C, D) from the base of the composite section to approximately 12 m stratigraphic height. The magnitude of the positive excursion is 3–4‰ in the $\delta^{13}C_{wood}$ data, compared to 1.5 ‰ in the $\delta^{13}C_{org}$ data. A subsequent decrease in $\delta^{13}C$ values from 12 m to approximately 25 m stratigraphic height has a magnitude of 2.5 ‰ in $\delta^{13}C_{org}$ and around 5 ‰ in $\delta^{13}C_{wood}$. $\delta^{13}C_{org}$ values increase from 25 m height to the top of the Kome Formation, but this is not observed in the corresponding $\delta^{13}C_{wood}$ data.

The Slibestensfjeldet Formation exhibits lower and less variable TOCs and a smaller "noise envelope" of $\delta^{13}C_{org}$ values. Typically the scatter is <0.5 ‰ from one sample to the next in the Slibestensfjeldet Formation, compared to around 1.0 ‰ variation in the other formations (Figure 3.27C).

Examination of the $\delta^{13}C_{org}$ and $\delta^{13}C_{wood}$ for the lower portion of the Ravn Kløft Member (Figure 3.27C, D) reveals a negative excursion in both datasets, but at slightly different stratigraphic heights and of different magnitudes. In the $\delta^{13}C_{org}$ data, a negative excursion of 1.5 ‰ at around 245 m height in the composite section compares to a larger magnitude excursion of 2.0 ‰ slightly higher in the section at around 248 m height in $\delta^{13}C_{wood}$. A general positive trend is identified through this part of the Ravn Kløft Member (244–284 m height in the composite section) on the order of 1 ‰ in both $\delta^{13}C_{org}$ and $\delta^{13}C_{wood}$. This trend continues in the $\delta^{13}C_{wood}$ dataset through the top of the Ravn Kløft Member (from

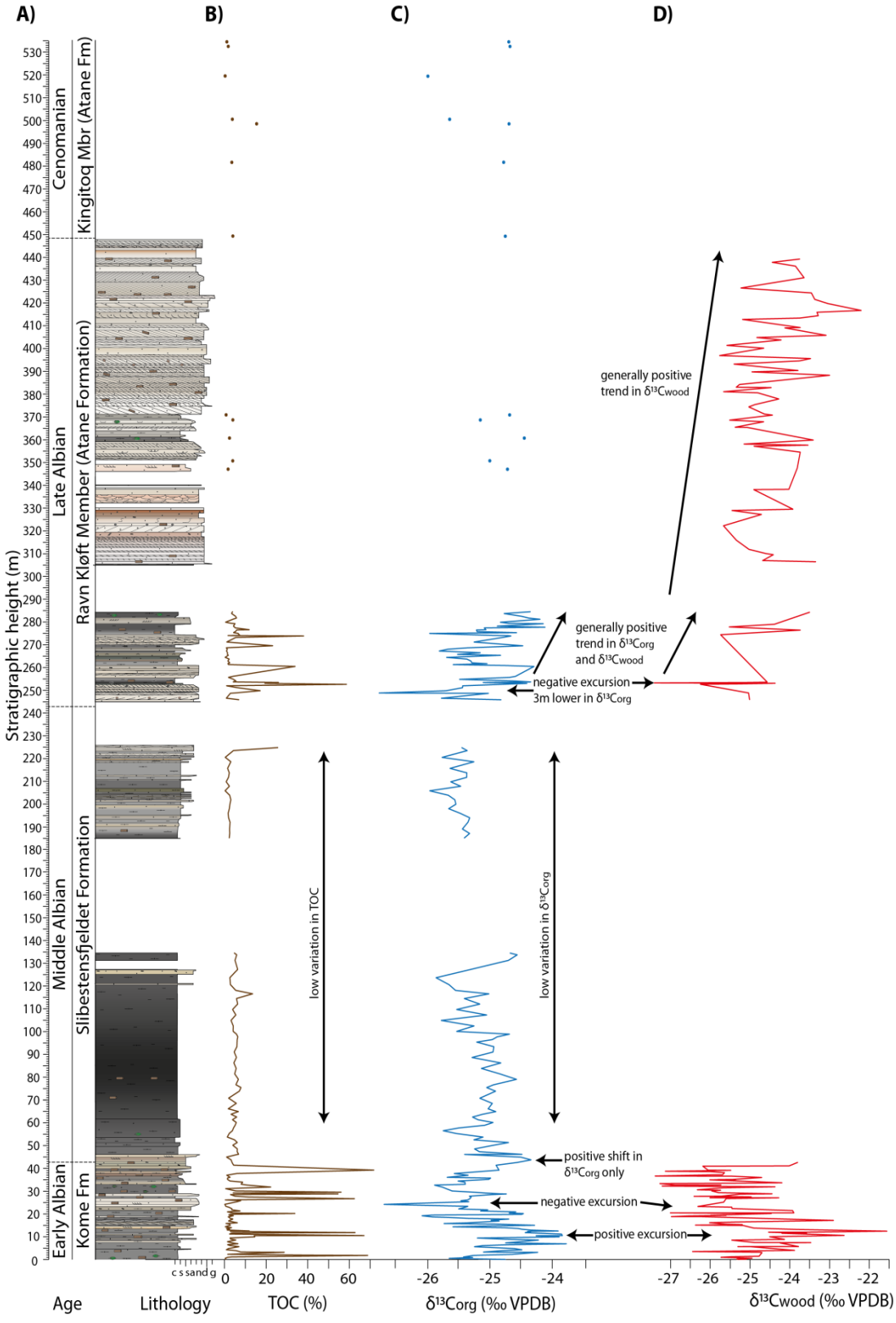

Figure 3.27: Summary of TOC, $\delta^{13}C_{org}$ and $\delta^{13}C_{wood}$ collected through the composite section presented with graphic log, Formation name and approximate age based on palynofloral estimates. Key to graphic log in Appendix A, Figure ii.

305–448 m height in the composite section), resulting in an overall increase in $\delta^{13}C_{wood}$ through the Ravn Kløft Member on the order of 1.5–1.8 ‰.

The noise evident in both $\delta^{13}C_{org}$ and $\delta^{13}C_{wood}$ datasets is representative of the natural variation in isotope ratios of higher plant organic material, with less noise presented in the bulk organic matter data likely due to an averaging effect of multiple plant pieces per sample (Section 2.2). However, the reduction of noise in the Slibestensfjeldet Formation $\delta^{13}C_{org}$ data most likely reflects a change in carbon sources, as part of a large, deep lacustrine system, producing more stable $\delta^{13}C_{org}$ with time.

The more sporadic fossil wood occurrence through the composite section compared to the averaged effect of $\delta^{13}C_{org}$ data may, in part, explain the difference in magnitude of excursions when compared to $\delta^{13}C_{wood}$. The reworking of fossil wood may also explain the stratigraphic offset between excursions, for example the negative excursion in the lower Ravn Kløft Member occurs approximately 3 m lower in the $\delta^{13}C_{org}$ data, compared to $\delta^{13}C_{wood}$ data.

3.5 Stratigraphic correlation

As preservation and organic source appear to have only minor effects on $\delta^{13}C$ variability, it is possible to use both the $\delta^{13}C_{org}$ and $\delta^{13}C_{wood}$ datasets as a chemostratigraphic tool to correlate to other published carbon isotope records (e.g. Gröcke *et al*., 1999, 2006; Hesselbo *et al*., 2000, 2002, 2003, 2007; Robinson and Hesselbo, 2004).

3.5.1 Aptian–Cenomanian carbon isotope reference curves

Previous studies of palynology and macrofossil palaeobotany suggest a broadly Albian–Cenomanian age for the West Greenland section of this thesis. However, it is instructive to consider the Aptian–Cenomanian, and so four published datasets spanning this interval were identified for inclusion in a reference curve. These data come from the Vocontian Basin (Gale *et al*., 2011; Herrle *et al*., 2004), the Isle of Wight, UK (Gröcke *et al.,* 1999) and California, USA (Robinson *et al.,* 2008). These datasets are calibrated here to a single timescale (Ogg *et al*., 2012) using their published marine biostratigraphies. The carbon isotope data from the Vocontian Basin and California are based upon bulk analysis of hemipelagic and pelagic marine carbonates, whereas the data from the Isle of Wight were generated from fossil wood deposited in a marginal marine setting.

The construction of an age-model for the four published sections relied on the conversion of depth to age, whereby biozone boundaries in the published biostratigraphic charts are used as tie-points to corresponding biozone boundaries in the Geological Timescale. With the corresponding ages assigned to these tie-points and a constant sedimentation rate assumed through the biozone, sample height is converted to age (example for the Isle of Wight shown Figure 3.28). However, the Geological Timescale is revised frequently; the most recent version is from 2012 (Ogg *et al.*, 2012 within Gradstein *et al.*, 2012) and the previous version is from 2004 (Gradstein *et al.* 2004). Using the most up-to-date biostratigraphic zonation from the Geological Timescale 2012 is important to ensure revisions in stage boundaries are translated into the age-model. The biostratigraphy used by Herrle *et al.* (2004) and Gröcke *et al.* (1999) most closely relate to that presented in the Geological Timescale 2004. The differences between the 2012 and 2004 Geological Timescale biostratigraphic charts (Figure 3.29) mostly concern the age of the ammonoid zones and the redefinition of many of the planktonic foraminifera biozones. The biozone boundaries used to calibrate the Gale *et al.* (2011) and Robinson *et al*. (2008) stratigraphy to the 2012 Geological Timescale are summarised in Table 3.9.

Biozone	Type	Age (Ma) G.T. 2012	Section present in	Type
base L. tardefurcata	ammonoid	111.3	Vocontian basin (Gale)	solid
base D. cristatum	ammonoid	107.5	Vocontian basin (Gale)	solid
base T. praeticinensis	p. forams	107.3	Vocontian basin (Gale)	solid
base M. pricei	ammonoid	106.9	Vocontian basin (Gale)	solid
base M. inflatum	ammonoid	103.9	Vocontian basin (Gale)	solid
base M. fallax	ammonoid	103.1	Vocontian basin (Gale)	solid
base M. rostratum	ammonoid	101.7	Vocontian basin (Gale)	solid
base M. perinflatum	ammonoid	101.4	Vocontian basin (Gale)	solid
base A. briacensis	ammonoid	101.0	Vocontian basin (Gale)	solid
base M. mantelli	ammonoid	100.3	Vocontian basin (Gale)	solid
base P. appenninica*	p. forams	102.0	California (Robinson)	dashed
base T. globotruncanoides	p. forams	100.5	California (Robinson)	dashed
base T. reicheli	p. forams	96.3	California (Robinson)	dashed
part T. reicheli	p. forams	96.0	California (Robinson)	dashed

*Table 3.9: Summary of biozones and boundaries used to calibrate the references curves to the Geological Timescale 2012, including details on the type, age according to the Geological Timescale, the section identified in and the corresponding certainty of the boundary within the section. (*previously T. appenninica in GTS 2004).*

Figure 3.28 (next page): Age-model construction using biostratigraphy from The Geological Timescale (left; Gradstein et al., 2004) whereby biozone boundaries are used to provide age tie-points to the corresponding biozone boundary depth in the published biostratigraphic charts (centre). This allows isotope data depth to be converted into age for each tie-point pair (right).

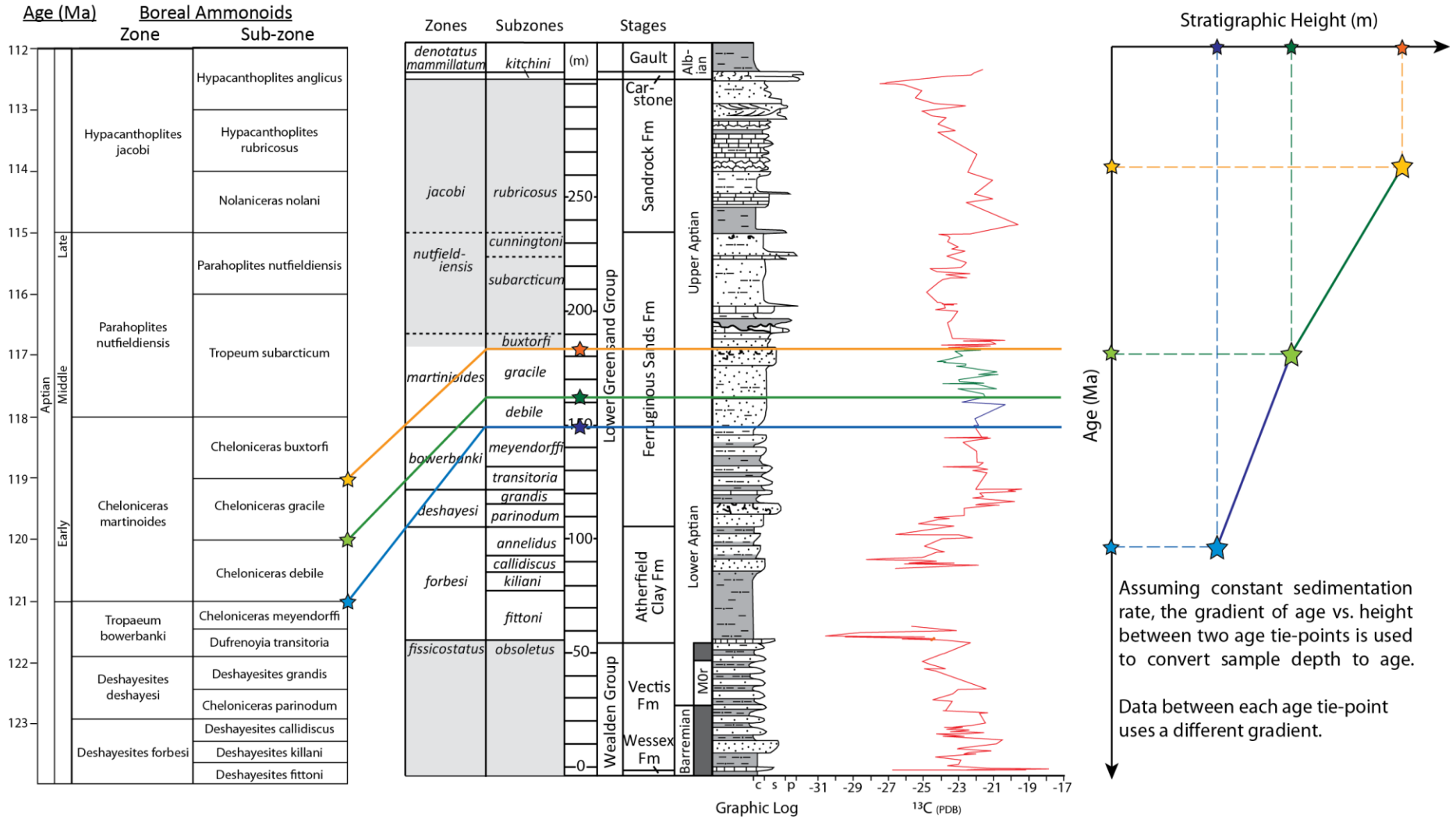
Age (Ma)
Boreal Ammonoids
Zone
Sub-zone
Aptian
Middle
Late
Early
Hypacanthoplites jacobi
Hypacanthoplites anglicus
Hypacanthoplites rubricosus
Nolaniceras nolani
Parahoplites nutfieldiensis
Parahoplites nutfieldiensis
Tropeum subarcticum
Cheloniceras martinoides
Cheloniceras buxtorfi
Cheloniceras gracile
Cheloniceras debile
Tropaeum bowerbanki
Cheloniceras meyendorffi
Dufrenoyia transitoria
Deshayesites deshayesi
Deshayesites grandis
Cheloniceras parinodum
Deshayesites forbesi
Deshayesites callidiscus
Deshayesites killani
Deshayesites fittoni
112
113
114
115
116
117
118
119
120
121
122
123
Zones
Subzones
Stages
(m)
denotatus mammillatum
kitchini
jacobi
rubricosus
nutfield-iensis
cunningtoni
subarcticum
buxtorfi
martinioides
gracile
debile
bowerbanki
meyendorffi
transitoria
deshayesi
grandis
parinodum
forbesi
annelidus
callidiscus
kiliani
fittoni
fissicostatus
obsoletus
250
200
150
100
50
0
Lower Greensand Group
Wealden Group
Gault
Car-stone
Sandrock Fm
Ferruginous Sands Fm
Atherfield Clay Fm
Vectis Fm
Wessex Fm
Alb-ian
Upper Aptian
Lower Aptian
M0r
Barremian
c
s
p
-31
-29
-27
-25
-23
-21
-19
-17
Graphic Log
13C (PDB)
Stratigraphic Height (m)
Age (Ma)
Assuming constant sedimentation rate, the gradient of age vs. height between two age tie-points is used to convert sample depth to age.
Data between each age tie-point uses a different gradient.

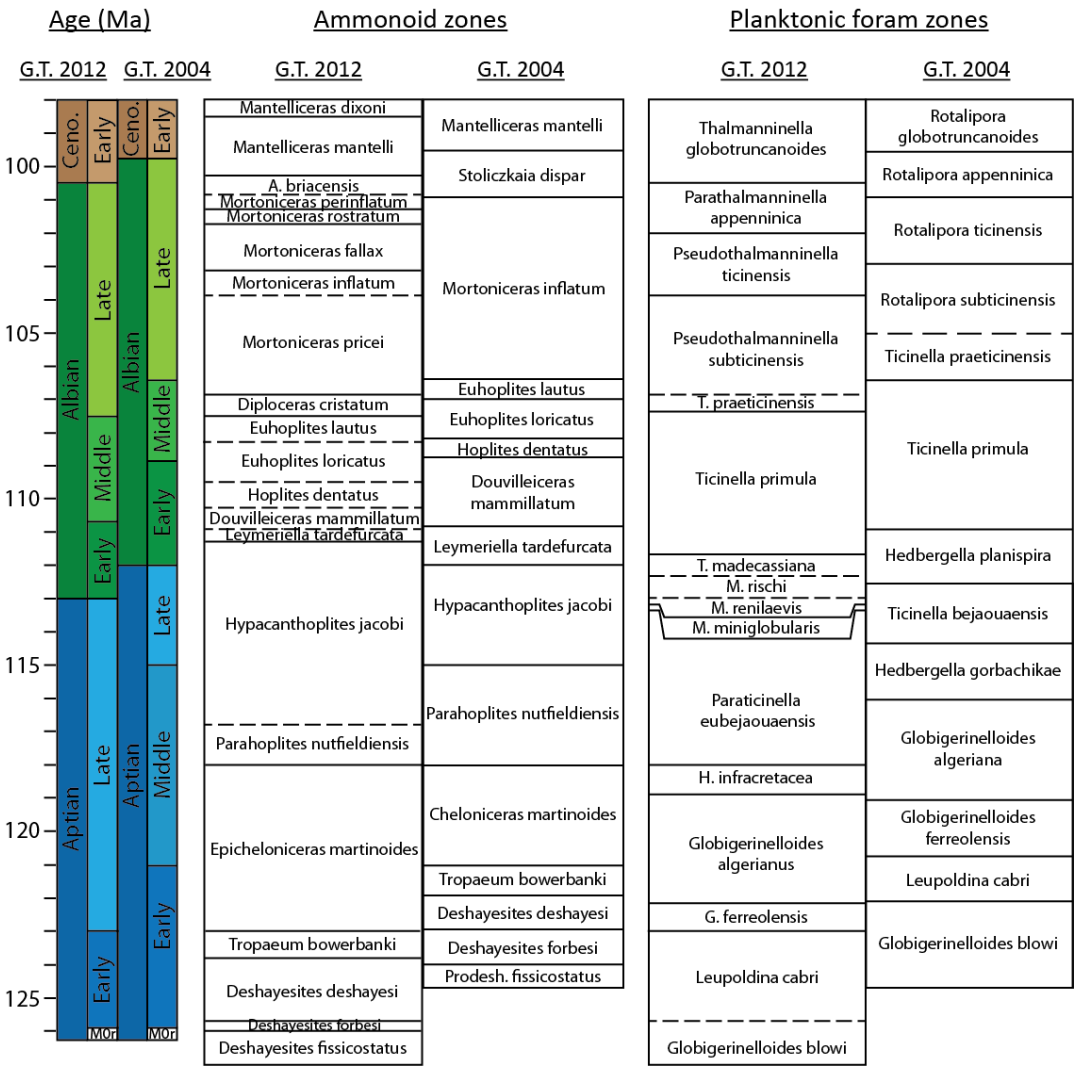

Figure 3.29: Comparison of stage boundaries, ammonoid zones and planktonic foraminifera zones for the Geological Timescale 2012 (G.T. 2012) and the Geological Timescale 2004 (G.T. 2004).

The biozone boundaries used to calibrate the Herrle *et al.* (2004) and Gröcke *et al*. (1999) stratigraphy to the 2004 Geological Timescale are summarised in Table 3.10. In order to take the age-model created using the 2004 Geological Timescale and translate the ages into the 2012 Geological Timescale, an additional calibration was performed by comparing biozone boundaries between the 2012 and 2004 timescale which had a consistent relationship with adjacent biozones across both sections, and are summarised in Table 3.11. These were used as age reference points to convert the Herrle *et al.* and Gröcke *et al.* stratigraphy into the 2012 Geological Timescale-based age-model.

Biozone	Type	Age (Ma) G.T. 2004	Section present in	Type
base NC7a	nannofossil	125.0	Vocontian basin (Herrle)	solid
top L. cabri	p. forams	120.9	Vocontian basin (Herrle)	solid
top G. ferreolensis	p. forams	119.2	Vocontian basin (Herrle)	solid
top G. algeriana	p. forams	116.2	Vocontian basin (Herrle)	solid
base T. bejaouaensis	p. forams	114.5	Vocontian basin (Herrle)	solid
base H. planispira	p. forams	112.7	Vocontian basin (Herrle)	solid
base M0r	magnetostrat.	126.3	Isle of Wight (Gröcke)	solid
top P. obsoletus	ammonoid (sub)	124.1	Isle of Wight (Gröcke)	solid
top D. fittoni	ammonoid (sub)	123.7	Isle of Wight (Gröcke)	solid
top D. forbesi	ammonoid	123.0	Isle of Wight (Gröcke)	solid
top C. parinodum	ammonoid (sub)	122.5	Isle of Wight (Gröcke)	solid
top D. grandis	ammonoid (sub)	122.0	Isle of Wight (Gröcke)	solid
top D. transitoria	ammonoid (sub)	121.5	Isle of Wight (Gröcke)	solid
top C. meyendorffi	ammonoid (sub)	121.1	Isle of Wight (Gröcke)	solid
top C. debile	ammonoid (sub)	120.1	Isle of Wight (Gröcke)	solid
top C. gracile	ammonoid (sub)	119.1	Isle of Wight (Gröcke)	solid
top C. buxtorfi	ammonoid (sub)	118.1	Isle of Wight (Gröcke)	dashed
part T. subarcticum	ammonoid (sub)	118.0	Isle of Wight (Gröcke)	dashed
part T. subarcticum	ammonoid (sub)	117.0	Isle of Wight (Gröcke)	dashed
top P. nutfieldiensis	ammonoid	115.1	Isle of Wight (Gröcke)	dashed
part H. jacobi	ammonoid	113.0	Isle of Wight (Gröcke)	dashed

Table 3.10: Summary of biozones and boundaries used to calibrate the references curves to the Geological Timescale 2004, including details on the type, age according to the Geological Timescale, the section identified in and the corresponding certainty of the boundary within the

Biozone	Type	Age (Ma) G.T. 2012	Age (Ma) G.T. 2004
base M0r	magnetostratigraphy	126.3	126.3
base D. forbesi	ammonoid	126.0	124.0
Base D. deshayesi	ammonoid	125.8	123.0
base T. bowerbanki	ammonoid	123.8	122.0
base E. martinoides	ammonoid	123.0	121.1
top L. cabri	p. forams	123.0	120.9
top G. ferreolensis	p. forams	122.2	119.2
base P. nutfieldiensis	ammonoid	118.0	118.1
base L. tardefurcata	ammonoid	111.3	112.0
top T. primula	p. forams	107.4	106.6
top P. subticinensis	p. forams	103.9	103.1
top P. ticinensis	p. forams	102.0	101.1
top P. appenninica	p. forams	100.5	99.7

Table 3.11: Summary of biozone boundaries used to calibrate the 2004 Geological Timescale (G.T. 2004) to the 2012 Geological Timescale (G.T. 2012).

The main problem associated with this method of age-model construction is incomplete biostratigraphic records in the published datasets. The Isle of Wight section is the most incomplete, whereby in the upper part of the section the authors provide partial ammonite zones or subzones, and, in places, tentative zonal boundaries. Tentative tie-points were assigned through these intervals, meaning the data between these tie-points may be more or less expanded than estimated in the age-model (listed as "Part" in the biozone description and dashed in the "Type" column of Table 3.10 respectively).

The calibration method relies on pairs of tie-points to convert depth to age of the isotope data between (Figure 3.28). In the cases where data ended in a biozone which had only one boundary defined, data was truncated at the last tie-point pair for all datasets with three exceptions: the first is an estimated end point of $\delta^{13}C_{wood}$ stratigraphy from the Isle of Wight, whereby there is an issue of uncertain biozone boundaries, in addition to, a large hiatus spanning from some point in the *H. jacobi* ammonite zone to some point in the *D. mammillatum* biozone. To avoid terminating the data at the last tie-point pair spanning the *P. nutfieldiensis* ammonite zone, an arbitrary termination point within the Geological Timescale *H. jacobi* zone was selected at 113 Ma for the top of the data at the hiatus point in the Isle of Wight section (Table 3.11; Part *H. jacobi*). This was considered acceptable given the uncertainty around the preceding three biostratigraphic zones, and indicates that the data terminates at some point in the *H. jacobi* ammonite zone.

The second exception concerns the Vocontian Basin stratigraphy: once the Herrle *et al.* (2004) stratigraphy was converted to the 2012 Geological Timescale, the Herrle *et al.* data beyond the last original tie-point (base *H. planispira*; Table 3.11) was matched to the Gale *et al.* data by using the ages of the LE and PE events, providing additional correlative constraints. The selection of two high-resolution studies of the same material from sections separated on the order of 25 km within the Vocontian Basin permits this additional correlative control since the sections are close and the isotopic events are deemed synchronous.

The final exception concerns the Robinson *et al.* (2008) stratigraphy from the Permanente Quarry in California. In order to represent the isotope stratigraphy beyond the last biozone boundary tie-point (base *T. reicheli*; Table 3.10), an arbitrary termination point within the *T. reicheli* biozone was selected at 96.0 Ma (part *T. reicheli*; Table 3.9). This portion of data in actuality may be more expanded or condensed than as presented in the calibrated summary (Figure 3.30), but the data is in the correct age range based on the biozone

information and within the general uncertainty in biostratigraphy of this section (Robinson, *pers. comms*.). Thus, similarly shaped isotope structures, which appear temporally offset are not necessarily asynchronous events, but could be the consequence of uncertainties in the construction of the age model. Similarly, the absolute ages of the events must be considered with the uncertainty in mind, particularly where there is a large age gap between selected biozone boundaries (Tables 3.9, 3.10).

3.5.2 Carbon isotope age framework

The veracity of the age models can be tested by considering the temporal alignment of isotopic events (Figure 3.30).

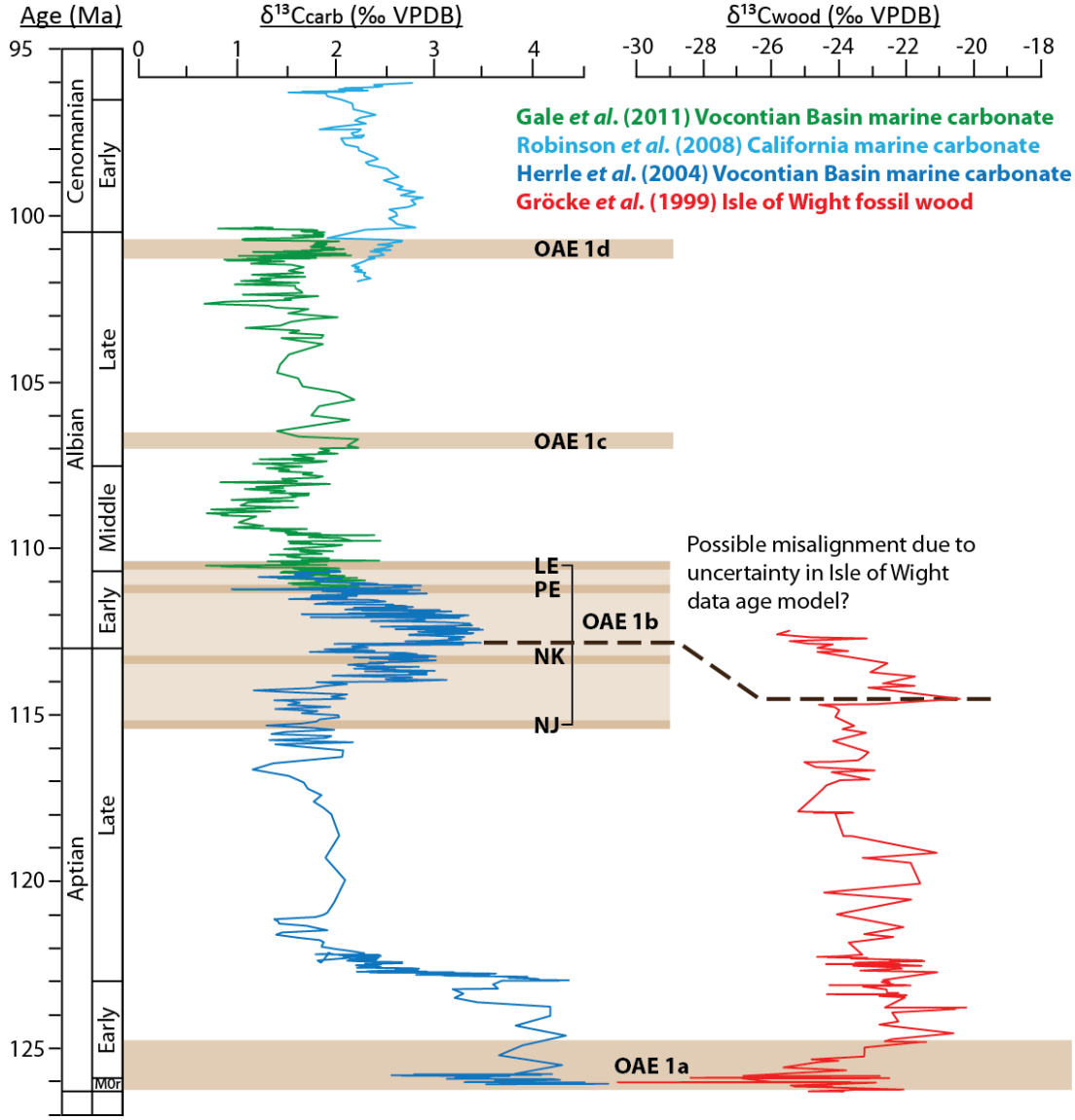

Figure 3.30: Reference curves calibrated to the 2012 Geological Timescale (Ogg et al., 2012) Recognised OAEs are labelled (brown shading), including: LE: Leenhardt Event, PE: Paquier Event, NK: Niveau Kilian, NJ: Niveau Jacobi associated with OAE1b.

3.5.2.1 Selli Event: OAE1a

Both the Isle of Wight $\delta^{13}C_{wood}$ and the Vocontian basin $\delta^{13}C_{carb}$ present a large negative isotope excursion associated with the Selli Event (OAE1a) in the early Aptian around 126 Ma (Figure 3.30).

3.5.2.2 OAE1b, Aptian-Albian Boundary

A positive excursion around 114 Ma observed in the Herrle *et al.* $\delta^{13}C_{carb}$, prior to a black shale event Niveau Kilian (NK in Figure 3.30), does not appear to be synchronous with the $\delta^{13}C_{wood}$ stratigraphy from the Isle of Wight, where the positive excursion occurred about 1 Myr earlier. However, given the uncertainty in the biostratigraphy of the Isle of Wight, these positive shifts are likely synchronous. In addition, the $\delta^{13}C_{wood}$ stratigraphy from the Isle of Wight subsequently follows a general negative trend, similar to the $\delta^{13}C_{carb}$ of the Vocontian Basin from around 113–111 Ma, although again the Isle of Wight negative trend occurs earlier. The negative excursion close to the Niveau Kilian black shale deposition (NK in Figure 3.30) is not resolved by the Isle of Wight data.

3.5.2.3 OAE 1d, Albian-Cenomanian Boundary

A general positive trend in $\delta^{13}C_{carb}$ from the Vocontian Basin and the Permanente Quarry, California occurs across the Albian–Cenomanian boundary on the order of +0.5 ‰ from 102–99 Ma. At the top of the interval identified as OAE 1d, around 100.5 Ma, a negative isotope excursion of short duration (<0.5 Myr) and around -0.7 ‰ magnitude is present in both the Vocontian Basin and Californian $\delta^{13}C_{carb}$ records (Figure 3.30). The Gale *et al.* Vocontian Basin isotope values are offset compared to the Californian data from Robinson *et al.*, but this is not unexpected given: the distances between sample locations, the likely differences in palaeo-ocean chemistry at each site, and the diagenetic and tectonic history of the Californian site (Robinson *et al.,* 2008). Nonetheless, the two datasets appear to track the same isotopic trends with similar sensitivity (similar excursion magnitudes). The Californian $\delta^{13}C_{carb}$ positive trend reverses at around 99 Ma, where a negative trend on the order of 1.0–1.5 ‰ continues until 96.5 Ma, at which point a positive trend resumes (but the rate unconstrained due to biostratigraphic uncertainty) in $\delta^{13}C_{carb}$ at the top of the Permanente Quarry section.

3.5.3 Greenland data correlation

The carbon isotope data from the present study are correlated to the reference curves through matching of isotopic excursions within the constraints of the palynofloral age

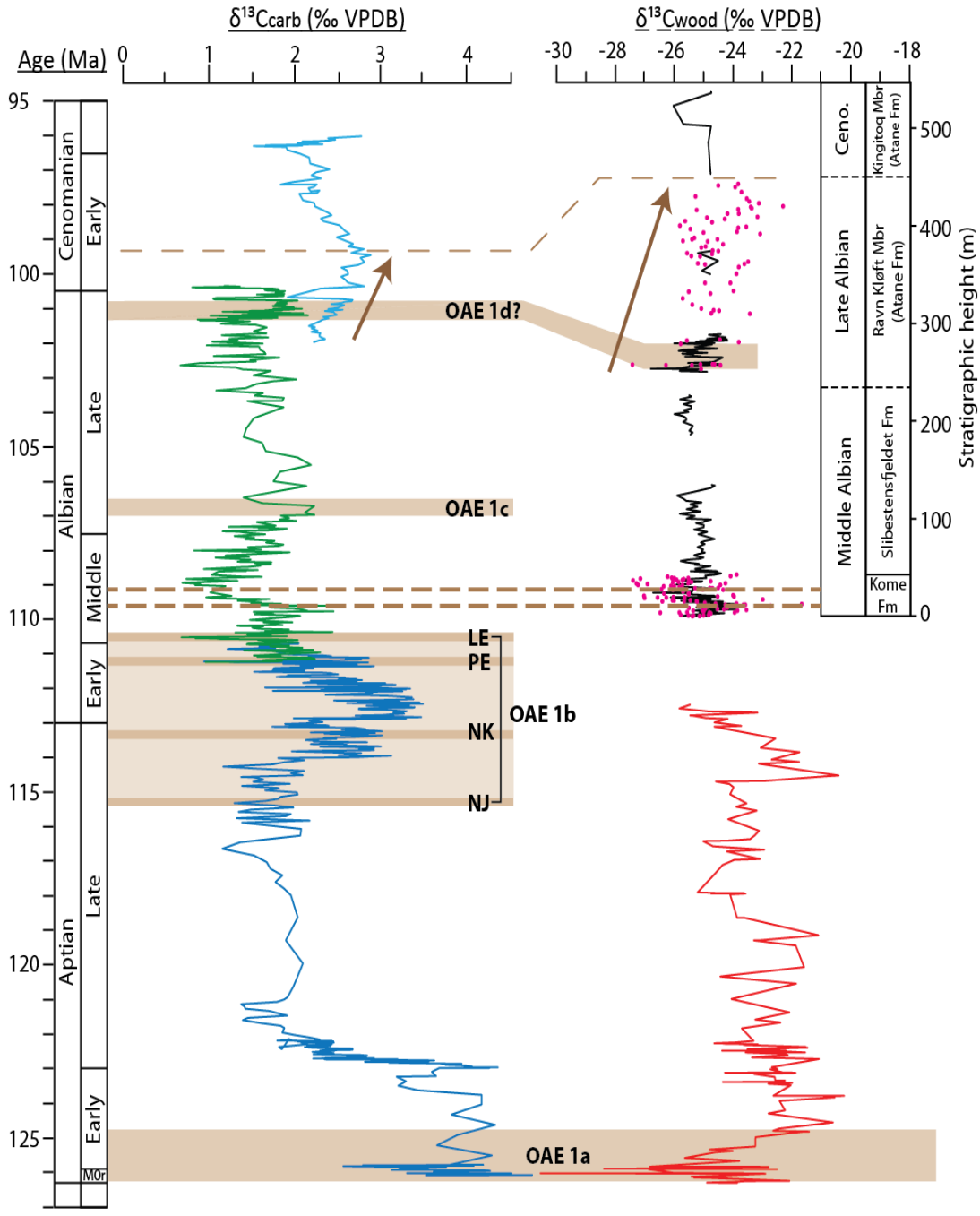

Figure 3.31: Present study isotope data ($\delta^{13}C_{org}$ = black line; $\delta^{13}C_{wood}$ = pink points) with palynological and floral age estimates and Formations correlated to reference curve isotope stratigraphy:

Red = Isle of Wight fossil wood from Gröcke et al. (1999)

Light blue = Vocontian Basin marine carbonate from Gale et al. (2011)

Dark blue = Vocontian Basin marine carbonate from Herrle et al. (2004).

Recognised OAEs are labelled, including LE: Leenhardt Event, PE: Paquier Event, NK: Niveau Kilian, NJ: Niveau Jacobi associated with OAE1b.

estimates (Figure 3.31). Comparison of the $\delta^{13}C_{org}$ (black line, Figure 3.31) and $\delta^{13}C_{wood}$ (pink points, Figure 3.31) values from West Greenland with the $\delta^{13}C_{wood}$ from the Isle of Wight (red line, Figure 3.31) indicates that the base of the West Greenland section must be younger than Early Albian. It is not possible to correlate the carbon isotope stratigraphy through the Slibestensfjeldet Formation to the $\delta^{13}C_{carb}$ record from the Vocontian Basin (green and dark blue in Figure 3.31) and this likely reflects the difference in carbon cycling between the lacustrine Slibestensfjeldet Formation and the marine Vocontian Basin.

The negative carbon isotope excursion identified near the base of the Ravn Kløft Member may correlate to the isotopic structure identified in the reference curves at the base of the interval labelled OAE 1d (around 101.5 Ma, Figure 3.31). However, there are many negative spikes throughout the chemostratigraphy of all studies, and the correlation of the stratigraphy on that basis would be subjective. Instead, the subsequent positive trend recorded in the Ravn Kløft Member correlates to the positive trend in the Californian $\delta^{13}C_{carb}$. The end of the positive trend exhibited in the $\delta^{13}C_{carb}$ records from California at around 99.4 Ma may correlate to somewhere in the boundary between the Ravn Kløft and Kingittoq Members where the present study $\delta^{13}C_{wood}$ shows a positive trend spanning from around 300 m until 450 m (Figure 3.31). The grab samples from the Kingittoq Member do not exhibit clear trends in $\delta^{13}C_{org}$, but indicate that $\delta^{13}C$ values in the Greenland section were slightly more negative compared to the top of the Ravn Kløft Member, and hence may correlate with the end of the positive trend exhibited in $\delta^{13}C_{carb}$ from California. This correlation places the base of the Ravn Kløft Member as Late Albian and extends in to the Early Cenomanian, with the Kingitoq Member entirely in the Cenomanian, supporting the previous palynological and floral age estimates (Section 2.5.5).

A closer examination of the Kome Formation isotope stratigraphy against the Vocontian Basin reference curves (Figure 3.32) confirms the Formation is not Early Albian in age. The isotopic excursions associated with the Leenhardt and Paquier Events are short duration negative spikes in $\delta^{13}C_{carb}$ on the order of 1.0–1.5 ‰. A general positive trend from around 110.4 Ma to around 109.7 Ma has a magnitude of around +0.5 ‰ (Figure 3.32). This may correlate to the positive shift in $\delta^{13}C$ values in the Kome Formation from 0–12 m height, although uncertainty surrounding the age of the base of the Greenland section (which is not the base of the Kome Formation) remains (Figure 3.32).

The subsequent negative shift in $\delta^{13}C_{carb}$ of the Vocontian Basin of a magnitude of around -1.0 ‰ agrees with the shape of the Kome Formation $\delta^{13}C$ values from 12–25 m height.

However, the excursion magnitude recorded in the terrestrial carbon reservoirs is greater than marine carbonate which may be due to possible changes in ε_p related to pCO_2 (Section 2.2.2). Despite the difference in sensitivity of carbon reservoir response, the ratio of excursion magnitude across the positive-negative shifts for both datasets are similar.

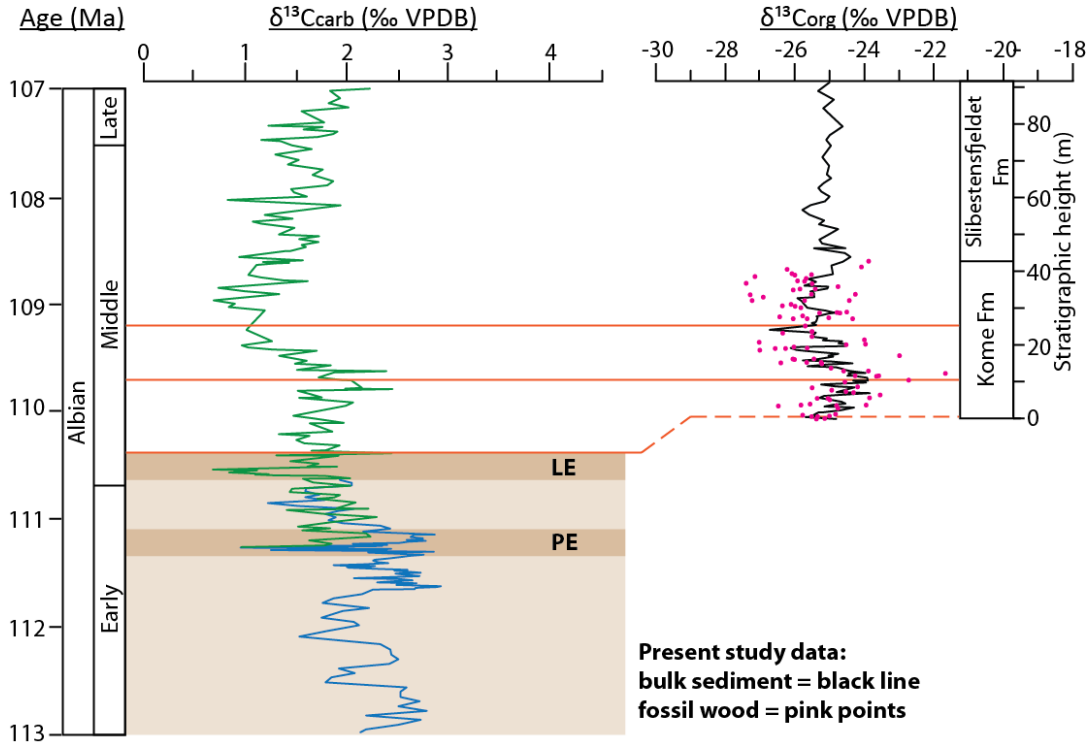

Figure 3.32: $\delta^{13}C$ from the Kome Formation isotope correlated to the Vocontian Basin reference curve. LE: Leenhardt Event, PE: Paquier Event.

The correlation agrees with the previous palynological and floral based estimates of age for the Greenland section (Section 2.5.5), with the Kome Formation thought to be Middle Albian, in addition to a brackish water dinoflagellate cyst tie-point from Nøhr-Hansen (2005) for the Slibestensfjeldet Formation. Floral estimates of Boyd (1998a, b, c, 2000, 2004) and those summarised by Dam *et al.* (2009) indicate a Late Albian to Cenomanian age for the remainder of the section. As a result, the correlation of the Greenland carbon isotope stratigraphy reinforces and refines the age-model for the stratigraphy across the Nuussuaq Peninsula, and provides a better framework within which changes in floral dynamics can be interpreted.

3.6 Summary

In conclusion, two portions of the Greenland stratigraphy yield isotopic structures which can be correlated to $\delta^{13}C_{carb}$ reference curves from the Vocontian Basin and California. A pronounced positive-negative excursion in the Kome Formation is correlated to a similar

isotope event in the Vocontian Basin after the series of events comprising OAE1b. The lower Ravn Kløft Member presents a positive trend in $\delta^{13}C$ values, which has been correlated to a similar isotopic disturbance recorded in the $\delta^{13}C_{carb}$ of the Vocontian Basin and California associated with OAE1d. If this correlation is correct, the data from the present study provides additional evidence for the global nature of OAE1d (e.g. Gröcke *et al.*, 2006).

These two intervals of isotopic structure in the Kome Formation and Ravn Kløft Member are suitable to address the research goals since they represent intervals of global disturbance of the carbon cycle, and occur in fluvio-deltaic depositional palaeoenvironments, and therefore, are likely to contain abundant fossil leaf cuticle for stomatal measurements.

4. Extraction and morphotyping of fossil leaf cuticle

4.1 Introduction

Cuticle covers all primary aerial surfaces of plants and is composed of chemically resistant insoluble biopolymers, including varying amounts of cutin and cutan depending on plant type (Figure 4.1; Eglinton and Hamilton, 1967; Tegelaar *et al.*, 1991; Lyons *et al.*, 1995 and references therein; Deshmukh *et al.,* 2005 and reference therein; Taylor *et al.,* 2009). In many cases the cuticle is covered with epicuticular waxes of varying form and structure (see Barthlott *et al.*, 1998 and references therein for review).

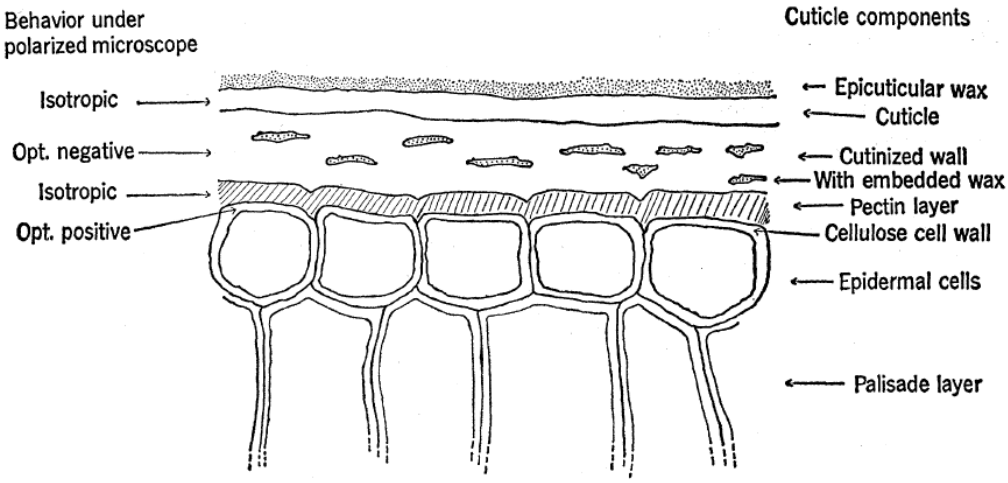

Figure 4.1: Early polarising light microscopy analysis of leaf material in cross-section, showing cellular detail and cuticle layers including epicuticular wax, from Eglinton and Hamilton (1967).

Components of leaf cuticle have been identified as resistant to the coalification process, whereby cutin and wax remain well preserved in even bituminous grade coals, whereas cellulose and water-soluble compounds are lost early during diagenesis (Lyons *et al.,* 1995; Gröcke, 2002).

In life, plant cuticle and waxes are important controls on water loss (which can occur through the leaf cuticle if it is thin) but they also serve to: repel excess water from the leaf surface, attenuate radiation of wavelengths for photosynthesis and filter UV-radiation, and protect the plant tissue from abrasion and pathogen infiltration (Haworth and McElwain, 2008 and references therein; Taylor *et al.,* 2009). Since cuticle closely conforms to the surface of the leaf, filling the gaps between epidermal cell walls and even partially or fully extending into the stomatal cavity (internal cuticle; Pesacreta and Hasenstein, 1999 and

references therein), the cuticle retains an impression of the epidermal surface long after the original tissue has decayed (Taylor *et al.*, 2009). Therefore, examination of the impression of epidermal cells and stomatal openings on fossil leaf cuticle can provide the measurements required for stomatal density, index and conductance.

This chapter describes how cuticle was retrieved from bulk sediment samples through acid digestion and examined under epifluorescence microscopy. Leaf cuticle features have been scored in a character matrix, which has been analysed to group cuticle features into morphotypes. Through comparisons of the morphotypes, collected macrofossils and published descriptions, it has been possible to tentatively assign plant types to the morphotypes.

4.2 Approach

4.2.1 Bulk maceration

The aim of bulk maceration was to retrieve large (mm to sub-mm) fossil leaf cuticle pieces from sedimentary rocks for the purpose of stomatal counting. Since the leaf cuticle was chemically resistant to acid, the method aimed to dissolve all other mineral material comprising the sediment. Through the process of sieving, the desired material was separated from smaller organic debris.

The method presented here was developed from that used by Barclay (2011) who adapted the method of Wellman and Axe (1999). The modifications to the published protocols are discussed in Appendix C. Approximately 100–200 g of sample was broken into 1 cm size pieces using a hammer and metal plate and placed into a labelled 250 ml polypropylene wide-neck bottle with screw cap. If samples contained obviously large pieces of cuticle (e.g. leaf mat samples) these were not broken into such small pieces. Some poorly cemented samples could be easily broken by hand (including the leaf mat samples).

Batches of ten sample bottles were placed in a non-HF fume hood, with just enough concentrated Hydrochloric acid (32 % HCl) to cover the sample and the caps screwed on loosely to allow gas to vent from the reaction. The HCl was added immediately to the samples because the carbonate content of the samples was low (Section 3.3.1). The samples were left for a week to digest the carbonate species present and were agitated daily by screwing the cap on tightly and shaking, before reopening the cap again for ventilation. Once the reaction with HCl was complete the samples were topped up with water and rinsed through a 500 µm sieve in order to remove fine mineral material which

can cause instantaneous reaction upon Hydrofluoric acid (HF) addition. The sample was returned to the bottle when nearly neutral - through trial it was found that leaving the sample slightly acidic prevented fluoride precipitates when HF was added.

For the steps involving HF, standard HF safety protocols were implemented. The samples were moved to a designated HF-hood, and placed in a large plastic tray. 68 % HF was added to one sample at a time, adding just enough to cover the sample. The cap was replaced promptly and left slightly loose for ventilation of gas from the reaction. The sample was watched for signs of reaction - in most cases some reaction would be visible and was kept under control by spraying with water from a wash bottle. Any HF spilt through an over-boiled reaction or from the stock bottle would be contained within the work tray, and neutralised with water and sodium bicarbonate. After one week digesting in HF, the samples were rinsed with large amounts of water through a 125 µm sieve until neutral. Excess acid was collected via a funnel into a 5 L bucket and neutralised with sodium bicarbonate. Once rinsed, the sample was stack sieved using three sieve sizes: the first (4 mm) sieve was used to separate out large unreacted material, which was returned to the sample bottle, where fused pieces could be broken down with a plastic stirring rod. The second sieve in the stack (500 µm) was used to separate out partially macerated pieces of a size suitable for stomatal counting. This material was placed into a labelled polypropylene vial (40 ml) ready for addition of HF to clean up the cuticle present and complete the acid digestion. The final fraction, from a 125 µm sieve, was placed into a labelled 40 ml polypropylene vial for storage (for future preparation should the need arise).

HF was re-added to the primary sample bottle and the vial containing the 500 µm cuticle fraction and left for another week. The process was repeated until as much of the sample was reacted as possible, generally taking a minimum of four weeks. In most cases there was a small volume of unreacted material after four weeks, which was not worth pursuing. Often this material was coaly debris, including fossil wood pieces which were not required at this stage. Removing HF from the pore spaces of unreacted rock was attempted by leaving the material in a beaker of water for several days, neutralising the excess and repeating, but even then the material was considered as hazardous (Barclay *pers. comm*). The material was dried, placed in polythene sample bags and clearly labelled for storage in a plastic container with the contents clearly labelled.

Initially, only one bottle per sample was processed, and the cuticle yielded was examined to assess the suitability for stomatal counting based on cuticle abundance and

preservational state (i.e. were stomata and cell detail preserved?). It was generally found that finer grained sediments provided well-preserved cuticle (based upon a pilot study under epifluorescence microscopy of the first batch of macerated cuticle) compared to coarser grained samples, but that fine-grained sediments required longer maceration times. When suitable samples were identified, an additional two to four bottles per sample were macerated. With two fume hoods being utilised in a lab dedicated to this maceration, it was possible to set up a batch system: with 10 bottles in HCl in the non-HF hood, and batches at various stages of HF digestion in the HF-only hood, in addition to the small vials. This allowed continuous processing of material for maximum efficiency. In addition, the small vials of material could be rinsed when desired to be examined under the microscope allowing access to cuticle material at all times.

4.2.2 Cuticle sorting (binning)

The end product of the maceration was a single 40 ml vial of mixed organic debris for each sample. In order to aid the morphotyping process, the cuticle was sorted based on suitability for stomatal counting and morphotyping.

4.2.2.1 Protocol

The first stage of separating the organic material was completed in the maceration stage, whereby the >500 µm and <4 mm material was retained as a size suitable for stomatal counting (except in the case of leaf mat samples where the 4 mm sieve was omitted since the cuticle material contained near complete pinnae up to 30 mm in length). Examination of leaf cuticle by normal light microscopy would require additional preparation of the material to clear the cuticle from the dark brown coalified state to clear/colourless through bleaching (Kerp and Krings, 1999). This potentially destructive step can be avoided if the cuticle has not been appreciably coalified and if the unsaturated organic compounds (including lignin and cutin) that comprise leaf cuticle, auto-fluoresce under UV, blue and violet excitation (Van Gijzel, 1979; Kerp, 1990; Rost, 1995 and references therein; Yeung, 1998; Doláková and Burešová, 2007). The colour of auto-fluorescence under UV light changes with increasing age and degree of coalification; from strong fluorescence of blue-green/white (youngest/least coalified), to bright yellow/orange-brown and weak auto-fluorescence (older/more coalified) before losing the ability auto-fluoresce completely (Van Gijzel, 1979; Kerp, 1990; Doláková and Burešová, 2007). Therefore, providing the cuticle material fluoresces well, epifluorescence microscopy is advantageous since it requires no additional preparation of material beyond acid digestion, preserving delicate features

which may otherwise be lost. The epifluorescence microscope used was a Zeiss UNIVERSAL microscope with an RSIII fluorescence condenser, UV and blue excitation filters and a mercury arc lamp light source. The imaging apparatus comprises a Jenoptik ProgRes® CCD camera supported by ProgRes® CapturePro software for image capture.

Cuticle fragments were picked out of water (from the vial which was kept slightly acidic to prevent bacterial and fungal decomposition) from a glass dish using a fine brush and placed onto a glass slide. A pipette was used to drop a small amount of water onto the cuticle fragment and a cover slip was placed over the top to prevent the cuticle from drying under the microscope and also to provide a clear, stable image. The pilot study examination of the cuticle indicated that the material fluoresced well, with the majority fluorescing bright yellow under the blue excitation filter, with some pieces fluorescing more poorly with an orange to brown colour, and some not at all indicating a greater degree of coalification. The positive results from the pilot study indicated there was sufficiently fluorescing pieces to use epifluorescence microscopy rather than a more aggressive cuticle clearing approach. Examination of the first bottle of each sample indicated the suitability of the horizon for the research goals by assessing the yield of well-fluorescing cuticle. As the cuticle was examined it was placed into a labelled vial based on the preservation type as outlined in Table 4.1.

Groups 1 to 4 did not contain suitable material or suitable preservation for morphotyping, so were not considered further. Groups 5, 6, 7A and 8A contained pieces that were suitable for morphotyping; the latter three were also suitable for stomatal density and index measurements. Groups 7B and 8B contained cuticle with well-preserved features but both groups lacked sufficient detail to be used as either morphotypes or for stomatal counting. Group 9 contained pieces of varying degrees of fluorescence but were identifiable structures associated with plants (including plant reproductive structures and Bennettite scales) but not leaf cuticle.

4.2.2.2 Summary of sorted cuticle

A total of 8300 macerated fragments across 79 horizons were sorted into the groups outlined in Table 4.1; of these, 35 horizons were deemed unsuitable after examination of the first macerated material bottle and were not pursued further (Table A, Appendix C). The remaining 44 horizons had a good yield of cuticle pieces categorised into groups 5, 6, 7

(A and B), and 8A, and form the source material for the morphotyping process and are summarised in Table 4.2.

Group	Classification	Description
1	Unsorted	500 µm to 4 mm size fraction of cuticle separated in the maceration stage.
2	Not leaf cuticle	Pieces that do not fluoresce and/or are not plant cuticle e.g. wood, pseudocuticle, sediment
3	Little/no cell detail, no character score	Pieces with little to no cell detail, no features allow it to be scored by character matrix, not morphotyped.
4	Cell detail, no stomata, no character score	Epidermal cells may be well preserved but with lack of stomata and other features of character matrix, cannot be scored. Not morphotyped.
5	Cell detail, stomata, character score but no SD/SI	Sufficient detail to score on character matrix but not able to count e.g. too small or patches obscured/poor preservation.
6	Cell detail, stomata, character score and SD/SI	Sufficient detail to score on character matrix and to count either SD or SI.
7	Exceptional preservation	Pieces with preserved internal tissue or useful pieces for structure of a morphotype e.g. leaf tip, leaf base etc.
7A		7A. Material that could be character scored and SD/SI counted.
7B		7B. Material that could not be character scored or SD/SI counted.
8	Fungal/algal specimens	Cuticle pieces bearing epiphyte structures
8A		8A. Material that could be character scored and SD/SI counted.
8B		8B. Material that could not be character scored or SD/SI counted.
9	Other structures	Other plant structures e.g. Bennettite scales, reproductive cuticle structures.

Table 4.1: Cuticle classification scheme based on degree of preservation (fluorescence) and structure type.

Sample	Composite height (m)	Cuticle Group										
		2	3	4	5	6	7A	7B	8A	8B	9	Total
LK-B-7	1.10		8	152	156	163			5	15	1	500
LK-B-9	1.87	47	33	80	19	21				6	4	210
LK-B-2	3.14	23	17	82	23	23					2	170
LK-B-3	3.26		35	47	29	21		9	3	24	2	170
LK-B-15	5.60	80	76	187	33	38		2	1	22	1	440
LK-B-20	7.78	9	21	5	2	3						40
LK-B-25	10.45	181	8	48	5	8						250
LK-B-28	11.60	41	205	96	24	25	1	4		2	2	400
LK-B-31	12.35	28	77	163	17	9		1		1	4	300
LK-B-42	16.08	13	81	204	62	54	1	3			2	420
LK-B-49	19.19	9	152	132	29	16	1	1				340

Table 4.2 continued. Sample	Composite height (m)	Cuticle Group										
		2	3	4	5	6	7A	7B	8A	8B	9	Total
LK-B-55	21.29	4	18	106		4		1		1	1	135
LK-B-56	21.79	8	33	86	4	8					1	140
LK-B-57	22.19		85	140	5	5						235
LK-B-67	27.39	98	83	263	20	44				2		510
LK-B-68	27.80	17	4	15	2							38
LK-B-74	30.06	23	9	14	2					2		50
LK-B-78	31.77	16	34	239	34	19			3	5		350
LK-B-79	32.17	12	13	341	101	7				26		500
LK-B-81	33.00	19	17	106	16	46		1	1	5		211
LK-B-82	33.45	18	18	41		3						80
LK-B-83	33.92	22	12	13		1				2		50
LK-B-87	35.72	5	7	1		2						15
LK-B-99	39.41	25	3	10		1				1		40
LK-B-119	40.95	24	46	18	7	5						100
ANE-B-477	173.96		28	28	4							60
RKE-B-3	182.11	21	12	8	3	6						50
RKE-B-4	183.17	23	30	6	1							60
RKE-B-5	183.30		32	13	4	4				4	23	80
RKE-B-9	187.00		29	6	4	11						50
RKE-B-13	187.57			19	11							30
RKE-B-14	187.92		17	143	5	6				1		172
RKE-B-16	188.18	4	15	43		1					1	64
RKE-B-17	188.58	12	13	30	1	4						60
RKE-B-18	188.98	13	20	84	1	9				1		128
RKE-B-23	194.97	1	18	103		4					4	130
RKE-B-33	198.95	32	42	58	11	7						150
RKE-B-35	199.85	1	11	215	8	8	5	2		15		265
RKE-B-44	203.54	16	37	34	4	12				1	1	105
RKE-B-102	209.49	5	4	8		3						20
RKE-B-128	210.63		23	79	17	11						130
RKE-B-105	210.69	24	46	147	14	8				1		240
RKE-B-133	212.50	21	5	3		1						30
RKE-B-119	217.40	4	44	63	9	14				2		136

Table 4.2 (previous page and continued above): List of samples with number of cuticle pieces sorted into groups defined in Table 4.1: samples with good cuticle yield and subsequent bottles of material macerated resulting in total number of pieces sorted as given in the total column.

4.2.3 Character matrix construction

4.2.3.1 The morphotyping approach

Fossil leaf cuticle has been demonstrated to have sufficiently different characters to distinguish between plant groups, even at genus and species level depending on preservation (e.g. angiosperm cuticle from the Ravn Kløft flora in West Greenland studied by Boyd, 1998c). Barclay *et al*. (2007) developed the Cuticle Database Project (CDP) - an online based resource of cuticle images for the purposes of identifying fossil material by comparing the sample material to an identification key structure. The CDP flowchart (Appendix C, Figure i) presents a path for identifying fossil material: at each comparison point the user is taken to a web page with images from the cuticle database to aid identification. The outcome in the decision making process takes the user to the relevant next page. Epidermal features that are likely environmentally controlled (phenotypic), for example the degree of cell wall crenulation, the stomatal density and the trichome density, are separated from factors controlled by genetics (genotypic) which are used to distinguish between plant types, e.g. stomatal complex type, stomatal distribution and relief (Figure 4.2; Barclay *et al.*, 2007).

When dealing with small fragments it may not be possible to be certain of taxonomic interpretation to a genus and species level, and so cuticle can be assessed in terms of morphotypes. The concept of morphotypes was used by Barclay (2011) to select suitable fossil material for stomatal density and index measurements based on the procedures outlined in the Manual of Leaf Architecture by the Leaf Architecture Working Group (1999).

	Major Characters	Genotype	Phenotype
CUTICLE	Papillae type and position	X	X
	Secretory structures (glands, glandular hairs)	X	
	Stomatal complex type	X	
	Stomatal distribution (rows, dispersed, sunken)	X	
	Stomatal position (amphistomatous, hypostomatous)	X	X
	Striations (intercellular, intracellular, epicuticular wax)	X	X
	Trichomes (type, complexity, location)	X	
	Trichome bases plus surrounding cell arrangement and number	X	
	Cell walls (degree of crenulation)		X
	Hydathodes (position, size, number)		X
	Papilla number and size		X
	Stomatal density		X
	Stomatal index		X
	Trichome density		X
LEAF	Palisade parenchyma (structure)		X
	Palisade to mesophyll parenchyma ratio		X

Figure 4.2: Summary of genotypic (genetic) controlled cuticle characters, compared with phenotypic (environmentally) controlled characters, summarised by Barclay et al. (2007).

A morphotype represents cuticle pieces sharing the same genotypic characteristics, which, by extension, are assumed to represent the same plant type. Cuticle pieces possessing all the cuticle traits required for identifying the morphotype are called holomorphotypes, and serve as the reference for comparison of cuticle pieces that may not have all traits but a sufficient number to distinguish them from other floral types. As a result, not just the cuticle that is sorted for stomatal density and index measurements can be used, but also other cuticle fractions that may have been deemed too small for stomatal density measurements, or have no stomata preserved, can be sorted into, at-worst, plant groups, and even genus or species levels, using the morphotyping method (e.g. Barclay *et al.,* 2007; Barclay, 2011).

Barclay (2011) recorded cuticle features in a character matrix, which is a table of features scored using a key system, whereby for a given characteristic (e.g. stomatal complex type), a description is recorded by using a number to represent a given characteristic state (e.g. 0 = cyclocytic, 1 = paracytic and so on). The benefit of using a character matrix is that it allows any user to continue the morphotyping process at a later date with reduced subjective input, and allows rapid data accumulation on not just genotypic features but also phenotypic features, so that environmental changes can also be tracked. The characters recorded in the present study matrix were based on the genotypic features identified by Barclay *et al*. (2007) and Barclay (2011), in addition to features identified in a pilot study of the cuticle (Table 4.3).

For most plants, if multiple stomata were preserved on a surface it was recorded in the "stomatal side" part of the matrix, if then on the reverse side of the same cuticle piece none to 1–2 stomata were preserved, this was the "non-stomatal side" to avoid the assumption that the side bearing more stomata was the abaxial surface prior to a more complete assessment through examination and interpretation of the selected holomorphotypes (Section 4.4), and for when only one side of cuticle was preserved. For amphistomatous pieces a note was made in the matrix of that character.

4.2.3.2 The character matrix

The keys to the character matrix record the descriptions for cuticle according to the features outlined in Table 4.3. Table 4.4 lists the character scores for general leaf shape, including the shape of the base, tip and margins, although, these characters were not always evident on small pieces of cuticle, particularly for the base and tip description.

Feature Scored		Stomatal side		Non-stomatal side	
		Outside	Inside	Outside	Inside
Stomata	Stomatal arrangement	x	x	x	x
	Number of bands	x	x	x	x
	Number of rows in band	x	x	x	x
	Stomatal orientation	x	x	x	x
	Stomatal relief	x	x	x	x
	Stomatal structure		x		x
	Florin ring	x		x	
	Stomatal pore ornamentation	x		x	
	Fluorescence colour	x	x	x	x
Epidermal cells and leaf surface	Surface ornamentation	x		x	
	Trichrome Bases	x		x	
	Stomata:Epidermal cell size	x	x	x	x
	Epidermal cell shape in stomatal band	x	x	x	x
	Epidermal cell shape across surface	x	x	x	x
	Epidermal cell wall shape	x	x	x	x
	Pellucid dots	x	x	x	x
	Fungal/algal fossils	x		x	
	Fluorescence colour	x	x	x	x
Leaf shape	General Shape	x	x	x	x
	Leaf tip shape	x	x	x	x
	Leaf margin	x	x	x	x
	Leaf base shape	x	x	x	x
	Cuticle thickness	x	x	x	x

Table 4.3: Summary of cuticle features scored in the character matrix and the surfaces on which they could be examined.

Leaf Shape	Score value	Character
General shape	0	not possible
	1	pinnate
	2	broad
	3	lobed
Leaf tip	0	not possible
	1	pointed
	2	rounded
	3	mucronate
Leaf margin	0	not possible
	1	entire
	2	toothed/serrated
Base shape	0	not possible
	1	flat
	2	concave
	3	convex
	4	tubular
Cuticle thickness	0	thin
	1	normal
	2	thick

Table 4.4: Character matrix key for leaf shape features.

The cuticle thickness was described for all pieces and the leaf margin and leaf shape could be scored if the cuticle fragment was sufficiently intact. The scoring of stomatal and epidermal features depended on the preservation state, but the keys to all characters scored are presented for stomatal features (Table 4.5) and epidermal features (Table 4.6). Description and explanation of characters are provided in Section 4.4.

Stomatal Features	Score	Character
Stomatal arrangement	0	unknown
	1	dispersed
	2	in furrow or groove
	3	rows, no bands
	4	rows, in bands
	5	in bands, disordered
	6	in bands either side of groove
Number of bands	value	number counted off cuticle
Number of rows in band	value	number counted off cuticle
Stomatal orientation	0	unknown
	1	random
	2	longitudinal to cell direction or leaf axis
	3	transverse to cell direction or leaf axis
Stomatal relief	0	unknown
	1	flush
	2	raised
	3	sunken
	4	crypted
Stomatal structure	0	unknown
	1	anamocytic
	2	cyclocytic
	3	paracytic
Florin ring	0	absent
	1	present
Pore ornamentation	0	none
	1	lobed margin
	2	papillose margin
	3	papillose pore
	4	combo 1+3
	5	combo 2+3
Stomatal cell fluorescence colour	0	unknown/poor fluorescence
	1	green
	2	yellow
	3	orange/brown
	4	brown

Table 4.5: Character matrix key for stomatal pore features.

Epidermal Features	Score	Character
Surface ornamentation - papillae	0	absent
	1	stomatal associated
	2	ED cell associated cobble
	3	ED cell associated longer, patchy
	4	ED cell associated longer, continuous
	5	furrow associated
Surface ornamentation - trichome base	0	absent
	1	present
Stomata:Epidermal Cell size	0	small
	1	similar
	2	large
Epidermal cell shape - in stomatal area	0	n/a
	1	irregular polygon
	2	longitudinal rectangle
	3	transverse rectangle
	4	square
	5	longitudinal hexagonal
	6	transverse hexagonal
Epidermal cell shape - outside stomatal area/across surface	0	irregular polygon
	1	longitudinal rectangle
	2	transverse rectangle
	3	square
	4	longitudinal hexagonal
	5	transverse hexagonal
Epidermal cell wall shape	0	straight
	1	wavy
	2	crenulate
Fungal/algal fossils	0	none
	1	network
	2	solitary
	3	lobed solitary
	4	hyphae
	5	internal lobed solitary
	6	puncture fungus
Pellucid dots	0	absent
	1	present
ED cell fluorescence colour	0	unknown/poor fluorescence
	1	green
	2	yellow
	3	orange/brown

Table 4.6: Character matrix key for epidermal surface features.

4.2.4 Character matrix analysis (cluster analysis)

PAST is free palaeontological software that can perform numerous statistical functions, including the handling and analysis of multivariate datasets like that collected in this thesis. The input is a spreadsheet format, with each sample represented by a row of data, with different character information presented in columns. The cluster analysis function in PAST is used to examine the possible morphotypes within the data. There are several ways to perform a cluster analysis on palaeontological and ecological data, but the PAST software uses a hierarchical cluster analysis. The function is specifically an agglomerative algorithm: taking an array of individual data points in multidimensional space and deciding which are nearest to each other and joining them in a cluster. These clusters are then compared iteratively to see which are nearest and joined in a super cluster (Figure 4.3 for a two dimensional dataset) and contrasts to, the more rarely used, divisive clustering which puts the original data into one large cluster and successively divides into smaller clusters (Hammer and Harper, 2006). The output of the clustering process is displayed in a dendrogram (Figure 4.3), whereby the branching point represents the joining of data in a cluster. The different heights of the branching points indicate the degree of separation

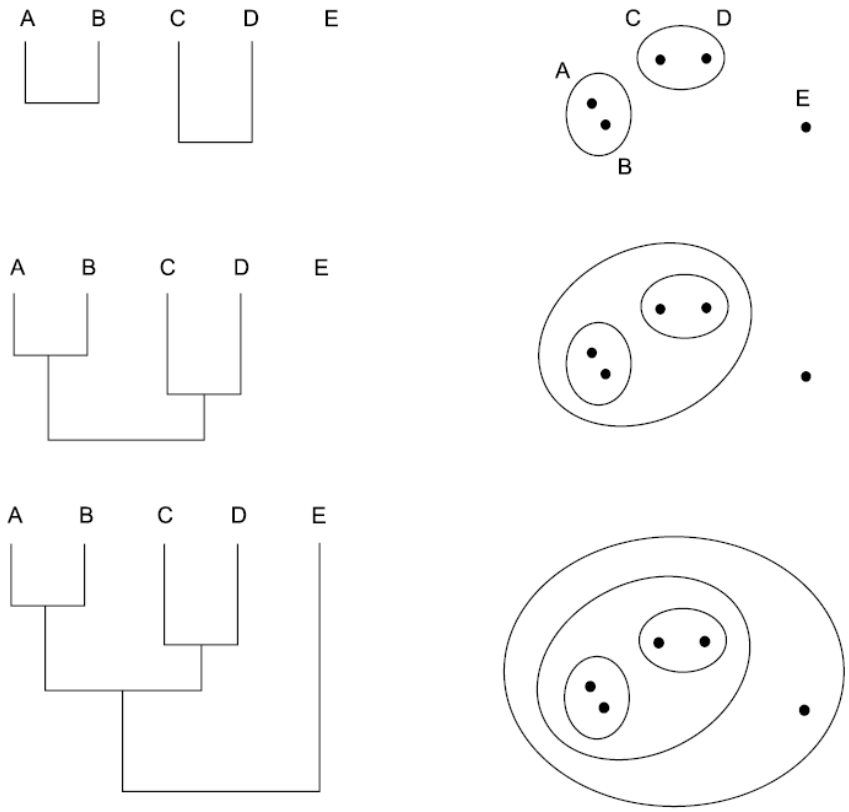

Figure 4.3: Agglomerative clustering method for two-dimensional data set from Hammer and Harper (2006).

between clusters. For example, in Figure 4.3, points A and B are closer than points C and D, so the branching point representing the respective merging is higher in the dendrogram (or tree) for A-B than C-D (Hammer and Harper, 2006). This means of data presentation is a simple but clear way to understand the likely number of groups in a dataset. However, there are some issues that need to be considered (Hammer and Harper, 2006):

1. Cluster analysis will cluster all datasets, including those that are very poorly separated or completely evenly spaced datasets, meaning a relationship hierarchy is assigned to data even if no hierarchical structure is present.
2. The cluster analysis will also eventually join data that is likely not related. For example, cuticle morphotypes that are clearly different plant types will at some stage in the tree (dendrogram) be linked at a low position. This means the user has to decide where to cut the tree and/or apply external information to the dataset.
3. Each branching point can be freely rotated, so the closeness of samples across the width of the tree is not significant (e.g. in Figure 4.3, B and C are no more closely related than A and D).
4. The output of the cluster analysis depends on the algorithm for cluster/data distance and the distance measure. The same dataset can produce many different dendrograms with samples in different clusters from one case to the next.

Of the three algorithms available in PAST (UPGMA – unweighted pair-group average; single linkage – nearest neighbour; Ward method), this thesis uses pair-grouping, whereby clusters are joined based on the average distance between all members in the two groups. Since cluster analysis is not a statistical tool, rather an exploratory method, clusters produced from analysis of the cuticle character matrix may contain more than one morphotype, or members of a morphotype may be split between clusters. Some user appreciation of the dataset is also required, for example selection of the distance calculation technique between data points (e.g. Euclidean, Gower, Chord) can result in vastly different trees, which for morphotyping purposes can result in different morphotype groupings. Therefore, it was important to refer back to the sample material and assess the apparent groupings from a given iteration of cluster analysis (Section 4.3.2).

An additional means of evaluating a cluster analysis is through the cophenetic correlation coefficient. The cophenetic correlation coefficient is returned upon creation of a dendrogram in PAST through cluster analysis, and represents the correlation coefficient of the linear correlation between cophenetic distances calculated from the tree compared to

the original distances used to calculate the tree, whereby a cophenetic correlation coefficient close to one indicates the dendrogram faithfully represents the distances between data points (Saraçli *et al.*, 2013).

4.3 Simplified character matrix analysis

4.3.1 Cuticle feature selection

In order to successfully separate morphotypes through cluster analysis of a simplified version of the character matrix, genotypic features which were frequently preserved were selected (e.g. stomatal complex type is a good feature to separate plant types but was not always present due to preservational issues). The original character matrix (Tables 4.5 and 4.6) was then used as a reference to compare features of the samples clustered by the matrix to confirm inclusion in the morphotype.

The features selected to comprise the simplified character matrix for analysis were:

1) Stomatal arrangement (as in Table 4.5).
2) Stomatal orientation (as in Table 4.5).
3) Stomatal ornamentation (simplified from the original matrix to: absent [0] and present [1]).
4) Surface ornamentation (simplified from the original matrix to: absent [0], papillae [1], furrow papillae [2], circular structures [3], ribbed [4]).
5) Trichome presence/absense – non-glandular hairs, often only identified by the trichrome base as a circular structure, larger than stomata or epidermal cells (as in Table 4.6).
6) Pellucid dots (glands in the mesophyll; Barclay, 2011) and other epidermal glandular structures – similar round structures, sometimes with associated epidermal cells and generally very brightly fluorescing (as in Table 4.6).

4.3.2 Matrix analysis

Only cuticle fragments which had complete entries in the character matrix for the selected cuticle features (Section 4.3.1) were analysed in PAST.

4.3.2.1 First analysis – paired-group (Gower distance)

After several attempts of cluster analysis on the character matrix, the paired-group (Gower distance) produced the highest cophenetic coefficient of 0.9288 (Figure 4.4); whereby the

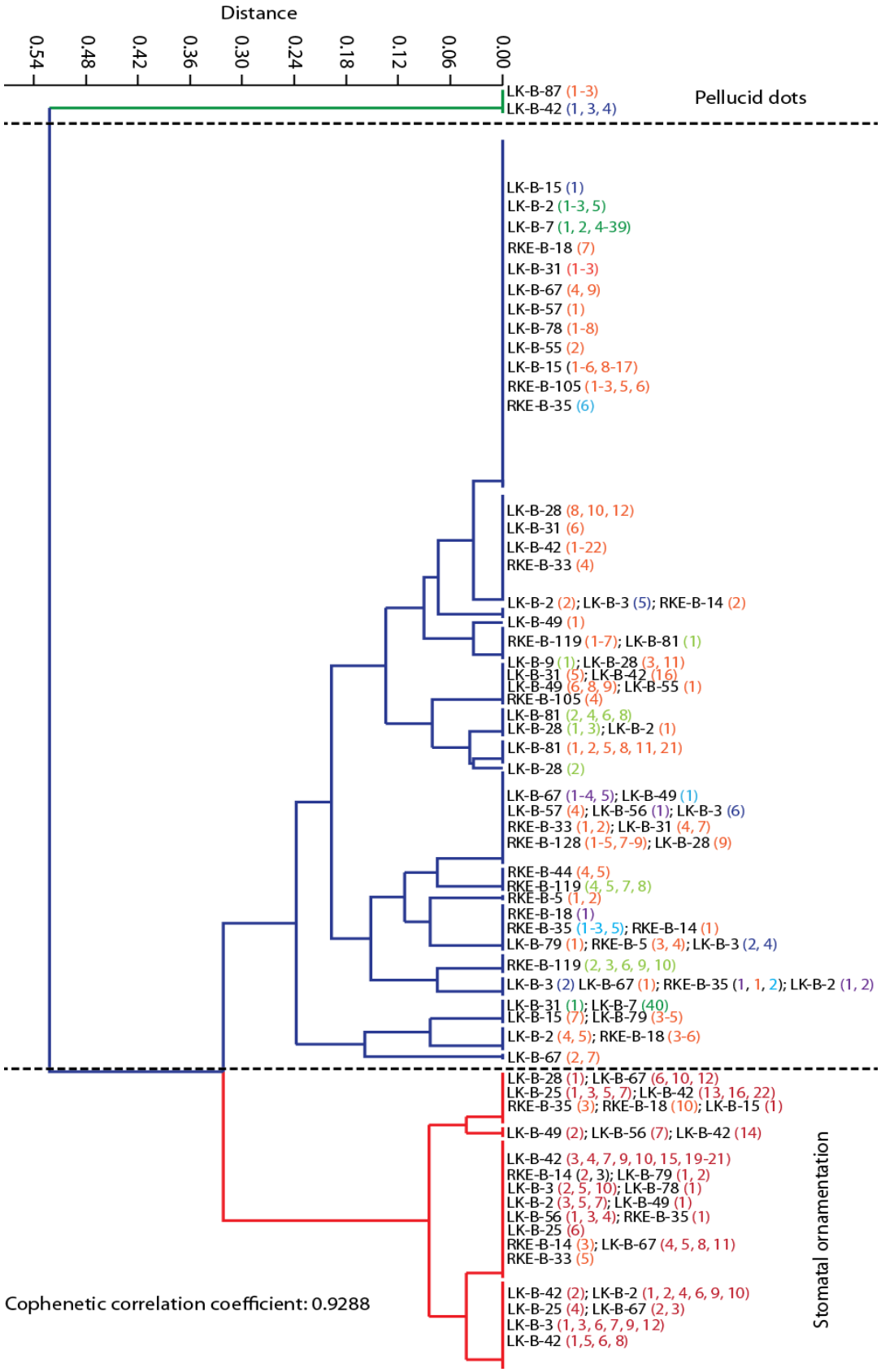

Figure 4.4: Paired-group cluster analysis using Gower distance, with a cophenetic correlation coefficient of 0.9288 for character matrix entries with complete records of cuticle features outlined in Section 4.2.2. Sample labels show horizon with cuticle piece in brackets colour-coded by sample vials.

Gower means of assessing sample distance (developed by Gower, 1971 based on a range-normalised Manhattan distance; Pavoine *et al.,* 2009) was calculated before the paired-group algorithm was applied to the resulting distance matrix. Examination of the character matrix and cuticle fragment images for the most distantly related groups (highlighted by green and red branches in Figure 4.4) reveals two likely morphotypes: the first containing cuticle pieces all with pellucid dots (green branch, Figure 4.4); and the second containing cuticle pieces which all possess stomatal ornamentation and dispersed-to-irregularly arranged into files stomatal arrangement (red branch, Figure 4.4). As such, the dendrogram can be divided into three groupings (Figure 4.4), whereby the middle set of branches contains numerous clusters, which on comparison to the original matrix did not immediately reveal intact groups which could be defined as morphotypes.

4.3.2.2 Second analysis – paired-group (Chord distance)

Reanalysis of the character matrix attempted to clarify morphotypes from the middle grouping (blue branches, Figure 4.4) by omitting the cuticle pieces with stomatal ornamentation (red branch, Figure 4.4) but retaining the apparent morphotype distinguished by pellucid dots (green branch, Figure 4.4) as a definite outlier (Barclay, 2011). The best cluster analysis using this data was a paired-group analysis using chord distance (a modification of Euclidean distance, Gan *et al.*, 2007) which produced a cophenetic correlation coefficient of 0.942 (Figure 4.5).

Since the cluster analysis is an exploratory tool, the clusters shown in Figures 4.4 and 4.5 may contain more than one morphotype, or may have divided morphotypes based on variations in the character matrix reflecting natural variation of a given plant form. Whilst the use of a character matrix reduced subjective input by limiting the character options through the use of the character key (Table 4.5, 4.6), some subjectivity may remain in the decision making process for character assignment which could be reflected in the cluster analysis distribution of morphotypes. However, additional information provided in the character matrix that was not used in the cluster analysis but still distinguishes plant types (e.g. stomatal complex type where recorded), can be used to clarify the clusters produced and aid morphotype definition.

In the same way as for the initial cluster analysis (Figure 4.4) possible morphotypes were deciphered from Figure 4.5 by dividing the dendrogram by the most distant branch division

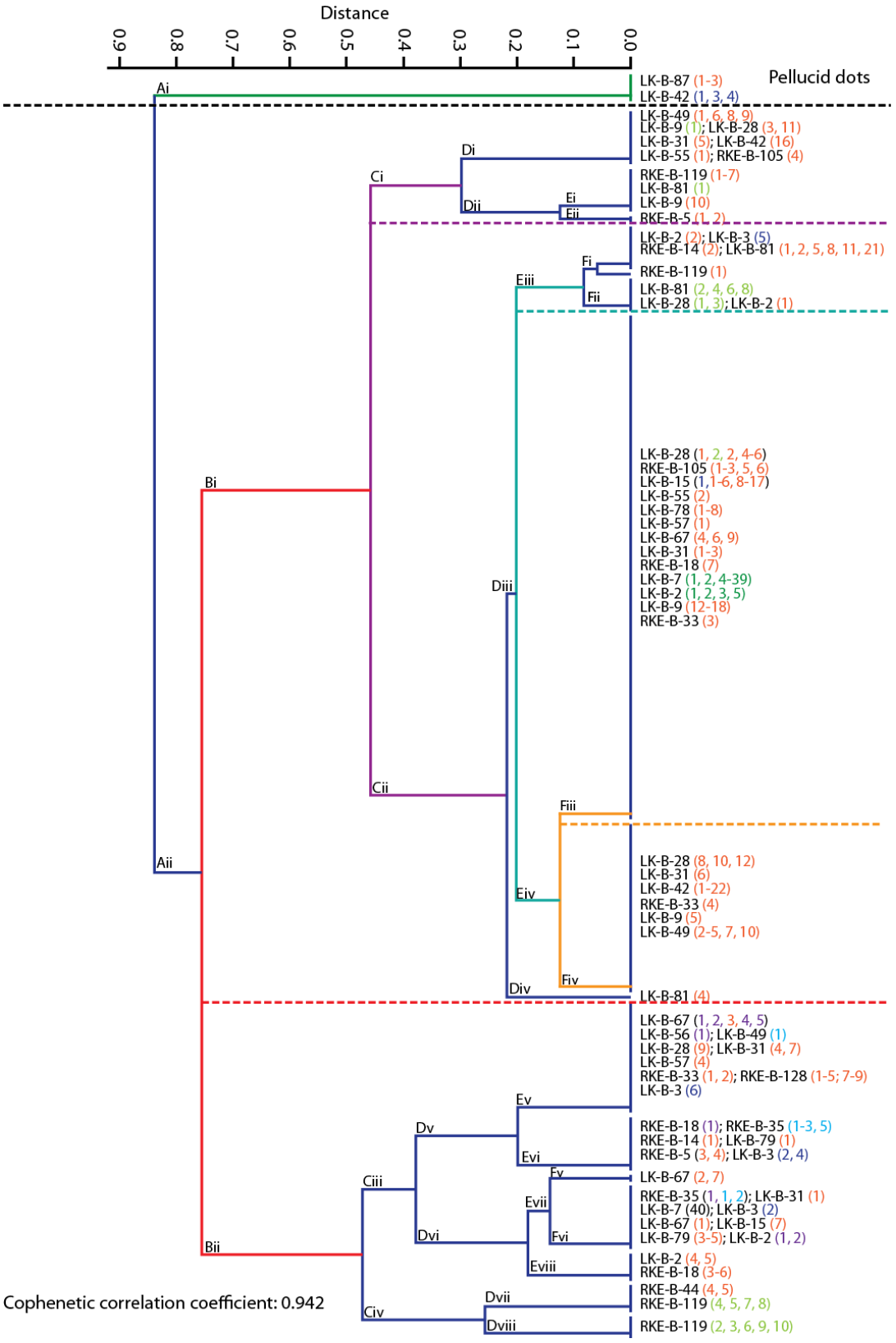

Figure 4.5: Paired-group cluster analysis using Chord distance, with a cophenetic correlation coefficient of 0.942 for character matrix entries with complete records of cuticle features outlined in Section 4.2.2, with the red branch data from Figure 4.5 omitted from the analysis. Sample labels show horizon with cuticle piece in brackets colour-coded by sample vials.

and comparing information in the original character matrix for samples either side of the divide to understand the differentiating feature causing the divide. The most distantly related divide shown in Figure 4.5 after the outlier branch (pellucid dot group, green branch in Figure 4.5) is shown by the red branch, dividing the cuticle pieces into two branch groups (Bi and Bii). Upon examination of the character matrix, cuticle fragments in the lower subdivision (Bii) are dominated by stomata arranged in a furrow, with the exception of the lowest three clusters (Dvii, Dviii and Eviii), which do not have stomata arranged in a furrow.

Examination of the subdivision of the Bi branch into Ci and Cii (purple branches and dashed line in Figure 4.5) divides cuticle fragments into those with stomata organised into rows or bands (Cii) from those which appear to have a dispersed stomatal arrangement (Cii). The further clustering from branch Ci (Figure 4.5) appears to separate cuticle fragments with randomly aligned stomata (Di) from those with aligned stomata (Dii). The further clustering of branch Cii (Figure 4.5) is less certain, since the Div branch (blue in Figure 4.5) separates out only one cuticle fragment (LK-B-81 [4]). Instead, if the subclusters of the Diii branch are considered (teal in Figure 4.5), branch Eiv contains cuticle fragments with stomata arranged into rows, either within a band (Fiii; orange in Figure 4.5) or not within a band (Fiv; orange in Figure 4.5). The cuticle fragments within the Eiii subcluster are less clear, containing fragments with a range of stomatal arrangement and orientation, some of which are similar to the Ci subcluster, indicating for these samples a closer examination of the character matrix is required to clarify possible morphotypes.

From the groupings described from the two cluster analyses (Figures 4.4 and 4.5), comparison to the complete character matrix supports the separation of twelve morphotypes, with identifying features listed in Table 4.7. An additional group contains cuticle fragments with cuticle characters different to the twelve morphotypes, but with too few pieces to create a new morphotype.

Morphotype	Feature matrix score										
	Stomatal arrangement	No. of bands	No. of rows in band	Veins	Stomatal orientation	Pellucid dots	Trichome	Stomatal pore ornamentation	Stomata:ED cell size	Stomatal complex type	Surface ornamentation
1	1 or 3				1	0	0	1, 2, 3	1, mainly 2	2	0 sometimes 2 or 3
2	4	1	9-25, average 14	Parallel, 1-3	2	0	0	0	1	2	0
3	2				2	0	0	2?	2	2	5
4	2	1			1 or 3	0	0		2	2	5
5	2	1	10		2	0	0	2	2	2	0
6	1				2	0	0		0 or 1	3	glands
7	1				1 or 2	0	0	0	1 or 2	3	glands, occasionally 2
8	2 or 5	1			1	0	0	0	2	3	glands
9	1				1	1	1	0	0	2?	0
10	4	2	3-6, average 5		2	0	0	0	1 or 2		0 or 5
11	6	2	4-6, average 5		2	0	0		2	2	0
12	3		4-12, average 8		2	0	0			2	0

Table 4.7: Summary of character matrix features defining twelve possible morphotypes, key to cuticle features in Table 4.6 and 4.7.

4.4 Morphotype descriptions

4.4.1 Morphotype 1

Morphotype 1 (Table 4.7) is readily identified by disperse-to-filed stomatal distribution, with sunken stomata protected by varying degrees of stomatal lobes or papillae (Figure 4.6B, C). This morphotype is separated by the Gower distance cluster analysis (Section 4.3.2.1; red branch Figure 4.4), with subclusters representing varying degrees of surface ornamentation (papillate to smooth).

Only the outside and inside cuticle surfaces from one side of the leaf are observed, suggesting that the plant may be amphistomatous (stomata on both leaf surfaces) or the leaf may be hypostomatous (stomata typically on the lower leaf surface only) and the upper cuticle surface was never identified from the Group 4 material at the binning stage (Table 4.1) because it was never found associated with the stomatal side. The cuticle is generally thick, with a strong yellow fluorescence, but the pieces are fragmentary, with no observed leaf margins, tips or bases.

The outside surface of the cuticle reveals a stomatal arrangement in vague rows (Figure 4.6A) or generally dispersed (Figure 4.6B). Typically, stomata are sunken and protected by varying degrees of stomatal papillae (Figure 4.6B) or lobes (Figure 4.6C) which match the number of subsidiary cells. The rest of the outside surface varies across cuticle fragment from smooth (e.g. Figure 4.6C) to varying concentrations of epidermal papillae (Figure 4.6D). Transitioning from smooth to papillate surface is observed on a single cuticle fragment, for which reason this morphotype has not been subdivided on the presence or absence of surface papillae.

Examination of the interior surface of the cuticle reveals randomly orientated cyclocytic stomatal apparatus (ring of smaller cells enclosing guard cells, generally 5-6 subsidiary cells in this case; Figure 4.6E) or, in rare cases, actinocytic (radially elongated ring of cells surrounding guard cells; Figure 4.6F) stomatal apparatus. The epidermal cells are irregular polygon in shape, with wavy cell walls, which are often smaller or similar in size to the stomata.

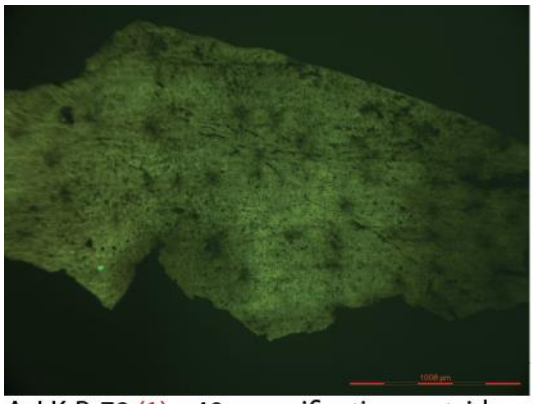

A: LK-B-78 (1), x40 magnification, outside surface (stomatal distribution - rows), 1000 µm

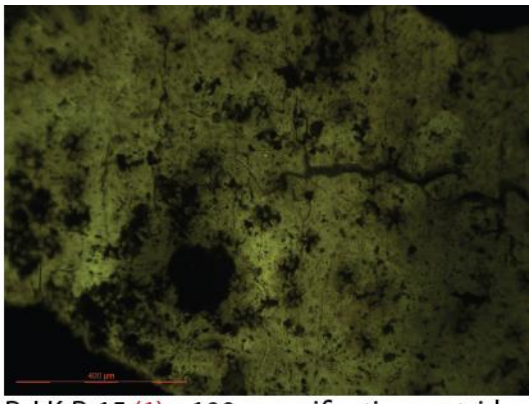

B: LK-B-15 (1), x100 magnification, outside surface (dispersed stomatal distribution and stomatal papillae), 400 µm

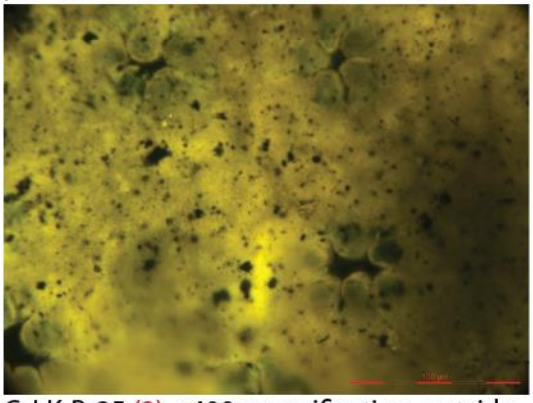

C: LK-B-25 (2), x400 magnification, outside surface (stomatal lobes), 100 µm

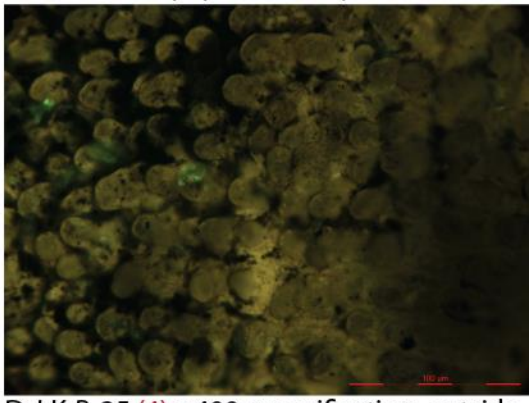

D: LK-B-25 (4), x400 magnification, outside surface (epidermal papillae), 100 µm

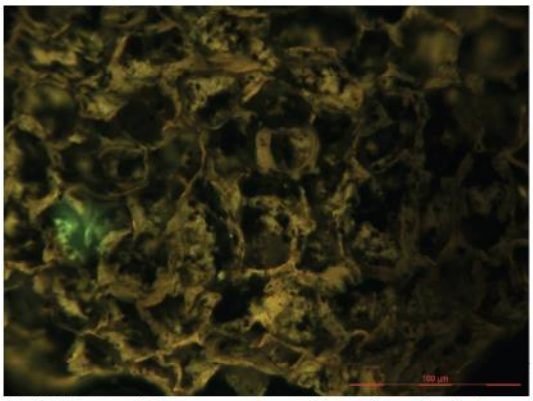

E: LK-B-25 (7), x400 magnification, inside surface (epidermal cells and cyclocytic stomata), 100 µm

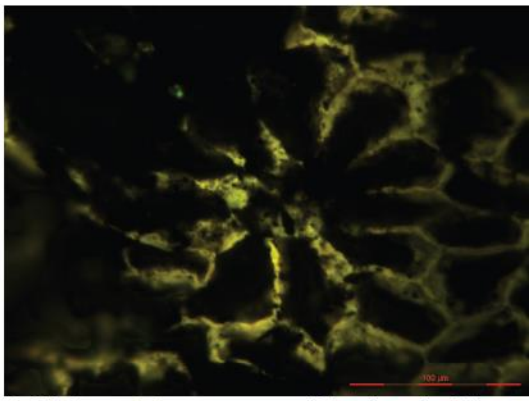

F: LK-B-67 (7), x400 magnification, inside surface (actinocytic stoma), 100 µm

Figure 4.6: Epifluorescence microscope images of morphotype 1 cuticle fragments, labelled with sample name and cuticle piece colour-coded by vial for reference within the character matrix, alongside the image magnification, which cuticle surface was examined, the feature captured in the image and the scale bar length.

4.4.2 Morphotype 2

The clustering process sorted cuticle fragments that possess a single stomatal zone with stomata arranged in files into a single group (Fiii in Figure 4.5). Examination of the cuticle fragments within this group reveal long strap-shaped leaves on the order of 20 mm in length (but never observed complete - leaf bases not observed) and on the order of 4 mm in width, with entire and generally parallel margins with a pointed or mucronate tip (Figure 4.7A, B).

Stomata are present only on one surface (hypostomatic), distributed in a wide central band arranged into rows which vary in number depending on the width of the leaf (typically 9–25 rows). Occasionally, there are gaps between stomatal rows, which may indicate veins running parallel to the leaf axis. The cuticle within the stomatal band is thinner than the rest of the leaf surface and does not fluoresce as strongly (Figure 4.7 A-D). The bright yellow fluorescing margin outside the stomatal band is between 200–300 µm wide. Stomata are flush to slightly sunken with respect to the cuticle surface (Figure 4.7C) but often this cannot be observed due to the poor preservation of the stomatal band cuticle. In these cases, the stomata can only be observed as darker areas, and the epidermal cell detail is lost (e.g. Figure 4.7D). Rarely, the inside surface of the stomatal side can be observed, revealing cyclocytic stomata with winged guard cells (Figure 4.7E). The stomatal complexes are generally a similar size to the epidermal cells, which are more irregular in shape than the rest of the leaf surface; although not as elongate and generally rectangular to irregular polygon in shape with wavy cell walls (Figure 4.7E).

There is no stomatal or surface ornamentation on either side of morphotype 2 (Figure 4.7 A-D, F), except the presence of epiphyllous structures (algal or fungal colonies that were hosted by the leaf surface; Section 5.5). Epidermal cells on the non-stomatal-side and stomatal-side marginal zones are elongate and irregularly rectangular to hexagonal with wavy cell walls (Figure 4.7A, C, F).

In exceptional cases, mesophyll tissue between the two cuticle surfaces is preserved (Figure 4.8), represented by finger-like extensions with brightly fluorescing tips, but dark shafts studded with small (<5 µm) structures which fluoresce less strongly than the tips.

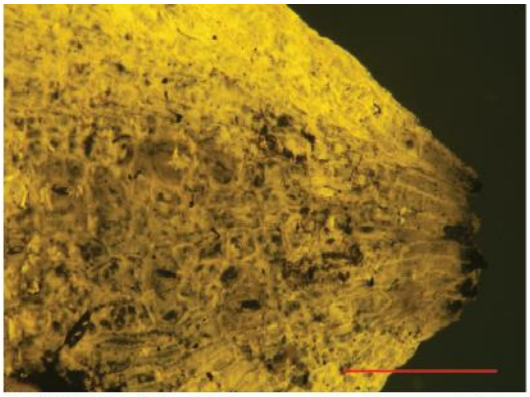

A: LK-B-42 (5), x100 magnification, outside stomatal-side (mucronate tip), 200 µm

B: LK-B-15 (11), x40 magnification, outside stomatal-side (thin cuticle in stomatal band, entire margins), 1000 µm

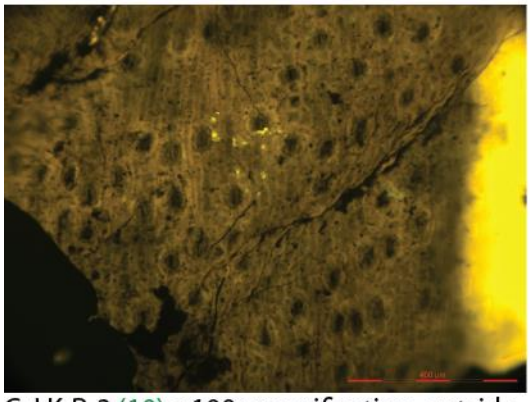

C: LK-B-3 (10), x100 magnification, outside stomatal-side (stomatal arrangement), 400 µm

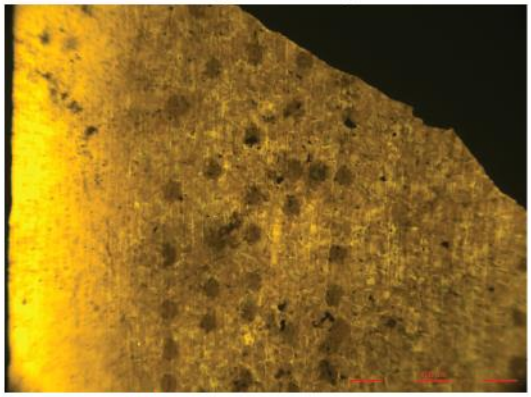

D: LK-B-7 (11), x100 magnification, outside stomatal-side (thin cuticle in stomatal zone), 400 µm

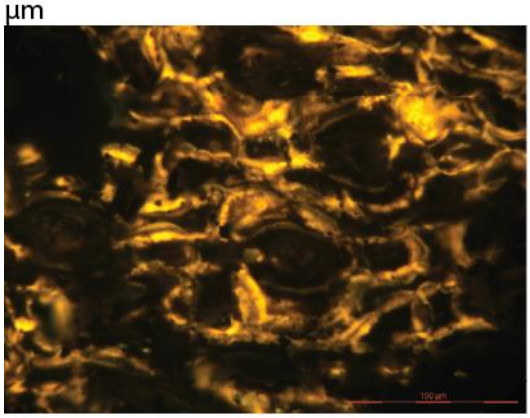

E: RKE-B-105 (3), x400 magnification, inside stomatal-side (cyclocytic stomata with winged guard cells), 100 µm

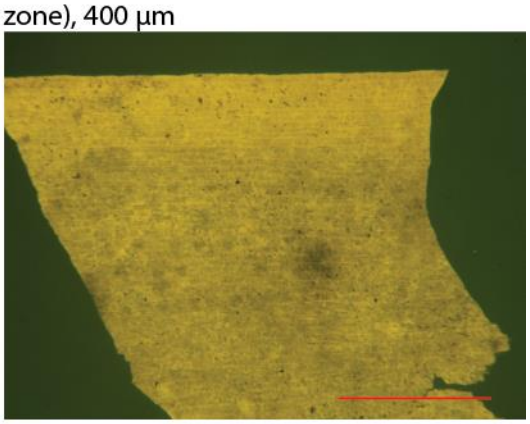

F: LK-B-42 (5), x40 magnification, outside non-stomatal side, 1000 µm

Figure 4.7: Epifluorescence microscope images of morphotype 2 cuticle fragments, labelled with sample name and cuticle piece colour-coded by vial for reference within the character matrix, alongside the image magnification, which cuticle surface was examined, the feature captured in the image and the scale bar length.

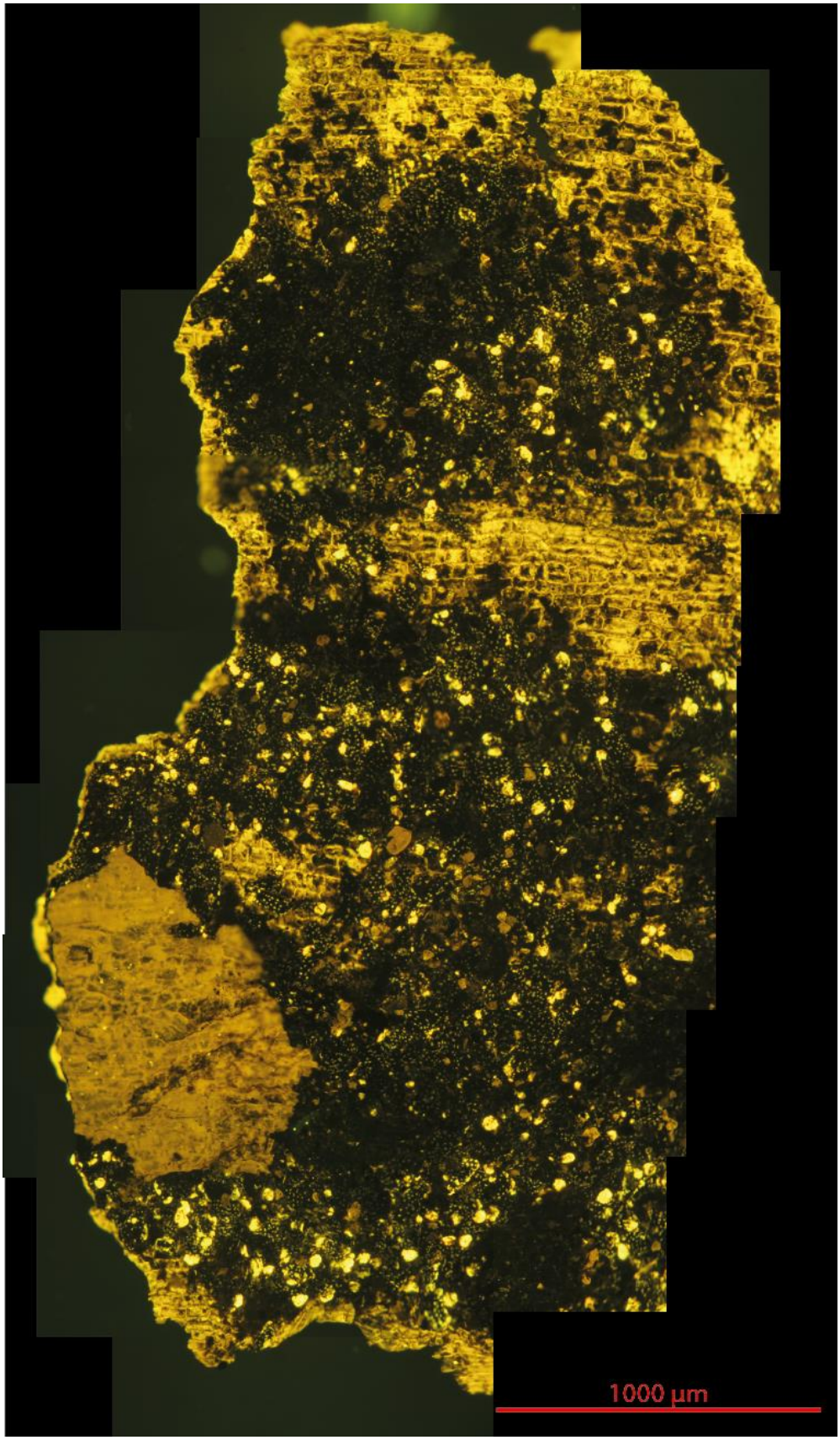

Figure 4.8: Epifluorescence microscope image of morphotype 2 cuticle fragment (LK-B-78 [1]) showing inside non-stomatal-side and outside stomatal side cuticle surfaces with mesophyll tissues preserved between.

4.4.3 Morphotype 3

The character matrix analysis separates cuticle fragments with stomata within a papillose furrow (branch Dv); and further subdivides those with longitudinally aligned stomata (branch Ev; Figure 4.5) which defines morphotype 3.

A: LK-B-42 (2), outside stomatal-side (mucronate tip and stomatal furrow terminating before tip, smooth to tuberculate papillae obscure stomata), 250 µm

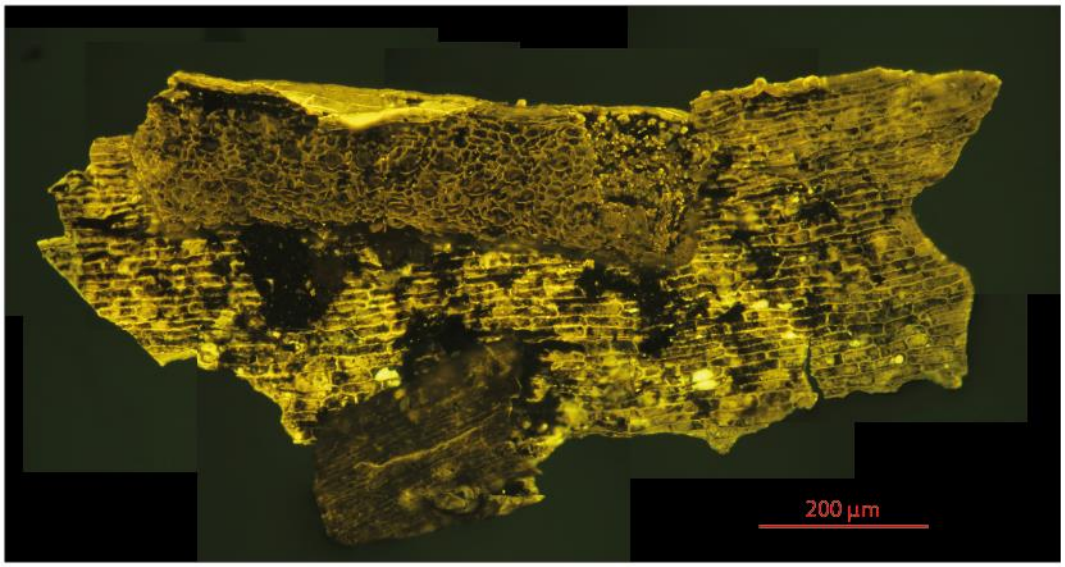

B: RKE-B-128 (2), inside stomatal-side (inside epidermal cell shapes and inside stomatal furrow surface; fold in cuticle reveals outside surface of stomatal furrow revealing tuberculate papillae), 200 µm

Figure 4.9: Epifluorescence microscope images of morphotype 3 cuticle fragments, labelled with sample name and cuticle piece colour-coded by vial for reference within the character matrix, alongside the image magnification, which cuticle surface was examined, the feature captured in the image and the scale bar length.

Cuticle fragments of this morphotype are often found with complete margins, indicating an elongate strap to lancolate-shaped leaf with entire margins and occasionally preserved mucronate tip (Figure 4.9A). The leaf base is never observed, but the leaves are at least 10 mm in length and 5 mm wide. The morphotype is hypostomatous with a characteristic narrow furrow that contains all the stomata, although, they are often obscured by smooth to tuberculate papillae (Figure 4.9B). The interior surface of the stomatal furrow reveals longitudinally orientated stomata parallel to the leaf axis (Figure 4.9B). The small stomata are cyclocytic with winged guard cells and are organised into uneven files. The epidermal cells within the stomatal furrow are irregularly shaped and are around twice to three times smaller than the epidermal cells across the rest of the leaf surface. The exterior of both sides of the leaf is smooth and without ornamentation (save for fossil epiphylls, Section 5.5), with elongate epidermal cells that are rectangular to pentagonal/hexagonal in shape with straight to wavy cell walls (Figure 4.9 A, B).

4.4.4 Morphotype 4

Morphotype 4 is distinguished from morphotype 3 in the character matrix analysis (branch Evi; Figure 4.5) on the basis of stomatal orientation. Morphotypes 3 and 4 are similar in form, sharing thick cuticle and elongate strap-shaped leaf form with entire margins, bearing a single papillose furrow (smooth-to-tuberculate papillae) within which all stomata are contained. However, the leaf tip of morphotype 4 where observed is obtuse, and the leaf base widens into a cylindrical opening (Figure 4.10 A-C) unlike morphotype 3.

Although the epidermal cell morphology on both leaf sides is similar to morphotype 3 (including the smaller irregularly shaped epidermal cells within the stomatal zone), the cyclocytic stomata are more globular in shape, tightly packed into the stomatal zone and are transversely to randomly aligned (Figure 4.10 D-F). On the interior surface of the non-stomatal-side, brightly fluorescing cells may represent preserved resin stores or strings of cutinised material (Figure 4.10G). In one cuticle fragment, mesophyll tissue is preserved (Figure 4.10H), which appears similar to that preserved in fragments of morphotype 2, with tightly packed cells bearing brightly fluorescing tips, which are orientated perpendicular to the non-stomatal-side cuticle surface.

Figure 4.10 (next page): Epifluorescence microscope images of morphotype 4 cuticle fragments, labelled with sample name and cuticle piece colour-coded by vial for reference within the character matrix, alongside the image magnification, which cuticle surface was examined, the feature captured in the image and the scale bar length.

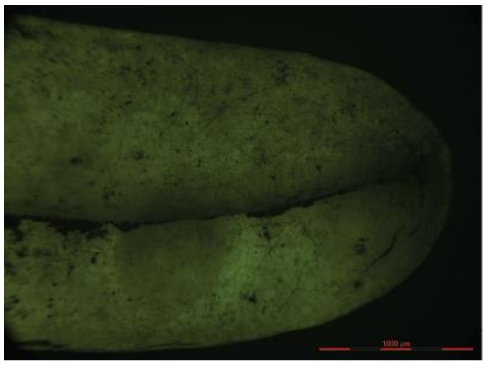

A: RKE-B-35 (1), x40 magnification, outside stomatal-side (rounded tip), 1000 µm

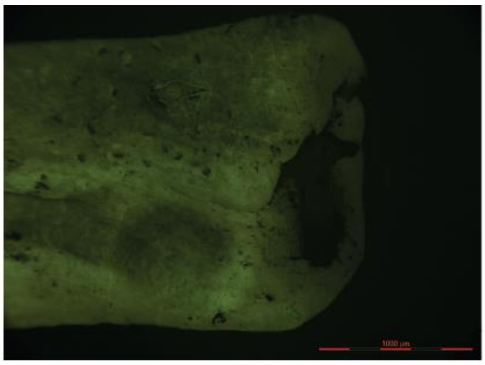

B: RKE-B-35 (1), x40 magnification, outside non-stomatal-side (cylindrical leaf base), 1000 µm

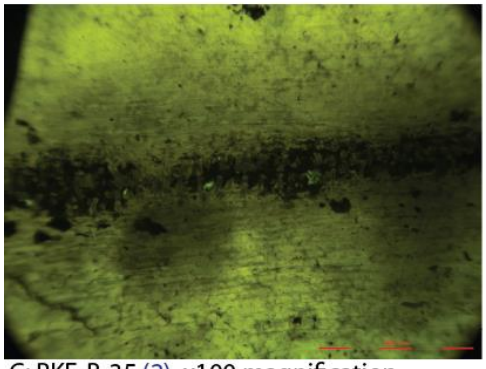

C: RKE-B-35 (2), x100 magnification, outside stomatal-side (smooth to spatulate papillae), 400 µm

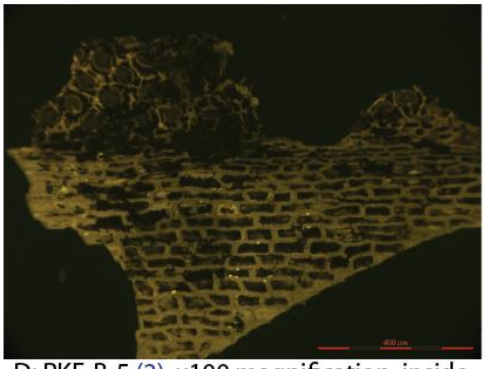

D: RKE-B-5 (2), x100 magnification, inside stomatal-side (aligned stomata in stomatal furrow), 400 µm

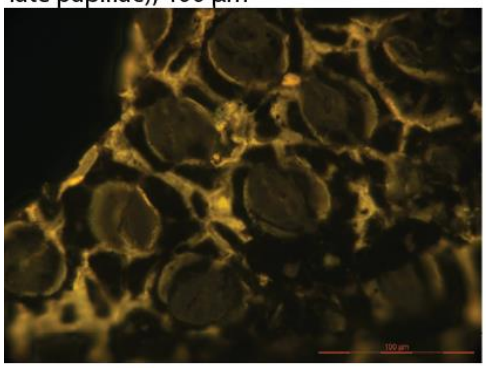

E: RKE-B-5 (2), x400 magnification, inside stomatal-side (cyclocytic stomata with winged guard cells), 100 µm

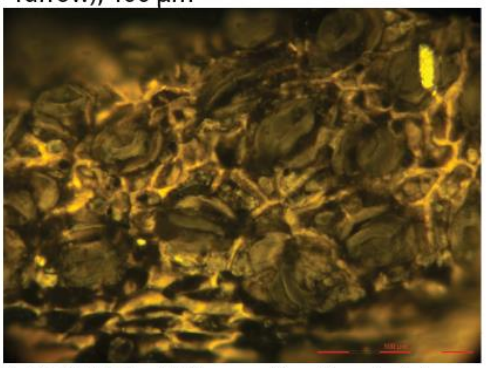

F: LK-B-3 (7), x400 magnification, inside stomatal-side (randomly aligned stomata in furrow), 100 µm

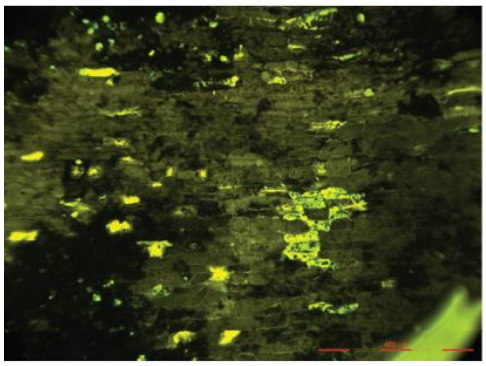

G: RKE-B-35 (4), x100 magnification, inside non-stomatal side (epidermal cell shape), 400 µm

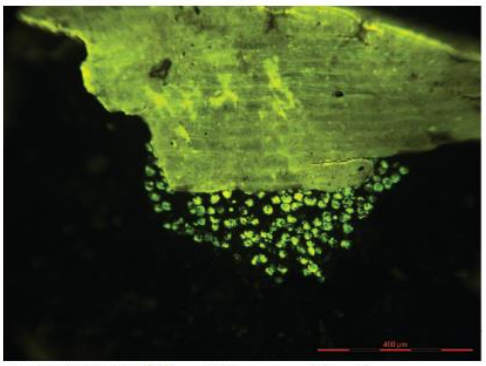

H: RKE-B-35 (5), x100 magnification, outside non-stomatal-side (mesophyll), 400 µm

Whilst only complete character matrix entries were clustered, it became apparent on inspection of the original character matrix and assessment of incomplete entries that mostly morphotypes 3 and 4 cannot be distinguished because the stomatal orientation and leaf tip and base were not always observed; the implications of this are explored in Section 5.2.

4.4.5 Morphotype 5

Morphotype 5 was grouped by the cluster analysis with morphotype 3 (branch Ev, Figure 4.5) but examination of the character matrix reveals why this morphotype should be separate from morphotype 3.

Similar to morphotype 3, morphotype 5 cuticle fragments possess parallel entire margins indicating a leaf width of around 5 mm (the leaf tip nor base are never observed), are hypostomatous with stomata organised into regular files in a single stomatal band. However, the stomatal band is not within a furrow and there are no overarching papillae at the band margins (Figure 4.11A). The epidermal cuticle across the stomatal band is thinner

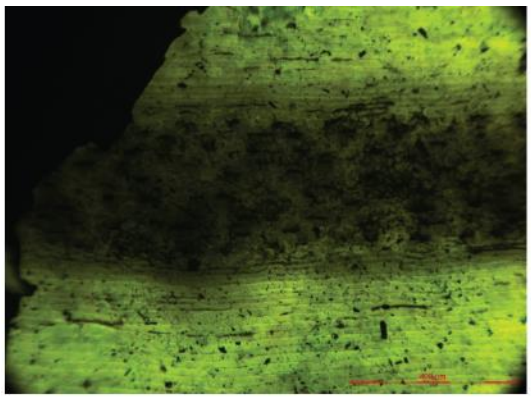

A: LK-B-49 (1), x100 magnification, outside stomatal-side (stomatal groove), 400 µm

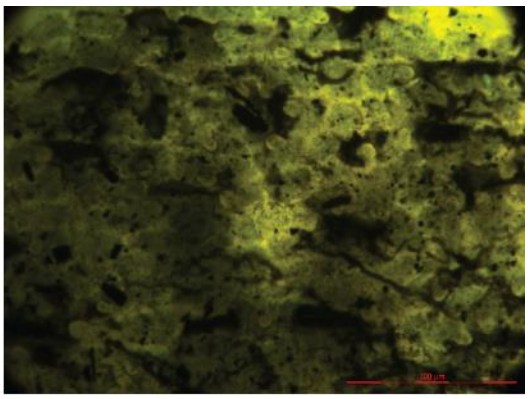

B: LK-B-49 (1), x400 magnification, outside stomatal-side (papillose stomatal rims), 100 µm

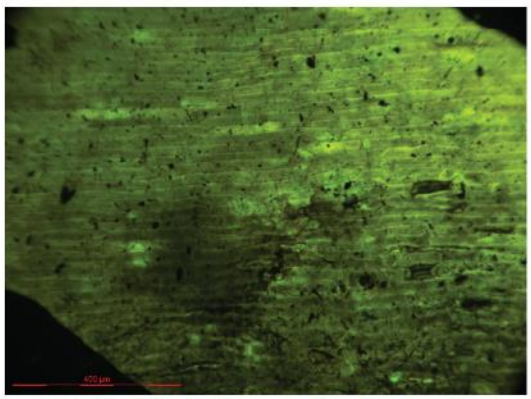

C: LK-B-49 (1), x100 magnification, outside non-stomatal-side (epidermal cell shapes), 400 µm

Figure 4.11: Epifluorescence microscope images of morphotype 5 cuticle fragments, labelled with sample name and cuticle piece colour-coded by vial for reference within the character matrix, alongside the image magnification, which cuticle surface was examined, the feature captured in the image and the scale bar length.

than the rest of the cuticle, like morphotype 2. However, the stomatal band curves into the cuticle surface, and is narrower than those of morphotype 2, with 9 files of stomata observed within a band. The stomata are sunken with slot-like openings and short, smooth papillae extend partially over the stomatal pores (Figure 4.11B). The stomatal complex type cannot be determined because a view of the interior cuticle surface was not available.

The epidermal cells within the stomatal zone are shorter than those outside the stomatal zone, and are square to irregular polygon in shape with wavy cell walls (Figure 4.11B). A few epidermal cells within the stomatal zone bear papillae. On the outside surface of the non-stomatal-side, some epidermal cells appear to fluoresce more brightly than those surrounding, suggesting strings of more cutinised material as identified in other morphotypes (Figure 4.11C).

4.4.6 Morphotype 6

Cuticle fragments separated by the character matrix analysis within branch Civ (Figure 4.5) are different from those of branch Ciii because stomata are not contained within a stomatal band or furrow like morphotypes (3–5) described previously. However, examination of the complete character matrix of samples from this branch reveals two morphotypes (6 and 7).

The outside (non-stomatal?) surface of cuticle fragments of this morphotype do not fluoresce well, and the fragmentary nature precludes identification of leaf shape, tip, base or margin shape. The cuticle is of medium thickness, and fluoresces orange-brown at lower

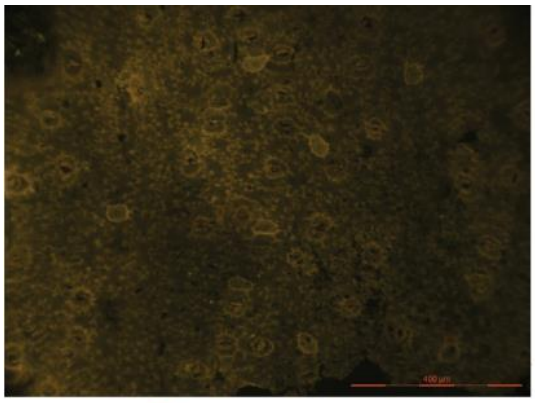

A: RKE-B-44 (1), x100 magnification, outside stomatal-side (stomata and circular structures), 400 µm

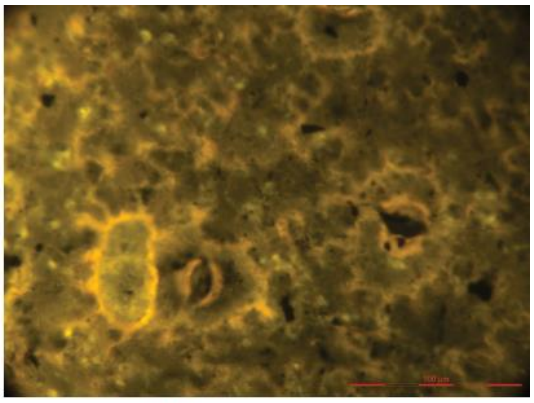

B: RKE-B-44 (1), x400 magnification, outside stomatal-side (paracytic stomata with circular structure), 100 µm

Figure 4.12: Epifluorescence microscope images of morphotype 6 cuticle fragments, labelled with sample name and cuticle piece colour-coded by vial for reference within the character matrix, alongside the image magnification, which cuticle surface was examined, the feature captured in the image and the scale bar length.

magnifications (Figure 4.12A). Stomata are randomly dispersed and orientated, with no obvious venation pattern across the epidermal surface (Figure 4.12A). The stomata are flush with the surface, with paracytic subsidiary cells which have heavily crenulated cell walls much like the rest of the epidermal cells across the leaf surface resulting in very irregular but generally four-sided epidermal cells (Figure 4.12A, B) and the subsidiary cells are occasionally larger on one side than the other (Figure 4.12A). Distributed across the surface (at a lower concentration than the stomata) are oval cells with less crenulated cell walls and slightly brighter fluorescence than the rest of the surface, of a length around 70 µm (Figure 4.12A, B).

4.4.7 Morphotype 7

Morphotype 7 fragments were sorted by the character matrix cluster analysis into branch Civ (Figure 4.5) along with morphotype 6, but comparison of the cuticular features reveals why these morphotypes are separate.

Similar to morphotype 6, the preservation of this apparently hypostomatous morphotype is poor. The outside stomatal-side cuticle is rarely preserved except for the stomata, resulting in an unusual view of the inside of the non-stomatal-side that is studded with stomata (Figure 4.13B, E). Rare examples of the outside stomatal side show that the cuticle is thin and that the epidermal cells are square to rectangular with crenulated cell walls. The stomata are of a similar size to the epidermal cells and are generally flush to slightly sunken with respect to the surface (Figure 4.13A). The stomata are paracytic, rarely hemiparacytic (or uneven subsidiary cell size), of similar appearance to those of morphotype 6: with wide and winged guard cells and crenulated subsidiary cells giving a star-like appearance (Figure 4.13B, C). The stomata are generally aligned but no leaf margins are preserved. The fluorescence of the external non-stomatal-side is poor and epidermal characters are not preserved except for a few pieces of very thin cuticle from which the only identifiable features are the presence of short epidermal papillae and a possible gland structure (oval to round outline, slightly crenulated wall, similar to those identified in morphotype 6) as shown in Figure 4.13D. However, the lack of occurrence of the oval structures on the stomatal side of morphotype 7 was the basis for separating from morphotype 6.

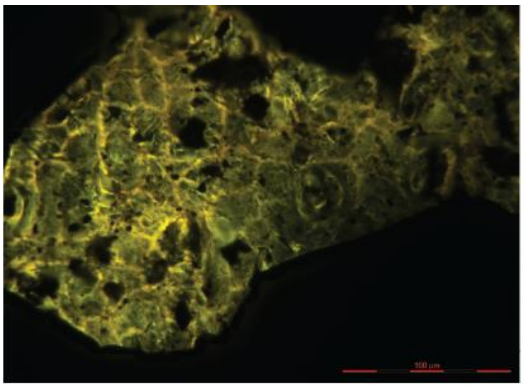

A: RKE-B-119 (6), x400 magnification, outside stomatal-side (epidermal cell shape and stomata), 100 µm

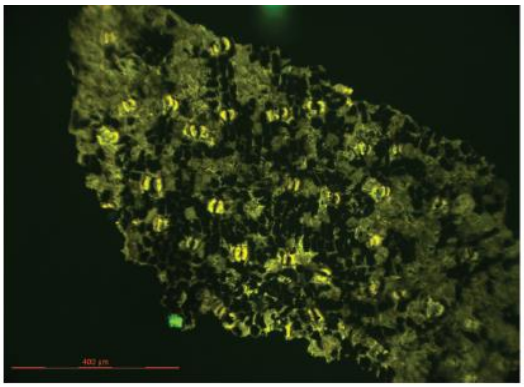

B: RKE-B-119 (3), x100 magnification, inside non-stomatal-side (with aligned stomata only remains of outside ss), 1000 µm

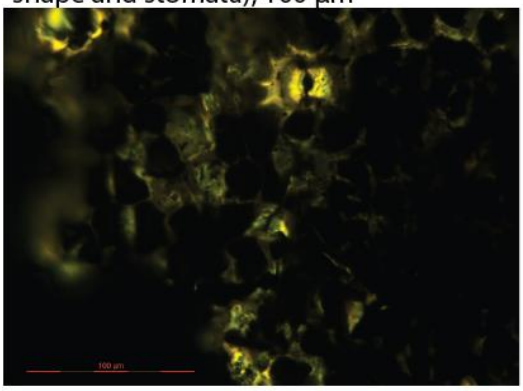

C: RKE-B-119 (5), x400 magnification, outside stomatal-side (paracytic or hemiparacytic stoma), 100 µm

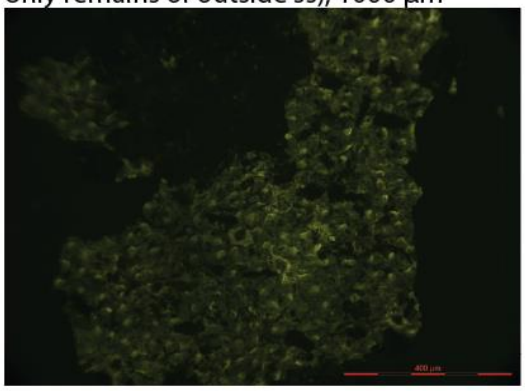

D: LK-B-9 (1), x100 magnification, outside non-stomatal-side (epidermal papillae and circular structures), 400 µm

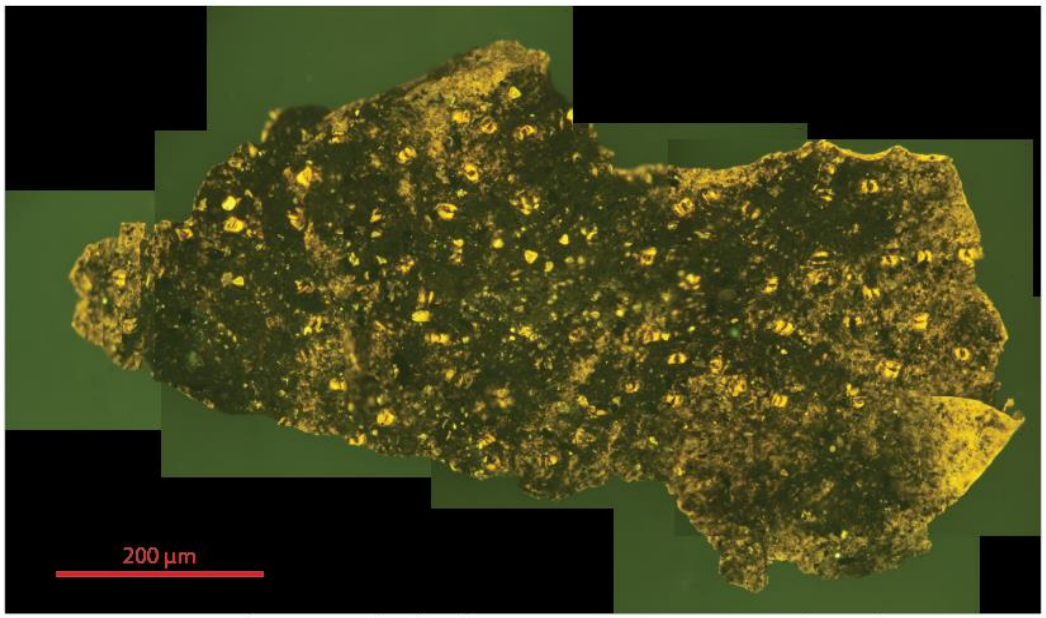

E: LK-B-28 (1), outside stomatal-side (showing poor preservation of cuticle - stomata studded in mesophyll), 200 µm

Figure 4.13: Epifluorescence microscope images of morphotype 7 cuticle fragments, labelled with sample name and cuticle piece colour-coded by vial for reference within the character matrix, alongside the image magnification, which cuticle surface was examined, the feature captured in the image and the scale bar length.

4.4.8 Morphotype 8

Cuticle fragments assigned to morphotype 8 are part of the Eiii branch (Figure 4.5) which was found to contain conflicting cuticle features which did not readily relate to a single morphotype (Section 4.3.2.2), highlighting the use of cluster analyses as an explorative tool. Since the paracytic stomatal complex identified in morphotypes 6 and 7 are particularly distinctive, cross-referencing to the original character matrix located the cuticle fragments sharing this stomatal type. Instead of being assigned to morphotypes 6 or 7, however, there are sufficiently different features to separate these fragments into an additional morphotype (8).

Only the external surfaces of this morphotype are preserved, and are found to be of medium thickness, with entire and parallel margins indicating a likely elongate leaf shape despite the fact that the leaf tips and based are not observed (Figure 4.14A, B).

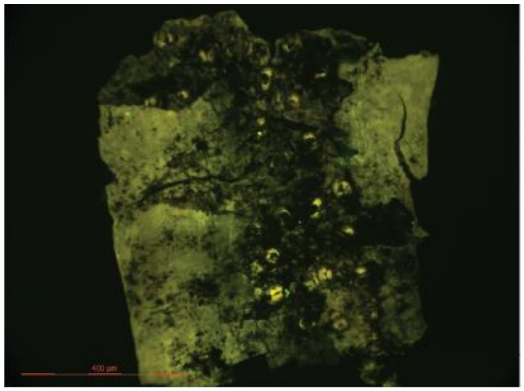

A: LK-B-28 (2), x100 magnification, outside stomatal-side (stomatal furrow), 400 µm

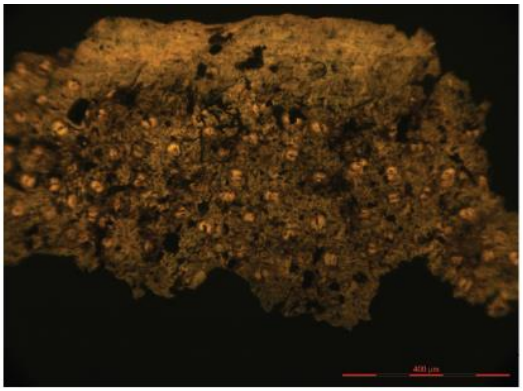

B: LK-B-49 (5), x100 magnification, outside stomatal-side (central stomatal band), 400 µm

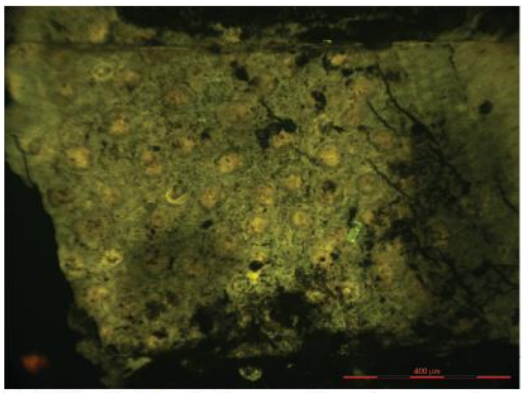

C: LK-B-81 (3), x100 magnification, outside non-stomatal-side (circular structures and pink colouration areas), 400 µm

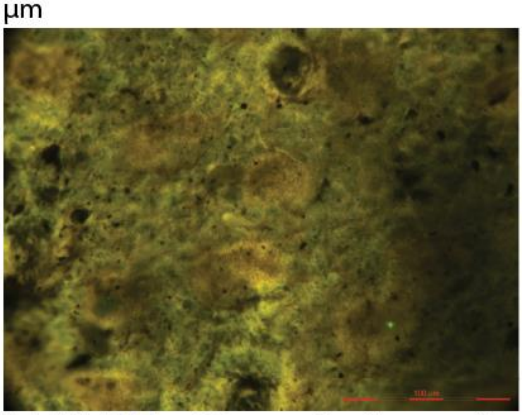

D: LK-B-49 (4), x400 magnification, outside non-stomatal-side (possible hair bases and pink areas), 100 µm

Figure 4.14: Epifluorescence microscope images of morphotype 8 cuticle fragments, labelled with sample name and cuticle piece colour-coded by vial for reference within the character matrix, alongside the image magnification, which cuticle surface was examined, the feature captured in the image and the scale bar length.

Stomata are observed on one side only (hypostomatous) and are randomly orientated within a stomatal zone running parallel to the leaf long axis, which varies from a distinct stomatal furrow (Figure 4.14A) to a stomatal zone apparently flush with the rest of the leaf surface (very rare; Figure 4.14B). The stomata are paracytic, sharing morphology with morphotypes 6 and 7 (Figure 4.14A, B). The epidermal cell morphology cannot be distinguished within the stomatal zone except that the cell walls are likely crenulate. Epidermal cells across the rest of the stomatal-side surface are generally square to elongate rectangular with the long axis parallel to the stomatal zone with crenulated cell walls (Figure 4.14A, B) and the surface is otherwise smooth.

The outside cuticle surface of the non-stomatal side shows generally square epidermal cells with crenulated cell walls, with circular to oval outlines sparsely dispersed across the surface possibly indicating hair bases or gland structures, in addition to unusual pink/orange fluorescing circular areas of slightly larger size (Figure 4.14C, D). However, comparison of the density of the larger pink/orange fluorescing areas to the stomatal density on the reverse side of the leaf indicates this may be a preservational effect on the cuticle of the non-stomatal side. Closer examination reveals no relief expression of these areas (Figure 4.14D).

4.4.9 Morphotype 9

Whilst cuticle fragments of morphotype 9 are rare (Section 5.2) they are sufficiently different that the cluster analysis consistently separated this group (Figures 4.4, 4.5). Generally, only one surface of the fragments fluoresces, with the reverse side likely comprising mesophyll tissue with no structural details preserved. The cuticle is thin and fluoresces green (Figure 4.15A) unlike the other morphotypes described (e.g. morphotypes 1–5), which may in part reflect the difference in cuticle thickness and/or the chemical composition of the cuticle. Since only one side of the leaf fluoresces, it is unknown if this morphotype is amphistomatous or hypostomatous.

The epidermal cells are irregular polygons in shape with straight cell walls (Figure 4.15B-D). Stomata are dispersed across the surface, and are randomly orientated and flush with the leaf surface, with simple slot-like openings, which are small compared to the epidermal cell size (Figure 4.15C, D). The inside surface of the cuticle cannot be examined; however, the stomata appear to be cyclocytic with possible amphicyclocytic forms (Figure 4.15D).

The outside surface of the cuticle is predominantly smooth, with venation of likely second order visible on the larger fragments (Figure 4.15A). Brightly fluorescing circular structures

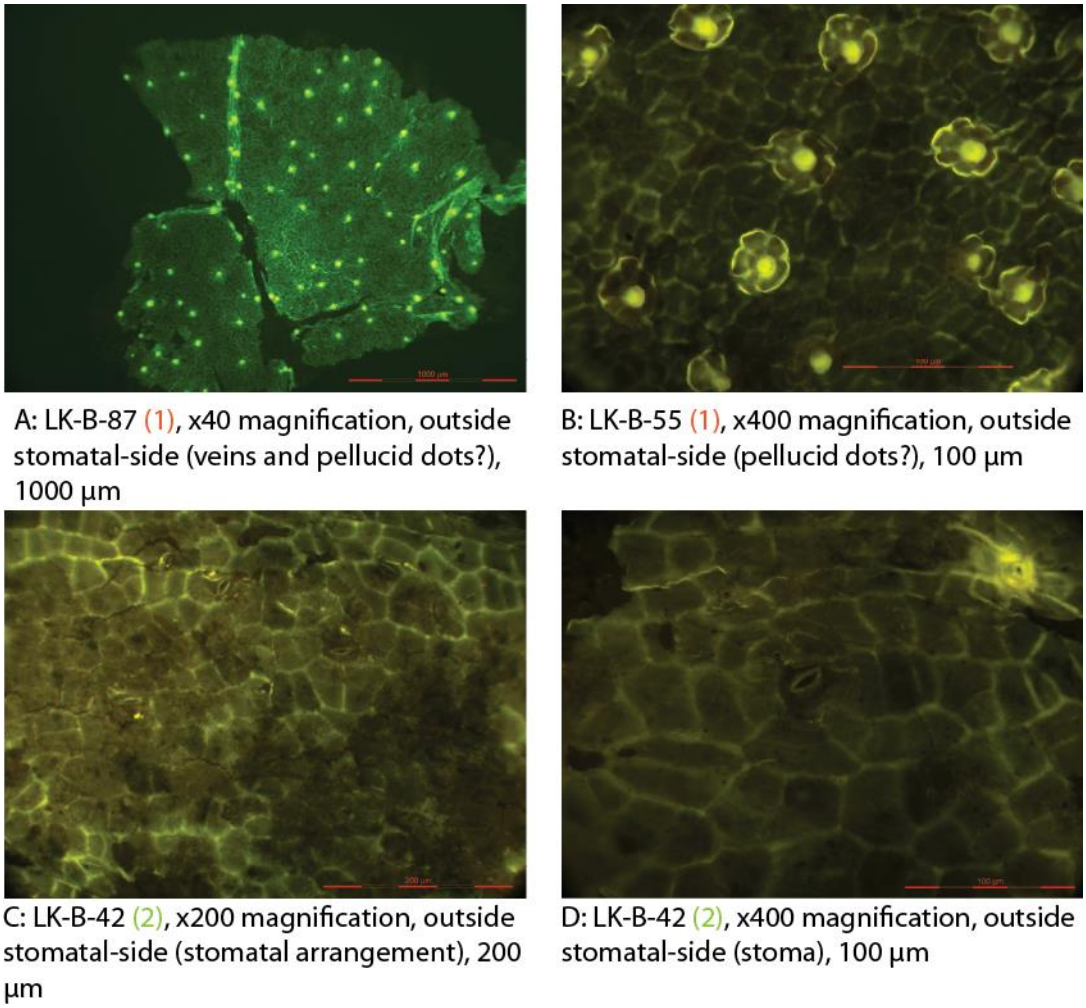

A: LK-B-87 (1), x40 magnification, outside stomatal-side (veins and pellucid dots?), 1000 µm

B: LK-B-55 (1), x400 magnification, outside stomatal-side (pellucid dots?), 100 µm

C: LK-B-42 (2), x200 magnification, outside stomatal-side (stomatal arrangement), 200 µm

D: LK-B-42 (2), x400 magnification, outside stomatal-side (stoma), 100 µm

Figure 4.15: Epifluorescence microscope images of morphotype 9 cuticle fragments, labelled with sample name and cuticle piece colour-coded by vial for reference within the character matrix, alongside the image magnification, which cuticle surface was examined, the feature captured in the image and the scale bar length.

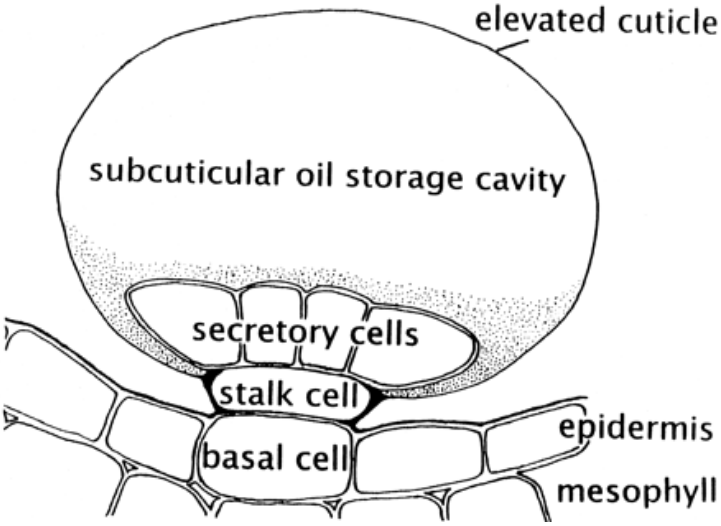

Figure 4.16: Cartoon cross-section of a peltate glandular trichome from Turner et al. (2000).

of about 30–40 µm diameter of two types are observed (Figure 4.15B, D), which were described in the character matrix as pellucid dots (or other glandular structure) and formed the basis of the separation of this morphotype from others in the character matrix analysis (Figures 4.4 and 4.5). The first type has a brightly fluorescing central spot and a rosette of outer cells and appear to be similar to peltate glandular trichomes (Figure 4.16), whereby the oil storage cavity is not preserved, revealing a stalk cell and the rosette-like secretory cells standing proud of the epidermis (Turner *et al.*, 2000).

Other brightly fluorescing structures appear simpler in construction, with no clearly defined outer rosette of cells, and may represent trichomes or capitate oil glands (e.g. Figure 4.15D) rather than pellucid dots specifically which are oil glands within the mesophyll (Barclay, 2011). However, the similar brightness of fluorescence in the same fashion as pellucid dots would suggest from a compositional point of view these structures are more glandular in origin than hair bases (Barclay, 2007).

4.4.10 Morphotype 10

In the process of exploring the less certain morphotype divisions from branch Cii (Figure 4.5), which contains cuticle fragments bearing stomata arranged into files, clear morphotypes based on the grouping of stomata either in two bands (morphotypes 10 and 11) or in files across the surface (morphotype 12) were identified through consultation and comparison with the original character matrix. The lack of resolution of these morphotypes through the cluster analysis likely reveals the issue of over-generalising the simplified character matrix and presents the fine balance of detail required for a successful cluster analysis (whereby too much detail results in too many clusters). Nonetheless, the basic grouping of the material into stomatal arrangement provides the starting point for identification of these final three morphotypes.

Morphotype 10 has hypostomatous leaves with thick cuticle and entire margins that are close to parallel suggesting the leaf is generally elongate, but the shape tapers towards the mucronate tip (Figure 4.17A). Stomata are organised in two stomatal bands, which are approximately a quarter of the leaf width each, around 250 µm wide (Figure 4.17A). There are around 6 files of stomata within each band, with stomata orientated with the long axis parallel to the leaf long axis, and are irregularly spaced along the length of the file (Figure 4.17B).

Stomata are simple in shape and generally slightly sunken into the surface, but the subsidiary cell arrangement cannot be determined from the pieces examined, but the

stomata appear to be of a similar size to the few, generally rectangular epidermal cells with wavy walls visible in the stomatal zone (Figure 4.17B). Epidermal cells across the rest of the leaf surface are elongated and rectangular in shape with wavy cell walls (Figure 4.17B).

In some cases, the epidermal cells bear short papillae in the stomatal zone which gives the rectangular elongate filed arrangement a ribbed-like texture in the stomatal zone where stomatal rims are raised but smooth (Figure 4.17C).

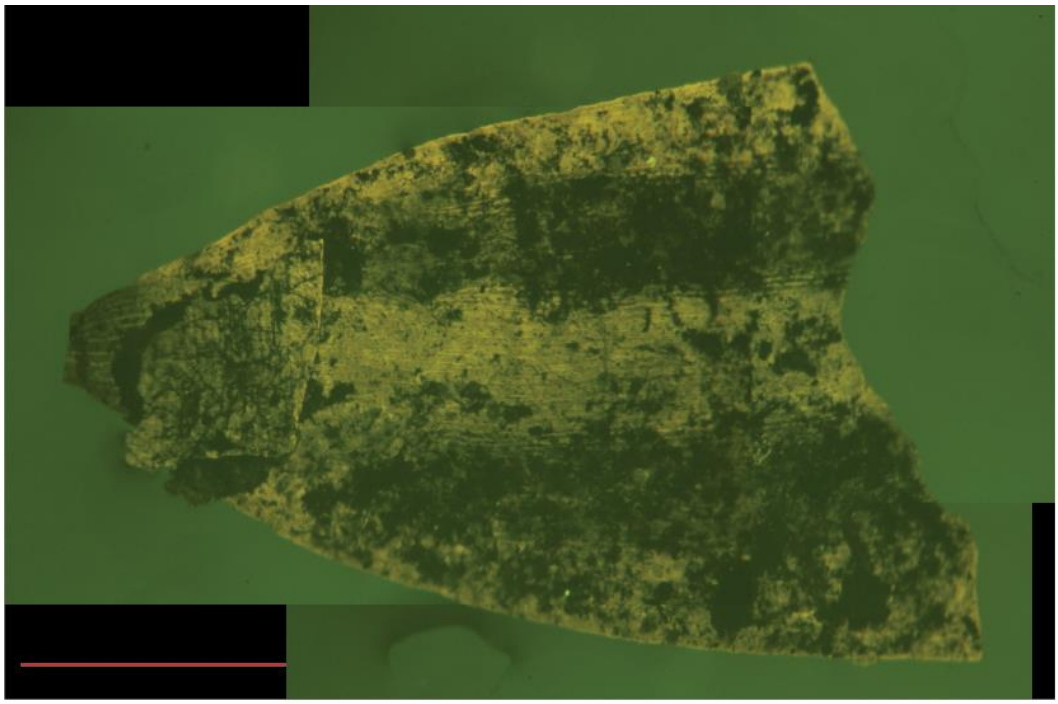

A: LK-B-3 (1), x40 magnification, outside stomatal-side (two stomatal bands and mucronate tip), 500 µm

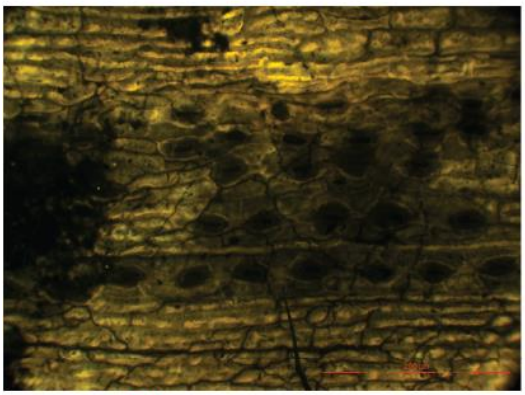

B: LK-B-3 (11), x200 magnification, outside stomatal-side (stomatal arrangement), 200 µm

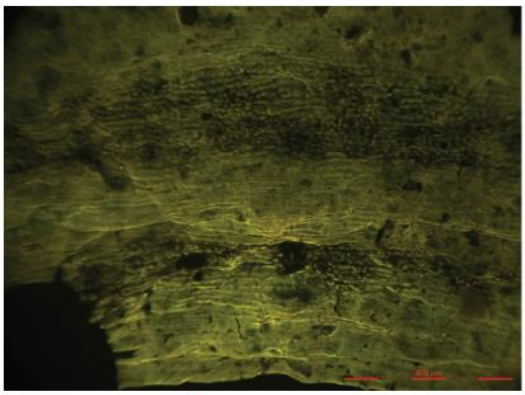

C: RKE-B-128 (8), x100 magnification, outside stomatal-side (two stomatal bands with papillose texture), 400 µm

Figure 4.17: Epifluorescence microscope images of morphotype 10 cuticle fragments, labelled with sample name and cuticle piece colour-coded by vial for reference within the character matrix, alongside the image magnification, which cuticle surface was examined, the feature captured in the image and the scale bar length.

4.4.11 Morphotype 11

Morphotype 11 is separated from branch Cii (Figure 4.5) from cross-referencing of features with the full character matrix. Fragments of this type are rare and similar in shape to other strap-shaped morphotypes (e.g. morphotype 10) with thick cuticle, and are likely elongate leaves, at least 2 mm wide. The entire margins taper towards the mucronate leaf tip (Figure 4.18A).

However, this morphotype is readily identified from other morphotypes by the hypostomatous stomatal zone comprising approximately one third of the leaf; which is distinctly divided into two by a poorly fluorescing central groove approximately 150 µm wide, running parallel to the leaf axis (Figure 4.18A). Stomata are organised into approximately 9 files per band, with the long axis orientated parallel to the leaf margin, and are sunken into the surface with simple slot-like openings orientated parallel to the leaf axis (Figure 4.18B). The stomatal complex type cannot be determined from the external surface, and the epidermal cell preservation is not clear but appears to be smaller than the epidermal cells outside the stomatal zone and less regular in shape with wavy cell walls (Figure 4.18B). The external cuticle surface is smooth but host to epiphyllous structures (Section 5.5); the epidermal cells outside of the stomatal zone are generally elongate rectangular with wavy to slightly crenulated cell walls (Figure 4.18B) and the epidermal cells within the mid-leaf groove are narrower and more pentagonal to hexagonal.

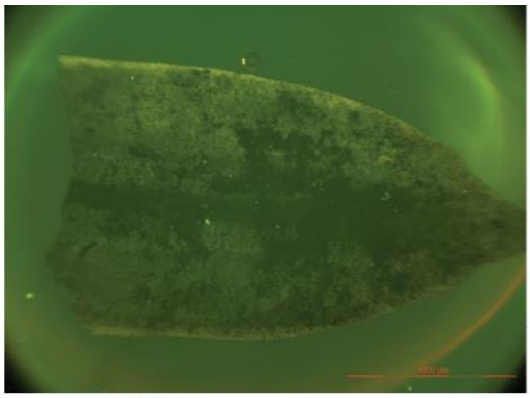

A: LK-B-3 (14), x40 magnification, outside stomatal-side (pointed to mucronate tip, rows of stomata either side of groove), 200 µm

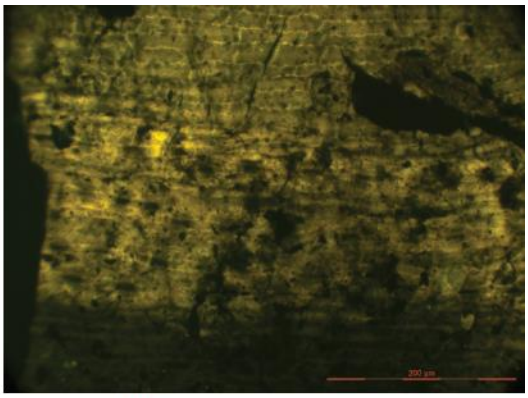

B: LK-B-3 (14), x200 magnification, outside stomatal-side (6 rows of stomata in band above groove), 200 µm

Figure 4.18: Epifluorescence microscope images of morphotype 11 cuticle fragments, labelled with sample name and cuticle piece colour-coded by vial for reference within the character matrix, alongside the image magnification, which cuticle surface was examined, the feature captured in the image and the scale bar length.

4.4.12 Morphotype 12

Morphotype 12 is separated from branch Cii (Figure 4.5) from cross-referencing of features with the full character matrix. Morphotype 12 fragments are characterised by amphistomatous strap-shaped leaves of unknown length but around 1 mm width (Figure 4.19A), which may originally have been needle-like in nature given the lack of leaf margin differentiation observed in other morphotypes (e.g. morphotype 2) and the continuation of cuticle characters on both sides. Only the outside surfaces are preserved, and the cuticle is fairly thin but smooth, with stomata arranged into evenly spaced files which continue across both leaf sides. The epidermal cells within the file appear to fluoresce more brightly than the rest of the cuticle surface (Figure 4.19A) and are slightly less regular in shape, shorter and less narrow than those outside of the files which are elongate hexagonal. All epidermal cells present wavy cell walls (Figure 4.19B). Stomata are unevenly spaced within the files, and slightly sunken into the cuticle surface, possessing five inflated-looking cyclocytic subsidiary cells (Figure 4.19B). The size of the stomata relative to the epidermal cells could not be determined.

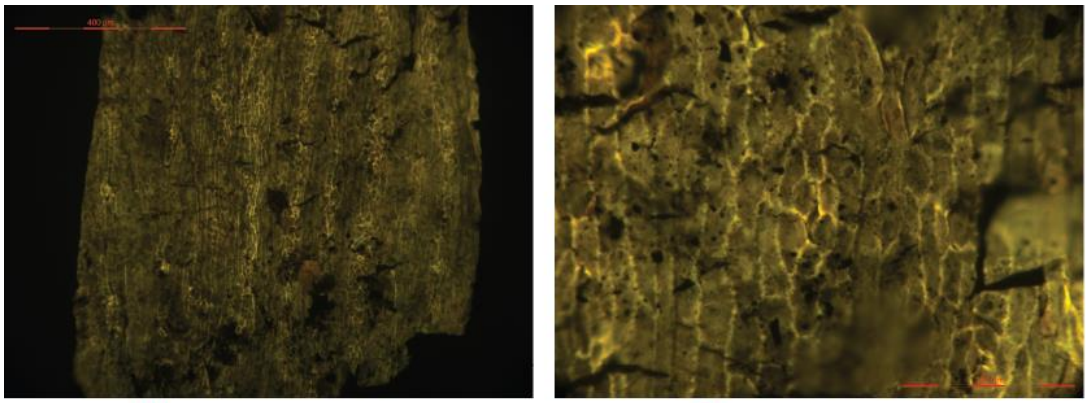

A: LK-B-42 (3), x100 magnification, outside stomatal-side (rows of stomata), 400 µm

B: LK-B-42 (3), x400 magnification, outside stomatal-side (stomata), 100 µm

Figure 4.19: Epifluorescence microscope images of morphotype 12 cuticle fragments, labelled with sample name and cuticle piece colour-coded by vial for reference within the character matrix, alongside the image magnification, which cuticle surface was examined, the feature captured in the image and the scale bar length.

4.5 Morphotype identification

The identified morphotypes (Table 4.7) were compared to published plant and cuticle descriptions, in particular to the work of Boyd (1998 a-c, 2000; 2004), to assign, where possible, plant types to the morphotypes.

4.5.1 Morphotype 1 (Cheirolepidiaceae)

Based on the unusual stomatal projections (papillae and lobes), morphotype 1 is compared to Cheirolepidiaceae conifers, some of which have been observed to possess such stomatal projections (Watson, 1977, 1988; Alvin *et al.* 1981; Haworth *et al.,* 2005; Aucour *et al.*, 2008; Passalia, 2009). Furthermore, Cheirolepidiaceae (*Cupressinocladus*) have previously been identified in Cretaceous samples from West Greenland by Seward (1927). There are seven main genera of Cheirolepidiaceae conifers (Watson, 1988): *Brachyphyllum* Lindley and Hutton *ex* Brongniart (in part); *Cupressinocladus* Seward (in part); *Frenelopsis* Schenk; *Hirmeriella* Hörhammer; *Pagiophyllum* Heer (in part); *Pseudofrenelopsis* Nathorst; and *Tomaxellia* Archangelsky.

Descriptions of *Pseudofrenelopsis* species (Watson, 1977, 1988) appear to closely resemble the material described in the present study by having thick cuticle, stomata organised into well-defined to scattered arrangements depending on leaf form (open or closed), normally possessing 5–6 subsidiary cells (more rarely up to 9), with papillae around the rim of the stomatal pit but no papillae inside the pit. Watson acknowledged the variety of form between species of *Pseudofrenelopsis* regarding the rim of the stomatal pit, the degree to which the rim of the stomatal pit was raised, and the epidermal cell papillae which varied from none to very long hairs. Comparison of *Pseudofrenelopsis* and other Cheirolepidiaceae to the present study material reveals consistent similarities including the generally large stomatal complex with respect to the epidermal cells, which are irregular polygon in shape like those of the present study morphotype (Figure 4.20A compared to Figure 4.20B). The stomatal rim of morphotype 1 material is generally (but not exclusively) flush with the cuticle surface; which is similar to another Cheirolepidiaceae, *Frenelopsis*, described by Watson (Figure 4.20C compared to Figure 4.20D).

The most certain way to distinguish between genera of Cheirolepidiaceae is by examination of shoots, whereby the scale-like leaves are radially attached around the rachis with varying leaf form (Figure i, Appendix C), but unfortunately no identifiable shoots were observed in the macrofossil samples collected from West Greenland. Despite this, the similarity of cuticle features of Morphotype 1 to the Cheirolepidiaceae conifers of Watson (1977, 1988) and Alvin *et al.* (1981) suggests morphotype 1 can be assigned to the Cheirolepidiaceae with confidence.

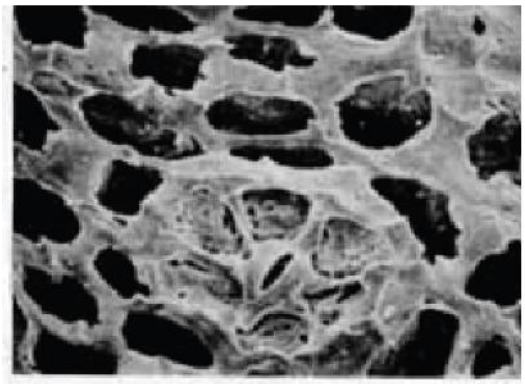

A: *Pseudofrenelopsis varians* inside surface showing stomatal complex with 6 subsidiary cells

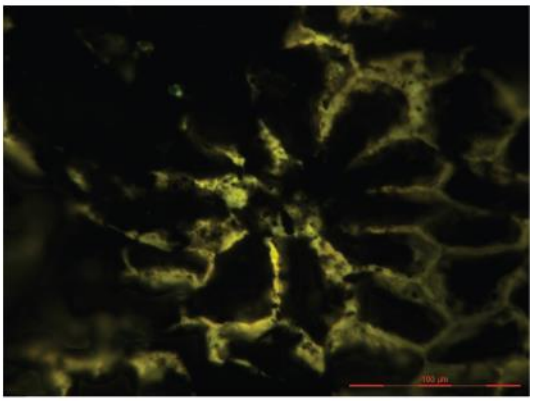

B: LK-B-67 (7), x400 magnification, inside surface (actinocytic stoma), 100 µm

C: *Frenelopsis alata* showing smooth outside surface with stomatal lobes

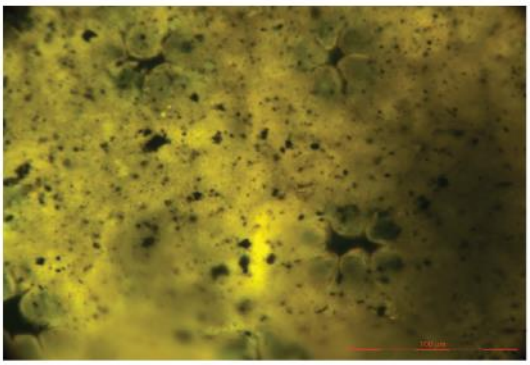

D: LK-B-25 (2), x400 magnification, outside surface (stomatal lobes), 100 µm

Figure 4.20: Comparison of morphotype 1 (Figures B and D) to Cheirolepidiaceae conifers from Watson (1988), showing A: Pseudofrenelopsis internal cuticle surface and stomatal apparatus, and C: Frenelopsis exterior cuticle surface showing stomatal pits with papillae.

4.5.2 Morphotypes 2–5 (Miroviaceae)

Bose and Manum (1990) studied extinct Cretaceous conifer leaves with a single central stomatal band similar to morphotypes 2–5, from high palaeolatitudes, including West Greenland. Since these fossil plants are only known from foliage, the family name, Miroviaceae, defined by Bose and Manum (1990) comprises form-genera (Watson *et al.*, 2001), including: *Holkopitys* Bose and Manum; *Sciadopityoides* Sveshnikova emend.; *Mirovia* Reymanówna emend.; *Oswaldheeria* Bose and Manum; and, later, a fifth genus (Bose and Manum, 1991), *Tritaenia* Maegdefrau and Rudolf. However, based on more recent observations of Miroviaceae leaf anatomy (Gordenko, 2007) and the abundance of Miroviaceae within the Greenland material (Section 5.2), the divisions of the family Miroviaceae from Bose and Manum (1990, 1991) are likely representative of a distinct plant type.

4.5.2.1 Morphotype 2 (Oswaldheeria)

Descriptions of *Oswaldheeria* species by Bose and Manum (1990) and *Oswaldheeria exima* sp. nov by Gordenko (2007) closely match the description of cuticle from morphotype 2, including the long linear hypostomatous leaves with mucronate tips, and a thick adaxial cuticle with elongate pentagonal cells with straight boundaries. On the abaxial surface, monocyclic stomata are organised into longitudinal rows and are longitudinally aligned to the leaf axis, similar to morphotype 2 (compare Figure 4.21 A-C to Figure 4.21E, F). The stomata are slightly sunken into the surface (Figure 4.21A, B) and have winged guard cells (Figure 4.21C). The shape of the epidermal cells within the stomatal zone and in the lower surface margins match the description of the leaf cuticle of morphotype 2, as does the

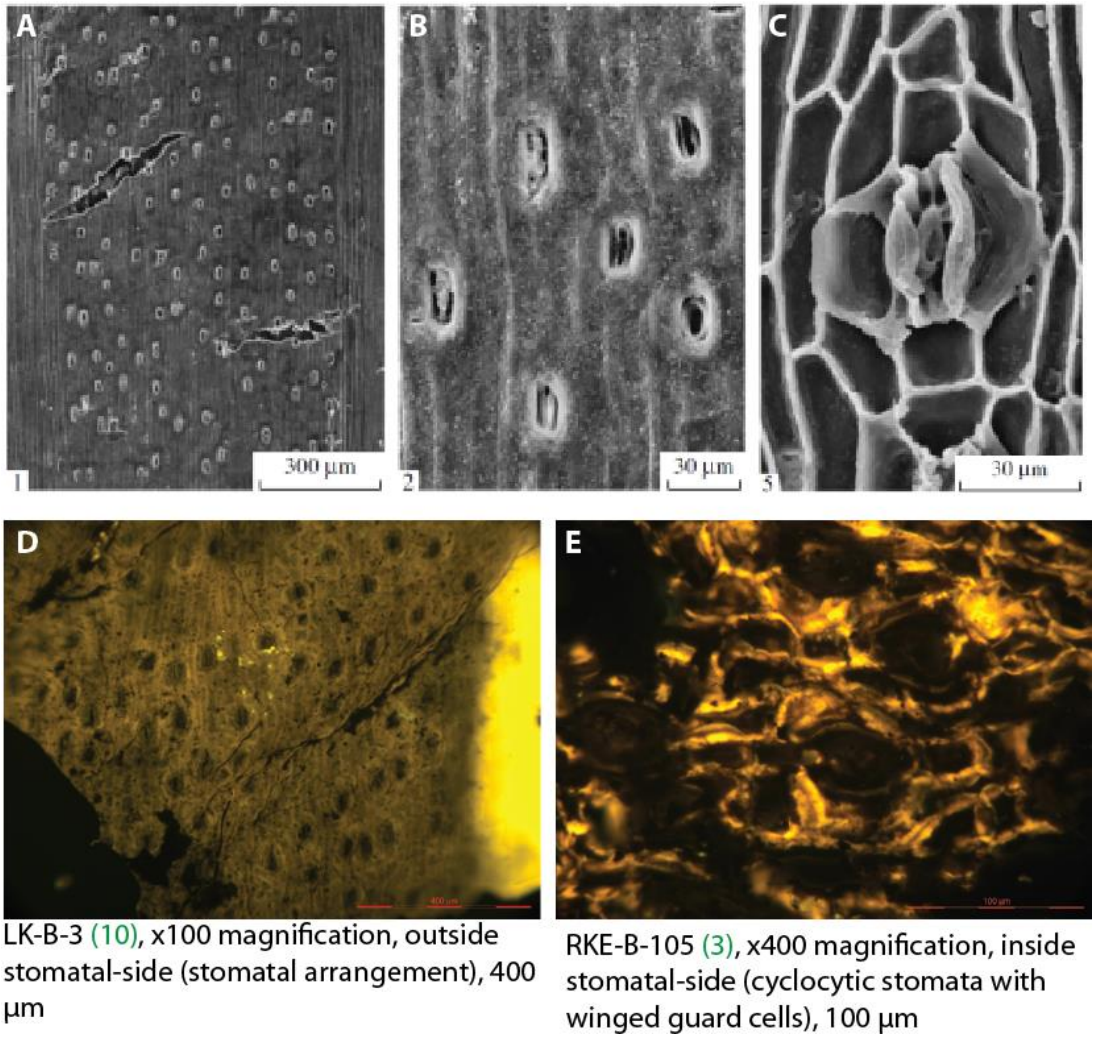

Figure 4.21: SEM images of Oswaldheeria exima from Grodenko (2007) showing A: outside lower surface showing stomata arranged into single broad zone, generally arranged in files and orientated parallel to the leaf long axis; B: close up of outside surface showing slightly sunken stomata; C: inside surface showing stomatal apparatus with winged guard cells. Comparison to present study morphotype 2 material D: stomatal arrangement, E: stomatal apparatus.

typical width of the lower surface margin (Gordenko, 2007). Preserved mesophyll tissue has been discovered previously for fossil plant samples (e.g. Chandrasekharam, 1972; Logan *et al.*, 1993; Axsmith *et al.*, 1998; Narkhede and Khursel, 2013) and comparison to extant plants has led to the view that many gymnosperms have differentiated mesophyll tissues of palisade and spongy parenchyma forms, like angiosperms (Dickison, 2000). Given the uncertain affinity of the Miroviaceae family, the potential to reveal additional anatomical information from the mesophyll tissue is particularly interesting.

A new species, *Oswaldheeria exima,* from the Kursk region, described by Gordenko (2007) also had exceptional preservation as seen in SEM images (Figure 4.22 A, B). These images reveal that the leaf had two conducting bundles, confirming the early inference of this form by Bose and Manum (1990). Gordenko (2007) also revealed that the conducting bundles are not analogous to modern *Sciadopitys* (which Bose and Manum compared he Miroviaceae to) because they are not inverted, supporting the notion that the leaf had multiple veins. Observations made on the morphotype 2 cuticle fragments further support this assertion. Finger-like projections in the mesophyll tissues observed in the West Greenland material closely resemble the mesophyll cells observed in *Oswaldheeria exima* (compare Figure 4.22B with Figure 4.22C and Figure 4.8).

The apparent auto-fluorescence of the mesophyll tissue in the cuticle is interesting when compared to the structure of the mesophyll cells of *Oswaldheeria exima*, which appear in many cases to be porous. This may suggest that the small green/yellow studs on the finger-like projections in Figure 4.22C represent auto-fluorescing material that fills the pores. These pores, therefore, may be the original site of plastids, perhaps chloroplasts (or other plastid types (e.g. those responsible for cuticle production, which could explain the fluorescence colour). The colour of the mesophyll fluorescence is similar to the rest of the cuticle suggesting it is compositionally similar and of a similar age (Section 4.2.2) and therefore may be original material that has been lost in other examples (e.g. Gordenko, 2007). The cause of the bright fluorescence in the tips of the mesophyll cells in the present

Figure 4.22 (next page): SEM images of Oswaldheeria exima from Gordenko (2007), A: transverse section of a long leaf showing the mesophyll, two conducting bundles and transfusion tissue. B: conducting bundle fragment (bottom of image, left-right across image) with mesophyll tissue (top of image, slightly oblique orientation to the bundle tissue by about 45°). Compare to C: close up of mesophyll tissue from present study morphotype 2, scale bar 50 µm showing unusual fluoresce, not previously thought to have been observed in mesophyll tissue.

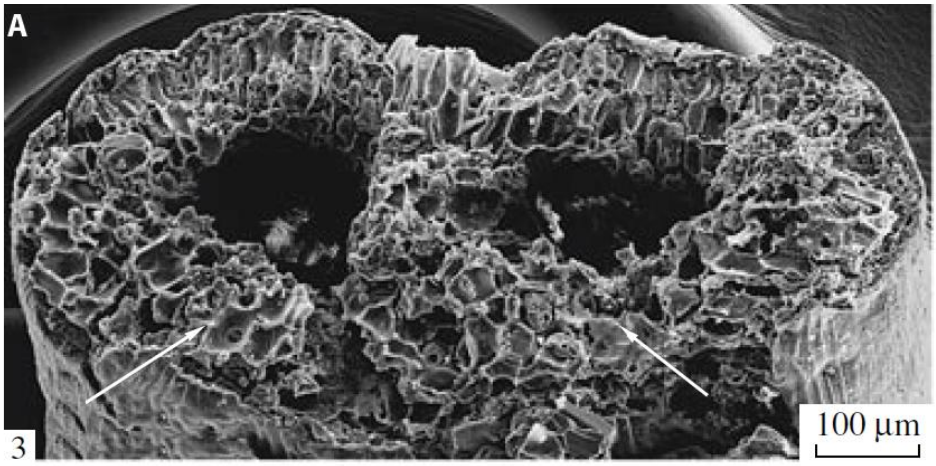
A
3
100 µm

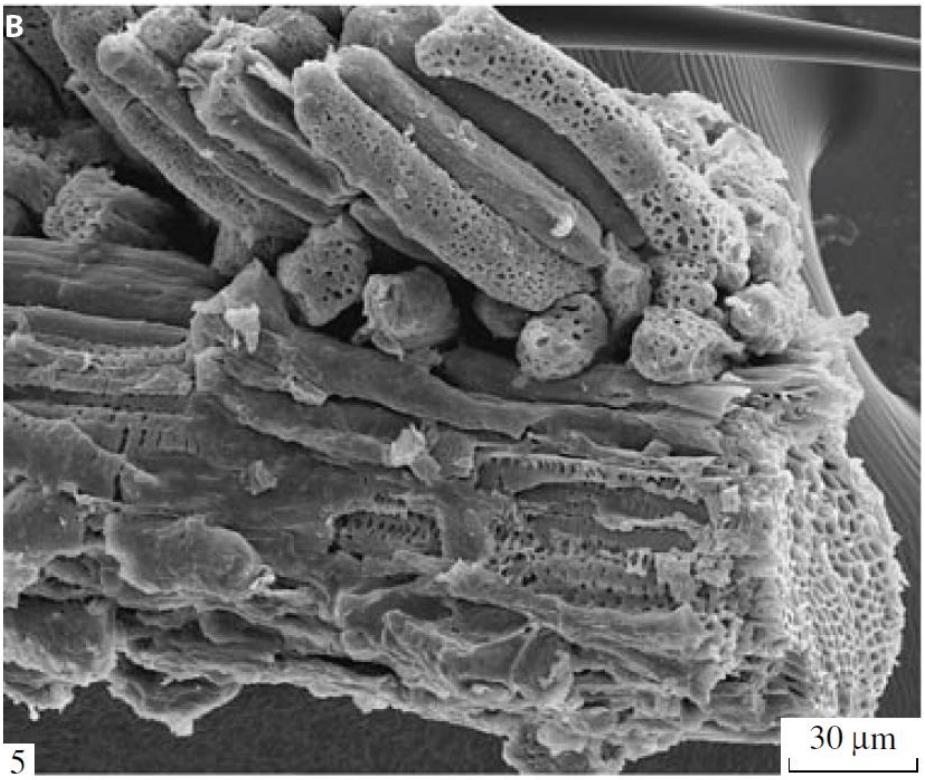
B
5
30 µm

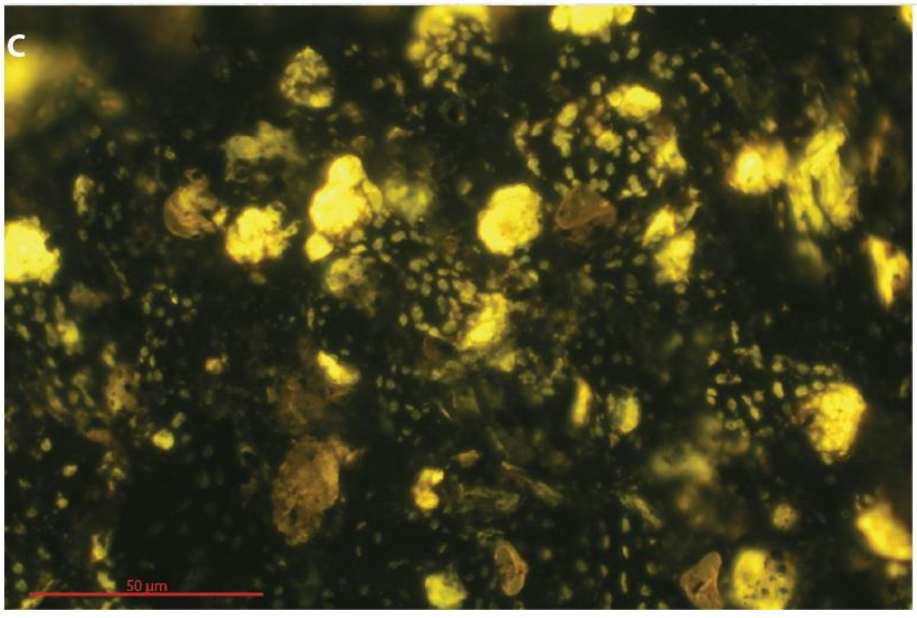
C
50 µm

study material is more difficult to explain since there is nothing comparable in the SEM images of Gordenko (2007) and, thus, may be a preservational effect or an additional structure that was not observed by SEM. Nonetheless, the identification of mesophyll tissue through epifluorescence microscopy has not to date (as far as known) been accomplished for fossil material of this nature and such exceptional preservation may reflect the minimal sample processing during bulk maceration.

4.5.2.2 Morphotype 3 (Sciadopityoides)

Bose and Manum (1990) describe several *Sciadopityoides* genera from the Miroviaceae family all characterised by a single stomatal zone, which closely resemble the cuticle fragments described in morphotypes 3 and 4. Some of the species described by Bose and Manum were found in West Greenland, for example *Sciadopityoides ikorfatensis*, which has long, linear leaves of 13–18 mm length and 2–3 mm width, with obtuse to occasionally acute tips and a cylindrical base (Figure 4.23A). The features unique to this *Sciadopityoides* species are the crowded tuberculate papillae and longitudinally orientated stomata in general files within the stomatal furrow and are a close fit to the present study material to be confident of this morphotype identification (compare sketches from Bose and Manum 1990, in Figure 4.23B-D to the morphotype 3 cuticle in Figure 4.23E).

4.5.2.3 Morphotype 4 (Sciadopityoides)

Morphotype 4 is very similar to morphotype 3 except that the stomata are more tightly packed and are generally transversely-to-obliquely orientated, which suggests the morphotypes may be similar and likely the same genus. Bose and Manum (1990) described *Sciadopityoides microphylla* from the Ikorfat area of West Greenland which closely matches the description of morphotype 4 cuticle: leaves are typically 10–14 mm long and around 2.5 mm wide, with obtuse tips and entire margins revealing a straight to slightly curved leaf with a widened cylindrical base (Figure 4.24A). The stomatal furrow contains crowded cyclocytic stomata and is protected, and often concealed, by papillae which are predominantly tuberculate, although some are smooth (Figure 4.24B). Around the stomata 5-6 subsidiary cells often abut but are never shared by stomata (Figure 4.24C); stomata are mostly obliquely or transversely orientated (Figure 4.24C). Therefore, on comparison of *Sciadopityoides microphylla* (Figure 4.24A-C) to morphotype 4 material (Figure 4.24D, E) this morphotype is confidently affiliated with *Sciadopityoides* genus.

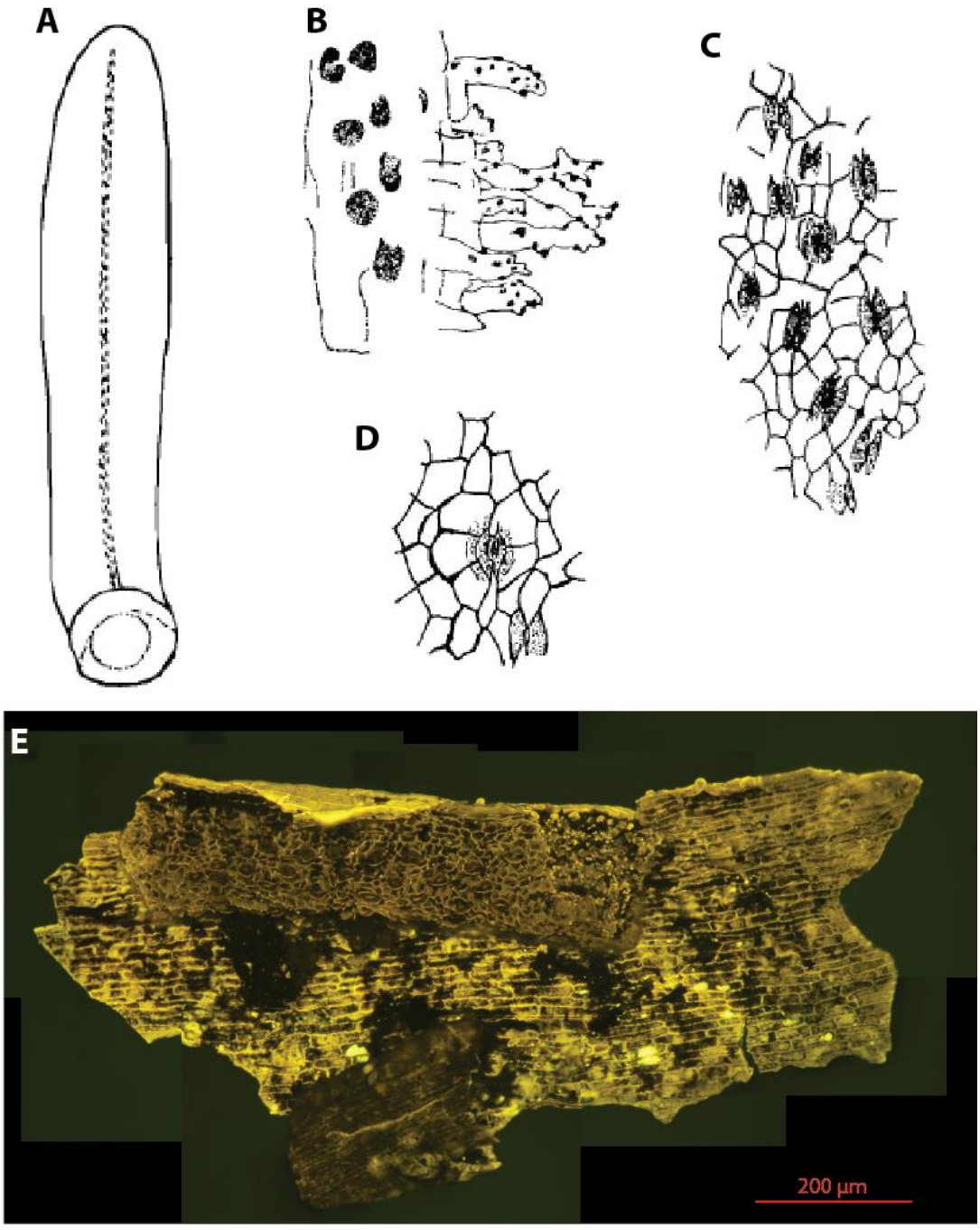

RKE-B-128 (2), inside stomatal-side (inside epidermal cell shapes and inside stomatal furrow surface; fold in cuticle reveals outside surface of stomatal furrow revealing tuberculate papillae), 200 µm

Figure 4.23: Sketches from Bose and Manum (1990) of Sciadopityoides ikorfatensis. A: leaf shape with obtuse tip and cylindrical base, with single stomatal zone. B: margin of stomatal zone showing tuberculate papillae extending over the furrow. C: stomatal distribution and alignment within stomatal furrow showing epidermal cell shape. D: more detailed sketch of cyclocytic stoma with 6 subsidiary cells. E: comparison to morphotype 3 cuticle from the present study.

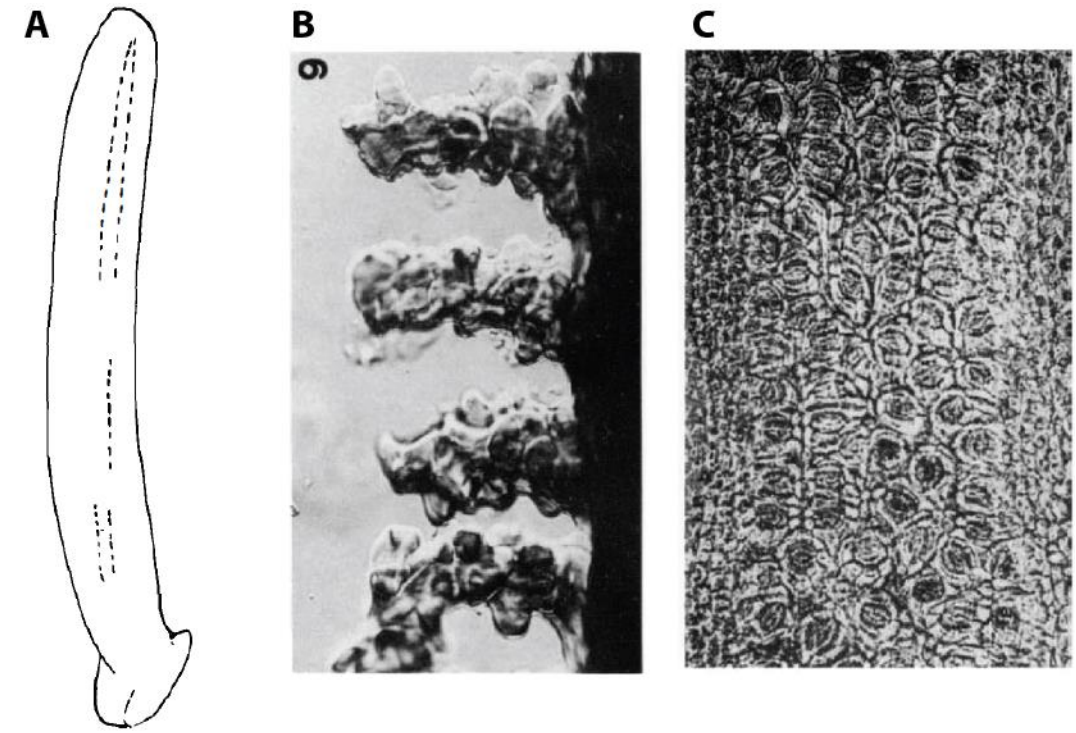

RKE-B-5 (2), x100 magnification, inside stomatal-side (aligned stomata in stomatal furrow), 400 µm

RKE-B-5 (2), x400 magnification, inside stomatal-side (cyclocytic stomata with winged guard cells), 100 µm

Figure 4.24: from Bose and Manum (1990) Sciadopityoides microphylla. A: sketch of leaf shape with obtuse tip and cylindrical base, with single stomatal zone. B: margin of stomatal zone showing tuberculate papillae extending over the furrow. C: stomatal distribution and alignment within stomatal furrow. Compared to present study morphotype 4 cuticle D: inside stomatal furrow, E: tightly packed stomatal apparatus.

4.5.2.4 Morphotype 5 (Oswaldheeria)

Morphotype 5 is similar to morphotype 2 in that the median stomatal zone is not in a furrow and has thinner cuticle than the rest of the surface, but in the case of morphotype 5 is curved into the leaf surface unlike the flush surface of morphotype 2. In addition, morphotype 5 also has papillate stomatal rims which are not observed in morphotype 2. Nonetheless it is possible that morphotype 2 and 5 could both be members of the genera

Oswaldheeria, particularly when the description of *O. arctica* by Bose and Manum (1990) is considered (Figure 4.25). *O. arctica* leaves are straight to curved in shape with entire margins, obtuse tips and cylindrical bases, around 8–15 mm in length and up to 2.5 mm wide. *O. arctica* has a broad stomatal zone on the abaxial surface, where the cuticle is thinner than the rest of the leaf and contains epidermal cells which are shorter and more irregular in shape than outside the stomatal zone (Figure 4.25B). Within the stomatal zone, stomata are arranged in loose files or randomly dispersed (Figure 4.25A), and are cyclocytic with 5–6 subsidiary cells bearing short papillae of similar length to that presented in morphotype 5 (Figure 4.25B, C compare to morphotype 5 material in Figure 4.25D). On comparison of the morphotype 5 material to the sketches in Bose and Manum (1990), morphotype 5 closely resembles the description of *Oswaldheeria arctica* and can be confidently placed in the *Oswaldheeria* genus.

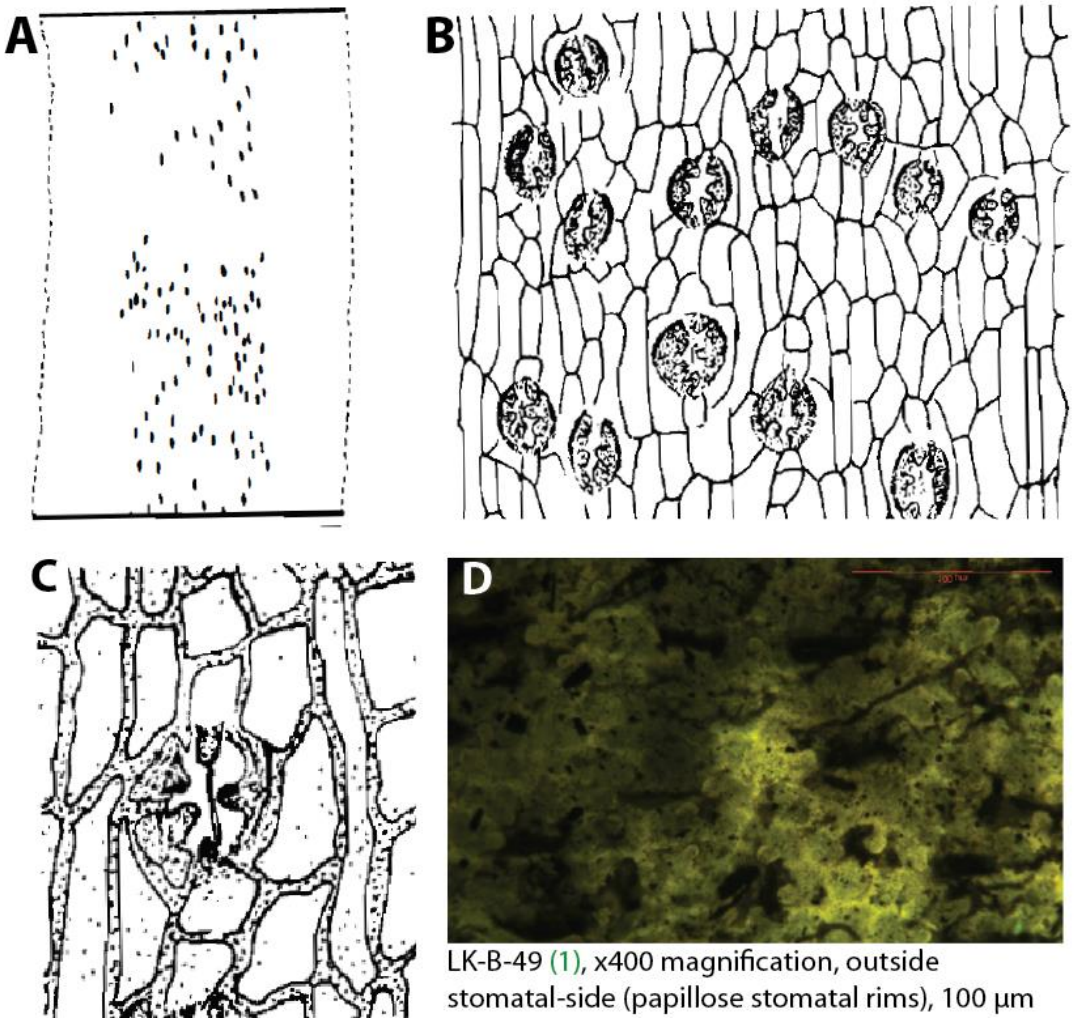

Figure 4.25: sketches from Bose and Manum (1990) of Oswaldheeria arctica. A: sketch of stomatal zone stomatal distribution. B: stomatal distribution in stomatal zone showing epidermal cell shape. C: stomatal complex showing papillate subsidiary cells. Comparison to D: morphotype 5 stomatal zone showing similar papillose stomatal margins.

4.5.3 Morphotypes 6–8 (Bennettitales)

Boyd (1998b, 2000) described Bennettitalean foliage form-genera from the Kome Formation on the northern coast of the Nuussuaq Peninsula and reported that the cuticle can appear quite similar for many species, and that much of the plant classification relies on examination of shoots. Despite this, the similarities in cuticle features can be used to determine that morphotypes 6–8 are Bennettitalean, and supplementary evidence from the macrofossil samples collected from the field area reveal some of the genera represented in the West Greenland floral community.

4.5.3.1 Morphotypes 6 and 7 (Nilssoniopteris or Pterophyllum)

Boyd (2000) described predominantly paracytic stomata from *Pterophyllum* (Figure 4.26A-C) and *Nilssoniopteris,* although occasionally, the stomata are brachyparacytic or hemiparacytic, with subsidiary cells often presenting a crenulate margin along with the remainder of the epidermal cells. These features are clearly observed in morphotype 6 (Figure 4.26E) and possible hemiparacytic and paracytic stomata with crenulate cell walls were observed in morphotype 7 (Figure 4.26F).

Boyd (2000) also identified "cuticular bodies" in most species of *Nilssoniopteris* and *Pterophyllum* (Figure 4.26D), which are similar in size and shape to the oval outlines identified in all three Bennettitalean morphotypes (most clearly seen in Figure 4.26E), suggesting that this is a feature shared by most Bennettitales. The oval structures are approximately 1–1.5 times longer than stomata with less crenulated margins than the epidermal cells (Figure 4.26D, E). Boyd (2000) observed that the centres of these structures were normally empty, supporting the idea that they are hair bases (Kvaček, 1995). However, in one example, Boyd identified a possible stoma within the cuticular body and therefore proposed this was a malformed or abandoned stoma (considering stomata can initiate from the same protodermal cells as hair bases). The function of these cuticular bodies is no clearer from examination of those preserved in morphotypes 6–8; no stomata were observed within the structures, supporting the idea these structures could be trichomes or glandular structures - possibly even salt glands as an adaptation to arid soils or brackish ground waters (Sincock and Watson 1988).

4.5.3.1 Morphotype 8 (Pseudocycas)

Morphotype 8 contains stomata within a distinct stomatal zone, or in many cases a furrow (Figure 4.27E, F), which are comparable to descriptions by Boyd (1998b) of *Pseudocycas ravnkloftensis* (Figure 4.27A, B): hypostomatous pinnae, with stomata in a single longitudinal furrow where papillae may be found only at the furrow margin (Figure 4.27A).

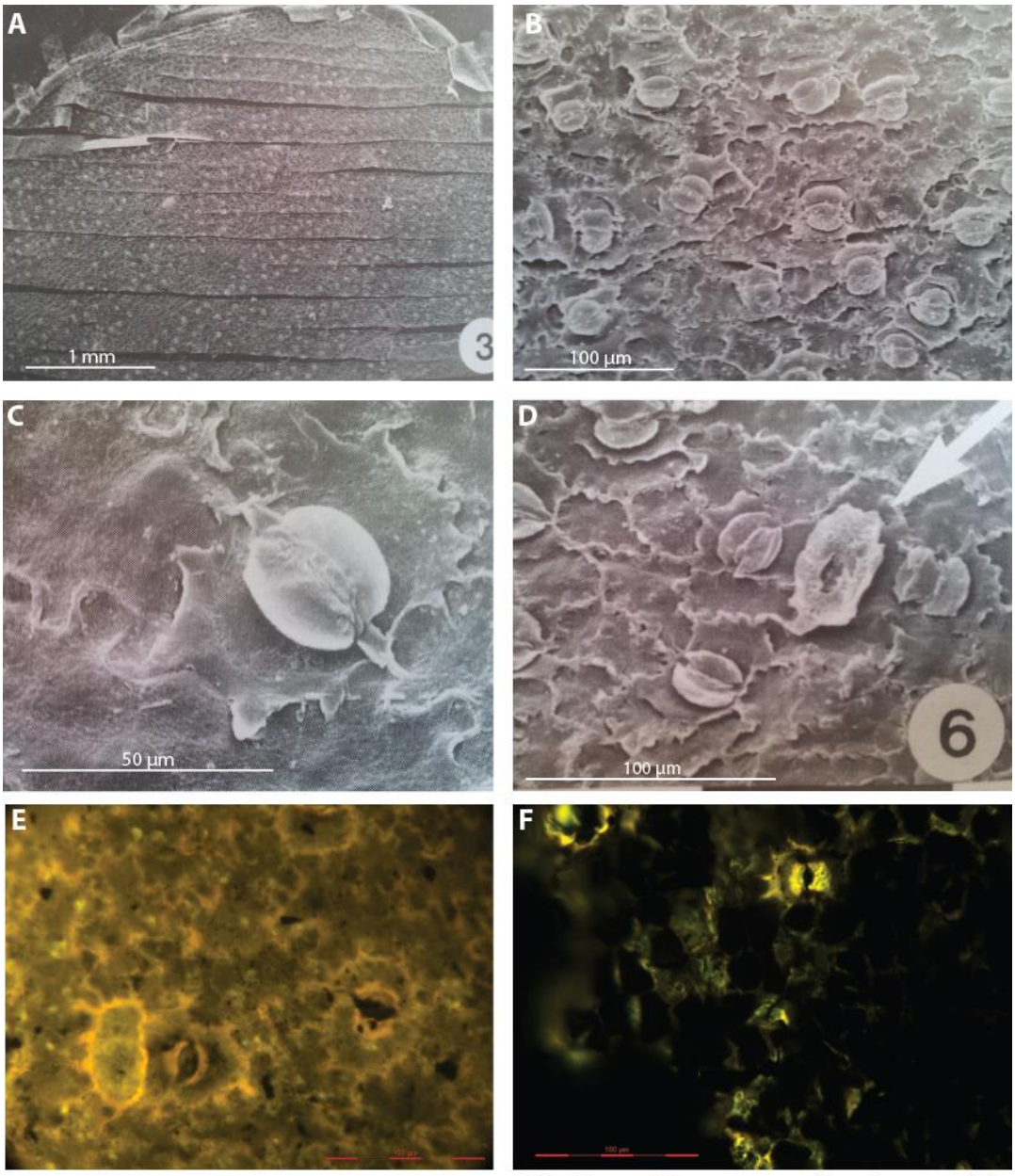

Figure 4.26: SEM images from Boyd (2000) of A: Pterophyllum lepidum stomatal distribution showing venation; B: Pterophyllum sp. B inside cuticle surface stomata; C: Pterophyllum markussenii stomatal complex; D: Nilssoniopteris ikorfatensis showing cuticular body (arrowed). Comparison to the present study material: E: morphotype 6 showing paracytic stomata and cuticular body; F: morphotype 7 showing paracytic stomata.

Stomata are randomly dispersed within the stomatal furrow predominantly but not strictly transversely oriented and brachyparacytic (Figure 4.27B). The presence of a furrow and transversely-to randomly orientated stomata matches the description of morphotype 8, including a similar stomatal groove (compare Figure 4.27A to Figure 4.27E, but note

that one is an external view rather than internal). The stomatal architecture could not be clearly identified in the stomatal zone of morphotype 8 since the epidermal cells were poorly preserved (where cell walls could be determined they appeared crenulated, similar to the descriptions by Boyd, 1998b) but the guard cells appeared winged with some polar extensions preserved in some cases, similar to stomata of *Pseudocycas thomasii* described by Boyd (compare Figure 4.27B to Figure 4.27C, D).

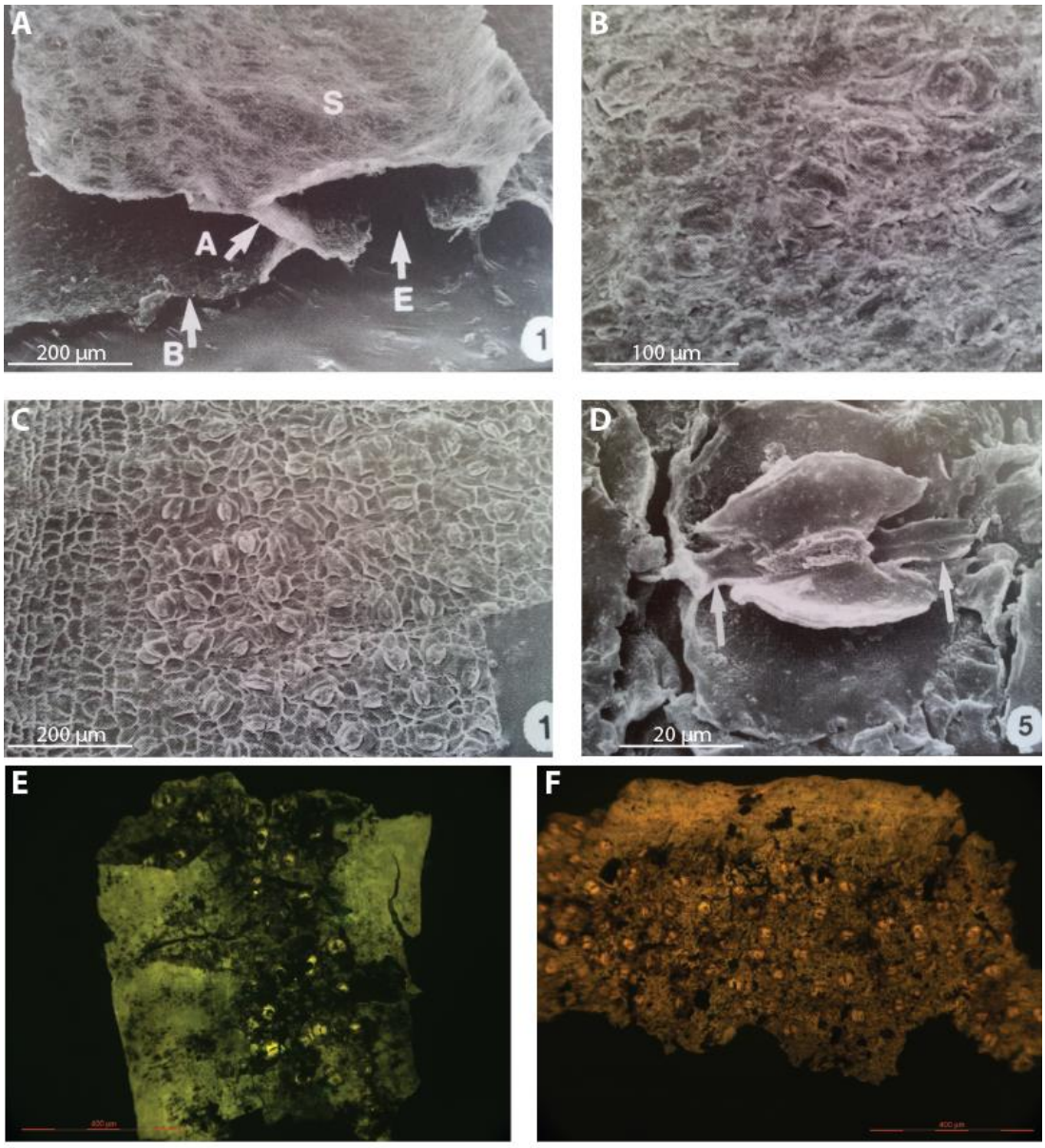

Figure 4.27: SEM images from Boyd (1998b) of A and B: Pseudocycas ravnkloftensis inside surface of stomatal furrow; C: Pseudocycas thomasii inside cuticle surface showing stomatal zone. D: Pseudocycas thomasii stomata showing polar extensions (arrowed). Comparison to morphotype 8 cuticle material from the present study E: stomatal furrow, F: single central stomatal band.

Of the six species of *Pseudocycas* described by Boyd (1998b), three species (*P. thomasii, P. speciosus, and P. arcticus)* did not have a stomatal furrow. Instead, the brachyparacytic stomata are confined to a single central stomatal zone, where they are transversely to randomly oriented (Figure 4.27C, D). Epidermal cells within the stomatal zone are irregular polygons in shape, whereas the non-stomatal margins are more square in shape with crenulated cell walls (Figure 4.27C). These descriptions compare closely with some of the material grouped in morphotype 8 (e.g. Figure 4.27F).

4.5.3.3 Macrofossil samples (morphotypes 6–8)

Additional information on the likely Bennettite genera represented by the cuticle of morphotypes 6 and 7 can be inferred from macrofossil specimens collected close to the sampled sections (Appendix A), since pinna morphology can be used to define Bennettitalean foliage genera (Figure 4.28). According to Barclay's field notes (Appendix A), fossil shoots of *Pterophyllum, Nilssoniopteris* and *Pseudocycas* were identified and

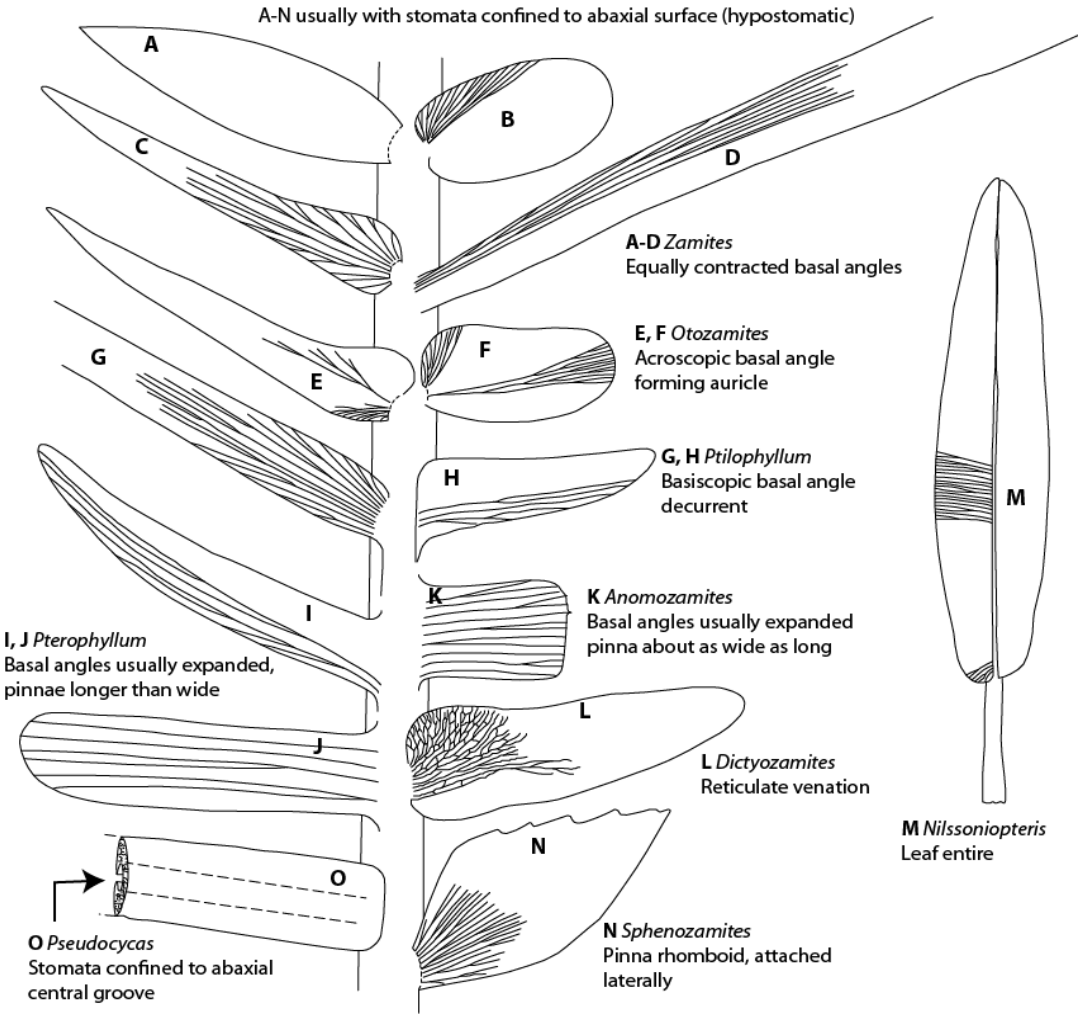

Figure 4.28: Bennettitalean leaf morphology from Taylor et al. (2009).

collected (e.g. Figure 5.16). However, pinnae where a central groove could be observed parallel to the leaf axis should not be interpreted as Pseudocycas exclusively, as the study of the cuticle has revealed in many cases the disarticulated pinnae bearing a median stomatal furrow are Sciadopityoides species (morphotypes 3 and 4).

Most macrofossil specimens collected from the present study are *Pterophyllum* (Figure 4.29) and are often found in great accumulations (e.g. Figure 5.16). The *Pterophyllum*

Figure 4.29: Photographs of Pterophyllum specimens collected from West Greenland. A: Below (EC) EC4. B: JCM1b cp of 1a EC gorge East side above EC4. C: LK-F-3P cp with parallel veins preserved in pinnae with widened bases.

specimens possess pinnae arranged opposite-to-alternately along the rachis, with 1–2 mm spacing (Figure 4.29). The pinnae are fairly broad with obtuse (Figure 4.29A, B) or acute (Figure 4.29C) tips, with straight to slightly broadened bases (Figure 4.29A-C) and in some cases parallel veins are preserved (Figure 4.29C).

These are all features described by Boyd for *Pterophyllum* species, for example: *Pterophyllum concinnum* (obtuse to acute pinna tips, pinna length decreases towards rachis apex; Figure 4.30A), *Pterophyllum markussenii* (acute pinna tips; Figure 4.30B) and *Pterophyllum lepidum* (pinna length decreases towards rachis apex; Figure 4.30C). However, without accompanying cuticular studies for macrofossil specimens it remains

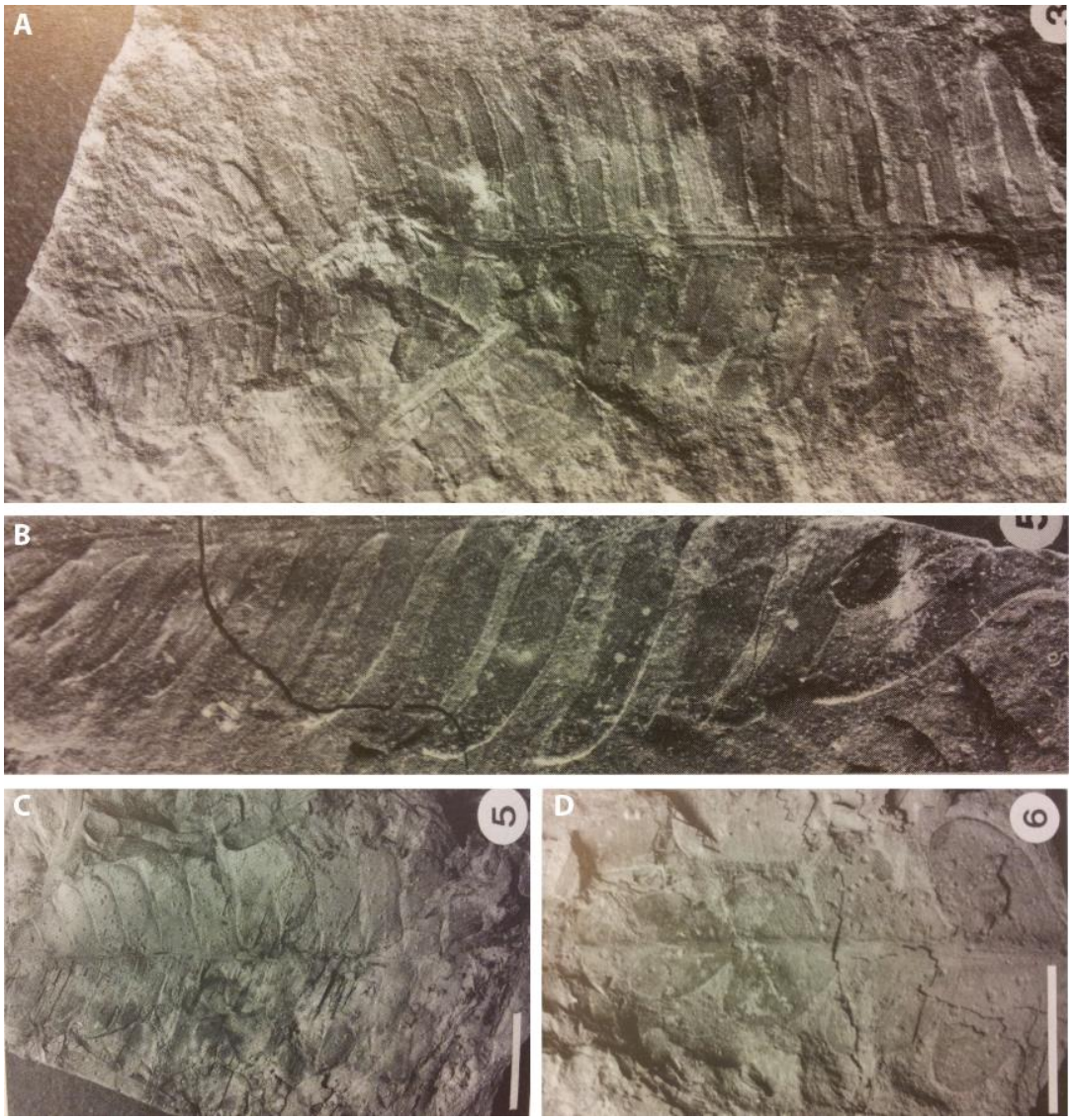

Figure 4.30: Photographs of Pterophyllum specimens collected from West Greenland by Boyd (2000). A: Pterophyllum concinnum, no scale bar provided. B: Pterophyllum markussenii, no scale bar provided; C: Pterophyllum lepidum, scale bar 1 mm; D: Pterophyllum lepidum, scale bar 1 mm.

impossible to identify morphotypes 6 and 7 with any certainty, but the co-occurrence of large numbers of *Pterophyllum* macrofossils collected in the present study and cuticle fragments sharing similarities with Boyd's description of *Pterophyllum* provides a tenuous link. However, as outlined previously, whilst the cuticle of morphotype 6 and 7 is likely Bennettitalean, it could not be unequivocally distinguished from *Nilssoniopteris* descriptions by Boyd (2000).

Other macrofossil specimens collected from the field area support the identification of *Pseudocycas* (morphotype 8) within the logged section. Close examination of preserved pinnae (Figure 4.31) reveals a median groove, and these shoots can be differentiated from *Scidopityoides* by the arrangement of pinnae along the rachis (Figure i, Appendix C, Watson, 1977), whereby the bipinnate fronds have acute tipped pinnae tightly packed around 20–30° from the wide (1 cm) and possibly woody rachis (cellular preservation, Figure 4.31A). These macrofossil specimens are very similar to specimens of *Pseudocycas steenstrupii* (Figure 4.31B) described by Boyd (1998b). Cuticle fragments identified as likely Bennettitalean scales supports the presence of Bennettites in the West Greenland stratigraphy (Appendix C).

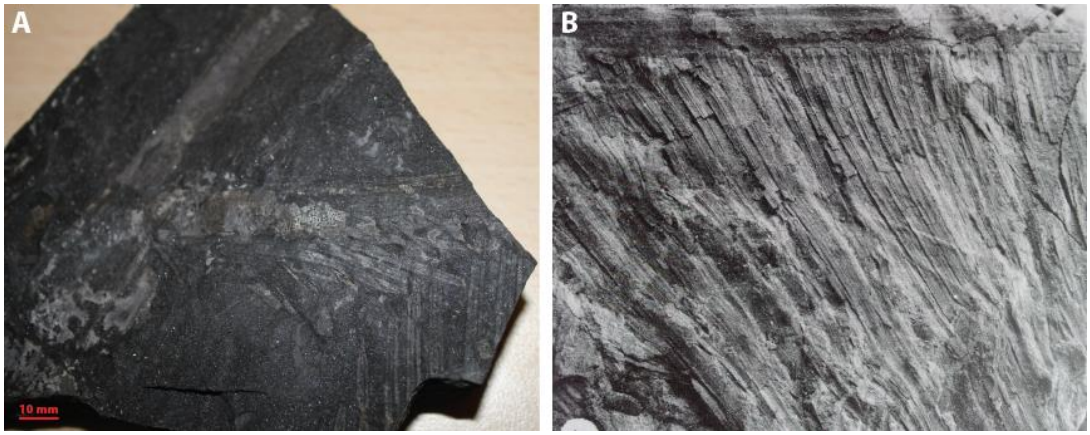

Figure 4.31: A: photograph of specimen RKW-F-Cycad Fcp, scale 10mm compared to B: Pseudocycas steenstrupii collected by Boyd (1998b).

4.5.4 Morphotype 9 (Angiosperm, Lauraceae?)

The presence of pellucid dots and other glandular structures are common on angiosperm leaf cuticle, in addition to relatively small stomata dispersed across the epidermal surface and second order venation (Barclay, 2011). Examination of the angiosperm macrofossil specimens collected in the present study provides a starting point for identifying suspected angiospermous leaf cuticle.

Boyd (1998c) discovered three-lobed (and occasionally unlobed) leaf fossils bearing resemblance to other leaves in the Lauraceae (Order: Laurales) primarily based on the intersection of the most basal second-order vein with sinuous and basilaminar veins, in addition to other venation and leaf shape similarities (Boyd, 1998c for review). Boyd placed these leaves in their own genus (*Trilaurus*) on the basis of the differences of these leaves to those in the Laurales, including more irregular and fewer higher order veins and differences in the size and shape of the leaf compared to other laurels (Boyd 1998c).

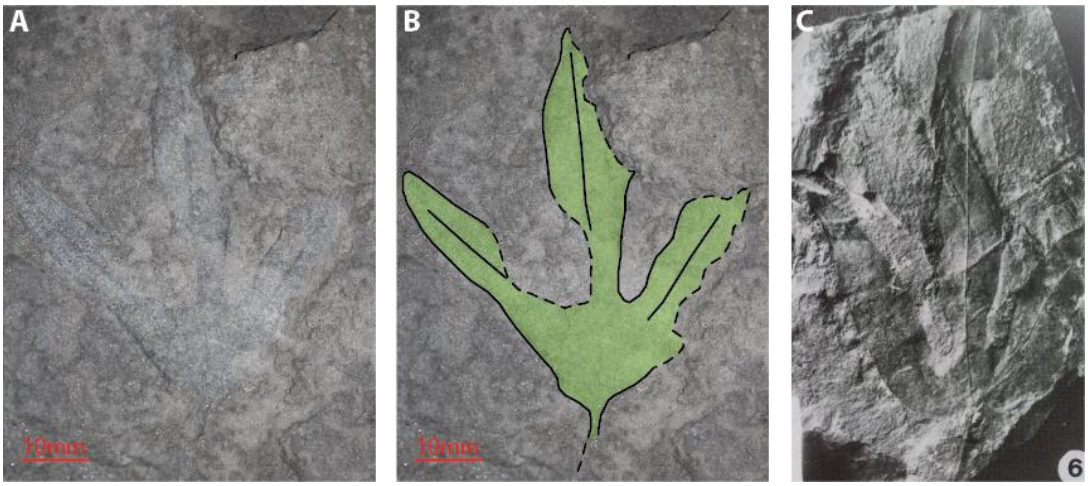

Figure 4.32: Trilaurus sassopsis fossil photographs. A: sample Boyd Loc M2 Dp, scale 10 mm. B: same sample as A, with the leaf outline and venation preserved annotated. C: Specimen of Trilaurus sassopsis from Boyd (1998c) for comparison, no scale published.

Comparison of the fossil material collected in the present study to that of Boyd reveals striking similarities in form despite the fact that venation, other than the mid-vein, was not preserved (a problem encountered by Boyd and attributed to thin veins and thick leaves; Figure 4.32). The fossil leaf discovered from the present study material (Figure 4.32A, B) is around 5 cm in width and length and elliptic in shape. The leaf is symmetrical, palmately lobed (tri-lobed) with fairly narrow lobes approximately 1.0–1.5 cm wide with pointed to rounded tips, possessing entire margins and an acute base. Only primary venation is preserved and is palinactinodromous, creating a midvein for each lobe (Figure 4.32A, B). This description fits the description of Boyd's specimen of *Trilaurus sassopsis* shown in Figure 4.32C, indicating despite the lack of additional information retrievable from the present study specimen, given the unusual form of *Trilaurus sassopsis*, the three-lobed specimens identified in the macrofossil specimens can be confidently identified as this leaf genus.

Linking morphotype 9 cuticle fragments to this, or any other, angiosperm macrofossil requires comparison of cuticle directly associated with the macrofossil to the cuticle fragments. Unfortunately, very little cuticle material was preserved after processing by Boyd (1998c), due to his use of Schulze's solution. Consequently, only the thickest cuticle of *Ceratophytum* and *Dicotylophyllum* angiosperms were preserved in any great detail in Boyd's study. Nonetheless, when the macrofossil specimens collected by this study are examined under a low power fluorescence microscope (UCL Cell Biology Department) it reveals that, in all likelihood, the cuticle is not preserved in any of the impressional angiosperm fossils since no fluorescence is observed. Given the rarity of apparently angiospermous leaf cuticle (which appears quite thin in Figure 4.15) compared to the macrofossil specimens collected, it would suggest the preservation of this cuticle is limited.

The poorly preserved cuticle retrieved by Boyd (1998c) from only one side of the leaf species did not possess stomata, suggesting the species was hypostomatous with disorganised epidermal cells outside of veins, and elongate cells with parallel long axes within the vein areas. Only the stomatal surface of morphotype 9 was observed, which makes comparison to Boyd's cuticle problematic; however, the limited description of epidermal cell morphology compares to morphotype 9, but this may be true of many angiosperm (and other) plants.

The identification of structures similar to pellucid dots in the cuticle fragments of morphotype 9 provide a tantalising comparison to modern Lauraceae which are characterised by essential oils derived from mesophyll oil cavities (Li and Christophel, 2000; Rowher, 2000; Judd *et al*., 2002; Barclay, 2011). Comparison of morphotype 9 cuticle material to extant Lauraceae (e.g. those described in Barclay, 2011) reveals significant similarities in stomatal arrangement, orientation, complex type and size with respect to epidermal cells, in addition to the epidermal cell shape and venation pattern (e.g. Figure 4.33) supporting the interpretation of morphotype 9 as likely Lauraceae and associated with the *Trilaurus* macrofossils collected.

However, the glandular structures identified on a single cuticle fragment (Figure 4.16B) appear to be subcuticular rather than mesophyll in origin, and appear more similar to the peltate glandular trichomes responsible for essential oils of the Lamiaceae (Dunkić *et al.*, 2007). There is insufficient information to confirm the identification of this particular cuticle fragment but if found to be correct, it would suggest the Lamiaceae first appeared

earlier than previously thought (Cenozoic; Drew and Sytsma, 2013; Tripp and McDade, 2014 and references therein).

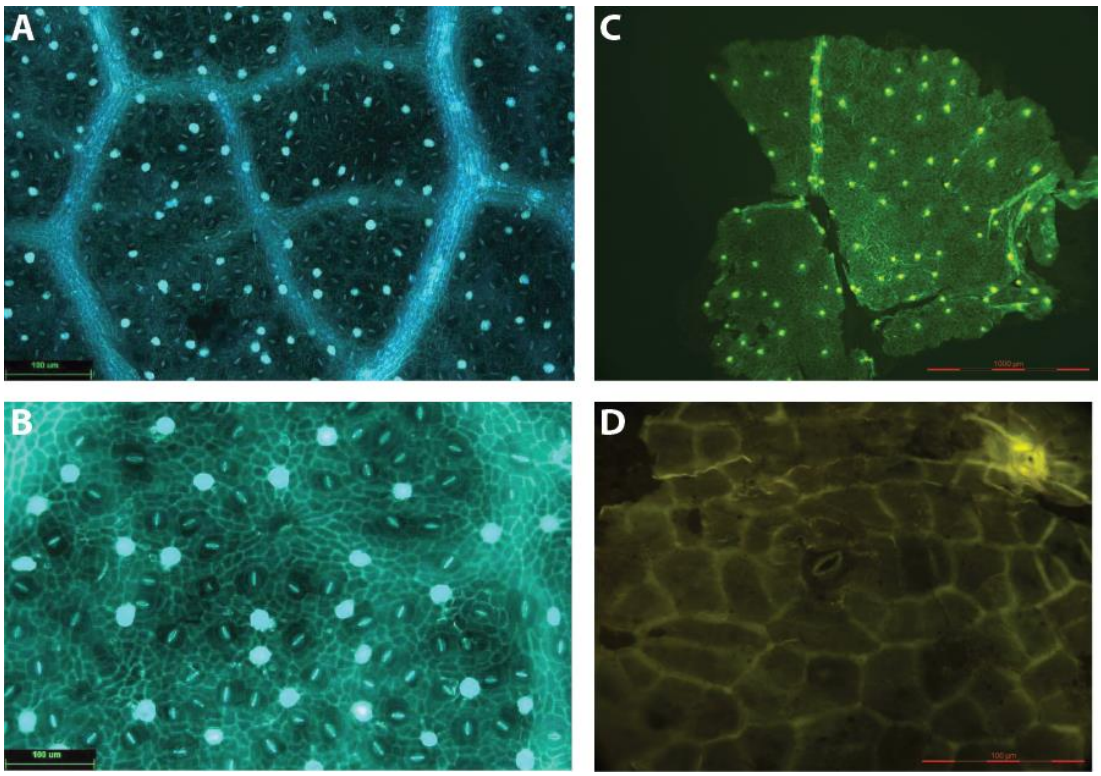

Figure 4.33: Comparison of extant Lauraceae to morphotype 9 cuticle. A and B: from Barclay (2011), epifluorescence image of Hypodaphnis zenkeri (scale in A = 200 µm; scale in B = 100 µm). Comparison to morphotype 9: C: entire cuticle fragment showing more sparse venation but similar pellucid dots or other glandular structure, scale = 1000 µm. D: lower view showing small slot-like stomata with similar brightly fluorescing rim as that of H. zenkeri, scale = 100 µm.

4.5.5 Morphotype 10 (Coniferale, *Taxus/Sequoia*?)

Dual stomatal bands occur in many Coniferales, as identified by this study (e.g. morphotypes 10, 11 and miscellaneous: Section 4.6) but subtle characteristics provide a means to separate the cuticle. Ma and Li (2002) described the epidermal characteristics of *Sequoia sempervirens*, an extant member of *Sequoia* which has generally hypostomatous, occasionally amphistomatous, linear leaves up to 2.3 cm long and 2.2 mm wide, with an acute to mucronate tip (Figure 4.34A). *S. sempervirens* has similar epidermal cell shapes on both sides of the leaf which are elongate with straight walls except on the lower surface within the stomatal bands where they are less regular (Figure 4.34A). The stomatal bands contain 3–8 rows of stomata per band either side of the mid-vein and are predominantly aligned with long axis parallel to the midvein, but occasionally found oblique or perpendicular. These features compare with the description of morphotype 10 (Figure

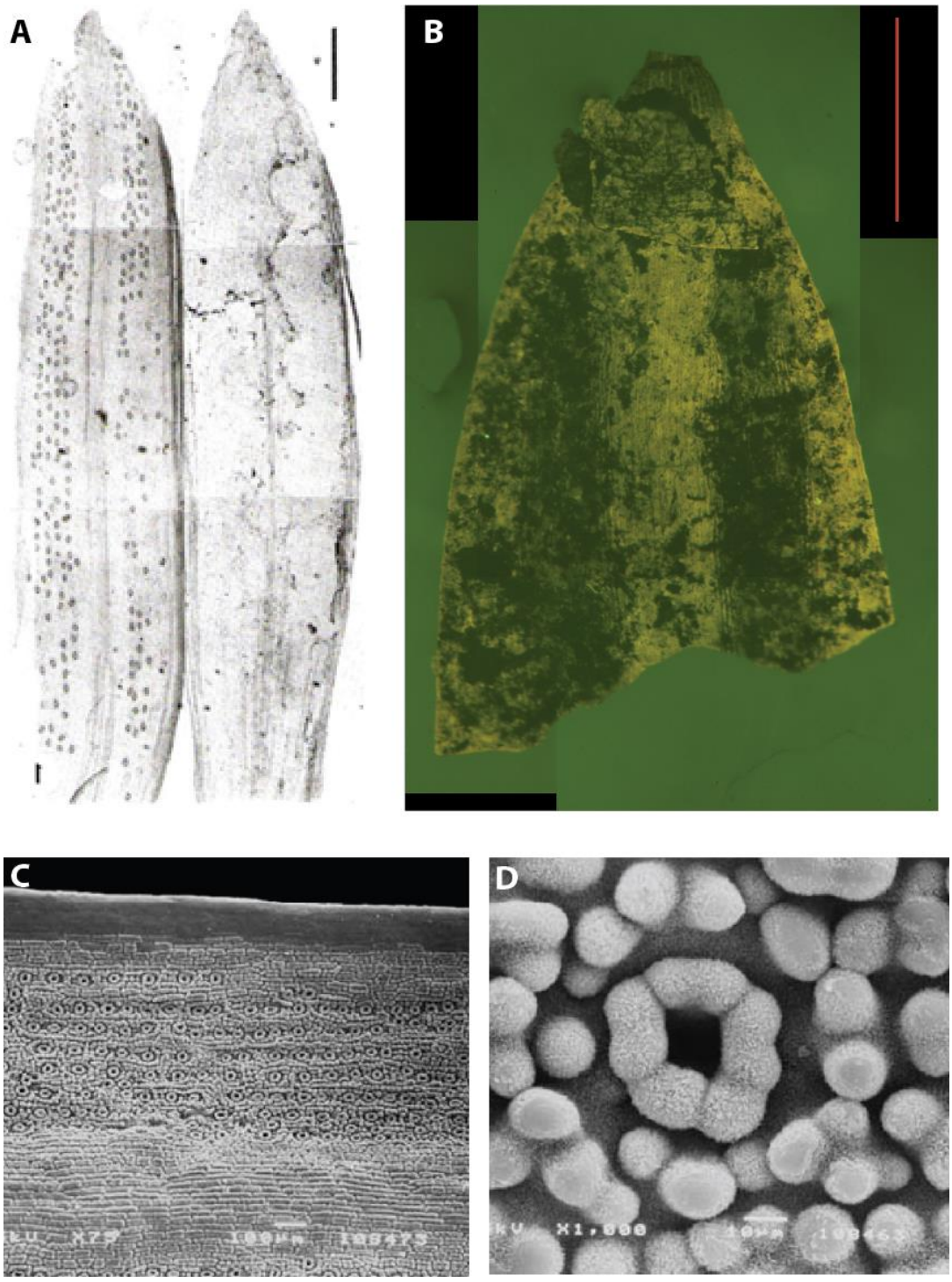

Figure 4.34: A: from Ma and Li (2002) image of Sequoia sempervirens leaf cuticle showing two linear leaves with the upper surface on the left, attached to the lower surface on the right with two bands of stomata and acuminate to acute tip. Scale bar = 5 mm. B: present study morphotype 10 cuticle fragment showing leaf tip and dual stomatal band, scale bar = 500 µm. C and D: from Schirone et al. (2010) SEM images of Taxus baccata leaf cuticle. C: SEM image of one stomatal band, scale bar = 100 µm; D: SEM image of papillose epidermal cells and florin ring around stomatal opening, scale bar = 10 µm.

4.34B) except that stomata are never observed on the adaxial surface of morphotype 10 cuticle. In addition, some cuticle fragments grouped into morphotype 10 possess epidermal papillae in the stomatal zone, with the stomatal opening protected by a raised rim, which is more comparable to *Taxus* (e.g. 4.34C, D) which shares all other features of *Sequoia* with up to 9 files of stomata in each stomata band (Schirone *et al.*, 2010).

Both *Sequoia* and *Taxus* have representatives in the Cretaceous: for example Spjut (2007 and references therein) describes the geographic distribution of *Taxus,* and Seward (1927) and Boyd (1998c) describe *Sequoia smittiana,* which shares many of the features of morphotype 10. In addition, *Cephalotaxus* is a closely related conifer family to *Taxaceae*, with similar cuticle characters except the stomatal bands are narrower, but this genus also possesses a fossil history through the Mesozoic (Hao *et al.,* 2008 and references therein). Based on comparisons of the material collected in morphotype 10 to the descriptions published by other studies, it seems likely that two genera are represented: one *Sequoia*-like (non-papillate) and one *Taxus*-like (papillate stomatal band).

4.5.6 Morphotype 11 (Pinaceae, *Tsuga?*)

Comparison of the cuticle of morphotype 11 to morphotype 10 reveals significant similarities between the stomatal form: two bands of stomata either side of a midvein on a single side of a linear leaf with an acuminate tip. However, the midvein width of morphotype 11 is narrower than morphotype 10, as are the stomatal bands, and the stomata are smaller and more slot-like than anything in morphotype 10.

Examination of other dual-stomatal band plant genera reveals the conifer *Tsuga* (Pinaceae) possesses a narrower midvein than *Taxus* and *Sequoia,* with linear leaves and pointed to mucronate tips (Matsumoto *et al.*, 1995; Kouwenberg *et al*., 2003, 2005; compare Figure 4.34 to 4.35) and in description is similar to the material of morphotype 11, except that the width of the external non-stomatal zones are generally wider in morphotype 11 (Figure 4.35). *Tsuga* fossils date to the Late Cretaceous, possibly as early as the Albian (LePage, 2003 and references therein) but to the best of available knowledge have not been described from West Greenland.

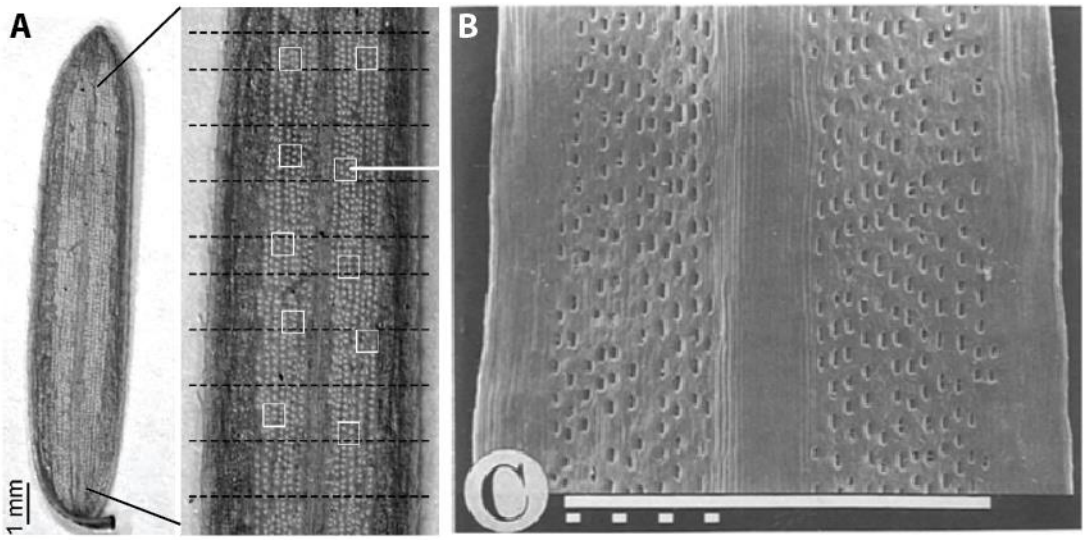

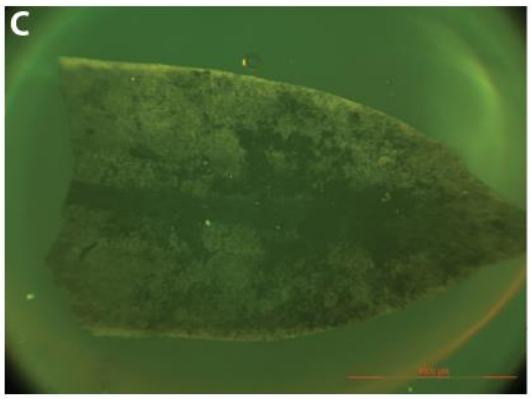

LK-B-3 (14), x40 magnification, outside stomatal-side (pointed to mucronate tip, rows of stomata either side of groove), 200 µm

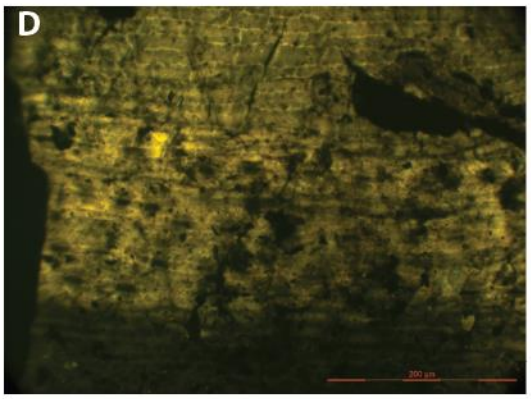

LK-B-3 (14), x200 magnification, outside stomatal-side (6 rows of stomata in band above groove), 200 µm

Figure 4.35: Comparison of extant Tsuga species - A: Tsuga heterophylla from Kouwenberg et al. (2003). B: SEM image of Tsuga chinensis from Matsumoto et al. (1995), to morphotype 11 cuticle fragments in C and D.

4.5.7 Morphotype 12 (Araucariaceae, *Araucaria?*)

Comparison of the limited amounts of cuticle comprising morphotype 12 to published descriptions would indicate that this morphotype is most similar to genera of the Araucariaceae and in particular members of the genus *Araucaria*. *Araucaria* has stomatal apparatus with common polar extensions and 4–5 subsidiary cells but no florin rings (unlike some Podocarpaceae – Section 4.6). The stomata of *Araucaria* are organised into irregular linear files spaced across the leaf and are typically amphistomatous (unlike *Agathis*), with elongate to slightly irregular epidermal cells possessing wavy to crenulate cell walls (Stockey and Taylor, 1978; Haworth *et al.*, 2011; compare Figure 4.36A, B to Figure 4.36C, D).

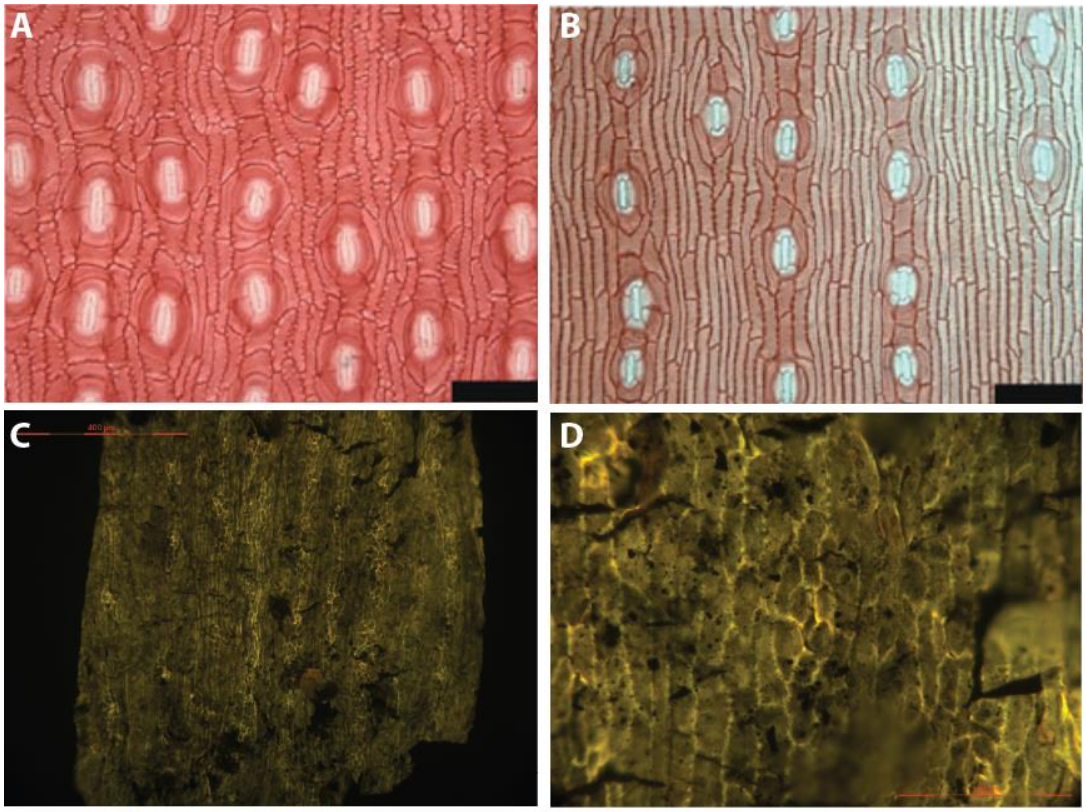

Figure 4.36: Light microscope images of Araucaria leaf cuticle from Haworth et al. (2011).A: A. angustifolia. B: A. bidwillii. Scale bar = 100 µm compared to cuticle from morphotype 12 (C and D).

Since the stomatal apparatus of morphotype 12 is not preserved, and due to the few number of pieces which were generally fragmentary (no information on the leaf base or tip was preserved), assigning this morphotype to the genus *Araucaria* remains tentative.

4.6 Other leaf cuticle fragments (not morphotyped)

The leaf cuticle fragments which were not sorted into any morphotype due to the small number of fragments (1 or 2 fragments) are summarised in this section to provide a "snapshot" of the lesser floral components. Nonetheless, the identification of these plants remains uncertain. Whilst some appear as though they could be grouped within an established morphotype, significant differences in cuticle features prevented inclusion. For example, the cuticle fragment shown in Figure 4.37A-B closely resembles the papillose variant of morphotype 10, but on closer examination the stomata are orientated perpendicular to the leaf axis (Figure 4.37B), suggesting this cuticle fragment likely represents another species of the proposed *Taxus* members of morphotype 10.

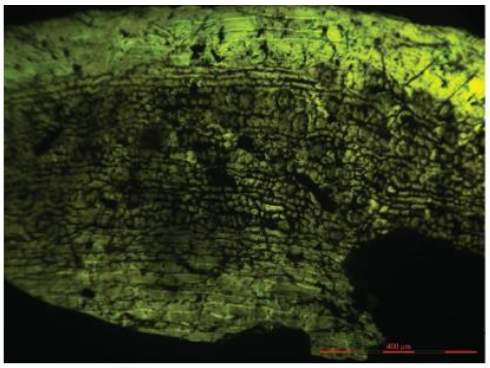

A: LK-B-67 (2), x100 magnification, outside stomatal-side (stomatal band with papille and transverse orientated stomata), 400 µm

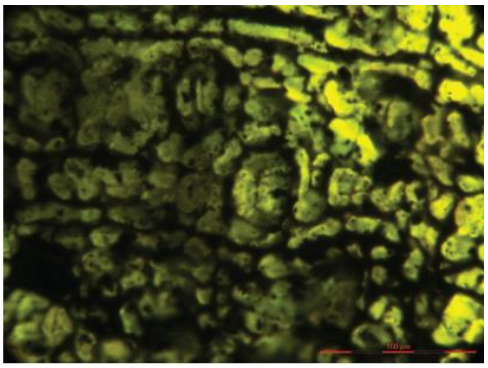

B: LK-B-67 (2), x400 magnification, outside stomatal-side (stomatal band papille and transverse orientated stomata), 100 µm

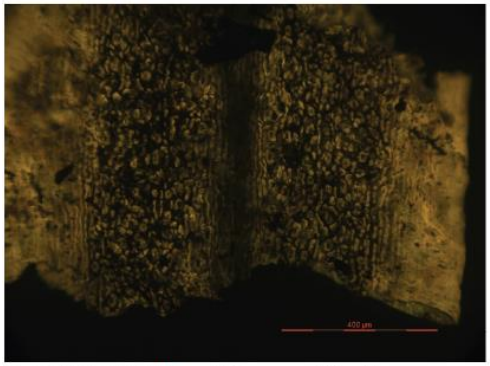

C: RKE-B-119 (5), x100 magnification, outside stomatal-side (stomatal bands either side of groove), 400 µm

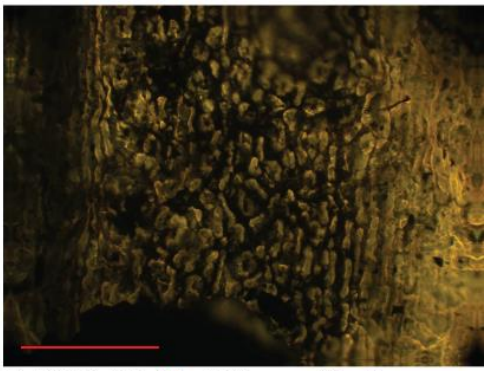

D: RKE-B-119 (5), x100 magnification, outside stomatal-side (papillose stomatal band, long axis orientation), 200 µm

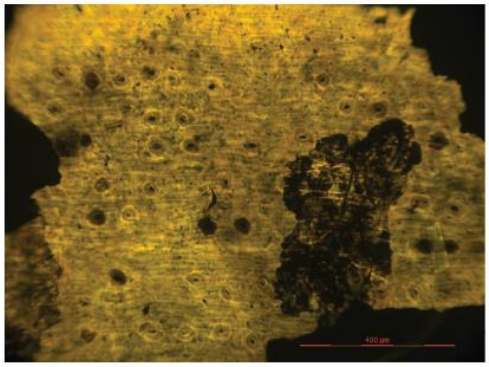

E: LK-B-28 (10), x100 magnification, outside stomatal-side (indistinct stomatal rows), 400 µm

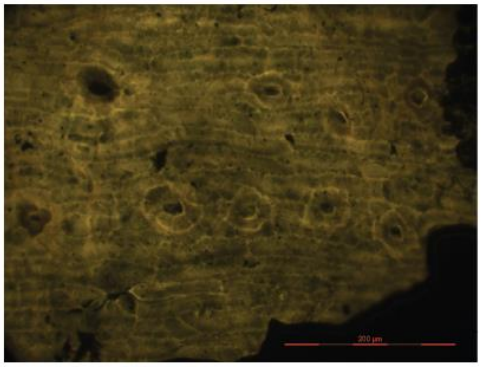

F: LK-B-28 (10), x200 magnification, outside stomatal-side (indistinct stomatal rows), 200 µm

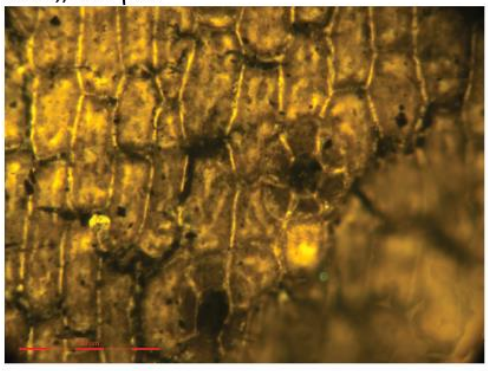

G: LK-B-28 (3), x400 magnification, outside stomatal-side (stomata), 90 µm

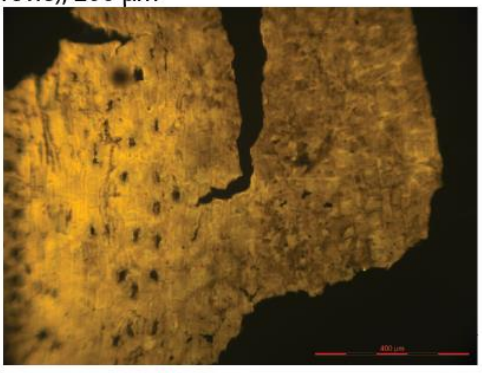

H: RKE-B-105 (7), x100 magnification, outside stomatal-side (stomatal band, indistinct rows), 400 µm

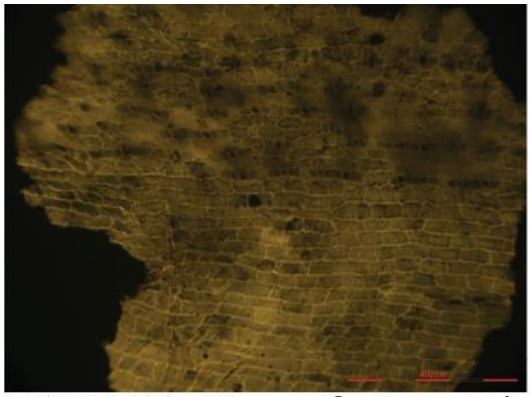

I: RKE-B-44 (2), x100 magnification, outside stomatal-side (stomatal band with transverse stomata), 400 µm

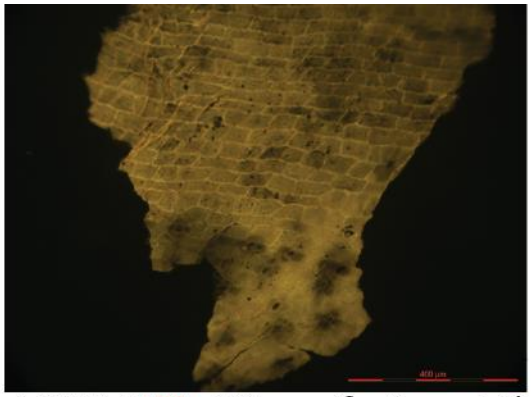

J: RKE-B-44 (2), x100 magnification, outside stomatal-side (stomatal band with transverse stomata), 400 µm

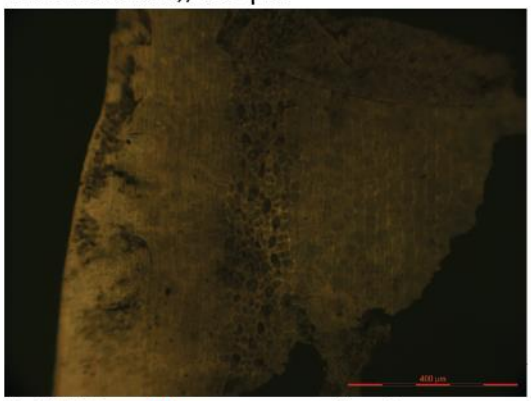

K: RKE-B-44 (3), x100 magnification, outside stomatal-side (stomatal? band), 400 µm

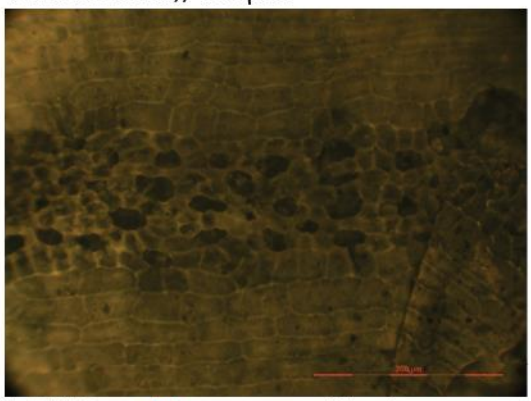

L: RKE-B-44 (3), x200 magnification, outside stomatal-side (stomatal? band), 200 µm

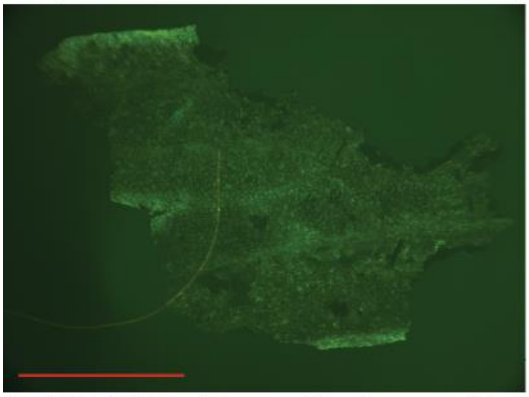

M: LK-B-49 (1), x40 magnification, outside stomatal-side (papillose surface with parallel veins), 1000 µm

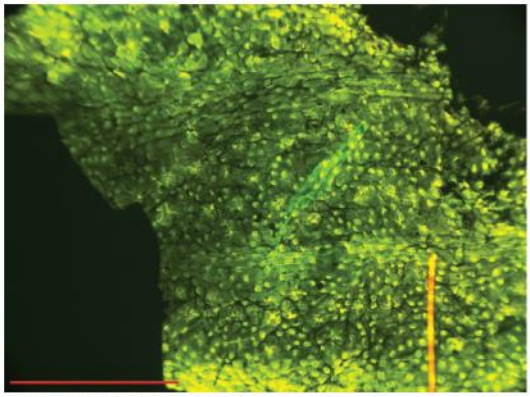

N: LK-B-49 (1), x100 magnification, outside stomatal-side (papillose surface with stomata), 400 µm

Figure 4.37 (above and previous page): Epifluorescence microscope images of cuticle fragments not assigned to any morphotype, labelled with sample name and cuticle piece colour-coded by vial for reference within the character matrix, alongside the image magnification, which cuticle surface was examined, the feature captured in the image and the scale bar length.

The cuticle fragment shown in Figure 4.37C-D also has dual-stomatal bands bearing papillae much like the fragments shown in Figure 4.37A-B and the proposed *Taxus* members of morphotype 10, except the stomatal distribution more closely resembles the configuration presented in morphotype 11, with a narrow midvein. The discovery of such a cuticle fragment with intermediary characteristics likely represents another genus of the Pinaceae.

The cuticle fragments presented in Figure 4.37E-G are quite thin with a stomatal distribution similar to morphotype 12, except the stomata are quite round and possess clear florin rings of six subsidiary cells (compare to Figure 4.36 C, D). These cuticle pieces can be compared to members of the Podocarpaceae (Stockey and Ko, 1988), which are characterised by stomata arranged into irregular files and possess distinct florin rings (Figure 4.38B) or sunken stomata (Figure 4.38A), with 5–6 subsidiary cells (Figure 4.38C). The preservation of the cuticle material represented in Figure 4.37E-G is such that the stomata are missing, leaving circular holes of the stomatal rim; alternatively, these structures may have been misinterpreted and may represent hair bases. However, comparison to Figure 4.38A and 4.38D reveals the stomata can be quite rounded and look like hair bases, and may have been prone to being blocked by debris or wax (Figure 4.38D).

The cuticle fragment shown in Figure 4.37H represents cuticle fragments with stomata arranged into uneven files, which appear to group into bands, but not strictly enforced. The limited availability and preservation of material of this type restricts affiliation to any plant type, but does resemble *Araucaria* (Figure 4.36) but is less regular in the stomatal distribution and some banding is present, perhaps like the upper surface of *Sequoia sempervirens* (Figure 4.34A).

The cuticle fragments in Figure 4.37I-J and Figure 4.37K-L are only identified in one horizon (RKE-B-44) and present unusual stomatal arrangement and morphology. The cuticle fragment in Figure 4.37I-J is characterised by at least two stomatal zones, where epidermal cells are smaller and less regular in shape compared to the non-stomatal zones (Figure 4.37I) and appear to be orientated perpendicular to the long axis of the epidermal cells with a halo of poorer fluorescence surrounding the stomatal opening (Figure 4.37J).

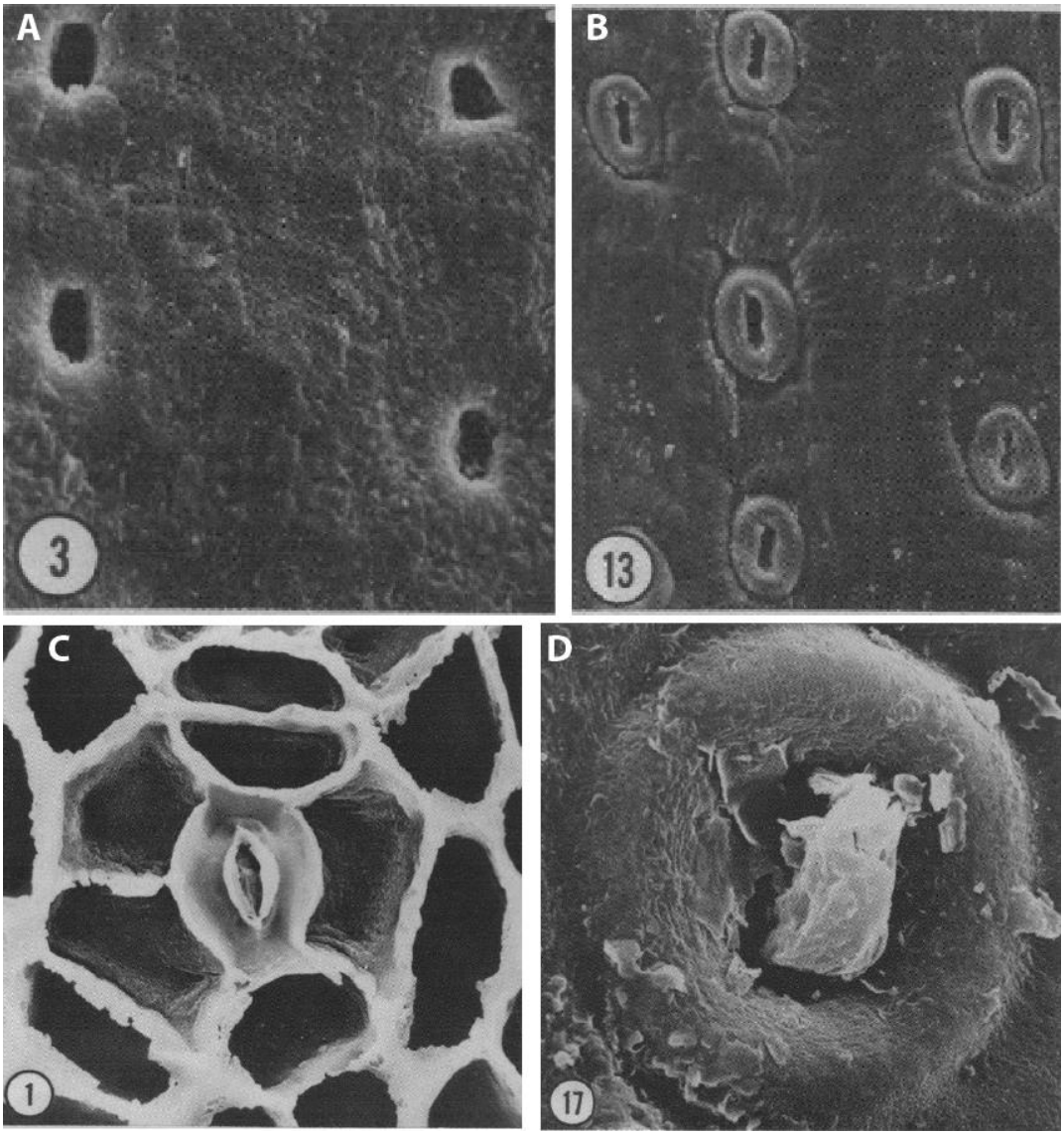

Figure 4.38: SEM images from Stockey and Ko (1988). A: Acmopyle pancheri showing no florin rings. B: Decussocarpus comptonii outer surface, clear florin rings. C: Acmopyle pancheri inside surface of stomata. D: Decussocarpus comptonii stoma with stomatal plug.

The cuticle fragment in Figure 4.37K-L presents the most unusual stomatal morphology if the circular voids are interpreted as stomatal rims (but the inside surface of this cuticle type was not observed); whereby stomatal openings are irregular in shape and size, occurring within a narrow ribbon parallel to the leaf axis (Figure 4.37K). The leaf margin is entire and indicates a linear leaf shape (but only one edge was preserved, and the number of stomatal bands across the surface could not be diagnosed). The epidermal cells across the surface are elongate and generally rectangular with wavy cell walls, but are more irregularly shaped in the stomatal band, whereby subsidiary cells appear to be shared by neighbouring stomata (Figure 4.37L).

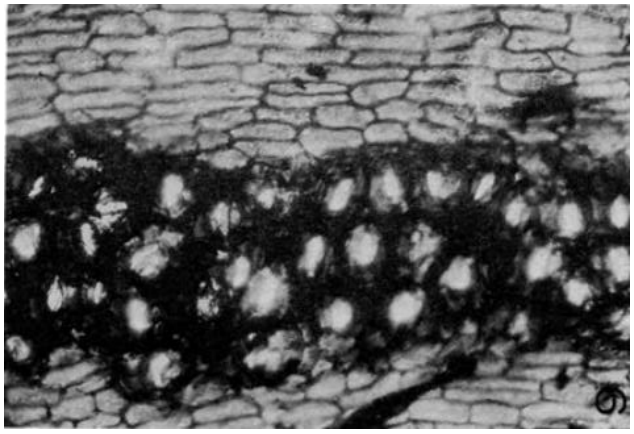

Figure 4.39: Light microscope image of Elatocladus areolatus from Vigran (1970) showing the densely packed stomata frequently sharing subsidiary cells within a narrow stomatal zone, surrounded by elongate epidermal cells.

Such densely packed stomata sharing subsidiary cells in narrow bands have been identified in species of *Elatocladus* (Vigran, 1970; Figure 4.39) from the Jurassic. Several species of *Elatocladus* have been identified from the Cretaceous of West Greenland (Seward, 1927), and are characterised by two stomatal bands that run close to the leaf margin as identified in Figure 4.37K).

The final cuticle fragment (Figure 4.37M-N) is thin, with green fluorescence, possesses an entire margin (inferred linear shape; Figure 4.37M), with a surface covered by epidermal papillae. Stomata are confined to bands separated by narrow elongate epidermal cells bearing smaller papillae, which are interpreted as veins running parallel to the leaf axis.

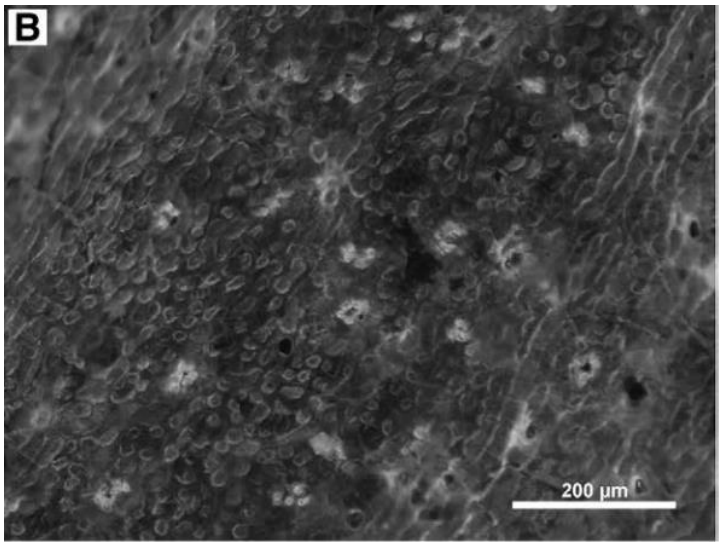

Figure 4.40: Epifluorescence microscope image of Ginkgo adiantoides from Smith et al. (2010).

This cuticle most closely resembles cuticle of *Ginkgo* which often has papillose epidermal cells and stomata protected by papillae with veins running parallel to one another (e.g. Smith *et al.*, 2010; Figure 4.40); *Ginkgo* species have been identified from the Cretaceous of West Greenland (e.g. Seward, 1927).

4.7 Summary

The cuticle fragments with sufficient abundance and preservation to be successfully sorted into morphotypes by cluster analysis of the character matrix are summarised in Table 4.8 and provide the basis for assessing floral changes through the Greenland stratigraphy (Chapter 5). However, minor components (Section 4.6) including possible *Elatocladus,* Ginkgoales, Pinaceae, Podocarpaceae, and other Coniferales were also present in low abundances according to the cuticle record.

Type	Morphotype	Family	Possible genera
Coniferales	1	Cheirolepidiaceae	Pseudofrenelopsis/ Frenelopsis?
	2	Miroviaceae	Oswaldheeria
	3	Miroviaceae	Sciadopityoides
	4	Miroviaceae	Sciadopityoides
	5	Miroviaceae	Oswaldheeria
Cycadoides	6	Bennettitales	Pterophyllum?
	7	Bennettitales	Pterophyllum?
	8	Bennettitales	Pseudocycas
Angiosperm	9	Lauraceae?	Trilaurus?
Coniferales (Pinales)	10	Cupressaceae/Pinaceae?	Sequoia/Taxus?
	11	Pinaceae?	Tsuga?
	12	Araucariaceae	Araucaria?

Table 4.8: Summary of morphotypes with the possible plant affinity based on the descriptions and comparisons outlined in this chapter.

5. Floral and palaeoclimate reconstruction

5.1 Introduction

This chapter uses cuticles, macrofossils and pollen to explore changes in floral abundances and palaeoecology, and to infer palaeoclimates during deposition of the Kome Formation and Ravn Kløft Member. The pollen data are derived from unpublished work by Horikx and Heimhofer. The macrofossil evidence is based upon a limited number of samples collected in 2009, integrated with the comprehensive studies of Boyd (1998a-c, 2000, 2004). The identification and prevalence of fossil epiphytes and other fungal structures on many cuticle fragments may have significant implications for both plant-fossil preparation techniques and the interpretation of plant behaviour, depositional environment, and palaeoclimate for the Cretaceous of West Greenland.

5.2 Record of floral changes from the Nuussuaq Peninsula

5.2.1 Morphotyped cuticle record

5.2.1.1 Bias considerations

The morphotyped cuticle record can be used to assess relative changes in abundance of floral groups. However, sources of bias must be considered in order to appreciate the limitations of data interpretation. The main issue concerns the sample size: both in terms of overall floral composition representation and the impact on comparisons between differing sample sizes across horizons. A total of 8300 fragments were sorted across 79 horizons, of which 44 had sufficient material to morphotype. However, not all of these fragments were identified as cuticle (Figure 5.1A, black data) and not all of these fragments were morphotyped (Figure 5.1A, grey data), meaning that the overall sample size was just 1506 (Figure 5.1B). Given that the sizes of many of the cuticle fragments were around 1–2 mm, the overall sample size is not particularly strongly representative of an intact floral community. Whilst the amount of material macerated varied between horizons (Figure 5.1B), the relative abundance of morphotypes is examined to correct for this potential bias.

A range of additional biases also likely persist through this data set: for example, the organic debris yield (cuticle plus non-cuticle; Figure 5.1A) and cuticle fragment yield (Figure 5.1B) are likely in part related to lithology and depositional environment. The lithology

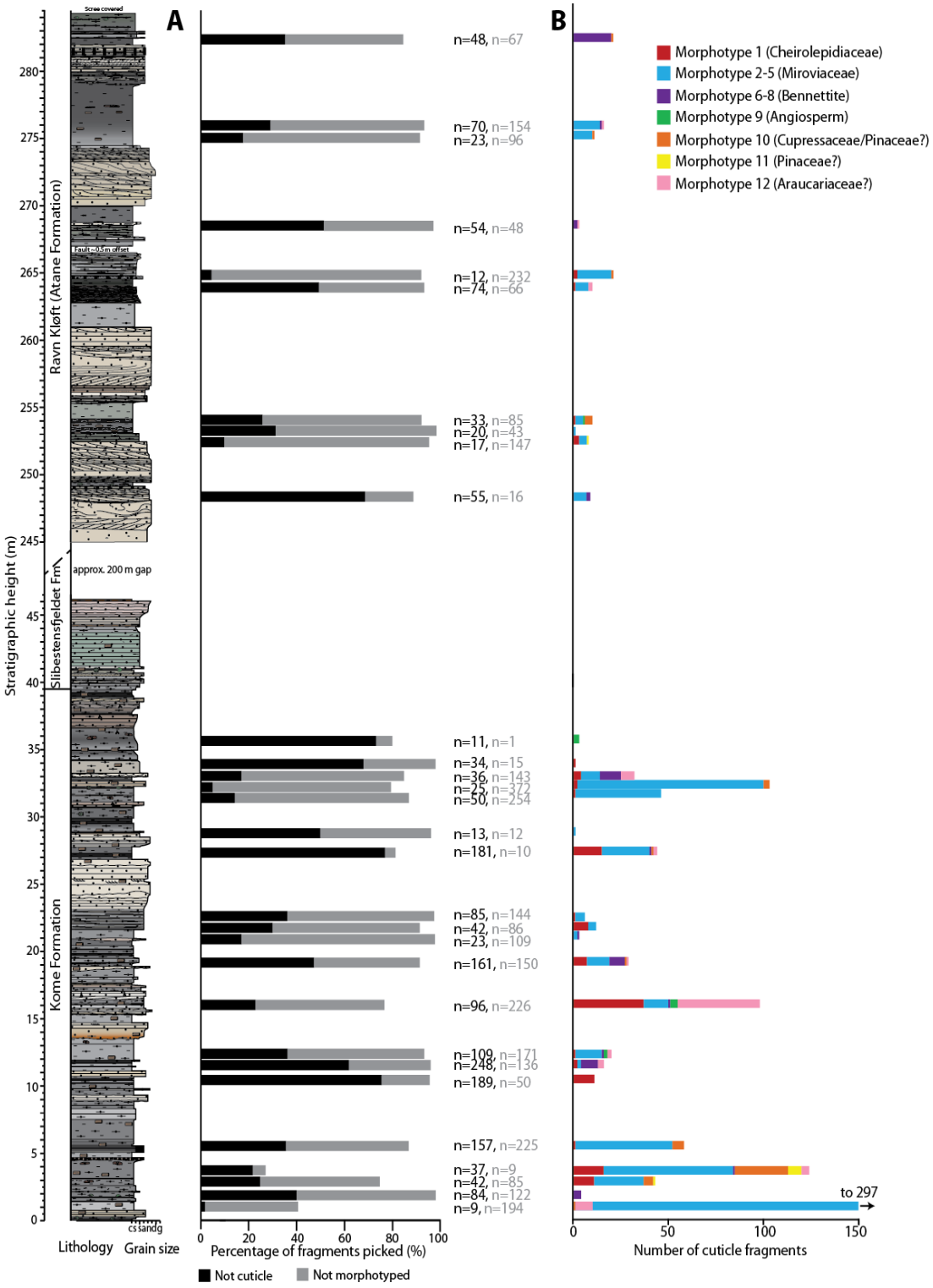

Figure 5.1: Graphic log for the Kome Formation and Ravn Kløft Member showing A: percentage of picked fragments which were either not cuticle (black) or could not be morphotyped (grey), n = number of fragments of each type. B: number of cuticle fragments of each morphotype as shown in legend examined for through the Kome Formation and Ravn Kløft Member.

could affect the floral yield by varying the potential for cuticle preservation. For example, in coarser grained sediment (particularly in the Ravn Kløft Member), cuticle was observed to

be more poorly preserved due to physical damage, where cuticle fragments were identified but the cellular detail was eradicated by damage from sand grains. The Ravn Kløft Member in general has a greater fluvial component than the Kome Formation, with more channel sands and in general coarser grain sizes and, on average, fewer organic fragments picked (Figure 5.1A). Preservation of plant material may also be selective depending on the proximity to the deposition site and preferred habitat of a given plant type (e.g. Coiffard *et al.*, 2007, Figure 5.13) or by processes transporting material to the site of deposition (e.g. selective fluvial transportation, Poole and Kürschner, 1999 and references therein).

Finally, assessment of diversity is not resolvable through the West Greenland stratigraphy because the twelve morphotypes (Chapter 4) do not represent total floral diversity. The morphotypes generally represent the most abundant plant groups in the West Greenland stratigraphy that were most readily preserved, and other plant types were identified in the cuticle but could not be grouped into morphotypes due to the small number of fragments of each type (Section 4.6). Furthermore, the identification of morphotypes is at best to genus-level, thus, the morphotypes were grouped into general plant families (Cheirolepidiaceae [1], Miroviaceae [2–5], Bennettitales [6–8], Angiosperms [9], with the gymnosperms of morphotypes 10–12 kept separate). Whilst this does reduce the quality of the record of floral changes by potentially masking genera-specific variation, this is the most reasonable approach given the biases outlined previously, and follows standard protocol from other palaeoecological studies (e.g. McElwain *et al.*, 2007; Section 1.5.2).

5.2.1.2 Relative distribution of morphotypes

The relative abundances of morphotyped cuticle fragments (Figure 5.2) reveal common associations of plant groups; for example, the Cheirolepidiaceae and Miroviaceae. In order to compare the stratigraphic horizons in terms of the floral composition, a detrended correspondence analysis (DCA) of the morphotype relative abundance was utilised as an explorative tool (using PAST freeware). The DCA compares the relative abundances of the plant groups (as in Figure 5.2) assigning a value (axis 1) to indicate the similarity of the horizons, such that similar axis 1 values indicate a similarity in floral abundance. The horizon at 35.72 m was omitted from the DCA because the floral composition of 100 % angiosperm morphotype (9) was so different from the rest of the horizons no other trends could be determined if it was included. The variation of axis 1 values through the West Greenland stratigraphy is shown in Figure 5.3C.

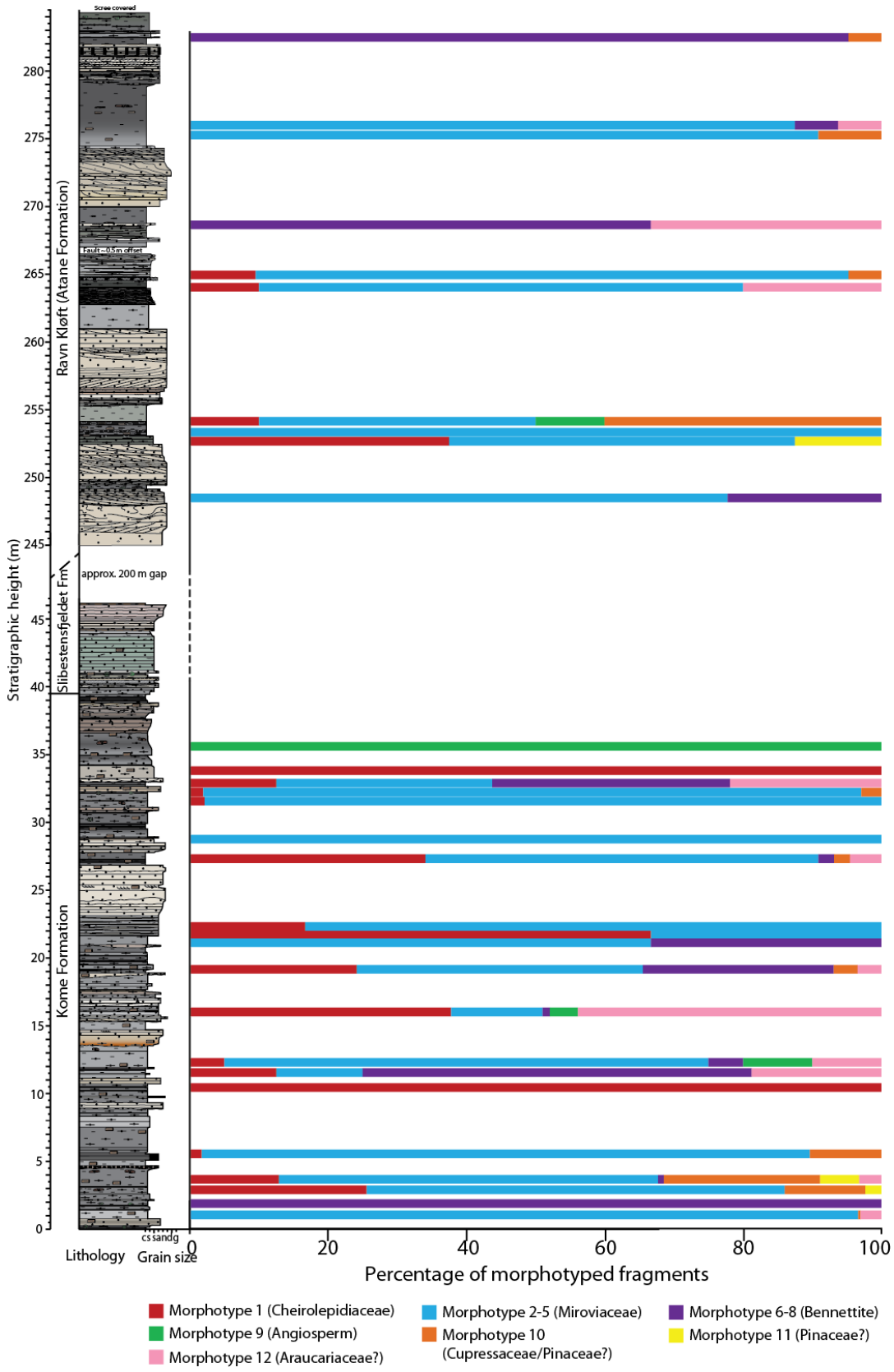

Figure 5.2: Relative abundance of plant groups (as shown in legend) through the Kome Formation and Ravn Kløft Member.

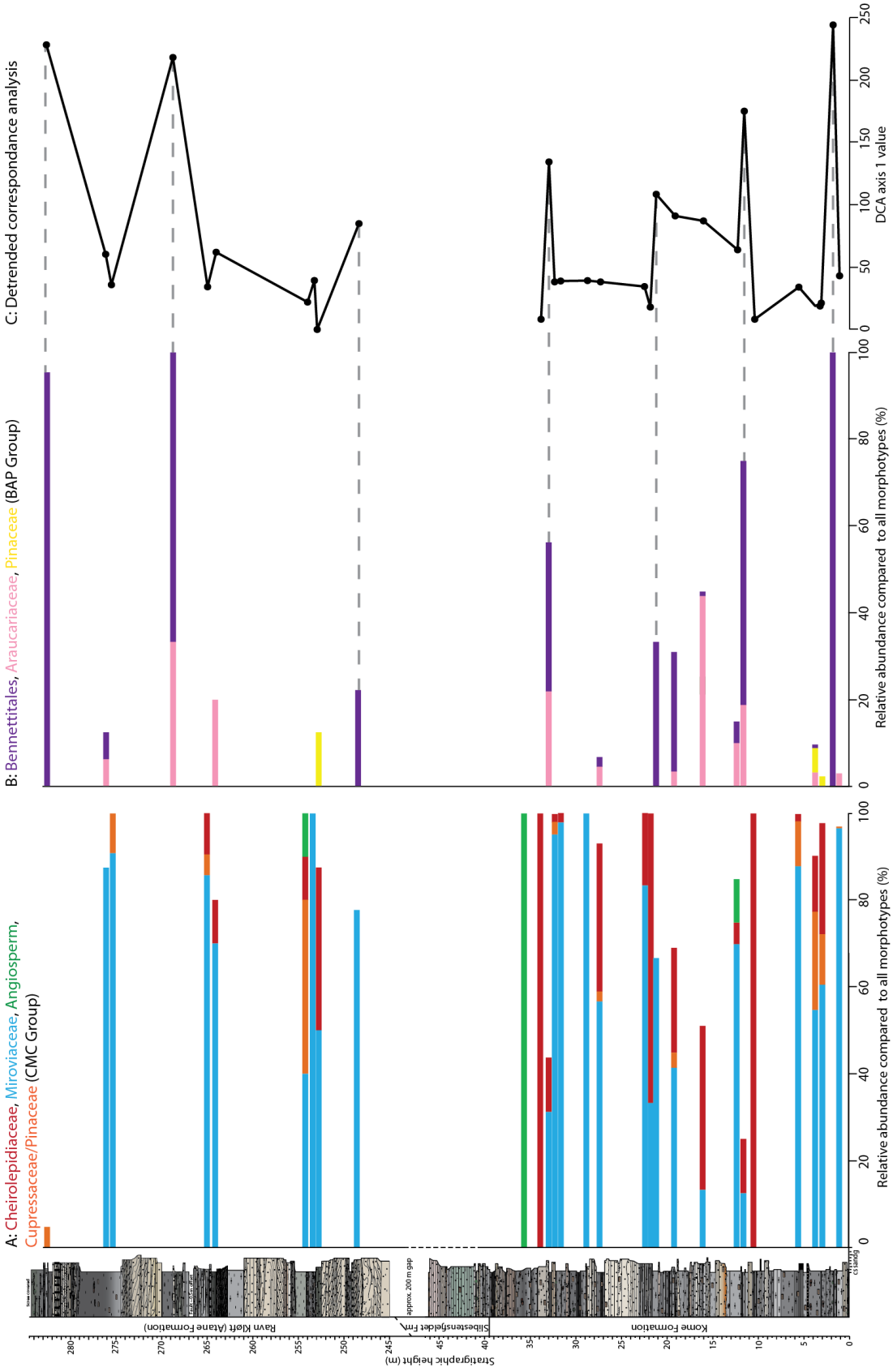

Figure 5.3: A and B: relative abundance of plant groups (as shown in legend) through the Kome Formation and Ravn Kløft Member. C: Detrended correspondence analysis axis 1 values, whereby similar axis 1 values reveal similar floral composition horizons.

If similar axis 1 values of the DCA analysis (Figure 5.3C) are considered to represent similar floral compositions, comparison to the relative abundance of morphotypes (Figure 5.3A, B) reveals the cause of generally lower axis 1 values <50 from those with axis 1 values >50. High axis values are observed when the relative abundance of Bennettitales (morphotypes 6–8), Araucariaceae (morphotype 12) and to a lesser extent Pinaceae (morphotype 11) increase above 12.5 % (Figure 5.4).

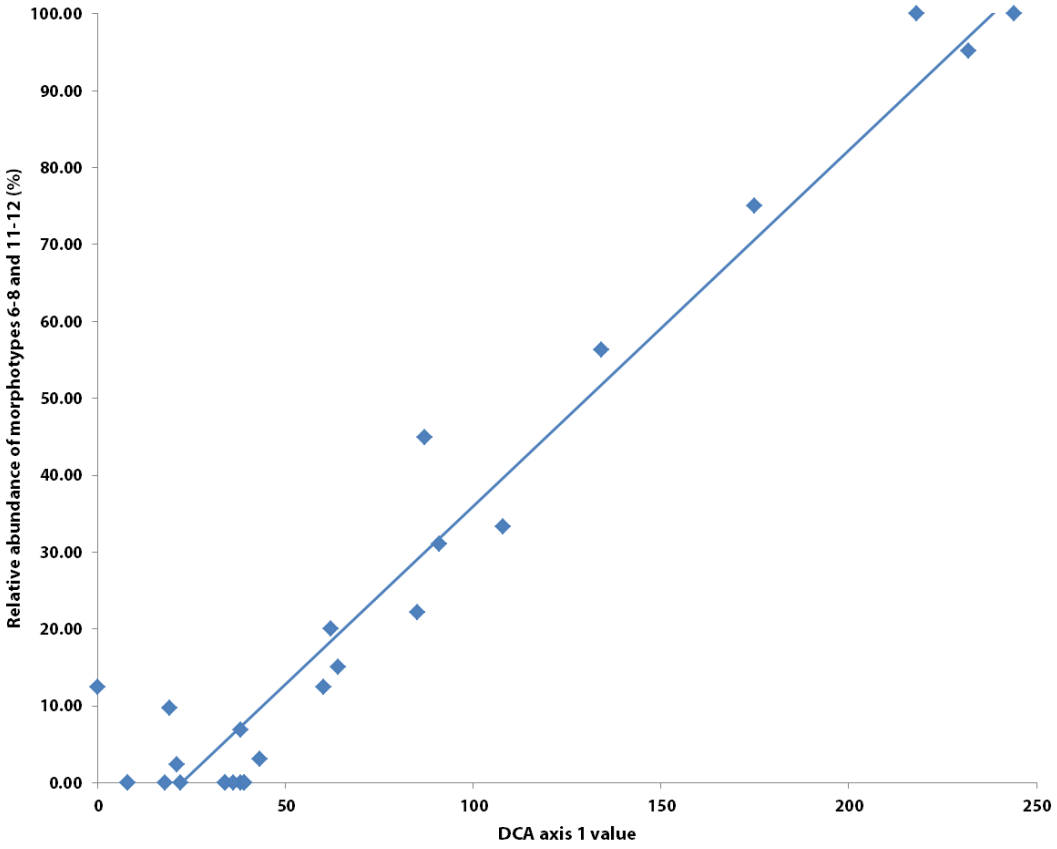

Figure 5.4: DCA axis 1 values against the combined relative abundance of morphotypes 6–8, 11 and 12 (BAP group) showing an increase in relative abundance of > 12.5 % with axis 1 values > 50. R^2 value of linear trendline = 0.93

Therefore, the DCA reveals the possibility of two floral groupings, one of which contains Bennettitales (morphotypes 6-8), Araucariaceae (morphotype 12) and Pinaceae (morphotype 11), hereafter the BAP group, which increases in relative abundance (Figure 5.3B) as the relative abundance of the Cheirolepidiaceae (morphotype 1), Miroviaceae (morphotypes 2–5) and Cupressaceae/Pinaceae (morphotype 10), hereafter the CMC group, decreases (Figure 5.3A). If the DCA does reveal a floral transition between these two floral groupings, the trend in axis 1 values through the stratigraphy reveals shifts in the relative dominance of these two plant groupings (Figure 5.3C).

Generally the middle portion of the Kome Formation (around 10 m to 27 m stratigraphic height in Figure 5.3) has coarser lithology than the rest of the Formation. Through this interval, the axis 1 values are generally >50 compared to above and below, indicating that this middle portion of the Kome Formation has a greater representation of the BAP group. Similarly, the Ravn Kløft Member is a coarse-grained lithology representing a significant fluvial channel component (channel sandstones shown in graphic log, Figure 5.3). In comparison to the Kome Formation, the Ravn Kløft Member has, in general, higher axis 1 values, suggesting that the relative importance of the BAP group is even greater, and is reflected in the relative abundance data (Figure 5.3B).

An additional possible relationship between plant groups can be observed between the Cheirolepidiaceae (morphotype 1) and Miroviaceae (morphotypes 2–5) families (Figure 5.3A). Generally, as the relative abundance of either Cheirolepidiaceae or Miroviaceae is higher, the other has a lower relative abundance. When the frequency distribution of the relative abundance of Miroviaceae with respect to just the Cheirolepidiaceae and Miroviaceae is considered, a skewed relationship is apparent (Figure 5.5).

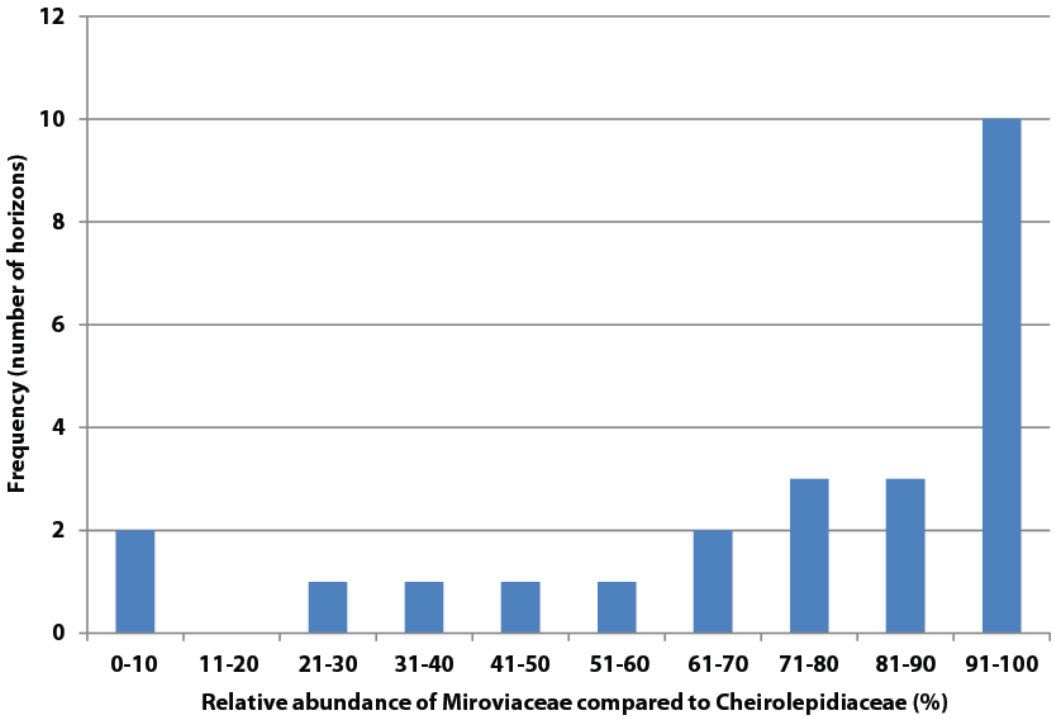

Figure 5.5: Frequency histogram of relative abundance of Miroviaceae compared to Cheirolepidiaceae (i.e. relative abundance of Miroviaceae plus relative abundance of Cheirolepidiaceae = 100%), showing greater dominance of high and low ratio of Miroviaceae versus Cheirolepidiaceae indicating a negative relationship between occurrence within a horizon.

The frequency distribution shows that, in general, there is a large proportion of Miroviaceae compared to Cheirolepidiaceae. If the two plant types were occupying the same environmental niche and responded to palaeoenvironmental changes in the same way, an equal distribution between the two plant families would be expected (i.e. a peak in relative abundance around 40–60 %). Therefore, the unequal distribution through the West Greenland stratigraphy may reveal a second order floral compositional change, which can be resolved by a DCA of the relative abundance of just Miroviaceae compared to Cheirolepidiaceae (Figure 5.6B).

There is no strong correlation between the two plant groupings described for the DCA of all morphotypes (CMC and BAP groups divided in Figure 5.6A by dashed line) to the changes in axis 1 values for the Miroviaceae-Cheirolepidiaceae DCA (Figure 5.6B). Based on comparisons to the relative abundance data, high axis 1 values in the Miroviaceae–Cheirolepidiaceae DCA correspond to a greater abundance of Cheirolepidiaceae. There is a tentative suggestion that, overall, the significance of the Cheirolepidiaceae decreases from around 10 m stratigraphic height to the top of the Kome Formation (dashed arrow, Figure 5.6B), except for the topmost Kome Formation data point which represents 100 % Cheirolepidiaceae. Within this declining trend are smaller oscillations in the relative dominance of either group, which may have lithological or ecological significance (Section 5.6.3).

Despite the possible relationships across floral groups, there is little information on the angiosperms based on morphotype 9 (the angiosperm morphotype) other than the abundance was low, comprising only 0.7 % of all the cuticle fragments morphotyped (10 angiosperm fragments out of the 1506 cuticle fragments morphotyped). In one horizon

Figure 5.6 (next page): DCA analyses of cuticle morphotype data through the Kome Formation and Ravn Kløft Member. A: Axis 1 values of relative abundance data of all morphotypes grouped into plant families as outlined in section 5.2.1, dashed line show division of two plant groupings, whereby everything to the left of the line is predominantly CMC group = Cheirolepidiaceae, Miroviaceae, Angiosperm and Cupressaceae/Pinaceae; everything to the right indicates an increased influence of the BAP group = Bennettitales, Araucariaceae and Pinaceae.

B: Axis 1 values of relative abundance data for Miroviaceae with respect to Cheirolepidiaceae only (i.e. relative abundance of Miroviaceae plus Cheirolepidiaceae for a given horizon = 100%) whereby higher axis 1 values indicate a greater dominance of Cheirolepidiaceae. The dashed arrow shows a possible general decline in the relative dominance of Cheirolepidiaceae through the Kome Formation.

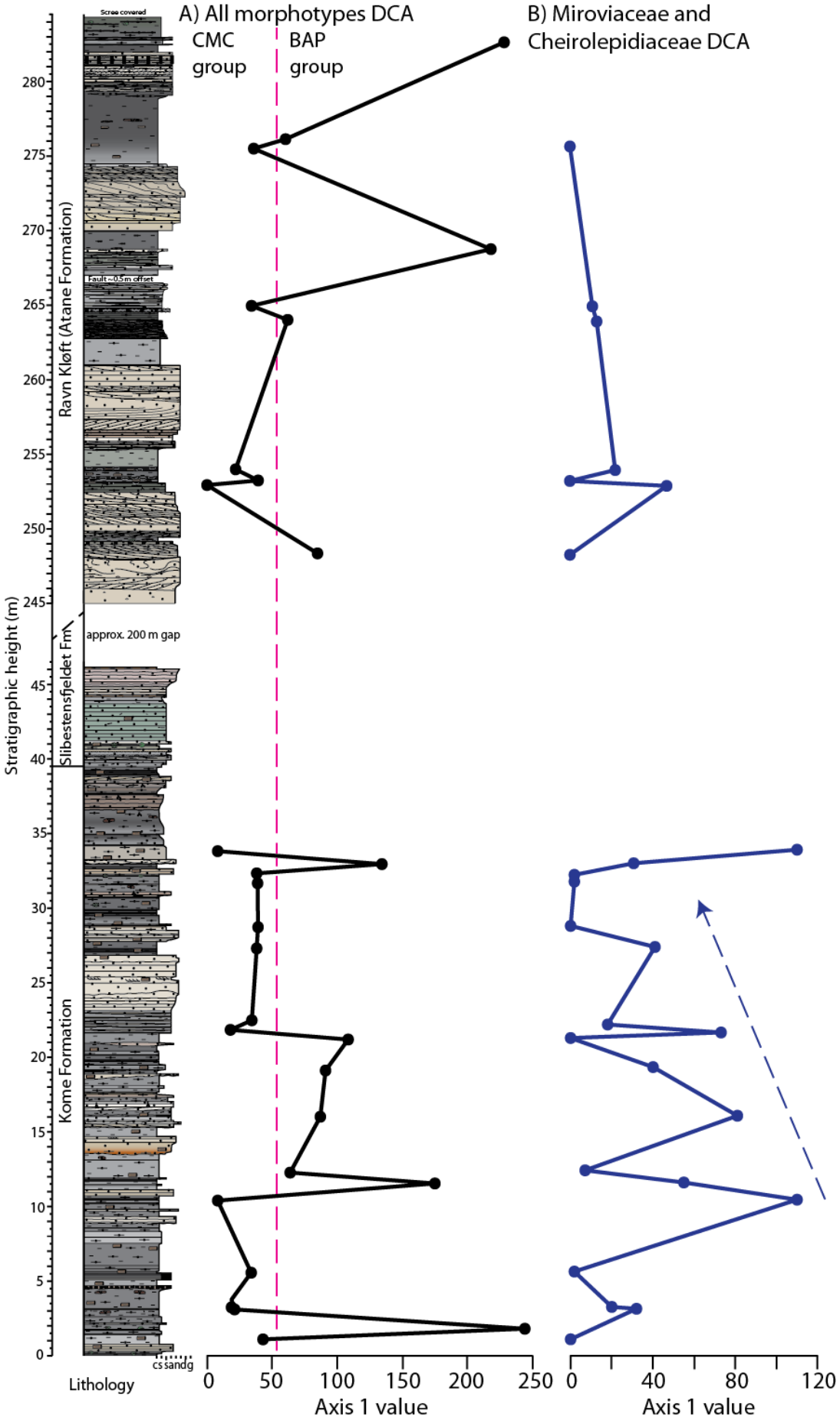
A) All morphotypes DCA
CMC group
BAP group
B) Miroviaceae and Cheirolepidiaceae DCA
Scree covered
Fault ~0.5 m offset
Ravn Kløft (Atane Formation)
approx. 200 m gap
Slibestensfjeldet Fm
Kome Formation
Stratigraphic height (m)
280
275
270
265
260
255
250
245
45
40
35
30
25
20
15
10
5
0
cs sandg
Lithology
0
50
100
150
200
250
Axis 1 value
0
40
80
120
Axis 1 value

(LK-B-87 at 35.72 m height in the Kome Formation) only angiosperm (morphotype 9) cuticle fragments were found, but this horizon also had a very low yield of organic material (15 organic fragments of which 3 were angiospermous, with no strong lithological clues as to why this was the case). In order to understand the apparent rarity of angiosperms through the West Greenland stratigraphy, and whether this is related to taphonomic biases of depositional environment and relative locations of floral occupation sites (i.e. were the angiosperms living elsewhere other than the site of deposition?), other means of assessing the angiosperm representation must be considered, namely pollen records and macrofossil records.

5.2.2 Pollen records

The palynological data of Horikx and Heimhofer (unpublished) provides a basic picture of terrestrial pollen through the Kome Formation, Slibestensfjeldet Formation and Ravn Kløft Member. However, the data presented in this thesis are absolute abundances only, and the amount of sample macerated or overall number of organic fragments is unknown, thus, relative abundances cannot be determined. The number of angiosperm pollen grains increases rapidly in the Kome Formation, from around 1–3 grains in the lower Kome Formation to around 23 by the top of the Kome Formation (Figure 5.7). Numbers remain fairly high through the lower to middle Slibestensfjeldet Formation (around 175 m height) before declining back to 1–3 grains by the top of the Slibestensfjeldet Formation and the lower portion of the Ravn Kløft Member (Figure 5.7). It may be expected that the lacustrine Slibestensfjeldet Formation would yield different concentrations of pollen than the more fluvially dominated deposits of the Kome Formation and Ravn Kløft Member, particularly if the pollen was wind-dispersed or the sedimentation rates were slower (Mander *et al.,* 2010). Nonetheless, the apparent increase in abundance of angiosperm pollen occurs at the top of the Kome Formation, around the same horizon as the increase in angiosperm cuticle abundance (Figure 5.7), providing a tantalising possibility that angiosperm abundances increased in the floral population towards the top of the Kome Formation. However, this remains tenuous given the lack of relative pollen abundance data and the low yield of angiosperm cuticle from West Greenland.

Examination of the pollen species identified from the pollen record reveals *Retimonocolpites* and *Clavatipollenites* in the lowest three horizons (which includes the horizon at the top of the Kome Formation where the five-fold increase in pollen abundance is observed; Figure 5.8) These two particular pollen species are significant because *Clavatipollenites* has been identified on the stamen of Lauraceae flowers of Cenomanian

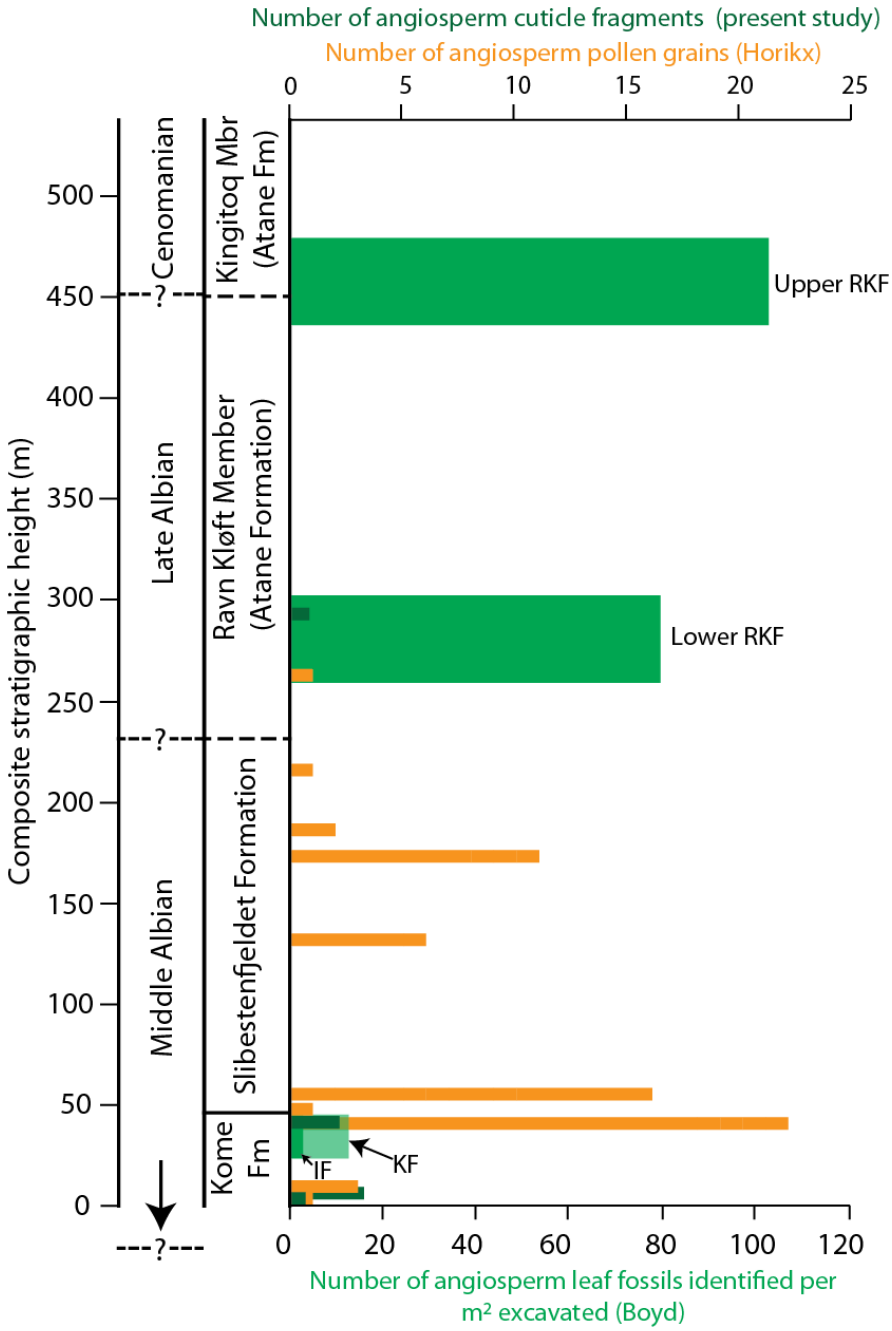

Figure 5.7: Summary of generalised angiosperm fossil records through the Nuussuaq section, showing present study cuticle record (dark green), pollen data from Horikx and Heimhofer (unpublished; orange) and generalised macrofossil data collected by Boyd (1998a-c, 2000, 2004).

age (Pedersen *et al.*, 1991), which further supports the interpretation of the angiosperm cuticle (morphotype 9) as likely Lauraceae. In the increased abundance horizon around 40 m height at the top of the Kome Formation (labelled LK-B-119 in Figure 5.8), the first *Tricolpites* pollen grain (only 1 grain) was identified, which are affiliated with the Eudicot clade (Friis *et al.*, 2011). Therefore the presence of both *Tricolpites* and *Clavatipollenites* pollen in the Kome Formation indicates the more basal angiosperms (Lauraceae, of the

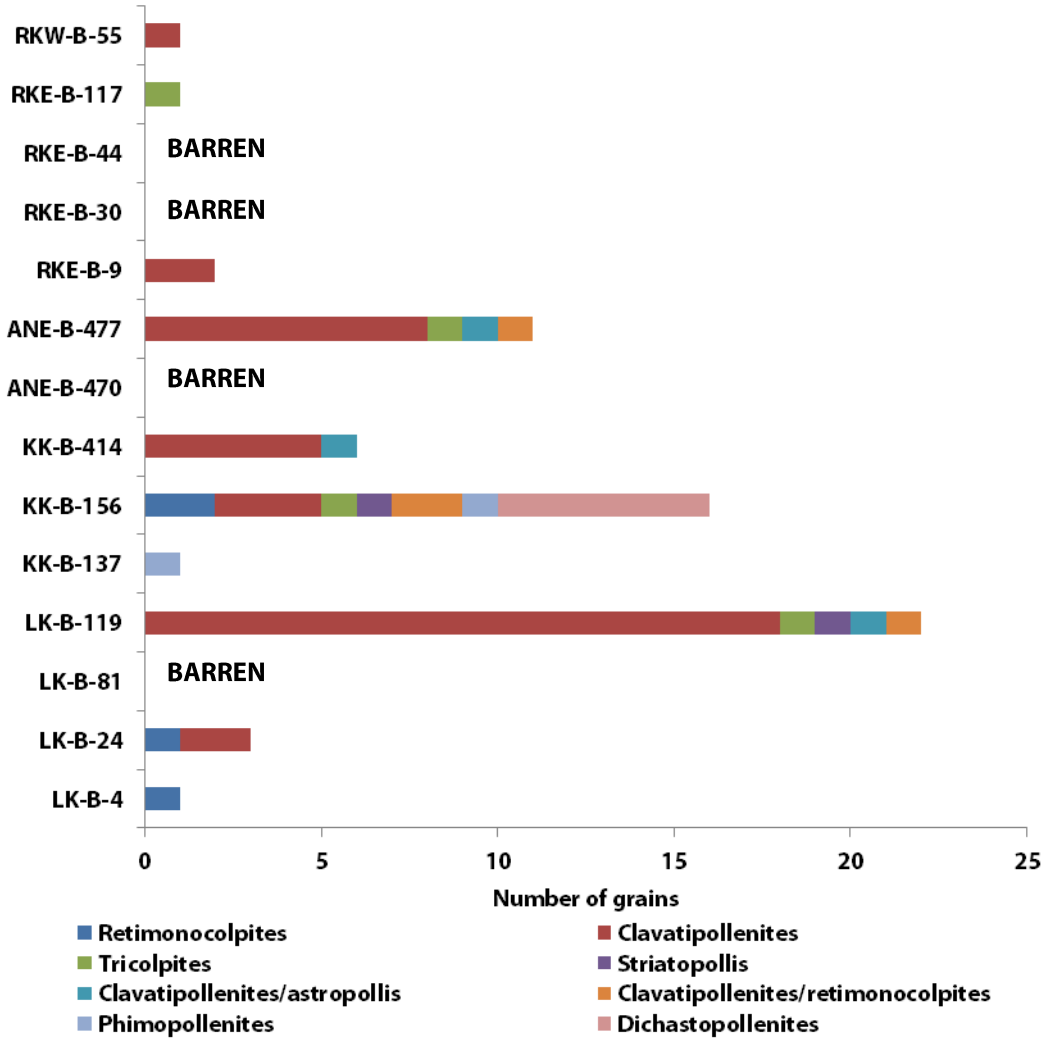

Figure 5.8: Pollen data collected by Horikx and Heimhofer (unpublished) using material from the present study, showing number of grains for labelled horizons in stratigraphic order as shown in Figure 5.7.

Magnoliid clade) and the later diverging Eudicots had already spread into this region by the Middle Albian.

5.2.3 Macrofossil records

As outlined previously, the rarity of all organic debris in the horizon which yielded only angiosperm cuticle (LK-B-87 at 35.72 m stratigraphic height), may indicate that the depositional environment in which angiosperms were deposited is either rarely encountered in the West Greenland stratigraphy and/or the depositional environment may not be conducive to cuticle preservation (for example in channel sands). A way of accounting for some of the lateral variation and to assess if this is a factor in angiosperm representation in the West Greenland stratigraphy is to explore the macrofossil record collected by Boyd (1998a-c, 2000, 2004) in the context of Floras as redefined by Boyd (1998c; Figure 5.9).

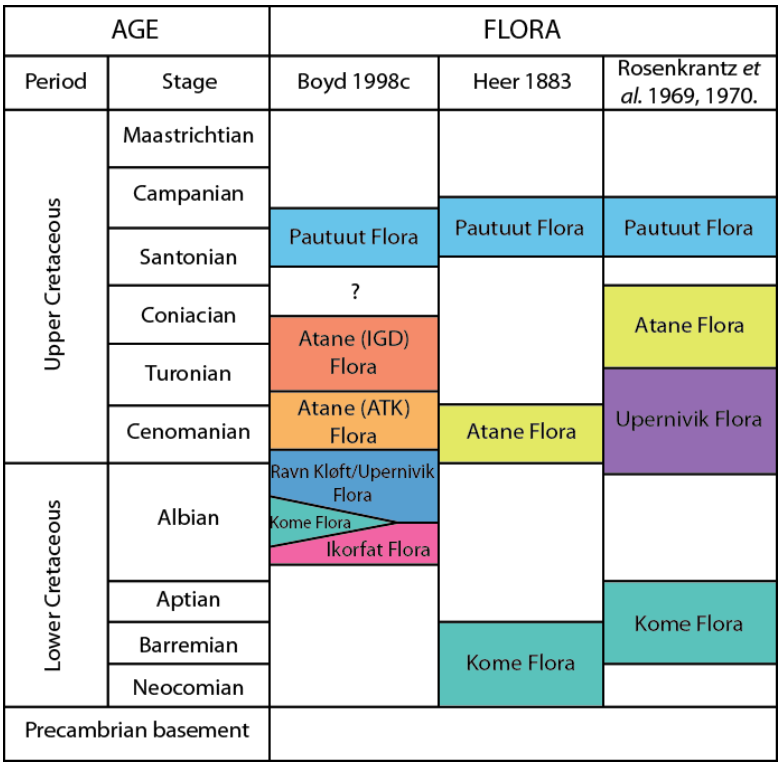

Figure 5.9: Redrawn from Boyd (1998c) showing approximate age relationship and newly defined Floras compared to previous studies.

Of Boyd's Floras, the Ikorfat Flora and Ravn Kløft Floras are geographically and stratigraphically the most applicable to the present study: the Ikorfat Flora is only found in the Kome Formation around Ikorfat, near the sections logged for the present study (Section 2.5; Figure 2.14). The Ravn Kløft Flora can be closely tied to the present study stratigraphy as Boyd's S sandstone was located in the field (Figure i, Appendix D) and correlated across to the RKE section permitting some, but not all, of Boyd's florules stratigraphic heights to be approximated to the present study stratigraphy (Figure 5.10).

The Ikorfat Flora has the lowest abundance of angiosperm material (IF in Figure 5.7) of less than 5 leaf fossils per m^2 excavated. Only a slightly greater abundance of around 15 fossils per excavated m^2 was identified by Boyd for the slightly younger Kome Flora (KF in Figure 5.7). Boyd documented a higher abundance of angiosperm leaf fossils in both the lower and upper Ravn Kløft Flora of 80 and 100 fossils per excavated m^2 respectively. This supports the evidence from the cuticle and pollen record that the West Greenland stratigraphy experienced an increase in angiosperm abundance, but given the uncertainty in the cuticle and pollen record (as set out in Section 5.2.1 and 5.2.2), the exact stratigraphic height of angiosperm abundance rise remains ambiguous, but likely occurred at some point between the upper Kome Formation and the Ravn Kløft Member.

Boyd also identified an apparent increase in angiosperm diversity on comparison of the stratigraphic ranges of different angiosperm genera in the Ikorfat and Ravn Kløft Floras

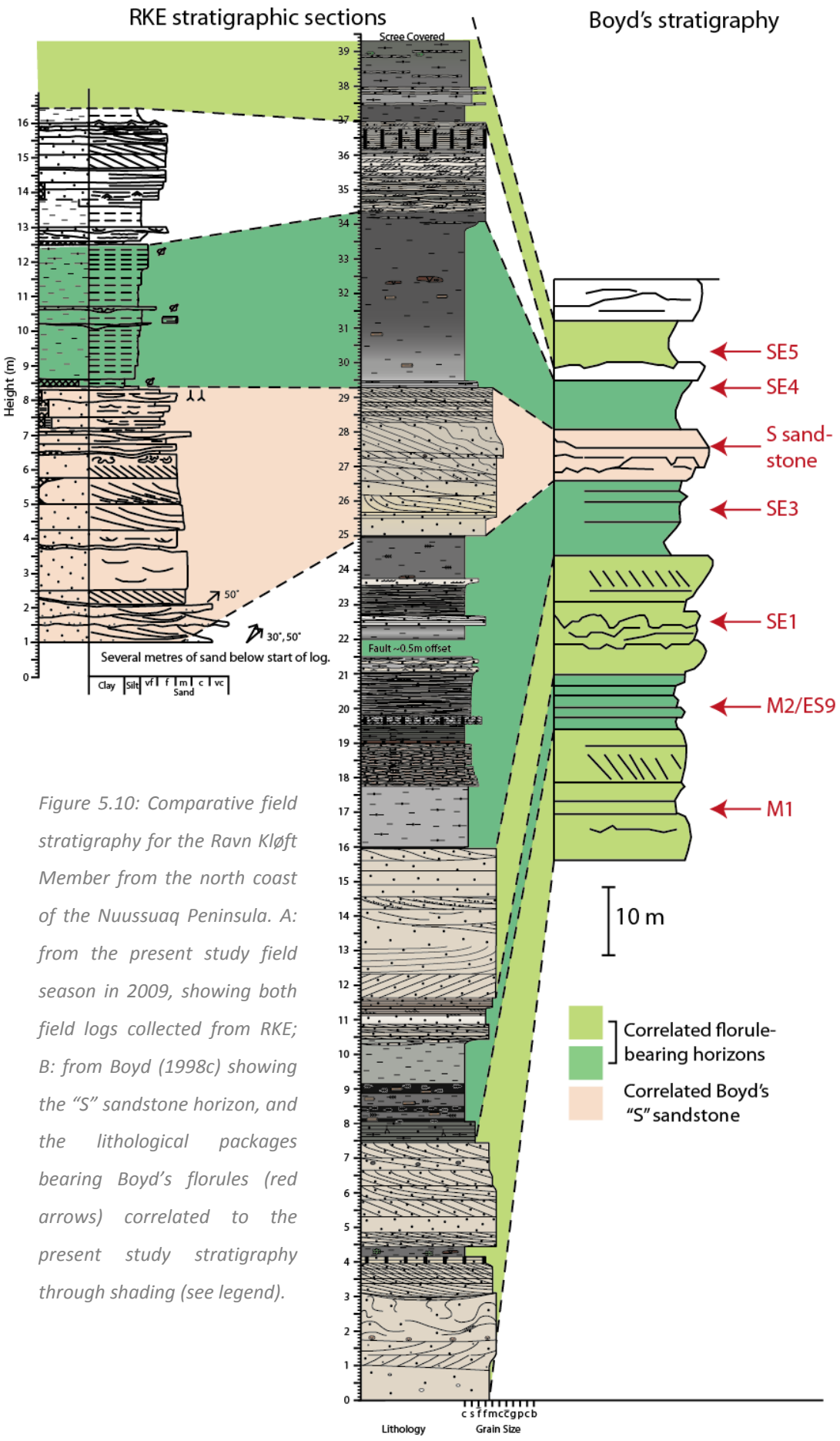

Figure 5.10: Comparative field stratigraphy for the Ravn Kløft Member from the north coast of the Nuussuaq Peninsula. A: from the present study field season in 2009, showing both field logs collected from RKE; B: from Boyd (1998c) showing the "S" sandstone horizon, and the lithological packages bearing Boyd's florules (red arrows) correlated to the present study stratigraphy through shading (see legend).

(Figure 5.10). Some additions to the stratigraphic ranges recorded by Boyd can be proposed based on the present study cuticle and macrofossil record. *Sapindopsis* macrofossil samples collected in the 2009 field season from the Kome Formation (Appendix D) indicates the stratigraphic range of *Sapindopsis* should be extended into the Kome Formation (Figure 5.11).

The predominant angiosperm cuticle identified from the Kome Formation was interpreted as most likely Lauraceae and tentatively assigned as *Trilaurus* on examination of the macrofossils available (Section 4.5.4); indicating *Trilaurus* was present in the Ikorfat Flora. Additionally, the occurrence of *Clavatipollenites* pollen in the Kome Formation (Horikx and Heimhofer; unpublished, Figure 5.8) indicates the stratigraphic range of *Trilaurus* also should be extended into the Kome Formation (Figure 5.11).

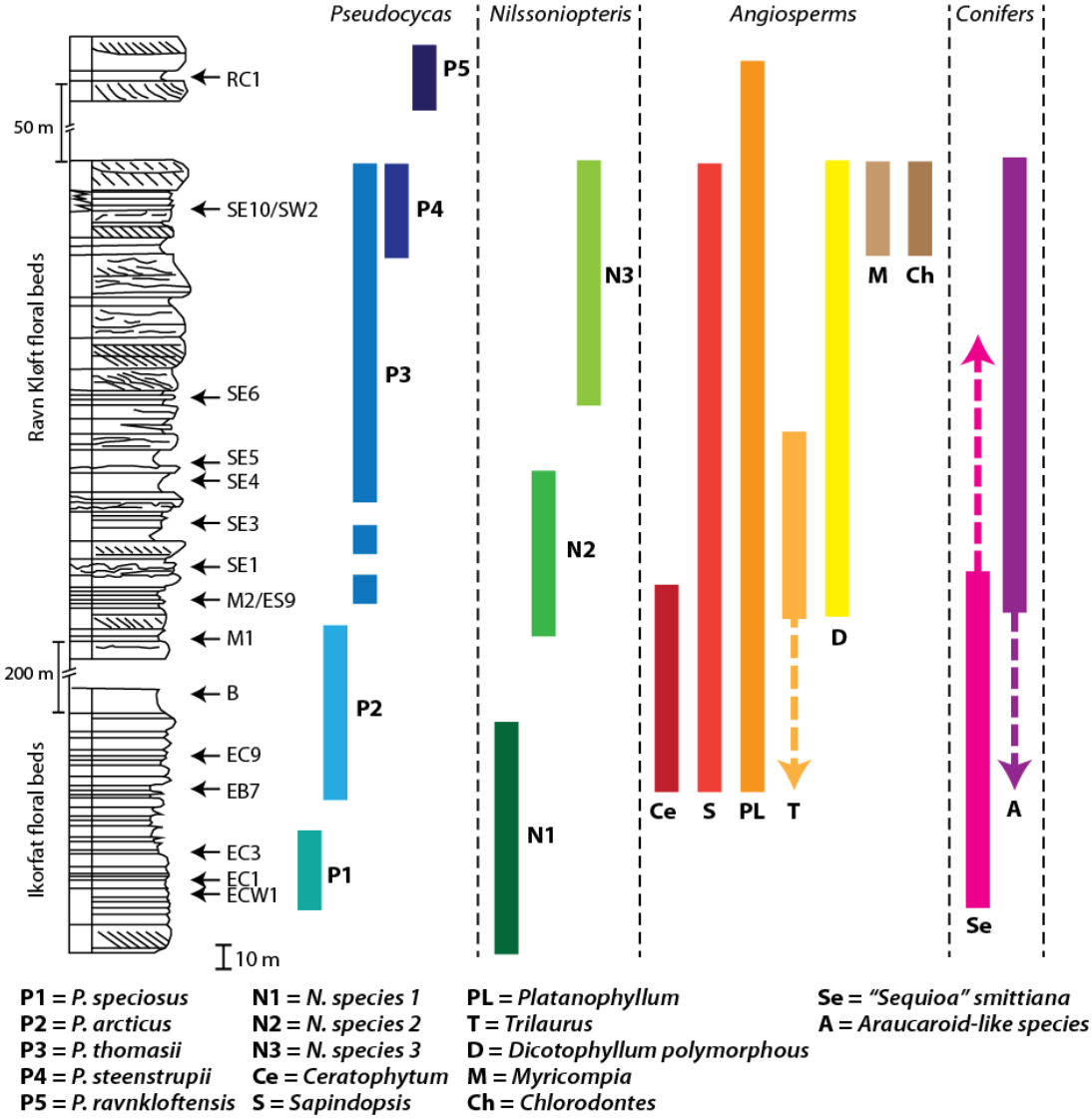

Figure 5.11: Redrawn from Boyd (1998c) showing the stratigraphic ranges of leaf fossils collected by Boyd through the Ikorfat and Ravn Kløft floras. Dashed arrows indicate extension of stratigraphic ranges based on present study cuticle.

Boyd's "*Sequoia" smittiana* (Figure 5.11) was described by Seward (1927) from West Greenland and has been tentatively reconciled with the descriptions of morphotype 10 (*Taxus* or *Sequoia* genus affinity; Section 4.5.5). If the identification of morphotype 10 is correct, the stratigraphic range of "*Sequoia" smittiana* could be extended further into the Ravn Kløft Flora through correlation to Boyd's stratigraphy (Figure 5.11).

Similarly, Boyd (1998 a-c) identified an Araucaroid-like conifer. Whilst the plant was never described by Boyd, it could tentatively be compared to an Araucaroid-like conifer identified in the cuticle record (morphotype 12, Section 4.5.7). Thus, Boyd's Araucaroid-like stratigraphic range can be extended into the Kome Formation but this remains ambiguous (Figure 5.11). If the association of morphotypes 10 and 12 cuticle is comparable to Boyd's macrofossil record, it would suggest that these two plant types persisted through the Nuussuaq Peninsula stratigraphy from at least the upper Kome Formation to the Ravn Kløft Member (Figure 5.11).

Boyd (1998c) reconstructs an apparent evolutionary transition in two Bennettitalean genera: *Pseudocycas* and *Nilssoniopteris* (Figure 5.11) which would not be resolved in the present study data since morphotypes 6–8 (*Pterophyllum*? [6–7] and *Pseudocycas* [8]) were grouped as a single Bennettitalean plant type. Nonetheless, Boyd's transitions may provide an additional indicator that the floral composition was responding to some driving factor at this time, although it did not affect all Bennettitalean genera, as *Pterophyllum* species showed no such trends (Boyd, 1998c).

5.3 Comparison to other records of angiosperm abundance

5.3.1 Global pollen first occurrences

Angiosperm floral abundance likely increased through the Albian–Cenomanian of West Greenland. This interpretation is supported by Boyd's macrofossil data, which indicates an increase in diversity (Figure 5.11) and abundance (Figure 5.7) between the Ikorfat and Ravn Kløft Flora, and within the Ravn Kløft Flora. Information from the cuticle and pollen records supports a low abundance of angiosperms in the Ikorfat Flora, but by extending the stratigraphic range of *Trilaurus*, this study suggests that some of the floral changes started earlier than previously suggested by Boyd (1998c), possibly around the top of the Kome Formation (Figure 5.7).

Adding the approximate stratigraphic range of the pollen record from the present study by Horikx and Heimhofer (unpublished) to the global summary of angiosperm pollen first

occurrences (Figure 5.12; Hickey and Doyle, 1977) suggests that Tricolpate and Monosulcate pollen may have appeared earlier than previously thought for around 55–60 °N palaeolatitude (Smith *et al.,* 1994).

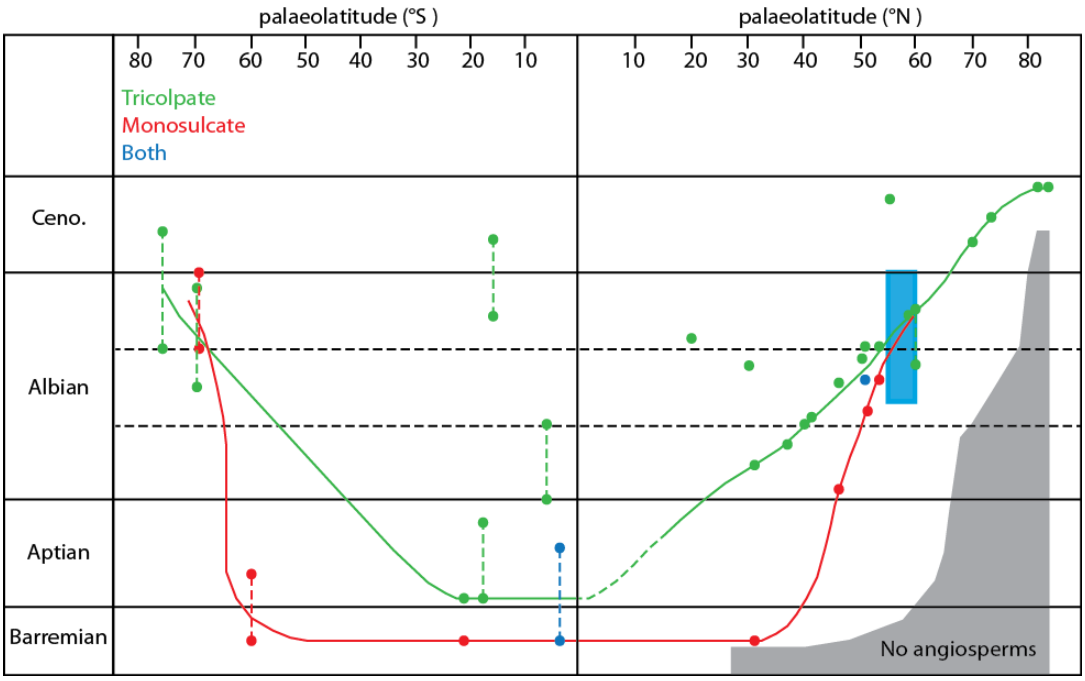

Figure 5.12: Adapted from Hickey and Doyle (1977), a summary of the first occurrences of Tricolpate and Monosulcate angiosperm pollen with palaeolatitude and time through the mid-Cretaceous, with site localities referenced within Hickey and Doyle (1977). Stratigraphic range of pollen record (including both tricolpate and monosulcate pollen) from the present study by Horikx and Heimhofer (unpublished), with uncertainty shown by light blue box.

However, the age constraints used by Hickey and Doyle (1977) are not calibrated to the Geological Timescale 2012, unlike the present study data. Therefore, the relative age association of stage boundaries may differ between the two datasets (present study data with respect to references within Hickey and Doyle, 1977). Age uncertainties are partially accounted for in Figure 5.12 by dashed lines (Hickey and Doyle, 1977). Additionally, there likely is variation in the method of palaeolatitude reconstruction, with estimates for the West Greenland section ranging between 55–60 °N (Smith *et al.,* 1994). Further compilations with more constrained palaeolatitude and age estimates are required to confirm if the Tricolpate pollen presence in the Middle Albian is the oldest record for this palaeolatitude (Horikx, *pers. comms.*).

5.3.2 North America

The increase in angiosperm abundance as indicated by the pollen and macrofossil records (Sections 5.2.2 and 5.2.3 respectively; Figure 5.7) can be compared to a compilation of angiosperm pollen abundance for North American sites above 42 °N palaeolatitude (Lupia

et al., 1999; Figure 5.13A) and a macrofossil summary (Lidgard and Crane, 1990; Figure 5.13B).

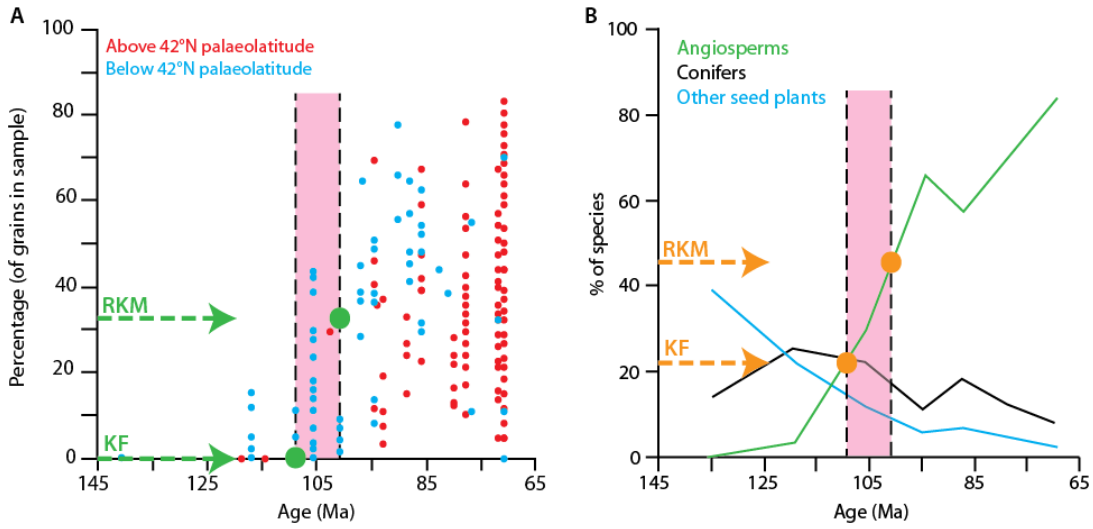

Figure 5.13: Redrawn and adapted comparisons of angiosperm abundance of the present study material (age range indicated by pink shading; KF = Kome Formation, RKM = Ravn Kløft Member). A: from Lupia et al. (1999) showing the percentage abundance of angiosperm pollen from North America sorted by palaeolatitude (see inset legend). B: from Lidgard and Crane (1990) showing macrofossil abundance changes from North America over the same interval.

Across the time interval from the Kome Formation to the Ravn Kløft Member (pink shading, Figure 5.13), angiosperm pollen abundance from North America above 42°N palaeolatitude increased from nearly 0 % to just over 30 %. This is comparable to the relative increase in abundance indicated by Horikx and Heimhofer's pollen record (unpublished; green points in Figure 5.13A) assuming the same amount of material was studied per horizon by Horikx and Heimhofer (but this remains unknown).

In order to accommodate the taphonomic differences between pollen and macrofossil data, generalised flora-based changes in abundance based on Boyd's macrofossil data (Ikorfat Flora compared to Ravn Kløft Flora; orange points, Figure 5.13B), were compared to the macrofossil compilation by Lidgard and Crane (1990; Figure 5.13B). Whilst the role of palaeolatitude is not included in the Lidgard and Crane dataset, the generalised angiosperm leaf fossil abundance increase (Figure 5.7) is of a similar magnitude to the increase indicated in the North American dataset (Figure 5.13B) from around 22 % to around 45 %.

Comparison of the West Greenland floral angiosperm abundance changes with the North American records strongly supports the radiation of angiosperms from the latest Middle Albian to Late Albian in West Greenland (equivalent to Upper Kome Formation to Ravn Kløft Member). The pollen records indicate that Eudicots had already spread into this

region by the late Middle Albian (Kome Formation; Section 5.2.2) which may be slightly earlier than previously thought for 60 °N palaeolatitude (Figure 5.12).

5.4 Comparison to floral assemblage of Europe

5.4.1 Records of floral change in Europe and the concept of landscape ecology

The European Cretaceous floral record is rich and reasonably well age-constrained (Coiffard *et al.*, 2012), with fossil collections obtained from numerous localities over the past 200 years (Coiffard *et al.*, 2006 and references therein). No synthesis of these records was attempted until the application of Wagner's Parsimony Method (WPM) by Coiffard *et al.* (2006, 2007). A strong relationship of floral composition to depositional environment was revealed through the Barremian to Cenomanian, reflecting the ecological landscape (the mosaic of juxtaposing environmental niches for a given geomorphological unit, Coiffard *et al.,* 2006, 2012; Figure 5.14A). The migration of the angiosperms between different

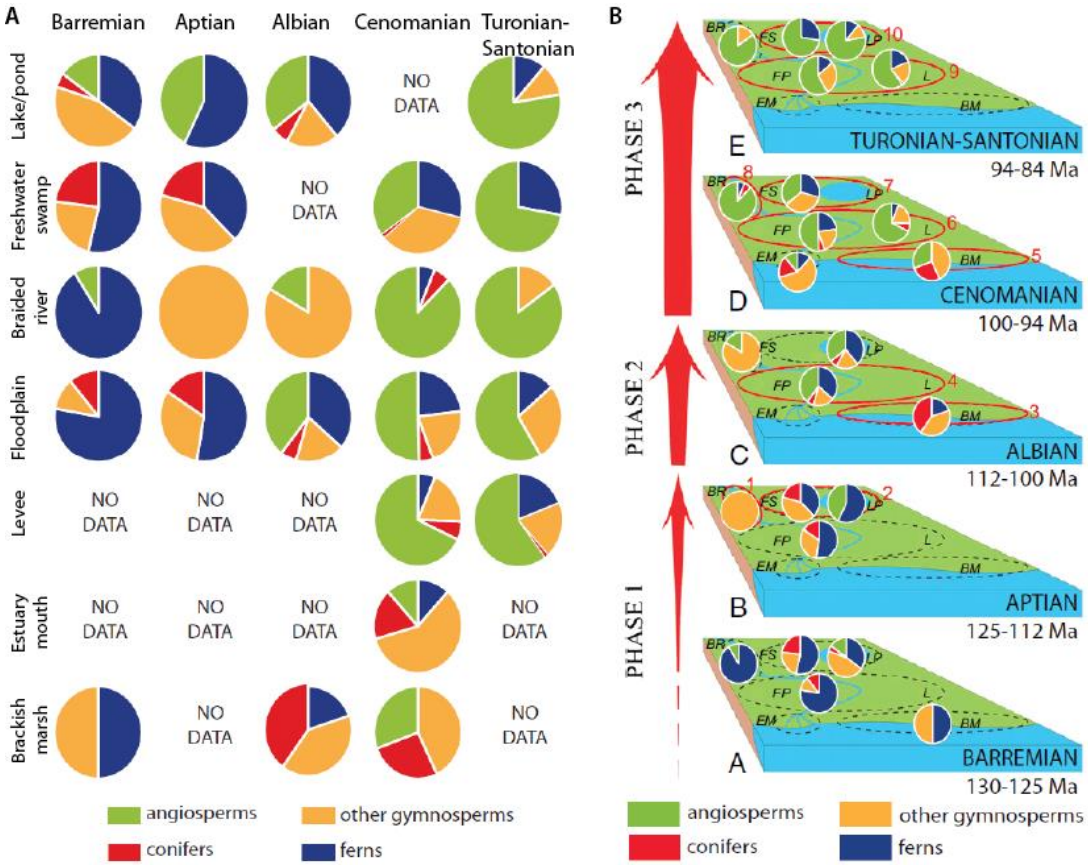

Figure 5.14: From Coiffard et al. (2012). A: pie diagrams showing vegetation compositional changes according to depositional environment for Barremian–Santonian. B: pie diagrams showing vegetational changes in a palaeoenvironmental context, showing the phases of floral migration.

palaeoenvironments was mapped and divided into three main phases through this interval based on the WPM analyses (Coiffard *et al.*, 2012, Figure 5.14).

The first phase (Barremian–Aptian, Figure 5.14) vegetation was dominated by fern thickets and conifer woodlands over floodplains, with restricted angiosperm presence as aquatics in freshwater wetlands, and chloranthoid, lauralean and magnolialean pollen representing the terrestrial angiosperms present by the late Aptian (Coiffard *et al.*, 2012). During the second phase (Albian, Figure 5.14), the European angiosperm floral record diversified, with an apparent spread onto floodplains as an understory under the coniferous canopy, whilst remaining dominant in the aquatic realm. The habit of the angiosperms contrasted with the ferns and gymnosperms which they replaced, with smaller leaves and a ramified habit (many active meristems regrow more readily if part of the plant is damaged, Coiffard *et al.*, 2012). By the beginning of the third phase (Cenomanian, Figure 5.14), the angiosperms occupied most environments including back swamps, coastal swamps and levees, but not estuaries (Coiffard *et al.,* 2012). Many angiosperms in the Cenomanian were arborescent, including the Lauraceae and Platanaceae, which inhabited river margins which were frequently disturbed (Coiffard *et al.*, 2012). Through phase three the angiosperms continued to spread over the floodplains, at the expense of other plant groups such as Bennettitales, which was suggested by Coiffard *et al.* as due in part to the angiosperm growth habit (e.g. the more energy efficient palm growth habit versus the Cupressacean conifers they replaced).

Coiffard *et al.* (2012) compared this tri-phase transition in angiosperm diversity and abundance to the North American floral records (Albian–Cenomanian; Hickey and Doyle, 1977) attributing the end of the second phase (understory angiosperm shrubs of Lower Albian age) and the beginning of the third phase (channel margin Platanoids of Albian to Cenomanian age) to the Potomac Group. The Albian–Cenomanian Dakota flora described by Retallack and Dilcher (1981) was compared to the third phase by Coiffard *et al.* (2012) due to the similarities in the range of palaeoenvironments in which angiosperm genera were found.

5.4.2 Ecological landscape from plant reconstructions of West Greenland

As identified previously in Chapter 5.2.1.2, attempts to resolve absolute changes in diversity and abundance cannot be assessed without consideration of taphonomic biases and an appreciation of plant ecology. Coiffard *et al.* (2006, 2007, 2012) have taken the ecological considerations a step further by considering the landscape ecology of a given

geomorphological unit, that ultimately, is represented by the fossil flora record. Therefore, in order to compare the present study floral changes to the European record and to test whether the phases in the European angiosperm floral record also occurred at higher latitudes, the ecology and typical palaeoenvironments of the floral components of the present study are assessed.

5.4.2.1 Angiosperms

The present study cuticle and macrofossil record identified two likely species of angiosperm present from the middle of the Kome Formation (*Trilaurus sassopsis* and *Sapindopsis Ravnkloftensis*), with additional species *Platanophyllum* spp. and *Ceratophytum schornii*, identified in the Kome Formation (Ikorfat Flora) by Boyd (1998c). The list of plants can be expanded for the Ravn Kløft Member from the fossil leaf record of Boyd (1998c) to also include *Panefolium*, *Chlorodontes*, *Myricompia* and *Dicotophyllum genera*. Of the angiosperms identified in the Kome Formation, *Trilaurus* is part of the more basal Magnollid clade, and was likely deposited in a floodplain. However, given the rarity of the cuticle fragments, the source of the cuticle fragments may have been further afield. The genera identified by Boyd (*Platanophyllum, Ceratophytum*, and *Sapindopsis*, all basal Eudicots) were located in lithologies interpreted as shallow lakes or bays (ECT, Figure 5.10) and fluvial sandstones and backwater swamps (EC9, Figure 5.10).

A greater range of angiosperm genera were identified by Boyd in the Ravn Kløft Member, some of which are basal ANITA grade angiosperms (Amborellales, Nymphaeales, Illiciaceae, Trimeniaceae and Austrobaileyales; Qiu *et al.*, 1999), which are not found in the Kome Formation, including *Chlorodontes* (of uncertain affiliation according to Boyd, 1998c, but most comparable to the Chloranthaeceae) and *Panefolium* (thought by Boyd to belong to the Nymphaeales). These taxa are found closely associated with aquatic palaeoenvironments (swamps, shallow lakes and over bank deposits; Florules SE2, SW2, SE10, Figure 5.10). The remainder of the angiosperm genera identified by Boyd in the Ravn Kløft Member are Eudicots, with the exception of *Trilaurus* (Magnoliid). Considering the greater fluvial component of the Ravn Kløft Member compared to the Kome Formation, the differences in the angiosperm record across this interval may indicate the expansion of more diversified angiosperms (Eudicots) into the disturbed fluvial channel environment by the Ravn Kløft Member.

5.4.2.2 Bennettitales

In order to understand the significance of the apparent spread of the angiosperms through different depositional environments, the spread or decline of other plant groups within the landscape ecology must also be considered. Both in the cuticle (Figure 5.6) and macrofossil records (Boyd 1998a, 2000), large accumulations of *Pseudocycas, Pterophyllum* and *Nilssoniopteris* leaf-form genera are found.

Currently, the growth habit of the Bennettitales is poorly constrained due to a lack of articulated fragments found in the fossil record. As a result, the two families of Bennettitales are distinguished upon plant habit and reproductive structures (Ryberg *et al*., 2007). Of these, members of the Williamsoniceae family have been reconstructed as slender palm-like and branching shrub and arborescent forms, and have been found associated with *Pterophyllum* and *Ptilophyllum* foliage genera (Delevoryas and Hope, 1976; Delevoryas, 1982; Govil, 2007 and references therein; Figure 5.15).

The identification of *Pseudocycas* associated with a fairly thick rachis from the present study macrofossil collection (around 1 cm; Figure 4.31A), which appears to be branching off another stem, and a similar specimen collected by Boyd (1998a; Figure 4.31B), could

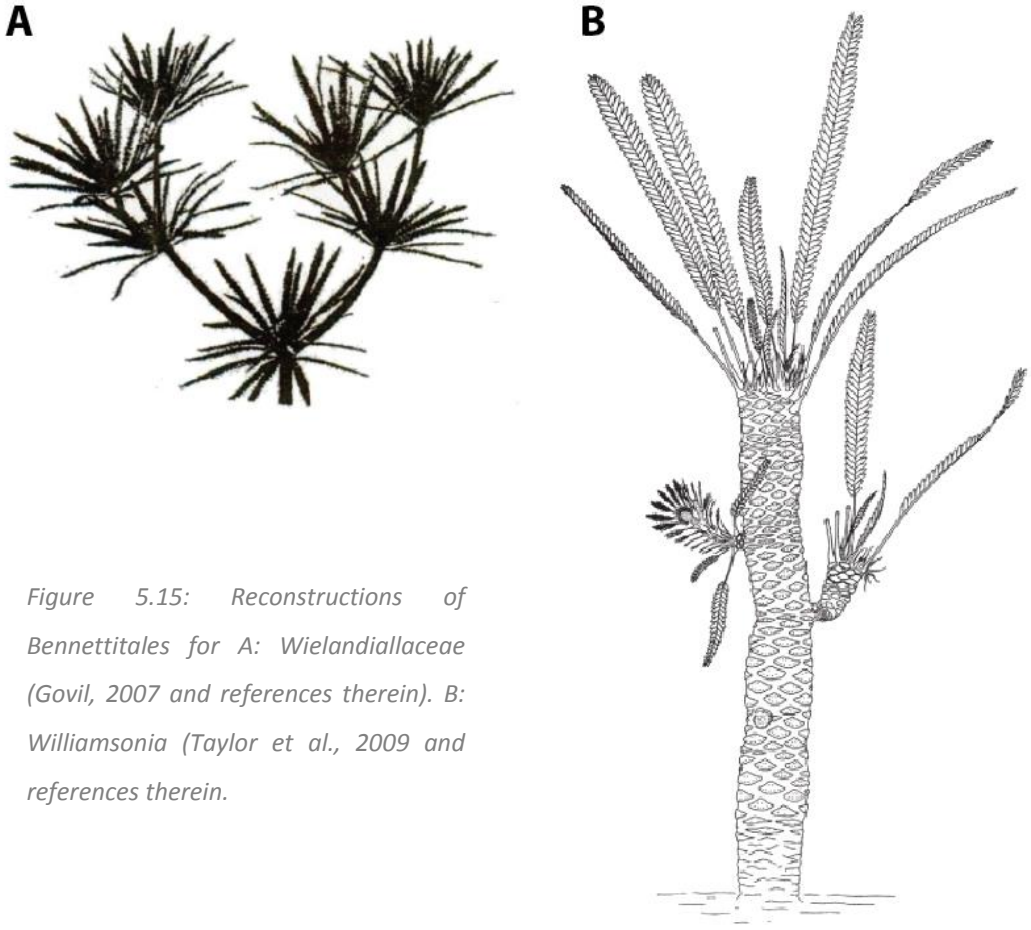

Figure 5.15: Reconstructions of Bennettitales for A: Wielandiallaceae (Govil, 2007 and references therein). B: Williamsonia (Taylor et al., 2009 and references therein.

indicate a branching habit of *Pseudocycas* from the field area. However, additional information on the likely stature of such a plant (shrub or tree) or the habit of the other Bennettitales identified from the macrofossils and cuticle records cannot be obtained due to the lack of associated stem and branch fossil information.

Figure 5.16: LK-F-3F cp of LK-F-2F ikorfat. Photograph showing Bennettite-rich horizon. A: non-annotated photograph, B: same photograph with overlay highlighting Pterophyllum (green), Nilssoniopteris (yellow) and likely Miroviaceae (blue).

Assemblages of *Pterophyllum, Nilssoniopteris* and *Pseudocycas* were identified in the field study and in some samples collected (e.g. Figure 5.16). However, pinnae where a central groove could be observed parallel to the leaf axis should not be interpreted as *Pseudocycas* exclusively: the study of the cuticle has revealed in many cases disarticulated pinnae bearing a median stomatal furrow are *Sciadopityoides* species (morphotypes 3 and 4) and appear to be commonly associated with *Pterophyllum* and *Nilssoniopteris* in fine grained lithologies of the Kome Formation (Figure 5.16). Boyd (1998a) also identified the common occurrence of *Pseudocycas* with Miroviaceae, and interpreted the Bennettitales in West Greenland were likely swamp margin dwellers, occupying slightly more drained soil on the overbank. This is supported by the assemblages identified in the present study, except, in addition, some of the compression fossil fronds of *Pterophyllum* were found in more sandy horizons in the Kome Formation (e.g. Figure 4.29A). Associated with fluvial sands, this may indicate Bennettitales bearing *Pterophyllum* foliage may also have persisted further from swampy sites, potentially in more drained river banks (and hence may have been transported). Given that previous reconstructions of associated foliage and stems have indicated *Pterophyllum* was found on tall slender arborescent Bennettitales (e.g. Figure 5.15B), it is suggested that some Bennettitales in West Greenland may have lined streams and swamp margins as trees, rather than as squat shrubs.

5.4.2.3 Miroviaceae

Previous studies reveal that the Miroviaceae were an important component of high latitude floras from the Jurassic onwards (Nosova and Wcisło-Luraniec, 2007; Nosova and Kiritchkova, 2008; ZiKun *et al.* 2012), despite only being represented in the fossil record by foliage, often in mass accumulations (e.g. Bose and Manum, 1990, 1991; Gomez, 2002; Gordenko, 2007). The palaeo-habitat of this plant in West Greenland is fairly consistent with these previous studies, with evidence for little transport, suggesting the Miroviaceae inhabited swamp-like waterlogged soils and the respective margins of such soils (Boyd, 1998c) or floodplain lakes where leaf litter collected parautochthonously (Manum *et al.*, 2000). The water source in the soil may vary from freshwater (e.g. Manum *et al.*, 2000) to brackish (e.g. brackish coastal floodplain, Gomez, 2002) indicating these plants may have been non-obligate halophytes since there is no evidence for brackish incursions in the Kome Formation or Ravn Kløft Member. Since the Miroviaceae are only known from shoot foliage, reconstructions of plant habit are limited. Miroviaceae leaves are strap-shaped, with rounded to acuminate tips, and in some morphotypes (*Sciadopityoides*) possess tubular leaf bases. A *Sciadopityoides* shoot fragment with leaves apparently still attached


A
7
8
9
10
11

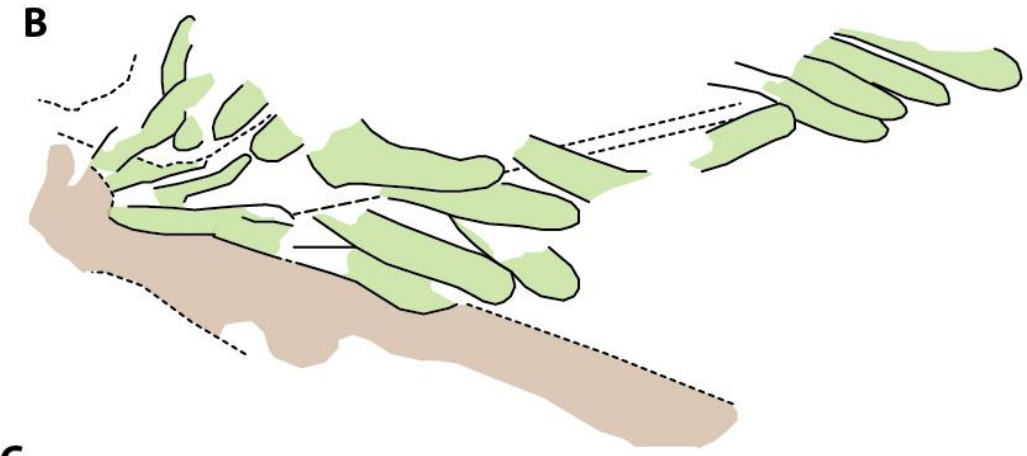
B

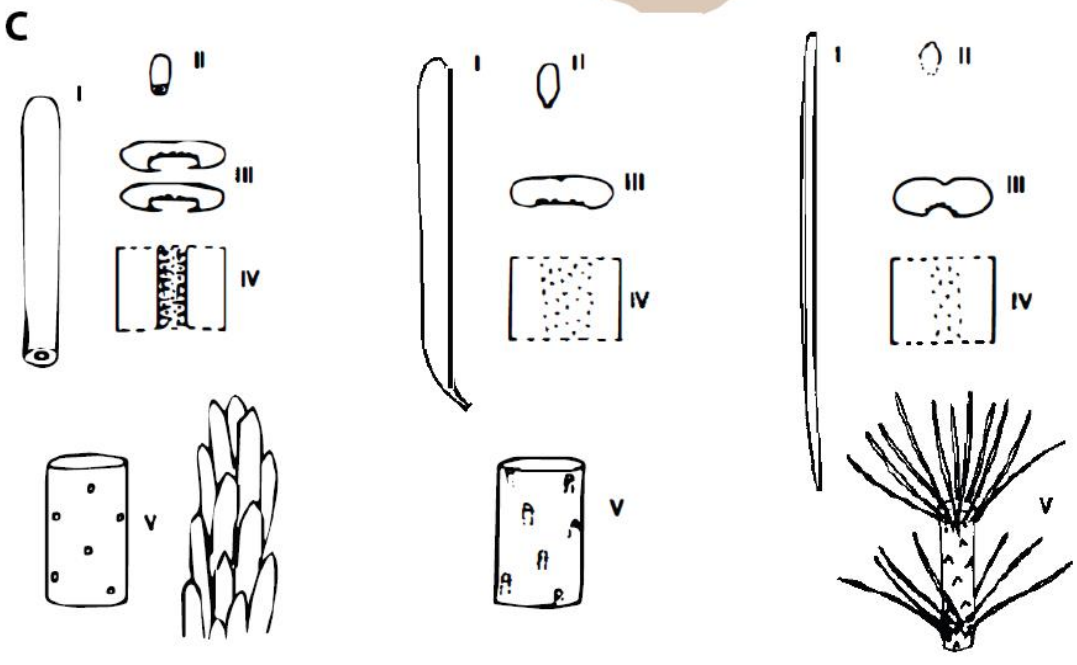
C
I
II
III
IV
V
Sciadopityoides
Oswaldheeria
Sciadopitys verticillata

to the stem was identified in one macrofossil sample collected during the field season in West Greenland (Figure 5.17A, B).

The specimen compares with the *Sciadopityoides* shoot form (Figure 5.17C), where the circular leaf base attached to the stem simply (i.e. not subtended by a scale leaf as is the case with *Sciadopitys verticillata*) in a spiral pattern, with leaves pointed upwards and appressed to the shoot (Bose and Manum, 1990). In addition, the shoot fossil also reveals a tentative association with fossilised wood (Figure 5.17B) indicating this plant may have had woody stems, similar to the extant *Sciadopitys verticillata* branching habit (Figure iii, Appendix D). The identification of a *Sciadopityoides* shoot fragment agrees with the cuticle morphotype identification (morphotypes 3 and 4). Shoot fragments of *Oswaldheeria* (morphotypes 2 and 5) were not identified in the macrofossil specimens, but have been described by Bose and Manum (1990) for material collected from Kome in West Greenland. Reconstructions of *Oswaldheeria* indicate leaves were attached to the shoot in a spiral arrangement as with Sciadopityoides, but leaf bases were decurrent and slightly twisted resulting in a more horizontal spreading of leaves (Figure 5.17C; Bose and Manum, 1990).

5.4.2.4 Conifers

Without shoot morphology, the cuticle fragments identified as Cheirolepidiaceae (morphotype 1) could not be assigned to a definite form-genus, but shared many features with *Pseudofrenelopsis* and *Frenelopsis* including: thick cuticle, stomata organised into scattered to well-defined rows, normally possessing 5–6 subsidiary cells, and papillae around the rim of the stomatal pit, but no papillae within the pit (Section 4.5.1). Unfortunately, reconstructions of plant habit vary across the form-genera; *Cupressinocladus valdensis* was reconstructed as a tall forest tree with a 1 m diameter trunk. In contrast, *Pseudofrenelopsis parceramosa* has been reconstructed with more succulent characteristics, with possibly less wood development, but still an arborescent habit and a more slender and uniform thickness trunk (Watson, 1988 and references therein). Other members of the Cheirolepidiaceae have been reconstructed as smaller

Figure 5.17 (previous page): Photograph and interpretation of collected macrofossil specimens. A: Sample "LK-F-3c"showing insitu Sciadopityoides leaves. B: sketch overlay of Sciadopityoides leaves showing leaf cuticle in green and possible wood in brown. Scale in cms. C: sketches of Miroviaceae compared to Sciadopitys verticillata from Bose and Manum (1990) showing: (i) long leaf morphology; (ii) short leaf morphology; (iii) leaf cross-section; (iv) stomatal distribution; (v) stem with leaf attachment position and reconstruction with leaves.

succulent plants and herbaceous forms with less wood development (e.g. *Frenelopsis ramosissima*, Watson, 1988 and references therein).

Previous interpretations of Cheirolepidiaceae conifer palaeo-habitat (e.g. Passalia 2009) generally agree with the present study: they are commonly found associated with floodplain and deltaic deposits, in generally wet settings. However, some Cheirolepidiaceae have been identified in palaeoenvironments which experienced at least seasonally prolonged aridity (Haworth *et al.*, 2005: English Wealden) and others were halophytes, with instances of brackish water conditions and tidal-estuarine influences (Haworth *et al.*, 2005; Aucour *et al.*, 2008; Potomac Group, North America). However, there is no direct evidence at present of brackish influences on the stratigraphy beyond that of the lacustrine Slibestensfjeldet Formation. However, given the likely proximity to the palaeocoastline (since there were brackish incursions of the Slibestensfjeldet Formation from a coastal lagoon, Dam *et al.*, 2009) the possibility of brackish incursions/influences cannot be totally ruled out.

The reconstructed habit of other Coniferales from West Greenland is unknown due to the sparse cuticle record and absence of identified macrofossil remains neither collected from the present study, nor described by Boyd. Seward (1927) did describe some conifer species, including Sequoineae (possibly similar to *Taxus* or *Sequoia*; morphotype 10) and Araucariaceae (morphotype 12) as well as Ginkgoales and *Elatocladus* (Section 4.6), all of which have been identified by few cuticle pieces from the present study. However, Seward fails to describe the lithology or depositional environment of the localities in which the fossils were found. The common association of *Taxus/Sequoia* (morphotype 10) with the Miroviaceae; and Araucariaceae (morphotype 12) with the Bennettitales (Figure 5.3; Figure 5.6 – CMC and BAP groups respectively), in addition to the stratigraphic ranges of these two morphotypes (10 and 12) persisting through the stratigraphy in West Greenland (Figure 5.11), may indicate these plants also inhabited the same or closely related respective ecological landscape. However, without an improved fossil record of other Coniferales and gymnosperms (e.g. the Ginkgoales; Seward, 1927), information on the significance of these plant groups on the radiation of the angiosperms into new environmental niches cannot be resolved.

5.4.2.5 Ferns

Ferns were not identified in the cuticle record, but are known to be part of the flora based on macrofossil specimens collected from the present study and by Seward (1927). A single

macrofossil specimen collected from the field area has been identified as *Sphenopteris.* The fossil frond (Figure iv, Appendix D) has oppositely arranged pinnae with notophyllous sized leaves along the rachis (see Ash *et al.*, 1999 for terminology). The leaves are pinnately lobed with rounded tips and have straight to decurrent bases and only the primary venation appears to be preserved in part. Seward described three species of *Sphenopteris* from the Cretaceous of West Greenland and found considerable overlap in form, with stems possessing alternate arranged leaves which are lobed at the base of the leaf and entire at the top (Figure iv; Appendix D). The unusual leaf morphology of the specimen is comparable to Seward's description, but further identification to species level is inhibited by the preservation.

Several other macrofossil samples collected during the present study possess poorly preserved bipinnate fronds with pinnules attached alternately along the rachis (Figure v; Appendix D). The pinnules are at least 10 cm in length, bearing rounded tipped leaflets, which were not always preserved. The leaflet-bearing pinnules are also found as individual fragments not associated with the rest of the stem (Figure v; Appendix D). The description of these fossil specimens compares to descriptions of *Gleichenites* species by Seward (1927; Figure v [C]; Appendix D), who found it to be the most abundant genus in the Cretaceous West Greenland vegetation. This was not the case in the present study, with no representation in the cuticle record (which may reflect the preservation potential of the fern cuticle) and limited numbers of macrofossil samples. This may highlight the significance of lateral variation in terrestrial palaeoenvironments, but Seward (1927) did not provide descriptions of sample sites, ages or lithologies, and thus can only provide a general floral assemblage for the Nuussuaq Peninsula.

5.4.3 Reconciliation of landscape ecology and floral compositional changes

The landscape ecology distilled from the available lithological and fossil evidence reveals the Miroviaceae likely represent the wettest soil occupiers, probably living either in swamp-like conditions or the margins of waterlogged areas (Section 5.4.2.3). Previous studies of Cheirolepidiaceae conifers (e.g. Passalia, 2009; Section 5.4.2.4) support the floral association of Cheirolepidiaceae and Miroviaceae, indicating they likely shared similar ecological niches. However, the possible negative abundance relationship between the two families (Figure 5.6B) suggests the Cheirolepidiaceae inhabited more drained soils than the Miroviaceae, perhaps further from the waterlogged margin. Therefore the shift in balance between the two families (Figure 5.6B) most likely reflect lateral variations in the

depositional environment (i.e. movement of water table or waterlogged condition margin), which would not be uncommon through time.

The identification of Bennettitales more closely associated with fluvial systems is reconciled with the identification of two floral groups in the DCA (Figures 5.3, 5.6A), and an apparent shift in lithology in the Kome Formation. Overall, the Bennettitales appear to have inhabited drained soils close to fluvial channel margins and possibly further from the site of deposition in the field localities, having been washed into floodplain deposits. As explained previously, the Cheirolepidiaceae and Miroviaceae are representative of more swampy conditions (high water content in soils), and the DCA (Figure 5.3 and 5.6A) reveals that through the Kome Formation, there was a shift from a more waterlogged and possibly swampy palaeoenvironment, to a greater role of the fluvial regime in the middle of the Kome Formation before returning to more waterlogged and swampy palaeoenvironments. The timescale of this shift is greater than the small scale oscillations in the interpreted waterlogged soil (or water table) margin movement (Figure 5.6B) and therefore may represent an ecological landscape shift imposed by palaeoclimatic variations rather than smaller scale lateral variations in terrestrial depositional environments (e.g. swampy margin movements).

The association of the other conifers identified in the cuticle record with the two groups of plants determined from the DCA (Figures 5.3, 5.6A) suggests morphotype 10 (*Taxus/Sequoia?*) may have occupied the wetter swamp-like environments (CMC Group; Figure 5.6A), whereas the Araucariaceae (morphotype 12) may have greater affiliation with the Bennettitales (BAP Group; Figure 5.6A); there is no contradictory evidence revealed by the limited ecological information for these two morphotypes (Section 5.4.2.4). The very low representation of the ferns in the studied West Greenland stratigraphy, despite being the dominant floral component in the study of Seward (1927), reveals the importance of consideration of complex and detailed lateral variation in landscape ecology, which is also suggested by the low yield of angiosperm cuticle in the present study, compared to the excellent macrofossil record collected close to the present study field sites (Figure 5.10). This summary highlights the importance of considering the broad scale ecological landscape when attempting to assess floral changes through time.

5.4.4 Landscape ecology comparison to Europe

The Kome Formation may be associated to Coiffard *et al.* (2012) phase two, since the West Greenland, European and North American records share similar genera (e.g. members of

the Lauraceae) but with different species between geographical regions. Similarly, both *Sapindopsis* and *Platanophyllum* genera of the present study were identified (but distinguished at a species level) in the Potomac Group Zone IIb and III from North America (Hickey and Doyle, 1977). In the Potomac Zone IIb, these genera were understory shrubs across floodplains and were correlated by Coiffard *et al.* (2012) to their phase two of angiosperm radiation. The age of the Kome Formation (early Middle Albian) agrees with the timings of floral change with respect to paleoenvironment from Coiffard *et al.* (2012) phase two.

The Ravn Kløft Member may represent an ecological landscape closer to Coiffard *et al.* phase three, on account of the greater range of angiosperm species identified by Boyd. Many were closely associated with aquatic palaeoenvironments (swamps, shallow lakes and over bank deposits; Florules SE2, SW2, SE10, Figure 5.10). However, the depositional environment of the Eudicots and *Trilaurus* (Magnoliid) may indicate the expansion of more diversified angiosperms into the disturbed fluvial channel environment on account of the greater dominance of channel sands in the Ravn Kløft Member. The occurrence of Lauraceae and Platanoids inhabiting, respectively, swampy woodland and on the banks of freshwater lakes and streams in the Dakota Flora (Albian–Cenomanian; Retallack and Dilcher, 1981), reflects a similar association of angiosperm with depositional environment to that observed in West Greenland. Angiosperms occupying such environments were considered by Coiffard *et al.* to represent the beginning of phase three. Phase three according to Coiffard *et al.* (2012) spanned from the Cenomanian onwards, but the Ravn Kløft flora is thought to be Late Albian in age based on the carbon isotope stratigraphy (Section 3.5), which may indicate the spread of angiosperms into the disturbed channel margins occurred earlier than previously thought for high palaeolatitudes, if the ecological landscape interpretation of floral migration is correct.

5.5 Palaeoclimate indicators – fungal/algal evidence

The identification of epiphyllous organisms (living on the leaf surface or phyllosphere) on both macerated and untreated cuticle using epifluorescence microscopy provides important palaeoenvironmental indicators to supplement the ecological landscape interpretations, since true epiphylls (not parasites) have unique demands of a host surface (i.e. water availability). They are described in the following sections along with other fossil structures which may indicate saprotrophic (decay) organisms. Altogether, these structures

provide an unprecedented snapshot of ancient microecology and insights into Cretaceous palaeohydrology.

5.5.1 Epiphyllous fungi (Microthyriaceae family)

5.5.1.1 Microthyriales subfamily?

The most common epiphyllous fossil identified consists of a 40–50 µm diameter disc-like thallus, within which small cells (<5 µm length) are radially arranged (Figure 5.18). The margins of the thallus are entire to slightly lobed, and are darker, which may indicate some change in thickness. Rarely, hyphal extensions are observed projecting from the thallus, the preservation of which is indistinct (Figure 5.18). The thallus appears to be only one cell layer thick and does not appear to autofluoresce (or at least poorly, such that it appears as a shadow on the brightly fluorescing thick cuticle of the fossil leaf).

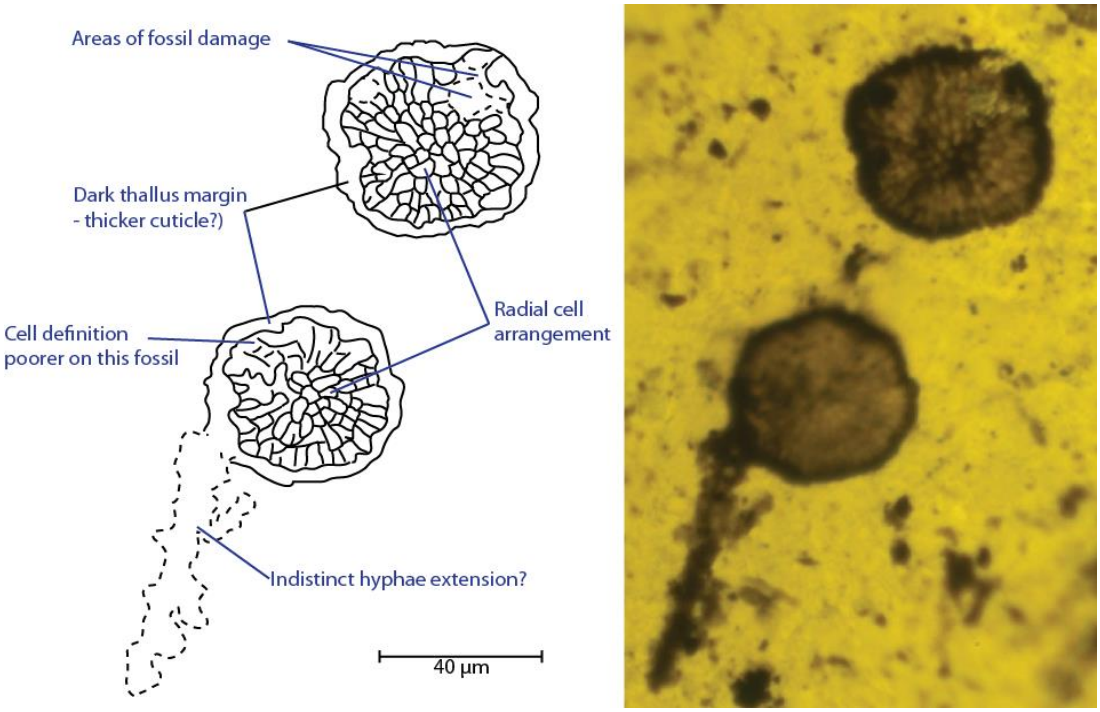

Figure 5.18: Possible fossil Microthyriales on the adaxial side of a Miroviaceae leaf cuticle, from horizon LK-B-3 (Kome Formation).

This fossil was identified mostly on the adaxial leaf surface (but not exclusively) of Miroviaceae (morphotypes 2–4) and on Taxiodiaceae (morphotype 10) cuticle fragments. The abundance on a single cuticle fragment varied, from an individual to up to 33 individuals, sometimes touching and occasionally interfering or overlapping (e.g. Figure 5.19). Seward (1927) described surface dwelling fossils from Skansen (southeast coast of Disko island, Figure 2.9) with *Asterina*-like fungi mycelium, with fruiting bodies "flattened, radiate, disc-shaped structures somewhat resembling in appearance the Green Alga *Coleochœte*". According to Dam *et al*. (2009) the strata of this area are part of the fluvio-

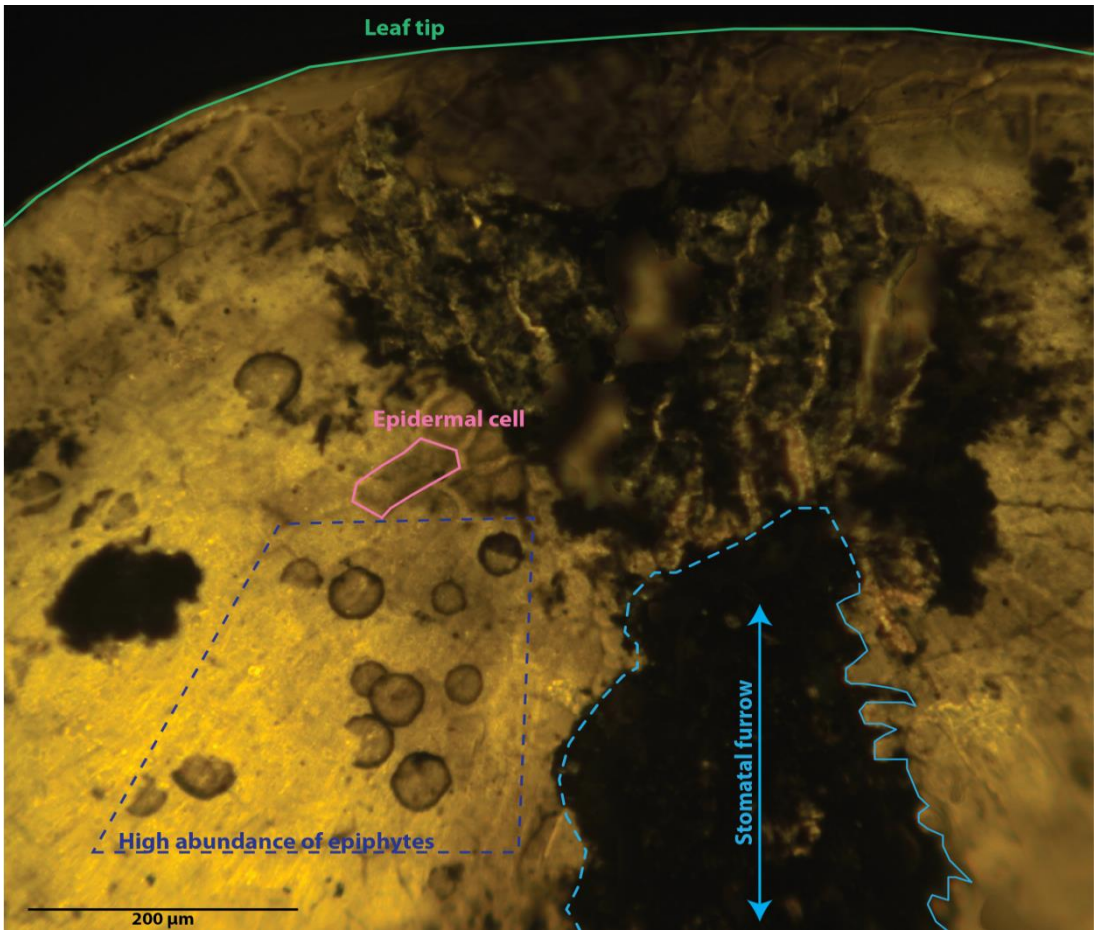

Figure 5.19: Cluster of fungal epiphytes (Microthyriales?) on the abaxial side of a Miroviaceae leaf cuticle, from horizon RKE-B-35 (Ravn Kløft Member).

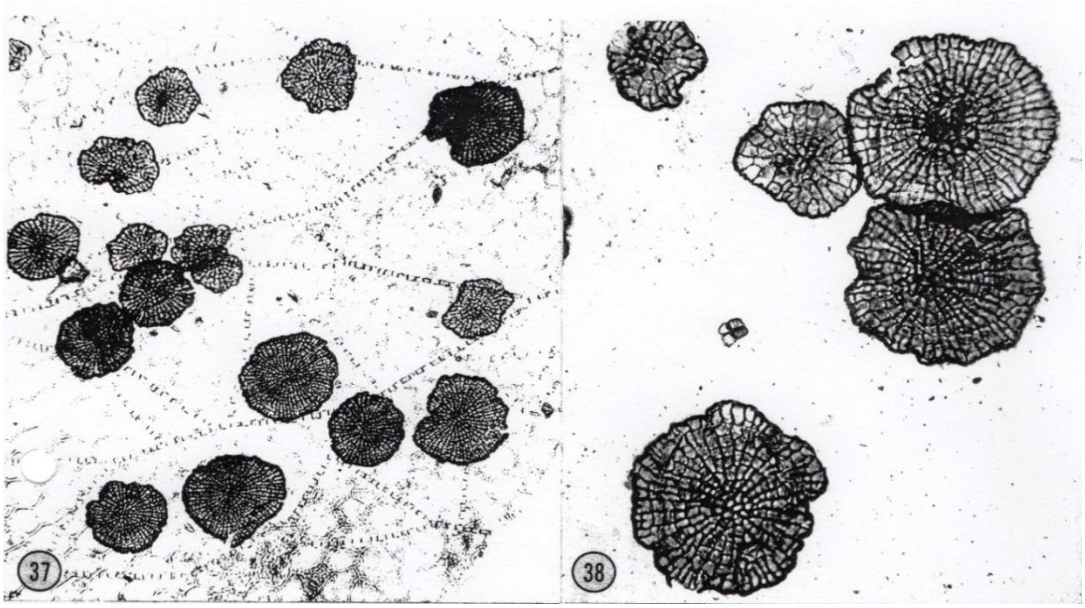

Figure 5.20: Callimothallus pertusus stromata on Sapindus sp. host leaf upper epidermis from Dilcher (1965). Left shown at x170 magnification (no scale supplied) and also shows associated hyphae of Shortensis memorabilis. Right: C. pertusus at x400 magnification

deltaic Atane Formation (Skansen Member). However, as outlined previously, Seward's (1927) paper lacks detailed site collection locations, in addition to no indication of the plant these fossils are associated with, nor a confirmed identification of whether the structures are algal or fungal in origin. Dilcher (1965) compiled all known epiphyllous fungi from Eocene deposits in Tennessee, USA, which includes detailed descriptions of Asterineae fungi. However, comparison of the material from the present study to that of Dilcher (1965) indicates that the fossil structures from West Greenland (Figures 5.18 and 5.19) are likely Microthyriaceae epiphyllous organisms, most comparable to the genus *Callimothallus* (Figure 5.20) from the Microthyrieae subfamily (after Dilcher, 1965). The fossil structures from West Greenland are also similar to fossil epiphylls on Miocene leaves from Northern Idaho, USA, identified by Sherwood-Pike and Gray (1988); in particular bearing a striking resemblance to members of the *Phragmothyrites* genus (Figure 5.21).

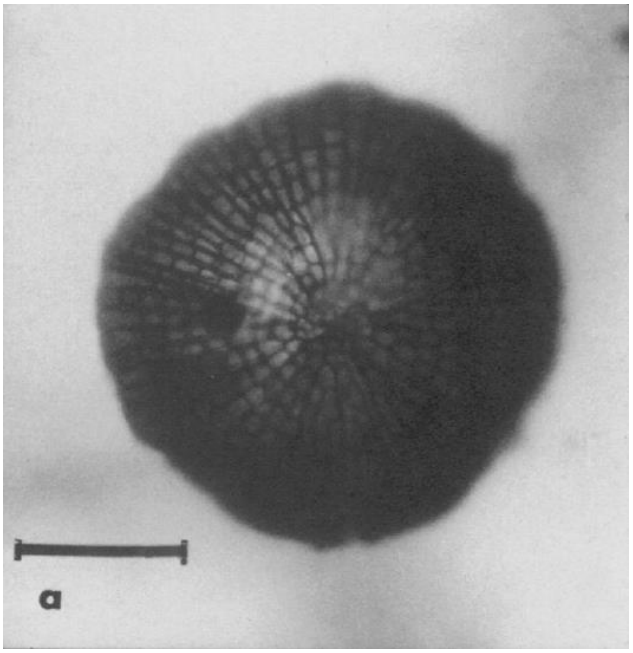

Figure 5.21: Phragmothyrites thyrothecium on Quercus simulate leaf from Sherwood-Pike and Gray (1988). Scale bar = 50 µm.

The question of whether these fossils are fungal or algal in origin remains largely unanswered. Originally the Microthyriaceae were considered as algal organisms, but were placed in the fungi by Dilcher (1965) through study of gametangial cells. However, other studies indicate the composition of other Microthyriaceae mycelium behaves much like sporopollenin rather than cellulose, chitin or lignin, which could suggest an algal origin (Germeraad, 1979 and references therein). As a result, the classification and affinity of the Microthyriales remains somewhat elusive and debated. For the purposes of this thesis, however, the classification based on Dilcher (1965) is utilised since the fossil material from West Greenland most clearly compares to the descriptions by Dilcher.

5.5.1.2 Trichopelteae subfamily?

Another epiphyllous fossil structure was identified on the adaxial surface of Miroviaceae cuticle fragments (Figure 5.22), possessing similarities with the Microthyriaceae fungi

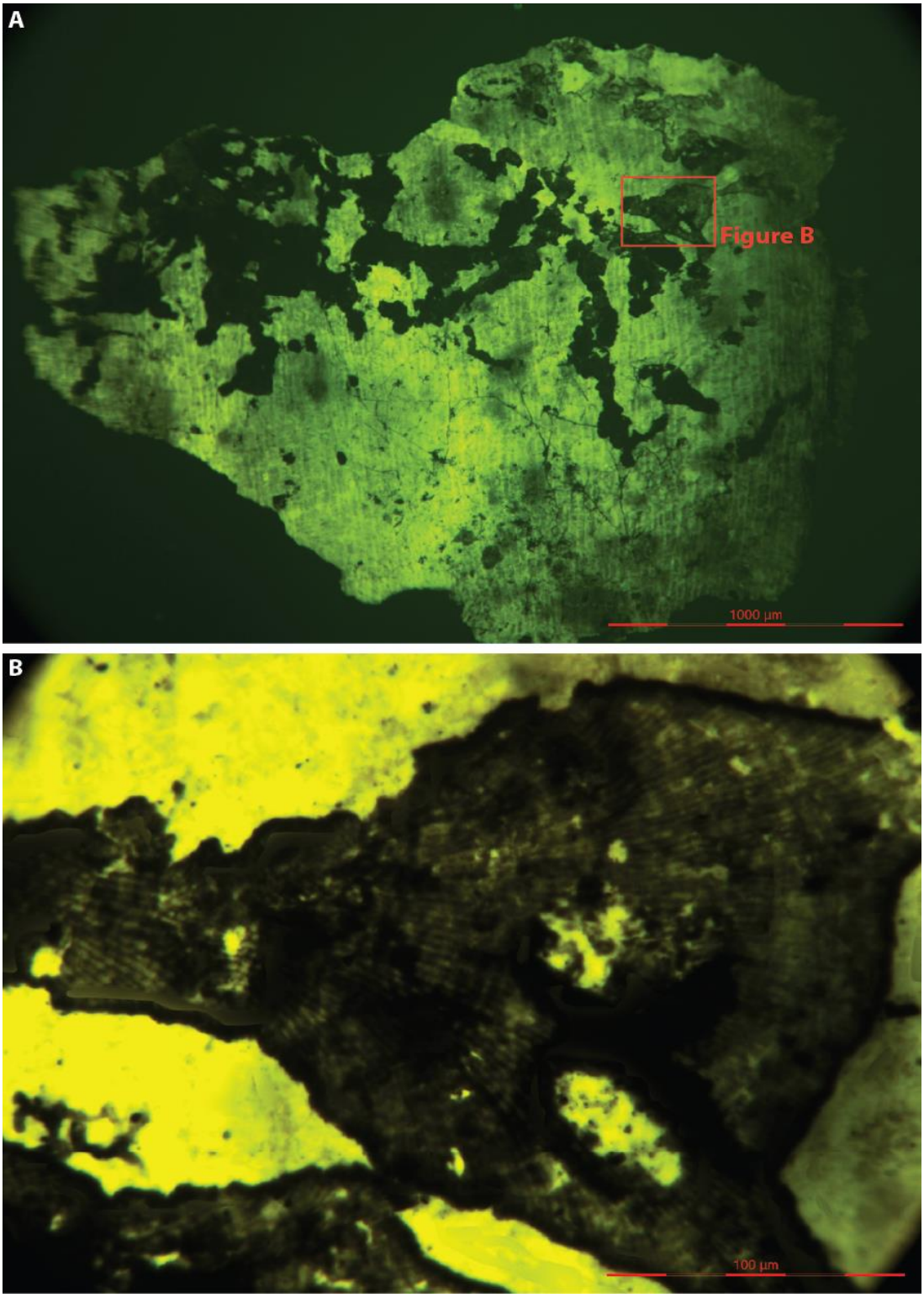

Figure 5.22: Fossil epiphyte, similar to members of the Trichopelteae subfamily from the Kome Formation (horizon LK-B-81). A: showing extensive network of fossil across the adaxial surface of host Miroviaceae cuticle. B: closer view of fossil showing cellular detail.

identified in section 5.5.1.1; namely the state of preservation (little to no autofluorescence compared to leaf cuticle), small cell sizes (<5 µm), and single cell thicknesses. However, the habit of this fossil differs, with branches of widths ranging around 50–100 µm spreading across the host surface, leading to hub-like structures which probably represent fruiting bodies (ascomata, Figure 5.22). Comparison of this fossil with the description of an Eocene example of *Trichopeltinites fusilis* (Dilcher 1965), reveals significant similarities (compare Figure 5.22 to 5.23) including darker areas representing mature stromata (Dilcher, 1965).

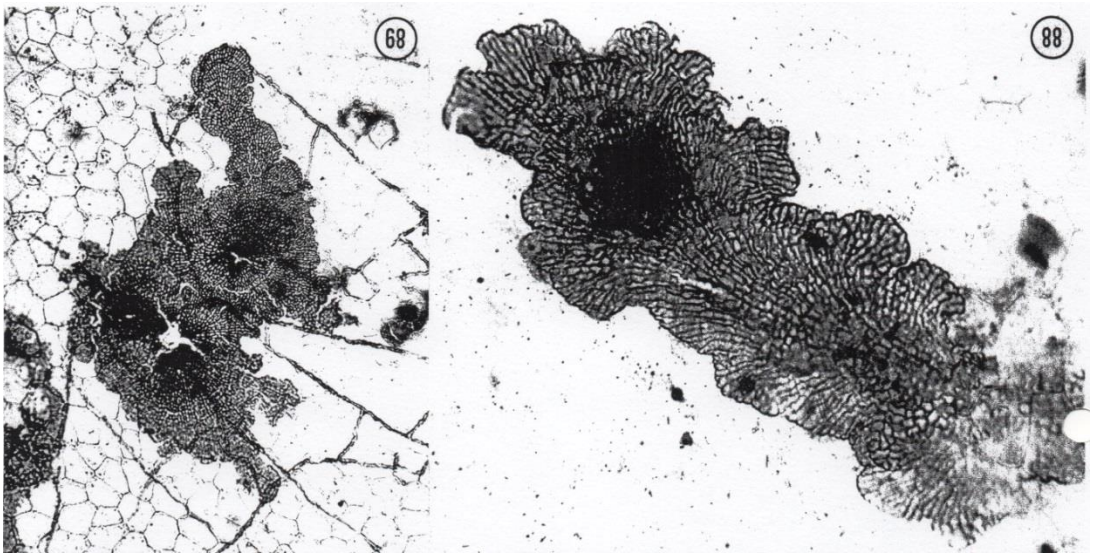

Figure 5.23: Fossil Trichopeltinites fusilis stromata on Sapindus sp. Host, showing mature stromata with ascomata (darker areas) from Dilcher (1965) Eocene deposits of Western Tennessee, USA. No scale provided, description indicates ascomata are 25-50 µm and cells are 8-25 µm long, and 2-4 µm wide.

5.5.2 Endophytic organisms

5.5.2.1 Fungal endophyte?

Fossil structures, thought to be unlike anything identified previously in published descriptions of the fossil fungal record, were commonly found on the adaxial surface of Miroviaceae cuticle (morphotypes 2 and 4) in the Kome Formation and Ravn Kløft Member, and are thought to represent endophytic organisms (living within a host). The structures comprised large areas (1 mm diameter) of slightly less brightly fluorescing cuticle, with radially arranged punctures or slits in the cuticle surface (Figure 5.24). These slits had one side that appeared to be more depressed than the other, and this side always faced the centre of the structure area (Figure 5.24).

In many cases, at the centre of the punctures is a split in the leaf cuticle orientated with the long axis of the cuticle epidermal cells (likely indicating the weakest direction in the cuticle

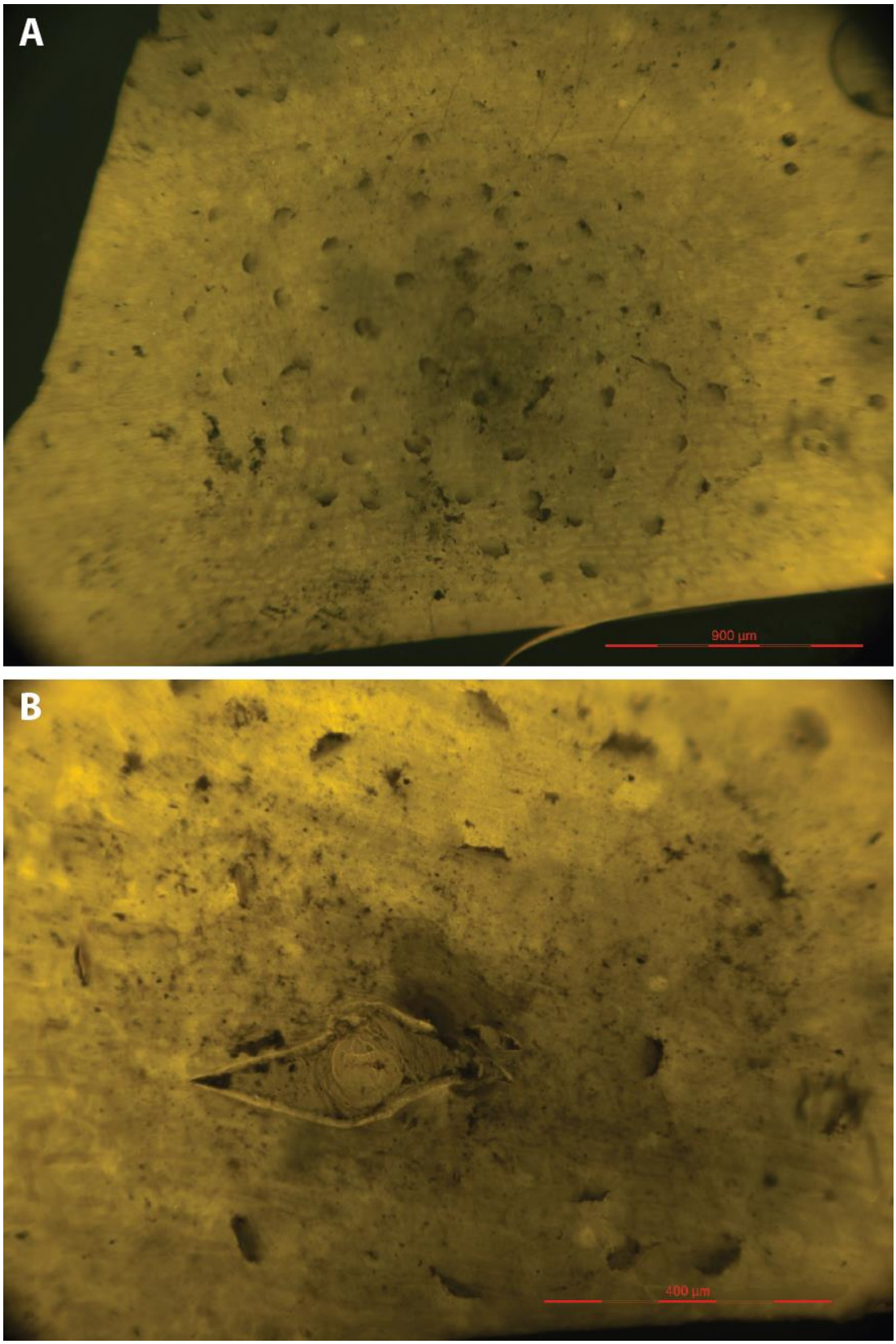

Figure 5.24: Enigmatic fungal structures on adaxial Miroviaceae cuticle surface on fragments from RKE-B-35 Ravn Kløft Member. A: radially arranged puncture-like structures and large area of less bright autofluorescence. B: similar puncture structures with a split in the cuticle revealing an intact protrusion.

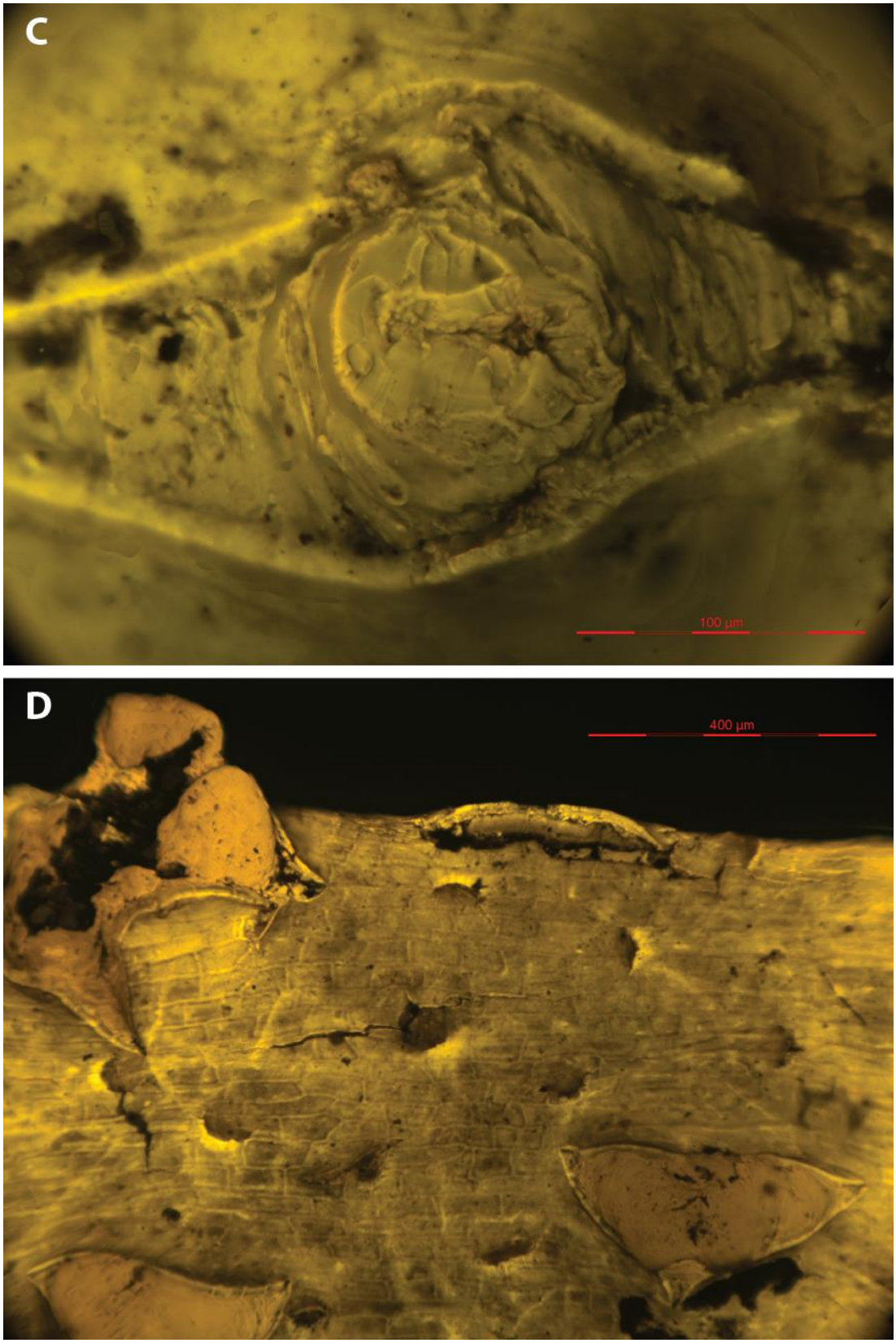

Figure 5.24 (continued): Enigmatic fungal structures on adaxial Miroviaceae cuticle surface on fragments from RKE-B-35 Ravn Kløft Member. C: closer view of intact protrusion of B showing small slit at the tip. D: three cuticle splits with protrusions, two intact and one torn wide open.

and epidermis), approximately 400 µm in length with a protrusion extending out of the cuticle (typically round, with a diameter of 150 µm protruding at the widest point in the cuticle split; Figure 5.24B, D). The colour of autofluoresce of the material protruding through the cuticle was similar to the cuticle, which would suggest the material is of a similar age (experienced the same burial temperatures and durations) as the cuticle (Chapter 4.2) and therefore is unlikely to be a later (or Recent) organism. In some cases, the protruding structure is intact (e.g. Figures 5.24B, C and two of the examples in D) but in others, the cuticle is widely torn open along with the protruding material (Figure 5.24D). There is no cellular detail preserved in these protrusions, but the intact examples appear in some cases to possess a slit (approximately 50 µm) at the tip (Figure 5.24C).

A fungal association is interpreted for these fossil structures because the protruding structures are interpreted as covered conidioma (or acervulus conidioma): these structures contain the conidia for asexual reproduction of the fungus and are found either subcuticular, intraepidermal or subepidermal, where conidia develop in a thin fertile layer such that pressure increases through the generation of spores, eventually splitting the cuticle and explosively releasing the spores (Alfieri, 1978). The torn open structure shown in Figure 5.24D appears to resemble an explosively opened conidioma, whereas the other structures are more intact and may indicate the spore release had yet to happen, or may have escaped from the smaller split at the tip of the protrusion (Figure 5.24C).

The cause of the radially arranged punctures remains problematic because the pattern of cuticle indentation appears as though something pushed through the cuticle from the outside of the plant, inwards, radiating from the central point. Whilst some fungal spores infect leaves by the development of appressoria from the spore (peg-like extensions from the spore which are capable of exerting sufficient pressure on the cuticle to pierce the surface, Deising *et al.,* 2000), the lack of any evidence of external structures, and the indication of an extensive subcuticular structure (area of less bright autofluorescence and conidioma), and the radial arrangement with clear orientation of the indentation path (rather than randomly distributed as would be expected with initial fungal infection) would indicate these smaller punctures are associated with the subcuticular body.

The suggestion that the fungal structures are representative of saprotrophs (obtaining nutrients from already dead plant matter, rather than a parasitic infection) is derived from the lack of any apparent plant response to infection. For example, despite the apparently explosive eruption of the possible conidia through the leaf surface in Figure 5.24D, the

cuticular impression of the epidermal cells shows no variation around the infected area. The same can be seen in the other examples shown in Figure 5.24, even where no protrusions are observed (Figure 5.24A). Alternatively, it could be suggested that the cuticle retains its form regardless of changes occurring beneath it – if the fungal organism was a pathogen the epidermal tissue would probably die (Wolf, 1930) as is seen in many common leaf spot disease, where necrosis expands from the point of infection eventually leading to leaf drop (Mahy and van Regenmortel, 2010).

5.5.2.2 Algal endophyte - Trentepohliales?

Another endophyte fossil structure was identified in cuticle fragments from the Kome Formation and Ravn Kløft Member, but the host cuticle fragments could not be assigned to a morphotype since only epidermal cells were preserved. In the fragment which most clearly shows the endophytic habit (Figure 5.25), the organism cells are small and rounded (approximately 15 µm diameter, Figure 5.25B). The total size of the fossil structure is around 1 mm in diameter, as seen by the less brightly fluorescing cuticle in Figure 5.25A. The margins of the subcuticular structure, inferred from the pattern of fluorescence, appear to be lobed, with a lobe width of around 200 µm (Figure 5.25A). There are no obvious reproductive structures protruding from the cuticle, despite the fact the missing cuticle revealing the cellular detail below occurs in the centre of the structure. This may indicate that the centre of the fossil body is likely thicker than the rest of the structure and therefore the cuticle was more prone to removal through diagenetic/degredational processes.

Isolated fragments with limited leaf epidermal cuticle preserved, but greater preservation of the endophyte, reveals a difference in surface texture each side of the fossil. One side (Figure 5.26A) has a smooth texture, whereas the other side (Figure 5.26B) has much more detail. Determining which side is the external surface is problematic since epidermal cuticle appears on both sides, but it is thought the smoother surface may reflect the internal surface between the cuticle and epidermal tissue (suggesting this organism was subcuticular). The thallus is elongate in shape, approximately 2.9 mm in length and 850 µm wide, with elongate lobed margins. The cells are small and rounded (Figure 5.26B; annotated in Figure 5.27), similar in size and shape to the structure presented in Figure 5.25B. However, studded across this surface are larger round cells (approximately twice the size of the cells) and places where these cells appear to be missing leave darker pores (Figure 5.27).

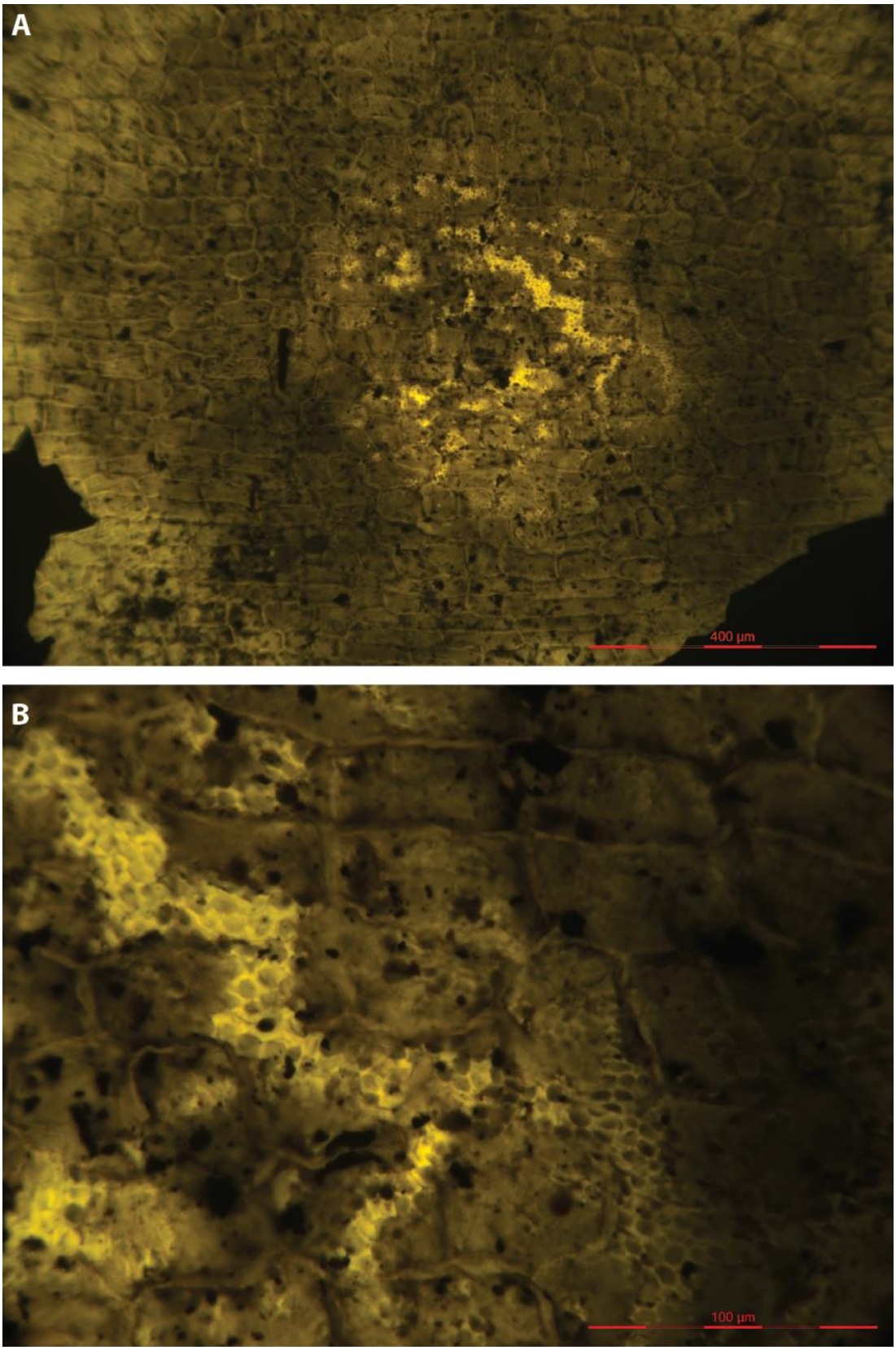

Figure 5.25: Possible algal endophyte from the Kome Formation (horizon LK-B-7) within unidentified epidermal cuticle. A: showing extent of subcuticular body by area of less brightly fluorescing cuticle. B: close up of missing cuticle revealing the cellular structure of the endophyte.

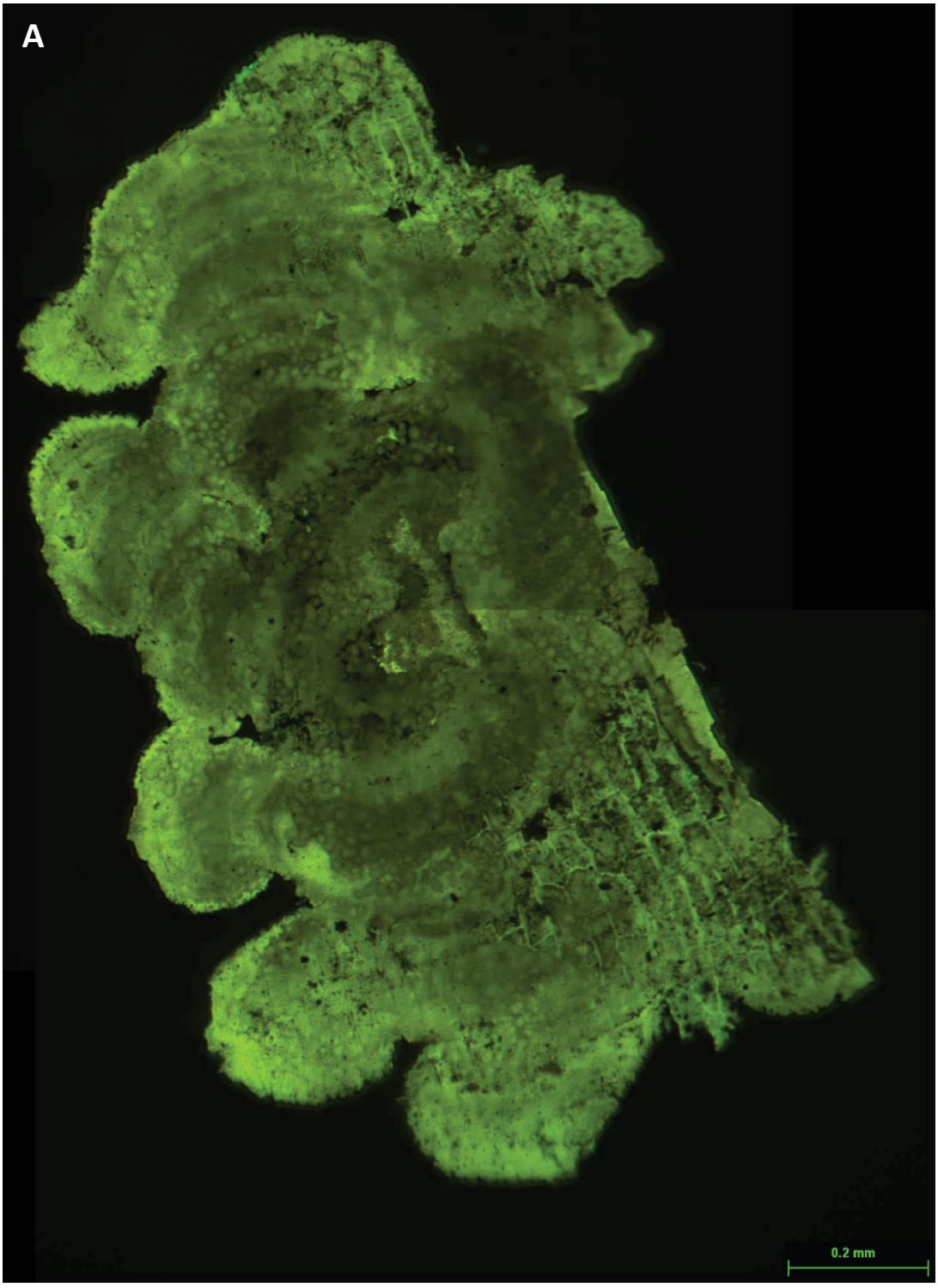

Figure 5.26: possible algal endophyte from the Kome Formation (LK-B-81). A: showing relatively smooth surface with little to no cellular structure, with epidermal cell impressions visible in leaf cuticle.

Figure 5.26 B (next page): Other side of algal fossil showing extensive cellular detail as described in text and annotated in Figure 5.27.

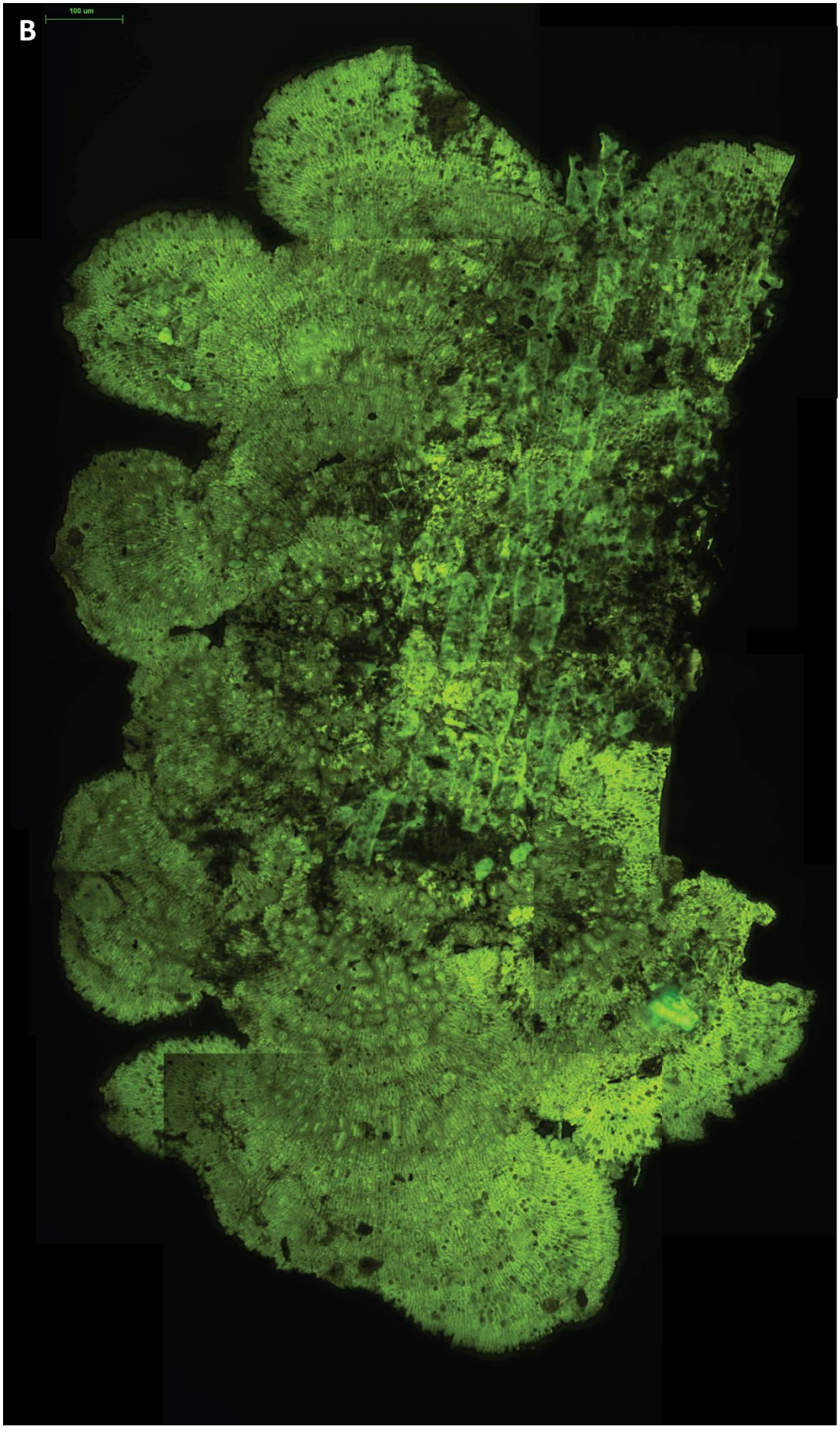
B
100 um

These round cells are larger towards the centre of the structure, and in places there are areas with a smooth texture where the small cells are not observed (except the large round cells; Figure 5.27). Since these regions occur where the fossil appears thickest, this would suggest that there is some depth-structure to this fossil and that the outermost layer may be missing, revealing the cellular detail.

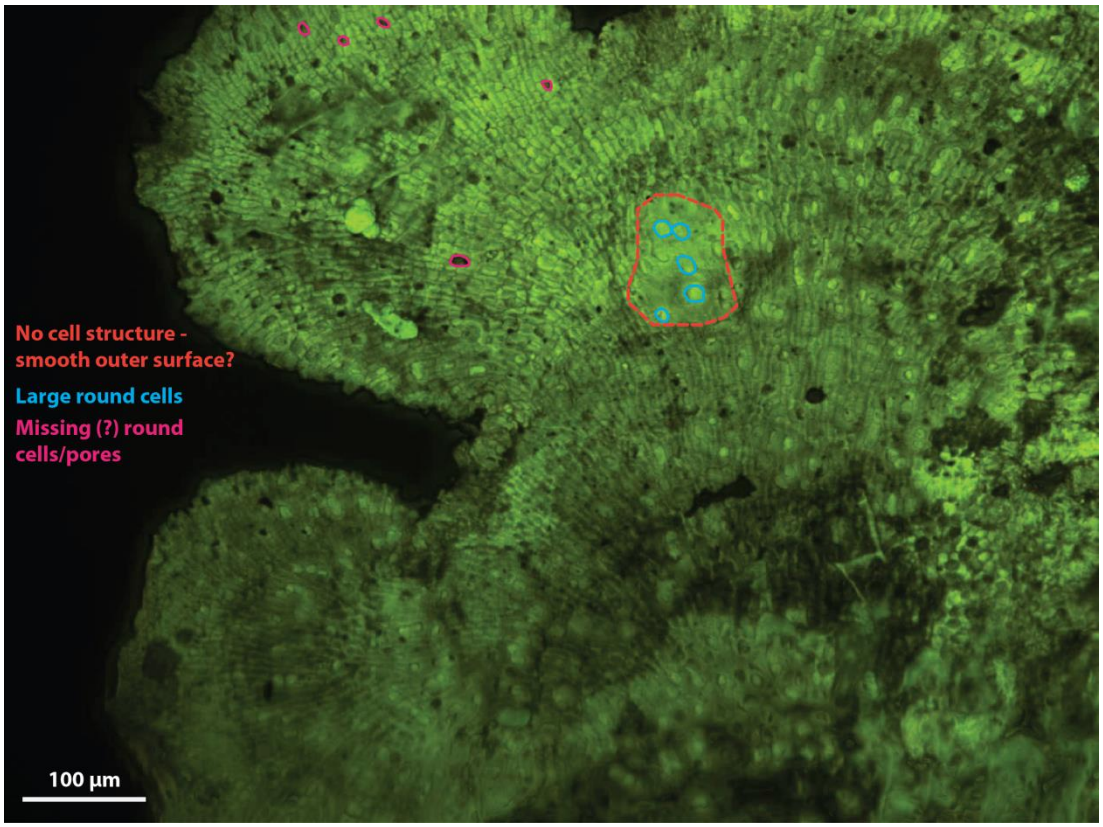

Figure 5.27: Annotated algal endophyte from Kome Formation (horizon LK-B-81) from Figure 5.26B, showing the small area of possible outermost algal layer (red) the large round cells which stud the surface and increase in size towards the centre (blue) places where the round cells appear to be missing leaving a pore behind (pink).

This fossil is most likely an algal endophyte colony, possibly from the family Trentepohliales based on similarities with extant examples, including: the thallus form, subcuticular habit and the presence of the larger round cells (Joubert and Rijkenberg, 1971; Germeraad, 1979; López-Bautista *et al.*, 2002; Neustupa, 2003). The large round cells are very similar to the gametangial cells of *Phycopeltis* species (Figure 5.28A-D; Germeraad, 1979; López-Bautista, 2002; Neustupa, 2003), whereby the cells expand and are eventually forced upwards through the cuticle where the gametes are exposed during algal colony sexual reproduction (Goff, 1983). Once their function is complete, the gametangial cell walls decay, resulting in gametangial holes (Figure 5.28D; Germeraad, 1979). Such gametangial holes are very similar to the smaller pores around the edge of the thallus. The once active (and therefore

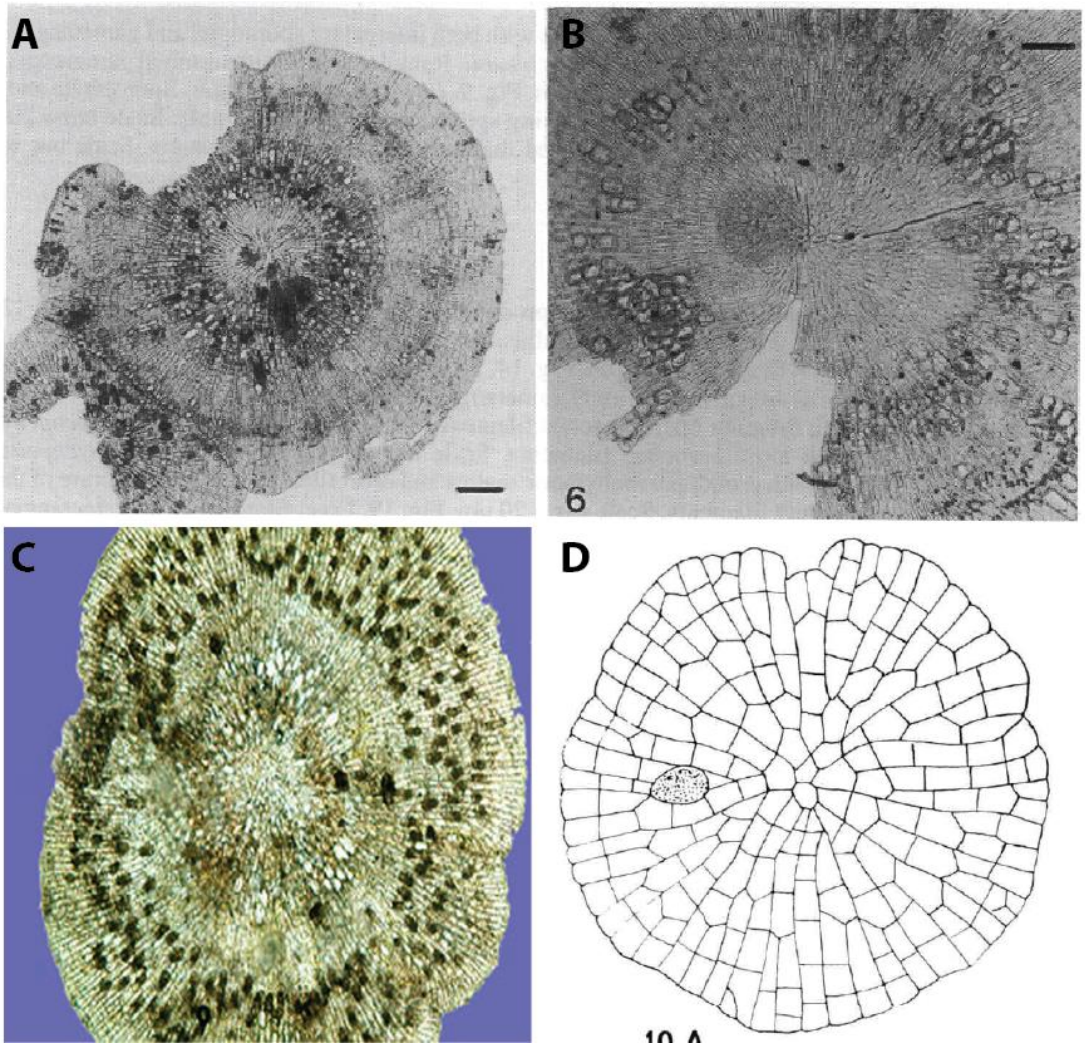

Figure 5.28: Phycopeltis species showing gametangial cells and holes. A and B: from Neustupa (2003) showing extant Phycopeltis theaensis intercalary gametangial forming circular ring, scale bars: 50 µm and 30 µm respectively. C: Discoid thallus of extant Phycopeltis sp. from López-Bautista et al. (2002). D: line drawing of extant Phycopeltis arundinacea thallus showing gametangial hole from Germeraad (1979).

larger) gametangial cells are those closer to the centre of the structure (Figure 5.26B), similar to some *Phycopeltis* species, which possess a ring of active gametangial cells (Figure 5.28A-C).

Without any other reproductive structures (in particular the identification of winged flagella-type gametes and zoospores), the identification of this fossil can only be tentatively assigned to the Trentepohliales. Nonetheless, the identification of likely gametangial cells rather than conidioma structures (like Figure 5.24) would strongly suggest an algal rather than fungal origin. As with the other fossil structures identified in this section, the similarity of autofluorescence colour and brightness indicates these structures are as ancient as the leaf cuticle and not a more recent contaminant.

The habit of this fossil organism is also largely unknown. Members of the Trentepohliales family are generally parasitic or epiphytic, living either on the cuticle surface, subcuticularly or deeper in the host tissue (e.g. *Cephaleuros* species, commonly observed as leaf spot disease on leaves; Joubert and Rijkenberg, 1971). However, as with the fungal endophyte structure (Section 5.5.2.1), there is no evidence of a host response expressed in the cuticle.

5.5.3 Untreated macrofossils

Whilst examining the macrofossil collection from the present study, a few fungal/algal fossil structures were observed on unidentified leaf cuticle from a single horizon in the Kome Formation (horizon LK-F-74).

5.5.3.1 Branching fungal/algal epiphytes?

Branching network thalli on unidentified cuticle (e.g. Figure 5.29) reveal consistent structural components common with other structures identified from the horizon (Figure vi; Appendix D). The thallus branches are of a similar width, around 200 µm with an irregular branching pattern, sometimes anastomosing. In one case, the branches lead to at least five hub-like structures (with one possible early stage development highlighted in blue in Figure 5.29B), which was common across all similar structures identified (Figure v, Appendix D). The hub-like structures are interpreted to be similar to the ascomata of the Trichopelteae (Figure 5.23) but appear more clearly defined. A close examination of these structures reveals the impression of epidermal cells from the cuticle below within these structures, but otherwise there is a lack of cellular detail of the actual fossil material for these reproductive structures. Some of the structures appear to have broken open, in a similar manner to the fungal endophyte in Figure 5.26D (although the fossil structure in Figure 5.29 appears to be epiphytic), suggesting these structures may have suffered an explosive release of spores as part of a fungal reproductive cycle.

There are brightly fluorescing structures which appear to occur in pairs along the length of the thallus branches, which are enigmatic in function, and are a common feature of all fossil structures studied on the untreated material. In one example (Figure 5.30), it appears that there may previously have been filaments extending from these points, which have either not been preserved or had gone before deposition. Such features might be

Figure 5.29 (next page): Fossil structure of uncertain affinity from the Kome Formation (LK-F-74). A: untreated fossil sample. B: annotated fossil sample to highlight structures with apparent fungal and algal affinities.

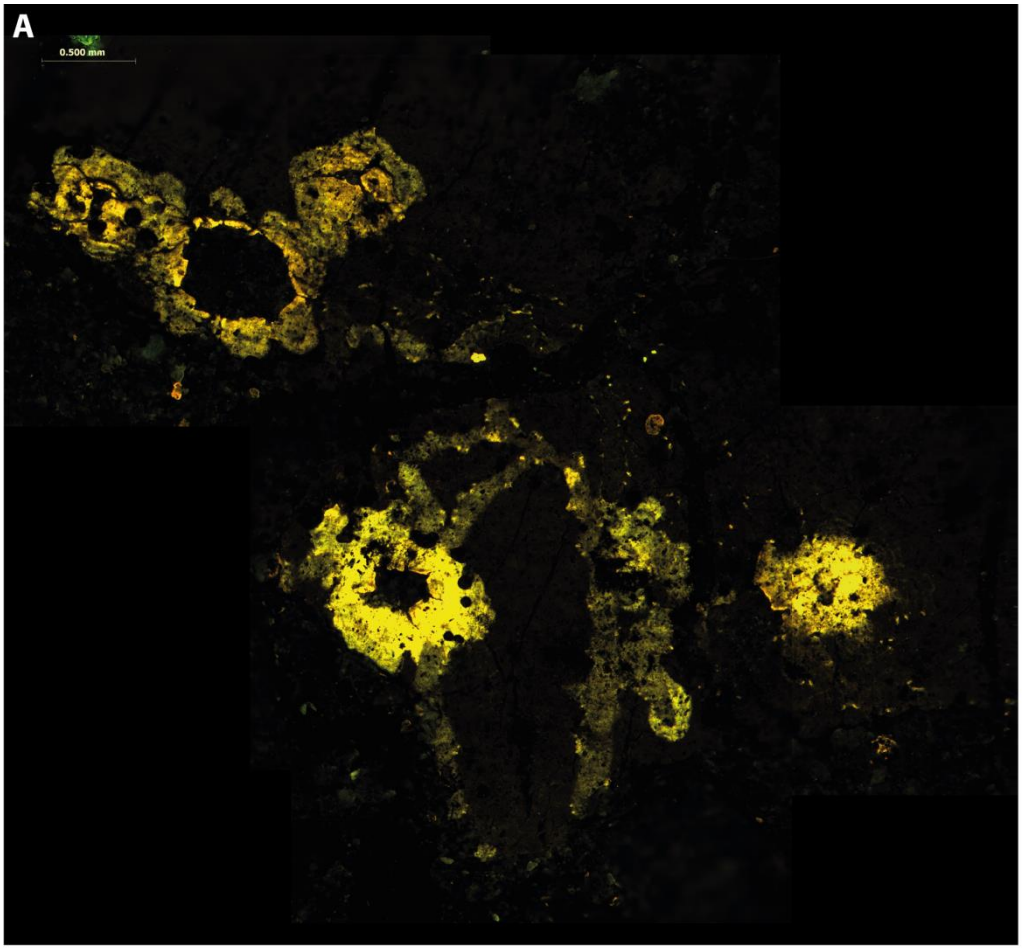
A
0.500 mm

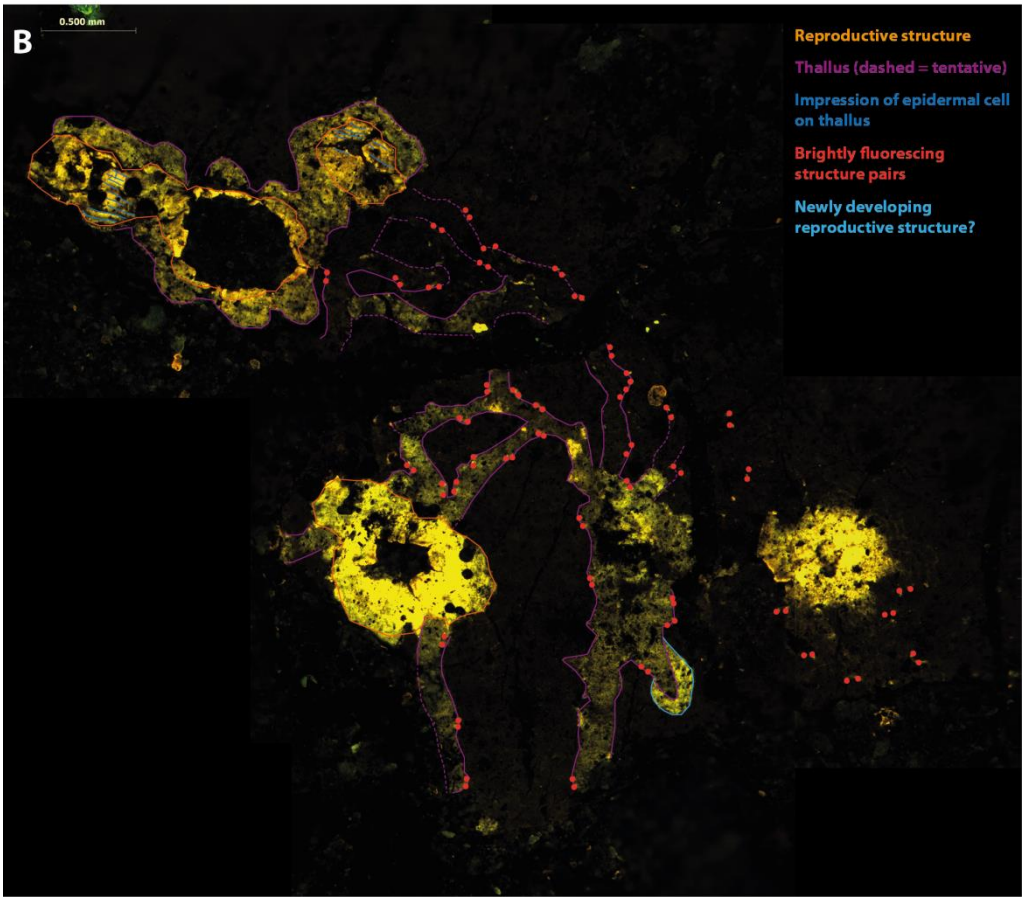
B
0.500 mm
Reproductive structure
Thallus (dashed = tentative)
Impression of epidermal cell on thallus
Brightly fluorescing structure pairs
Newly developing reproductive structure?

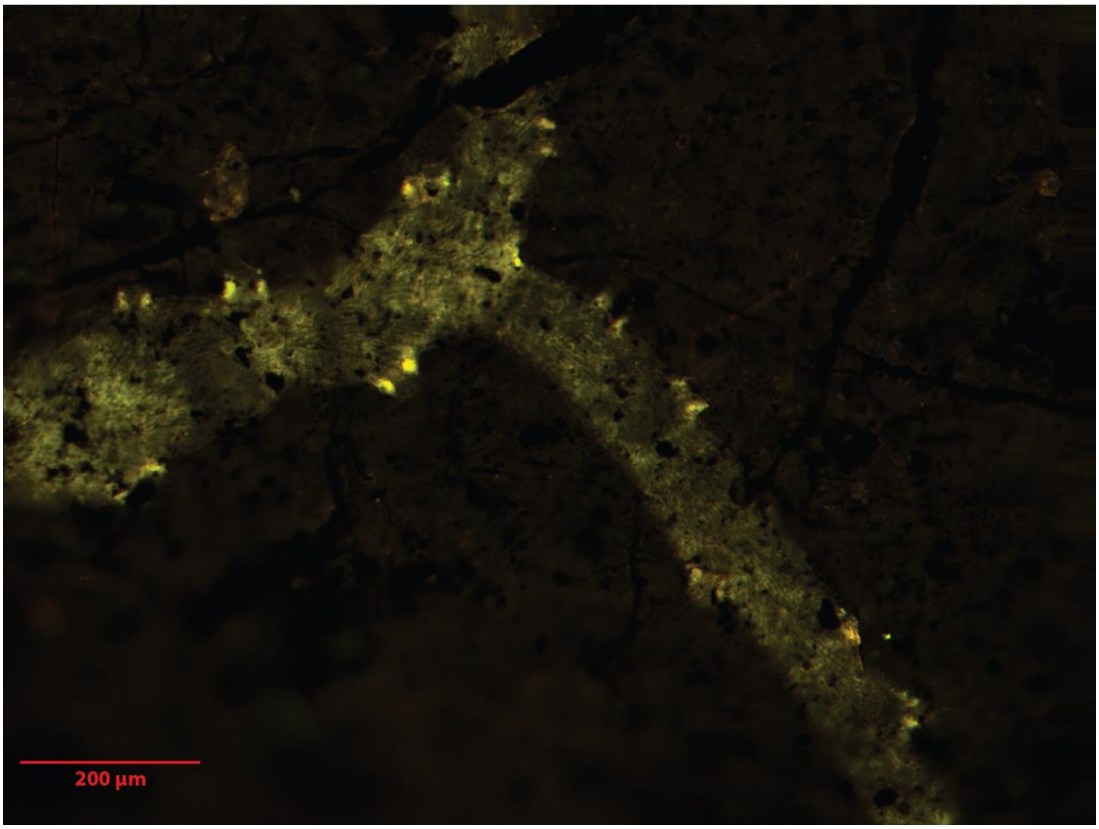

Figure 5.30: Fossil structure of uncertain affinity from the Kome Formation (LK-F-74); image of branching thallus with brightly fluorescing features in pairs along branch with indications of filamentous extensions from these points previously.

considered more comparable to algal descriptions of *Phycopeltis* by Neustupa (2003), which can bear sterile hairs and sporangiaphores, both of which extend from the thallus. Whilst the function and origin of the brightly fluorescing structure pairs remains enigmatic, the fossil structures are most likely epiphyllous fungi or algal colonies. The difficulty of identifying fossil alga and fungi from thallus structure alone is well cited in the literature as outlined in previous sections, and without additional reproductive information the identification of these structures cannot be completed and is beyond the scope of this thesis.

5.5.3.2 Epiphyllous lichen?

One fossil structure from the untreated material is slightly different from all others described. Found on an unidentified cuticle fragment (most likely the adaxial surface), the fossil structure is circular in shape (approximately 450 µm in diameter) with a lobed margin (Figure 5.31). The thallus appears thick; the outer margins of the thallus preserves the impression of the long axis of the epidermal cells from the host cuticle below, but such an impression is absent from the centre of the structure (Figure 5.31B). Aside from these

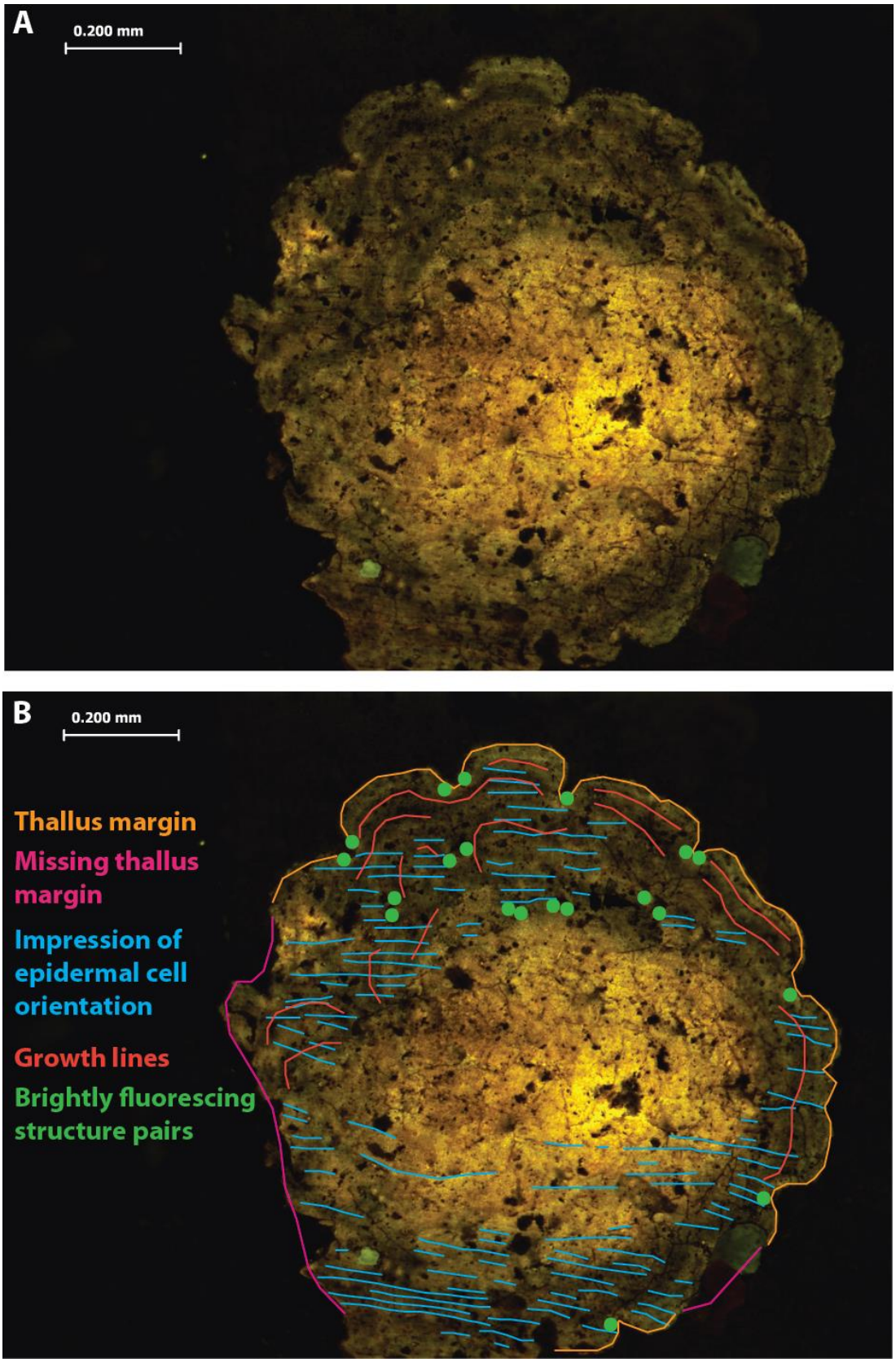

Figure 5.31: Fossil structure of uncertain affinity (possibly epiphyllous lichen) from the Kome Formation (LK-F-74). A: untreated fossil sample, where paired structures show growth of thallus. B: annotated image of fossil structure showing comparable features to previous structures.

impressions of the epidermal cells, the outermost layer of the fossil is smooth, appears quite thick, with little to no cellular detail preserved.

Brightly fluorescing paired structures are found along the thallus margin between lobes and in roughly concentric rings towards the centre of the structure. Additionally, variation in the thallus autofluorescence brightness also picks out evenly spaced concentric rings mimicking the outer margin, which may be indicative of thallus growth phases.

Upon consultation with Professor Duckett at the Natural History Museum, London, this particular fossil structure is very tentatively identified as an epiphytic lichen on the basis of the size, lack of associated projections/thallus branches and concise form, and by the thickness of the thallus which may suggest additional layering of the structure compared to the other fossils in Section 5.5.3.1. Such layering may include a symbiont required for lichenisation of the host organism (fungal or algal, Grube *et al.* 2012). Given the structural similarities identified in Figure 5.31B, it may be possible a similar species of algae/fungi to those presented in Section 5.5.3.1 took on a symbiont to form lichen. However, the only way to determine if this is the case, would be to obtain a cross-section through the thallus to look for clear layering, one of which bearing evidence of symbionts, which is beyond the scope of the thesis.

5.5.4 Stratigraphic occurrences, palaeoclimate interpretations and the fossil record of epiphytes and endophytes

5.5.4.1 Stratigraphic occurrences

Figure 5.32A presents the percentage of morphotyped cuticle fragments which yield interpreted epiphytic and endophytic fossil structures. Epiphytic fossils were more common than endophytic remains, with apparently a greater relative abundance in the Ravn Kløft flora. An unconstrained bias in the record of epiphyte and endophytes through the stratigraphy concerns the preservational bias of the host material. If the organism has an apparent preference for a given host, the relative abundance of that host will affect the apparent relative frequency of the epiphyte or endophyte. The fossil structures are all found in fine-grained lithologies with a high organic content (Figure 5.32A), often associated with mass accumulations of leaves (particularly in the case of the endophytes), indicating a low energy, waterlogged or marginally-waterlogged depositional environment, possibly swampy or floodplain deposits in small stagnant ponds where leaf litter collected parautochthonously based on the ecological landscape interpretation (Section 5.4.2). In addition to the habitat range of the host, the preservation potential of the host cuticle may

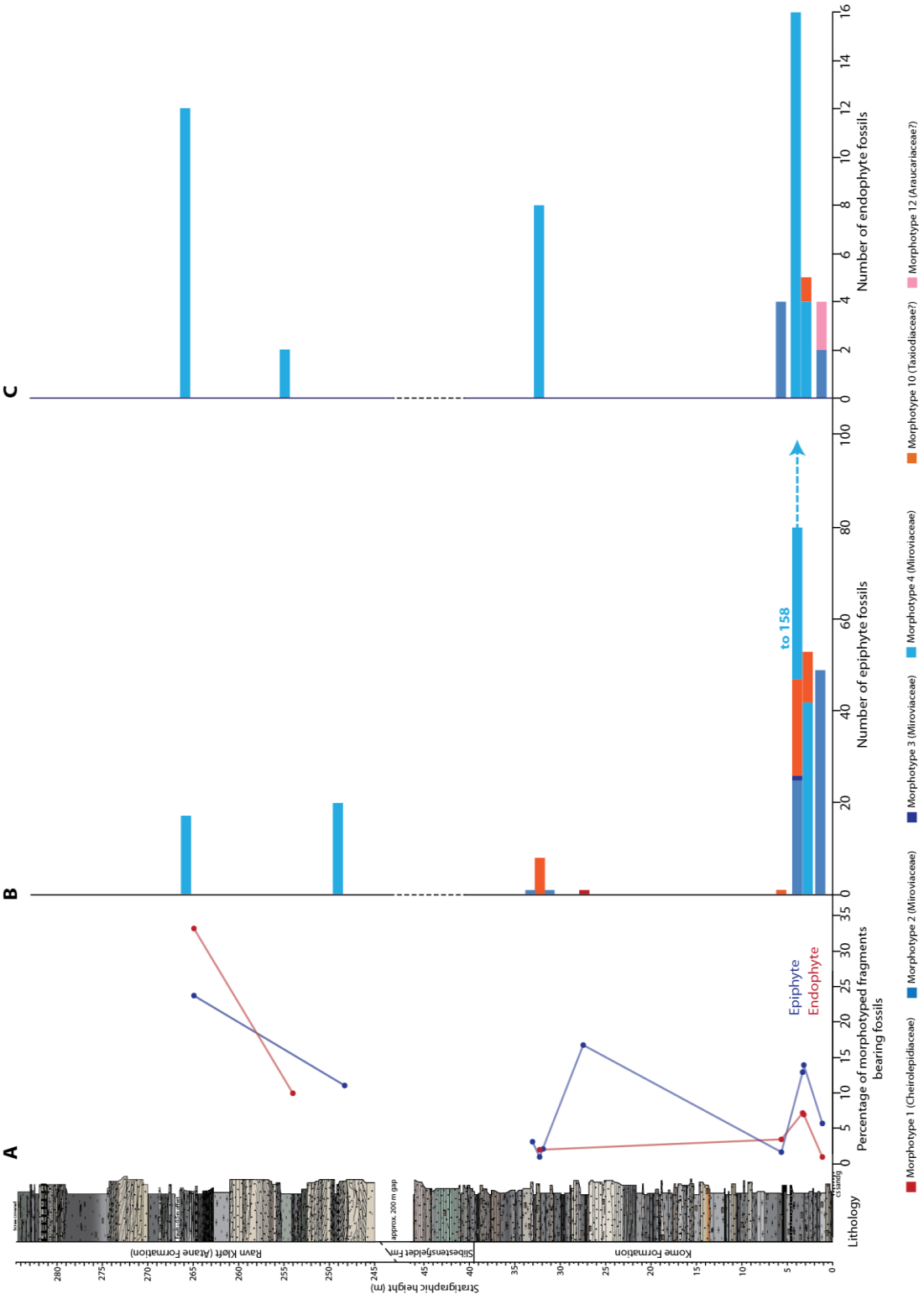

Figure 5.32: Stratigraphic occurrence of epiphyte and endophyte fossils through the West Greenland stratigraphy. A: percentage of morphotyped cuticle fragments bearing epiphyte and endophyte fossils. B: Absolute number of epiphyte individuals identified per horizon colour-coded according to host morphotype. C: Absolute number of endophyte individuals identified per horizon colour-coded according to host morphotype.

affect the apparent abundance of the fossil structures through the stratigraphy. The most common hosts were Miroviaceae (morphotypes 2–4) and *Taxus/Sequoia?* (morphotype 10). These morphotypes were the most intact remains of all the fragments sorted (Figure 5.1), with particularly thick cuticle, which may be more robust for preservation, particularly when only one Cheirolepidiaceae (morphotype 1) fragment was identified as bearing just a single epiphytic fossil structure. On consideration of these biases, it is clear that these fossil structures persisted through the West Greenland stratigraphy, and have a clear affiliation with waterlogged soil-dwelling (or slightly more marginal) plants, but the extent of these fossil structures further from this palaeoenvironment is unknown and unresolvable based on the present study material.

5.5.4.2 Palaeoclimatic interpretation

The possible fungal endophyte described in Section 5.5.2.1 and the association with mass accumulation of leaves is consistent with a saprotrophic interpretation of leaf litter decomposition. The preservation of the fossil fungus is also consistent with the inferred depositional environment of the mass accumulations of leaves, which were likely rapidly buried after a local flooding event which collected the leaf litter parautochthonously, thus preserving the fungal fossil prior to complete decomposition of the leaf.

The occurrence of true epiphytic organisms living on (but not negatively interacting with) a host leaf provides important palaeoclimatic information, since the organisms rely on water from the host surface and not the host itself (Dilcher, 1965; Anthony *et al*,. 2002). The dominance of epiphytes occurring on the adaxial surface (upward facing) of leaves, or the tips of the abaxial (downward facing) surface (e.g. Figure 5.19) is consistent with areas likely to accumulate water, whilst maintaining the positional requirement to photosynthesise.

The demand for free water means most modern epiphyllous fungi are found in humid climates, but are not restricted to tropical or subtropical temperatures, with epiphyllous fungi identified from more temperate regions (Worobiec and Worobiec, 2013 and references therein). Instead, high annual rainfalls of greater than 1000–1500 mm yr^{-1} (Kemp, 1978; Taylor *et al.*, 2009 and references therein) and high humidity play the main role in epiphyll distribution, predominately as the water source for the organism, but also for reproduction. Therefore, free water on the surface in the form of dew, fog, and rain are important as a spore distribution mechanism (Andrews and Harris, 2000).

The occurrence of epiphyllous organisms on Miroviaceae, *Taxus/Sequoia* (morphotype 10) and the single occurrence on a Cheirolepidiaceae cuticle fragment, supports the grouping of these floral types by the DCA (Section 5.1; CMC group) and a humid and wet, swampy palaeoenvironment interpretation. Interestingly, no epiphyte fossils were identified in the middle Kome Formation interval from around 10 m to 25 m, despite the presence of Miroviaceae and *Taxus/Sequoia* throughout this interval. However, across this interval a possible shift in landscape ecology occurred as interpreted from the DCA of all morphotypes (BAP Group; Figures 5.3, 5.6), whereby Bennettitales (morphotype 6–8), Araucariaceae (morphotype 12) and possibly Pinaceae (morphotype 11) became more important in the floral composition. These are interpreted to have inhabited better drained soils and are possibly more representative of floral communities surrounding fluvial channels and floodplains (Section 5.4). It is tentatively suggested that the shift in floral composition either was a long-lived lateral change in facies, or, on a broader scale, a change in overall climate to drier conditions which were not conducive to epiphyll growth.

5.5.4.3 The fossil record of epiphytes and leaf endophytes.

Most of the published records of members of the Microthyriaceae family are from Cenozoic deposits, mainly Miocene–Oligocene (e.g. Dilcher, 1965; Germeraad, 1979; Sherwood-Pike and Gray, 1988; Phipps and Rember, 2004; Worobiec and Worobiec, 2013). However, fossil structures with discoid thalli like those described here have been identified previously from the Early Cretaceous (e.g. Shao-Lin and Wu, 1986, epiphyllous fungi on *Nilssoniopteris* host; Tripathi, 2001) and even the Jurassic (Harris, 1961). Whilst the fossil structures identified from the present study are therefore not the oldest representation of the Microthyriaceae family, their presence confirms the existence of epiphyllous fungi in the Mesozoic. The high abundance of these structures (Figure 5.32) may also suggest that the maceration method and the use of epifluorescence microscopy helps to increase the yield of retrieved fossil structures, and that the oxidative cuticle clearing for light microscopy (applied in most previous studies of Mesozoic and Cenozoic flora) may destroy these delicate structures.

Similarly, the algal endophyte described in Section 5.5.2.2 tentatively assigned to the Trentepohliales is, to the best of available literature studied, the oldest representative of this family, with previously identified fossils reported from the Eocene (around 40 Ma) by Tappan (1980). Without reproductive structures the identification of this fossil remains tenuous, but if the fossil record range is extended to around 110 Ma in the Middle Albian as suggested in this thesis, this may go part way in reconciling the large span of time

between the first occurrence of Dasycladales and Charales (500 Ma and 420 Ma respectively) thought to be the marine ancestors of the Trentepohliales (López-Bautista *et al.*, 2002).

5.6 Palaeoclimate indicators – floral evidence

5.6.1 Mass accumulations of Miroviaceae – a seasonality red herring?

In the present study, the Miroviaceae (morphotypes 2–5) are most commonly found in mass accumulations, within which they are the dominant floral component (Figure 5.6). From the sedimentological and fossil evidence outlined in this Chapter, the Miroviaceae leaf accumulations are interpreted as the result of short distance accumulation of leaf litter, followed by fairly rapid burial through a likely flooding event. However, this is not the first demonstration of mass accumulations of this plant group; many previous studies of the Miroviaceae through the Mesozoic encounter mass accumulations of leaves with defoliated shoots bearing abscission scars from circum-Arctic localities (Manum *et al.*, 2000 and references therein). These nearly monospecific accumulations were thought to indicate all Miroviaceae were deciduous (Bose and Manum, 1990). The assumption that mass accumulations of leaves must dictate deciduousness is debatable, since this implies a complete drop of leaves instigated by seasonal climate changes (Manum *et al.,* 2000; Gordenko, 2007). However, some members of the Miroviaceae were interpreted to have shed leaves incompletely, on discovery of partially denuded *Sciadopityoides* and *Mirovia* shoots (Gordenko, 2007), which indicates the leaf shedding was the result of dead leaf drop employed by all plants, both deciduous and evergreen. The single *Sciadopityoides* shoot fragment from the macrofossil specimens of the present study (Figure 5.18) also still had leaves attached, and would also suggest that the mass accumulations of Miroviaceae is likely the collection of dead leaves dropped by the plants over an interval of time which have been parautochthonously concentrated. True deciduousness is unlikely in the Miroviaceae since the examination of the leaf cuticle reveals the thickness which permits such good preservation, would be expensive to lose seasonally. In addition, whilst some of the epiphylls are small (Section 5.5.1) and therefore may have grown quickly, some of the more extensive structures (like those described in Section 5.5.3) may be expected to be more common on evergreen leaves than deciduous, providing more time for successful propagation. In addition, overabundance of epiphylls may inhibit leaf photosynthesis and instigate leaf death and drop (Anthony *et al.*, 2002). Therefore, a seasonal component to palaeoclimate should not be inferred from mass accumulations of Miroviaceae (unlike previous studies, e.g. Manum *et al.*, 2000; Gordenko, 2007).

5.6.2 Charcoalified wood fragments – forest fires

The presence of charcoalified fossil wood fragments is commonly interpreted as a sign of forest fires in a seasonally regulated climatic regime (e.g. Patterson *et al.* 1987). In the present study, charcoalified wood fragments predominantly occur in the fluvial sands of the Ravn Kløft Member (Figure 3.22), which may in part reflect the change in the floral composition upstream through the Middle to Late Albian. In particular, with the increased abundance of angiosperms through the West Greenland stratigraphy, the palaeoenvironment may have become more prone to wildfire due to the more rapid generation of a flammable mass in a world with higher modelled atmospheric O_2 (Bond and Scott, 2010).

If the occurrence of charcoalified wood represents episodes of forest fire in the Albian of West Greenland, there may also have been dry periods upstream from the Nuussuaq stratigraphy conducive to wild fire initiation (seasonally dry, but not necessarily causing fire annually), although there is no irrefutable evidence of arid periods extending for long periods of time: the episodes of drying may have prompted Miroviaceae leaf drop, but the time between leaf drop and parautochthonous burial through flooding may have been quite short due to the early stage leaf litter-decomposing fungal structures identified in Section 5.5.2.1.

5.6.3 Miroviaceae and *Taxus/Sequoia* drip tips?

In some intact cuticle remains, distinct mucronate leaf tips were identified in *Sciadopityoides*, and *Taxus/Sequoia* (morphotype 10). The presence of an extended pointed tip is common in tropical rainforest foliage in order to drain water from the leaf surface, whereby the narrow tip encourages a drop of water to form at the tip and fall away (Lücking and Bernecker-Lücking, 2005). It is possible the mucronate leaf tips, albeit shorter than the elongated pointed drip-tips of tropical rainforest foliage, may have helped flush standing water from the surface of the leaf. However, as previously outlined, the water demand for epiphytes doesn't automatically indicate high rainfall, but high humidity, and therefore these smaller tips may serve a function to promote dew drips in the case of excessive condensation from conditions such as fog.

As outlined in Chapter 4, the plant types with this tip type were hypostomatous, with the stomata confined to the lower (abaxial) surface. The need to remove water from the surface therefore cannot be to prevent water clogging the stomatal pores, but has been proposed by studies of tropical rainforest flora as a means of drying the leaf to prevent the

overpopulation of epiphytes which intercept the light source. However, the verdict on the efficiency of these structures in accomplishing this task remains debated (Ivey and DeSilva, 2001; Lücking and Bernecker-Lücking, 2005; Burd, 2007).

5.6.4 The multiple function of "xeromorphic" cuticle features

Cuticular papillae are often grouped with other features such as thick cuticle, sunken stomata and trichomes as "arid-form" xeromorphic features (discussed by Haworth and McElwain, 2008 and references therein). Xeromorphic features reduce transpirational losses of the plant in conditions of water-stress (e.g. extended arid periods, Haworth *et al.,* 2005; or saline soil conditions, Passalia, 2009). However, it is becoming increasingly apparent that the identification of these features do not exclusively relate to water-stressed environments (Haworth and McElwain, 2008 and references therein), and are commonly associated with wetlands (e.g. Stull *et al.*, 2012). The Cheirolepidiaceae conifers are one example of a plant group which inhabited a wide range of palaeoenvironments: sometimes associated with arid, coastal or brackish regimes (e.g. Haworth *et al.*, 2005; Aucour *et al.*, 2008), the family did not consist entirely of xerophytes. Representatives of the clade are also found in entirely freshwater fluvio-deltaic regimes with stable climate and water supply (Gomez *et al.,* 2002; Yang *et al.*, 2009; Passalia, 2009).

Haworth and McElwain (2008) re-evaluated the function that arid-form features could serve a plant in addition to anti-transpiration (Table 5.1), including micromorphological traits which could serve a specific function in a wet climate. The possession of such features therefore may enhance the plant group's ecological range by providing a range of benefits in many different environments (Haworth and McElwain, 2008). Interesting parallels can be drawn between the Cheirolepidiaceae and the angiosperm family Proteaceae, which share many apparently succulent adaptations, but may also share some reproductive elements; for example the pollen responsive surfaces of the Cheirolepidiaceae may be similar to the angiosperm recognition system (Alvin, 1983). Whilst many members of the Proteaceae family are salt marsh shrubs (again a similar ecology interpreted for some of the Cheirolepidiaceae conifers), there are representatives of Proteaceae in a swathe of environments, including rainforest and wet sclerophyll forests of Australia and Tasmania (Myerscough *et al.*, 2001), for example *Helica glabriflora, Banksia integrifolia, Stenocarpus salignus* and *Lomatia myricoides*.

Feature	Anti-transpirational function	Wet climate function	Other function
Thick cuticle	Physical barrier to water loss through cuticle	Resistance to fungal invasion which increases in wet conditions	Physical barrier to abrasion and protection from absorption of toxic atmospheric components (SO_2, H_2S), rates of absorption increase in wet climates
Surface and stomatal papillae	Increases boundary layer resistance reducing transpirational wicking	Prevents a film of water forming on the leaf surface or blocking stomata	Stomatal papillae may prevent debris blocking pores and reduce pathogen infection. Epidermal papillae may serve as physical impediment insect/herbivore defence
Trichomes	Increases boundary layer resistance reducing transpirational wicking	Prevents a film of water forming on the leaf surface or blocking stomata	Trichomes may serve as insect/herbivore defence through physical impediment or chemical deterrent
Stomatal pits or furrow	Increases transpiration pathway length, increasing boundary layer resistance		Prevents debris blocking stomata and pathogen infection when combined with papillae

Table 5.1: Summary of apparently xeromorphic features with alternative function in wet climates and other considerations from Haworth and McElwain (2008).

The leaf form and growth habit of the Proteaceae are not comparable to the scale-leaves of the Cheirolepidiaceae, but some species of Proteaceae possess sunken stomatal pits with papillae or lobes protecting the stomatal rim (Jordan *et al.*, 2008), which are similar to the papillose stomata of the Cheirolepidiaceae (morphotype 1). There is a great diversity of stomatal form within the Proteaceae family, ranging from papillae-free to deeply encrypted stomata with papillae within the pit in addition to the rim (Jordan *et al.*, 2008). However, Jordan *et al.* mapped the evolution of these stomatal forms through the history of the family with respect to independently derived palaeoclimatic interpretation, and found that only the deepest stomatal encryption could consistently be attributed to arid conditions. The less extreme forms of stomatal protection, similar to those of the Cheirolepidiaceae, evolved multiple times in the history of the Proteaceae but with no great correlation with climatic aridity (Jordan *et al.*, 2008). *Sciadopitys verticillata*, the extant species to which the Miroviaceae were first compared (based on the presence of a deep stomatal furrow protected by papillae) is native to the cloud forests of Japan, growing in high rainfall and humidity, representing another plant with apparently xeromorphic conditions which is sensitive to water levels.

Whilst it would be unwise to draw too many comparisons between the evolution of features between angiosperms and gymnosperms, there are striking parallels in the story

of the two plant families. Both groups are often assumed to be exclusively adapted to climatic aridity but can actually thrive across a great range of environments. Ultimately, the interpretation of the ecology of fossil groups from the present study, which possess many of the features listed in Table 5.1 (including the Cheirolepidiaceae and Miroviaceae), and the lithology in which they were encountered, indicate a palaeoenvironment which did not suffer from water stress for extended periods of time, or any evidence of brackish influences. Thus, the present study supports the growing concept of the multiple functions of apparently xeromorphic traits.

5.7 Summary

The morphotypes resolved by the cluster analysis (Chapter 4) are suitable for reconstructing changes in major floral component abundances through the West Greenland stratigraphy, but not diversity changes. DCA of all morphotype relative abundances reveals two floral affiliations, the CMC group (Cheirolepidiaceae, Miroviaceae and Coniferales of morphotype 10) and the BAP group (Bennettitales, Araucariaceae and Pinaceae). Increases in the relative abundance of the BAP group > 12.5 % appear to correspond to a change from waterlogged soils to more fluvially-dominated depositional regime in the middle Kome Formation (10–25 m; Figure 5.3). DCA of Miroviaceae and Cheirolepidiaceae relative abundances only also reveals a smaller scale oscillation in relative abundance between the two plant families through the Kome Formation (Figure 5.6), which may reflect lateral movement of the water table and/or waterlogged soil margins. Interpretations of plant ecology (Section 5.4.2) support the DCA interpretation, indicating the BAP group likely occupied better drained soils, with the Miroviaceae occupying the wettest soils (and the Cheirolepidiaceae, intermediary).

The angiosperm cuticle record was extremely sparse, comprising 0.7 % of all the cuticle fragments morphotyped. The pollen record indicates a possible increase in angiosperm abundance at the top of the Kome Formation (Figure 5.7) but this cannot be confirmed as the relative pollen abundance is unknown. However, the macrofossil record collected by Boyd (1998a-c, 2000, 2004) reveals an increase in abundance (Figure 5.7) and possibly diversity (Figure 5.11) on comparison of the Kome Formation and the Ravn Kløft Member floral assemblages. This indicates at some point between the Ikorfat Flora and the Ravn Kløft Flora there was an increase in angiosperm abundance (the exact stratigraphic height remains unconstrained).

Assessment of the angiosperm role in the ecological landscape suggests the Kome Formation is comparable to phase 2 of Coiffard *et al.* (2012) method of angiosperm radiation into new ecological niches (as documented in the European floral record and interpreted by Coiffard *et al.* from the North American floral record). On comparison, the increase in abundance of angiosperm macrofossils (particularly the Lauraceae and Platanaceae) in the Ravn Kløft Member compared to the Kome Formation is interpreted as the beginning of the transition between Coiffard *et al*. phase two and three, whereby angiosperms expanded from the understory of a gymnosperm forest to occupation of swamps, levees and disturbed channel margins. If the landscape ecology angiosperm phase interpretations from the West Greenland stratigraphy are valid, the present study data indicates that angiosperms may have spread to higher latitudes earlier (Late Albian) than the lower palaeolatitude sites from Europe indicate (Cenomanian; Coiffard *et al.,* 2012). This is further indicated by the presence of Tricolpate pollen in the Kome Formation (Horikx and Heimhofer, unpublished; Figure 5.8), which indicates the Eudicots had already spread to higher palaeolatitudes (55–60 °N) by the Middle Albian.

The possible leaf litter subcuticular fungi (Section 5.5.2.1), unlike any known published descriptions, reveals a unique ecological snapshot of leaf litter decomposition halted at an early stage likely through rapid parautochthonous burial due to flooding. The possible subcuticular algal colonies (Section 5.4.2.2), tentatively affiliated to the Trentepohliales, may represent the oldest known occurrence of this family but more reproductive detail is required to confirm the identification, which was not available from the present study material. The palaeoclimatic requirements (high humidity and likely high mean annual rainfall) interpreted from the epiphytes supports the interpretation that the CMC group (Cheirolepidiaceae, Miroviaceae and Coniferales *Taxus/Sequoia*) shared the same ecological landscape setting as alluded to from the DCA. In addition, the absence of epiphytes in the middle portion of the Kome Formation (10–25 m) coincides with the interval of increased significance of the BAP group of plants (Bennettitales, Araucariaceae and Pinaceae) derived from the DCA (Figure 5.3), which may suggest either an overall palaeoclimate change towards less humid conditions, or a long-term lateral shift in landscape ecology.

The overall interpretation from floral and fungal/algal ecology indicates the palaeoclimate in West Greenland in the Middle to Late Albian was significantly humid, probably with mean annual rainfall estimates of >1000–1500 mm yr^{-1} (Kemp, 1978; Taylor *et al.*, 2009).

The presence of mucronate leaf tips in multiple morphotypes may support the interpretation of a highly humid climate, which given the proximity to the palaeo-coastline, may indicate sea fog was a common feature like that experienced along the northern Pacific coast of the USA.

The occurrence of charcoalified wood fragments, predominantly in the Ravn Kløft Member, indicates there may have been wildfires in drier upstream areas, which may have been propelled by the increase in angiosperm abundance (Bond and Scott, 2010). The possibility of wildfires suggests there may have been a seasonal component to climate, in terms of a period of lower rainfall in inland areas. If this decrease in rainfall also affected more coastal areas (i.e. the sampled stratigraphy), this may have caused leaf drop in Miroviaceae plants (collected in mass accumulations through subsequent flooding) and the oscillating inverse abundance relationship between the Miroviaceae and Cheirolepidiaceae (Figure 5.6B).

6: Stomatal measurements and pCO_2

6.1 Introduction

This chapter contains all data concerning measurements made from stomata of leaf cuticle, including stomatal density, index and conductance. Three morphotypes (morphotype 1 – Cheirolepidiaceae, morphotype 2 – Miroviaceae and morphotype 9 – angiosperms) are deemed most suitable for these measurements because they have sufficient cuticle yield and preservation. Stomatal index data are used to reconstruct atmospheric pCO_2 using the nearest living equivalent stomatal ratio approach for the Cheirolepidiaceae and angiosperm material. Data from morphotype 2 (Miroviaceae) are calibrated to the morphotype 1 (Cheirolepidiaceae) reconstruction due to a lack of a suitable nearest living equivalent for the Miroviaceae. Stomatal conductance data (g_{wmax}) are used to provide an indication of possible hydrological changes through the section, ecophysiological information about the three morphotype plant types and as a novel means of estimating relative pCO_2 changes.

6.2 Stomatal measurement methods

6.2.1 Stomatal density, index and frequency measurements

6.2.1.1 Sampling strategy

Stomatal density and index were calculated using the standard protocol from Poole and Kürschner (1999), to enable comparison to other datasets: counts were made over the same area for each fossil leaf cuticle fragment. A Zeiss UNIVERSAL microscope with RSIII fluorescence condenser with blue and UV filters was used to examine the cuticle, generally at x100 magnification, but higher magnification (x200) was used where autofluorescence of cuticle fragments was poor. All stomatal counts were made from images of the field of view captured using the Jenoptik Progres® CCD camera and annotated with a calibrated scale bar in Progres® CapturePro software. After capture, images were annotated with a square counting area of 0.09 mm^2 for both x100 and x200 magnification images. This area is greater than the minimum area recommended by Poole and Kürschner (>0.03 mm^2), and represents the largest area possible where stomata and epidermal cells could be readily identified for a given magnification.

However, the use of fragmentary cuticle prevents the optimum sampling protocol of Poole and Kürschner from being employed and, consequently, variables such as position on the

leaf and leaf type (e.g. sun vs. shade morphology) cannot be constrained easily. These factors are in addition to the uncertainties associated with identifying species from cuticle morphotypes discussed in Chapter 4. To overcome some of the issues with using cuticle fragments, other authors (e.g. Haworth *et al.*, 2005; Aucour *et al.,* 2008; Passalia, 2009; Barclay *et al.*, 2010) collected large datasets of stomatal information, which are thought to encompass this natural variation and thereby still successfully provide a measure of average changes in stomatal density and index (McElwain, 1998).

In the present study, an appropriate count sample size for a given morphotype horizon was determined from the cumulative mean versus sample count number (Poole and Kürschner, 1999; Figure 6.1), where abundant material was available. The cumulative mean typically stabilises between 5 and 10 counts, indicating that an appropriate number of counts have been made. However, this was not always possible due to the rarity of many morphotypes in certain horizons.

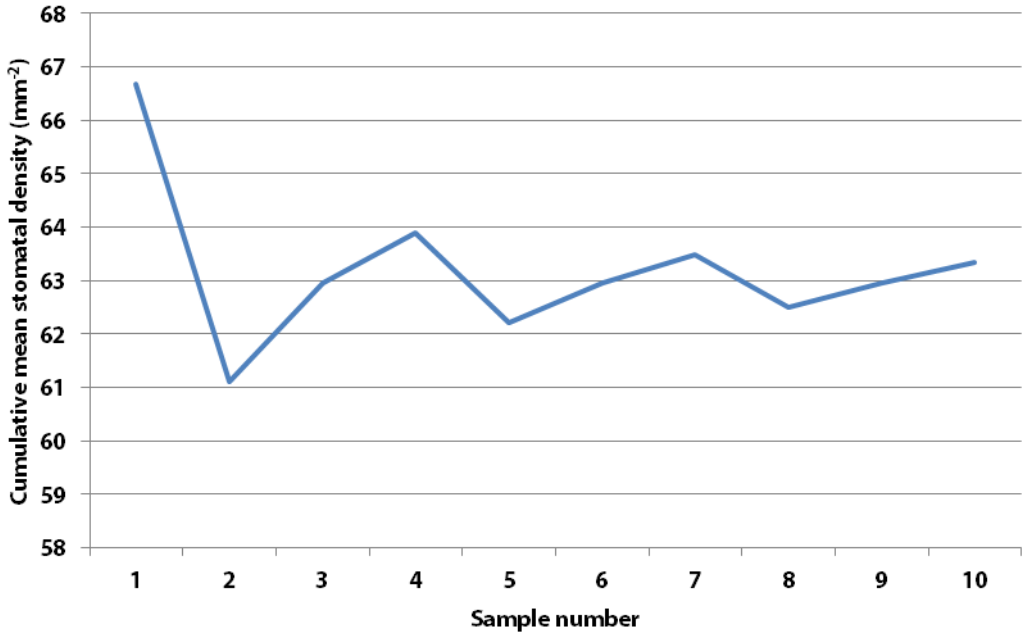

Figure 6.1: Stomatal density counts on cuticle fragment LK-B-2 (1) of morphotype 1 (Cheirolepidiaceae), showing the stabilising of the cumulative mean after 6–7 areas counted.

6.2.1.2 Stomatal density

Stomatal density is defined as the total number of stomata per mm^2 area. (Equation 2.2, page 43). The square of area 0.09 mm^2 annotated on the image is the area over which stomatal density and index counts were made (Figure 6.2A).

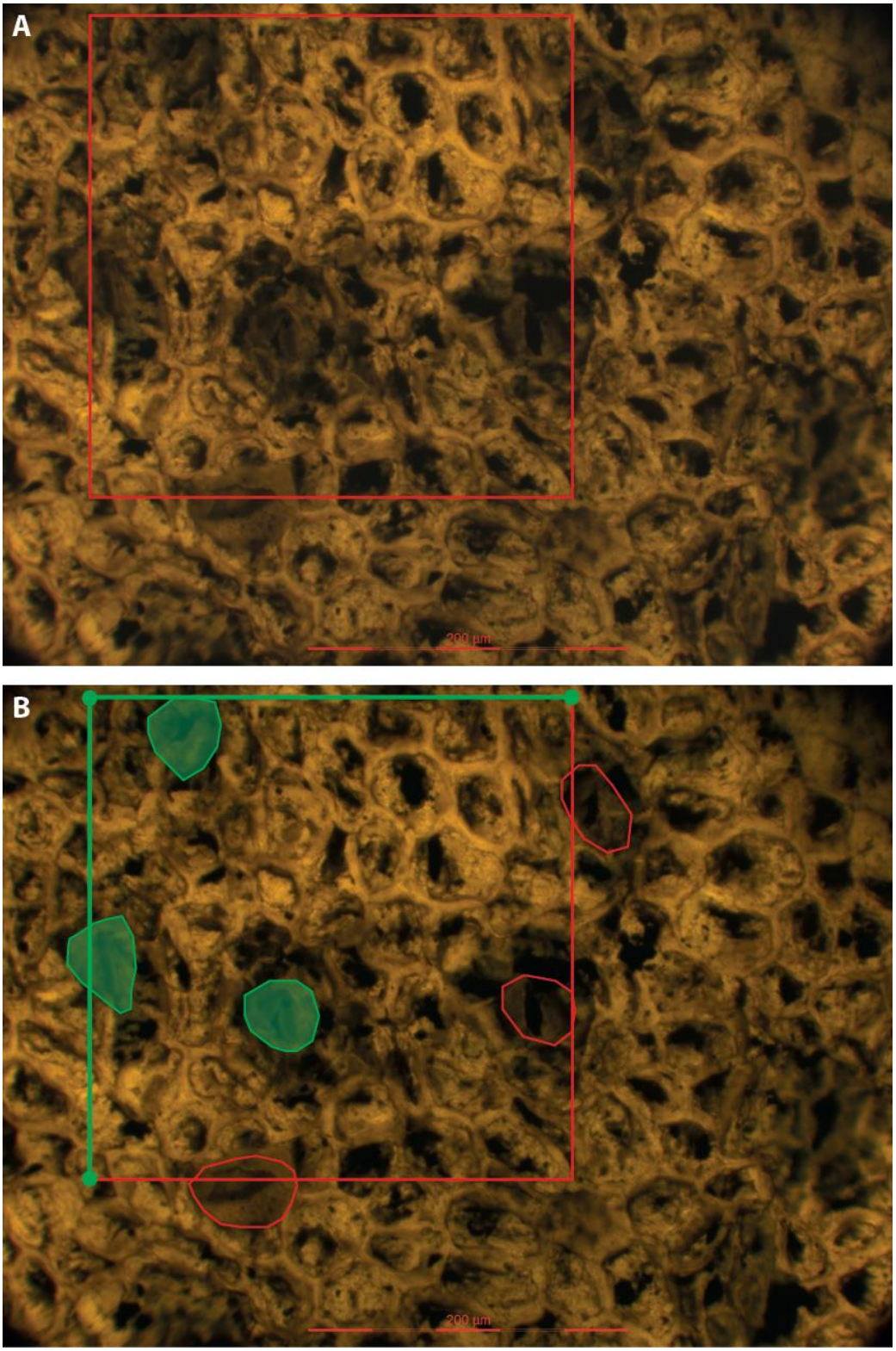

Figure 6.2: Epifluorescence image at x200 magnification of Cheirolepidiaceae cuticle fragment (morphotype 1) LK-B-28 (2) inside cuticle surface showing stomata and epidermal cells within the count area shown in red (Figure A). Scale bar shown = 200 µm. B: same image with annotations of stomata counted because they intersect the green areas or interior (green) and those not counted as they intersect the red edges (red outline) based on Poole and Kürschner (1999).

According to the standard protocol for cell inclusion for stomatal and epidermal counts (Kubínová, 1994; Poole and Kürschner, 1999), stomata within the count area, in addition to any stomata crossing the top and left sides and corners (Figure 6.2B) were counted. Any stomata which crossed the right or bottom edge of the area were not counted, even if they only crossed over by a small amount (Figure 6.2B).

Stomatal density per mm^2 (as defined in Equation 2.2, page 61) was calculated by scaling up the stomatal density measured over the count area (by dividing the measured stomatal density by the count area). The standard deviation was calculated to reflect the variation of density measurements per fragment.

6.2.1.3 Stomatal index

Stomatal index (Salisbury, 1927) is defined as the stomatal density divided by the sum of the epidermal cell density plus the stomatal density, all multiplied by 100 (Equation 2.3, page 62); stomatal index is dimensionless. Measurement of epidermal cell density follows the same protocol as described for stomatal density and was measured from the same areas. Generally, it was found the interior cuticle surface (like that shown in Figure 6.2) provided the best detail of epidermal cells. The only additional factor to consider in the case of epidermal cell density, is whether the subsidiary cells are included as part of the stomatal complex or as individual epidermal cells. In the present study, subsidiary cells were counted as epidermal cells in line with similar studies in order to produce comparable datasets (e.g. Haworth *et al.,* 2005).

6.2.1.4 Stomatal frequency

Kouwenberg *et al.* (2003, 2005) compared the influence of stomatal initiation on stomatal number measurements for broad leaved angiosperms (and other plant groups which initiate stomata fairly evenly across the developing leaf surface), and needle conifers (where initiation occurs at the leaf base resulting in files of stomata along the length of the leaf with needle growth; Croxdale, 2000; Kouwenberg *et al*., 2003). The stomatal frequency for needle conifers can be defined as the number of stomata per mm length, calculated by multiplying the stomatal density by the number of rows within the stomatal band.

Only morphotype 2 (Miroviaceae) had a suitable stomatal arrangement to explore this measure of stomatal numbers since morphotypes 1 (Cheirolepidiaceae) and 9 (angiosperm) possessed dispersed stomatal distribution (Chapter 4.4.1 and 4.4.9 respectively). However, the number of cuticle fragments with a completely preserved stomatal band was rare.

Instead, the stomatal density of each count area was divided by the number of stomatal files within the area, giving the average number of stomata per mm length in each file. According to the data for some conifer species from Kouwenberg *et al.* (2003, 2005), this is a sensitive measure of pCO_2 response.

6.2.2 Stomatal conductance measurements

Stomatal conductance can be estimated from the theoretical maximum stomatal conductance for water vapour (g_{wmax}) by measuring the stomatal density and size (Franks and Beerling, 2009; Equation 6.1).

Equation 6.1: stomatal conductance calculation.

$$g_{wmax} = \frac{\frac{d}{v} \times D \times a_{max}}{\left(l + \frac{\pi}{2}\sqrt{\frac{a_{max}}{\pi}}\right)}$$

$$a_{\max} \approx \pi \left(\frac{\rho}{2}\right)^2$$

$$l = \frac{W}{2}$$

Where:

d = diffusivity of water vapour in air at 25°C and 1 atm (2.49 x 10^{-5} m^2s^{-1})

v = molar volume of air at 25°C and 1 atm (2.44 x 10^{-2} m^3mol^{-1})

D = stomatal density (m^{-2})

a_{max} = maximum open area of stomatal pore (m^2)

l = pore depth (m)

ρ = stomatal pore length (m)

W = guard cell pair width (m)

Based on Franks and Beerling's calculation, the measurements required from the leaf cuticle are: the stomatal density, the pore length, and guard cell pair width (Figure 6.3). The guard cell length is not required for the g_{wmax} calculation but is useful if the stomatal size (S) is to be estimated (S = W x L; Franks and Beerling, 2009).

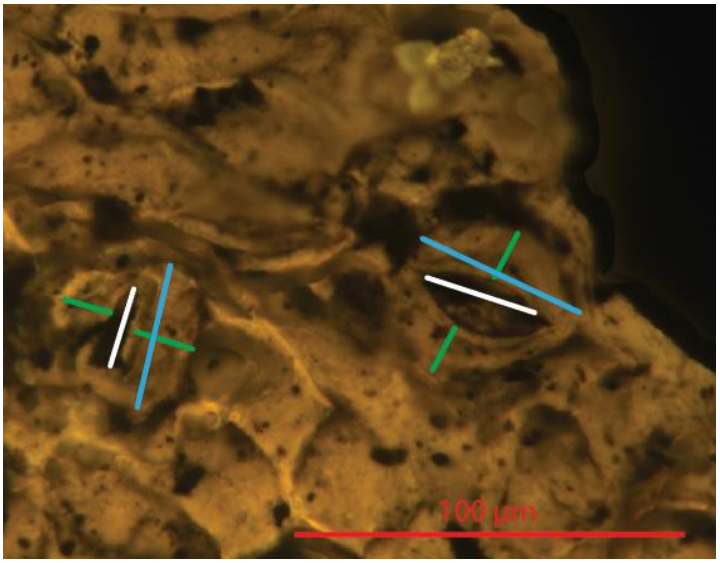

Figure 6.3: Morphotype 1 cuticle fragment (LK-B-42_9) at x400 magnification, epifluorescence image of inside cuticle surface, showing two stomata. White line – pore length, green lines = guard cell width (pair), blue line – guard cell length.

Stomatal measurements were made from epifluorescence images at either x200 or x400 magnification depending on the autofluorescence, and were captured and scaled in the same way as for stomatal density and index measurements. The measurements were made

in Image J freeware using the scaled measuring tool for morphotypes 1, 2 and 9 for all fragments with sufficiently preserved stomatal detail, in order to calculate g_{wmax}.

6.3 Results

6.3.1 Stomatal density, index and frequency measurements

6.3.1.1Cheirolepidiaceae (morphotype 1)

Morphotype 1 produced the largest yield of cuticle suitable for stomatal measurements, with 455 stomatal density and 188 stomatal index measurements made over 83 and 46 cuticle fragments respectively (Figure 6.4). There are fewer stomatal index measurements due to the demand for epidermal cell preservation.

There is a large range in stomatal densities measured at horizons with multiple fragments, on the order of 20–30 mm^{-2} which remains fairly consistent through the Kome Formation and Ravn Kløft Member stratigraphy (Figure 6.4A). Despite this variation, there appears to be a decrease in stomatal density from around 60–70 mm^{-2} in the first 6 m of stratigraphy, to around 40 mm^{-2} by 11 m stratigraphic height. This trend is less strongly represented in the stomatal index data, where a decrease of around 1 unit is represented in the first 11 m of the Kome Formation, with a high stomatal index of around 12 measured at 5.6 m (Figure 6.4B). However, the standard deviation of this horizon large since it is represented by just two measurements from just one cuticle fragment.

The stomatal density and index through the middle portion of the Kome Formation, from around 11 m to 32 m stratigraphic height, are fairly stable within the 1σ error bars (Figure 6.4). The stomatal density values average around 40–50 mm^{-2} (Figure 6.4A), whereas there is slightly more variation in the corresponding stomatal index data but is generally around 6–8 (Figure 6.4B). The resolution of stomatal density and index data for the Ravn Kløft Member is low, but yield comparable values to the Kome Formation (Figure 6.4).

6.3.1.2 Angiosperm (morphotype 9)

As identified in Chapter 5, angiosperm cuticle is very rare in the macerated record; two horizons in the Kome Formation produced just five fragments from which stomatal measurements could be made (24 stomatal density, and 18 stomatal index measurements in total). Nonetheless, there is a significant increase in stomatal density from around 75 mm^{-2} to a greater range around 150–200 mm^{-2} (Figure 6.5A). This increase in stomatal

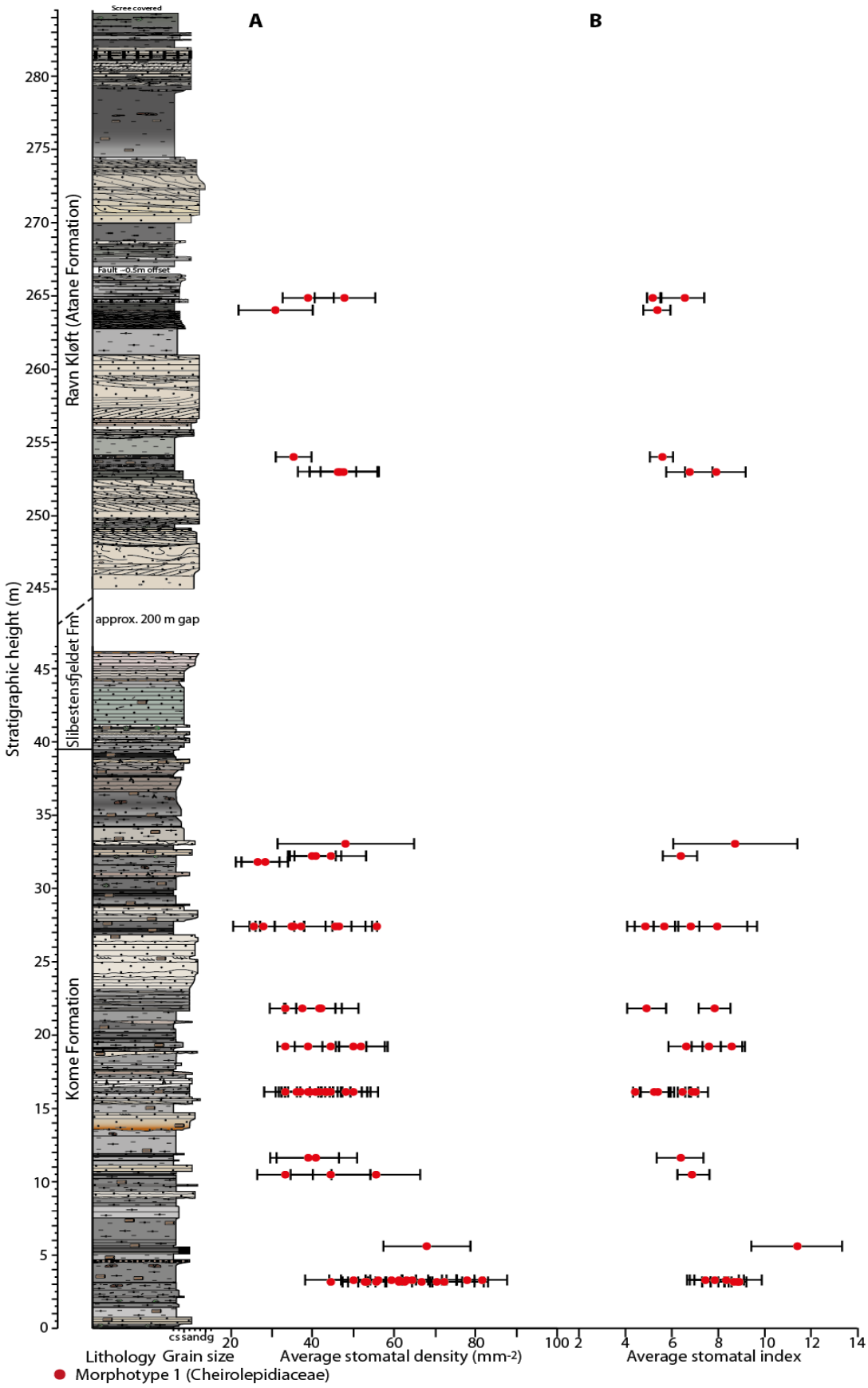

Figure 6.4: Cheirolepidiaceae (morphotype 1) fragment average stomatal density (A) and index (B) with ±1σ error bars.

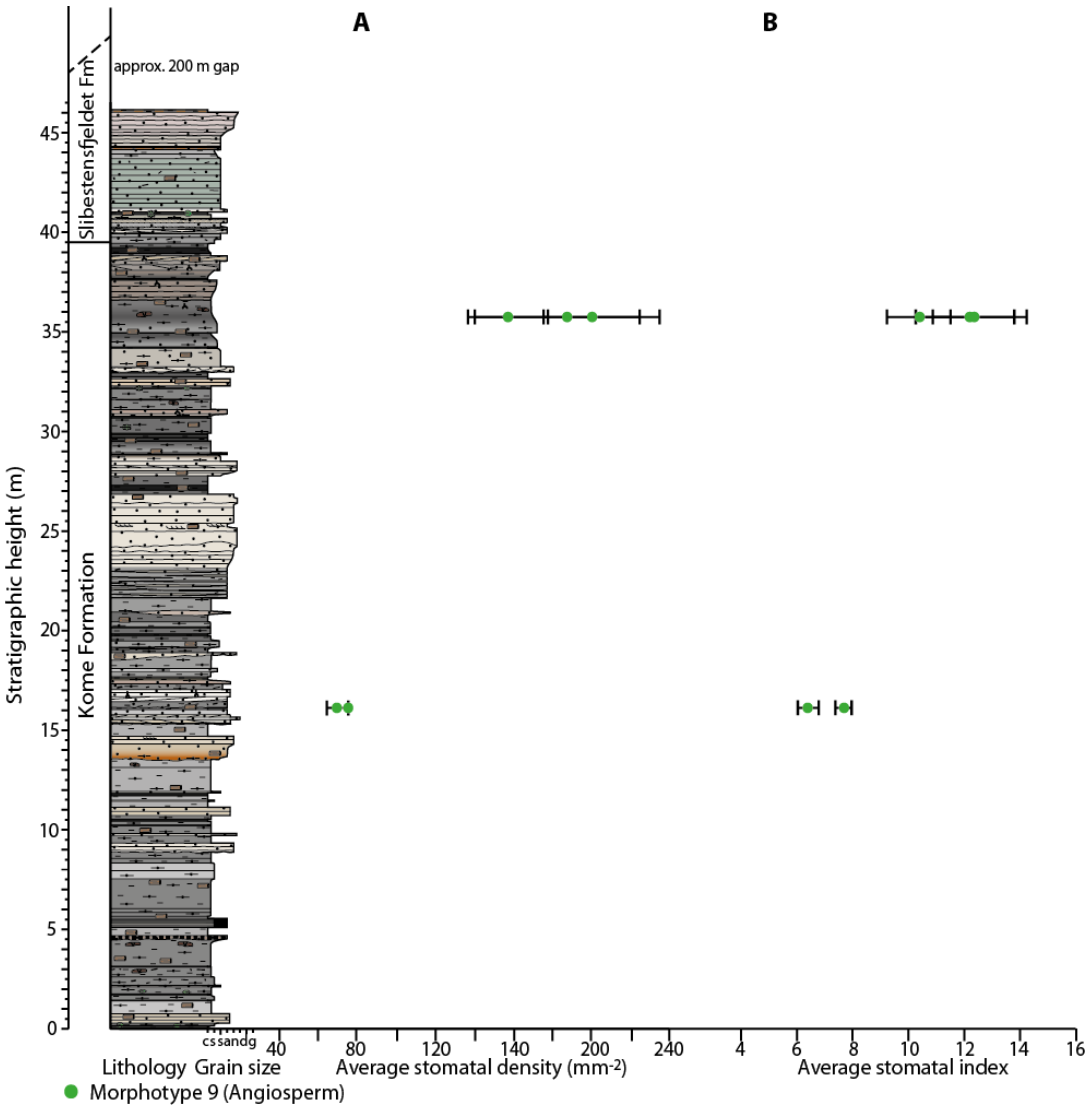

Figure 6.5: Angiosperm (morphotype 9) fragment average stomatal density (A) and index (B) with ±1σ error bars.

density is also reflected in the stomatal index data, which increases from around 7 at around 16 m stratigraphic height to around 10–12 at around 36 m height (Figure 6.5B).

6.3.1.3 Miroviaceae (morphotype 2)

Morphotype 2 fragment average stomatal densities (calculated from 228 measurements in total) present the widest range in density for a given horizon of the three morphotypes measured, up to 60 mm^{-2}, representing a difference of 50 % in the lowest range compared to the upper range: e.g. at 1.1 m stratigraphic height (Figure 6.6A). The uncertainty caused by this variation make trend identification outside of this range difficult, but there is a suggestion of a decrease in stomatal density from 1.1 m height to more consistently around 70 mm^{-2} at around 12 m height (but composed of fewer data points).

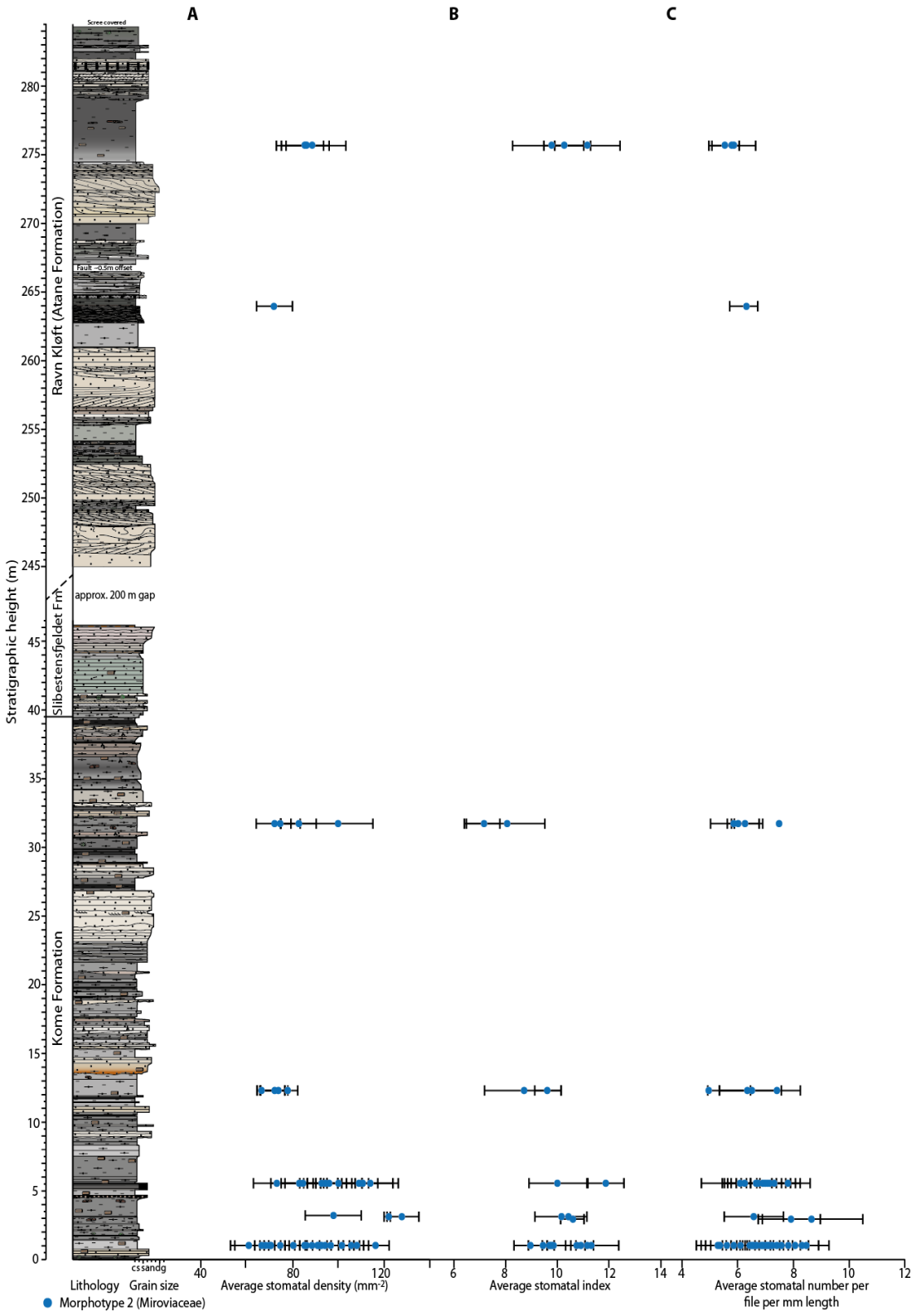

Figure 6.6: Miroviaceae (morphotype 2) fragment average stomatal density (A), stomatal index (B) and stomatal number per mm length in each file (C) with ±1σ error bars.

The variation within-horizon of the stomatal index data ranges at a maximum of 3.5 units (Figure 6.5B). There is a tentative decrease from a stomatal index of around 10–11 in the lower 6 m of stratigraphy in the Kome Formation to around 9–10 by around 13 m stratigraphic height, although the variation within-horizon is greater in the lower 6 m of stratigraphy. Stomatal index remains similar near the top of the Kome Formation with an index value around 8 at 32.17 m stratigraphic height. Whilst the data resolution through the Ravn Kløft Member is poor, the stomatal density and index values for morphotype 2 are similar to those in the Kome Formation (Figure 6.6 A, B).

The new stomatal length measure of number of stomata per file over 1 mm length, based on that of Kouwenberg *et al.* (2003), shows similar degrees of within-horizon variation as the stomatal density and index data, making identification of any trends within the dataset problematic. Overall, the range within-horizon remains fairly similar (around 3) for horizons with multiple fragment measurements, with a general value of around 7 throughout the Kome Formation and Ravn Kløft stratigraphy (Figure 6.6C).

6.3.2 Stomatal conductance and pore length

A total of 902 stomata were measured from 120 cuticle fragments from the three morphotypes (1, 2 and 9) in order to calculate g_{wmax} (Figure 6.7A). The Cheirolepidiaceae (morphotype 1, red in Figure 6.7) have an average g_{wmax} value of around 1000 ± 225 (1σ) mmol m^{-2} s^{-1} for the lower 5 m of stratigraphy of the Kome Formation (Figure 6.7A). The average g_{wmax} value for the remainder of the Kome Formation (above 5.60 m) is around 814 ± 167 (1σ) mmol m^{-2} s^{-1}. The stomatal conductance at 5.60 m is considered cautiously since this horizon is represented by only one cuticle fragment, but does support higher g_{wmax} values for the lower 6 m of Kome Formation stratigraphy, with a value around 1200 mmol m^{-2} s^{-1} (Figure 6.7A). Similarly, the highest horizon in the Kome Formation and two horizons in the Ravn Kløft Member are represented by single cuticle fragments, but fall within the range of the other horizon box plots of around 700–900 mmol m^{-2} s^{-1}.

The angiosperm (morphotype 9, green in Figure 6.7A) average g_{wmax} values almost double from 924 ± 131 (1σ) mmol m^{-2} s^{-1} at 16.08 m, to 1828 ± 258 (1σ) at 35.72 m. However, it is noted that only five cuticle fragments comprise the entire angiosperm dataset, and the interquartile range on the higher horizon is on the order of 400 mmol m^{-2} s^{-1}.

The Miroviaceae (Morphotype 2, blue in Figure 6.7A) presents the greatest interquartile range in g_{wmax} of the three morphotypes, from around 300–900 mmol m^{-2} s^{-1} despite having

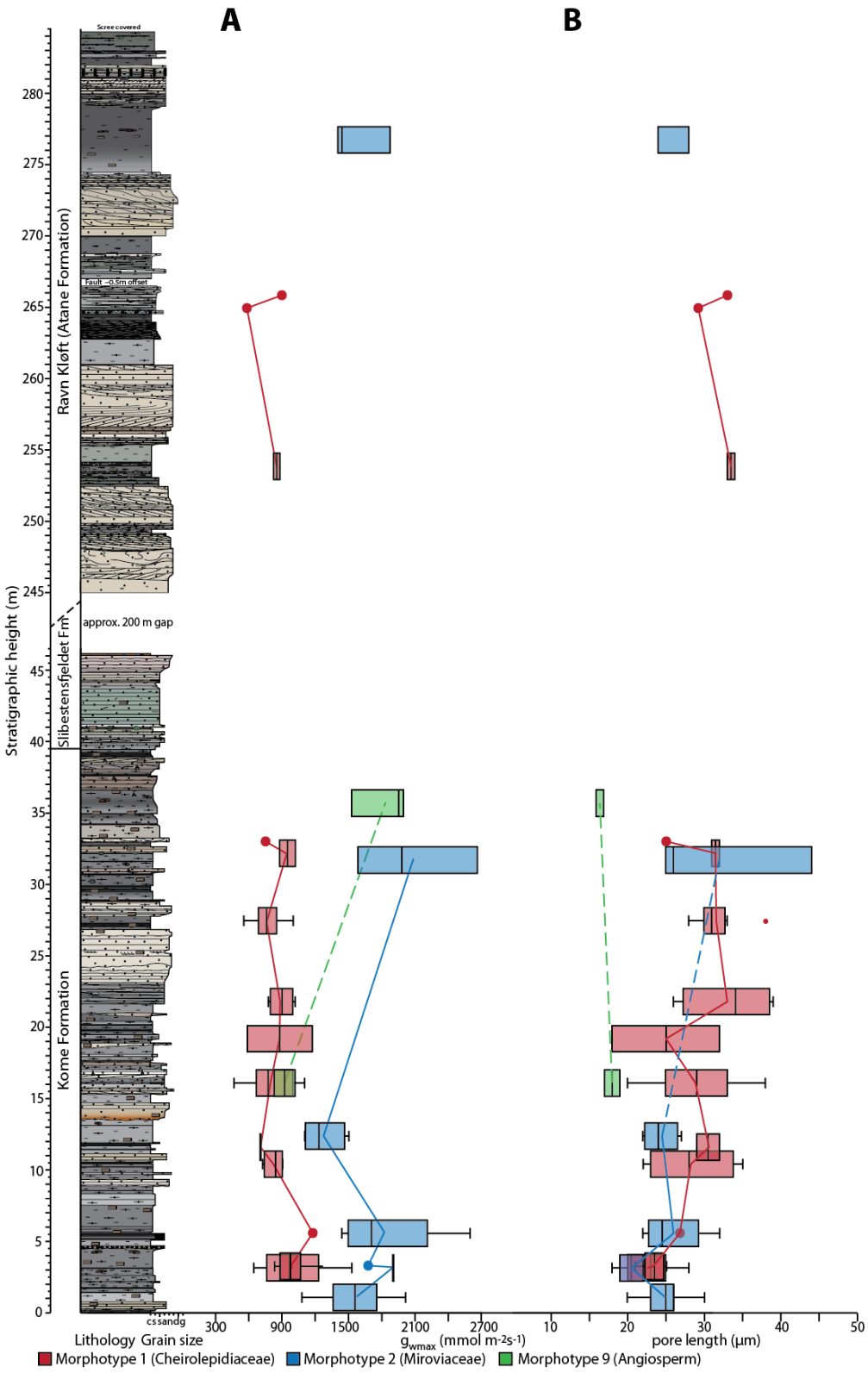

Figure 6.7: Fragment average g_{wmax} data (A) and pore length (B) presented as box and whisker diagrams showing interquartile range as box edges, the median value dividing the box and the whiskers represent 2 % and 98 % values where applicable. Single data points are shown for horizons represented by a single cuticle fragment. Horizon average value trend indicated by colour-coded lines.

the largest sample of cuticle fragments for some horizons (at 1.1 m and 5.6 m). The average value for the lower 5.6 m of stratigraphy is 1657 ± 322 (1σ) mmol m^{-2} s^{-1} compared to 1271 ± 191 (1σ) mmol m^{-2} s^{-1} for 12.35 m height, and 2079 ± 545 (1σ) mmol m^{-2} s^{-1} for 31.77 m stratigraphic height. The single horizon from which g_{wmax} was measured in the Ravn Kløft Member, reveals similar values to the lower Kome Formation, around 1500–1800 mmol m^{-2} s^{-1}

The variation within-horizon is large for the g_{wmax} and pore length data, as shown by the interquartile range and whiskers of the box plots in Figure 6.7; as a result, in many cases, horizon ranges overlap, making it difficult to determine statistically significant variations. Therefore, in this thesis the average value trends are described, but it is acknowledged that some of these variations are small and within the error as shown in Figure 6.7. Nonetheless, comparison of all three morphotype g_{wmax} reveals coeval trends in horizon average values (Figure 6.7A), which would indicate that the trends in average gwmax are likely representative of the true stratigraphic trends. A decrease in average g_{wmax} values are indicated in the first 12 m of Kome Formation stratigraphy by the Cheirolepidiaceae (morphotype 1) and Miroviaceae (morphotypes 2), followed by a subsequent increase in average g_{wmax} by around 33 m height recorded by the Miroviaceae and angiosperm (morphotype 9) values. However, the average g_{wmax} of the Cheirolepidiaceae remains fairly stable through the interval from around 10 m to 33 m. The absolute values of g_{wmax} of the Cheirolepidiaceae are the lowest of the three morphotypes, with the Miroviaceae possessing the highest stomatal conductance (Figure 6.7A).

The changes in pore length with stratigraphy are less concordant across the three morphotypes (Figure 6.7B): despite the great change in stomatal conductance, the angiosperm data (morphotype 9) shows no significant change in pore length, and has the smallest stomata measured of the three morphotypes, around 17 μm. The Cheirolepidiaceae (morphotype 1) which possesses more stable g_{wmax} values throughout the stratigraphy have the largest stomata of the three morphotypes, and shows a small increase in average pore length though the Kome Formation of around 10 μm, but the significance of this increase is lost within the large interquartile ranges (Figure 6.7B). The pore lengths of Cheirolepidiaceae are around 30 μm in the Ravn Kløft Member (Figure 6.7B). The Miroviaceae (morphotype 2) possess generally similar pore lengths throughout the entire stratigraphy, of around 20–25 μm (Figure 6.7B) despite the apparent increase in pore length at the top of the Kome Formation, which on appreciation of the median value

indicates the horizon average is likely skewed to larger values on account of considerable variation in pore lengths at this horizon (Figure 6.7B). The pore lengths of the Cheirolepidiaceae and Miroviaceae are more comparable in size with each other than that of the angiosperm material.

6.4 Preliminary discussion

6.4.1 Stomatal number measurements - data trends

Similar to the g_{wmax} and pore length data, the large error on the stomatal frequency measurements means many trends based on average values are within the error of the horizons (e.g. Figure 6.8). Whilst trends in the average data are still discussed in this thesis, it is recognised that some of the variation is within the error range. However, average trends are supported by consistent trends across all datasets, which likely reveal true variation through the stratigraphy (Figure 6.8). In the first 5.6 m of Kome Formation stratigraphy, a small increase in stomatal index is recorded by the Cheirolepidiaceae (Figure 6.8B) and the number of stomata per mm of a stomatal file of the Miroviaceae (Figure 6.8C), which exceeds the 1σ error bars. This is followed by a decrease by around 13 m height in all stomatal measures (density – Figure 6.8A, index – Figure 6.8B and the stomatal frequency measure – Figure 6.8C) for the Cheirolepidiaceae and Miroviaceae, which also indicate a change in values outside of the 1σ error bars.

Relatively stable low values persist from around 13 m height to around 32 m height in the Cheirolepidiaceae stomatal density (Figure 6.8A) and index (Figure 6.8B) data, supported by low values of stomatal density and index of angiosperm and Miroviaceae data. The angiosperm stomatal density and index data reveal a large increase (well outside the 1σ error range) from around 16 m height to the top of the Kome Formation. This trend is supported by a smaller increase in the topmost Cheirolepidiaceae density and index data, although the increase is only just outside the 1σ error range. However, the stability of the Cheirolepidiaceae density and index data from 13–32 m height may suggest the increase in frequency through this interval was quite rapid and confined to the topmost of the Kome Formation if the two morphotype datasets can be reconciled.

The resolution of data in the Ravn Kløft Member is insufficient for any strong trends to be identified, but the general values and error ranges on the data are comparable to the Kome Formation, and the values of all three stomatal measurements appear fairly stable and

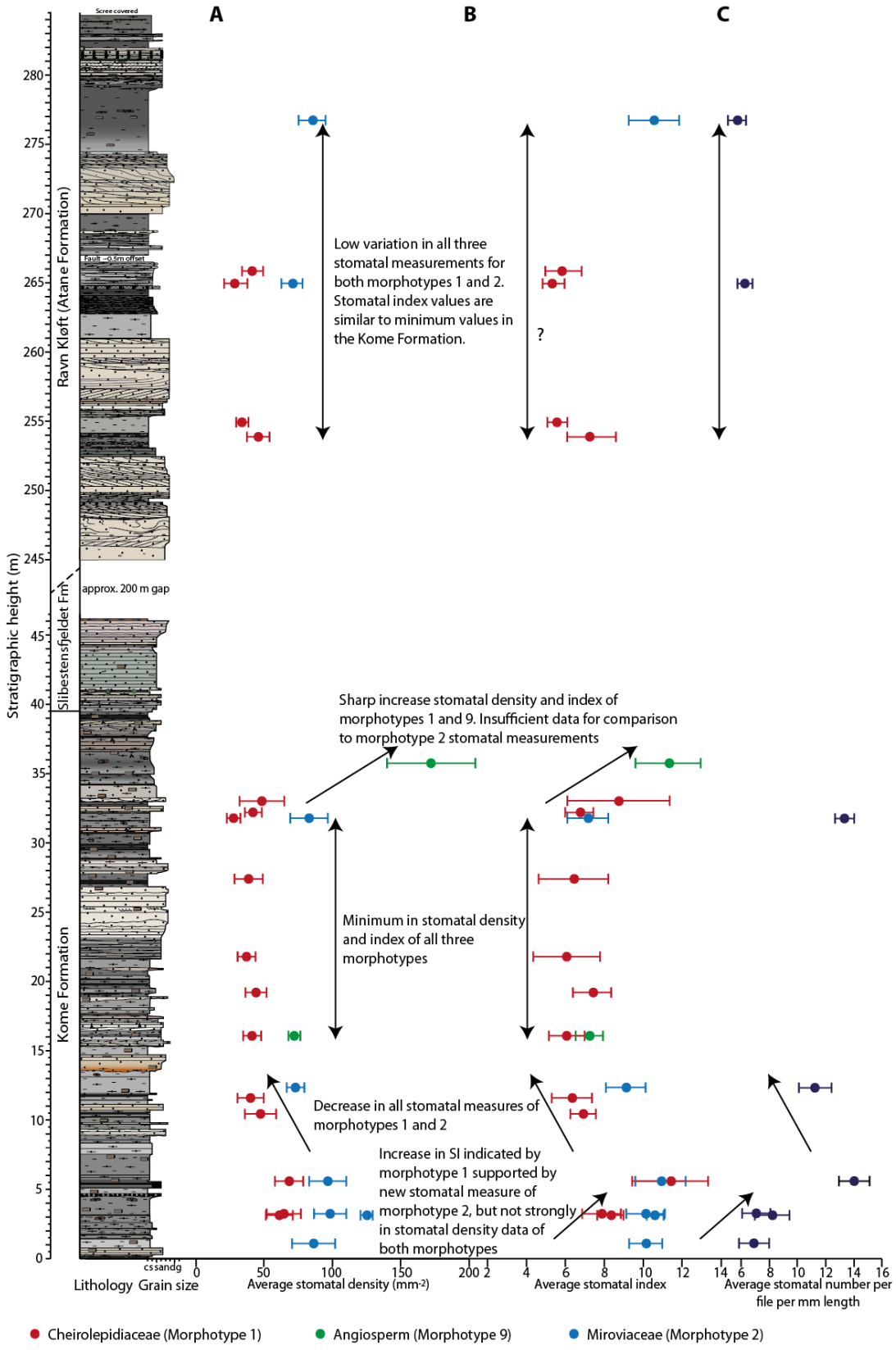

Figure 6.8: Horizon average stomatal measurements through the Kome Formation and Ravn Kløft Member for all three morphotypes (morphotype 1, 9 and 2) showing A: stomatal density. B: stomatal index. C: new measure of stomatal frequency: stomatal density divided by the number of rows per mm. Error bars = ±1σ.

similar to the minimum values of density and index recorded between 13 m and 32 m in the stratigraphy.

Overall, the Cheirolepidiaceae possess the lowest stomatal density and index of the three morphotypes, whereas the angiosperms possess the highest values. The offset between the three morphotypes remain fairly consistent throughout the stratigraphy, which is a good indicator that the relative trends are caused by a single driving factor. Given the trends are apparent in all stomatal number measurements, this driving factor is most likely pCO_2 rather than environmental factors (Section 2.3.3).

6.4.2 Stomatal conductance and pore length

When the stomatal density is compared with pore length as a proxy for stomatal size (Figure 6.9A), a negative relationship is identified in the Cheirolepidiaceae (morphotype 1) and angiosperms (morphotype 9). This is the first high-resolution dataset for a given morphotype (assumed to approximate to a single species) supporting Franks and Beerling's (2009) hypothesis: that in order to achieve higher stomatal conductance, higher densities of smaller stomata are required, since fewer but larger stomata will suffer from a longer diffusion path as the guard cell width (and therefore pore depth) increases (Figure 6.9B). The gradient of the angiosperm data trend (shown as a linear relationship since the scale is greatly expanded compared to that of Franks and Beerling in Figure 6.9B that the relationship approximates to linear) is less than that of the Cheirolepidiaceae, indicating a much greater change in stomatal density compared to pore length (Table 6.1). The general range of stomatal density and pore length of these two morphotypes is supported by a selection of extant angiosperm and gymnosperm species measured by McElwain and Lawson (*in press*), but reveals the Cheirolepidiaceae pore lengths are up to 10 µm longer than the other gymnosperm species of Lawson and McElwain.

Plant	Equation of linear trend line
Cheirolepidiaceae (M.1)	y = -0.2389x + 39.391
Gymnosperms (McElwain & Lawson)	y = -0.1584x + 33.769
Angiosperm (M.9)	y = -0.0395x + 20.578
Angiosperms (McElwain & Lawson)	y = -0.023x + 17.285
Miroviaceae (M.2)	**y = 0.0494x + 21.372**

Table 6.1: trend line equations for relationship between pore length and stomatal density (Figure 6.9A).

The data from the Cheirolepidiaceae and angiosperm of the present study and the selection of angiosperm and gymnosperm species from McElwain and Lawson reveal a

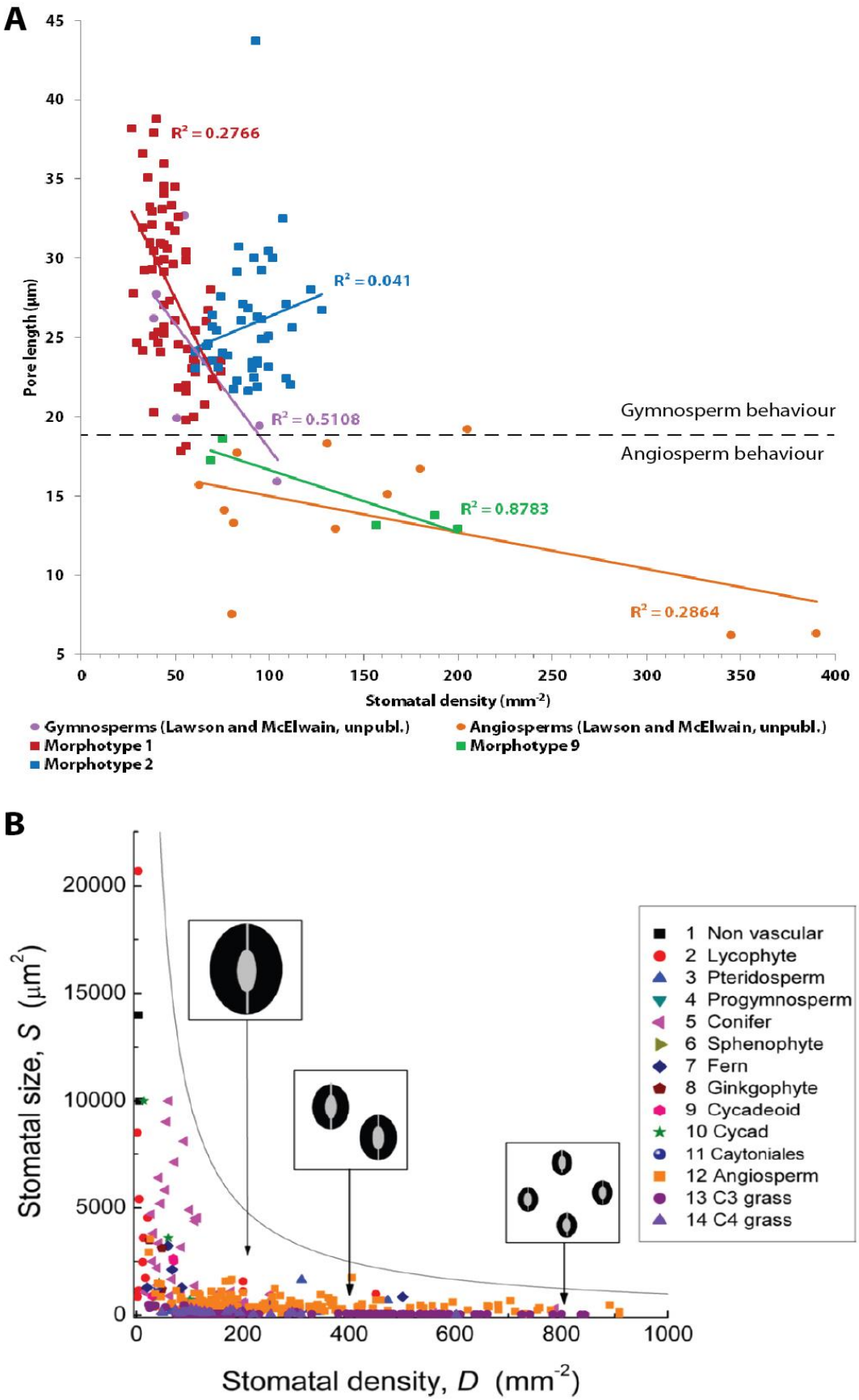

Figure 6.9: Relationship between stomatal pore length (A) and stomatal size (B, from Franks and Beerling, 2009) with stomatal density for various plant species from the present study, McElwain and Lawson (in press) and Franks and Beerling (2009).

subdivision in general plant behaviour, which can also be observed in the data from Franks and Beerling (2009), whereby gymnosperms have a smaller range in stomatal density and greater variation in pore length, whereas angiosperms experience greater variation in stomatal density with limited pore lengths which are often considerably smaller than gymnosperms (Figure 6.9A), although there is some overlap between these two "behavioural types". However, the Miroviaceae data (morphotype 2) does not appear to follow the same trend, with a low r^2 value for the trend line, which has a small positive gradient (Table 6.1) unlike the other plant data in Figure 6.9A. The pore lengths are more comparable to the "gymnosperm behaviour" but generally have higher stomatal density than the Cheirolepidiaceae.

The implications of this apparent physiological difference between angiosperms and gymnosperms on the stomatal conductance are explored within the context of Franks and Beerling's hypothesis. A positive relationship between stomatal density and g_{wmax} is observed for all three morphotypes (Figure 6.10A), as expected from the g_{wmax} calculation (Equation 6.1). The gradient of the trend lines for the Cheirolepidiaceae (morphotype 1) and Miroviaceae (morphotype 2) are similar and possess comparable degrees of scatter from each trend line (with r^2 values around 0.39 and 0.31 respectively). The angiosperm (morphotype 9) has a steeper gradient (and a high r^2 value of 0.97 reflecting the low sample size), indicating comparatively the angiosperm morphotype experiences a greater change in stomatal density to achieve the same difference in g_{wmax}.

When the pore length is considered against g_{wmax}, different responses across the three plant types are observed (Figure 6.10B). The angiosperm data (morphotype 9) presents a negative relationship between pore length and g_{wmax}, as predicted from Franks and Beerling's (2009) hypothesis. Therefore, the angiosperms possess a greater degree of plasticity in stomatal initiation: by keeping stomatal sizes small, the angiosperm morphotype is capable of great density change of at least twice that of the Cheirolepidiaceae and Miroviaceae. Thus, for angiosperms, stomatal density is the dominant factor in the g_{wmax} calculation.

However, both the Cheirolepidiaceae and Miroviaceae indicate a positive relationship between g_{wmax} and pore length, such that fragments with longer pores have a high calculated g_{wmax} (Figure 6.10B). At first instance, this positive relationship appears at odds with the hypothesis of Franks and Beerling and the relationship between stomatal density and pore length (Figure 6.9A): how can g_{wmax} be higher in both cases of higher stomatal

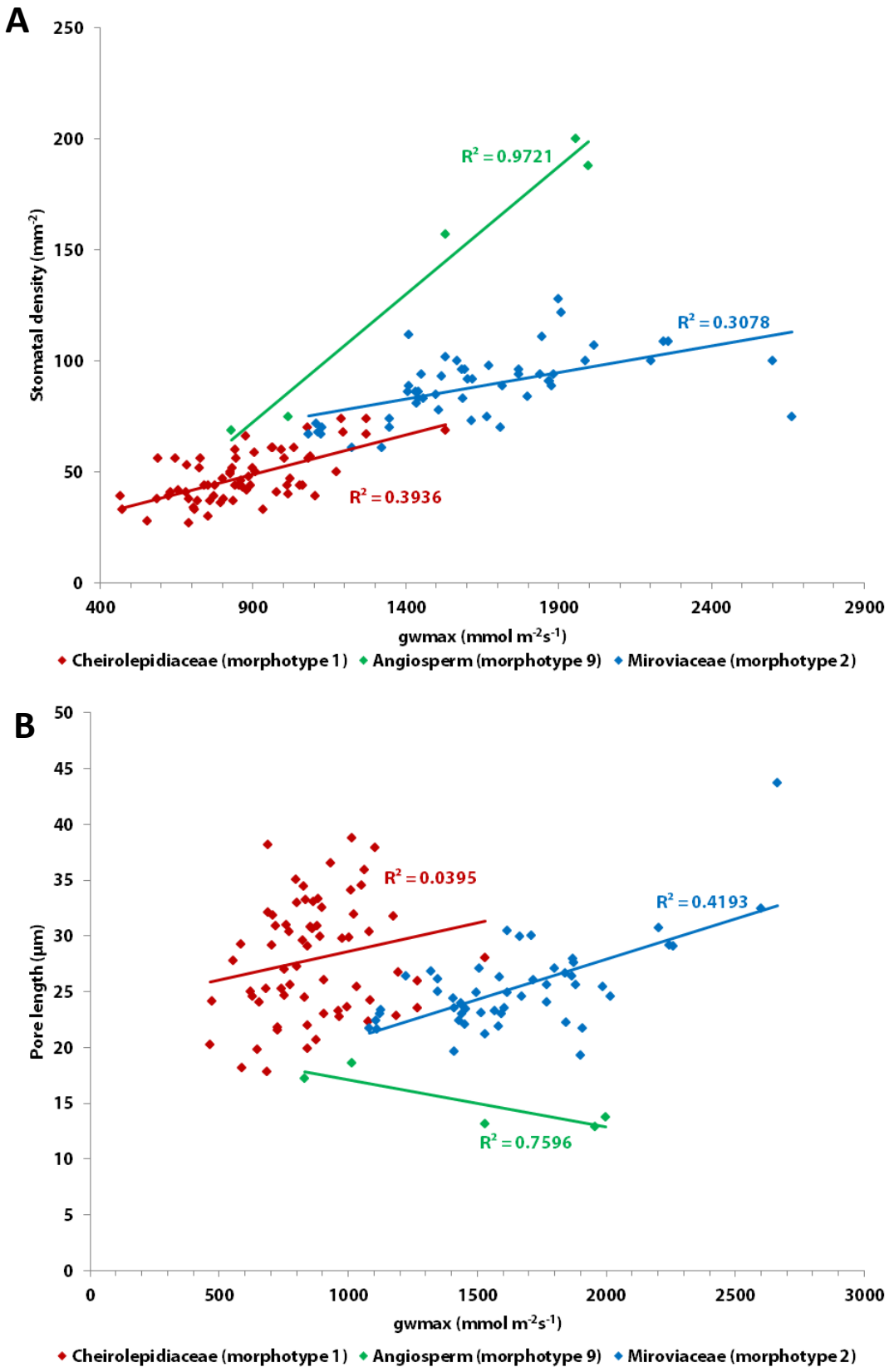

Figure 6.10: Fragment average stomatal measurements versus g_{wmax} showing trend lines with r^2 values for A: stomatal density versus g_{wmax} and B: pore length versus g_{wmax}.

density (Figure 6.10A) and longer pore lengths (Figure 6.10B) when in general there are fewer larger stomata for a given cuticle fragment (Figure 6.9A)? This reveals the relative importance of pore length compared to stomatal density (the two main variables in the calculation, Equation 6.1) on g_{wmax} for this plant type, and suggests the Cheirolepidiaceae could not accomplish great changes in stomatal density and instead possessed greater variation in pore lengths at a time when they were not physiologically constrained (Section 6.6). The Miroviaceae appear to share this characteristic, as shown in the positive relationship between stomatal density and pore length with respect to g_{wmax} (Figure 6.10). However, the relationship between stomatal density and pore length (Figure 6.9A) is less defined compared to the angiosperms and gymnosperms (McElwain and Lawson, in press), suggesting a more unusual behaviour of this plant. The stomatal density is more constrained than that of the angiosperms, but on average is higher than other gymnosperms, with a very tentative indication that higher stomatal densities were accompanied by larger stomata. This is contrary to the hypothesis of Franks and Beerling (2009) and all the other plant data presented, possibly indicating a significantly unrestricted physiology to afford a transpiration-expensive form (Section 6.6).

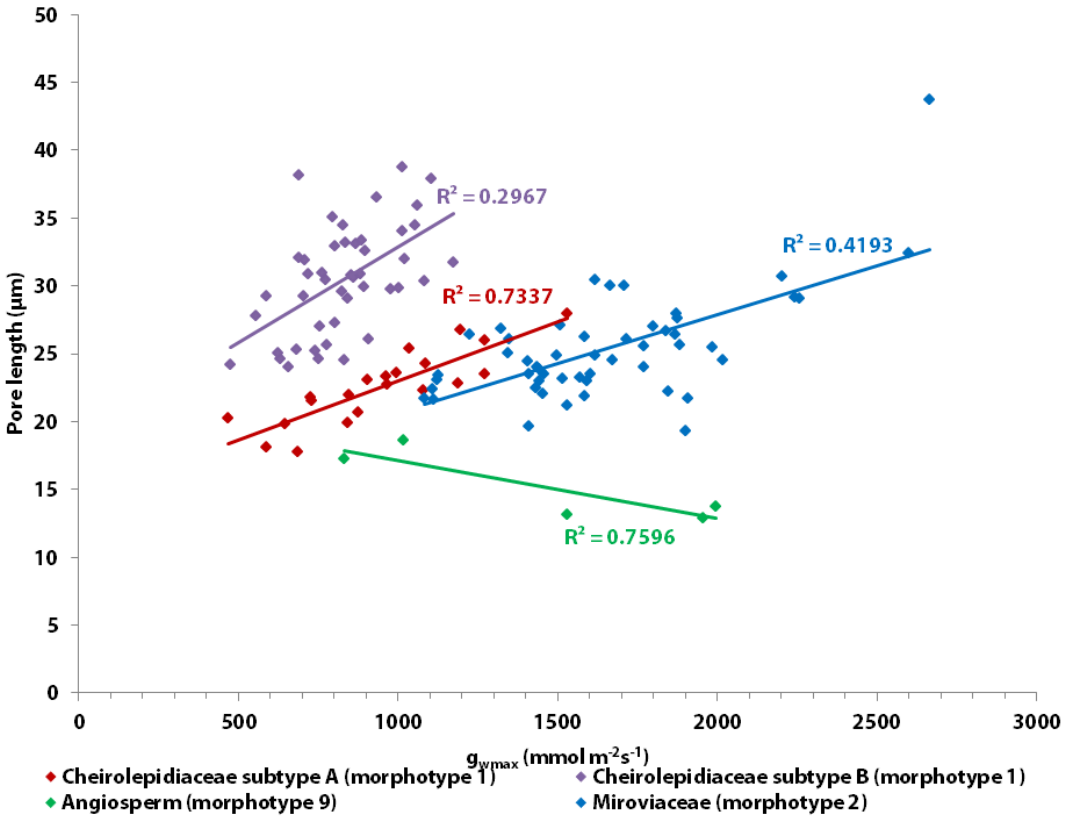

Figure 6.11: Fragment average stomatal pore length versus g_{wmax} showing trend lines with r^2 values showing the division of the Cheirolepidiaceae data into two subtypes.

Closer inspection of the relationship between Cheirolepidiaceae pore length and g_{wmax} (Figure 6.10B), reveals a possible bi-modal split of the data into two separate trends (Figure 6.11) but no such division can be observed in the relationship between stomatal density and g_{wmax} (Figure 6.10A). The gradient of subtype B trend line is slightly greater than subtype A which is more similar to the Miroviaceae, and may indicate a greater reliance on pore length changes on controlling of stomatal conductance than subtype A. The pore length of subtype B is also generally higher than subtype A, by about 5–10 µm. This may indicate the presence of more than one species or genera is represented within the morphotype 1 definition (Cheirolepidiaceae) which should be taken into consideration for pCO_2 reconstructions (Section 6.5).

6.5 pCO_2 reconstruction

6.5.1 Method

Section 2.3.3 introduced the concept of the stomatal ratio where, for Mesozoic studies, the closest approximation to ancient pCO_2 is most comparable to the Recent Standardisation: 1SR unit = 1 RCO_2 unit, where 1 RCO_2 unit = 300 ppm (McElwain, 1998). However, in order to use a NLE grown at pCO_2 levels of greater than 300 ppm, a correction must be applied. For example, in McElwain (1998), the NLE material for fossil Lauraceae-based reconstructions was collected from an atmosphere of 360 ppm. Assuming a linear relationship between SI and pCO_2, NLE material collected at 360 ppm would have a stomatal index 1.2 times lower than if it were collected at 300 ppm. Therefore, for the Recent standardisation to be applied, the SR must be multiplied by the ratio of collection pCO_2 value to 300 ppm (in the cited case 360/300 = 1.2) before being equated to 1RCO_2 unit.

The transfer function approach can be used for fossil plants with extant living representatives as outlined in Section 2.3.3. A linear regression of either historical herbarium data or growth chamber experiments of stomatal index against the known pCO_2 is used to calculate the pCO_2 for the fossil material by using the equation of the line of best fit for the calibration dataset (e.g. Kürschner *et al.*, 2008; Barclay, 2011).

6.5.2 NLE selection

6.5.2.1 Cheirolepidiaceae (morphotype 1)

As discussed previously, the cuticle fragments identified in morphotype 1 could not be assigned to a definite form-genus, but shared many cuticle features with *Pseudofrenelopsis*

and *Frenelopsis* (Section 4.5.1). Reconstructions of plant habit vary across the Cheirolepidiaceae form-genera: *Pseudofrenelopsis parceramosa* has been reconstructed as trees with succulent characteristics, wood development and an arborescent habit (Watson, 1988 and references therein), whereas other members of the Cheirolepidiaceae, such as *Frenelopsis ramosissima* (e.g. Watson, 1988 and references therein) have been reconstructed as smaller succulent plants and herbaceous forms with less wood development. Phylogenetic affinities for the Cheirolepidiaceae remain conjectural without associated reproductive fossils (Watson, 1988). However, for the purposes of pCO_2 reconstruction, previous studies (e.g. Haworth *et al.*, 2005; Aucour *e al.*, 2008; Passalia, 2009) mostly compare the Cheirolepidiaceae to cupressacean conifers based on the similarities of form (Watson, 1977), and thus provide a starting point for NLE selection.

Haworth *et al.* (2005) reconstructed pCO_2 from macerated leaf cuticle from *Pseudofrenelopsis parceramosa* through the Wealden and Lower Greensand Groups (South England) and the Potomac Group (USA) using the stomatal ratio method with a generalised "Frenelopsid-like" NLE. The generalised NLE was defined by the average stomatal index of three modern cupressacean conifers and a halophyte angiosperm *Salicornia virginica*. The selection of *Salicornia* by Haworth *et al.* covered the likely ecological range of *Pseudofrenelopsis*, which included coastally influenced localities (Potomac Group) and seasonally dry fluvial settings (Wealden Group). Whilst the Nuussuaq Group along the Nuussuaq Peninsula was likely deposited close to the coastline at a palaeoaltitude close to sea-level (Dam *et al.*, 2009; Chapter 2.5), there is no direct evidence of brackish or saltwater influence in the Kome or Atane Formations, which have been interpreted as exclusively freshwater, thereby precluding the requirement for a halophyte NLE.

Of the three Cupressacean conifers used by Haworth *et al*. (2005), only *Callitris oblonga* (Figure 6.12A), occurs in habitats analogous to the depositional environments of the Nuussuaq Group. Extant *Callitris oblonga* is found in river habitats (rarely more than 100 m from water source) in Australia and Tasmania at altitudes ranging from 10–1300 mabsl (Haworth *et al*., 2010), with leaves sheathing around the stem in a scale-like fashion, comparable to many of the Cheirolepidiaceae form genera. However, the cuticular morphology is not identical to morphotype 1 as there are no stomatal papillae, and the stomata of *Callitris* species occur in bands, ordered into approximate files (Figure 6.12A, B), where epidermal cell walls are generally straight and are rectangular to irregular polygon in shape, being more irregular in shape in the stomatal zones.

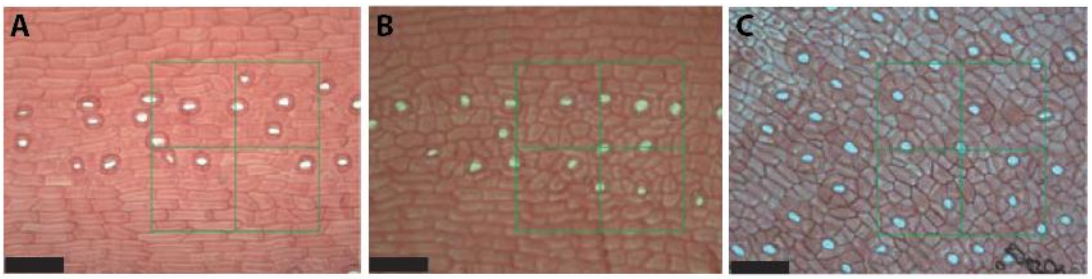

Figure 6.12: From Haworth et al. (2010) cuticle images of selected NLEs, with 100 µm scale bar. A: Callitris oblonga; B: Callitris rhomboidea; C: Athrotaxis cupressoides.

Haworth *et al.* (2010) found *Callitris rhomboidea* (Figure 6.12B) presents a significant stomatal index response to pCO_2 through study of stomatal index of historical herbarium samples. *C. rhomboidea* is found in temperate areas of Australia and Tasmania with higher precipitation but more drained soil than *Callitris oblonga* (Figure 6.12A; Haworth *et al*., 2010) indicating a suitable NLE choice for the present study Cheirolepidiaceae material. Whilst Haworth *et al.* identified no significant response of *C. oblonga* to below ambient pCO_2 based on historical herbarium samples, another cupressacean conifer, *Athrotaxis cupressoides* (Figure 6.12C) was found by Haworth *et al.* to demonstrate no response to below-ambient pCO_2 based on herbarium material, but a strong relationship was identified in growth chamber experiments where pCO_2 was varied from 370–670 ppm. This indicates *A. cupressoides* is a good candidate for pCO_2 reconstructions for times of past high pCO_2 like the Cretaceous (Haworth *et al.*, 2010) and that other conifer species may also still retain responses to above ambient pCO_2 despite the lack of historical response for lower pCO_2. The stomatal distribution of *A. cupressoides* is comparable to the Cheirolepidiaceae (with broader stomatal zones than *Callitris*, cyclocytic stomata are arranged into irregular files; Figure 6.12C). *A. cupressoides* is found at higher altitudes (900–1300 mabsl) than the *Callitris* species, but is found close to water sources (Haworth *et al*., 2010).

On that basis, these three conifers (*Callitris oblonga, Callitris rhomboidea* and *Athrotaxis cupressoides*) were selected as the NLE for the present study morphotype 1 (Cheirolepidiaceae) material. Using the data provided in Haworth *et al.* (2010), a generalised Frenelopsid-like NLE stomatal index (SI) value of 9.8 ± 1.2 for 367 ppm pCO_2 is based on averaged values for the three conifer species (summarised in Table 6.2). The stomatal index values for these three species are similar, which according to Haworth *et al.* (2005) would suggest convergent stomatal adaptations and gas exchange relationship (Table 6.2).

Species	Average pCO_2	Average SI	Standard deviation of SI
Athrotaxis cupressoides (growth chamber)	370	10.0	0.3
Callitris oblonga	367	10.5	1.4
Callitris rhomboidea	364	9.8	1.0

Table 6.2: From Haworth et al. (2010) average pCO_2 and corresponding average stomatal index values for three NLE conifer species.

6.5.2.2 Angiosperm (morphotype 9)

Although morphotype 9 could not be unequivocally assigned to a plant genus all cuticle fragments (except one bearing possible peltate glandular trichomes which was not used for stomatal measurements) possessed Laurel-like trichomes across the epidermal surface and other similar cuticular features of Lauraceae (Section 4.5.1) In addition, the identification of *Trilaurus sassopsis* macrofossils (Section 4.5.1) supports the case for selecting a Lauraceae NLE for morphotype 9.

Greenwood *et al.* (2003) measured the clear stomatal response of the Laurel *Neolitsea dealbata* through historical herbarium sets (reflecting an inverse response in stomatal index to changes in pCO_2), in addition to the lack of response of stomatal index to changes in temperature and mean annual and seasonal rainfall. *Neolitsea dealbata* is found in tropical to subtropical environments along the east coast of Australia, with mean annual temperatures of 14–26 °C, and mean annual precipitation ranging 1000–4000 mm yr^{-1}, generally favouring disturbed habitats as a small tree in multiple-level canopies of lowland rainforest up to 900 m and higher altitude single layer forests around 1100 m altitude (Greenwood *et al*., 2003 and references therein). Based on the sedimentological and palaeobotanical evidence (Dam *et al.*, 2009; Chapter 5) from the Nuussuaq Group, this is a suitable ecological comparison. The leaf form and cuticular morphology of *N. dealbata* and morphotype 9 are also similar: whilst *Trilaurus sassopsis* is palmately-lobed (tri-lobed) and *N. dealbata* has a simple elliptical to obovate form (Figure 6.13), both species possess notophyllous leaf sizes and share eucamptodromous secondary venation (Boyd, 1998c; Greenwood *et al*., 2003). The epidermal cell walls of *N. dealbata* are sinuously crenulated compared to the straight cell walls of morphotype 9 but otherwise appear to form irregular polygon shapes like morphotype 9 material. *N. dealbata* has paracytic stomata randomly orientated within the aureoles, and are flush with the epidermal surface (Greenwood *et al.*, 2003), which is not always the case in Lauraceae (Barclay, 2011) but is similar to morphotype 9 cuticle.

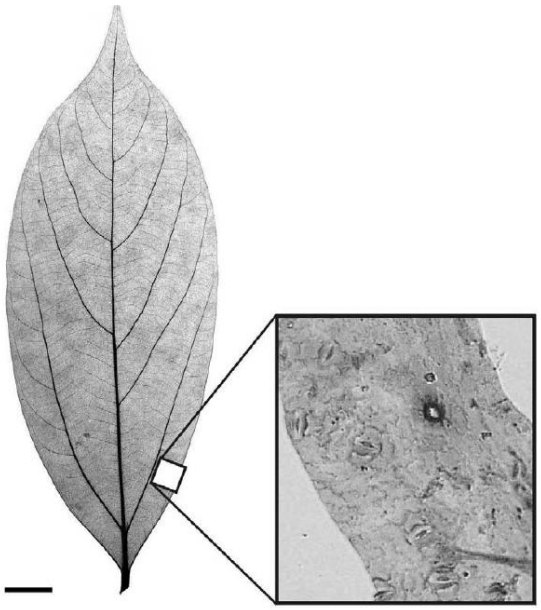

Figure 6.13: From Greenwood et al. (2003). X-ray image of Neolitsea dealbata leaf (left, scale bar = 10 mm). Inset: close up light microscope image of cleared cuticle showing stomata and sinuously crenulated epidermal cell walls with a single trichome base.

Kürschner *et al.* (2008) used the transfer function of extant *Laurus nobilis* and *Ocotea foetens* to calibrate fossil material from the Miocene. Of these two species, the ecology and cuticular features of *O. foetens* are considered most similar to the Nuussuaq Group angiosperms. *O. foetens* is a Lauraceae found in Macaronesia (the North Atlantic archipelagos off the coast of Africa and Spain: including Madeira, the Azores and the Canary Islands), inhabiting a similar humid Mediterranean climate as *L. nobilis*, but with higher mean annual precipitation on some archipelagos than others (e.g. Madeira; Marrero and Nogales, 2005). *O. foetens* is hypostomatic, with an irregular polygon pavement of epidermal cells in areole areas (which are larger than *L. nobilis*), which contain randomly orientated paracytic stomata, and non-glandular hairs occur across the epidermal surface similar to morphotype 9 material (Figure 6.14).

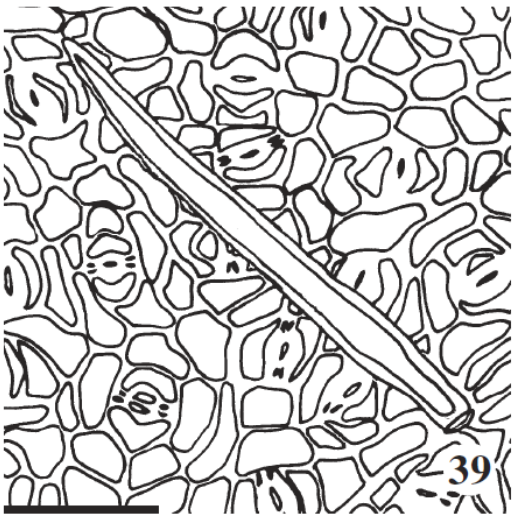

Figure 6.14: From Marrero and Nogales (2005). Sketch of abaxial side of O. foetens leaf epidermis, showing outlines of irregular polygon-shaped epidermal cells, randomly orientated paracytic stomata, and a non-glandular trichome running diagonally across the field of view. Scale bar = 25 µm.

The leaf size and shape of *O. foetens* is similar to that of *N. dealbata* but the second order venation is more brochidodromous. However, combining these two species as a generalised NLE is supported by the average stomatal index values obtained from the training sets of Greenwood *et al.* (2003) for *N. dealbata* (15.0 ± 2.5 at 301 ppm) and Kürschner *et al*. (2008) for *O. foetens* (14.0 ± 1.0 at 301 ppm), giving an average Lauraceae NLE stomatal index of 14.5 ± 1.8 for approximately 300 ppm.

If the angiosperm morphotype has been correctly identified as a member of the Lauraceae, pCO_2 can also be estimated from the transfer functions derived from the training sets of *N. dealbata* and *O. foetens* (Table 6.3). Since the transfer function is normally used for fossil and modern plants of the same species, the use of *N. dealbata* and *O. foetens* transfer function will yield loosely estimated pCO_2, since the relative responses to pCO_2 between the fossil material and the modern material is unknown.

Dataset	Species	Transfer function equation
Greenwood *et al*. (2003)	*Neolitsea dealbata*	SI = -0.1163 [CO_2] + 50.248
Kürschner *et al.* (2008)	*Ocotea foetens*	SI = -0.0552 [CO_2] + 30.245

Table 6.3: Summary of transfer function equations for the two Lauraceae species adopted in the present study used to find pCO_2 (ppm).

6.5.2.3 Miroviaceae (morphotype 2)

No living equivalent is available for the Miroviaceae *Oswaldheeria* (morphotype 2); therefore neither the transfer function nor the NLE stomatal ratio approach could be applied to this data. Instead, the data is tied to the Cheirolepidiaceae record by constructing a linear regression through the three most closely overlapping horizons (LK-B-2, LK-B-3 and LK-B-31 tied to LK-B-28 as the nearest other horizon), essentially adopting the method of the transfer function by using the Cheirolepidiaceae data as the training set. This is a reasonable approach given the similarities in stomatal response in the relationships of pore length and stomatal density (Figure 6.10A and 6.11).

6.5.3 pCO_2 reconstruction

The reconstructed pCO_2 through the stratigraphy was completed for all three morphotypes by the methods outlined in section 6.4.2 (Figure 6.15). Based on the bimodal distribution of Cheirolepidiaceae pore lengths with respect to g_{wmax} (Figure 6.11) the stomatal index data was divided into the two subtypes accordingly. Cheirolepidiaceae subtype A occurred in four horizons in the Kome Formation, and in each horizon has consistently higher

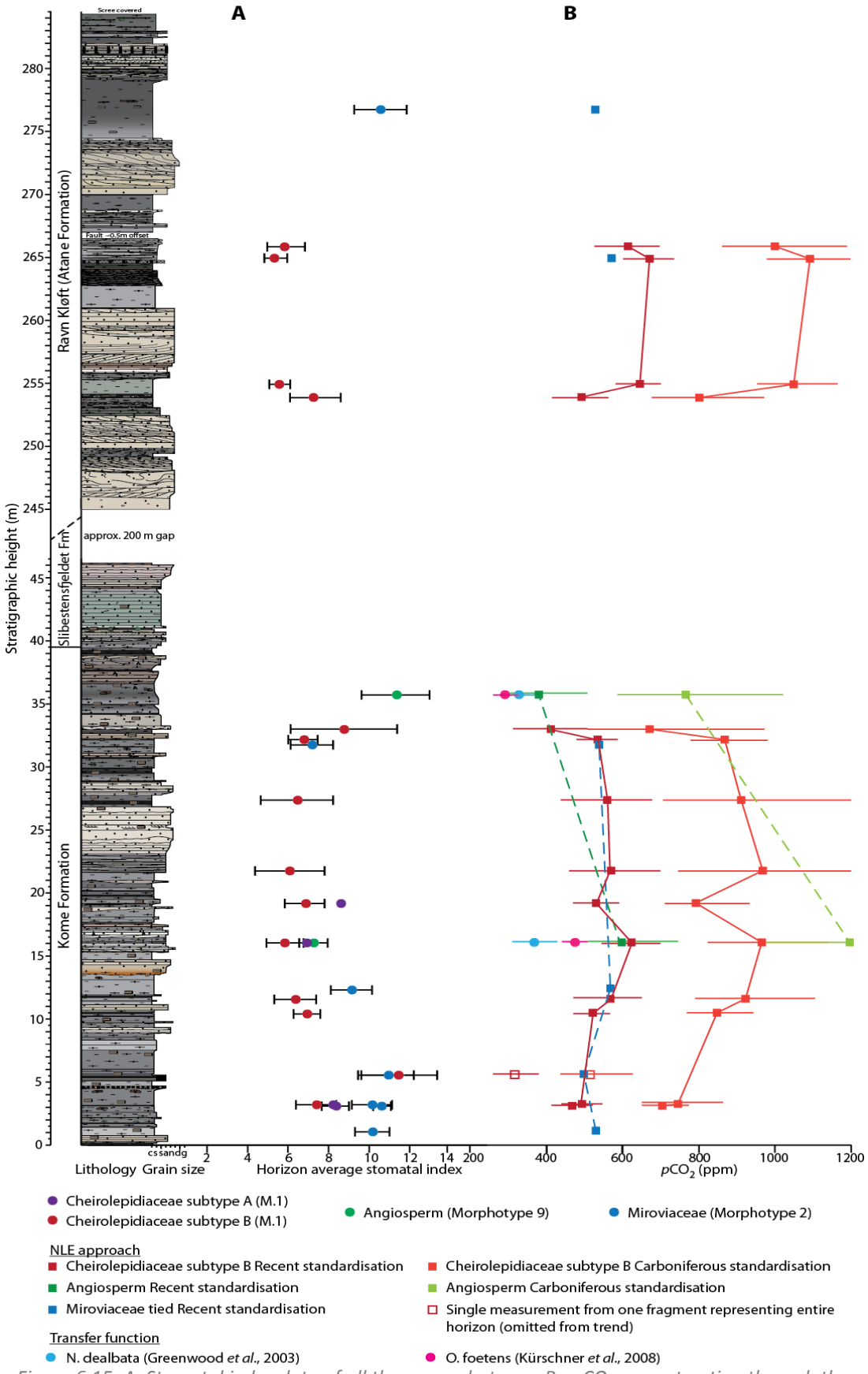

Figure 6.15: A: Stomatal index data of all three morphotypes, B: pCO_2 reconstruction through the Nuussuaq stratigraphy using the NLE stomatal ratio and transfer function approach. Error bars = propagation of SI 1σ in pCO_2.

stomatal index by 1–2 units. Therefore pCO_2 has been calculated on the basis of Cheirolepidiaceae subtype B of which there was more data (Appendix E). The pCO_2 value reconstructed at 5.6 m height in the Kome Formation has been omitted from the reconstructed pCO_2 trend for both the Recent and Carboniferous standardisation because, as outlined previously, this horizon is represented by two measurements from a single fragment, and the high stomatal index values were not supported by any of the stomatal measures of the Miroviaceae (morphotype 2) nor was the stomatal density of the Cheirolepidiaceae high at this point (Figure 6.8).

As with the stomatal density and index data, the error on the pCO_2 reconstructions is large (Figure 6.15), and as a result the trends in average pCO_2 of each morphotype largely fall within the ±1σ error range. Nonetheless, the trends in average pCO_2 are considered significant because they are identified in more than one morphotype. Reconstructed pCO_2 based on the Cheirolepidiaceae (Recent Standardisation) indicates a slight increase from average values of 446 ppm in the first 5 m of stratigraphy to around 520–560 ppm by 11 m stratigraphic height. The average pCO_2 remains fairly consistent throughout the remainder of the Kome Formation, around 550 ppm. However, as stated there is overlap of the error bars between these two intervals, which casts doubt on whether the increase of 100 ppm in the first 11 m of stratigraphy is real or artefact.

The topmost Cheirolepidiaceae horizon in the Kome Formation reconstructs a decrease in pCO_2 to 413 ppm, although again the error bars overlap, casting large uncertainty on the reliability of this apparent 150 ppm decrease. However, the stomatal ratio approach of pCO_2 reconstruction for the angiosperm (morphotype 9) reconstructs a decrease in pCO_2 from around 598 ppm ±151 (1σ) at 16 m height to 384 ppm ± 125 (1σ) by the top of the Kome Formation, with the apparent 214 ppm decrease falling just outside of the error bars of this dataset, supporting a decline in pCO_2 in the upper Kome Formation as purported from the Cheirolepidiaceae data as a statistically significant trend. The transfer function-based pCO_2 reconstruction using *N. dealbata* and *O. foetens* training sets (Figure 6.15B) both record a decrease across this interval, but the response of *N. dealbata* is less than that of *O. foetens* and the stomatal ratio reconstruction, indicating a decline of around 40 ppm, compared to 84 ppm estimated by *O. foetens*. Whilst the transfer function approach in this case was always going to be a loose estimate (since the relatedness of these two species to the fossil material is unknown), the closeness of the values to the NLE stomatal ratio method (falling within the error bars for the horizon at 35.72 m, but outside the error bar

range in the case of both transfer function reconstructions at 16 m) indicates the Recent standardisation is the most appropriate pCO_2 estimation for this time in the Mesozoic as previously suggested by McElwain (1998).

The tied Miroviaceae pCO_2 reconstruction demonstrates a low degree of variability, with an average value of 516 ppm ± 49 (1σ) through the entirety of the Nuussuaq stratigraphy. The absolute values of this reconstruction are, through the tying process, intrinsically similar to the Cheirolepidiaceae reconstruction, but the coherence of the tied reconstruction at horizons where the two morphotypes do not overlap provides some additional confirmation of the stability of pCO_2 at least in the middle portion of the Kome Formation.

The Ravn Kløft Member has few reconstructed pCO_2 values but the Cheirolepidiaceae reconstruction presents on average higher pCO_2 values than the Kome Formation, around 607 ppm ±79 (1σ).

The Carboniferous standardisation presents the upper estimation limit for the stomatal ratio approach of pCO_2 reconstruction, and therefore demonstrates the same trend in pCO_2, but much higher values between 700–1100 ppm and greater exaggerated responses of pCO_2 to changes in stomatal index as part of the calibration process. Since the transfer function approach yields values similar to the Recent Standardisation, the Carboniferous Standardisation values are not considered further.

6.5.4 Comparison to other Cretaceous pCO_2 reconstructions

6.5.4.1 Comparison of stomatal index data

The Cheirolepidiaceae stomatal index data of the present study can be compared to that of previous Cretaceous studies which were used to reconstruct pCO_2 (e.g. Haworth *et al.*, 2005; Aucour *et al.*, 2008; Passalia, 2009; Figure 6.16). There is a general agreement in the values of stomatal index produced by different species of Cheirolepidiaceae, which indicates members of this family likely possessed similar physiological controls in terms of stomatal initiation. The present study data overlaps in the Late Albian with all three published datasets; the present study data and that of Aucour *et al.* produce slightly higher stomatal index values but these are still within the error range of the other two datasets. The data collected from the Kome Formation of Middle Albian age records stomatal index values more similar to that of Aucour *et al.* (2008) than Haworth *et al.* (2005). The new data from this thesis suggests a possible increase in stomatal index from around 6 to 7–8 in the Middle Albian (LOESS smoothing: black line in Figure 6.16).

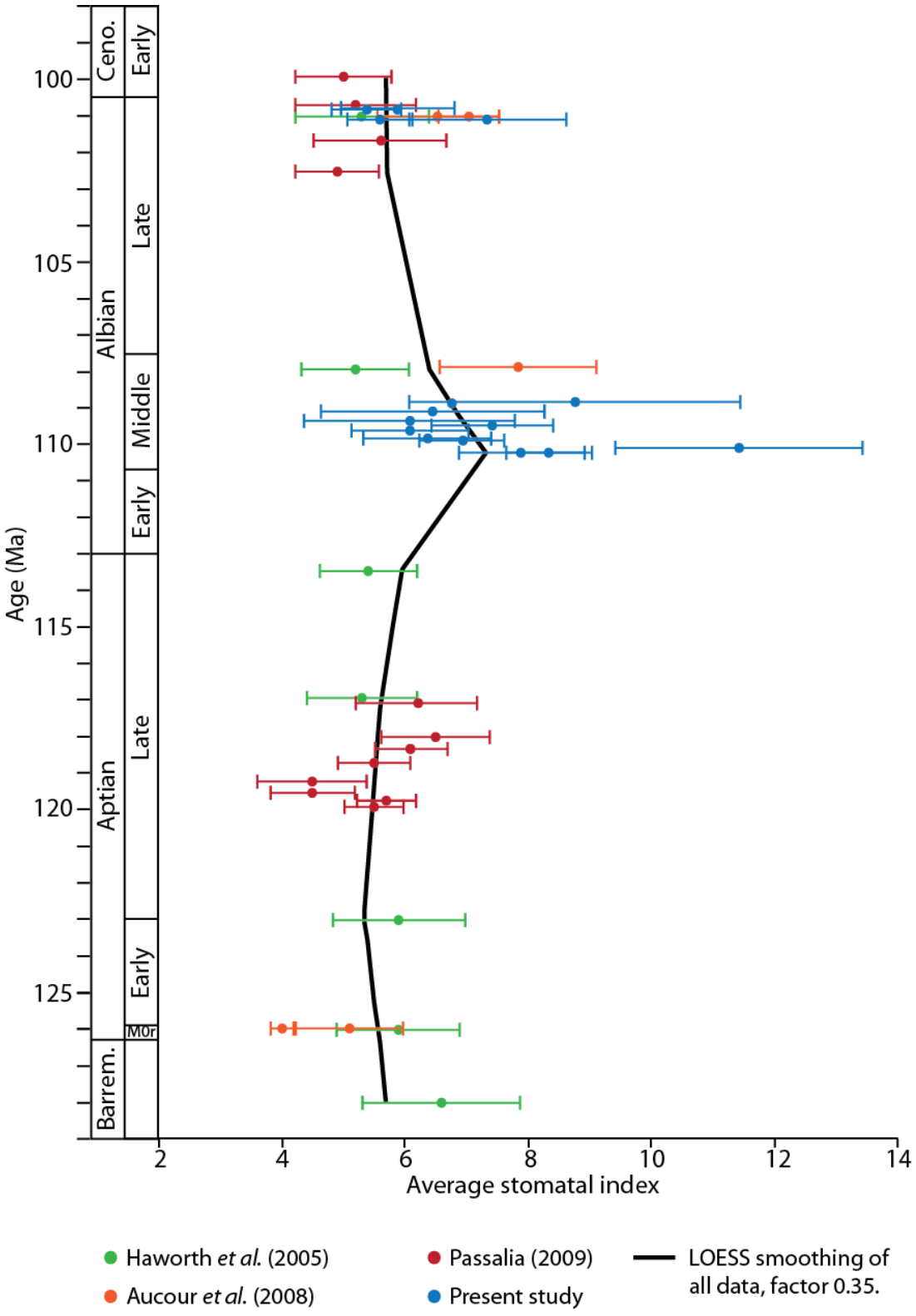

Figure 6.16: Average stomatal index for previously published studies and the horizon average present study data shown with ± 1σ error bars for Cheirolepidiaceae. The combined data long-term average trend is LOESS smoothed.

6.5.4.2 Scenario 1: pCO_2 reconstruction with previously published data

Given the similarity of the stomatal index data and the same stomatal ratio approach applied to all index data shown in Figure 6.16, a direct comparison of reconstructed pCO_2 should faithfully reconstruct pCO_2 through the Aptian–Early Cenomanian, with a predicted lower pCO_2 for the Middle Albian on account of the higher stomatal index indicated by the present study data (Figure 6.17).

The present study reconstructed pCO_2 values are significantly lower than the published reconstructions throughout the Albian, not just in the Middle Albian as predicted, but also in the Late Albian where the stomatal index data of all studies overlapped (Figure 6.16). The absolute values of the present study data are comparable with some reconstructions such as those of Aucour *et al.* (2008), Retallack (2001) and Passalia (2009), but there are occasions where the previously published reconstructions fall outside of the respective error bars (e.g. Aucour *et al.* versus Passalia in the Late Albian).

The greatest error source for the West Greenland dataset is the sample size, which was preservation dependant. Given the uncertainty of the low sample size, the error on the data is quite large. Small sample size might be expected to introduce noise into the pCO_2 reconstruction and a greater range of values would be expected. On the contrary, the pCO_2 reconstruction through the Nuussuaq stratigraphy shows a reasonable interval of stability (Figure 6.15) which would point to a different cause of the apparent present study data offset in pCO_2 values.

6.5.4.3 Scenario 2: pCO_2 reconstruction (re-examination of NLEs)

The single greatest source of variability in stomatal index-based reconstructions stems from the choice of NLE. The NLE for the present study was carefully selected based on similar species as those employed by previous studies of Haworth *et al.* (2005) and Passalia (2009) but with a thorough consideration of the palaeoclimate and environment (Chapter 5). However, the NLEs selected by other reconstructions could be re-examined; for example the use of the angiosperm *Salicornia virginica* by Haworth *et al.* (2005) and Passalia (2009) as a NLE for the Cheirolepidiaceae is contentious for a Cretaceous coniferous plant.

Haworth *et al*. (2010) identified a number of suitable coniferous NLEs for the Cheirolepidiaceae in addition to those originally used by Haworth *et al.* (2005), which occupy ecological niches comparable to those described in the studies of Haworth *et al*., (2005) and Aucour *et al*. (2008) (Table 6.4). These NLEs can be used to create a new

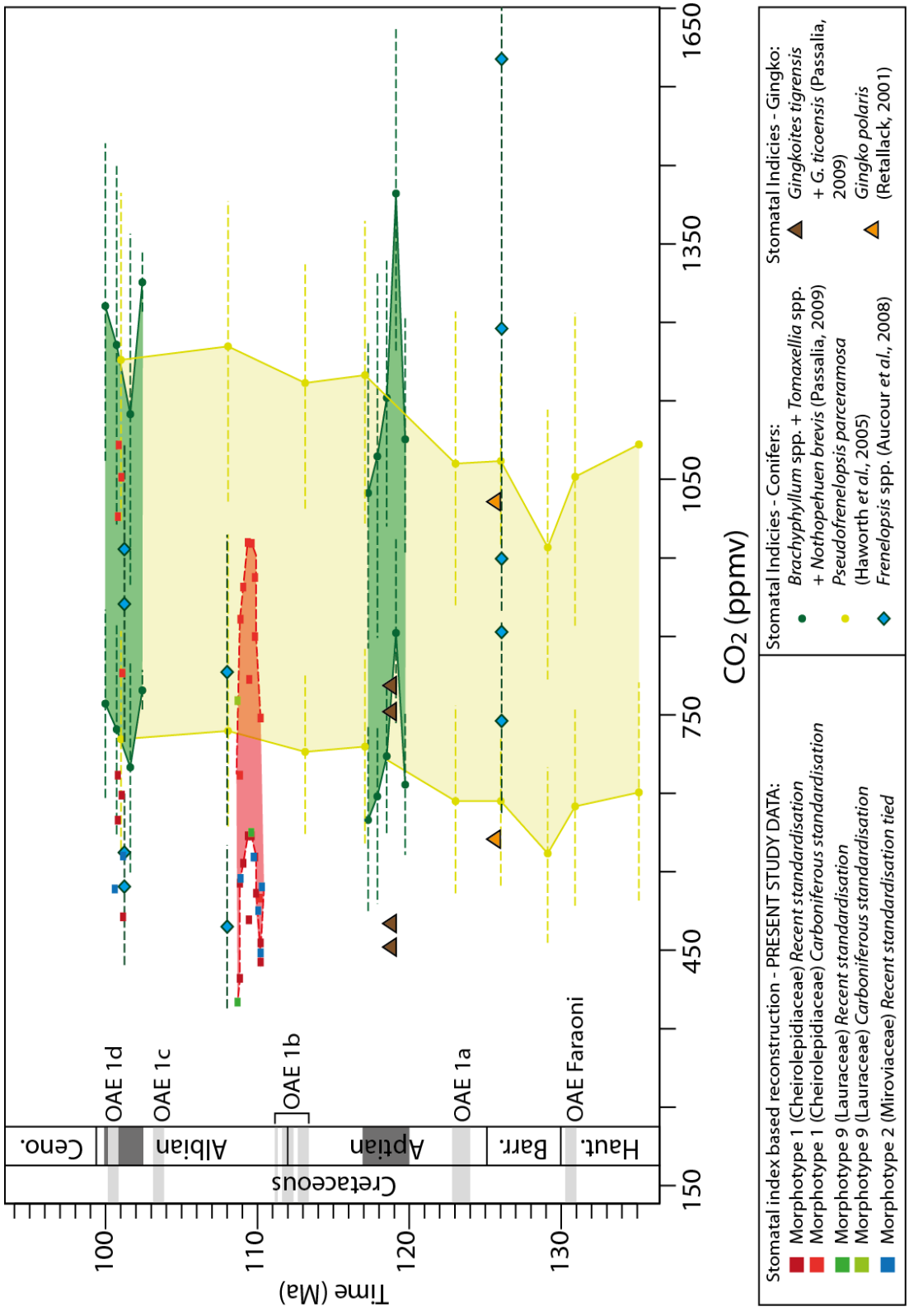

Figure 6.17: Adapted from Passalia (2009), previous pCO_2 reconstructions through the Cretaceous using stomatal index methods from studies shown in legend. Present study morphotype pCO_2 reconstructions represented by squares colour-coded as in legend.

generalised NLE with a stomatal index of 10.2 ± 1.2 for 307 ppm (Table 6.4) in order to recalibrate the pCO_2 data of Haworth *et al*., (2005) and Aucour *et al*. (2008).

Species	Annual pCO_2 (ppm)	Stomatal index (± 1σ)	Ecology
Callitris oblonga	305	10.2 ± 2.4	Drained soil but near water source
Callitris rhomboidea	303	11.0 ± 1.4	Drained soil but near water source
Callitris columnaris	308	9.2 ± 0.6	Can endure water stress, found in coastal and inland areas of Australia
Callitris preissii	311	9.6 ± 1.4	Can endure water stress, found in coastal and inland areas of Australia
Tetraclinis articulata	307	13.1 ± 0.8	Tolerant of extended dry periods
Athrotaxis cupressoides	306	8.3 ± 0.5	Similar cuticular morphology
Generalised (average) NLE	307	10.2 ± 1.2	

Table 6.4: Annual CO_2 and average stomatal index of species used for new calibration of the Haworth et al. (2005) and Aucour et al. (2008) datasets.

Conversely, the Cheirolepidiaceae cuticle from Argentina studied by Passalia (2009), possessed apparently xerophytic features (stomatal papillae) similar to those of the present study. It was argued by Passalia that the occurrence of these features was linked to impoverished soils (despite this palaeoenvironmental interpretation being restricted in stratigraphic extent), justifying the inclusion of drought-tolerant *Calocedrus decurrens* and *Tetraclinis articulata* in their generalised NLE. However, such traits have been observed in the present study where water-stress and impoverished soils are not thought to have been prevalent features of the palaeoenvironment (Section 5.6.4). Therefore, *Calocedrus decurrens* and *Tetraclinis articulata* should not be applied to the Argentinian dataset as they are not suitable ecological morphotypes. Instead, the same generalised NLE (9.8 ± 1.2 (1σ) at 367 ppm) as the present study material is applied to recalibrate the data from Argentina.

When the recalibrated data is considered (Figure 6.18), there is greater agreement in the stomatal index-based pCO_2 reconstructions from the three published datasets (Haworth *et al.*, 2005; Aucour *et al.*, 2008; Passalia, 2009) and the present study data. One of the issues with this summary presentation concerns the age of the reconstructions, and how well the ages of each dataset were constrained, for example the Haworth *et al.* (2005) data was published with descriptive ages (e.g. Early Aptian etc.), which have been plotted as an absolute age by Passalia and not edited for the present study. Parts of the Passalia (2009) dataset were constrained by radiometric dating of ash falls (118.56 ± 1.4 and 119.7 ± 0.4 Ma) giving a more certain age estimate for some parts of this dataset, but the remainder

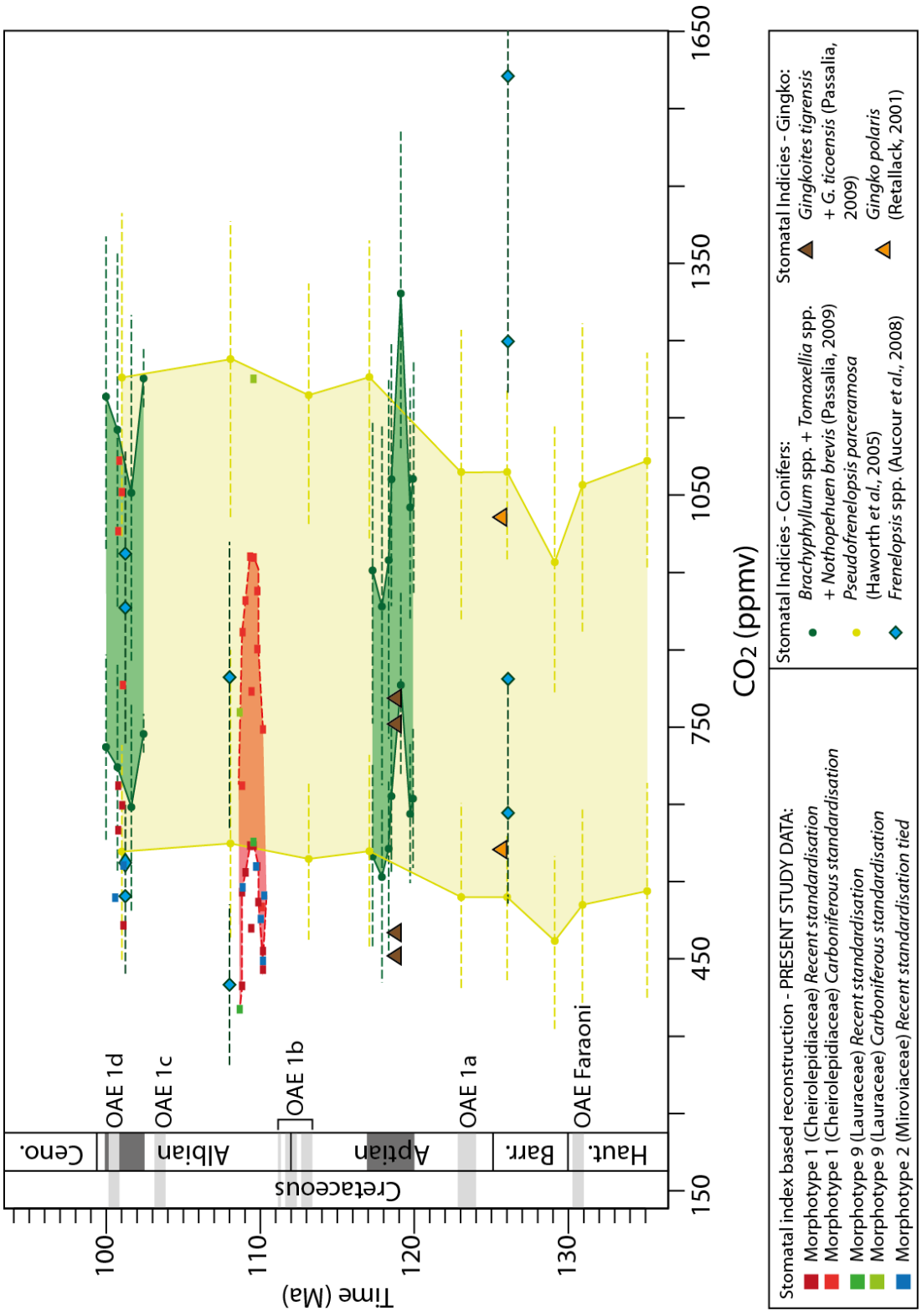

Figure 6.18: Adapted from Passalia (2009), previous pCO_2 reconstructions through the Cretaceous using stomatal index methods from studies shown in legend, recalibrated using two new generalised NLEs outlined in the text. Present study morphotype pCO_2 reconstructions represented by squares colour-coded as in legend.

were dated through palaeobotanical, invertebrate and dinoflagellate cyst stratigraphy. The present study dataset was age constrained by carbon isotope stratigraphy, which for the Kome Formation was fairly certain, but the isotope stratigraphy through the Ravn Kløft Member was more tentative (Chapter 3) resulting in some age uncertainty in the position of the pCO_2 reconstruction from the Ravn Kløft Member. When the age uncertainties of each dataset are taken together, this may account for the noise in reconstructions around 100–102 Ma. As this interval overlaps with OAE 1d (Passalia, 2009), pCO_2 may have been variable around this time, which may be reflected in the 200–250 ppm spread of pCO_2 values in the recalibrated data compilation over this interval (Figure 6.18). Unfortunately, the resolution of data from the Ravn Kløft Member is not sufficient to test for pCO_2 changes over OAE1d (according to the carbon isotope stratigraphy correlation; Chapter 3).

6.5.5 "Best-estimate" pCO_2 reconstruction through the Cretaceous

Both pCO_2 reconstruction compilations (Figures 6.17 and 6.18) reveal how sensitive the NLE stomatal ratio approach is to NLE selection. The implications of this sensitivity to NLE means the absolute values for both the Recent and Carboniferous standardisations should be treated cautiously, although the transfer function approach supports the Recent Standardisation reconstruction values.

Therefore, the overall "best-estimate" of Cretaceous pCO_2 is based on the re-evaluated NLE Recent Standardisation of Cheirolepidiaceae stomatal indices in addition to the morphotype data from this thesis (Figure 6.19). This newly calibrated compilation reconstructs an average pCO_2 level through the Aptian–Early Cenomanian of 576 ppm ± 111 (1σ). A long-term trend in pCO_2 is apparent (black line – LOESS smoothing, Figure 6.19), whereby average pCO_2 decreases from the Middle Aptian to the Early Albian by almost 150 ppm, before returning to similar values in the Late Albian. However, as stated previously, the apparent decline and subsequent rise in pCO_2 is mostly contained within the 1σ error of most data sources (error bars in Figure 6.19), with the exception of the most extreme high and low reconstructed values. This would indicate that the decline in pCO_2 was likely a real phenomenon, particularly given that the trend in average pCO_2 between the Early and Late Albian is not only recognised from three distinct plant groups from the present study data, but is also indicated by the *Frenelopsis* reconstruction from Aucour *et al.* (2008). The gaps between the main data intervals preclude the interpretation of the rate of decline and subsequent rise in pCO_2 since only the Haworth *et al.*(2005) data spans the entire Aptian–Cenomanian, but at a low temporal resolution with very loose age references (Passalia, 2009).

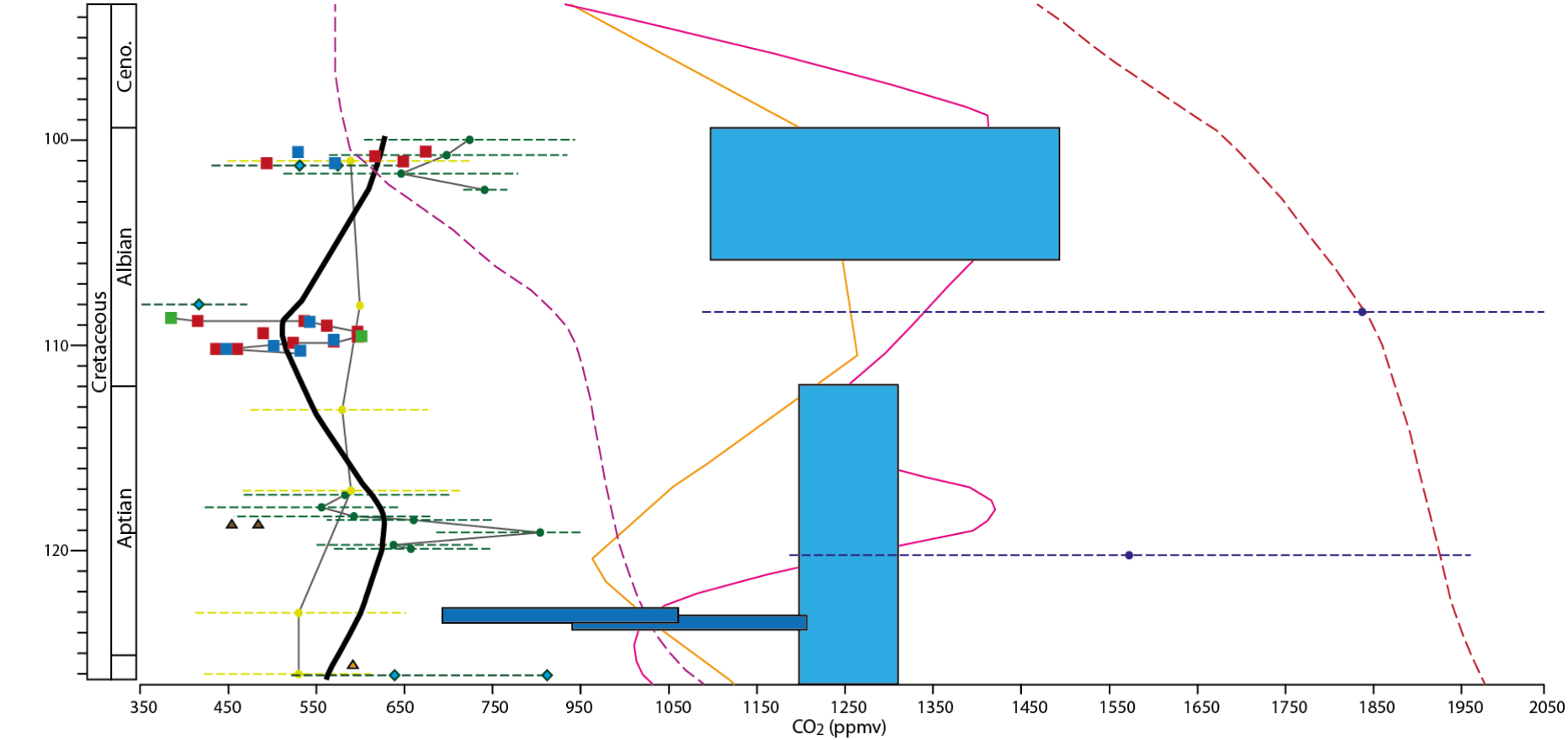
Cretaceous
Albian
Aptian
Ceno.
100
110
120
350
450
550
650
750
950
1050
1150
1250
1350
1450
1550
1650
1750
1850
1950
2050
CO2 (ppmv)
Biogeochemical models:
GEOCARB II (Berner, 1994)
GEOCARB III (Berner + Kothavala, 2001)
GEOCARBSULF (Berner, 2006, 2008)
Tajika (1998)
Carbon isotopes:
Heimhofer et al. (2004)
Fletcher et al. (2005, 2008)
Ekart et al. (1999)
Stomatal indicies - conifers:
Brachyphyllum spp. + Tomaxellia spp. + Nothopehuen brevis (Passalia, 2009)
Pseudofrenelopsis parceramosa (Haworth et al., 2005)
Frenelopsis spp. (Aucour et al., 2008)
Present study data:
Morphotype 1 (Cheirolepidiaceae)
Morphotype 9 (Lauraceae)
Morphotype 2 (Miroviaceae) tied
Stomatal indicies - Gingko:
Gingkoites tigrensis + G. ticoensis (Passalia, 2009)
Gingko polaris (Retallack, 2001)

The present study data indicates that pCO_2 may have been variable on shorter timescales (few Myr) as described in Section 6.5.3 and shown in Figure 6.19 for the Kome Formation in the Middle Albian. The pCO_2 reconstruction from Passalia (2009) supports the possibility of short-term variability in pCO_2 of a similar magnitude to the present study data (Figure 6.19). However, as outlined previously, the error on the pCO_2 reconstructions based on stomatal indices will always prevent small magnitude variations from being resolved. The error bars on the Passalia data partly overlap but there is still statistically significant change in pCO_2 (of at least 50 ppm) shown in the Middle Aptian (Figure 6.19). The alternative approach adopted in this thesis of using multiple plant types to resolve average trends in pCO_2 also confirms the likelihood of smaller magnitude variation in pCO_2.

The stomatal index-based "best-estimate" of pCO_2 through the Cretaceous reveals significantly lower pCO_2 values compared to other proxy and model reconstructions (Figure 6.19). The geochemical models in some instances estimate pCO_2 values either double or quadruple than the stomatal index-based "best-estimate". The exception is the GEOCARB II model, which is unsurprising given the use of the model in the stomatal ratio method (McElwain, 1998; see pg. 63). In the Late Albian, the GEOCARB II model predicts values similar to those estimated from stomatal indices. However in the Aptian and Albian, GEOCARB II predicts values almost double those indicated by the new reconstruction (Figure 6.19). The apparent deviation from the GEOCARB II trend, therefore, may in part reflect the capacity of the stomatal index-based proxy to resolve smaller scale changes in pCO_2, in addition to considerations of the limitations of carbon cycle models (as reflected in the great range in pCO_2 predictions from the other models and a lack of coherence in relative trends both between geochemical models and on comparison to the new "best-estimate" reconstruction).

The other proxy methods show an intermediary difference in reconstructed pCO_2 compared to the new stomatal index-based reconstruction. The fossil bryophyte-based proxy from Fletcher *et al*. (2005, 2008) has a very large error range that precludes the identification of any trends in pCO_2, but would indicate values at least double the average value reconstructed from stomatal index. The error range of part of the $\delta^{13}C_{phytoplankton}$ proxy

Figure 6.19 (previous page): Aptian to Early Cenomanian pCO_2 reconstructions based on proxy and model data as indicated in the legend. The "best-estimate" pCO_2 reconstruction based on recalibrated stomatal index data is shown with LOESS smoothing (factor 0.4) through the compilation.

from Heimhofer *et al.* (2004) overlaps with the upper range of the stomatal index reconstruction through the Early Aptian (Figure 6.19). The pedogenic carbonate proxy (Ekart *et al.*, 1999) reconstructs extremely high pCO_2 values through the Cretaceous, and most likely in part reflects the sensitivity of the method to estimated soil temperature (Section 2.3.2.2). Reconciling the cause of variation in other proxy-based methods of pCO_2 reconstructions is beyond the scope of this thesis, but the present study data would indicate pCO_2 may not have been as high during this interval of the Cretaceous as indicated by some proxy data and geochemical model predictions (Figure 6.19). Since some of the lower ranges in proxy pCO_2 estimates overlap within the upper ranges of the error on the present study reconstruction it is suggested that the stomatal index-based "best-estimate" of pCO_2 should be considered the lower limit of Aptian–Early Cenomanian pCO_2.

6.6 g_{wmax}, pCO_2 and ecological interpretations

6.6.1 g_{wmax} considerations

The trends of g_{wmax} through the West Greenland stratigraphy have been described (Section 6.3.2), but before the data can be interpreted, two aspects must be considered. Firstly, the study of pore length data (Figure 6.11) revealed two possible subtypes of morphotype 1 (Cheirolepidiaceae). However the range of g_{wmax} of these two possible subtypes is similar, indicating that the variation in stomatal density between the two types may accommodate the difference in pore length (i.e. the morphotype 1 data collectively adheres to the relationship from Franks and Beerling, 2009 shown in Figure 6.9A). Therefore, for all g_{wmax}-based considerations, morphotype 1 data is not divided into subtypes as was the case for pCO_2 reconstructions. Secondly, Franks and Beerling's (2009) equation for g_{wmax} as an estimate for maximum theoretical conductance (Equation 6.1) has been altered on the basis that an ellipse is a more appropriate approximation of a_{max} than a circle (e.g. Lammertsma *et al.*, 2011; McElwain and Lawson, *in press.*), such that the two radii of the ellipse are ½ pore length and ¼ pore length. Therefore, in order to compare the present study material to studies exploring the ecological significance of g_{wmax}, all data has been recalculated resulting in lower values of g_{wmax} compared to the circular pore area (Figure 6.20).

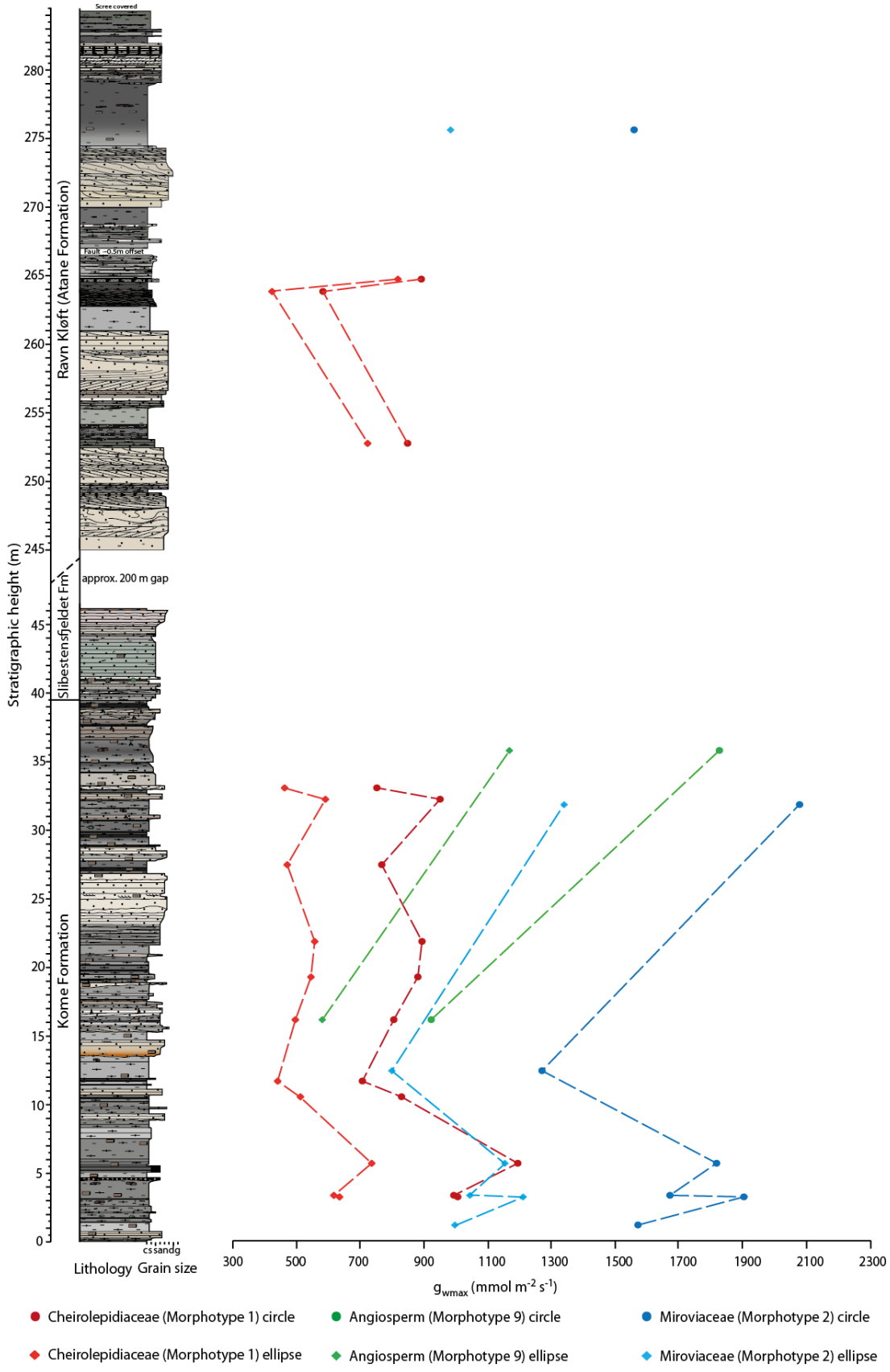

Figure 6.20: Comparison of horizon average g_{wmax} calculation based on a circular pore area (filled circles) and elliptical pore area (diamonds) for morphotypes 1, 2 and 9.

6.6.2 g_{wmax} and relation to pCO_2

Lammertsma *et al.* (2011) explored the response of stomatal conductance for several plants to the anthropogenic rise in pCO_2 over the past 150 yrs. They found a consistent response of stomatal conductance in both angiosperms and gymnosperm species: a 34 % (± 12 %) reduction in g_{wmax} was observed with 100 ppm rise in pCO_2 (Figure 6.21). Whilst the response of stomatal conductance was consistent across plant groups, the strategy to achieve the response varied between plant types, whereby angiosperms exhibit a greater tendency towards smaller, but more numerous stomata, than gymnosperms.

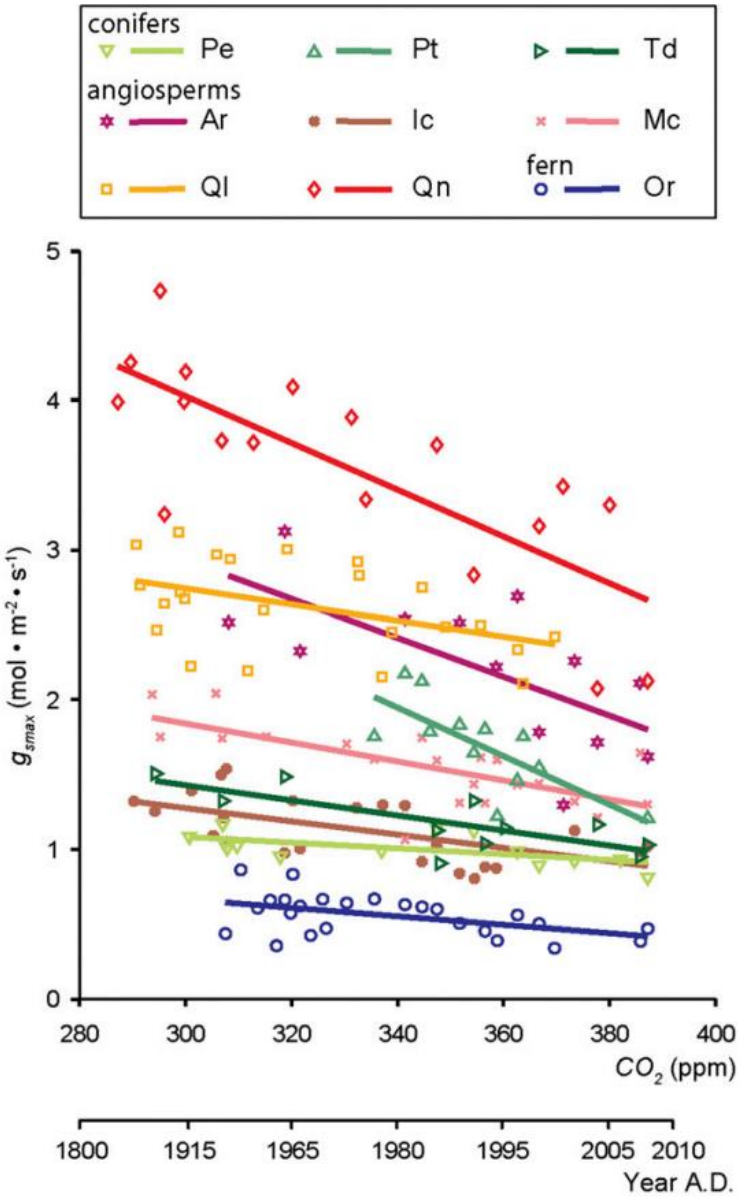

Figure 6.21: From Lammertsma et al. (2011) showing relationship between g_{wmax} and pCO_2 over past 150 yrs. Pe = Pinus elliottii; Pt = Pinus taeda; Td = Taxiodium distichum; Ar = Acer rubrum; Ic = Ilex cassine; Mc = Myrica cerifera; Ql = Quercus laurifolia; Quercus nigra; Or = Osmunda regalis.

The relative changes in stomatal conductance can be expressed as a percentage change from the highest conductance through the Kome Formation for each morphotype (Figure 6.21A). Overall, a consistent response of each morphotype is recorded through the stratigraphy. In the lower 5 m, both the Cheirolepidiaceae (morphotype 1) and Miroviaceae (morphotype 2) possess stomatal conductances around 10–20 % less than the maximum value recorded for both morphotypes (i.e. 0 %). By 10–25 m the relative change in stomatal conductance decreases to around 30–40 % of the maximum conductance value for the Cheirolepidiaceae and Miroviaceae. The angiosperm (morphotype 9) shows an increase in stomatal conductance of around 50 % from around 16 m to 36 m height, supported by around a 40 % increase in conductance represented by Miroviaceae, from around 13 m to 32 m height compared to the respective largest conductance value.

If the relationship between pCO_2 and g_{wmax} is assumed to be universal across all plant species, and applicable to the Cretaceous, the relative changes in g_{wmax} can be converted into relative changes in pCO_2 (Figure 6.22B). When this is compared to the relative changes in average pCO_2 derived from the NLE stomatal ratio method (Recent standardisation) of pCO_2 reconstruction (Figure 6.22C), broadly consistent trends in relative changes in pCO_2 are apparent. Both records of relative change in pCO_2 indicate an increase in pCO_2 from the first 5 m of stratigraphy to around 12 m stratigraphic height in the Kome Formation, with high values indicated for the middle portion of stratigraphy, followed by a decline in pCO_2 from around 23 m height to the top of the data section. The consistency of the trends of the two approximations of pCO_2 change (Figure 6.22B, C) is strong evidence for pCO_2 variation through the West Greenland stratigraphy as described.

However, comparisons of the relative magnitude of the pCO_2 rise and fall through the Kome Formation reveals different apparent sensitivity in recording pCO_2 change. The g_{wmax}-based relative pCO_2 change is smaller magnitude than that derived from the stomatal ratio. For example, the rise in pCO_2 over the first 12 m based on g_{wmax} data is on the order of 60–100 ppm for morphotypes 1 and 2 (Cheirolepidiaceae and Miroviaceae). However,

Figure 6.22 (next page): Kome Formation stratigraphy with A: Change in g_{wmax} expressed as a percentage change of the lowest value; B: Relative change in pCO_2 calculated from scaling relation from Lammertsma et al. (2011) whereby 34 % decline in g_{wmax} corresponds to 100 ppm increase in pCO_2, error bars accommodate the ±12 % uncertainty in the scaling relationship across species from Lammertsma et al.; C: relative change in pCO_2 based on NLE stomatal ratio (Section 6.5.3).

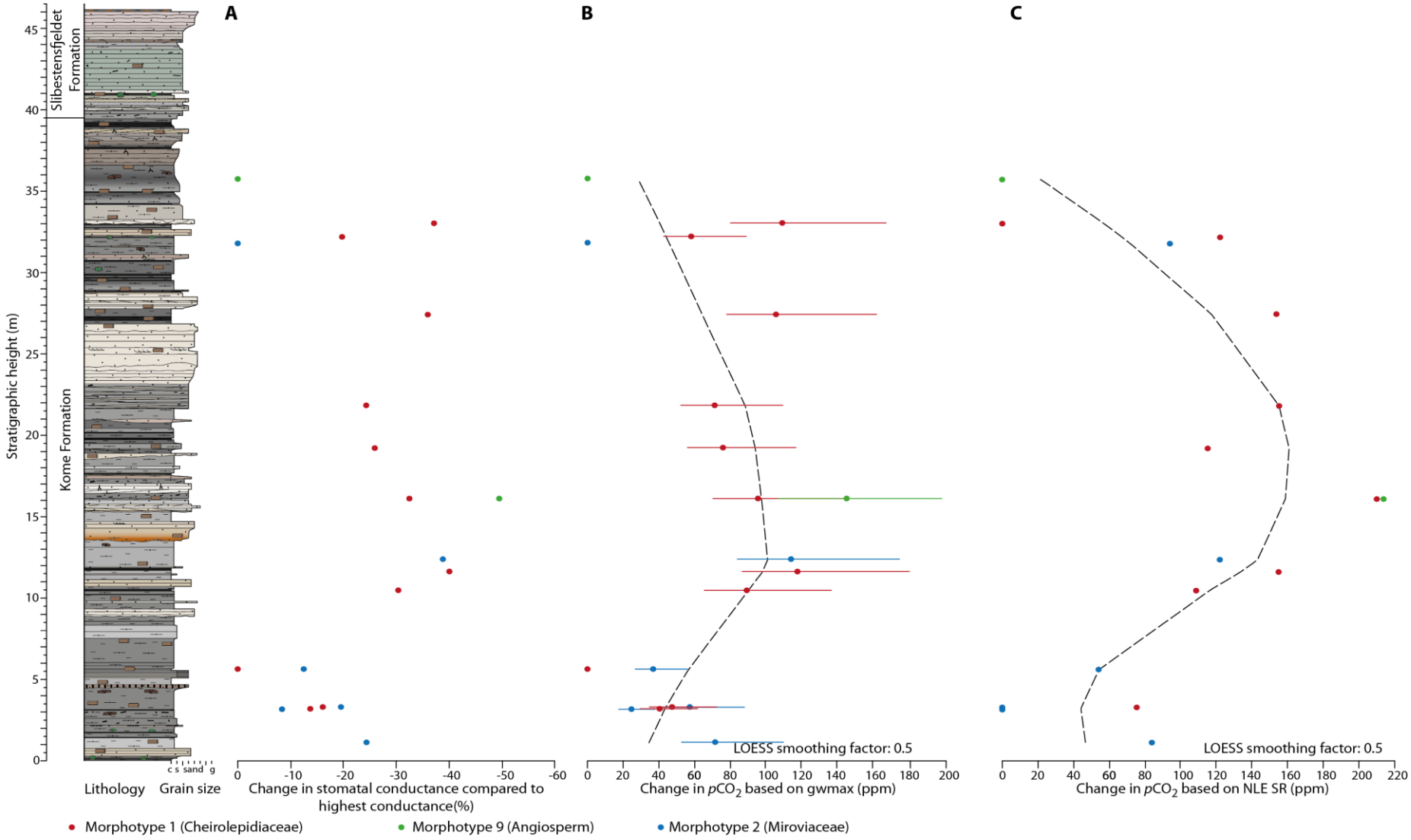
A
B
C
Slibestensfjeldet Formation
Kome Formation
Stratigraphic height (m)
Lithology
Grain size
c s sand g
Change in stomatal conductance compared to highest conductance(%)
Change in pCO_2 based on gwmax (ppm)
Change in pCO_2 based on NLE SR (ppm)
LOESS smoothing factor: 0.5
LOESS smoothing factor: 0.5
Morphotype 1 (Cheirolepidiaceae)
Morphotype 9 (Angiosperm)
Morphotype 2 (Miroviaceae)

comparison to the pCO_2 rise derived from the stomatal ratio method reveals an increase almost double that based on g_{wmax}, of 100–120 ppm (Figure 6.21). This is repeated in the pCO_2 decline between 13 m and 35 m, whereby the g_{wmax}-based data for the angiosperm shows a decrease of around 140 ppm; and a decline of around 120 ppm for the Miroviaceae data Figure 6.22B). In the stomatal ratio-based reconstruction for the angiosperm material, the decline in pCO_2 is on the order of 220 ppm (Figure 6.22C).

Comparison of these two methods of estimating pCO_2 change for three different plant types reveals the likely complicated response to pCO_2 changes by plants: the difference in magnitude between the two estimates (Figure 6.22B, C) reveals that stomatal size plays a part in regulating the stomatal conductance of plants during times of pCO_2 change in order to regulate their water-use efficiency (WUE; McElwain and Lawson, *in press.*). This also accounts for the almost twice smaller response of the g_{wmax}-based pCO_2 variation compared to those based on the stomatal ratio NLE approach, which implies assessing pCO_2 changes based on stomatal index alone may be oversimplified and results in a more exaggerated response to pCO_2 variations. This is supported by the more subdued inferred changes in pCO_2 from the transfer function approach of pCO_2 reconstruction of morphotype 9 (angiosperm), which indicated the fall in pCO_2 from 16 m to 35 m was on the order of 40–80 ppm (Figure 6.15).

Whilst it is clear that the angiosperms and gymnosperms adopted different strategies to achieve similar changes in stomatal conductance (Section 6.4.2), the relative importance of these two factors may be the cause of the apparently subdued response in the Cheirolepidiaceae g_{wmax}-based pCO_2 changes, which after the increase in pCO_2 in the first 10 m of stratigraphy of the Kome Formation remains fairly constant throughout the rest of the stratigraphy whilst the other two morphotypes (2 and 9) presents a decline in pCO_2 (Figure 6.22B). The importance of stomatal size in dictating this trend is apparent on comparison to the pCO_2 variations based on stomatal density, where a pCO_2 decline comparable to that indicated by the angiosperm morphotype is observed (Figure 6.22C) and in the discordant trends in pore length between the morphotypes (Figure 6.7). Therefore, whilst the use of g_{wmax} as a realistic tracker of pCO_2 changes is promising, particularly in light of coeval trends in measures of pCO_2 change through the West Greenland stratigraphy for ancient angiosperm and gymnosperm plants, it appears that the response of some species needs to be closely scrutinised (i.e. the Cheirolepidiaceae). Therefore, more research is required to determine if the 34 % decline in g_{wmax} for every 100 ppm increase in pCO_2 is universal and

applicable to ancient plants; the early evidence would suggest it may not be true for all plants. In addition, the g_{wmax} approach only produces relative changes in pCO_2, not absolute values. Therefore, the results of the present study would indicate that a multiple species approach using both NLE stomatal index and g_{wmax}-based pCO_2 reconstructions is likely the best method to attempt to account for the complications described, and provides the best overall appreciation of pCO_2 variation over an interval of time.

6.6.3 g_{wmax} and vein density

McElwain and Lawson (*in press*) explore the differences in the relationship between leaf vein density and g_{wmax} for extant gymnosperms and angiosperms (data points in Figure 6.23). Whilst g_{wmax} is the maximum theoretical stomatal conductance, the finer scale control of stomata, which plants utilise on a daily basis, means the overall stomatal conductance of a plant is lower than the maximum theoretical value, defined by McElwain and Lawson as G_{op}, the operational stomatal conductance (box plots in Figure 6.23).

McElwain and Lawson's data supports and elaborates on the leaf vein density hypothesis (Section 1.5.3; Figure 1.15; Feild *et al.*, 2011; Jan de Boer *et al.,* 2012), whereby the angiosperms present a positive relationship between vein density and g_{wmax}, with an increasing difference between g_{wmax} and G_{op} as vein density increases. This has been interpreted by McElwain and Lawson to indicate that a vein density of >4–6 mm mm^{-2}, permits a greater range in G_{op} ("G_{op} niche" in inset Figure 6.23), such that angiosperms can operate around 600–1000 mmol $m^{-2}s^{-1}$ below the maximum theoretical conductance (g_{wmax}), compared to only around 400 mmol $m^{-2}s^{-1}$ for gymnosperms (Figure 6.23). Crucially, this reveals that angiosperms have greater capacity to manage G_{op} in suboptimal conditions and as a result, are more adaptable (McElwain and Lawson). The vein density at which this occurs is the modelled transition in Jan de Boer *et al.* (2012) vein density (2.5–5 mm mm^{-2}) beyond which angiosperms exhibit smaller but more numerous stomata.

Since the smaller but more numerous stomatal strategy has already been identified in the present study data (Section 6.4.2), comparison of the fossil material to that of McElwain and Lawson (*in press.*) may illuminate whether this transition in strategy had already occurred by the Middle Albian in West Greenland. In order to do so, assumptions about the likely vein density of each morphotype have been estimated based on comparison of the leaf cuticle to NLEs identified previously, due to the fragmentary nature of the sample material. The vein density of the angiosperm (morphotype 9) has been approximated to around 4.8, which is slightly less than other Lauraceae species from McElwain and Lawson

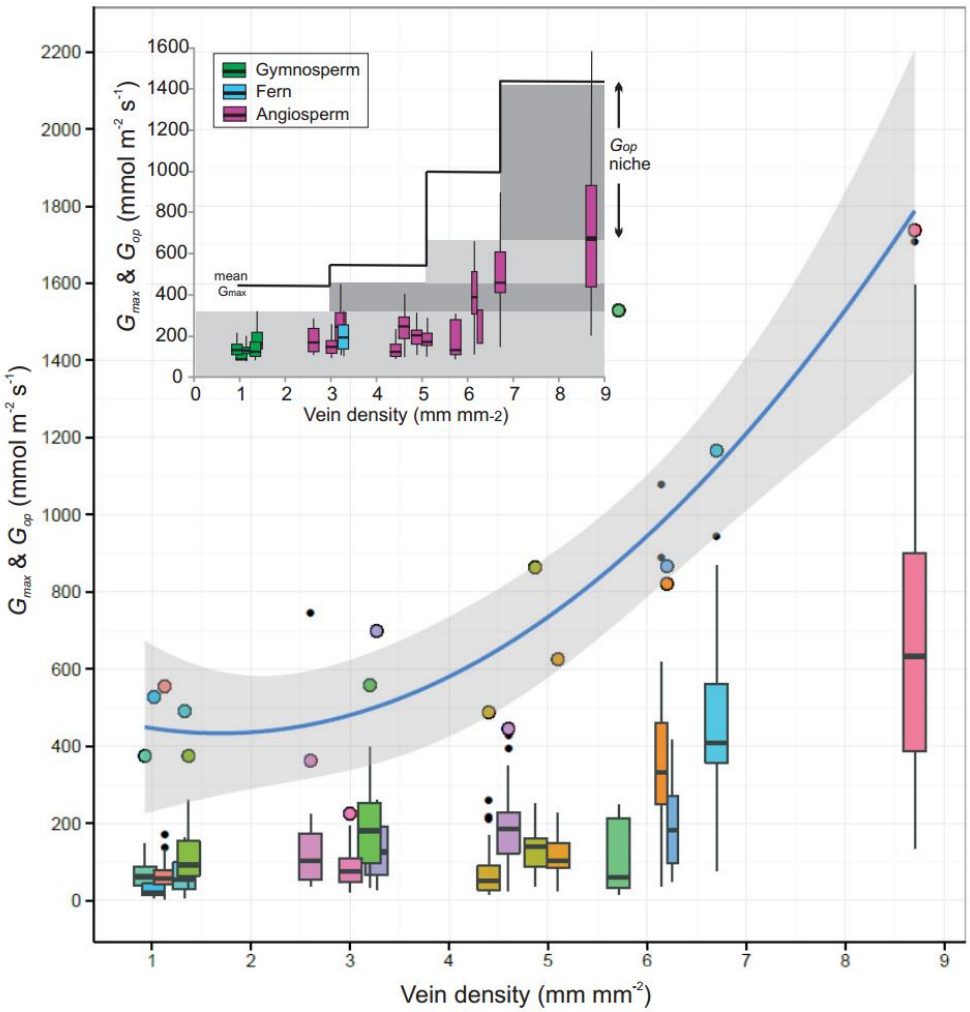

Figure 6.23: From McElwain and Lawson (in press) showing the relationship between vein density, g_{wmax} and G_{op} for angiosperm, gymnosperm and fern species (for species refer to McElwain and Lawson. Inset figure shows the generalised plant groupings according to the legend. Box plots = G_{op} data, data points = g_{wmax}.

(*in press*) based on the comparison of the leaf cuticle to other Lauraceae species (e.g. Figure 4.33) and the descriptions from Boyd (1998 c). The anatomical information from a fossil leaf of *Oswaldheeria exima* (Gordenko, 2007; Figure 4.23) supports a vein density of 2 mm mm^{-2} for morphotype 2 (Miroviaceae – *Oswaldheeria*). The Cheirolepidiaceae have a low vein density of around 1.5 inferred from examination of the cuticle record (no veins were observed in the cuticle fragments) providing vein densities for morphotypes 1 (Cheirolepidiaceae) and 2 (Miroviaceae) which are consistent with the rest of the gymnosperms and conifers studied by McElwain and Lawson.

When these vein densities and the corresponding g_{wmax} values for the three morphotypes are compared to the angiosperms and gymnosperms from McElwain and Lawson (*in press*), the angiosperm and Cheirolepidiaceae lie close to the trend from the extant data, and well within the range of uncertainty of the fossil plant vein densities (Figure 6.24).

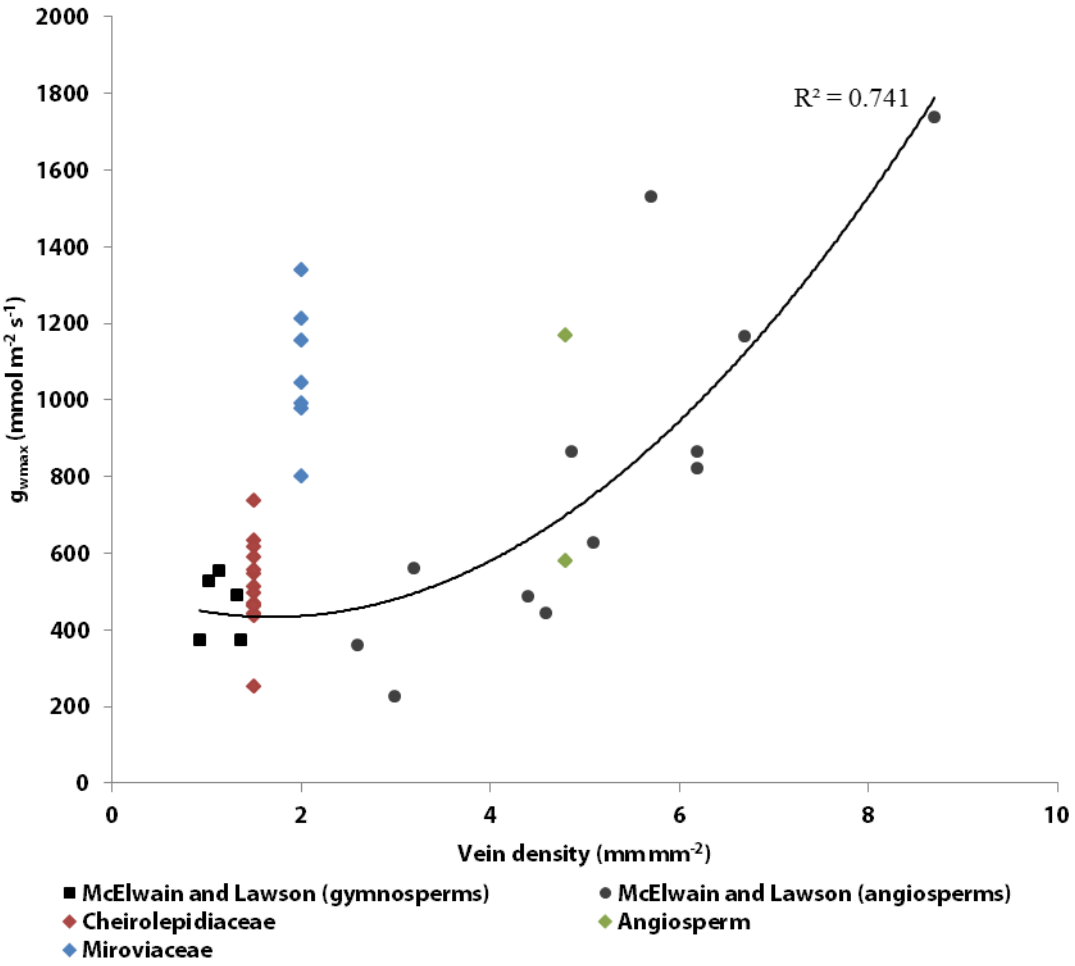

Figure 6.24: Adapted from McElwain and Lawson (in press; Figure 6.23) showing the relationship between vein density and g_{wmax} of extant angiosperm and gymnosperm species (from McElwain and Lawson) compared to present study morphotypes 1, 2 and 9.

However, morphotype 2 (Miroviaceae) lies significantly above the line, with extremely high stomatal conductance, higher even than the angiosperm data (and as seen in Figure 6.7).

Such high stomatal conductance for a plant which almost certainly had a low vein density (Gordenko, 2007), would imply that during the growing season of this plant, the ecophysiological constraints were not limiting, which may be reconciled with the ecological interpretation that the Miroviaceae grew in wet conditions (Chapter 5). Since water was so readily available, the plant had no restrictions in terms of stomatal regulation for water-use efficiency, enabling high theoretical g_{wmax}.

An alternative scenario reassesses the g_{wmax} values based on the pore lengths measured, which were slightly offset with respect to other gymnosperm material in Figure 6.9A and may suggest that the pore lengths were consistently overestimated. Inspection of the best preserved material has revealed the possibility of pore length overestimation as the result

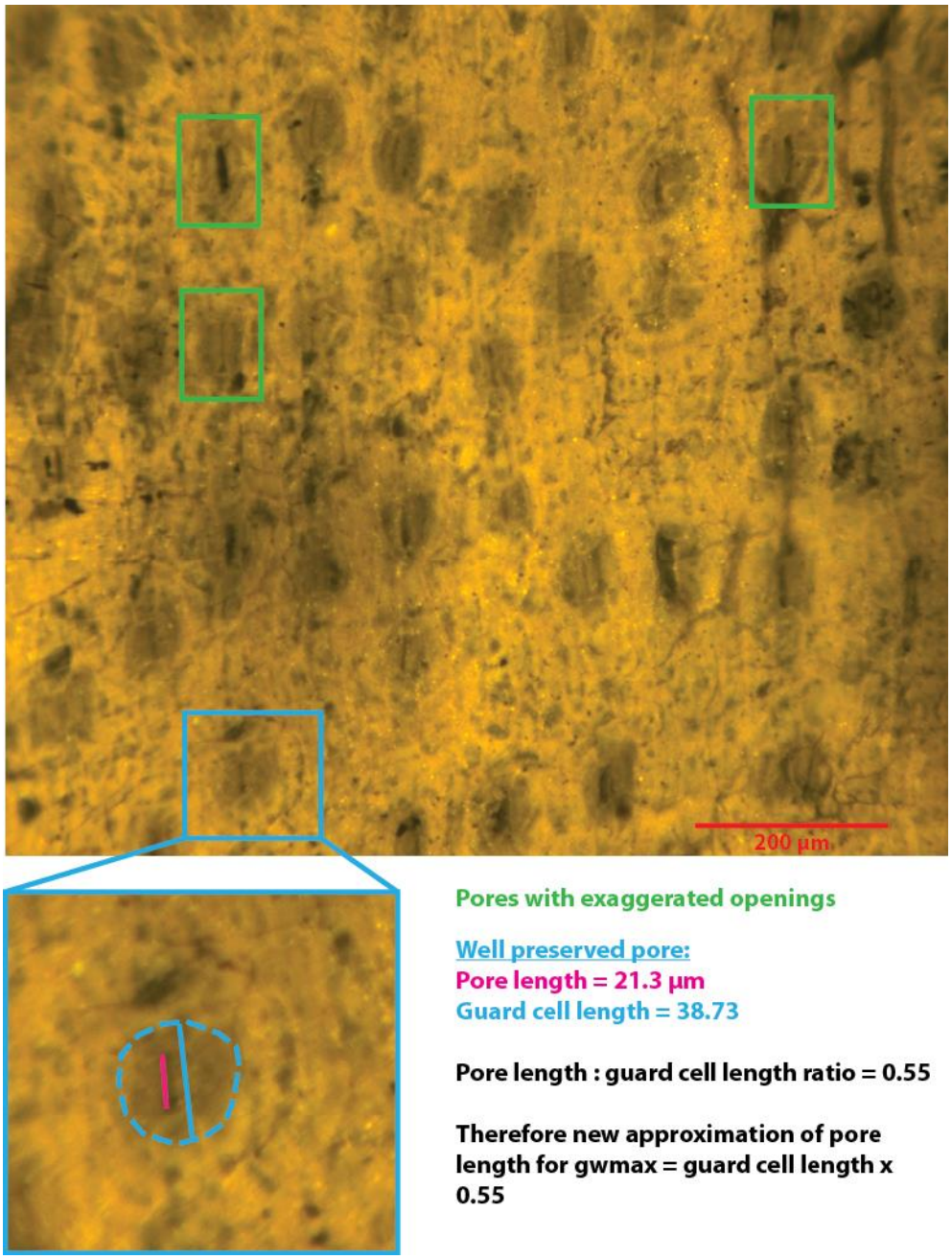

Figure 6.25: Re-examination of pore lengths of morphotype 2 (Miroviaceae) using excellently preserved samples (LK-B-7 (2)). New pore length approximation derived from ratio between well-preserved pore length and easily identified guard cell length.

of preservational effects of the cuticle causing pores to be drawn open (Figure 6.25) and as a result, the ratio of true pore length to guard cell length, which is clearly and reliably preserved, provides a new means of assessing pore length for calculation of g_{wmax} (Figure 6.25). Converting the pore length using the ratio between true pore length and guard cell length results in significantly lower g_{wmax} estimates, which conform to the relationship identified by McElwain and Lawson (Figure 6.26).

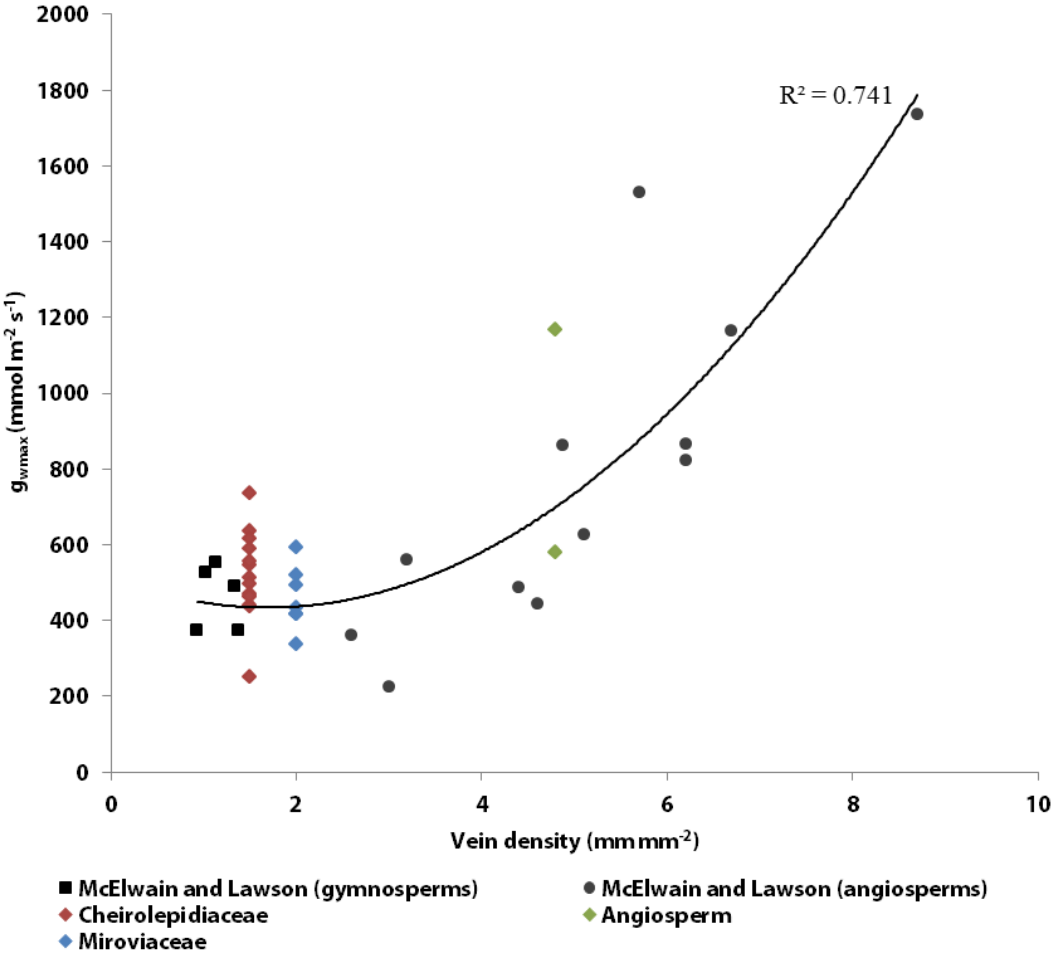

Figure 6.26: Adapted from McElwain and Lawson (in press; Figure 6.22) showing the relationship between vein density and g_{wmax} of extant angiosperm and gymnosperm species (from McElwain and Lawson) compared to present study morphotypes 1, 2 and 9 where g_{wmax} of morphotype 2 has been calculated using the estimation of stomatal pore length as shown in Figure 6.24.

If the pore length has been over estimated, and the new means of scaling pore length from guard cell length is the better measure of pore length, the previously discussed relative changes in pCO_2 based on the g_{wmax} may be called into question. However, since the possible overestimate appears to be consistent, the resulting effect on the relative changes in pCO_2 estimated from the percentage change in g_{wmax} between horizons is negligible. The verdict on whether the pores were consistently overestimated in length or that the high stomatal conductance reflects a lack of ecophysiological constraint remains inconclusive.

Nonetheless, the relationship between vein density and g_{wmax} for the angiosperm morphotype is strong evidence that the angiosperms had already developed higher leaf vein densities (permitting the attainment of higher theoretical stomatal conductance) and the smaller but more numerous stomatal strategy by the Middle Albian (Kome Formation).

6.7 Summary

Stomatal measurements can reveal a significant amount of information about palaeoclimates and palaeoenvironments. The clear difference in stomatal strategy between angiosperms and gymnosperms has been identified through several means (Sections 6.4.2, 6.6.2, 6.6.3), whereby angiosperms by this point in the Middle Albian had adopted the smaller but more numerous stomatal strategy through a higher vein density than gymnosperms, permitting a higher stomatal conductance capacity. This supports the evidence for the vein density hypothesis of Feild *et al.* (2011); Jan de Boer *et al.* (2012) and McElwain and Lawson (*in press*).

Despite this difference in stomatal strategy (density changes versus stomatal size changes) of angiosperms and gymnosperms, the resulting response of g_{wmax} to changes in pCO_2 appears to be fairly consistent across the three morphotypes (1, 2 and 9) as previously discovered by Lammertsma *et al*. (2011) for extant species. The changes in pCO_2 derived from changes in g_{wmax} (Section 6.6.2) correspond to the trends interpreted from the NLE stomatal ratio method of pCO_2 reconstruction (Figure 6.22) but differ in magnitude by a factor of around 0.5, indicating that pore length plays a role in managing plant WUE in response to pCO_2 changes.

Nonetheless, comparison of the two approaches to estimating changes in pCO_2 (Figure 6.22), in addition to the identification of coeval trends in average pCO_2 reconstructions across morphotypes (Figure 6.15), reveals there likely was a "real" and significant increase in pCO_2 in the first 10 m of the Kome Formation, on the order of 60–100 ppm, followed by a decline in pCO_2 from around 16 m to 35 m stratigraphic height in the Kome Formation on the order of 120–200 ppm.

Through reassignment of NLEs selected for previous studies of Cheirolepidiaceae stomatal indices, a new "best-estimate" of pCO_2 has been compiled (Figure 6.19), revealing an average value of around 575 ppm through the Aptian–Early Cenomanian. A long-term fall and subsequent rise in average reconstructed pCO_2 values of around 150 ppm is apparent (Figure 6.19) from the Early Aptian–Early Albian (fall) and the Early Albian–Late Albian (rise). Comparisons to most biogeochemical models and some proxy-based pCO_2 reconstructions (e.g. pedogenic carbonate pCO_2 reconstructions by Ekart *et al.*, 1999) indicate pCO_2 levels were double to quadruple the values generated by the stomatal ratio "best-estimate" compilation. However, the lower error range of some proxy data (e.g. $\delta^{13}C_{phytoplankton}$ proxy by Heimhofer *et al.*, 2004; Figure 6.19) overlaps with the upper error

range in values of the stomatal ratio based compilation during the Aptian. Therefore the recalibrated compilation of pCO_2 reconstructed using the stomatal ratio method is considered here as the "best-estimate" lower limit of pCO_2 during the Aptian–Early Cenomanian.

7: Synthesis and conclusions

7.1 Kome Formation: integration of palaeoclimate, palaeoenvironment and ecology data

This thesis has produced a detailed reconstruction of palaeoclimate, palaeoenvironment and ecology through the stratigraphy of West Greenland, particularly for the Kome Formation. Analysis of macerated leaf cuticle (Chapter 4) has revealed the dominant floral composition of Cheirolepidiaceae, Miroviaceae, Bennettitales, other conifers (including Pinaceae, Cupressaceae and Araucariaceae) and, most rare, angiosperms (Lauraceae). Comparison to the lithology reveals the palaeoenvironment was fluvio-deltaic, with common waterlogged areas associated with Miroviaceae, Cheirolepidiaceae and Pinaceae/Cupressaceae conifers. Better drained areas were more closely associated with fluvial channel margins and were associated with Bennettitalean and Araucariaceae foliage (Chapter 5).

The use of epifluorescence microscopy precluded the need for cuticle clearing, which may have prevented the loss or damage of delicate phyllosphere fossils. This may account for their poor pre-Cenozoic fossil record. The epiphyllous structures, in addition to the presence of mucronate leaf tips in some morphotypes (Chapter 5), indicate a humid climate, possibly with common coastal fog, like the Pacific coast of North America (McElwain, *pers. comms.*). The region also probably had a high mean annual rainfall (>1000–1500 mm yr^{-1}; Kemp, 1978; Taylor *et al.*, 2009 and references therein). This interpretation agrees with previously modelled mean annual precipitation for the Albian at ~60 °N palaeolatitude of around 2000 mm yr^{-1}, and reveals Albian precipitation rates were at least double that of modern 60 °N latitude (Ufnar *et al.*, 2008).

Detrended correspondence analyses (DCA; Chapter 5.1) revealed changes in the floral

Figure 7.1 (next page): Summary of data collected through the Kome Formation. A: carbon isotope stratigraphy with positive excursion marked by (iii). B: relative changes in pCO_2 inferred from the stomatal ratio method and g_{wmax} based method. Interval of pCO_2 change marked by (i), top of section marked by (ii) as reference points in the text. C: DCA analysis of all morphotypes revealed axis 1 values associated with relative abundance of Bennettitalean and Araucariaceae component. D: DCA analysis of just Cheirolepidiaceae and Miroviaceae relative abundances. E: Presence/absence of epiphyll fossils. F: Palaeoclimate and palaeoenvironmental interpretation.

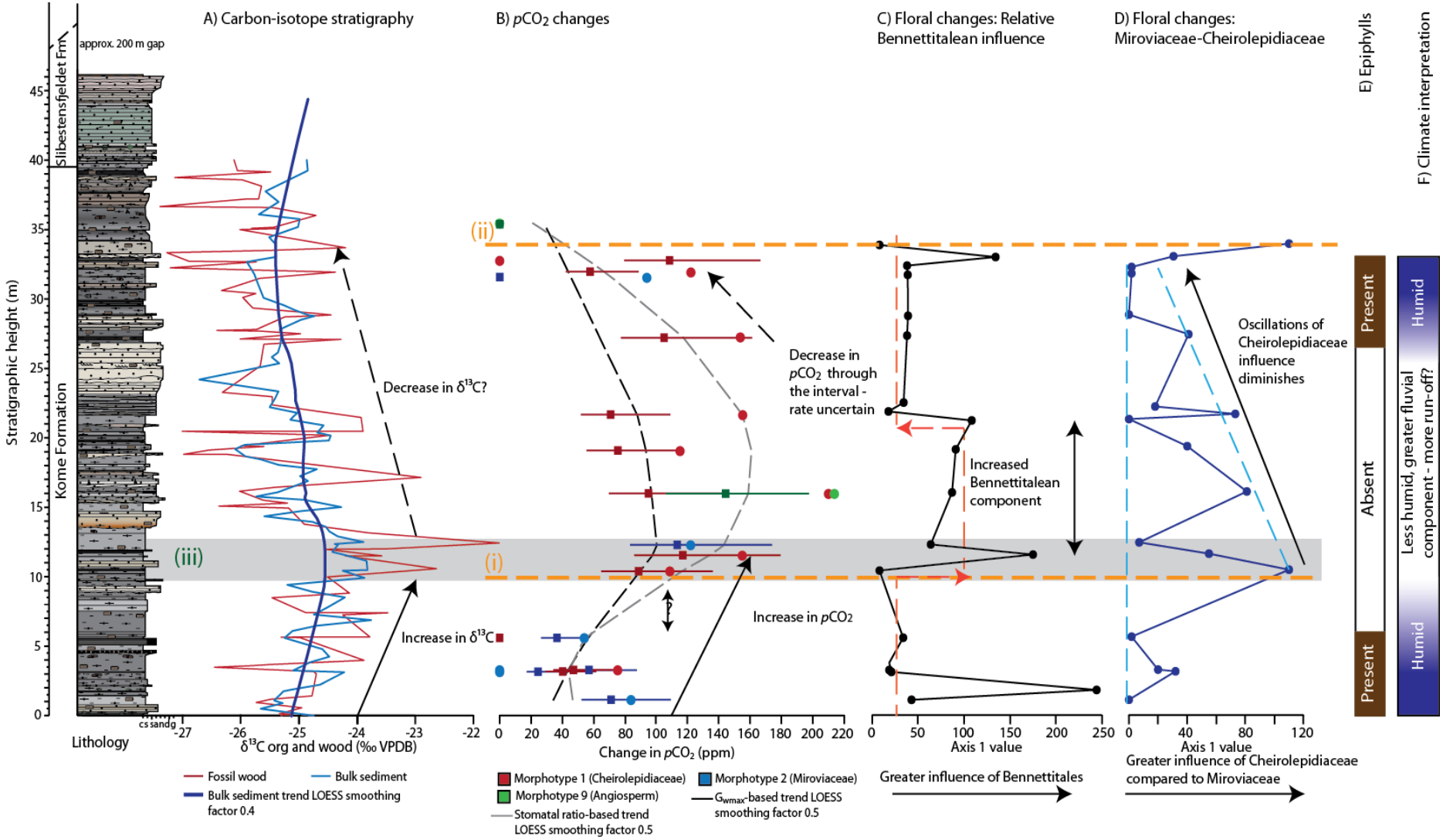
A) Carbon-isotope stratigraphy
B) pCO2 changes
C) Floral changes: Relative Bennettitalean influence
D) Floral changes: Miroviaceae-Cheirolepidiaceae
E) Epiphylls
F) Climate interpretation
Slibestensfjeldet Fm
approx. 200 m gap
Kome Formation
Stratigraphic height (m)
Lithology
cs sandg
δ13C org and wood (‰ VPDB)
Change in pCO2 (ppm)
Axis 1 value
Axis 1 value
Greater influence of Cheirolepidiaceae compared to Miroviaceae
Greater influence of Bennettitales
(i)
(ii)
(iii)
Decrease in δ13C?
Increase in δ13C
Decrease in pCO2 through the interval - rate uncertain
Increase in pCO2
Increased Bennettitalean component
Oscillations of Cheirolepidiaceae influence diminishes
Present
Absent
Present
Humid
Less humid, greater fluvial component - more run-off?
Humid
Fossil wood
Bulk sediment
Bulk sediment trend LOESS smoothing factor 0.4
Morphotype 1 (Cheirolepidiaceae)
Morphotype 2 (Miroviaceae)
Morphotype 9 (Angiosperm)
Gwmax-based trend LOESS smoothing factor 0.5
Stomatal ratio-based trend LOESS smoothing factor 0.5

composition through the Kome Formation (Figure 7.1C, D). The relative abundance of Cheirolepidiaceae compared to Miroviaceae oscillated through the Kome Formation (Figure 7.1D), and it is suggested that the Miroviaceae inhabited the wettest soils of swampy or waterlogged areas, with the Cheirolepidiaceae inhabiting more marginal areas. The apparent oscillations in the relative abundances of Cheirolepidiaceae compared to Miroviaceae are thought to represent the lateral movement of the swampy margin as may be expected through time in a dynamic depositional environment.

At around 10 m height in the Kome Formation (labelled (i) in Figure 7.1) there is a shift in axis 1 values of the DCA (Figure 7.1C), revealing the floral composition shifted to a greater influence of the Bennettitalean and Araucariaceae vegetation (BAP group). The lithology through this interval is generally coarser than the preceding swampy floodplain lithology and is interpreted as likely a greater role of fluvial channel activity at this time (Dam *et al.*, 2009). This interval of a greater Bennettitalean and Araucariaceae floral component also coincides with an absence of epiphylls on the Miroviaceae and Pinaceae/Cupressaceae cuticle through this interval (Figure 7.1E).

pCO_2 (Figure 7.1B) increased by around 60–100 ppm, from the lowest 5 m of Kome Formation, to the time of increased Bennettitalean influence and absent epiphylls (from around 500 ppm to around 600 ppm; Figure 7.2B). Comparison to the corresponding g_{wmax} data from the lower Kome Formation reveals that the stomatal conductance of the Cheirolepidiaceae (morphotype 1) decreases from around 700 mmol m^{-2} s^{-1} to around 500 mmol m^{-2} s^{-1} (Figure 7.2C). As the stomatal conductance fell (as may be expected with higher pCO_2), the rate of transpiration may also have decreased (e.g. Steinthorsdottir *et al.*, 2011). If transpiration decreased, there may have been less uptake of water by the flora, resulting in greater surface run-off, and possibly reduced humidity, which may account for the increased fluvial association floral composition (Bennettitales and Araucariaceae; Figure 7.1C, F) and the absence of epiphylls on the wettest soil-dwelling plants.

The apparent role of pCO_2 on floral composition continues through the Kome Formation (between (i) and (ii) in Figure 7.1), whereby pCO_2 decreases by as much as 200 ppm by 35 m stratigraphic height, to values <400 ppm (Figure 7.2B). Over this interval, the floral composition (Figure 7.1C) indicates a return of primarily swampy hydrophilic floral dominance, and a return of epiphyll presence (Figure 7.1D. E). The oscillations of the Cheirolepidiaceae component compared to Miroviaceae also diminishes from the maximum in pCO_2 (at (i) in Figure 7.1), towards the top of the Kome Formation. The

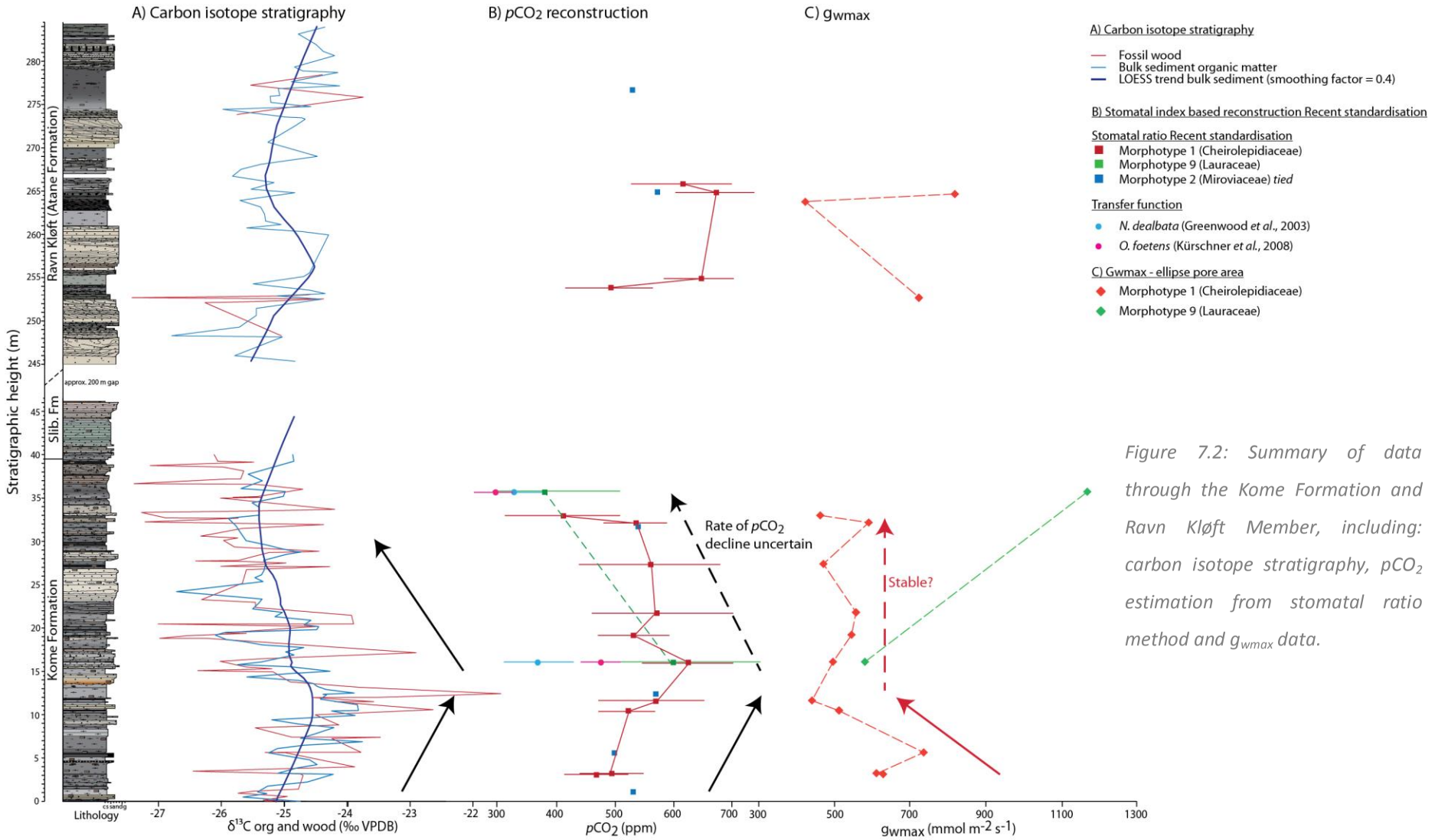

Figure 7.2: Summary of data through the Kome Formation and Ravn Kløft Member, including: carbon isotope stratigraphy, pCO_2 estimation from stomatal ratio method and g_{wmax} data.

changes in floral composition (Figures 7.1C, D) therefore indicate a transition to more humid and possibly wetter palaeoenvironments between (i) and (ii) as pCO_2 falls. This is supported by the g_{wmax} values of the angiosperms (morphotype 9), which show a large increase, almost doubling to values around 1200 mmol m^{-2} s^{-1}. The rate of pCO_2 decline through this interval is difficult to constrain as the angiosperm morphotype is only represented by two horizons, one at 16.08 m and the other at 35.72 m. The Cheirolepidiaceae data has a fairly large uncertainty in pCO_2 reconstruction (Figure 7.2B) but indicates that pCO_2 may have remained high for a while (from (i) to around 25–30 m stratigraphic height, Figures 7.1B; 7.2B) before falling. This is consistent with the pattern of floral change represented by the relative Bennettitalean and Araucariaceae component (Figure 7.1C).

Whilst the carbon isotope stratigraphy through the Ravn Kløft Member may correlate to the isotopic expression of OAE1d in other stratigraphies (Figure 7.3A), there is insufficient palaeobotanical data from the present study to interpret palaeoclimatic and ecological changes through this interval. Comparison of $\delta^{13}C_{org}$ and pCO_2 reconstructions through the Kome Formation (Figure 7.2 A, B) is inhibited by the incomplete pCO_2 record (particularly between 5–10 m; Figure 7.1B, 7.2B), in addition to the uncertainty surrounding the rate of subsequent pCO_2 decline as inferred from the stomatal ratio and g_{wmax} approaches (Figure 7.1B). As identified when describing the data, the relative changes in pCO_2 are also fairly small (a 60–100 ppm rise followed by up to 200 ppm fall through the Kome Formation) and average trends often fall within the error range on the data. However, the consistent average pCO_2 trends from multiple plant types through two approaches (stomatal ratio and g_{wmax}; Figure 7.1B) in the present study and comparison to other previously published reconstructions (e.g. Aucour *et al.*, 2008) reveals the trends in average reconstructed pCO_2 are likely a true representation of changes in pCO_2 through the Kome Formation (Figure 7.3B).

Figure 7.3 (below and next page): Summary of Cretaceous palaeoclimate – see legend below.

A) Carbon isotope stratigraphy

Marine carbonate
- Gale *et al.* (2011)
- Robinson *et al.* (2008)
- Herrle *et al.* (2004)

Present study
- Bulk sediment
- Fossil wood

B) Stomatal index based reconstruction Recent standardisation
- Morphotype 1 (Cheirolepidiaceae)
- Morphotype 9 (Lauraceae)
- Morphotype 2 (Miroviaceae) *tied*
- *Brachyphyllum* spp. + *Tomaxellia* spp. + *Nothopehuen brevis* (Passalia, 2009)
- *Pseudofrenelopsis parceramosa* (Haworth *et al.*, 2005)
- *Frenelopsis* spp. (Aucour *et al.*, 2008)
- *Gingkoites tigrensis* + *G. ticoensis* (Passalia, 2009)
- *Gingko polaris* (Retallack, 2001)

C) Angiosperm relative abundance

Lupia *et al.* (1999)
- Angiosperm pollen above 42 °N
- Angiosperm pollen below 42 °N

Lidgard and Crane (1990)
- Angiosperm macrofossils

West Greenland
- Angiosperm macrofossils (Boyd, 1998c)
- Angiosperm pollen (Horikx and Heimhofer, unpublished)

D) Benthic temperature estimates
- $\delta^{18}O$-based temperature reconstruction (Friedrich *et al.*, 2012)

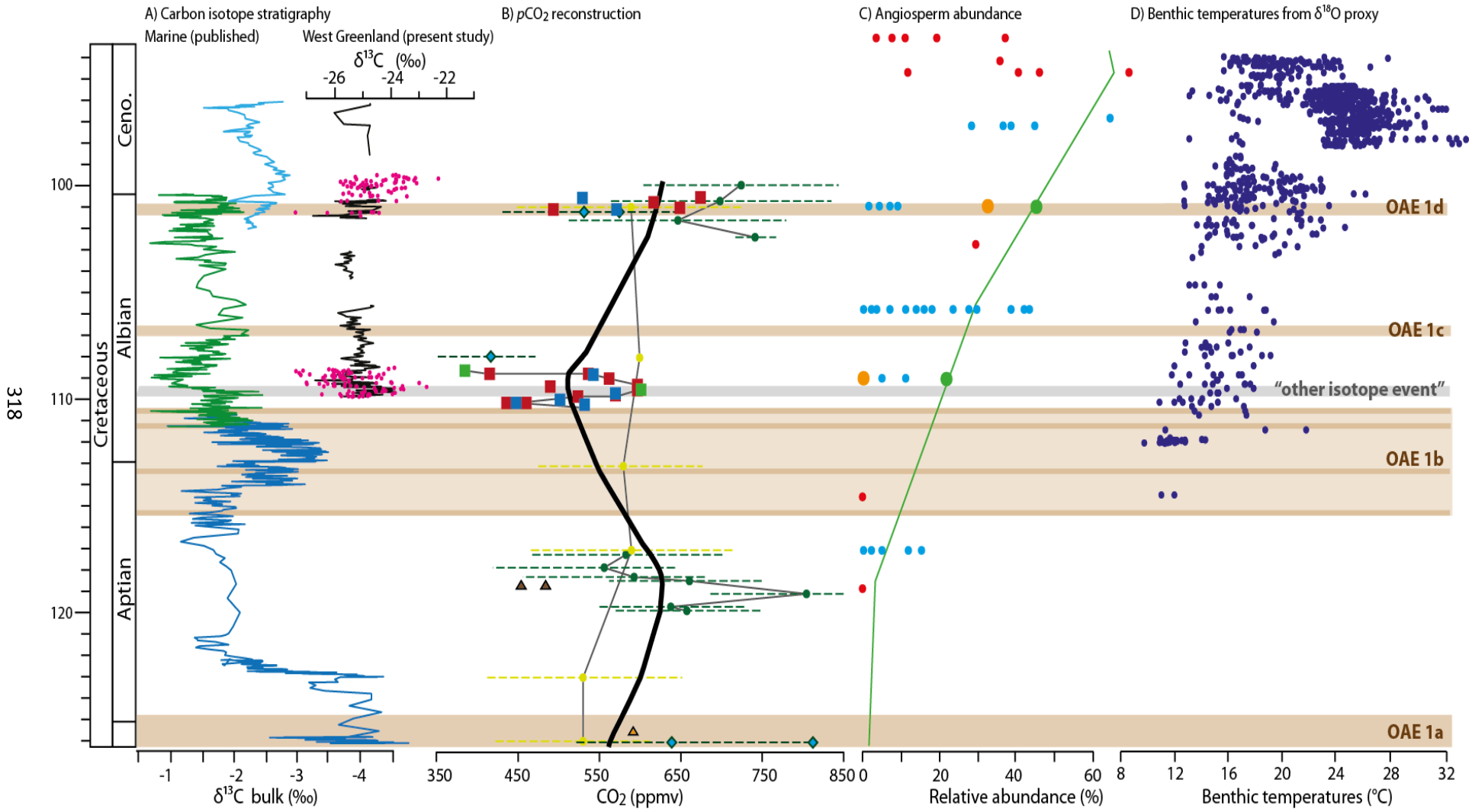
A) Carbon isotope stratigraphy
Marine (published)
West Greenland (present study)
δ13C (‰)
-26
-24
-22
B) pCO2 reconstruction
C) Angiosperm abundance
D) Benthic temperatures from δ18O proxy
Cretaceous
Ceno.
Albian
Aptian
100
110
120
OAE 1d
OAE 1c
"other isotope event"
OAE 1b
OAE 1a
-1
-2
-3
-4
δ13C bulk (‰)
350
450
550
650
750
850
CO2 (ppmv)
0
20
40
60
Relative abundance (%)
8
12
16
20
24
28
32
Benthic temperatures (°C)

The change in $\delta^{13}C_{org}$ is small (around 2.5 ‰ in the Greenland stratigraphy, and up to 1 ‰ in the Vocontian Basin $\delta^{13}C_{carb}$ record; Figure 7.3A), particularly when compared to the variation earlier around the Aptian–Albian boundary (Figure 7.3A). The subsequent negative shift of larger magnitude and short duration (of up to 4 ‰ in the Greenland stratigraphy and 1.5 ‰ in the Vocontian Basin $\delta^{13}C_{carb}$ record; Figure 7.3A) may represent an isotope event of greater palaeoclimatic significance.

Comparison of the carbon isotope stratigraphy to the pCO_2 record through the Kome Formation reveals the positive trend in $\delta^{13}C_{org}$ is exhibited in the lower 12 m or so of stratigraphy, with an unclear end height as indicated by grey shading (labelled iii) in Figure 7.1A. The lack of constraint in the pCO_2 rate of decline makes it difficult to correlate the negative trend in $\delta^{13}C_{org}$ to pCO_2 levels. However, more negative $\delta^{13}C_{org}$ values are commonly attributed to high pCO_2, on account of the balance of the carbon cycle (Chapter 2; Kump and Arthur, 1999). As indicated in Figure 7.3, the Kome Formation does not cover an OAE, but occurs <1 Myr after the series of events comprising OAE1b. Therefore, deviation to lower pCO_2 levels, as indicated by the "best-estimate" pCO_2 reconstruction from stomatal indices (Figure 7.3B), is not surprising if the supposition that CO_2 may have been drawn down during OAE1b that had a residual signature in the $\delta^{13}C_{org}$ of the Kome Formation. However, this remains conjectural without any pCO_2 reconstructed through OAE1b.

The apparent rise in pCO_2, therefore, appears at odds with the rise in $\delta^{13}C_{org}$ through the same interval. This, accompanied by the fact that the Kome Formation does not cover an OAE and the relative changes in both records are small in magnitude, would suggest other processes within the carbon cycle balance were likely occurring to cause a positive excursion in $\delta^{13}C_{org}$ during apparent pCO_2 rise, such as changes in ocean circulation (Kump and Arthur, 1999).

7.2 Angiosperm radiation in West Greenland

This thesis set out to explore the role of CO_2 starvation (Robinson, 1994; McElwain *et al.*, 2005) on the development and radiation of the angiosperms; such that angiosperms were more adapted to withstand the physiological drought imposed during lower pCO_2 (Chapter 1.5.5) compared to the poleward shifting of climate belts imposing evolutionary bottlenecks through which the angiosperms passed and flourished at the expense of other floral groups (Chapter 1.5.4; Coiffard *et al.*, 2012; Coiffard and Gomez, 2012).

To test the two hypotheses, the expectation from the geological record for both scenarios is compared to the palaeoclimatic, palaeoenvironmental and ecological observations from the West Greenland stratigraphy. In the case of CO_2 starvation (Robinson, 1994), an increase in angiosperm diversity and abundance is expected to occur with a low in atmospheric pCO_2 (McElwain *et al.*, 2005a). The thesis aimed to capture a pCO_2 fall during an OAE to see if these carbon cycling events may have forced a floral compositional change. However, if the angiosperms spread as a result of poleward movements of the climate belts in response to temperature increases (Coiffard and Gomez, 2012), the radiation and diversification of angiosperms would be expected to occur under increasing pCO_2 (whereby pCO_2 is positively correlated to temperature). As outlined in Section 7.1, the West Greenland stratigraphy did not cover an OAE with sufficient data resolution to test the OAE hypothesis. Nonetheless, the palaeoclimatic, palaeoenvironmental and ecological data integrated in this thesis provide important information on the state of "big picture" Cretaceous climate, in addition to greater insights into the development of angiosperms by the Albian.

The cuticle record of angiosperms through the West Greenland stratigraphy does not provide sufficient information to resolve changes in angiosperm abundance, but the record can be integrated with pollen (Horikx and Heimhofer, unpublished) and macrofossil (Boyd, 1998c) records as a means to compare angiosperm abundances between the Kome Formation and the Ravn Kløft Member (Figure 5.6; Figure 7.3C). Stomatal measurements through the Ravn Kløft Member reveal pCO_2 levels were higher than parts of the Kome Formation (Figure 7.2B), around 550–650 ppm (similar to the interval of increased pCO_2 in the Kome Formation). The low resolution of data in the Ravn Kløft Member makes deciphering any trends impossible, and the g_{wmax} values based on the Cheirolepidiaceae are variable. The lithology of the Ravn Kløft Member has a stronger fluvial component (Dam *et al.*, 2009), with common channel sandstones. The floral composition varies as a result, including a greater relative abundance of Bennettitales and Araucariaceae (Figure 5.3A) in addition to increased angiosperm abundance reflected in the macrofossil record (Figure 5.6, Figure 7.3C). However, in low energy depositional environments, in which mass accumulations of Miroviaceae occur and likely reflect locally swampy conditions, fossil epiphylls are present, indicating the climate was still humid like the Kome Formation (Kemp, 1978; Taylor *et al.*, 2009 and references therein). However, a seasonally drier component upstream, which may have led to forest fires (not necessarily annually), is indicated by increased charcoal content in the Ravn Kløft Member compared to the Kome

Formation (Figure 3.22), although this may in part be propelled by increased angiosperm abundance more rapidly generating a flammable leaf mass (Bond and Scott, 2010).

Coiffard and Gomez (2012) related phases in landscape ecology and the expansion of the occupational niches of angiosperms (from Coiffard *et al*., 2006, 2007, 2012) to the poleward spread of megathermal forests. The West Greenland floral composition can be compared to the phases of angiosperm niche occupation of Coiffard *et al.*, whereby the Kome Formation may represent phase 2, and the Ravn Kløft Member may represent an early stage of phase 3 (Section 5.4.4). However, the age associated with the beginning of this phase represented in the Ravn Kløft Member is earlier (Late Albian, Figure 7.3) than indicated for the lower palaeolatitude European region (Cenomanian; Coiffard *et al.*, 2012).

Nonetheless, examination of the pollen and macrofossil changes from West Greenland and the North American record (Lidgard and Crane, 1990; Lupia *et al*., 1999; Figure 7.3C) reveals an increase in relative abundance on the order of 30 % from the Kome Formation compared to the Ravn Kløft Member. The pCO_2 derived from stomatal ratios of fossil leaves of the present study also reveal an increase in pCO_2 across this interval of 100–200 ppm (with considerable uncertainty). At face value, this would appear to support the hypothesis of latitudinal climate belt shift with increasing temperatures, particularly when the high relative abundances in the Late Albian–Early Cenomanian (Figure 7.3C) coincides with increasing benthic sea temperatures, which likely reflect warming of Earth in general through the Albian (Friedrich *et al.*, 2012; Figure 7.3D; and Figure 1.1).

However, the pollen data from West Greenland (Horikx and Heimhofer, unpublished) reveals Tricolpate pollen in the Kome Formation, indicating Eudicots had already spread to 60 °N palaeolatitude by the Middle Albian, which may be earlier than previously thought (Figure 5.12; Hickey and Doyle, 1977). In addition, assessment of the stomatal parameters of the angiosperms compared to the gymnosperms measured in the present study reveals angiosperms had already adapted the “more numerous but smaller” stomatal strategy (Franks and Beerling, 2009), along with likely higher leaf vein density by the Middle Albian (Sections 6.3.2 and 6.5.3) and were therefore capable of higher stomatal conductance control as suggested by McElwain and Lawson (in press). Whilst the taphonomic bias cannot be ruled out, the limited pollen data available from the present study suggests an increase in angiosperm abundance at the top of the Kome Formation. In addition, previous compilations from North America (Figure 7.3C) reveal angiosperm abundance had already started to increase from the Middle Aptian in the case of macrofossils (Lidgard and Crane,

1990) and pollen records from below 42 °N (Lupia *et al.*, 1999), and at some point between the Late Aptian and mid-to Late Albian for above 42 °N. However, the present study would suggest that increased angiosperm pollen abundance had begun by the Middle Albian (Horikx and Heimhofer, unpublished).

When the angiosperm abundance (Figure 7.3C) is compared to the "best-estimate" pCO_2 compilation (Figure 7.3B), a minimum in pCO_2 occurs in the Middle Albian. As outlined previously, the low reconstructed pCO_2 values occur after OAE1b (Figure 7.3), where a large positive excursion is recorded in marine carbonate of around 2 ‰ from the late Aptian to the Aptian–Albian boundary, which could reflect the net result of carbon burial during OAEs through the interval. If so, this provides the exciting prospect that angiosperms may have developed the markedly different stomatal response strategy compared to gymnosperms at some time prior to the West Greenland stratigraphy, with a possibility that this was during an interval of reduced pCO_2. Nonetheless, this remains conjectural until pCO_2 is reconstructed with associated angiosperm records through the interval of OAE1b to test this hypothesis.

The "best-estimate" pCO_2 reconstruction (Figure 7.3B) provides a new more cohesive picture of changes in pCO_2 through the Cretaceous, and through comparison to other Cretaceous proxy and model-based reconstructions (Section 6.5.5), likely represents the lower limit of pCO_2 through the Aptian–Early Cenomanian. The average trend in the "best-estimate" pCO_2 reconstruction exhibits decreases in pCO_2 coinciding with intervals known to have experienced episodes of marine anoxia (OAEs), including OAE1a (Figure 7.3). However, the present study data also indicates there may have been smaller scale variation in pCO_2 through the West Greenland stratigraphy, with the rise and fall of pCO_2 in the Kome Formation occurring over approximately 1.5–2.0 Myrs, and is comparable in magnitude and duration to other studies in the Cretaceous (e.g. Passalia, 2009; Figure 7.3B). However, the resolution of small changes in pCO_2 is limited by the large error on the data, which can in part be countered by identifying coeval trends in average pCO_2 reconstructions of multiple plant types. If these small-scale variations are real indicators of Cretaceous pCO_2, Cretaceous climate must have been quite dynamic, and may have implications in reconstructing Cretaceous climate sensitivity (Royer *et al.*, 2012).

7.3 Conclusions

The research questions of the thesis were to investigate the relationship between carbon cycling, variations in pCO_2 and the rapid diversification and radiation of the flowering plants (angiosperms) during the mid-Cretaceous (Albian–Cenomanian), so that competing hypotheses regarding the roles of climate and pCO_2 on angiosperm diversification could be tested. In doing so, an improved understanding of Cretaceous carbon cycling through comparison of new, detailed reconstructions of pCO_2 with pre-existing Cretaceous data was required. Finally, the thesis aimed to improve our understanding of the stratigraphy and palaeoenvironments of the Nuussuaq Group, and to use palaeoenvironmental and palaeoecological information from the floral assemblage contained within the sediments to provide new insights into mid-Cretaceous climate variability. Exploration of these research themes revealed the following:

1. The carbon isotope stratigraphy of bulk organic matter and fossil wood revealed trends which could be correlated to published marine $\delta^{13}C_{carb}$ records. This provided a refined age-model for the West Greenland stratigraphy (Figure 3.31) when combined with published palynological estimates (summarised in Figure 3.27). The correlation of two isotopic events (one in the Kome Formation and one in the Ravn Kløft Member) to trends in $\delta^{13}C_{carb}$ revealed intervals of variation in global carbon cycling which could be used to test the hypothesis of the thesis.
2. Examination of 8300 macerated fossil leaf cuticle fragments permitted the identification of twelve floral groups (morphotypes), which likely reflected the most dominant local flora from the stratigraphic sections, with some other floral groups acknowledged but too few in abundance to be classed as a morphotype (Chapter 4). The morphotypes were affiliated with a likely plant family, and tentative genus associations through comparisons to other fossil and extant leaf cuticles and macrofossil specimens.
3. The changes in relative abundance of plant groups identified from the twelve morphotypes revealed changes in floral components through the West Greenland stratigraphy, but the data was not suitable for determining diversity changes. Two floral associations were discovered from detrended correspondence analysis (the CMC group: Cheirolepidiaceae-Miroviaceae-Coniferales [other], and the BAP group: Bennettitales-Araucariaceae-Pinaceae). Based on the floral ecology of these plant associations, a trend to more drained soil-favouring plants (the BAP group) was apparent in the middle of the Kome Formation (Chapter 5).

4. The identification of fossil epiphylls on CMC group hosts indicated high humidity and mean annual rainfalls (>1000–1500 mm yr^{-1}; Kemp, 1978) during the deposition of the Kome Formation (Chapter 5). However, the epiphyllous fossils were absent from CMC group cuticles during the interval of increased BAP group abundance, indicating perhaps a reduction in humidity during the middle Kome Formation.
5. The angiosperm cuticle record was rare, but was supplemented by pollen occurrences (Horikx and Heimhofer, unpublished) and macrofossil records (Boyd, 1998a-c, 2000, 2004), revealing a significant increase (on the order of 30 %) in abundance of angiosperms at some point between the Kome Formation and the Ravn Kløft Member (Chapter 5). Comparison to the North American floral records (Lidgard and Crane, 1990; Lupia *et al.*, 1999) revealed consistent changes in both magnitude and timing for above 42 °N palaeolatitude. Comparison to the European floral record (Coiffard *et al.*, 2006, 2007, 2012) was facilitated by an interpretation of landscape ecology, in order to understand the radiation of angiosperms into new ecological niches. The possible affiliation of angiosperms in West Greenland with fluvial channel margins indicated that by the Ravn Kløft Member (Late Albian) angiosperms had expanded into the breadth of ecological niches represented by Coiffard *et al.* (2012) phase 3, earlier than the European record (Cenomanian). In combination with the identification of Tricolpate pollen in the Kome Formation (Horikx and Heimhofer, unpublished) this indicates the angiosperms were already quite evolved by the Middle Albian, which may cast some doubt on the radiation of angiosperms in response to poleward shift of megathermal forests.
6. The different stomatal initiation response of angiosperms (the “smaller but more numerous strategy”; Franks and Beerling, 2009) compared to gymnosperms was revealed in Chapter 6 through: the relationship between vein density and stomatal conductance (McElwain and Lawson, *in press*) when fossil angiosperm and gymnosperm morphotypes were compared to extant examples; and the relationship between stomatal density and pore length to stomatal conductance for angiosperm and gymnosperm fossils when compared to extant examples (Franks and Beerling, 2009; McElwain and Lawson, *in press*). The identification of this difference in stomatal initiation response revealed angiosperms were already much more plastic in the capacity to respond to changes in pCO_2 than the gymnosperms by the Middle Albian (Chapter 6).

7. A "best-estimate" of pCO_2 was reconstructed through the interval by combining the stomatal ratio reconstruction from three plant types from the present study (Cheirolepidiaceae, Miroviaceae and angiosperm - Lauraceae) with previous stomatal indices-based reconstructions, which were recalibrated through reassessment of NLE suitability (Chapter 6). Comparisons to other model and proxy-based reconstructions indicate the "best-estimate" based on stomatal indices is likely the lower range in pCO_2 through the Aptian–Cenomanian, with an average value of around 575 ppm, but with lower values of pCO_2 reconstructed for the Middle Albian by around 150 ppm (Chapter 6). Small-scale variations (1–2Myr duration) in pCO_2 on the order of 60–200 ppm are recorded in the present study data, in addition to previous reconstructions (e.g. Passalia, 2009), which may have important implications for Cretaceous climate sensitivity (Royer *et al.*, 2012).
8. Stomatal conductances of the Cheirolepidiaceae decreased by around 200 mmol m^{-2} s^{-1} in the first 12 m of the Kome Formation, which was unsurprising given pCO_2 increased by approximately 60–100 ppm over the same interval (Chapter 6; Figure 7.2). A similar trend was identified in the angiosperm data, whereby stomatal conductances increased significantly (by around 500 mmol $m^{-2}s^{-1}$) from the middle to the top of the Kome Formation, with an associated pCO_2 fall on the order of 200 ppm. The low g_{wmax} values for the middle of the Kome Formation coincides with the interval of increased BAP group abundance and apparent decrease in humidity (interpreted from the absence of epiphylls on host CMC Group plants). This indicated that with increased pCO_2, plants may not have taken up as much water through root systems due to reduced rates of transpiration (reduced stomatal conductance). Therefore, the surface run-off may have increased, resulting in the shift in depositional environment to more fluvial channel dominated depositional environments (and associated landscape ecology – the BAP group) for both the middle of the Kome Formation and the Ravn Kløft member (Chapter 7).

7.4 Future work – revised hypothesis

There is evidence supporting both apparently contradictory hypotheses regarding the driving force of angiosperm radiation and diversification: there is an increase in angiosperm abundance which coincides with an increase in pCO_2 (and inferred temperatures, Friedrich *et al.*, 2012) recorded in the West Greenland stratigraphy, supporting the thermally driven spread of angiosperms towards the poles (Coiffard *et al.*, 2012). However, from the

conclusions of this thesis, the angiosperms had already adapted a markedly different stomatal regulation strategy to gymnosperms by the Middle Albian (Kome Formation) and Eudicots were already present in the West Greenland high palaeolatitude site. Pollen and macrofossil evidence from North America (Lidgard and Crane, 1990; Lupia *et al.*, 1999), in addition to the pollen record from West Greenland (Horikx and Heimhofer, unpublished), indicates the radiation may have already begun before the Middle Albian, possibly around the Aptian–Albian boundary.

If this is the case, there may be greater support for the CO_2 starvation, since the carbon isotope ratios reveal the series of events comprising OAE1b spans the Aptian–Albian boundary, and the present study pCO_2 reconstruction reveals pCO_2 levels just after the end of this event were lower than previous estimates elsewhere in the Aptian and Albian. The carbon isotope ratios through the interval of OAE1b also show a significant positive excursion, which could be suggested may be the result of carbon burial during OAEs. This new hypothesis for an earlier adaptation of angiosperms does not preclude the importance of thermally driven poleward spread of ecological landscapes in the radiation of angiosperms, but this may not have been the cause for the angiosperm physiological adaptations which are advantageous over gymnosperms, but rather the result of possession of such features.

Therefore, future work should precede the interval studied in this thesis, in an attempt to improve the resolution of floral changes over the Aptian–Albian boundary and reconstruct pCO_2 levels in order to test this new hypothesis. An approach similar to the present study is recommended, in particular the use of autofluorescence to study fossil leaf cuticle (with no cuticle clearing methods) as outlined in Section 4.1, since this has yielded unique insights into the phyllosphere through preservation of delicate structures, which may inherently be destroyed by cuticle clearing. The fossil structures identified in the present study expand the Mesozoic record for Microthyriaceae epiphylls and tentatively extends the fossil record of Trentepohliales by 70 Myrs. More detailed anatomical studies of these algal, fungal and possibly lichenised structures should be undertaken in future work as a relatively underappreciated ecological trove.

References

Ainsworth, E.A., S.P. Long (2005). What have we learned from 15 years of free-air CO_2 enrichment (FACE)? A meta-analytic review of the responses of photosynthesis, canopy properties and plant reproduction to rising CO_2. *New Phytologist*, **165**, 351-372, doi: 10.1111/j.1469-8137.2004.01224.x.

Alfieri, S.A. (1978). Black spot of Elm. *Plant Pathology Circular*, **189**, 2pgs.

Alvin, K.L., C.J. Fraser, R.A. Spicer (1981). Anatomy and palaeoecology of *Pseudofrenelopsis* and associated conifers in the English Wealden. *Palaeontology,* **24**, 759-778.

Alvin, K.L., (1983). Reconstruction of a Lower Cretaceous conifer. *Botanical Journal of the Linnean Society*, **86**, 169-176.

Andrews, J.H., R.F. Harris (2000). The ecology and biogeography of microorganisms on plant surfaces. *Annual Reviews of Phytopathology*, **38**, 145-180.

Anthony, P.A., J.A.M. Holtum, B.R. Jackes (2002). Shade acclimation of rainforest leaves to colonization by lichens. *Functional Ecology*, **16**, 808-816.

Arens, N.C., A.H. Jahren, R. Amundson (2000). Can C3 plants faithfully record the carbon isotopic composition of atmospheric carbon dioxide? *Paleobiology*, **26**, 137-164.

Armstrong, H.A., M.D. Brasier (2004). Microfossils 2nd Edition. Blackwell Publishing, Oxford, UK, 296 pgs.

Ash, A., L.J. Hickey, P. Wilf, B. Ellis, K. Johnson, S. Wing (1999). Manual of Leaf Architecture – morphological description and categorization of dicotyledonous and net-veined monocotyledonous angiosperms by Leaf Architecture Working Group, Smithsonian Institution, Washington DC, 65 pgs.

Aucour, A., B. Gomez, S.M.F. Sheppard, F. Thévenard (2008). $\delta^{13}C$ and stomatal number variability in the Cretaceous conifer *Frenelopsis*. *Palaeogeography, Palaeoclimatology, Palaeoecology*, **257**, 462-473.

Axsmith, B., T. Taylor, E. Taylor (1998). Anatomically preserved leaves of the conifer *Notophytum krauselii* (Podocarpaceae) from the Triassic of Antarctica. *American Journal of Botany*, **85**, 704-713.

Barclay, R.S. (2011). Testing the driving mechanisms for Oceanic Anoxic Event 2 (94 Ma) using pCO_2 estimates and carbon isotopes derived from fossil plant material in the Dakota Formation of Southwestern Utah (PhD Thesis, Northwestern University), 336 pgs.

Barclay, R., J. McElwain, D. Dilcher, B. Sageman (2007). The Cuticle Database: Developing an interactive tool for taxonomic and paleoenvrionmental study of the fossil cuticle record. *Courier Forschungsinstitut Senckenberg*, **258**, 39-55.

Barclay, R.S., J.C. McElwain, B.B. Sageman (2010). Carbon sequestration activated by a volcanic CO_2 pulse during Ocean Anoxic Event 2. *Nature Geoscience,* **3**, 205-208, doi: 10.1038/NGEO757.

Barron, E.J., W.M. Washington (1985). Warm Cretaceous climates: High atmospheric CO_2 as a possible mechanism. *Geophysical Monograph Series*, **32**, 546-553.

Barron, E.J., W.W. Hay, S. Thompson (1989). The hydrological cycle: a major variable during earth history. *Palaeogeography, Palaeoclimatology, Palaeoecology*, **75**, 157-174.

Barthlott, W., C. Neinhuis, D. Cutler, F. Ditsch, I. Meusel, I. Theisen, H. Wilhelmi (1998). Classification and terminology of plant epicuticular waxes. *Botanical Journal of the Linnean Society*, **126**, 237-260.

Becker, P. (2000). Competition in the regeneration niche between conifers and angiosperms: Bond's slow seedling hypothesis. *Functional Ecology*, **14**, 401-412.

Beerling, D.J. (1999). Stomatal density and index: theory and application. *In: Fossil Plants and Spores: Modern Techniques*, eds. T.P.

Jones, N.P. Rowe, *Geological Society, London*, 251–256.

Beerling, D.J., F.I. Woodward (2001). Vegetation and the terrestrial carbon cycle. Modelling the first 400 million years. *Cambridge University Press, Cambridge*, 405 pgs.

Berner, R.A. (1991). A model for atmospheric CO_2 over the Phanerozoic time. *American Journal of Science*, **291**, 339-376.

Berner, R.A. (1994). GEOCARB II: a revised model of atmospheric CO_2 over Phanerozoic time. *American Journal of Science*, **294**, 56-91.

Berner, R.A. (2003). The long-term carbon cycle, fossil fuels and atmospheric composition. *Nature*, **426**, 323-326.

Berner, R.A. (2006). Inclusion of the weathering of volcanic rocks in the GEOCARBSULF model. *American Journal of Science,* **294**, 295-302.

Berner, R.A. (2008). Correction of "Inclusion of the weathering of volcanic rocks in the GEOCARBSULF model". *American Journal of Science,* **308**, 100-103.

Berner, R.A., Z. Kothavala (2001). GEOCARB III: a revised model of atmospheric CO_2 over Phanerozoic time. *American Journal of Science*, **301**, 182-204.

Betts, R.A., O. Boucher, M. Collins, P.M. Cox, P.D. Falloon, N. Gedney, D.L. Hemming, C. Huntingford, C.D. Jones, D.M.H. Sexton, M.J. Webb (2007). Projected increase in continental runoff due to plant responses to increasing carbon dioxide. *Nature*, **448**, 1037–1041, doi: 10.1038/nature06045.

Bice, K.L., B.T. Huber, R.D. Norris (2003). Extreme polar warmth during the Cretaceous greenhouse? Paradox of the late Turonian $\delta^{18}O$ record at Deep Sea Drilling Project Site 511. *Paleoceanography,* **18**, 7pgs, doi: 10.1029/2002PA000848.

Bice, K.L., D. Birgel, P.A. Meyers, K.A. Dahl, K-U, Hinrichs, R.D.Norris (2006). A multiple proxy and model study of Cretaceous upper ocean temperatures and atmospheric CO_2 concentrations. *Paleoceanography*, **21**, 17 pgs., doi: 10.1029/2005PA001203.

Blakey, R. Palaeogeographic reconstructions. http://cpgeosystems.com. Last modified March 2014.

Bocherens, H., E.M. Friis, A. Mariotti, K.R. Pedersen (1994). Carbon isotopic abundances in Mesozoic and Cenozoic fossil plants: Palaeoecological implications. *Lethaia*, **26**, 347-358.

Bond, W.J. (1989). The tortoise and the hare: ecology of angiosperm dominance and gymnosperm persistence. *Biological Journal of the Linnean Society,* **36**, 227-249.

Bond, W.J., A.C. Scott (2010). Fire and the spread of flowering plant in the Cretaceous. *New Phytologist*, **188**, 1137-1150.

Bonis, N.R., J.H.A. Van Konijnenburg-Van Cittert, W.M. Kürschner (2010). Changing CO_2 conditions during the end-Triassic inferred from stomatal frequency analysis on *Lepidopteris ottonis* (Goeppert) Schimper and *Ginkgoites taeniatus* (Braun) Harris. *Palaeogeography, Palaeoclimatology, Palaeoecology*, **295**, 146-161.

Bornemann, A., J. Pross, K. Reichelt, J.O. Herrle, C. Hemleben, J. Mutterlose (2005). Reconstruction of short-term palaeoceanographic changes during the formation of the Late Albian 'Niveau Breistroffer' black shales (Oceanic Anoxic Event 1d, SE France). *Journal of the Geological Society, London,* **162**, 623-639.

Bose, M.N., S.B. Manum (1990). Mesozoic conifer leaves with 'Sciadopitys-like' stomatal distribution. A re-evaluation based on fossils from Spitsbergen, Greenland and Baffin Island. *Norsk Polarinsitutt Skrifter*, **192**, 1-81.

Bose, M.N., S.B. Manum (1991). Addition to the Family Miroviaceae (Coniferae) from the Lower Cretaceous of West Greenland and Germany: *Mirovia groenlandica* n. sp., *Tritaenia crassa* (Seward) comb. Nov., and *Tritaenia linkii* Mägdefrau et Rudolf emend. *Polar Research*, **9**, 9-20.

Boyd, A**.** (1998a). Macroleaf biostratigraphy of the Early Cretaceous beds in West Greenland. *Zentralblatt für Geologie und Paläontologie*, **1**, 1455-1468.

Boyd, A. (1998b) The Bennettitales of the Early Cretaceous floras from West Greenland: Pseudocycas. *Palaeontographica Ableitung B*, **247**, 123-155.

Boyd, A. (1998c). Cuticular and impressional Angiosperm leaf remains from the Early Cretaceous floras of West Greenland. *Palaeontographica Ableitung B*, **247**, 1-53.

Boyd, A. (2000). Bennettitales from the Early Cretaceous floras of West Greenland: *Pterophyllum* and *Nilssoniopteras*. *Palaeontographica Ableitung B*, **255**, 47-77.

Boyd, A. (2004). Bennettitalean fruits, flowers, and flower bracts from the Early Cretaceous floras of West Greenland. *Palaeontographica Ableitung B*, **268**, 113-172.

Brenner, G.J. (1996). Evidence for the earliest stage of angiosperm pollen evolution: a palaeoequatorial section from Israel. In: *Flowering plant origin, evolution and phylogeny* (eds. D.W. Taylor & L.J. Hickey), Chapman & Hall, New York, 91-115.

Brodribb, T.J., T.S. Feild (2010). Leaf hydraulic evolution led a surge in leaf photosynthetic capacity during early angiosperm diversification. *Ecology Letters,* **13**, 175-183, doi: 10.1111/j.1461-0248.2009.01410.x.

Bryan, S.E., R.E. Ernst (2008). Revised definition of Large Igneous Provinces (LIPs). *Earth-Science Reviews*, **86**, 175-202, doi: 10.1016/j.earscirev.2007.08.008.

Burd, M. (2007). Adaptive function of drip tips: a test of the epiphyll hypothesis in *Psychotria marginata* and *Faramea occidentalis* (Rubiaceae). *Journal of Tropical Ecology*, **23**, 449-455.

Caldeira, K., M.R. Rampino (1991). The mid-Cretaceous super plume, carbon dioxide, and global warming. *Geophysical Research Letters*, **18**, 987-990.

Cerling, T.E. (1991). Carbon dioxide in the atmosphere: evidence from Cenozoic and Mesozoic paleosols. *American Journal of Science*, **291**, 377-400.

Chalmers, J.A., T.C.R. Pulvertaft (2001). Development of the continental margins of the Labrador Sea: a review. *Geological Society of London Special Publications*, **187**, 77-105.

Chaloner, W.G., J.C. McElwain (1997). The fossil plant record and global climatic change. *Review of Palaeobotany and Palynology*, **95**, 73-82.

Chandrasekharam, A. (1972). Spongy mesophyll remains in fossil leaf compressions. *Science*, **177**, 354-356.

Chumakov, N.M., M.A. Zharkov, A.B. Herman, M.P. Doludenko, N.N. Kaldadze, E.L. Lebedev, A.G. Ponomarenko, A.S. Ratian (1995). Climatic belts of the mid-Cretaceous time. *Stratigraphy and Geological Correlation*, **3**, 241-260.

Clarke, L.J., H.C. Jenkyns (1999). New oxygen isotope evidence for long-term Cretaceous climatic change in the Southern Hemisphere. *Geology*, **27**, 699-702.

Coiffard, C., B. Gomez (2012). Influence of latitude and climate on spread, radiation and rise to dominance of early angiosperms during the Cretaceous in the Northern Hemisphere. *Geologica Acta*, **10**, 181-188, doi: 10.1344/105.000001701.

Coiffard, C., B. Gomez, V. Daviero-Gomez, D.L. Dilcher (2012). Rise to dominance of angiosperm pioneers in European Cretaceous environments. *PNAS*, **109**, 20955-20959, doi: 10.1073/pnas.1218633110.

Coiffard, C., B. Gomez, J. Kvaček, F. Thévenard (2006). Early angiosperm ecology: Evidence from the Albian-Cenomanian of Europe. *Annals of Botany*, **98**, 495-502.

Coiffard, C., B. Gomez, F. Thévenard (2007). Early Cretaceous angiosperm invasion of Western Europe and major environmental changes. *Annals of Botany*, **100**, 545-553, doi: 10.1093/aob/mcm160.

Colombo, U., F. Gazzarrini, R. Gonfiantini, G. Kneuper, M. Teichmiiller, R. Teichmiiller (1968). Das Verhaltnis der stabilen Kohlenstoff-Isotope von Steinkohlen und kohlenbiirtigem Methan in Nordwestdeutschland. *Zeitschrift für Angewandte Geologie*, **14**, 257-265.

Courtillot, V.E., P.R. Renne (2003). On the ages of flood basalt events. Comptes Rendus Geoscience, **335***,* 113-140.

Cowan, I. (1977). Stomatal behaviour and environment. *Advances in Botanical Research*, **4**, 117-219.

Cowan, I.R., G.D. Farquhar (1977). Stomatal function in relation to leaf metabolism and environment. *In: Integration of Activity in the Higher Plan, Society for Experimental Biology Symposium*, Cambridge University Press, Cambridge, ed. D.H. Jennings, **31**, 471-505.

Cowling, S.A. (2001). Plant carbon balance, evolutionary innovation and extinction in land plants. *Global Climate Biology*, **7**, 231-237.

Crane, P.R. (1985). Phylogenetic analysis of seed plants and the origin of angiosperms. *Annals of the Missouri Botanical Garden,* **72**, 716-793.

Croxdale, J.L. (2000). Stomatal patterning in angiosperms. *American Journal of Botany,* **87**, 1069-1080.

Croxton, C.A. (1978). Report of field work undertaken between 69°and 72°N, central West Greenland in 1977 with preliminary palynological results. *Unpublished report, Geological Survey of Greenland, Copenhagen* (in archives of Geological Survey of Denmark and Greenland, GEUS Report File 28069), 24 pgs.

Dam, G., H. Nøhr-Hansen (2001). Mantle plumes and sequence stratigraphy; Late Maastrichtian – Early Paleocene of West Greenland. *Bulletin of the Geological Society of Denmark*, **48**, 189–207.

Dam, G., G.K. Pedersen, M. Sønderholm, H.H. Midtgaard, L.M. Larsen, H. Nøhr-Hansen, A.K. Pedersen (2009). Lithostratigraphy of the Cretaceous-Paleocene Nuussuaq Group, Nuussuaq Basin, West Greenland. *Geological Survey of Denmark and Greenland Bulletin*, **19**, 171pgs.

Deising, H.B., S. Werner, M. Wernitz (2000). The role of fungal appressoria in plant infection. *Microbes and Infection*, **2**, 1631-1641.

Delevoryas, T. (1982). Perspectives on the origin of Cycads and Cycadeoids. *Review of Palaeobotany and Palynology*, **37**, 115-132.

Delevoryas, T., R.C. Hope (1976). More evidence for a slender growth habit in Mesozoic cycadophytes. *Review of Palaeobotany and Palynology,* **21**, 93-100.

Demaison, G.J., G.T. Moore (1980). Anoxic environments and oil source bed genesis. *Organic Geochemistry,* **2**, 9-31.

Deshmukh, A.P., A.J. Simpson, C.M. Hadad, P.G. Hatcher (2005). Insights into the structure of cutin and cutan from *Agave americana* leaf cuticle using HRMAS NMR spectroscopy. *Organic Geochemistry*, **36**, 1072-1085, doi:10.1016/j.orggeochem.2005.02.005.

Dickens, G.R., J.R. O'Neil, D.K. Rea, R.M. Owen (1995). Dissociation of oceanic methane hydrate as a cause of the carbon isotope excursion at the end of the Paleocene. *Paleoceanography*, **10**, 965-971.

Dickison, W.C. (2000). Integrative plant anatomy, Elsevier Science Academic Press, Florida, USA, 573 pgs., ISBN: 0-12-215170-4.

Dilcher, D.L. (1965). Epiphyllous fungi from the Eocene deposits in Western Tennessee, USA. *Palaeontographica Ableitung B*, **116**, 1-54.

Dilcher, D.L. (1989). The occurrence of fruits with affinity to Ceratophyllaceae in Lower and mid-Cretaceous sediments. *American Journal of Botany*, **76**, 162.

Doláková, N., A. Burešová (2007). Use of fluorescent microscopy in the study of redeposited palynomorphs in the cave and marine sediments of Moravia (Czech Republic). *Acta Palaeobotanica*, **47**, 275-279.

Doyle, J.A., M.J. Donoghue (1993). Phylogenies and angiosperm diversification. *Paleobiology*, **19**, 141-167.

Doyle, J.A. (2012). Molecular and fossil evidence on the origin of angiosperms. *Annual Reviews of Earth and Planetary Sciences*, **40**, 301-326.

Drew, B.T., K.J. Sytsma (2013). The South American radiation of *Lepechinia* (Lamiaceae): phylogenetics, divergence times and evolution of dioecy. *Botanical Journal of the Linnean Society*, **171**, 171-190.

Dunkić, V., N. Bezić, N. Ljubešić, I. Bočina (2007). Glandular hair ultrastructure and essential oils in *Satureja subspicata* Vis. ssp. *Subspicata* and ssp. *Liburnica* Šilić*. Acta Biologica Cracoviensia Series Botanica*, **49**, 45-51.

Eglinton, G., R.J. Hamilton (1967). Leaf epicuticular waxes. *Science*, **156**, 1322-1335.

Ekart, D.D., T.E. Cerling, I.P. Montañez, N.J. Tabor (1999). A 400 million year carbon isotope record of pedogenic carbonate: implications for palaeoatmospheric carbon dioxide. *American Journal of Science*, **299**, 805-827.

Erba, E. (1994). Nannofossils and superplumes: The early Aptian "nannoconids crisis". *Paleoceanography,* **9**, 483-501.

Erbacher, J., J. Thurow, R. Littke (1996). Evolution patterns of radiolarian and organic matter variations: A new approach to identify sea-level changes in mid-Cretaceous pelagic environments. *Geology,* **24**, 499-502, doi: 10.1130/0091-7613(1996)024<0499:EPORAO>2.3.CO;2.

Erbacher, J., B.T. Huber, R.D. Norris, M. Markey (2001). Increased thermohaline stratification as a possible cause for an ocean anoxic event in the Cretaceous period. *Nature*, **409**, 325-327.

Erbacher, J., O. Friedrich, P.A. Wilson, J. Lehmann, W. Weiss (2011). Short-term warming events during the boreal Albian (mid-Cretaceous). *Geology,* **39**, 223-226, doi: 10.1130/G31606.1.

Eriksson, O., E.M. Friis, P. Löfgren (2000). Seed size, fruit size and dispersal systems in angiosperms from the Early Cretaceous to the Late Tertiary. *The American Naturalist,* **156**, 47-58.

Farquhar, G.D., J.R. Ehleringer, K.T. Hubick (1989). Carbon isotope discrimination and photosynthesis. *Annual Reviews of Plant Physiology and Molecular Biology*, **40**, 503-537.

Fay, C.A. (2010). Comparative study of Early Cretaceous oceanic anoxic events and related phenomena. Lower Greensand Group, Isle of Wight. *University of Oxford, Master's Thesis*, (Sup. S.P. Hesselbo, H.C. Jenkyns), 68pgs.

Feild, T.S., N.C. Arens, J.A. Doyle, T.E. Dawson, M.J. Donoghue (2004). Dark and disturbed: a new image of early angiosperm ecology. *Paleobiology,* **30**, 82-107.

Feild, T.S., D.S. Chatelet, T.J. Brodribb (2009). Ancestral xerophobia: a hypothesis on the whole plant ecophysiology of early angiosperms. *Geobiology,* **7**, 237-264, doi: 10.111/j.1472-4669.2009.00189x.

Feild, T.S., G.R. Upchurch Jr., D.S. Chatelet, T.J. Brodribb, K.C. Grubbs, M. Samain, S. Wanke (2011a). Fossil evidence for low gas exchange capacities for Early Cretaceous angiosperm leaves. *Paleobiology,* **37**, 195-213.

Feild, T.S., T.J. Brodribb, A. Iglesias, D.S. Chatelet, A. Baresch, G.R. Upchurch Jr., B. Gomez, B.A.R. Mohr, C. Coiffard, J. Kvacek, C. Jaramillo (2011b). Fossil evidence for Cretaceous escalation in angiosperm leaf vein evolution. *PNAS*, **108**, 8363-8366, doi: 10.1073/pnas.1014456108.

Fletcher, B.J., D.J. Beerling, S.J. Brentnall, D.L. Royer (2005). Fossil bryophytes as recorders of ancient CO_2 levels: experimental evidence and a Cretaceous case study. *Global Biogeochemical Cycle*, **19**, 1-13.

Fletcher, B.J., S.J. Brentnall, C.W. Anderson, R.A. Berner, D.J. Beerling (2008). Atmospheric carbon dioxide linked with Mesozoic and early Cenozoic climate change. *Nature Geoscience,* **1**, 43-48.

Föllmi, K.B. (2012). Early Cretaceous life, climate and anoxia. *Cretaceous Research,* **35**, 230-257, doi: 10.1016/j.cretres.2011.12.005.

Forster, A., S. Schouten, M. Baas, J.S. Sinninghe Damsté (2007). Mid-Cretaceous (Albian-Santonian) sea surface temperature record of the tropical Atlantic Ocean. *Geology*, **35**, 919-922, doi: 10.1130/G23874A.1.

Frakes, L.A. (1999). Estimating the global thermal state from Cretaceous sea surface and continental temperature data. In: Evolution of the Cretaceous Ocean-Climate System, Eds: E. Barrera, C.C. Johnson, Boulder, Colorado, *Geological Society of America Special Paper*, **332**, 49-58

France, R.L. (1995). Differentiation between littoral and pelagic food webs in lakes using stable carbon isotopes. *Limnology and oceanography*, **40**, 1310-1313.

Francis, J.E., I. Poole (2002). Cretaceous and early Tertiary climates of Antarctica: evidence from fossil wood. *Palaeogeography, Palaeoclimatology, Palaeoecology*, **182**, 47-64.

Franks, P.J., D.J. Beerling (2009). Maximum leaf conductance driven by CO_2 effects on stomatal size and density over geologic time. *PNAS*, **106**, 10343-10347, doi: 10.1073/pnas.0904209106.

Freeman, K.H., J.M. Hayes (1992). Fractionation of carbon isotopes by phytoplankton and estimate of ancient CO_2 level. *Global Biogeochemical Cycles*, **6**, 185-198.

Friedrich, O. R.D. Norris, J. Erbacher (2012). Evolution of middle to Late Cretaceous oceans – A 55 m.y. record of Earth's temperature and carbon cycle. *Geological Society of America*, **40**, 107-110.

Friis, E.M., P.R. Crane, K.R. Pedersen (2011). Early flowers and angiosperm evolution. *Cambridge University Press*, *Cambridge,* 585 pgs.

Friis, E.M., K.R. Pedersen, P.R. Crane (2010). Diversity in obscurity: fossil flowers and the early history of angiosperms. *Philosophical transactions of the Royal Society B*, **365,** 369-382.

Friis, E.M., K.R. Pedersen, P.R. Crane (2006). Cretaceous angiosperm flowers: Innovation and evolution in plant reproduction. *Palaeogeography, Palaeoclimatology, Palaeoecology*, **232**, 251-293.

Friis, E.M., K.R. Pedersen, P.R. Crane (1999). Early angiosperm diversification: the diversity of pollen associated with angiosperm reproductive structures in Early Cretaceous floras from Portugal. *Annals of the Missouri Botanical Garden*, **86**, 259-266.

Gale, A.S., P. Bown, M. Caron, J. Crampton, S.J. Crowhurst, W.J. Kennedy, M.R. Petrizzo, D.S. Wray (2011). The uppermost Middle and Upper Albian succession at the Col de Palluel, Hautes-Alpes, France: An integrated study (ammonites, inoceramid bivalves, planktonic foraminifera, nannofossils, geochemistry, stable oxygen and carbon isotopes, cyclostratigraphy). *Cretaceous Research*, **32**, 59-130.

Gan, G., C. Ma, J. Wu (2007). Data clustering: theory, algorithms, and applications, Society for Industrial and Applied Mathematics, 184 pgs., ISBN-13: 978-0898716238.

Germeraad, J.H. (1979). Fossil remains of fungi, algae and other organisms from Jamaica. *Scripta Geologica*, **52**, 1-39.

Goff, L.J. (1983). Algal Symbiosis: A continuum of interaction strategies. (Eds.: L.J. Goff), Cambridge University Press, Cambridge, ISBN: 9780521177429.

Gomez, B. (2002). A new species of *Mirovia* (Coniferales, Miroviaceae) from the Lower Cretaceous of the Iberian Ranges (Spain). *Cretaceous Research*, **23**, 761-773, doi: 10.1006/cres.2002.1023.

Gomez, B., M. Bamford, X. Martínez-Delclòs (2002). Lower Cretaceous plant cuticles and amber (Kirkwood Formation, South Africa). *C.R. Palevol*, **1**, 83-87.

Gower, J.C. (1971). A general coefficient of similarity and some of its properties. *Biometrics*, **27**, 857-874.

Grace, J., J. Lloyd, J. McIntyre, A.C. Miranda, P. Meir, H.S. Miranda, C. Nobre, J. Moncrieff, J. Massheder, Y. Malhi, I. Wright, J. Gash (1995). Carbon dioxide uptake by an undisturbed tropical rain forest in Southwest Amazonia, 1992 to 1993. *Science,* **270**, 778-780.

Gradstein, F.M., F.G. Ogg, A.G. Smith, F.P. Agterberg, W. Bleeker, R.A. Cooper, V. Davydov, P. Gibbard, L.A. Hinnov, M.R. House, L. Lourens, H-P. Luterbacher, J.

McArthur, M.J. Melchin, L.J. Robb, J. Shergold, M. Villeneuve, B.R. Wardlaw, J. Ali, H. Brinkhuis, F.J. Hilgen, J. Hooker, R.J, Howarth, A.H. Knoll, J. Laskar, S. Monechi, J. Powell, K.A. Lumb, I. Raffi, U. Röhl, A. Sanfilippo, B. Schmitz, N.J. Shackleton, G.A. Shields, H. Strauss, J. Van Dam, J. Veizer, Th. van Kolfschoten, D. Wilson (2004). A Geologic Time Scale 2004. *Cambridge University Press, Cambridge*, 500pgs.

Grimaldi, D. (1999). The co-radiations of pollinating insects and angiosperms in the Cretaceous. *Annals of the Missouri Botanical Garden,* **86**, 373-406.

Gordenko, N.V. (2007). A new species of the Conifer Genus *Oswaldheeria* with well-preserved leaf anatomical elements from the Bathonian of the Kursk region. *Paleontological Journal*, **41**, 319-326.

Govil, C.M. (2007). Gymnosperms: Extinct and extant. Krishna Prakashan Media (P) Ltd, Delhi, 333 pgs.

Gröcke, D.R., S.P. Hesselbo, H.C. Jenkyns (1999). Carbon-isotope composition of Lower Cretaceous fossil wood: Ocean-atmosphere chemistry and relation to sea-level change. *Geology*, **27**, 155-158, doi: 10.1130/0091-7613(1999)027<0155:CICOLC>2.3.CO;2.

Gröcke, D.R. (2002). The carbon isotope composition of ancient CO_2 based on higher-plant organic matter. *Philosophical Transactions: Mathematical, Physical and Engineering Sciences*, **360**, 633-658.

Gröcke, D.R., G.A. Ludvigson, B.L. Witzke, S.A. Robinson, R.M. Joeckel, D.F. Ufnar, R.L. Ravn (2006). Recognizing the Albian-Cenomanian (OAE1d) sequence boundary using plant carbon isotopes: Dakota Formation, Western Interior Basin, USA. *Geology*, **34**, 193-196, doi: 10.1130/G21998.1.

Grube, M., M. Cardinale, G. Berg (2012). Bacteria and the Lichen Symbiosis. *In: Fungal Associations 2nd Edition: The Mycota IX.* Ed.: B. Hock. Springer-Verlag, Berlin, 363-372.

Hammer, O., D.A.T. Harper (2006). Paleontological data analysis, Blackwell Publishing Lts, Oxford, 368 pgs, ISBN-10: 1-4051-1544-5.

Hansen, H.N. (1992). Cretaceous marine and brackish (?) dinoflagellates cysts, West Greenland. *8th International Palynological Congruence*, Aix-en-Provence, Programme and Abstracts, page 107.

Hao, D.C., P.G. Xiao, B. Huang, G.B. Ge, L. Yang (2008). Interspecific relationships and origins of Taxaceae and Cephalotaxaceae revealed by partitioned Bayesian analyses of chrotoplast and nuclear DNA sequences. *Plant systematics and evolution*, **276**, 89-104.

Harris, T.M (1961). The Yorkshire Jurassic Flora, Volume 1 Thallophyta-Pteridophyta. *British Museum, Natural History*, 220pgs.

Haworth, M., S.P. Hesselbo, J.C. McElwain, S.A. Robinson, J.W. Brunt (2005). Mid-Cretaceous pCO_2 based on stomata of the extinct conifer *Pseudofrenelopsis* (Cheirolepidiaceae). *Geology*, **33**, 749-752.

Haworth, M., J. McElwain (2008). Hot, dry, wet, cold or toxic? Revisiting the ecological significance of leaf and cuticular micromorphology. *Palaeogeography, Palaeoclimatology, Palaeoecology,* **262**, 79-90, doi: 10.1016/j.palaeo.2008.02.009.

Haworth, M., J. Heath, J.C. McElwain (2010). Differences in the response sensitivity of stomatal index to atmospheric CO_2 among four genera of Cupressaceae conifers. *Annals of Botany*, **105**, 411-418, doi: 10.1093/aob/mcp309.

Haworth, M., C. Elliott-Kingston, J.C. McElwain (2011). The stomatal CO_2 proxy does not saturate at high atmospheric CO_2 concentrations: evidence from stomatal index responses of Araucariaceae conifers. *Oecologia*, **167**, 11-19, doi: 10.007/s00442-011-1969-1.

Hay, W.W. (2010). Can humans force a return to 'Cretaceous' climate? *Sedimentary Geology*, **235**, 5-26.

Hay, W.W., S. Flögel (2012). New thoughts about the Cretaceous climate and ocean. *Earth Science Reviews*, **115**, 262-272.

Heer, O. (1874a). Nachträge zur miocenen Flora Grönlands. *Kungliga Svenska Vetenskaps-Akademiens Handlingar*, **13**, 29pgs.

Heer, O. (1874b). Die Kreide-Flora der arctischen Zone. *Kungliga Svenska Vetenskaps-Akademiens Handlingar,* **12**, 138 pgs.

Heer, O. (1880). Nachträge zur fossilen Flora Grönlands. *Kungliga Svenska Vetenskaps-Akademiens Handlingar*, **18**, 17 pgs.

Heer, O. (1882). Flora fossilis Grönlandica. *Die fossile Flora Grönlands. Erster Theil,*. Zurich, Verlag von J. Wurster & Comp, 112 pgs.

Heer, O. (1883a). Flora fossilis Grönlandica. *Die fossile Flora Grönlands. Zweiter Theil*, Zurich, Verlag von J. Wurster & Comp, 275 pgs.

Heer, O. (1883b). Oversigt over Grønlands fossile flora. *Meddelelser om Grønland*, **5**, 79–202.

Heimhofer, U., P.A. Hochuli, J.O. Herrle, N. Andersen, H. Weissert (2004). Absence of major vegetation and palaeoatmospheric pCO_2 changes associated with oceanic anoxic event 1a (Early Aptian, SE France). *Earth and Planetary Science Letters*, **223**, 303-318.

Heimhofer, U., P.A. Hochuli, S. Burla, J.M.L. Dinis, H. Weissert (2005). Timing of Early Cretaceous angiosperm diversification and possible links to major palaeoenvironmental change. *Geology,* **33**, 141-144, doi: 10.1130/G21053.1.

Heimhofer, U., P.A. Hochuli, S. Burla, H. Weissert (2007). New records of Early Cretaceous angiosperm pollen from Portuguese coastal deposits: Implications for the timing of the early angiosperm radiation. *Review of Palaeobotany and Palynology*, **144**, 39-76.

Herman, A.B. (2002). Late Early-Late Cretaceous floras of the North Pacific Region: florogenesis and early angiosperm invasion. *Review of Palaeobotany and Palynology,* **122**, 1-11.

Herrle, J.O. (2002). Paleoceanographic and paleoclimatic implications on mid-Cretaceous black shale formation in the Vocontian Basin and the Atlantic: evidence from calcareous nannofossils and stable isotopes. Tübinger Mikropaläontologische Mitteilungen, **27**, 114 pgs.

Herrle, J.O., J. Pross, O. Friedrich, P. Kößler, C. Hemleben (2003). Forcing mechanisms for mid-Cretaceous black shale formation: evidence from the Upper Aptian and Lower Albian of the Vocontian Basin (SE France). *Palaeogeography, Palaeoclimatology, Palaeoecology,* **190**, 399-426.

Herrle, J.O., P. Kößler, O. Friedrich, H. Erlenkeuser, C. Hemleben (2004). High-resolution carbon isotope records of the Aptian to Lower Albian from SE France and the Mazagan Plateau (DSDP Site 545): a stratigraphic tool for paleoceanographic and palaeobiological reconstruction. *Earth and Planetary Science Letters*, **218**, 149-161, doi: 10.1016/S0012-821X(03)00646-0.

Hesselbo, S.P., D.R. Gröcke, H.C. Jenkyns, C.J. Bjerrum, P. Farrimond, H.S. Morgans Bell, O.R. Green (2000). Massive dissociation of gas hydrate during a Jurassic oceanic anoxic event. *Nature*, **406**, 392-395.

Hesselbo, S.P., S.A. Robinson, F. Surlyk, S. Piasecki (2002). Terrestrial and marine extinction at the Triassic-Jurassic boundary synchronised with major carbon-cycle perturbation: A link to initiation of massive volcanism? *Geology*, **30**, 251-254.

Hesselbo, S.P., H.S. Morgans-Bell, J.C. McElwain, P. McAllister Rees, S.A. Robinson, C.E. Ross (2003). Carbon-cycle perturbation in the Middle Jurassic and accompanying changes in the terrestrial paleoenvironment. *The Journal of Geology*, **111**, 259-276.

Hesselbo, S.P., H.C. Jenkyns, L.V. Duarte, L.C.V. Oliveira (2007). Carbon-isotope record of the Early Jurassic (Toarcian) Oceanic Anoxic Event from fossil wood and marine carbonate (Lusitanian Basin, Portugal). *Earth and Planetary Science Letters*, **253**, 455-470.

Hickey, L.J., J.A. Doyle (1977). Early Cretaceous fossil evidence for angiosperm evolution. *The Botanical Review,* **43**, 3-104.

Hilton, J., R.M. Bateman (2006). Pteridosperms are the backbone of seed-plant phylogeny. *Journal of the Torrey Botanical Society*, **133**, 119-168.

Houtte, L.V. (1845). Sciadopitys verticillata (Thunb.) Siebold & Zucc. *Flore des serres et des jardin de l'Europe*, **14**¸ illustration ID: 147253.

Huber, B.T., R.D. Norris, K.G. MacLeod (2002). Deep-sea palaeotemperature record of extreme warmth during the Cretaceous. *Geology*, **30**, 123-126.

Hughes, N.F. (1994). The enigma of angiosperm origins. *Cambridge University Press, Cambridge,* 303pgs, doi: 10.1130/0091-7613.

Ivey, C.T., N. DeSilva (2001). A test of the function of drip trips. *Biotropica*, **33**, 188-191.

Jahren, A.H., N.C. Arens, G. Sarmiento, J. Guerrero, R. Amundson (2001). Terrestrial record of methane hydrate dissociation in the Early Cretaceous. *Geology,* **29**, 159-162.

Jan de Boer, H., M.B. Epinga, M.J. Wassen, S.C. Dekker (2012). A critical transition in leaf evolution facilitated the Cretaceous angiosperm revolution. *Nature communications*, doi: 10.1038/ncomm2217 11pgs.

Jenkyns, H.C. (1999). Mesozoic anoxic events and palaeoclimate. *Zentralblatt für Geologie und Paläontologie*, **1997**, 943-949.

Jenkyns, H.C. (2003). Evidence for rapid climate change in the Mesozoic-Palaeogene greenhouse world. *Philosophical Transactions: Mathematical, Physical and Engineering Sciences,* **361**, 1885-1916.

Jenkyns, H.C., L. Schouten-Huibers, S. Schouten, J.S. Sinninghe Damsté (2012). Warm Middle Jurassic-Early Cretaceous high-latitude sea-surface temperatures from the Southern Ocean. *Climate of the Past*, **8**, 215-226, doi: 10.5194/cp-8-215-2012.

Jordan, G.J., P.H. Weston, R.J. Carpenter, R.A. Dillon, T.J. Brodribb (2008). The evolutionary relations of sunken, covered and encrypted stoma to dry habitats in Proteaceae. *American Journal of Botany*, **95**, 521-530.

Jones, T.P., W.G. Chaloner (1991). Fossil charcoal, its recognition and palaeoatmospheric significance. *Palaeogeography, Palaeoclimatology, Palaeoecology*, **97**, 39-50.

Jones, C.E., H.C. Jenkyns (2001). Seawater strontium isotopes, oceanic anoxic events, and sear floor hydrothermal activity in the Jurassic and Cretaceous. *American Journal of Science*, **301**, 112-149.

Joubert, J.J., F.H.J. Rijkenberg (1971). Parasitic green algae. *Annual Review of Phytopathology*, **9**, 45-64.

Judd, W.S., C.S. Campbell, E.A. Kellogg, P.F. Stevens, M.J. Donoghue (2002). Plant systematics: a phylogenetic approach. Sinauer Associates, Inc., Sunderland, Mssachusetts.

Kemp, E.M. (1978). Tertiary climatic evolution and vegetation history in the Southeast Indian Ocean region. *Palaeogeography, Palaeoclimatology, Palaeoecology*, **24**, 169-208.

Kerp, H. (1990). The study of fossil gymnosperms by means of cuticular analysis. *PALAIOS*, **5**, 548-569, doi: 10.2307/3514861.

Kerp, H., M. Krings (1999). Light microscopy of fossil cuticles. *In: Fossil plants and spores; modern techniques*, Eds.: T.P. Jones, N.P. Rowe, The Geological Society, London, 52-56.

Kohn, M.J. (2010). Carbon isotope compositions of terrestrial C3 plants as indicators of paleoecology and paleoclimate. *PNAS*, **107**, 19691-19695, doi: 10.1073/pnas.1004933107.

Koppelhus, E.B., G.K. Pedersen (1993). A palynological and sedimentological study of Cretaceous floodplain deposits of the Atane Formation at Skansen and Igdlunguaq, Disko, West Greenland. *Cretaceous Research*, **6**, 707-734.

Kouwenberg, L.L.R., J.C. McElwain, W.M. Kürschner, F. Wagner, D.J. Beerling, F.E.

Mayle, H. Bisscher (2003). Stomatal frequency adjustment of the four conifer species to historical changes in atmospheric CO_2. *American Journal of Botany*, **90**, 610-619.

Kouwenberg, L., R. Wagner, W. Kürschner, H. Visscher (2005). Atmospheric CO_2 fluctuations during the last millennium reconstructed by stomatal frequency analysis of *Tsuga heterophylla* needles. *Geology*, **33**, 33-36, doi: 10.1130/G20941.1.

Kubínová, L. (1994). Recent stereological methods for measuring leaf anatomical characteristics: Estimation of the number and sizes of stomata and mesophyll cells. *Journal of Experimental Botany*, **45**, 119-127.

Kump, L.R., M.A. Arthur (1999). Interpreting carbon-isotope excursions: carbonates and organic matter. *Chemical Geology*, **161**, 181-198.

Kürschner, W.M., Z. Kvaček, D.L. Dilcher (2008). The impact of Miocene atmospheric carbon dioxide fluctuations on climate and the evolution of terrestrial ecosystems. *PNAS*, **105**, 449-453, doi: 10.1073/pnas.0708588105.

Kuypers, M.M., R.D. Pancost, J.S. Sinninghe Damsté (1999). A large and abrupt fall in atmospheric CO_2 concentration during Cretaceous times. *Nature*, **399**, 342-345.

Kvaček, J. (1995). Cycadales and Bennettitales leaf compressions of the Bohemian Cenomanian, Central Europe. *Review of Paleobotany and Palynology*, **84**, 389-412.

Lammertsma, E.I., H.J. de Boer, S.C. Dekker, D.L. Dilcher, A.F. Lotter, F. Wagner-Cremer, (2011). Global CO_2 rise leads to reduced maximum stomatal conductance in Florida vegetation. *National Academy of Sciences Proceedings*, **108**, 10,4035-10,4040, doi:10.1073/pnas.1100371108.

Larson, R.L. (1991). Latest pulse of Earth: Evidence for a mid-Cretaceous superplume. *Geology,* **19**, 547-550.

Larson, R.L., E. Erba (1999). Onset of the mid-Cretaceous greenhouse in the Barremian-Aptian: Igneous events and the biological, sedimentary, and geochemical responses. *Paleoceanography,* **14**, 663-678.

Leavitt, S.W., A. Long (1986). Stable-carbon isotope variability in tree foliage and wood. *Ecology*, **67**, 1002-1010.

Leckie, R.M., T.J. Bralower, R. Cashman (2002). Oceanic anoxic events and plankton evolution: Biotic response to tectonic forcing during the mid-Cretaceous. *Paleoceanography,* **17**, 28pgs, doi: 10.1029/2001PA000623.

LePage, B.A. (2003). A new species of *Tsuga* (Pinaceae) from the middle Eocene of Axel Heiberg Island, Canada, and an assessment of the evolution and biogeographical history of the genus. *Botanical Journal of the Linnean Society*, **141**, 257-296.

Li, J., D.C. Christophel (2000). Systematic relationships within the *Litsea* complex (Lauraceae): a cladistic analysis on the basis of morphological and leaf cuticle data. *Australian Systematic Botany*, **13**, 1-13.

Lidgard, S., P.R. Crane (1988). Quantitative analyses of the early angiosperm radiation. *Nature,* **331**, 344-346.

Lidgard, S., P.R. Crane (1990). Angiosperm diversification and Cretaceous floristic trends: a comparison of palynofloras and leaf macrofloras. *Paleobiology,* **16**, 77-93.

Lücke, A., G.H. Schleser, B. Zolitschka, J.F.W. Negendank (2003). A Lateglacial and Holocene organic carbon isotope record of lacustrine palaeoproductivity and climatic change derived from varved lake sediments of Lake Holzmaar, Germany. *Quaternary Science Reviews*, **22**, 569-580.

Logan, G.A., J.J. Boon, G. Eglinton (1993). Structural biopolymer preservation in Miocene leaf fossils from the Clarkia site, northern Idaho. *Proceedings of the National Academy of Science, USA*, **90**, 2246-2250.

López-Bautista, J.M., D.A. Waters, R.L. Chapman (2002). The Trentepohliales revisited. *Constancea*, **83**, 23 pgs.

Lücking, R., A. Bernecker-Lücking (2005). Drip-tips do not impair the development of epiphyllous rain-forest lichen communities.

Journal of Tropical Ecology, **21**, 171-177, doi: 10.1017/S0266467404002093.

Lupia, R., S. Lidgard, P.R. Crane (1999). Comparing palynological abundance and diversity: implications for biotic replacement during Cretaceous angiosperm radiation. *Paleobiology,* **25**, 305-340.

Lyons, P.C., W.H. Orem, M. Mastalerz, E.L. Zodrow, A. Vieth-Redemann, R.M. Bustin (1995). $\delta^{13}C$ NMR, micro-FTIR and fluorescence spectra, and pyrolysis–gas chromatograms of coalified foliage of Late Carboniferous medullosan seed ferns, Nova Scotia, Canada: implications for coalification and chemotaxonomy. *International Journal of Coal Geology*, **27**, 227-248.

Ma, Q.W., C.S. Li (2002). Epidermal structures of *Sequoia sempervirens* (D. Don) Endl. (Taxodiaceae). *Taiwania*, **47**, 194-202.

Magallón, S. (2009). Flowering plants (Magnoliophyta). *In: The Timetree of Life,* Oxford University Press, Oxford, (Eds. Hedges, S.B., Kumar, S.).

Mahy, B.W.J., M.H.V. van Regenmortel (2010). Desk encyclopedia of Plant an Fungal Virology. *Academic Press, Elsevier*, Oxford, (Eds: B.W.J. Mahy and M.H.V. van Regenmortel), 587 pgs.

Mander, L., W.M. Kurschner, J.C. McElwain (2010). An explanation for conflicting records of Triassic-Jurassic plant diversity. *PNAS*, **107**, 15351-15356, doi: 10.1073/pnas.1004207107.

Manum, S.B., J.H.A. Van Konijnenburg-Van Cittert, V. Wilde (2000). *Tritaenia* Maegdefrau et Rudolf, Mesozoic '*Sciadopitys*-like' leaves in mass accumulations. *Review of Palaeobotany and Palynology*, **109**, 255-269.

Marrero, P., M. Nogales (2005). A microhistological survey on the trees of a relict subtropical laurel forest from the Macaronesian Islands as a base for assessing vertebrate plant diet. *Botanical Journal of the Linnean Society*, **148**, 409-426.

Maslin, M., Y. Malhi, O. Phillips, S. Cowling (2005). New views on an old forest: assessing the longevity, resilience, and future of the Amazon rainforest. *Transactions of the Institute of British Geographers*, **30**, 477-499.

Matsumoto, M., T. Ohsawa, M. Nishida (1995). *Tsuga shimokawaensis*, a new species of permineralised conifer leaves from the middle Miocene Shimokawa Group, Hokkaido, Japan. *Journal of Plant Research*, **108**, 417-428.

McCarroll, D., N.J. Loader (2004). Stable isotopes in tree rings. *Quaternary Science Reviews*, **23**, 771-801, doi: 10.1016/j.quascirev.2003.3.06.017.

McDowell, N.G., B.J. Bond, L.T. Dickman, M.G. Ryan, D. Whitehead (2011). Relationships between tree height and carbon isotope discrimination. *In: Size- and age-related changes in tree structure and function*, eds. F.C. Meinzer, B. Lachenbruch, T.E. Dawson, *Tree Physiology*, **4**, 255-286, doi: 10.1007/978-94-007-1242-3_10.

McElwain, J.C. (1998). Do fossil plants signal palaeoatmospheric CO_2 concentration in the geological past? *Philosophical Transactions of the Royal Society of London B*, **353**, 83-96.

McElwain, J.C., W.G. Chaloner (1995). Stomatal density and index of fossil plants track atmospheric carbon dioxide in the Palaeozoic. *Annals of Botany*, **76**, 389-395.

McElwain, J.C., D.J. Beerling, F.I. Woodward (1999). Fossil plants and global warming at the Triassic-Jurassic boundary. *Science,* **285**, 1386-1390.

McElwain, J.C., K.J. Willis, R. Lupia (2005). Cretaceous CO_2 decline and the radiation and diversification of angiosperms. *A History of Atmospheric CO_2 and its Effects on Plants, Animals and Ecosystems Ecological Studies,* **177**, 133-165.

McElwain, J.C., M.E. Popa, S.P. Hesselbo, M. Haworth, F. Surlyk (2007). Macroecological responses of terrestrial vegetation to climatic and atmospheric change across the Triassic/Jurassic boundary in East Greenland. *Paleobiology*, **33**, 547-573.

McElwain, J.C., T. Lawson (in press). A rise in maximum stomatal conductance facilitated the ecological radiation and diversification of angiosperms. *New Phytologist*.

Méhay, S., C.E. Keller, S.M. Bernasconi, H. Weissert, E. Erba, C. Bottini, P.A. Hochuli (2009). A volcanic CO_2 pulse triggered the Cretaceous Oceanic Anoxic Event 1a and a biocalcification crisis. *Geology*, **37**, 819-822.

Meyers, P.A. (1994). Preservation of elemental and isotopic source identification of sedimentary organic matter. *Chemical Geology*, **114**, 289-302.

Meyers, P.A., R. Ishiwatari (1993). Lacustrine organic geochemistry – an overview of indicators of organic matter sources and diagenesis in lake sediments. *Organic Geochemistry*, **20**, 867-900.

Midgley, J.J., W.J. Bond (1991). Ecological aspects of the rise of angiosperms: a challenge to the reproductive superiority hypotheses. *Biological Journal of the Linnean Society,* **44**, 81-92.

Mook, W.G. (2000). Environmental isotopes in the hydrological cycle: Principles and applications, Volume 1. *Technical Documents in Hydrology*, **39**, UNESCO, Paris, 271 pgs.

Moor, P.D. (1983). Plants and the palaeoatmosphere. *Journal of the Geological Society,* **140**, 13-25, doi: 10.1144/gsjgs.140.1.0013.

Myerscough, P.J., R.J. Whelan, R.A. Bradstock (2001). Ecology of the Proteaceae with special reference to the Sydney region. *Cunninghamia*, **6**, 951-1015.

Nagalingum, N.S., A.N. Drinnan, R. Lupia, S. McLoughlin (2002). Fern spore diversity and abundances in Australia during the Cretaceous. *Review of Paleobotany and Palynology,* **2431**, 1-24.

Narkhede, S.D., A.S. Khursel (2013). A fossil gymnospermous leaf *Gnetalophyllum deccanii* gen. et sp. Nov. from the Deccan intertrappean beds of Mohgaonkalan M.P., India. *Journal of Pharmacy and Biological Sciences*, **6**, 7-10.

Neustupa, J. (2003). The genus *Phycopeltis* (Trentepohliales, Chlorophyta) from tropical Southeast Asia. *Nova Hedwigia*, **76**, 487-505.

Nøhr-Hansen, H. (2005). Composition and distribution of Lower Cretaceous brackish water dinoflagellate cyst assemblages. *Palynology, Palaeolatitudes, Paleoaltitudes, Joint meeting APLF-TMS-LSPG,* Paris 3–7 October 2005 Abstract volume, pg. 87.

Norris, R.D., P.A. Wilson (1998). Low-latitude sea-surface temperatures for the mid-Cretaceous and the evolution of planktic foraminifera. *Geology*, **26**, 823-826, doi: 10.1130/0091-7613(1998)026<0823:LLSSTF>2.3.CO;2.

Nosova, N., E. Wcisło-Luraniec (2007). A reinterpretation of *Mirovia* Reymanówna (Coniferales) based on the reconsideration of the type species *Mirovia szaferi* Reymanówna from the Polish Jurassic. *Acta Palaeobotanica*, **47**, 359-377.

Nosova, N.V., A.I. Kiritchkova (2008). First records of the genus *Mirovia* Reymanówna (Miroviaceae, Coniferales) from the Lower Jurassics of Western Kazakhstan (Mangyshlak). *Paleontological journal*, **42**, 1383-1392.

O'Leary, M.H. (1981). Carbon isotope fractionation in plants. *Phytochemistry*, **20**, 553-567.

Ogg, J.G., L.A. Hinnov, C. Huang (2012). Chapter 27: Cretaceous, *In: The Geologic Time Scale 2012, (eds.) F. Gradstein, J. Ogg, M. Schmitz, G. Ogg, Elsevier, Volume 2,* 794-842, doi: 10.1016/B978-0-444-59425-9.00027-5.

Osborne, C.P., L. Sack (2012). Evolution of C4 plants: a new hypothesis for an interaction of CO_2 and water relations mediated by plant hydraulics. *Philosophical Transactions of The Royal Society, B,* **367**, 583-600.

Pagani, M., K.H. Freeman, M.A. Arthur (1999). Late Miocene atmospheric CO_2 concentrations and the expansion of C4 grasses. *Science*, **285**, 876-879.

Pallardy, S.G. (2008). Physiology of woody plants 3rd Edition. *Academic Press, Elsevier Inc. USA*, 464pgs, ISBN: 978-0-12-088765-1.

Passalia, M.G. (2009). Cretaceous pCO_2 estimation from stomatal frequency analysis of gymnosperm leaves of Patagonia, Argentina. *Palaeogeography, Palaeoclimatology, Palaeoecology,* **273**, 17-24, doi: 10.1016/j.palaeo.2008.11.010.

Patterson, W.A., K.J. Edwards, D.J. Maguire (1987). Microscopic charcoal as a fossil indicator of fire. *Quaternary Science Reviews*, **6**, 3-23.

Pavoine, S., J. Vallet, A. Dufour, S. Gachet, H. Daniel (2009). On the challenge of treating various types of variables: application for improving the measurement of functional diversity. *Oikos*, **118**, 391-402, doi: 10.1111/j.1600-0706.2008.166668.x.

Pearce, C.R., S.P. Hesselbo, A.L. Coe (2005). The mid-Oxfordian (Late Jurassic) positive carbon-isotope excursion recognised from fossil wood in the British Isles. *Palaeogeography, Palaeoclimatology, Palaeoecology*, **221**, 343-357.

Pearson, P.N., M.R. Palmer (2000). Atmospheric carbon dioxide concentrations over the past 60 million years. *Nature*, **406**, 695-699.

Pedersen, K.R., P.R. Crane, E.M. Friiss (1991). Fruits from the mid-Cretaceous of North America with pollen grains of the *Clavatipollenites* type. *Grana*, **30**, 577-590.

Pesacreta, T.C., K.H. Hasenstein (1999). The internal cuticle of *Cirsium horridulum* (Asteraceae) leaves. *American Journal of Botany*, **86**, 923-928.

Phipps, C.J., W.C. Rember (2004). Epiphyllous fungi from the Miocene of Clarkia, Idaho: reproductive structures. *Review of Palaeobotany and Palynology*, **129**, 67-79.

Pole, M. (2010). Cuticle morphology of Australasian Sapindaceae. *Botanical Journal of the Linnean Society*, **164**, 264-292

Poole, I., W.M. Kürschner (1999). Stomatal density and index: the practice. *In*: Fossil plants and spores: modern techniques, Geological Society London, 257-260, (*Eds)* Jones, T.P., Rowe, N.P.

Qiu, Y., J. Lee, F. Bernasconi-Quadroni, D.E. Soltis, P.S. Soltis, M. Zanis, E.A. Zimmer, Z. Chen, V. Savolainen, M.W. Chase (1999). The earliest angiosperms: evidence deom mitochrondrial, plastid and nuclear genomes. *Nature,* **402**, 404-407, doi: 10.1038/46536.

Rau, G.H., M.A. Arthur, W.E. Dean (1987). 15N/14N variations in Cretaceous Atlantic sedimentary sequences: implication for past changes in marine nitrogen biogeochemistry. *Earth and Planetary Science Letters,* **82**, 269-279.

Reichelt, K. (2005). Late Aptian-Albian of the Vocontian Basin (SE France) and Albian of NE Texas: biostratigraphic and paleoceanographic implications by planktic Foraminifera fauna. PhD thesis, Eberhard Karls Universität Tübingen.

Regal, P.J. (1977). Ecology and evolution of flowering plant dominance. *Science*, **196**, 622-629.

Retallack, G.J. (2001). A 300-million-year record of atmospheric carbon dioxide from fossil plant cuticles. *Nature*, **411**, 287-290.

Retallack, G.J., D.L. Dilcher (1981). A coastal hypothesis for the dispersal and rise to dominance of flower plants. In: *Paleobotany, Paleoecology, and Evolution* (ed. K.J. Niklas), Praeger Press, New York, 27-77.

Robinson, J.M. (1994). Speculations on carbon dioxide starvation, late Tertiary evolution of stomatal regulation and floristic modernization. *Plant Cell and Environment*, **17**, 1-10.

Robinson, S.A., J.E. Andrews, S.P. Hesselbo, J.D. Radley, P.F. Dennis, I.C. Harding, P. Allen (2002). Atmospheric pCO_2 and a dispositional environment from stable-isotope geochemistry of calcrete nodules (Barremian, Lower Cretaceous, Wealden Beds, England). *Journal of the Geological Society, London*, **159**, 215-224.

Robinson, S.A., S.P. Hesselbo (2004). Fossil-wood carbon-isotope stratigraphy of the non-marine Wealden Group (Lower Cretaceous, southern England). *Journal of the Geological Society, London*, **161**, 133-145.

Robinson, S.A., L.J. Clarke, A. Nederbragt, I.G. Wood (2008). Mid-Cretaceous oceanic anoxic events in the Pacific Ocean revealed by carbon-isotope stratigraphy of the Calera Limestone, California, USA. *Geological Society of America Bulletin,* **120**, 1416-1426, doi: 10.1130/B26350.1.

Romero, E.J., S. Archangelsky (1986). Early Cretaceous angiosperm leaves from southern South America. *Science*, **234**, 1580-1582.

Rost, F.W.D. (1995). Fluorescence Microscopy, Volume 2. Cambridge University Press, Cambridge, 473 pgs.

Rothman, D.H. (2002). Atmospheric carbon dioxide levels for the last 500 million years. *PNAS,* **99**, 4167-4171.

Rowher, J.G. (2000). Towards a phylogenetic classification of the Lauraceae: evidence from *mat*K sequences. *Systematic Botany*, **25**, 60-71.

Royer, D.L. (1999). Depth to pedogenic carbonate horizon as a paleoprecipitation indicator? *Geology*, **27**, 1123-1126, doi: 10.1130/0091-7613(1999)027<1123:DTPCHA>2.3.CO;2.

Royer, D.L., R.A. Berner, D.J. Beerling (2001). Phanerozoic atmospheric CO_2 change: evaluating geochemical and paleobiological approaches. *Earth-Science Reviews*, **54**, 349-392.

Royer, D.L., M. Pagani, D.J. Beerling (2012). Geobiological constraints on Earth system sensitivity to CO_2 during the Cretaceous and Cenozoic. *Geobiology*, **10**, 298-310, doi: 10.1111/j.1472-4669.2012.00320.x

Rundgren, M., D. Beerling (1999). A Holocene CO_2 record from the stomatal index of subfossil *Salix herbacea* L. leaves from northern Sweden. *The Holocene*, **9**, 509-513, doi: 10.1191/095968399677717287.

Runnegar, B. (1991). Nucleic acid and protein clocks. *Philosophical Transactions of the Royal Society of London B*, **333**, 391-397.

Ryberg, P.E., E.L. Taylor, T.N. Taylor (2007). Secondary phloem anatomy of *Cycadeoidea* (Bennettitales). *American Journal of Botany*, **94**, 791-798.

Salisbury, E.J. (1927). On the causes and ecological significance of stomatal frequency, with special reference to the woodland flora. *Philosophical Transactions of the Royal Society London B*, **216**, 1-65.

Sageman, B.B., S.R. Meyers, M.A. Arthur (2006). Orbital time scale and new C-isotope record for Cenomanian-Turonian boundary stratotype. *Geology*, **34**, 125-128, doi: 10.1130/G22074.1.

Saraçli, S., N. Doğan, İ. Doğan (2013). Comparison of hierarchical cluster analysis methods by cophenetic correlation. *Journal of Inequalities and Applications,* **203**, 8 pgs, doi: 10.1186/1029-242X-2013-203.

Schirone, B., R.C. Ferreira, F. Vessella, A. Schirone, R. Piredda, M.C. Simeone (2010). *Taxus baccata* in the Azores: a relict form at risk of imminent extinction. *Biodiversity Conservation*, doi: 10.1007/s10531-010-9786-0, 19 pgs.

Schlanger, S.O., H.C. Jenkyns (1976). Cretaceous oceanic anoxic events: causes and consequences. *Geologie en Mijnbouw,* **55**, 179-184.

Schouten, S., M. Woltering, W.I.C. Rijpstra, A. Sluijs, H. Brinkhuis, J.S. Sinninghe Damsté (2007). The Paleocene-Eocene carbon isotope excursion in higher plant organic matter: Differential fractionation of angiosperms and conifers in the Arctic. *Earth and Planetary Science Letters*, **258**, 581-592, doi: 10.1016/j.epsl.2007.04.024.

Schubert, B.A., A.H. Jahren (2012). The effect of atmospheric CO_2 concentration on carbon isotope fractionation in C3 land plants. *Geochimica et Cosmochimica Acta*, **96**, 29-43, doi: 10.1016/j.gca.2012.08.003.

Scotese, C.R. (1991). Jurassic and Cretaceous plate tectonic reconstructions. *Palaeogeography, Palaeoclimatology, Palaeoecology,* **87**, 493-501.

Scott, R.A., C.J. Smiley (1979). Some Cretaceous plant megafossils and microfossils from the Nanushuk Group, Northern Alaska: a preliminary report. *Circular of the United States Geological Survey*, **795**, 89-117.

Scott, A.C. (2009). Forest fire in the fossil record. *In: (Eds.) A. Cerdà, P.R. Robichaud, Fire effects on soils and resoration strategies,* Science Publishers, New Hampshire, 1-40.

Scott, A.C., D.M.J.S. Bowman, W.J. Bond, S.J. Pyne, M.E. Alexander (2014). Fire on Earth:

An introduction. Wiley & Sons, Ltd., West Sussex, UK, ISBN: 978-1-119-95356-2.

Seward, A.C. (1927). The Cretaceous plant-bearing rocks of western Greenland. *Philosophical Transactions of the Royal Society of London, Series B*, **215**, 57–175.

Seward, A.C., V.M. Conway (1935). Additional Cretaceous plants from western Greenland. *Kungliga Svenska Vetenskaps-Akade-miens Handlingar*, **15**, 51 pgs.

Seward, A.C., V.M. Conway (1939). Fossil plants from Kingigtoq and Kagdlunguak, West Greenland. *Meddelelser om Grønland*, **93**, 41 pgs.

Shao-Lin, Z., Z. Wu (1986). The cuticle of two fossil cycads and epiphytic fungi. *Acta Botanica Sinica*, **28**, 427-436.

Sherwood-Pike, M., J. Gray (1988). Fossil leaf-inhabiting fungi from northern Idaho and their ecological significance. *Mycologia*, **80**, 14-22.

Sincock, C.A., J. Watson (1988). Terminology used in the description of bennettitalean cuticle characters. *Botanical Journal of the Linnean Society*, **97**, 179-187.

Smith, A.G., D.G. Smith, B.M. Funnel (1994). Atlas of Mesozoic and Cenozoic coastlines. Cambridge University Press, Cambridge, 99 pages.

Smith, R.Y., D.R. Greenwood, J.F. Basinger (2010). Estimating palaeoatmospheric pCO_2 during the Early Eocene Climatic Optimum from stomatal frequency of *Ginkgo*, Okanagan Highlands, British Columbia, Canada. *Palaeogeography, Palaeoclimatology, Palaeoecology*, **293**, 120-131, doi: 10.1016/j.palaeo.2010.05.006.

Spicer, R.A. (1991). Plant taphonomic processes. *In: Topics in Geobiology*, **9**, Plenum Press, New York, 71-113 (Eds. Allison, P.A., Briggs, D.E.G.).

Spicer, R.A., A.B. Herman, A.T. Ahlberg, M.I. Raikevich, P.M.A. Rees (2002). Mid-Cretaceous Grebenka flora of Northeastern Russia: stratigraphy, palaeobotany, taphonomy and palaeoenvironment. *Palaeogeography, Palaeoclimatology, Palaeoecology*, **184**, 65-105.

Spiker, E.C., P.G. Hatcher (1987). The effects of early diagenesis on the chemical and stable carbon isotopic composition of wood. *Geochimica et Cosmochimica Acta*, **51**, 1385-1391.

Spjut, R.W. (2007). A phytogeographical analysis of *Taxus* (Taxacea) based on leaf anatomical characters. *Journal of the Botanical Research Institude*, **1**, 291-332.

Stebbins, G.L. (1981). Why are there so many species of flowering plants? *Bioscience,* **31**, 573-577.

Steinthorsdottir, M., F.I. Woodward, F. Surlyk, J. C. McElwain (2012). Deep-time evidence of a link between elevated CO_2 conditions and perturbations in the hydrological cycle via drop in plant transpiration. *Geology*, 4pgs, doi: 10.1130/G33334.1.

Stockey, R.A., T.N. Taylor (1978). Cuticular features and epidermal patterns in the genus *Araucaria* de Jussieu. *Botanical Gazette*, **139**, 490-498.

Stockey, R.A., H. Ko (1988). Cuticle micromorphology of some new Caledonian Podocarps. *Botanical Gazette*, **149**, 240-252.

Stull, G.W., W.A. DiMichele, H.J. Falcon-Lang, W.J. Nelson, S. Elrick (2012). Palaeoecology of *Macroneuropteris scheuchzeri*, and its implications for resolving the paradox of 'xeromorphic' plants in Pennsylvanian wetlands. *Palaeogeography, Palaeoclimatology, Palaeoecology*, **331**, 162-176.

Suarez, M.B.L.A. González. G.A. Ludvigson (2011). Quantification of a greenhouse hydrologic cycle from equatorial to polar latitudes: The mid-Cretaceous water bearer revisited. *Palaeogeography, Palaeoclimatology, Palaeoecology,* **307**, 301-312, doi: 10.1016/j.palaeo.2011.05.027.

Sun, G., M.A. Akimetiev, L. Golovneva, E. Bugdaeva, C. Quan, T.M. Kodrul, H. Nishida, Y. Sun, C. Sun, K. Johnson, D. Dilcher (2008). Late Cretaceous plants from Jiayin along

Heilongjiang River, Northeast China. *Courier Forschungsinstitut Senckenberg*, **258**, 75-83.

Tajika, E. (1998). Climate change during the last 150 million years: reconstruction from a carbon cycle model. *Earth and Planetary Science Letters,* **160**, 695-707.

Tajika, E. (1999). Carbon cycle and climate change during the Cretaceous inferred from a biogeochemical carbon cycle model. *The Island Arc*, **8**, 293-303.

Talbot, M.R., T. Johannessen (1992). A high resolution palaeoclimatic record for the last 27,500 years in tropical West Africa from the carbon and nitrogen isotopic composition of lacustrine organic matter. *Earth and Planetary Science Letters*, **110**, 23-37.

Tappan, H. (1980). The Paleobiology of plant protists, W.H. Freeman, San Francisco.

Tarduno, J.A., W.V. Sliter, L. Kroenke, M. Leckie, H. Mayer, J.J. Mahoney, R. Musgrave, M. Storey, E.L. Winterer (1991). Rapid formation of the Ontong Java Plateau by Aptian mantle plume volcanism. *Science,* **18**, 399-403.

Taylor, D.W., L.J. Hickey (1992). Phylogenetic evidence for the herbaceous origin of angiosperms. *Plant Systematics and Evolution,* **180**, 137-156.

Taylor, T.N., E.L. Taylor, M. Krings (2009). Paleobotany: The biology and evolution of fossil plants. *Elsevier Academic Press*, *USA,* 1230 pgs.

Tegelaar, E.W., H. Kerp, H. Visscher, P.A. Schenck, J.W. de Leeuw (1991). Bias of the paleobotanical record as a consequence of variation in the chemical composition of higher vascular plants cuticiles. *Paleobiology*, **17**, 133-144.

Tejada, M.L.G., K. Suzuki, J. Kuroda, R. Coccioni, J.J. Mahoney, N. Okouchi, T. Sakamoto, Y. Tatsumi (2009). *Geology*, **37**, 855-858, doi: 10.1130/G25763A.1.

Teslenko, Y.V. (1967). Some aspects of evolution of terrestrial plants. *Geologia I Geofizica (Novosibirsk),* **11**, 58-64.

Thornton, S.F., J. McManus (1994). Application of organic carbon and nitrogen stable isotopes and C/N rations as source indicators of organic matter provenance in estuarine systems: Evidence from the Tay Estuary, Scotland. *Estuarine, Coastal and Shelf Science*, **38**, 219-233.

Thurow, J., R. Littke, P. Meyers (1992). The Cenomanian/Turonian boundary event in the Indian Ocean – a key to understand the global picture. *Geophysical monograph,* **70**, 253-273.

Tieszen, L.L. (1991). Natural variations in the carbon isotope values of plants: Implications for archaeology, ecology and paleoecology. *Journal of Archaeological Science*, **18**, 227-248.

Tripathi, A. (2001). Fungal remains from Early Cretaceous Intertrappean Beds of Rajmahal Formation in Rajmahal Basin, India. *Cretaceous Research*, **22**, 565-574.

Tripp, E.A., L.A. McDade (2014). Time-calibrated phylogeny of Acanthaceae (Lamiales) A rich fossil record yields calibrated phylogeny for Acanthaceae (Lamiales) and evidence for marked biases in timing and directionality of intercontinental disjunctions. *Systematic Biology*, accepted manuscript April 2014, doi: 10.1093/sysbio/syu029.

Truswell, E.M. (1990). Cretaceous and Tertiary vegetation of Antarctica: a palynological perspective. In: *Antarctic Palaeobiology*, eds. Taylor, T.N., Taylor, E.L., 71-88, doi: 10.1007/978-1-4612-3238-4_7.

Tsikos, H., V. Karakitsios, Y. van Breugel, B. Walsworth-Bell, L. Bombardiere, M.R. Petrizzo, J.S. Sinninghe Damsté, S. Schouten, E. Erba, I. Premoli. Silva, P. Farrimond, R.V. Tyson, H.C. Jenkyns (2004). Organic-carbon deposition in the Cretaceous of the Ionian Basin, NW Greece: the Paquier Event (OAE 1b) revisited. *Geological Magazine*, **141**, 401-416.

Turner, G.W., J. Gershenzon, R.B. Croteau (2000). Distribution of peltate glandular trichomes on developing leaves of peppermint. *Plant Physiology*, **124**, 655-664.

Ufnar, D.F., G.A. Ludvigson, L. González; D.R. Gröcke (2008). Precipitation rates and atmospheric heat transport during the Cenomanian warming in North America: Estimates from a stable isotope mass-balance model. *Palaeogeography, Palaeoclimatology, Palaeoecology*, **266**, 28-38.

Urban, M.A., D.M. Nelson, G. Jiménez-Moreno, J. Châteauneuf, A. Pearson, F.S. Hu (2010). Isotopic evidence of C4 grasses in southwestern Europe during the Early Oligocene-Middle Miocene. *Geology*, **38**, 1091-1094, doi: 10.1130/G31117.1.

van Breugel, Y., S. Schouten, H. Tsikos, E. Erba, G.D. Price, J.S. Sinninghe Damsté (2007). Synchronous negative carbon isotope shifts in marine and terrestrial biomarkers at the onset of the early Aptian oceanic anoxic event 1a: Evidence for the release of 13C-depleted carbon into the atmosphere. *Paleoceanography,* **22**, 13 pgs., doi: 10.1029/2006PA001341.

Van Gijzel, P. (1979). Manual of the techniques and some geological applications of fluorescence microscopy. *American Association of Stratigraphic Palynologists*, **12**, Annual Meeting, Dallas, 55 pgs.

Vigran, J.O. (1970). Fragments of a middle Jurassic Flora from Northern Trøndelag, Norway. *Norsk Geologisk Tidsskrift*, **50**, 193-214.

Vogel, J.C. (1993). Variability of carbon isotope fractionation during photosynthesis. *In: Stable Isotopes and Plant Carbon-water Relations*, eds. J.R. Ehleringer, A.E. Hall, G.D. Farquhar, Academic Press Ltd., London, 555pgs.

von Caemmerer, S., J.R. Evans (1991). Determination of the average partial pressure of CO_2 in chloroplasts from leaves of several C3 plants. *Australian Journal of Plant Physiology*, **18**, 287-306.

Wagner, T., K. Wallman, J.O. Herrle, P. Hofmann, I. Stuesser (2007). Consequences of moderate ~25,000 yr lasting emission of light CO_2 into the mid-Cretaceous ocean. *Earth and Planetary Science Letters,* **259**, 200-211.

Wang, L., A.W. Mackay, M.J. Leng, P. Rioual, V.N. Panizzo, H. Lu, Z. Gu, G. Chu, J. Han, C.P. Kendrick (2013). Influence of the ratio of planktonic to benthic diatoms on lacustrine organic matter $\delta^{13}C$ from Erlongwan maar lake, northeast China. *Organic Geochemistry*, **54**, 62-68.

Watson, J. (1977). Some Lower Cretaceous conifers of the Cheirolepidiaceae from the USA and England. *Palaeontology*, **20**, 715-749.

Watson, J. (1988). The Cheirolepidiaceae, *in: Origin and Evolution of Gymnosperms*, Columbia University Press, New York, (Ed.) Beck, C.B., 383-447.

Watson, J., K.L. Alvin (1996). An English Wealden floral list, with comments on possible environmental indicators. *Cretaceous Research*, **17**, 5-26.

Watson, J., S.J. Lydon, N.A. Harrison (2001). A revision of the English Wealden Flora, III: Czekanowskiales, Ginkgoales and allied Coniferales. *Bulleting of the Natural History Museum, London (Geology)*, **57**, 29-82.

Watson, J., S.J. Lydon (2004). The Bennettitalean trunk genera *Cycadeoidea* and *Monanthesia* in the Purbeck, Wealden and Lower Greensand of southern England: a reassessment. *Cretaceous Research*, **25**, 1-26.

Weissert, H., E. Erba (2004). Volcanism, CO_2 and palaeoclimate: a Late Jurassic-Early Cretaceous carbon an oxygen isotope record. *Journal of the Geological Society, London,* **161**, 1-8.

Wellman, C.H., L. Axe, L. (1999). Extracting plant mesofossils and megafossils by bulk acid maceration. *In: Fossil plants and spores; modern techniques*, Eds.: T.P. Jones, N.P. Rowe, The Geological Society, London, 11-14.

Willis, K.J., J.C. McElwain (2014). The evolution of plants, second edition, Oxford University Press, Oxford.

Wilson, P.A., R.D. Norris (2001). Warm tropical ocean surface and global anoxia during the mid-Cretaceous period. *Nature*, **412**, 425-429.

Wing, S.L., L.D. Boucher (1998). Ecological aspects of the Cretaceous flowering plant radiation. *Annual Reviews of Earth and Planetary Science,* **26**, 379-421.

Wolf, F.A. (1930). A parasitic alga, *Cephaleuros virescens* Kunze, on citrus and certain other plants. *Journal of Elisha Mitchell Scientific Society*, **44**, 187-205.

Woodward, F.I. (1987). Stomatal numbers are sensitive to increases in CO_2 from pre-industrial levels. *Nature*, **327**, 617-618.

Woodward, F.I., F.A. Bazzaz (1988). The responses of stomatal density to CO_2 partial pressure. *Journal of Experimental Botany*, **39**, 1771–1781.

Worobiec, G., E. Worobiec (2013). Epiphyllous fungi from the Oligocene shallow-marine deposits of the Krabbedalen Formation, Kap Brewster, central East Greenland. *Acta Palaeobotanica*, **53**, 165-179, doi: 10.2478/acpa-2013-0014.

Wuchter, C., S. Schouten, M.J.L. Coolen, J.S. Sinninghe Damsté (2004). Temperature-dependent variation in the distribution of tetraether membrane lipids of marine Crenarchaeota: Implications for TEX_{86} paleothermometry. *Paleoceanography,* **19**, 10pgs, doi: 10.1029/2004PA001041.

Yang, X-J., G. Guignard, F. Thévenard, Y-D. Wang, G. Barale (2009). Leaf cuticle ultrastructure of *Pseudofrenelopsis dalatzensis* (Chow et Tsao) Cao ex Zhou (Cheirolepidiaceae) from the Lower Cretaceous Dalazi Formation of Jilin, China. *Review of Palaeobotany and Palynology*, **153**, 8-18.

Yeung, E.C. (1998). A beginner's guide to the study of plant structure. *In: Tested studies for laboratory teaching*, **19**,Ed. S.J. Karcher, Proceedings of the 19th Workshop/Conference of the Association for Biology Laboratory Education (ABLE), 125-142.

Zeebe, R.E. (2012). History of seawater carbonate chemistry, atmospheric CO_2 and ocean acidification. *Annual Reviews of Earth and Planetary Sciences,* **40**, 141-165, doi: 10.1146/annurev-earth-042711-105521.

ZiKun, J., W. YongDong, Z. ShaoLin, Z. Wu, T. Ning (2012). Occurrence of *Sciadopitys*-like fossil wood (Coniferales) in the Jurassica of western Liaoning and its evolutionary implications. *Chinese Science Bulletetin*, **57**, 569-572, doi: 10.1007/s11434-011-4850-z.

Appendix A: Field data

- Figure i: summary stratigraphic sections with depositional environment of Late Cretaceous to Palaeogene sediments across West Greenland from Dam *et al.* (2009). Sections presented in an approximate transect (exact locations numbered with references within Dam et al.) from Svarten-Halvø, across the Nuussuaq Peninsula, to sections across the Isle of Disko further south. Depositional environment is colour-coded, and the lithology and fossil distribution and type indicated by symbols.

- Figure ii: Graphic logs for all stratigraphic sections drawn from field notes and includes lithological information detailed in the key, grain size, approximate colour, additional notes made on the field logs and bulk, lithology and fossil wood sample horizons plotted against section stratigraphic height.

- Table A: list of fossil samples collected from Richard Barclay's field notes, listing the sample labels with equivalent location to the stratigraphic sections or Boyd's locality, and includes first observations on possible species present in the sample.

Figure i

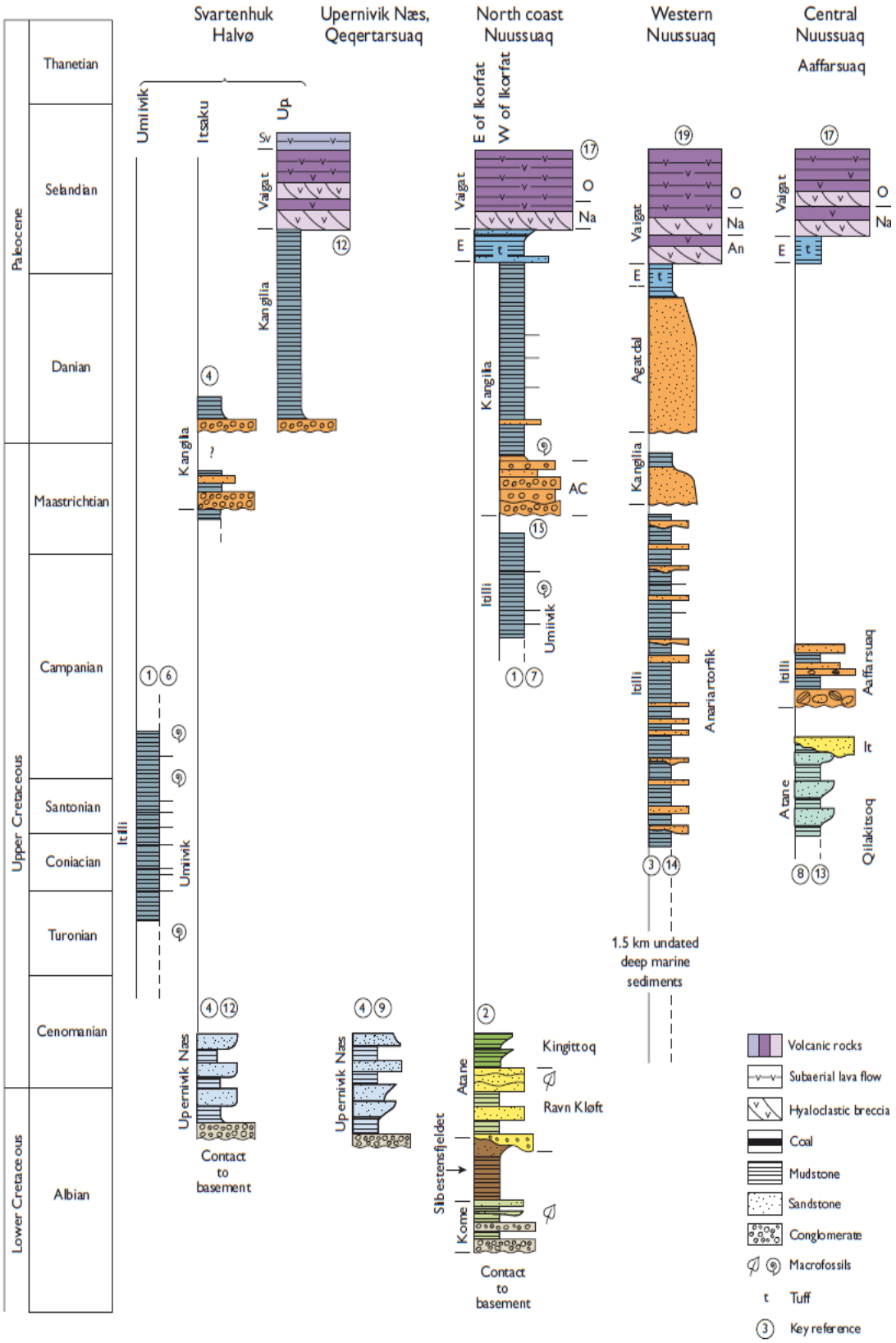
Svartenhuk Halvø
Upernivik Næs, Qeqertarsuaq
North coast Nuussuaq
Western Nuussuaq
Central Nuussuaq
Aaffarsuaq
Thanetian
Selandian
Danian
Maastrichtian
Campanian
Santonian
Coniacian
Turonian
Cenomanian
Albian
Paleocene
Upper Cretaceous
Lower Cretaceous
Umiivik
Itsaku
Up.
Sv
Vaigat
Kangilia
Itilli
Umiivik
Upernivik Næs
Contact to basement
E of Ikorfat
W of Ikorfat
O
Na
An
E
AC
Agatdal
Anariartorfik
1.5 km undated deep marine sediments
Aaffarsuaq
Atane
It
Qilakitsoq
Kingittoq
Ravn Kløft
Sibestensfjeldet
Kome
Volcanic rocks
Subaerial lava flow
Hyaloclastic breccia
Coal
Mudstone
Sandstone
Conglomerate
Macrofossils
Tuff
Key reference

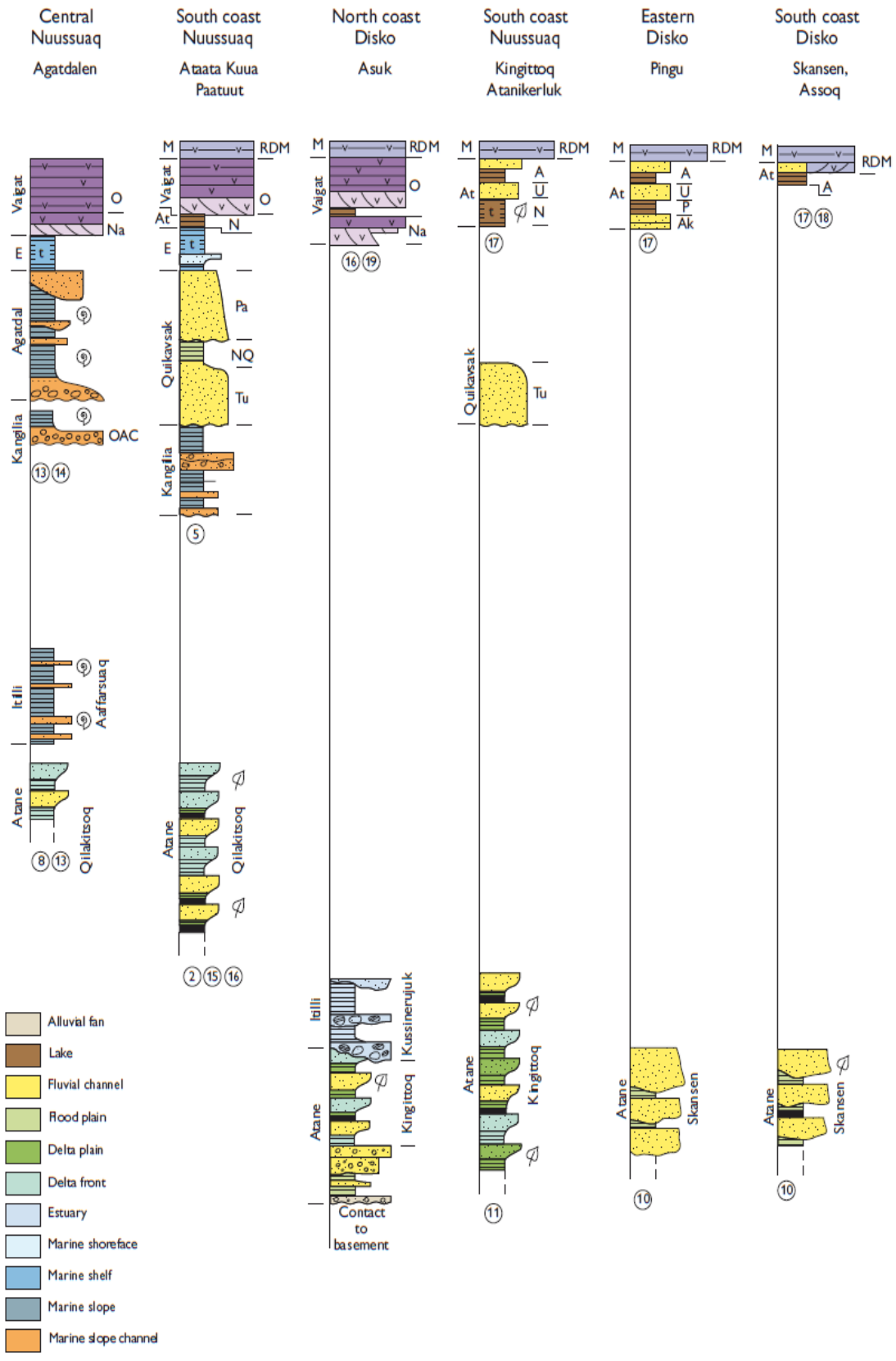
Central Nuussuaq
Agatdalen
South coast Nuussuaq
Ataata Kuua Paatuut
North coast Disko
Asuk
South coast Nuussuaq
Kingittoq Atanikerluk
Eastern Disko
Pingu
South coast Disko
Skansen, Assoq
Vaigat
Agatdal
Kanglilia
Itilli
Atane
Qilakitsoq
Aaffarsuaq
Quikavsak
Kanglia
Kussinerujuk
Kingittoq
Skansen
Contact to basement
M
RDM
At
E
O
Na
OAC
N
Pa
NQ
Tu
A
U
P
Ak
Alluvial fan
Lake
Fluvial channel
Flood plain
Delta plain
Delta front
Estuary
Marine shoreface
Marine shelf
Marine slope
Marine slope channel

LK Section (part 1)

Figure ii

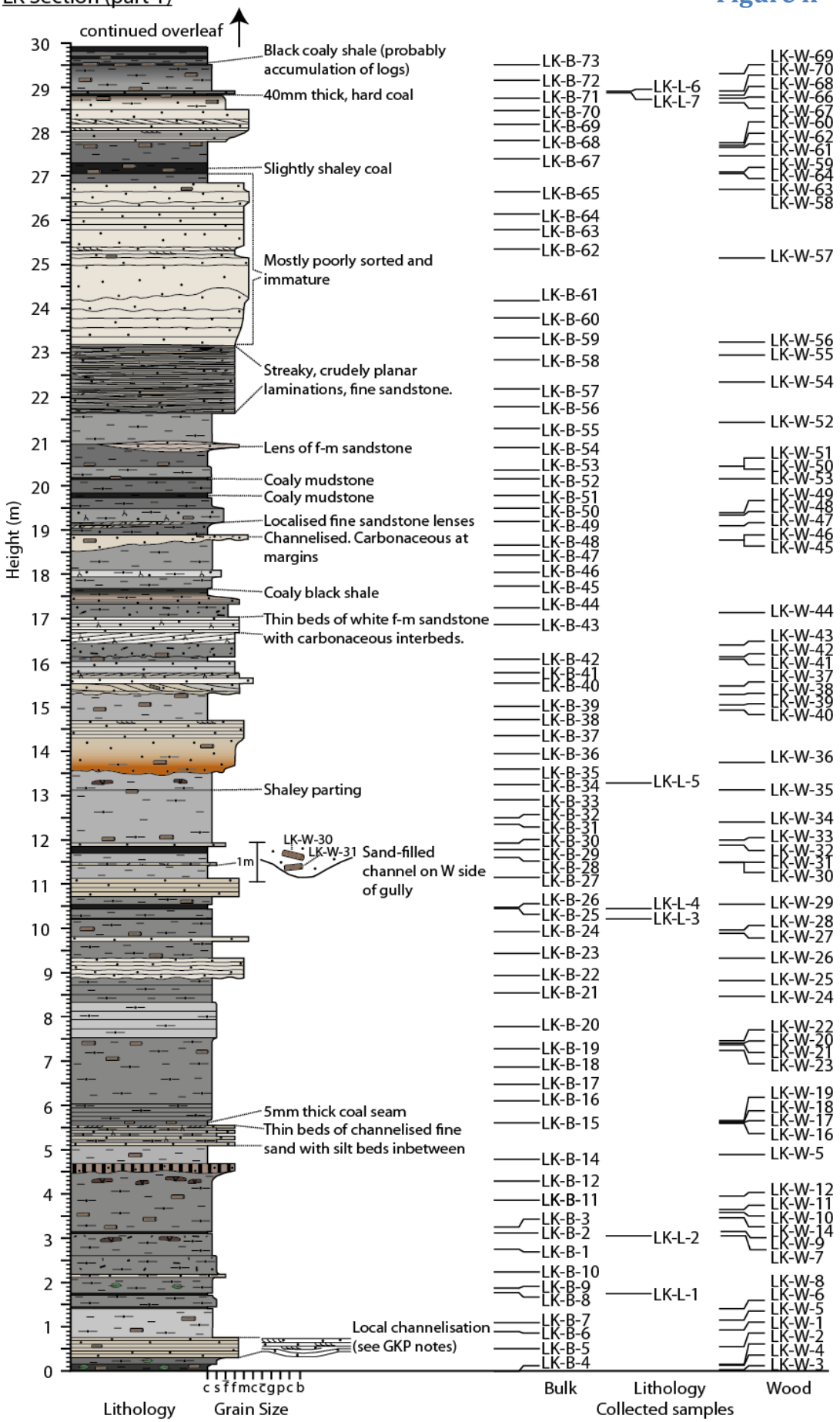

Graphic Log Key

Lithology

- Clay
- Silt
- Sand
- Coarse sand
- Siderite nodules
- Cemented sediment
- Weathering

Bedding

- Parallel bedding/laminations
- Cross-bedding
- Irregular bedding
- Flaggy bedding
- Wave-ripples/wavy bedding
- Current-ripples
- Lens/dicontinuous bedding

Organic Material

- Fossil wood fragment
- Carbonaceous fragments
- Fossil leaf - fern
- Fossil leaf - angiosperm
- Equisitites
- Rootlets
- Coal

Little Kussinikassaq (LK Section part 2)

27/07/2009 - 29/07/2009

Detailed section from stream West of Kussinikassaq named 'Little Kussinikassaq'. Starts with Kome Fm in good exposures on E and W of stream. There are good exposures of transitions into Slibestensfjeldet Fm, but faults cut up the latter formation so a complete section cannot be measured.

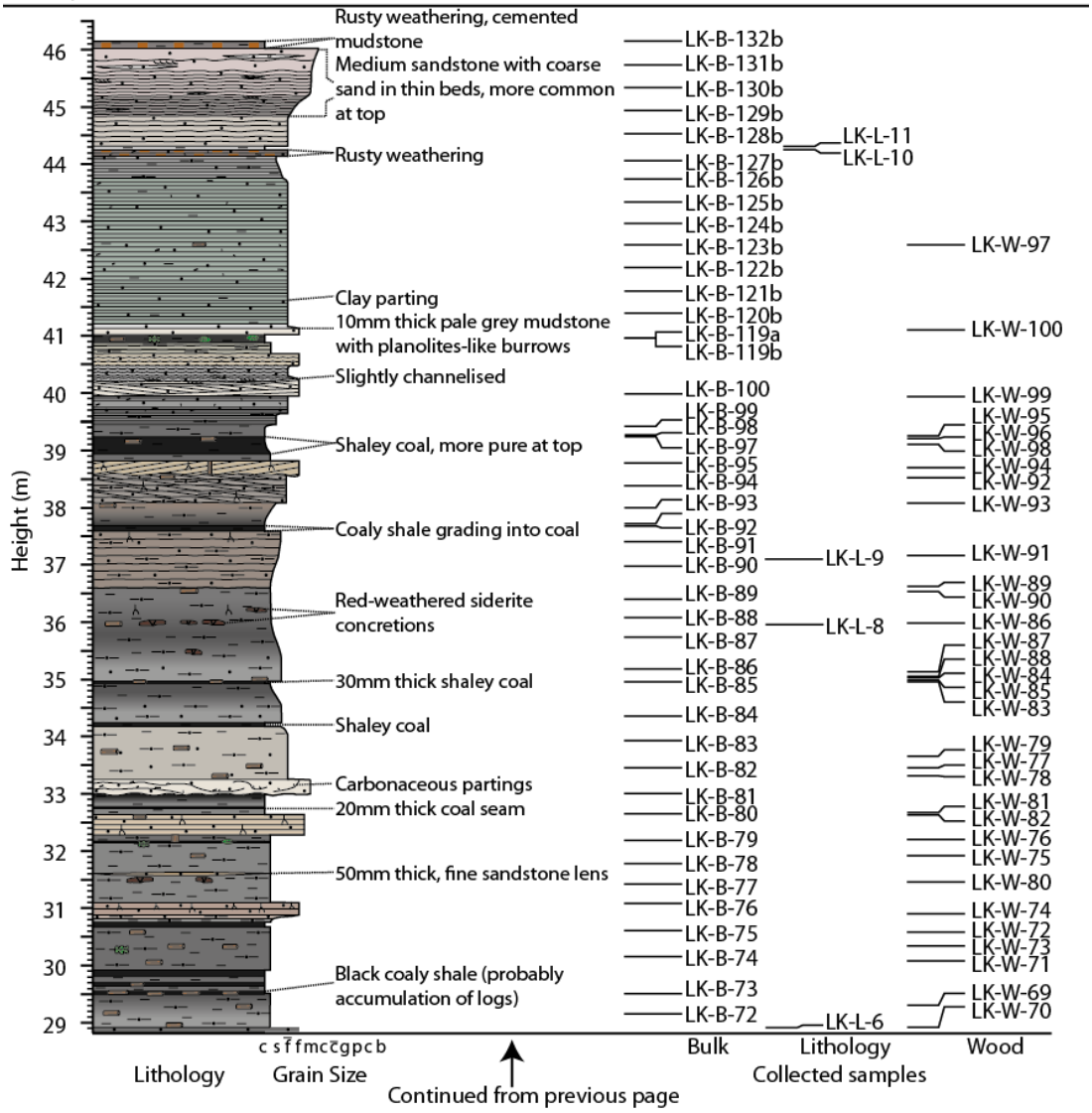

KK Section (part 1)

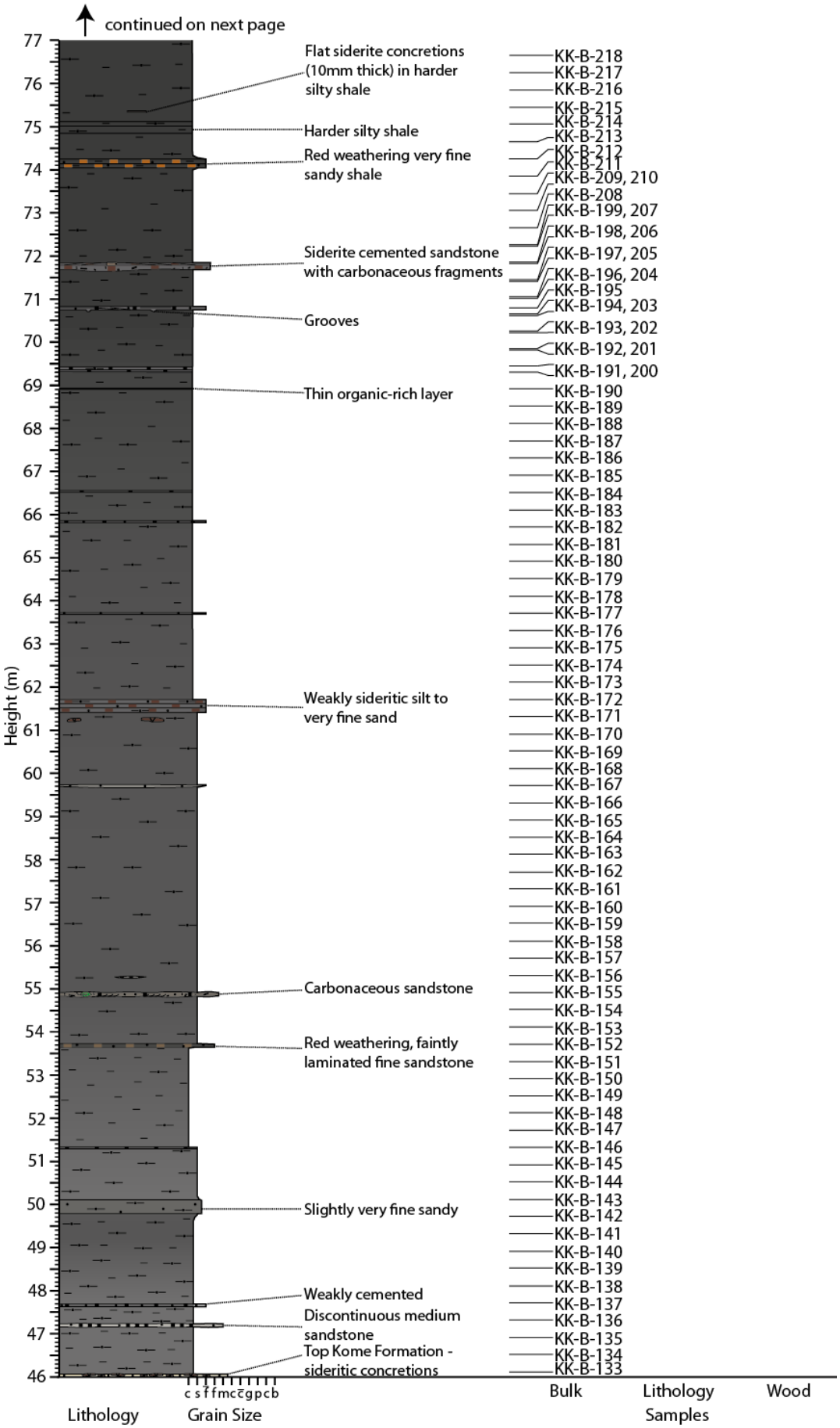

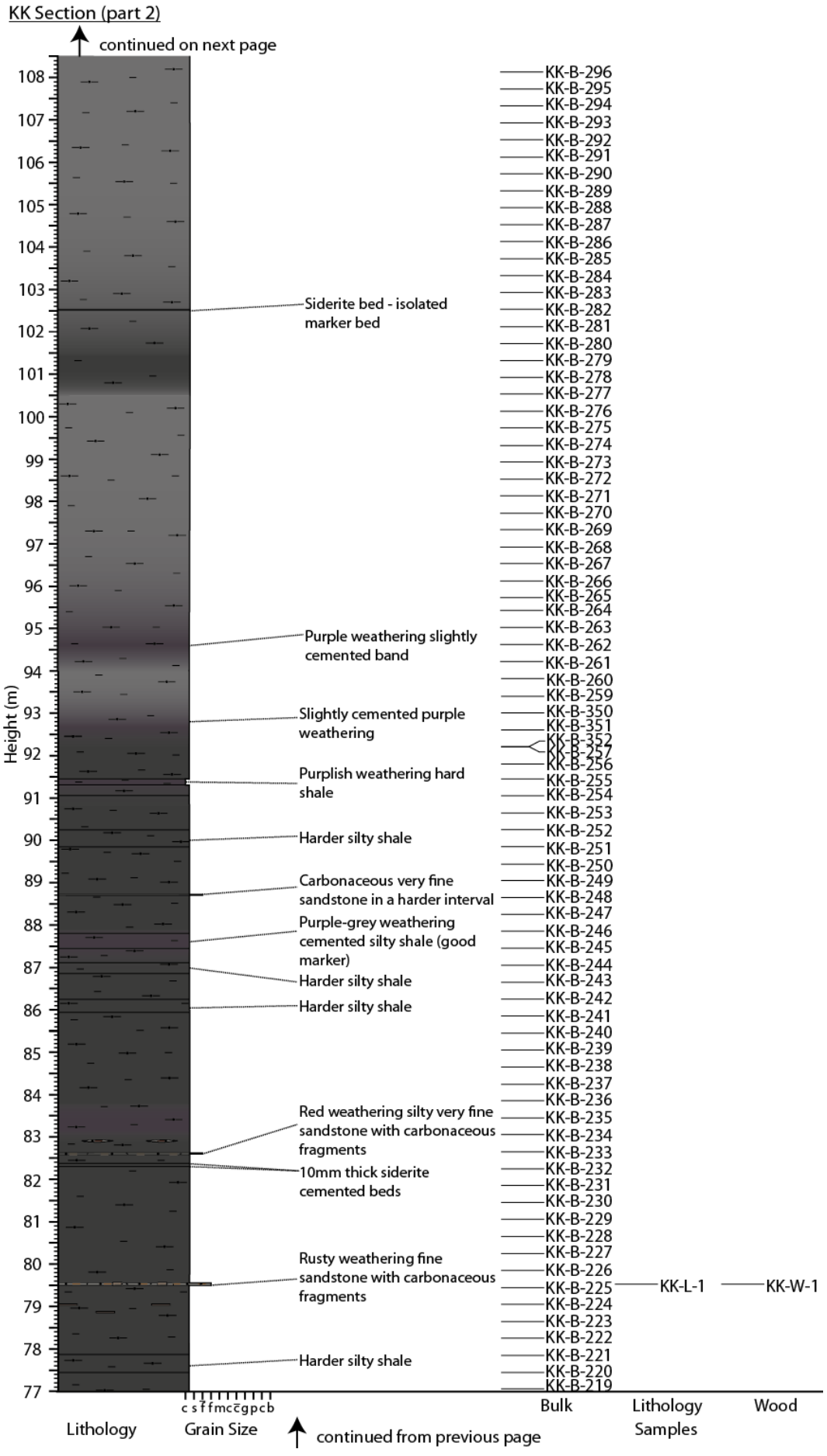
KK Section (part 2)
continued on next page
Height (m)
108
107
106
105
104
103
102
101
100
99
98
97
96
95
94
93
92
91
90
89
88
87
86
85
84
83
82
81
80
79
78
77
Siderite bed - isolated marker bed
Purple weathering slightly cemented band
Slightly cemented purple weathering
Purplish weathering hard shale
Harder silty shale
Carbonaceous very fine sandstone in a harder interval
Purple-grey weathering cemented silty shale (good marker)
Harder silty shale
Harder silty shale
Red weathering silty very fine sandstone with carbonaceous fragments
10mm thick siderite cemented beds
Rusty weathering fine sandstone with carbonaceous fragments
Harder silty shale
KK-B-296
KK-B-295
KK-B-294
KK-B-293
KK-B-292
KK-B-291
KK-B-290
KK-B-289
KK-B-288
KK-B-287
KK-B-286
KK-B-285
KK-B-284
KK-B-283
KK-B-282
KK-B-281
KK-B-280
KK-B-279
KK-B-278
KK-B-277
KK-B-276
KK-B-275
KK-B-274
KK-B-273
KK-B-272
KK-B-271
KK-B-270
KK-B-269
KK-B-268
KK-B-267
KK-B-266
KK-B-265
KK-B-264
KK-B-263
KK-B-262
KK-B-261
KK-B-260
KK-B-259
KK-B-350
KK-B-351
KK-B-352
KK-B-257
KK-B-256
KK-B-255
KK-B-254
KK-B-253
KK-B-252
KK-B-251
KK-B-250
KK-B-249
KK-B-248
KK-B-247
KK-B-246
KK-B-245
KK-B-244
KK-B-243
KK-B-242
KK-B-241
KK-B-240
KK-B-239
KK-B-238
KK-B-237
KK-B-236
KK-B-235
KK-B-234
KK-B-233
KK-B-232
KK-B-231
KK-B-230
KK-B-229
KK-B-228
KK-B-227
KK-B-226
KK-B-225
KK-B-224
KK-B-223
KK-B-222
KK-B-221
KK-B-220
KK-B-219
KK-L-1
KK-W-1
c s f f m c c̄ g p c b
Lithology
Grain Size
Bulk
Lithology Samples
Wood
continued from previous page

KK Section (part 3)

Kussinikassaq (KK)
Stratigraphic Height 46.07-72.22m
Location: 70°46'02.3"N 53°03'24.8"W

Stratigraphic Height 69.34-92.21m
Location: 70°76'61.5"N 53°05'78.1"W
Elevation (GPS) 104 ± 6m

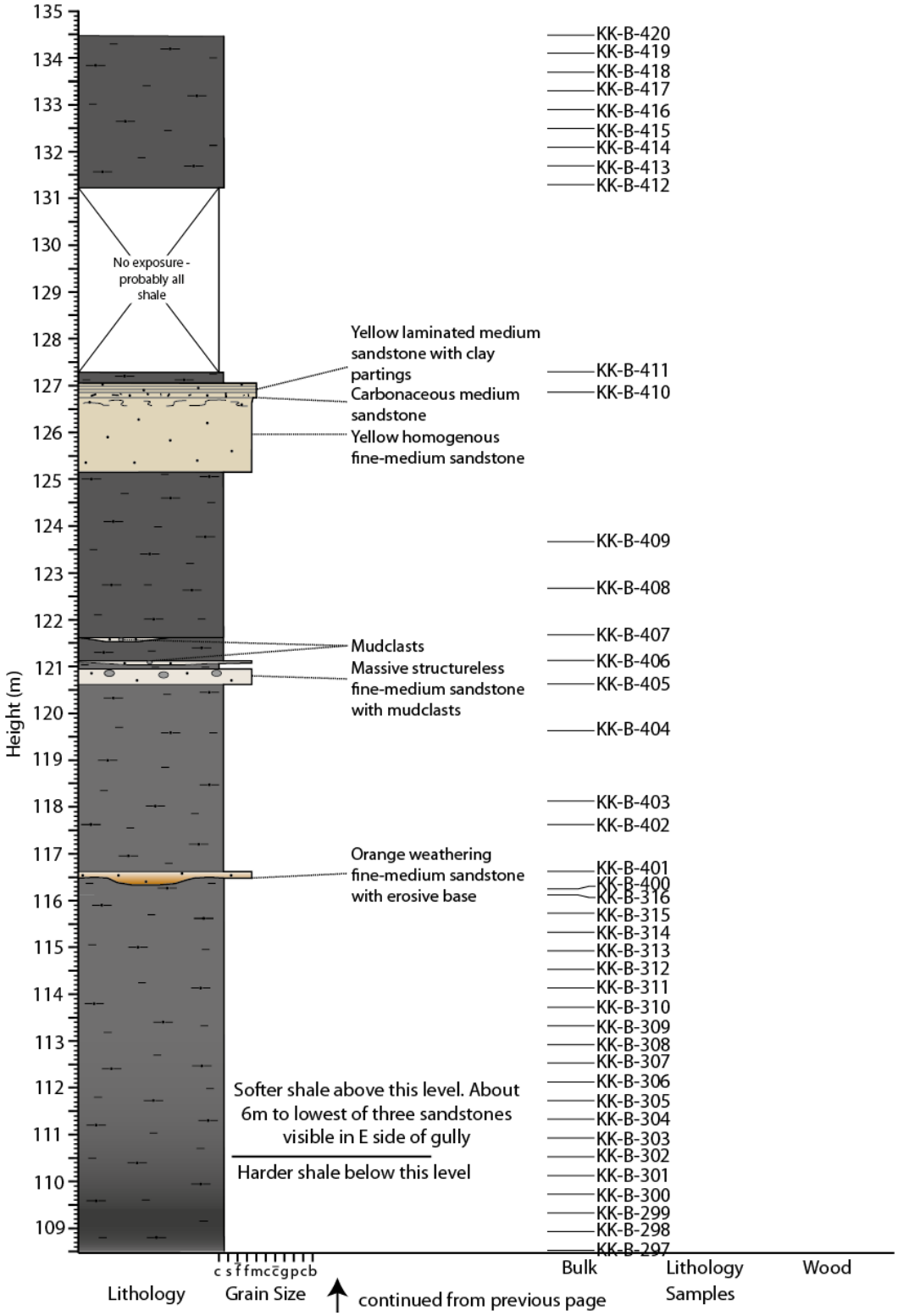

ANE Section (part 1)

continued on next page

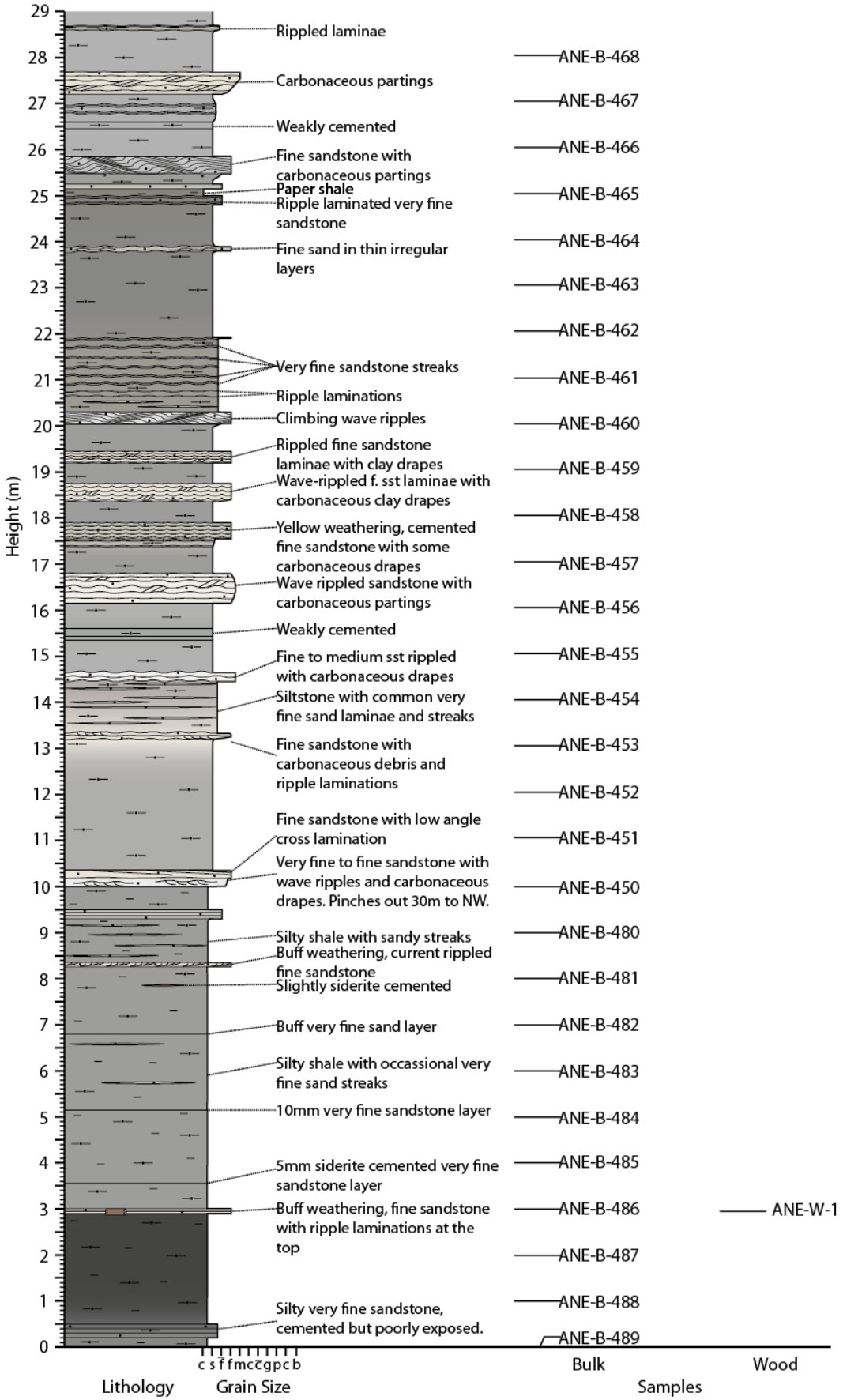

ANE Section (part 2)

Angiarsuit East (ANE) 03/08/2009 - 04/08/2009

0-10m West side of Angiarsuit East Gully. 10m to top = East side of Angiarsuit East Gully.

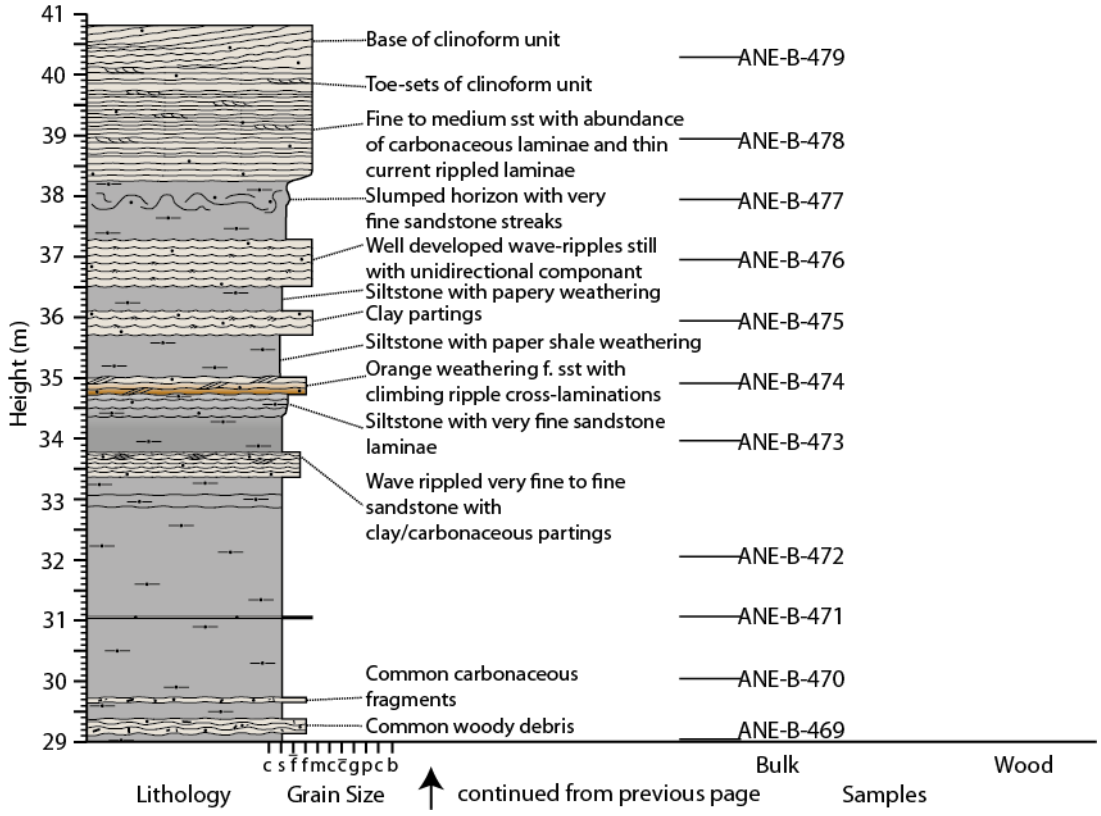

RKE Section (part 1)

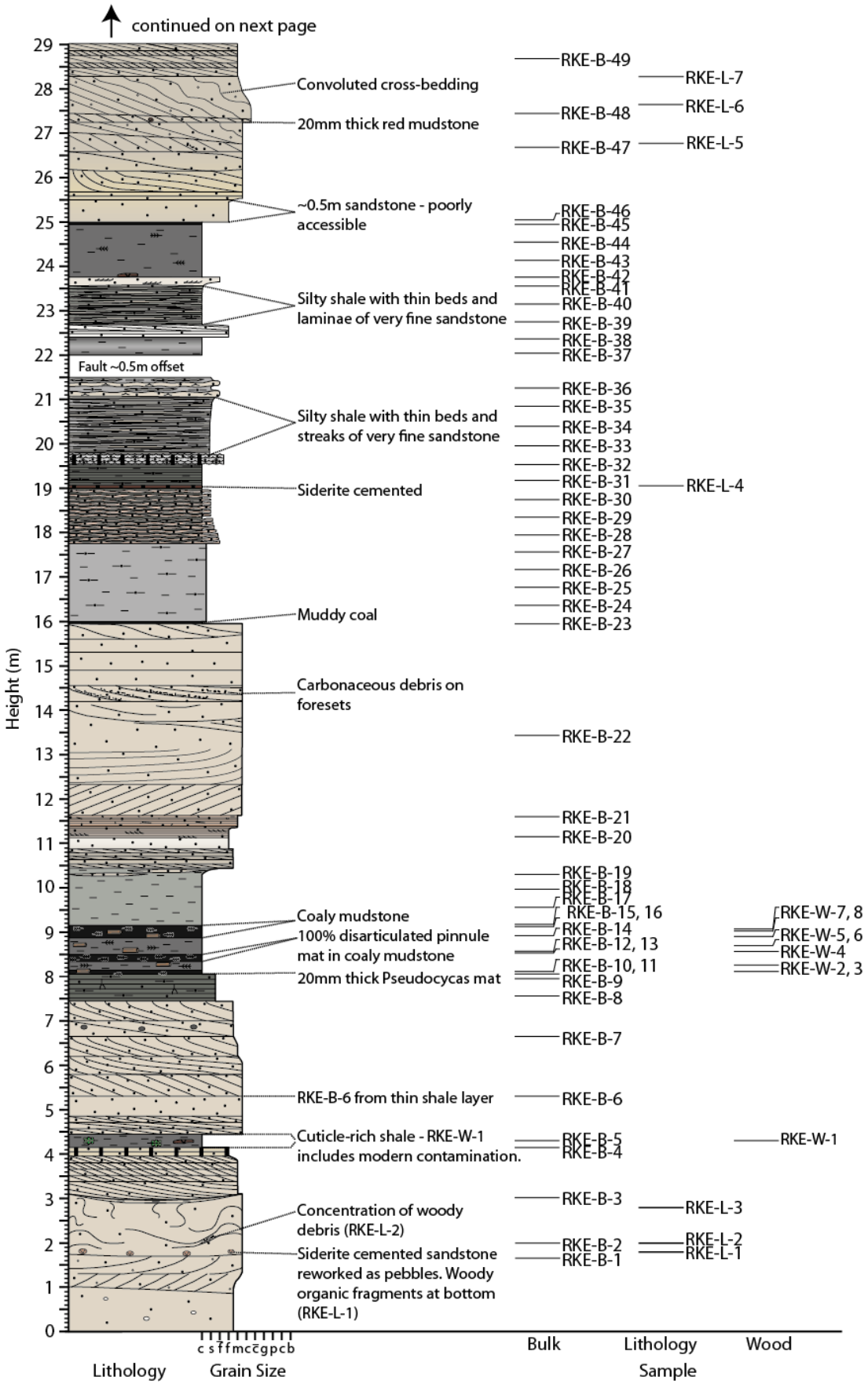

RKE Section (part 2)

08/08/2009

Ravn Kløft East (RKE)

Location: 70°45'09.2"N 52°55'00.6"W
150m elevation

Detailed section on bend in river. Ravn Kløft E.
Probably equivalent to Helle Midtgaard's Log 35.

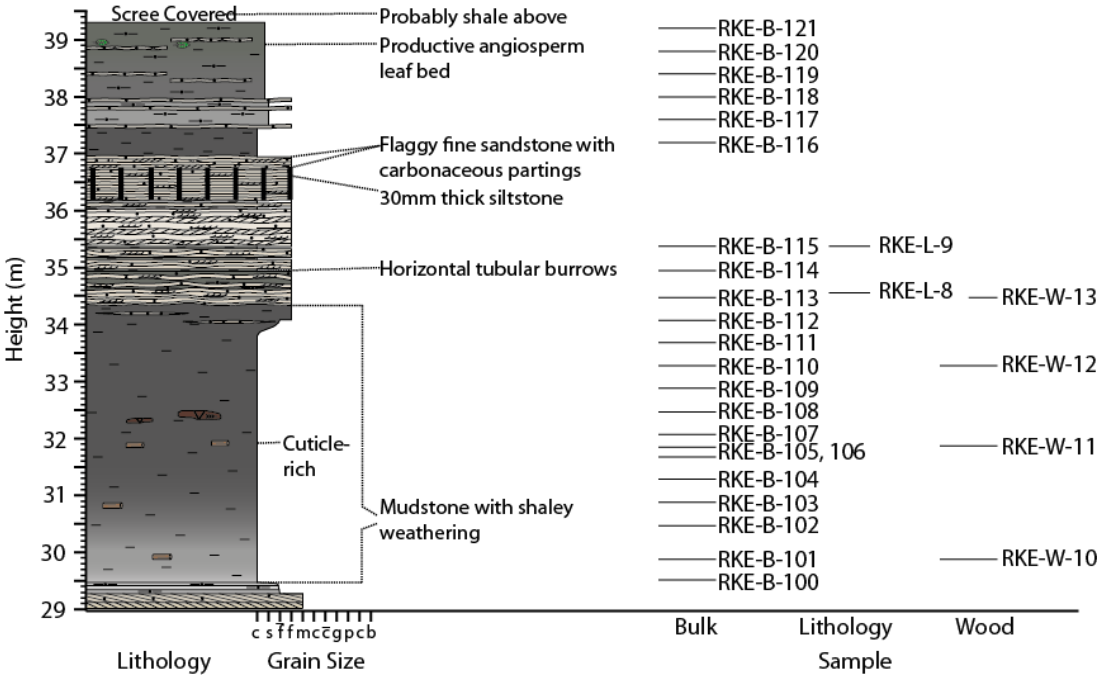

RKE parallel section

Additional section logged by G. Pedersen. Fluvial channel thicker in this section but still correlated to Boyd's SS sandstone.

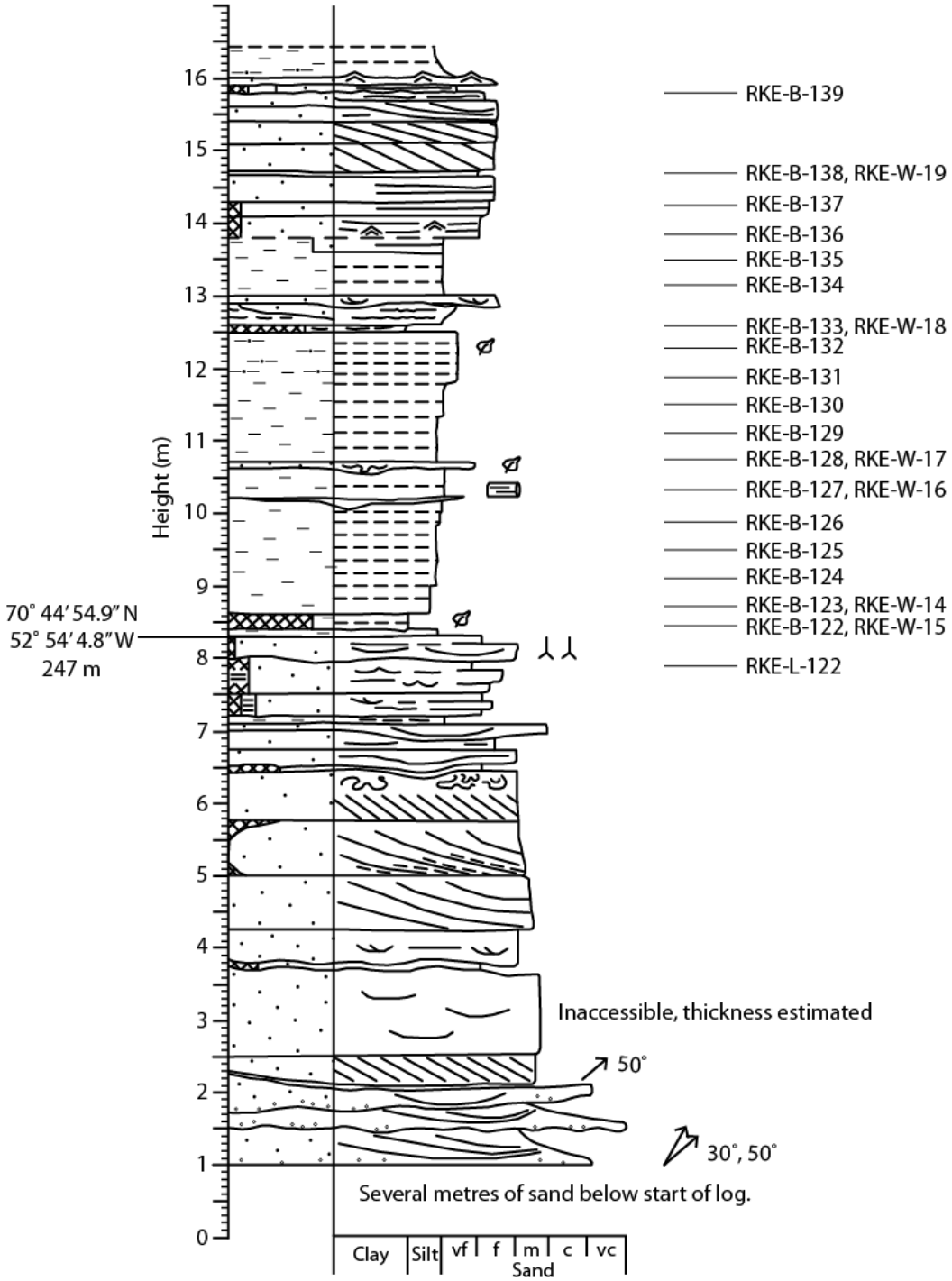

RKW Section (part 1)

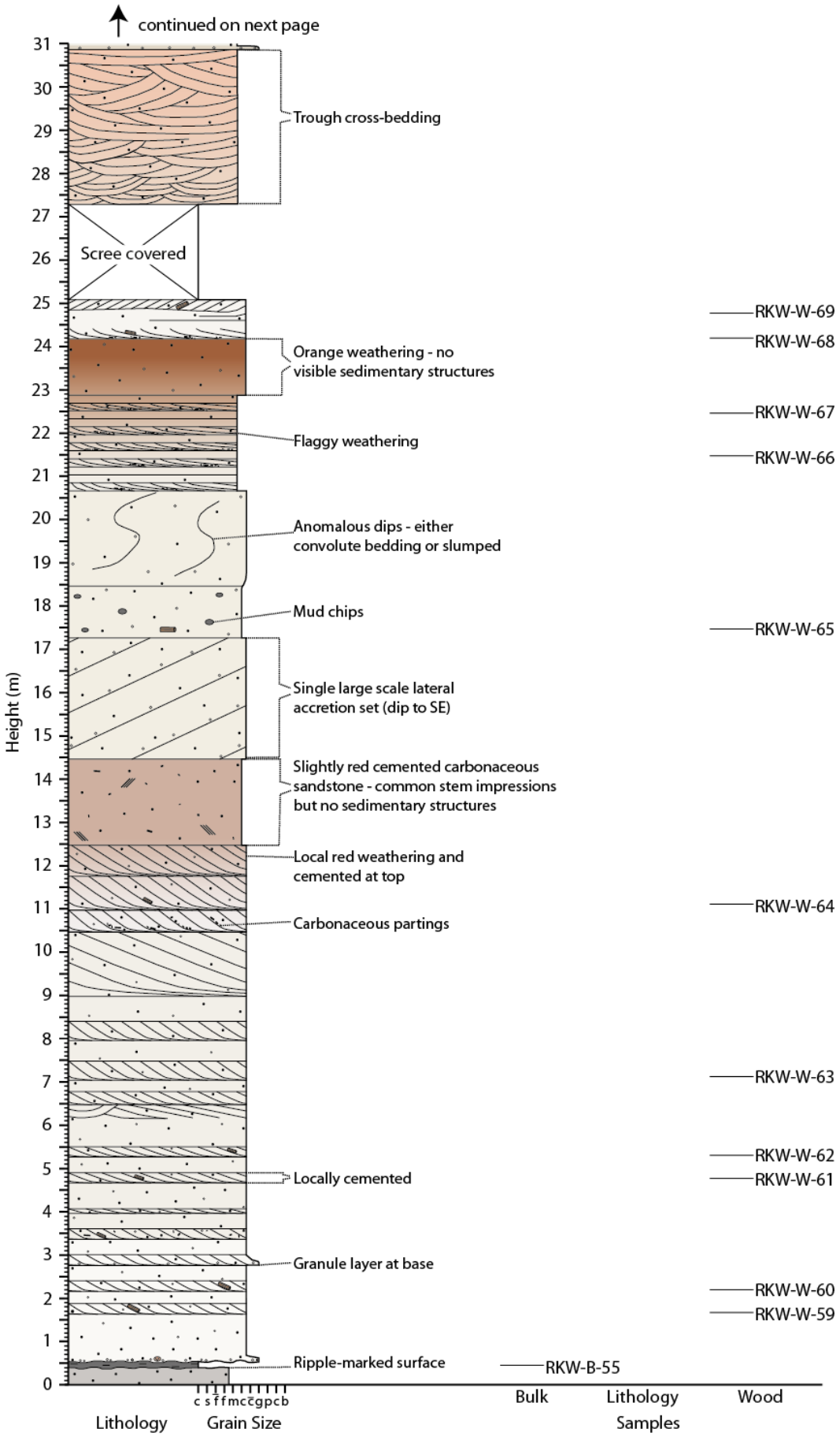

RKW Section (part 2)

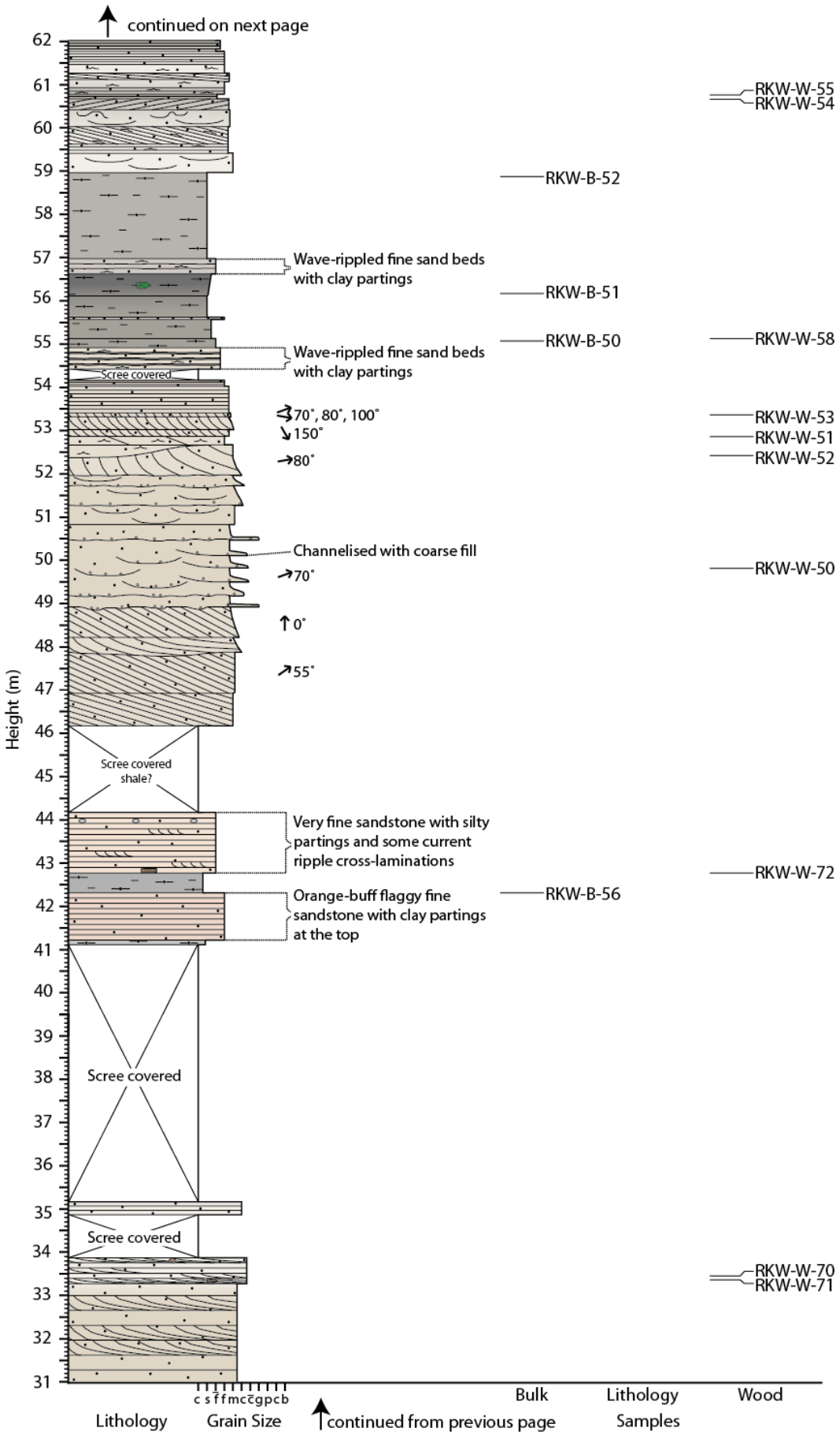

RKW Section (part 3)

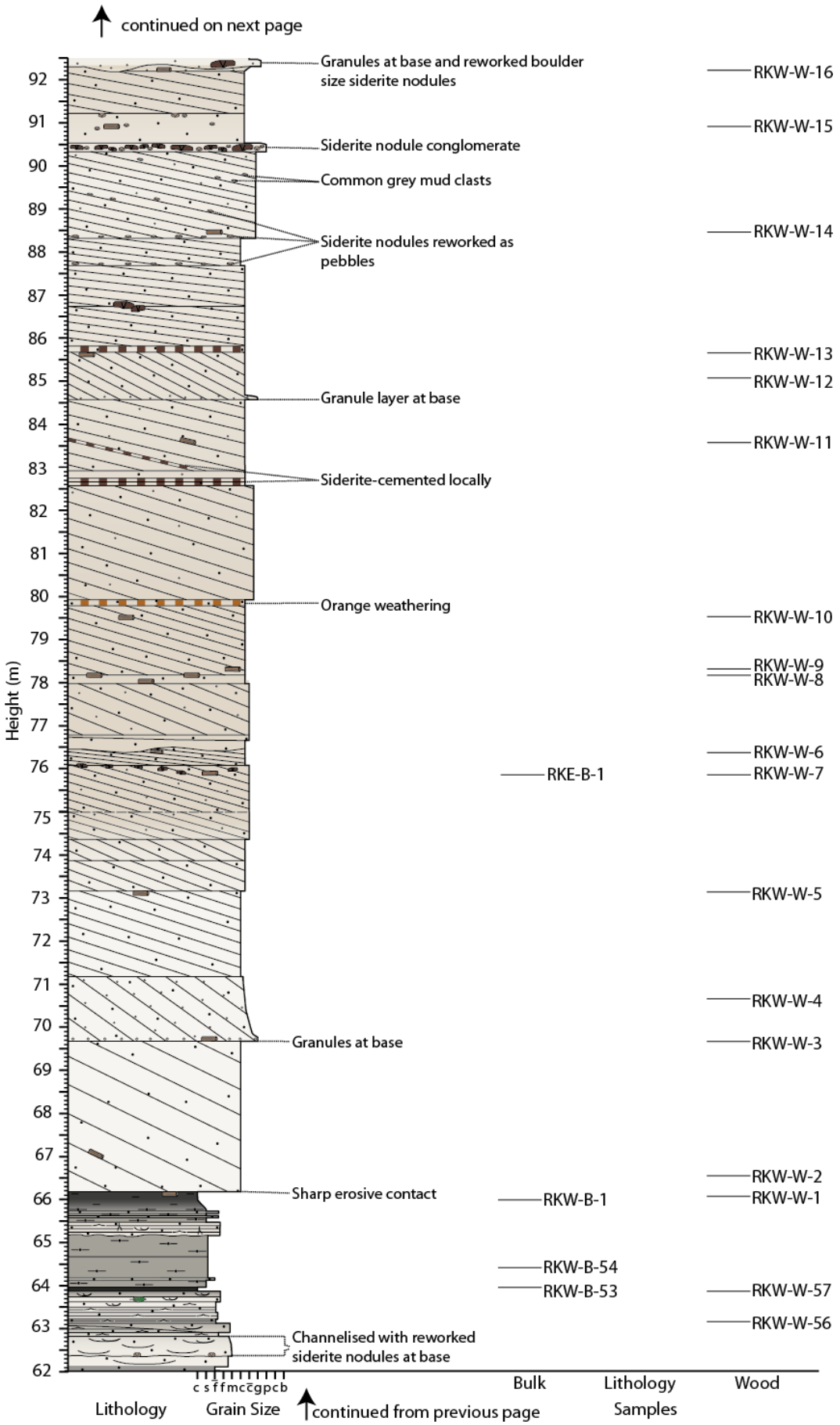

RKW Section (part 4)

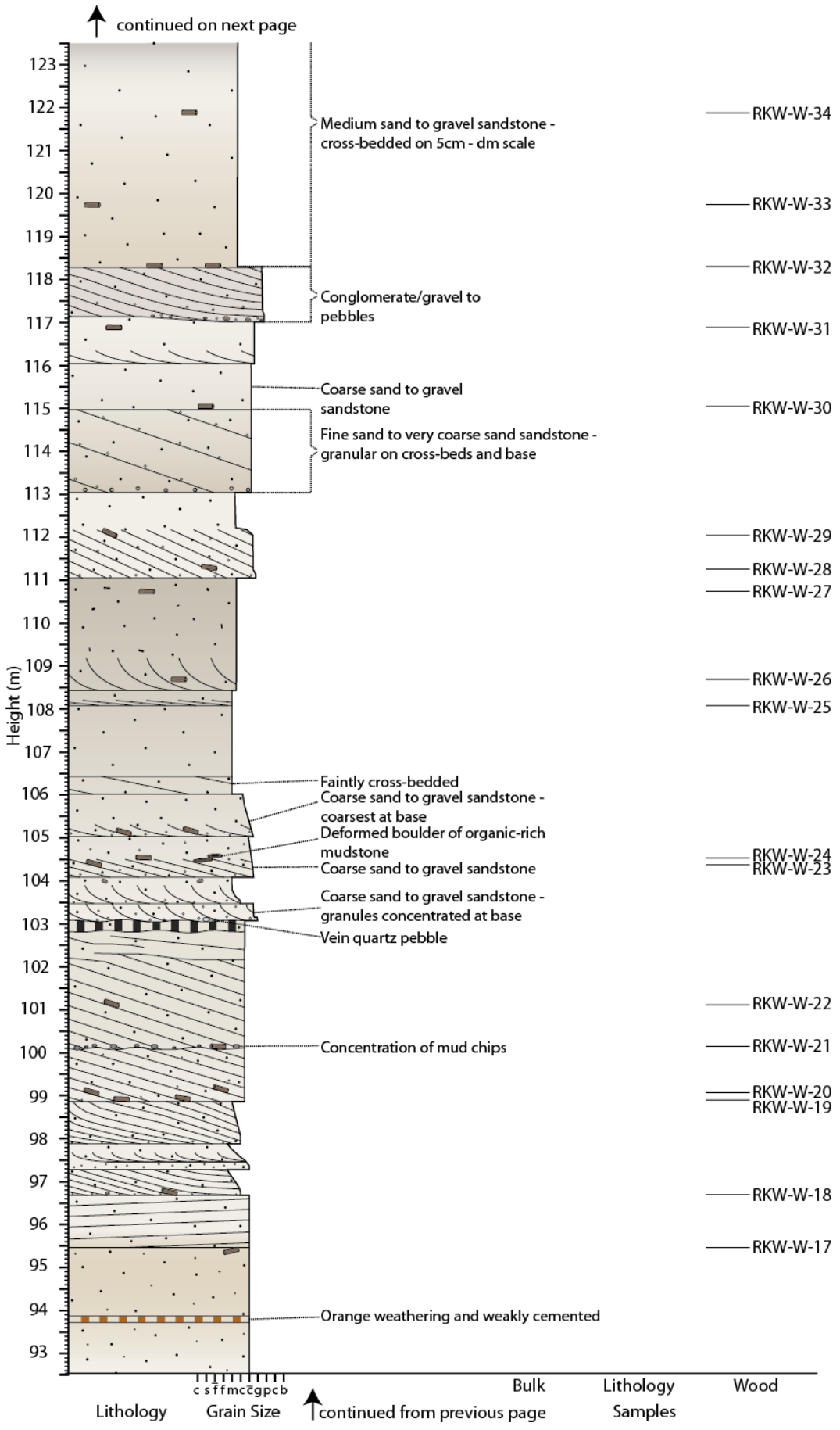

RKW Section (part 5)

Ravn Kløft West (RKW)

Location: 70°44'39.0"N 52°57'48.9"W 473m elevation (GPS)
Log complied from different field worker sections:
12/08/09 : 46.17 - 66.17m and 66.17 - 103.07
14/08/09 : 0.00 - 46.17m and 103.07 - 142.79

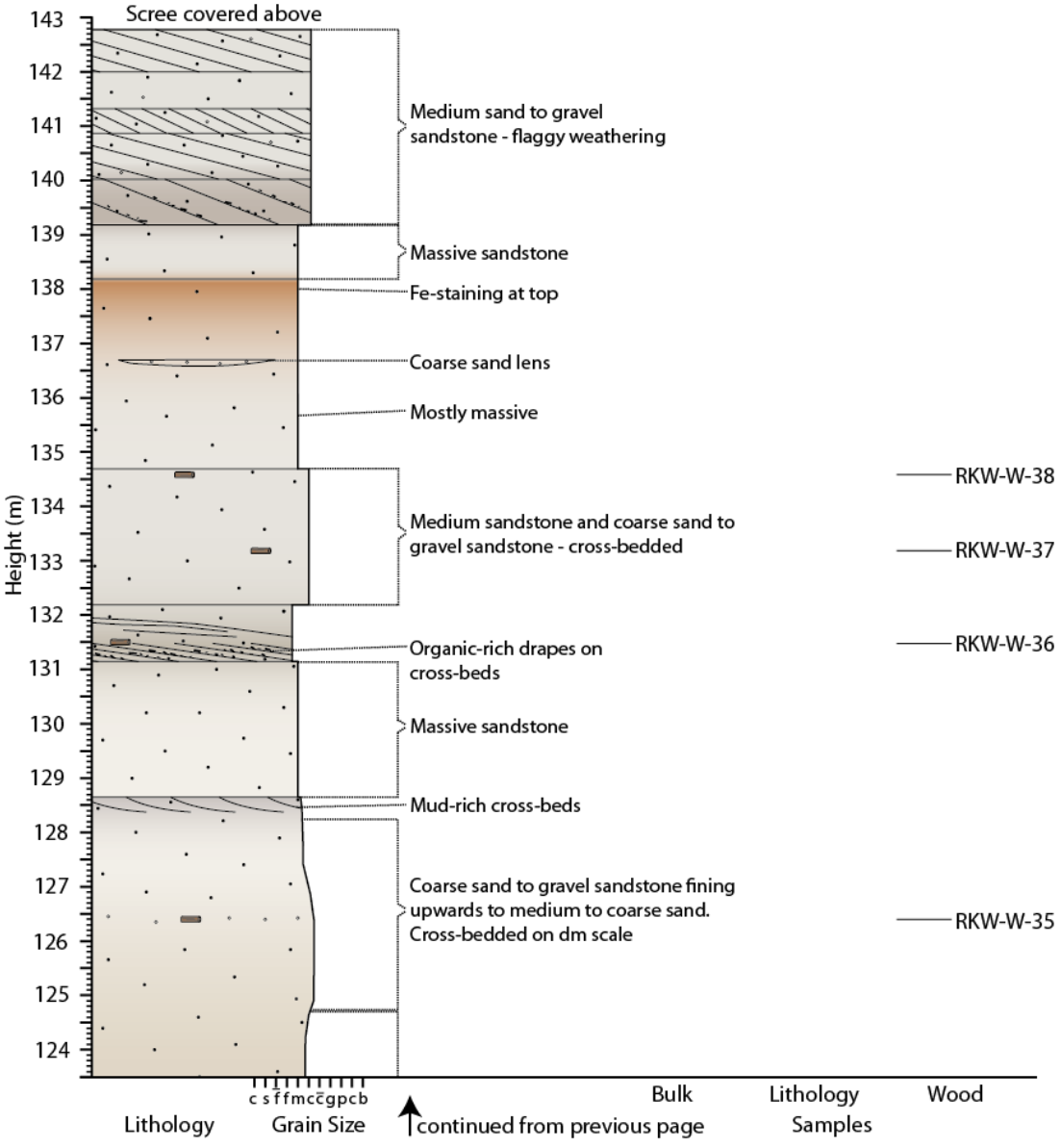

Table A

Locality	Sample Labels	Equivalent locality	Collecting Time	Sample Size	Species List
LK-B-4	n/a	LK-B-4	40 min; 1m^3	zero	mostly transported stems; no leaves seen or collected
LK-B-6	n/a	LK-B-6			
LK-F-3	A-P	LK-B-2	2 hrs	100+	Dispersed Pseudocycas; intact spec. of Pterophyllum sp., Pseudocycas speciosus (grooved), Nilsoniopteris cf. ikorfatensis.
LK-B-119	n/a	~1m above LK-B-100	20 min; 0.2m^2	zero	only transported sticks and unid. coalified leaves
LK-F-74	A-R	LK-B-74	2 hrs max; 0.3 m$^{2;}$	15 to 20	Articulated ferns (many - 1 w/ reticulated venation; conifers (3), plus 1 possible Bennetite
LK-F-33/34/35	A-D	LK-B-33-35	1.5 hrs max; 1m^3	4	
Below EC1	n/a	Austin Boyd ECW1			Articulated ferns; Pseudocycas spp.; Conifer cones and leaves + ferns in ss; 2 Sapindopsis leaflets at level of ECT loc of Boyd in topmost ss cap within Kome Fm.
ANE	n/a	n/a	1 hr max;	5 to 10	predominantly Pseudocyas sp.; possible angiosperm; Nilsoniopteris sp.; conifer shoot; poss. Fern
RKW-F-Cycad	A-F	n/a		5 to 10	Pseudocyas steensrupi
Wedge between stream	n/a	n/a			Pseudocycas ravnkloftensis
RKE	n/a	n/a			1 leaf of cf. Platanophytum; Pseudocyas cf. ravnkloftensis
RKE-B-10	unknown	RKE-B-10		hundreds	leaf mat of Pseudocycas cf. ravnkloftensis
RKE-B-44	unknown	RKE-B-44		several	good conifers
RKE-B-45	unknown	RKE-B-45		several	macro Pseudocycas
RKE-F-120	A-P	RKE-B-120	1 hr; 0.5 m^2	6 to 8	Sapindopsis w/ attached leaflets; Dicotylophyllum cf. polymorpum; dispersed Pseudocycas sp.; Conifer shoot (?); elliptical dicot leaf; Nisoniopteris sp.
Boyd M1	n/a	Boyd M1		zero	
Boyd M2	A-G	Boyd M2	40 min; 0.5 m^3	7 to 10	Trilaurus sassopsis; Pseudocycas sp.; Dicot type C (oblong, entire mgn); conifer shoot; fern frond, Cordate base dicot; Sapindopsis ravnkloftensis; cf. Platanophytum sp. (trinevate)

Appendix B: Geochemistry

- Table A: TC, TOC, TIC and $\delta^{13}C_{org}$ data with age from carbon isotope correlation (digital file).
- Table B: $\delta^{13}C_{wood}$ data with age from carbon isotope correlation (digital file)
- Table C: Fossil wood descriptions and classifications (digital file)
- Figure i: RKW section and grab samples TOC and TIC data
- Figure ii: RKW section and grab samples $\delta^{13}C_{org}$ data

Figure i

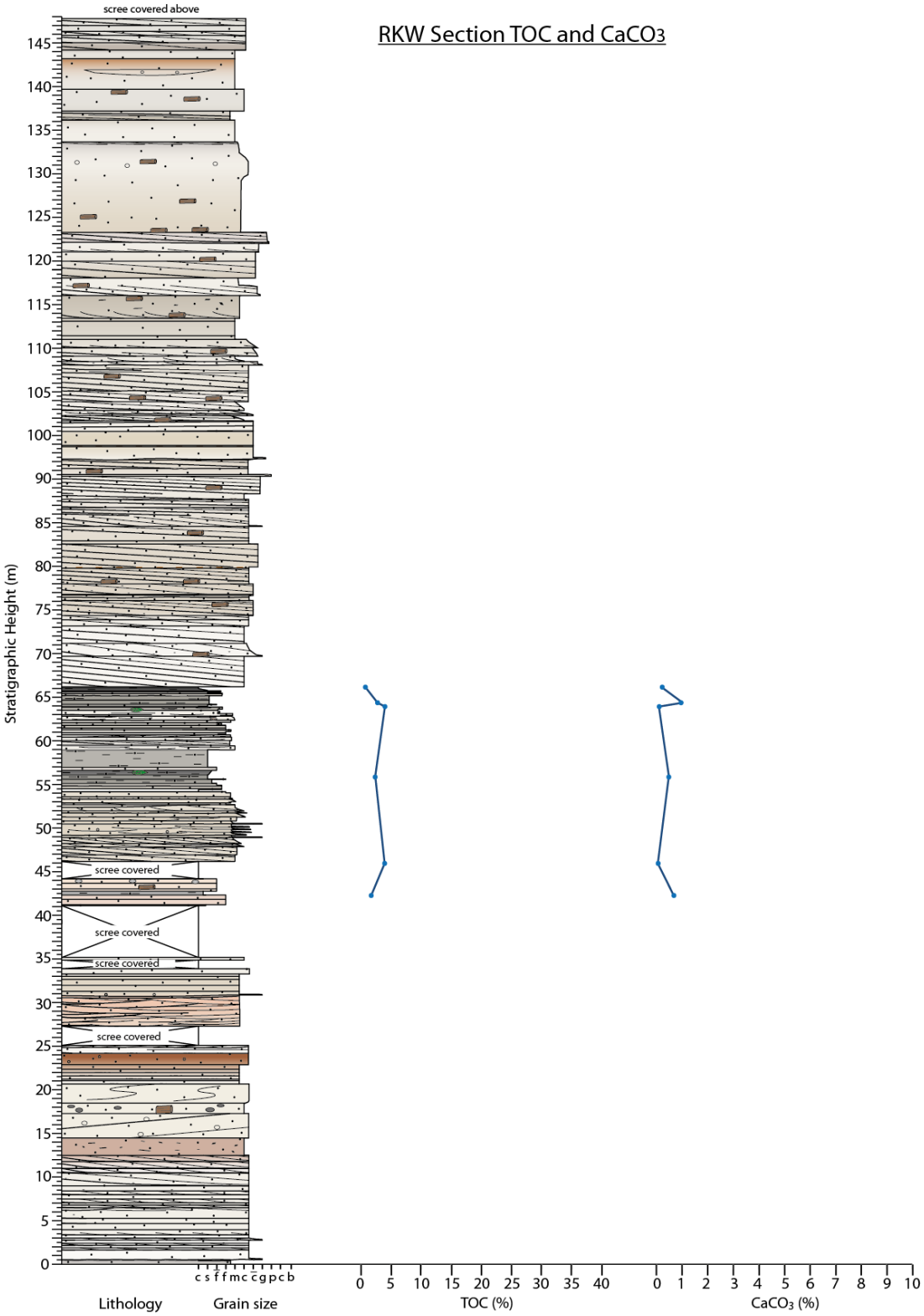
RKW Section TOC and CaCO3
scree covered above
Stratigraphic Height (m)
scree covered
scree covered
scree covered
scree covered
Lithology
Grain size
c s f f m c c g p c b
TOC (%)
CaCO3 (%)

Figure i (continued)

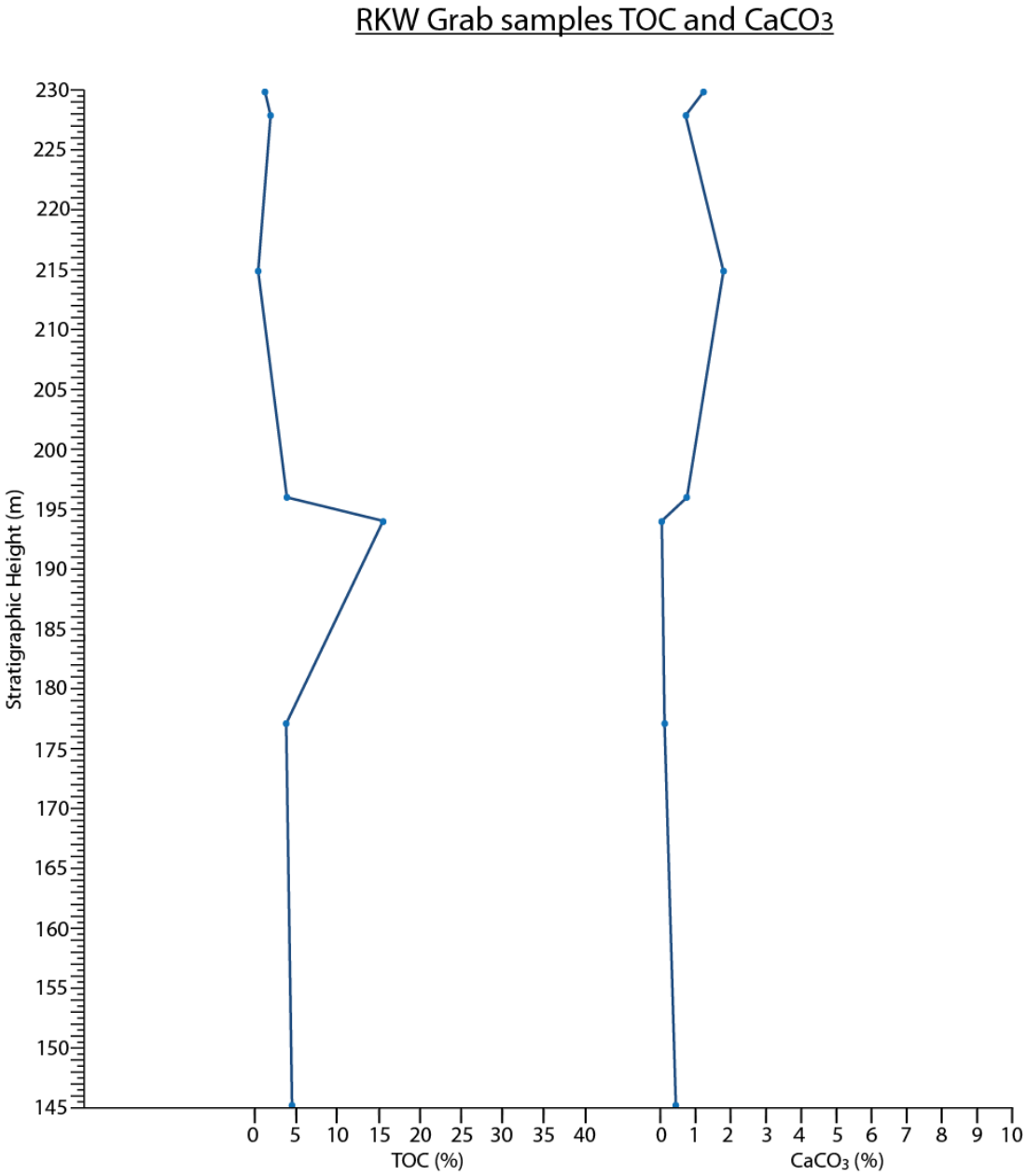

Figure ii

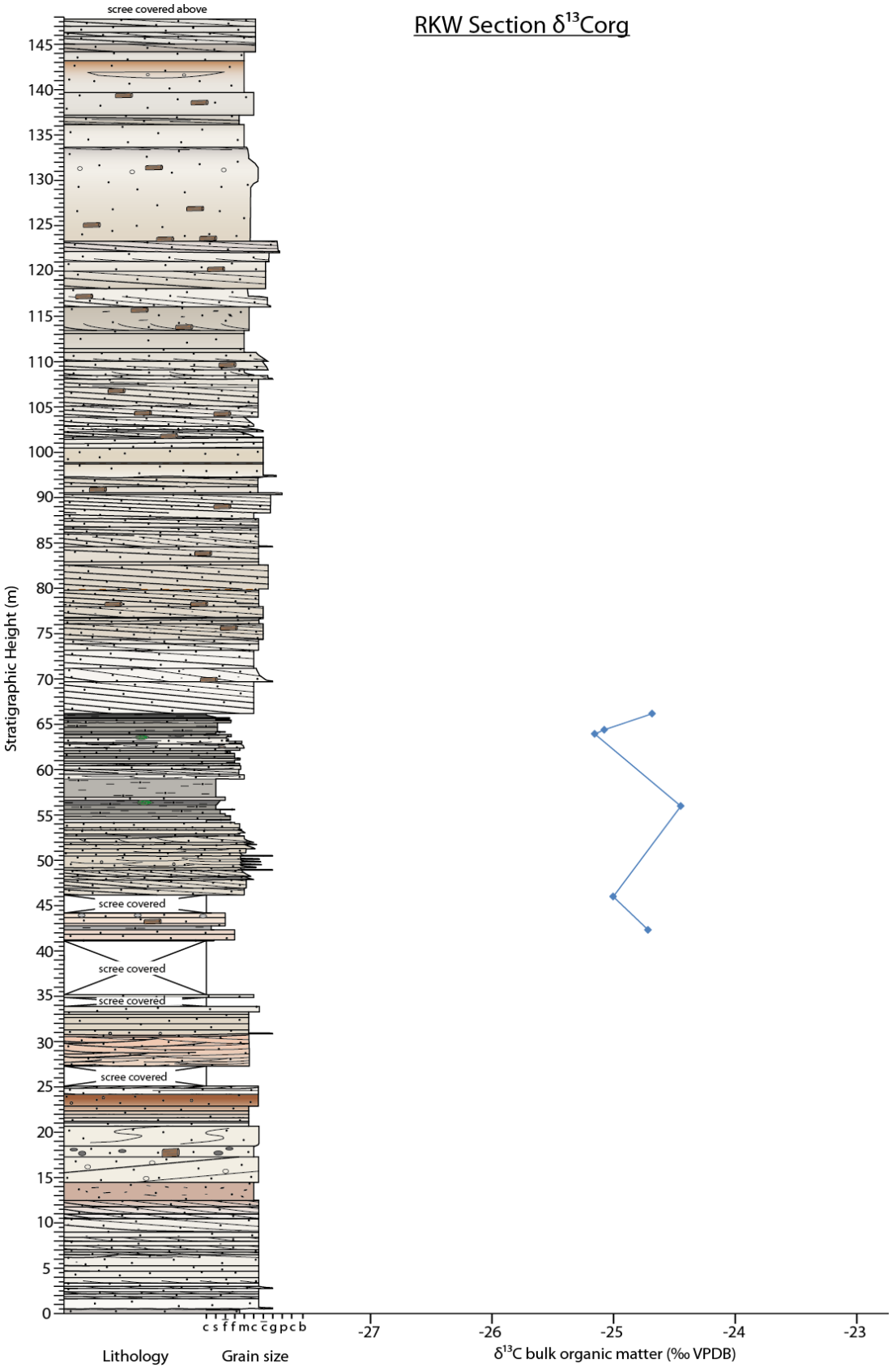
RKW Section δ13Corg
scree covered above
scree covered
scree covered
scree covered
scree covered
Stratigraphic Height (m)
0
5
10
15
20
25
30
35
40
45
50
55
60
65
70
75
80
85
90
100
105
110
115
120
125
130
135
140
145
c s f f m c c g p c b
Lithology
Grain size
-27
-26
-25
-24
-23
δ13C bulk organic matter (‰ VPDB)

Figure ii (continued)

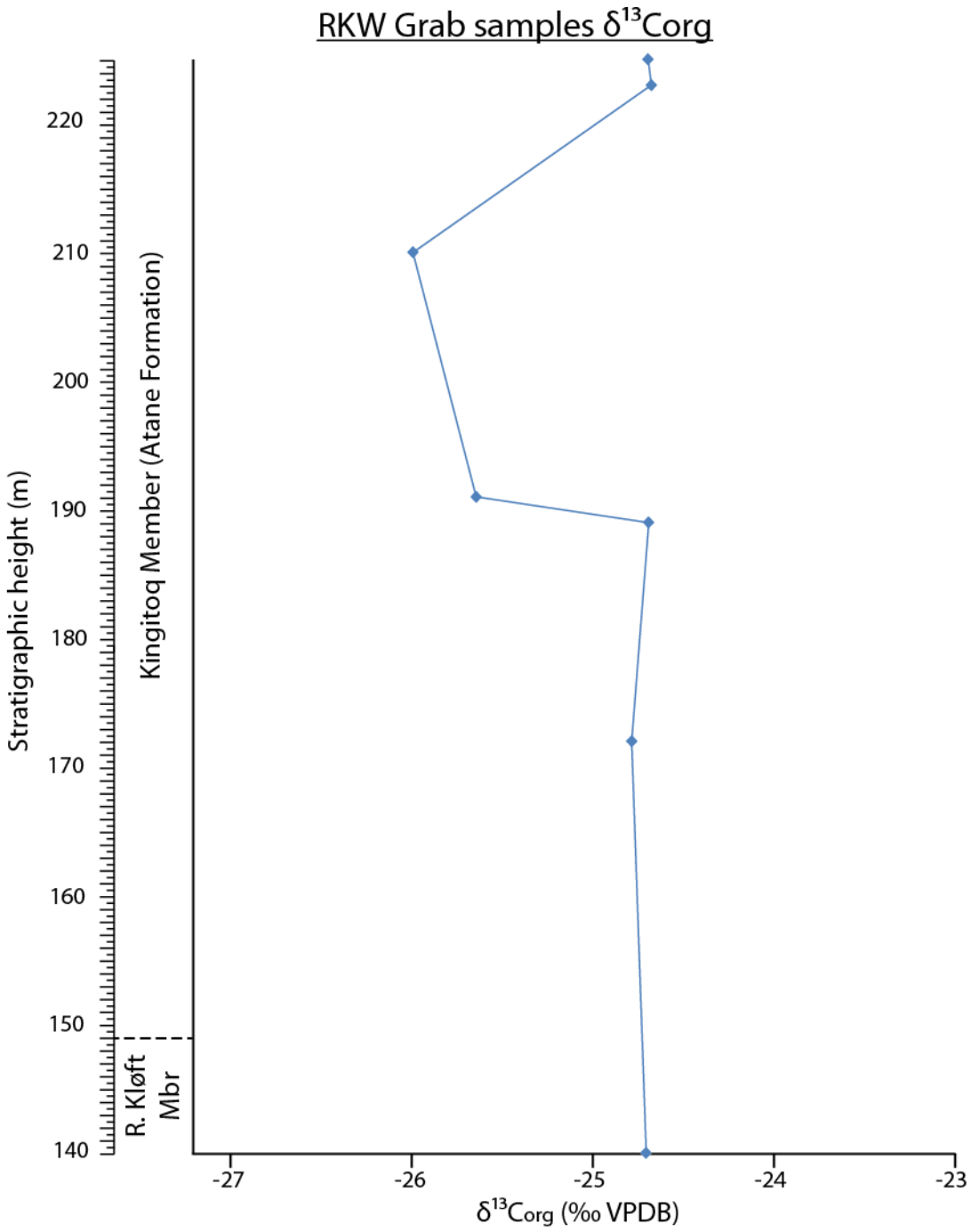

Appendix C: Cuticle record

- Bulk maceration protocol development.
- Table A: List of cuticle sorted from unsuitable horizons for morphotyping.
- Table B: Simplified character matrix (digital file).
- Table C: Full character matrix (digital file).
- Figure i: Sketches of Cheirolepidiaceae shoots from Watson (1977).
- Additional cuticular evidence of Bennettitales – scales. Includes the following figures:

  Figure ii: sketches of Bennettitalean flower *Williamsonia gigas* from Reddy (2003) showing A: female flower; B: floral bud surrounded by bracts.

  Figure iii: Epifluorescence microscope images of Bennettitalean bract fragments, labelled with sample name and cuticle piece colour-coded by vial for reference within the character matrix, alongside the feature captured in the image and the scale bar.

  Figure iv: SEM image from Boyd (2004) of Cycadolepsis mancheseriana showing inside cuticle surface with irregularly shaped epidermal cells and small paracytic stomata. Scale increments 100 µm.

Bulk maceration protocol development

The method described in Chapter 4 is a modification of protocols outlined by Barclay (2011; itself modified from Wellman and Axe, 1999). Barclay's technique uses 150 g of sample broken into pieces no bigger than 4 cm in size in a 1 L beaker, with 10 samples processed in a batch. The first of three chemical stages is the addition of concentrated HCl. However, after rinsing until neutral, Barclay (2011) uses 0.1 M sodium pyrophosphate solution to disperse clay material. After rinsing the sodium pyrophosphate, a small amount of HF (about 250 ml) is added slowly and stirred with a plastic rod. Barclay calculates the amount of HF required to fully digest the material, but does not add all immediately due to the likelihood of vigorous reaction. Once left for 24 hours, additional HF is added so that in some cases, as much as 600 ml of HF would be required. Once fully reacted, which could take as long as a month, the samples are rinsed to neutral and stack sieved to separate the desired size fractions.

Through a pilot study using this method, adaptations were made to the Barclay protocol, comprising:

1. From examination of the cuticle of the present study, the small cuticle piece sizes (generally less than 1 mm) meant the rock samples could be broken into pieces 1 cm in size to speed up reaction times with little risk of damaging the cuticle. In the rare cases that cuticle pieces were whole or large (e.g. in the case of the leaf mats) samples were not broken into such small pieces.
2. The current study used 250 ml polypropylene bottles with screw caps that were left partially loosened for venting. The neck on the bottle and the lid, although not sealed, would reduce the amount spilt if tipped compared the 1 L beakers of Barclay's technique. Also, the samples were agitated after 24 hours in HF by completely tightening the lid and shaking from side to side. This removed all possibility of contact with the HF, which could occur if the samples were agitated by stirring with a plastic rod, particularly if the HF had just been added. The lids also restrict the loss of material in the case of an over-boiled reaction. However, the bottles have a lower capacity than the beakers, so not as much HF can be added compared to the Barclay protocol. This was resolved by changing the acid weekly, and the small footprint of the bottles allowed for the continuous maceration system to be implemented.
3. The second chemical step of 0.1 M sodium pyrophosphate addition was omitted from the present study protocol - through trial it was found that many samples

were more likely to produce a precipitate if this step is included. There was little visible evidence of increased reaction time through clay dispersal and it was decided that the other adaptations such as regular agitation and smaller starting rock piece size were more beneficial. This likely reflects the difference in sedimentology between the two studies, and sodium pyrophosphate addition should not be ruled out for clay-rich samples.

4. Additional sieving stages were used in this study compared to Barclay to increase the efficiency of sorting material suitable for microscopy.

Table A

Sample	Composite height (m)	Cuticle Group									
		2	3	4	5	6	7A	7B	8A	8B	9	Total
LK-B-10	2.23	5	25									30
LK-B-11	3.86	7	10	3								20
LK-B-18	6.88	1	4	7						8		20
LK-B-19	7.28	18	18	4								40
LK-B-21	8.53	21		1								22
LK-B-24	9.91	6	1									7
LK-B-29	11.78	8	1	1								10
LK-B-30	12.30	12										12
LK-B-32	12.50	10										10
LK-B-34	13.25	40										40
LK-B-44	17.23	10										10
LK-B-45	17.73	10										10
LK-B-52	20.16	2	8									10
LK-B-58	22.84	1	4	4								9
LK-B-62	25.34	5	4	1								10
LK-B-63	25.79		10									10
LK-B-65	26.64	10										10
LK-B-70	28.48	1	14	11								26
LK-B-71	28.81		13	11						2		26
LK-B-73	29.51	12										12
LK-B-77	31.41	39	1									40
LK-B-85	34.95	39	1									40
LK-B-90	36.97	39								1		40
LK-B-125	43.33		16	14								30
RKE-B-8	186.47	1	9	10								20
RKE-B-19	189.30	1	26	13								40
RKE-B-32	198.53		8	1	1							10
RKE-B-40	202.16	20		8								28
RKE-B-122	208.35		8	2								10
RKE-B-123	208.60											0
RKE-B-106	210.84		10									10
RKE-B-132	212.20		2	2								4
RKE-B-110	212.29		10									10
RKE-B-111	212.69	10										10
RKE-B-120	217.80		5	5								10

Figure i

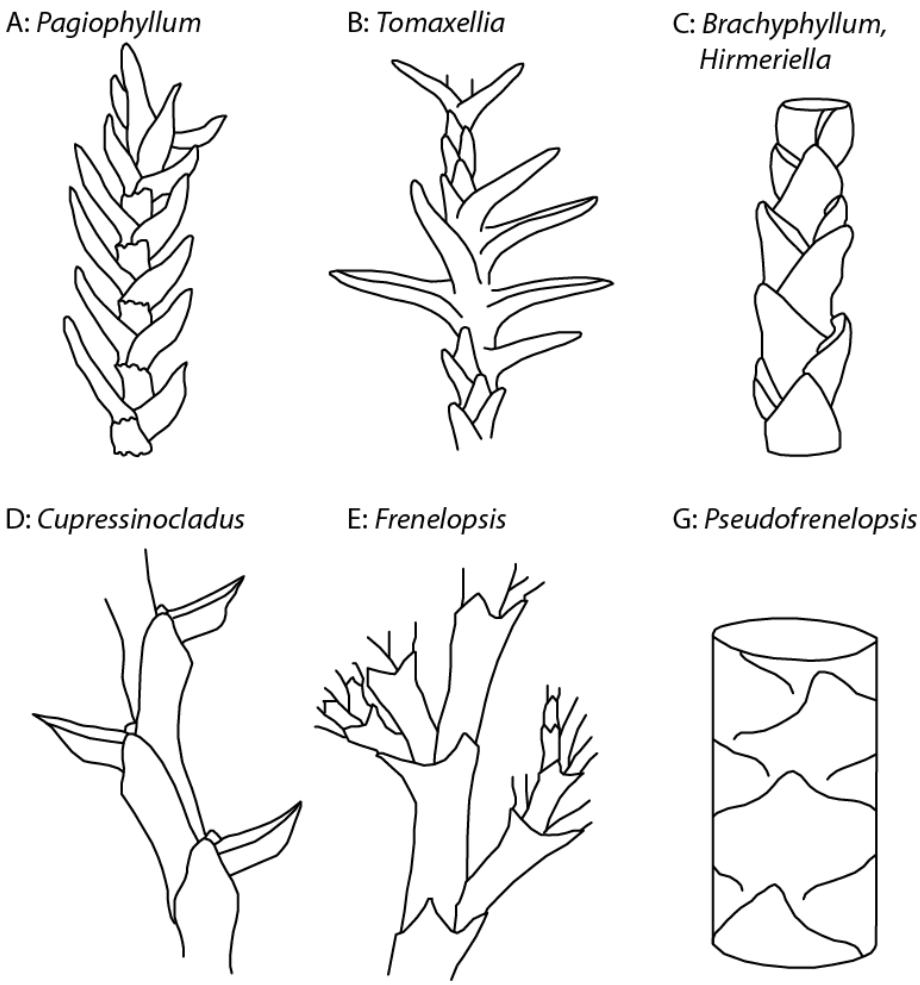
A: *Pagiophyllum*
B: *Tomaxellia*
C: *Brachyphyllum*, *Hirmeriella*
D: *Cupressinocladus*
E: *Frenelopsis*
G: *Pseudofrenelopsis*

Additional cuticular evidence of Bennettitales – scales

Additional evidence of the presence of Bennettitales in the floral community is in the form of bracts, which form part of the reproductive organs of Bennettitales (Figure ii).

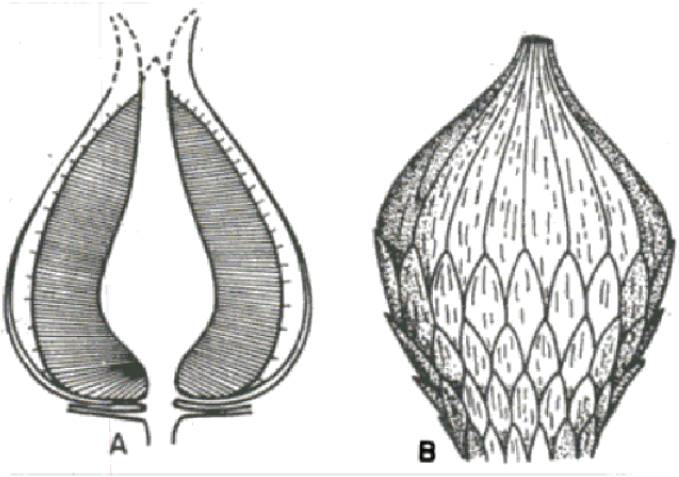

Figure ii: sketches of Bennettitalean flower Williamsonia gigas from Reddy (2003) showing A: female flower; B: floral bud surrounded by bracts.

Two cuticle fragments were identified from the macerated material from West Greenland that likely represent Bennettitalean bracts. The first (Figure iii-A) is a smooth elongate arrow-shaped scale, with no other preserved detail. However, comparison to the sketch in Figure ii reveals the possibility that this scale could have formed part of the overlapping array of scales covering a Bennettitalean flower bud.

The other cuticle fragment identified (Figure iii B-D) has more epidermal features preserved, which can be viewed on both the outside and inside surfaces, including a heavily textured external surface (Figure iii B) with a cobblestone-like appearance. The tip of the possible bract appears to be rounded rather than pointed as was the case for the other fragment (Figure iiiA). The inside surface reveals small irregularly shaped and size epidermal cells, with smaller and higher density paracyctic stomata (Figure iii C, D) compared to the Bennettitalean leaf samples (morphotypes 6–8). Boyd (2004) described several *Cycadolepsis* (form-genus for Bennettite bracts) specimens from West Greenland, which are similar in cuticular features to the piece identified in Figure iii B-D. For example, comparison to the description of the internal cuticle surface of *Cycadolepsis manchesteriana* reveals similar stomatal and epidermal characters (Figure iv), but unfortunately, since the cuticle piece identified from the present study material was small, the shape of the bract and therefore a clearer idea on the likely species of *Cycadolepsis* could not be determined.

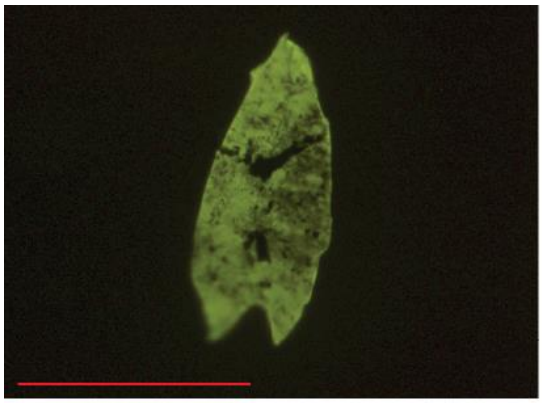

A: LK-B-3 (A), Bennettitalean bract (arrow-shaped), 500 µm

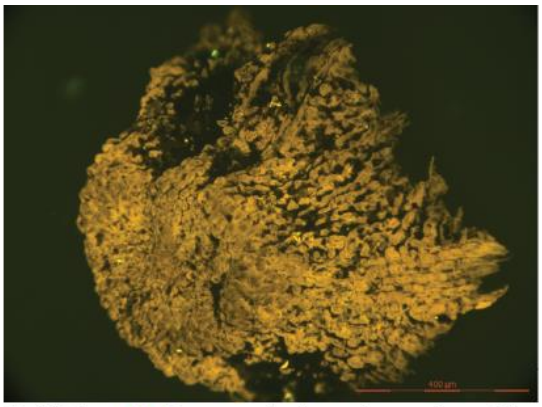

B: LK-B-9 (1), Bennettitalean bract (outside surface texture), 400 µm

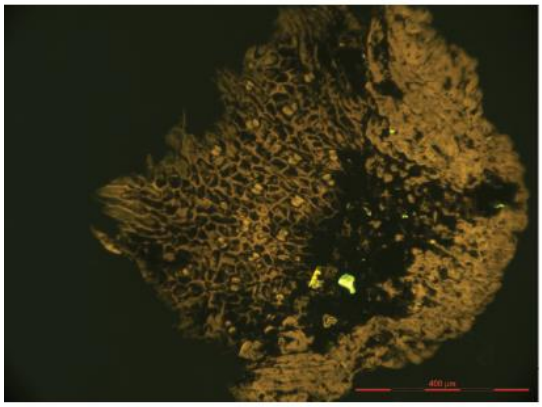

C: LK-B-9 (1), Bennettitalean bract (inside surface showing epidermal cells and stomata), 400 µm

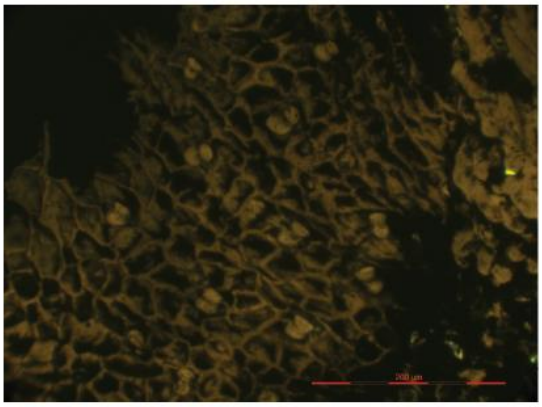

D: LK-B-9 (1), Bennettitalean bract (inside surface showing paracytic stomata), 200 µm

Figure iii: Epifluorescence microscope images of Bennettitalean bract fragments, labelled with sample name and cuticle piece colour-coded by vial for reference within the character matrix, alongside the feature captured in the image and the scale bar

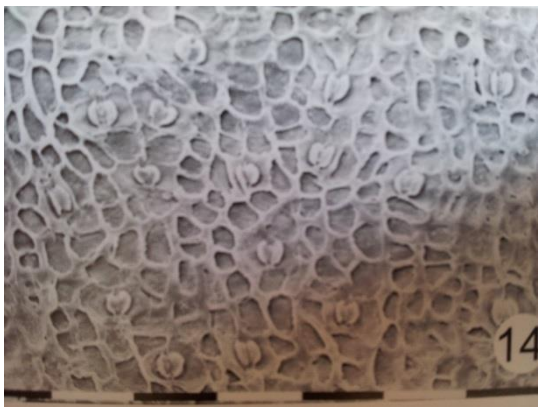

Figure iv: SEM image from Boyd (2004) of Cycadolepsis mancheseriana showing inside cuticle surface with irregularly shaped epidermal cells and small paracytic stomata. Scale increments 100 µm.

Appendix D: Floral reconstruction

- Table A: Morphotype relative abundance data (digital file).
- Table B: DCA axis 1 values (digital file).
- Figure i: Comparative field photographs of same stratigraphy from the north coast of the Nuussuaq Peninsula - A: from the present study field season in 2009, B: from Boyd (1998c) showing same S sandstone horizon, and the location of Boyd's florules SE3, SE4 and SE5, with a basalt horizon B also indicated in both.
- Identification of *Sapindopsis ravnkloftensis* macrofossils, including:

  Figure ii: Examples of Sapindopsis ravnkloftensis A: RKE-F-120 O showing leaves attached to stem. B: same specimen as A with annotation to show leaf area (green), stem (brown) and venation. C: Specimen from Boyd (1998c) showing leaves attached to stem. D: Specimen from Boyd (1998c) showing irregular toothed margin. E: RKE-F-120 Q showing elongate oblongate leaves with acute tips and irregular toothed margin. F: same specimen as E annotated to show leaf area (green) and venation. G: RKE-F-120G showing irregularly distributed toothed margin and second order venation. H: same sample as G but with annotations to highlight the leaf area (green) and second order venation.
- Figure iii: anatomical drawing of *Sciadopitys verticillata* from Houtte (1845) showing shoot attachment to branches.
- Figure iv: Sample photographs of *Sphenopteris*. A: BOYD LOC M2 B showing *Sphenopteris* frond. B: same sample as A with annotation to highlight leaf area (green) and rachis (brown). C: *Sphenopteris psilotoides* specimen from Seward (1927) no scale. D: *Sphenopteris dentatas* specimen from Seward (1927) no scale. E: *Sphenopteris psilotoides* specimen from Seward (1927) no scale.
- Figure v: Sample photographs of *Gleichenites*. A: Below ECW1 (EC) Ecp showing intact *Gleichenites* frond and individual pinnules. B: same sample as A with annotation to highlight leaf area (green) and rachis (brown). C: *Gleichenites gieseckiana* from Seward (1927) showing nearly complete bipinnate frond with alternately attached pinnules bearing rounded to acute tipped leaflets.
- Figure vi: Epifluorescence images of fossil structures of uncertain affinity from the Kome Formation untreated macrofossil collection (LK-F-74). A: branching thallus with brightly fluorescing features in pairs along branch with indications of filamentous extensions from these points previously. Branches leading to hub-like

structures. B: more crustose thallus, where paired structures show growth of thallus. C: closer image of structure shown in B, showing lobed thallus margin with brightly fluorescing features in pairs between lobes, with no indication of extensions from these points unlike in A.

Figure i

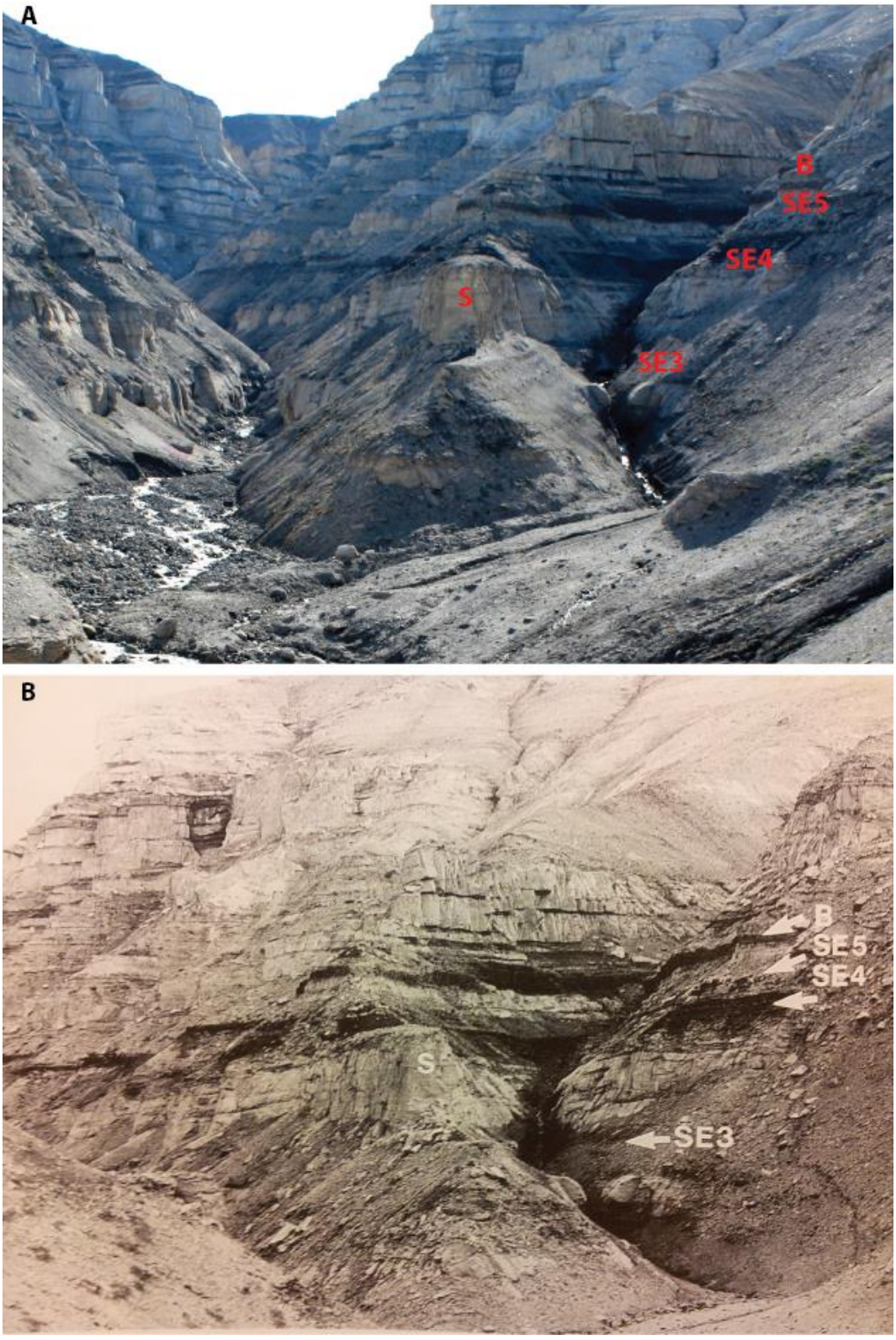

Identification of *Sapindopsis ravnkloftensis* macrofossils

Boyd (1998c) described stems and individual linear leaves with occasional toothed but normally entire margins. Boyd identified this material as a new species of *Sapindopsis* (order Rosales), and comparable specimens have been identified in the fossil material collected from the field area of the present study (Figure ii).

Examples collected from the present study include a stem specimen with leaves arranged oppositely at each node (Figure ii A, B). The leaves are notophyll in size (up to 1.5 cm wide and a minimum of 7 cm in length); symmetrical; and oblong in shape, with apparently parallel, entire margins in the middle portion of the leaf (see definitions in Ash *et al.,* 1999). The leaves have an acute basal angle but the tips in this particular specimen are not observed. Only the primary venation is preserved, which is pinnate (single primary vein; Figure ii A, B). This specimen description matches the description by Boyd (1998c) for *Sapindopsis ravnkloftensis* and strikingly resembles a more complete stem specimen collected and described by Boyd (Figure ii C), where the oppositely arranged leaves and the attachment to the rachis are preserved in considerable detail.

Other individual samples collected from the present study are more complete, showing leaf length of at least 10 cm, oblong leaf shape, and parallel margins for the majority of the leaf length and an acute leaf base (Figure ii E, F), and are comparable to the descriptions by Boyd (1998c). The margin of the leaf fossils collected of this type is not always entire, but occasionally and incompletely toothed (e.g. Figure ii G, H and also seen more rarely in Figure ii E, F). The teeth are large, with generally only one tooth per cm which are convex (apical side) straight (basal side; see Ash *et al.*, 1999), which are consistent with the description of the margin of this species from Boyd (1998c) in addition to their sporadic occurrence (Figure iiD). Second order venation was partially identified in one of the

Figure ii (next two pages): Examples of Sapindopsis ravnkloftensis A: RKE-F-120 O showing leaves attached to stem. B: same specimen as A with annotation to show leaf area (green), stem (brown) and venation. C: Specimen from Boyd (1998c) showing leaves attached to stem. D: Specimen from Boyd (1998c) show irregular toothed margin. E: RKE-F-120 Q showing elongate oblongate leaves with acute tips and irregular toothed margin. F: same specimen as E annotated to show leaf area (green) and venation. G: RKE-F-120G showing irregularly distributed toothed margin and second order venation. H: same sample as G but with annotations to highlight the leaf area (green) and second order venation.

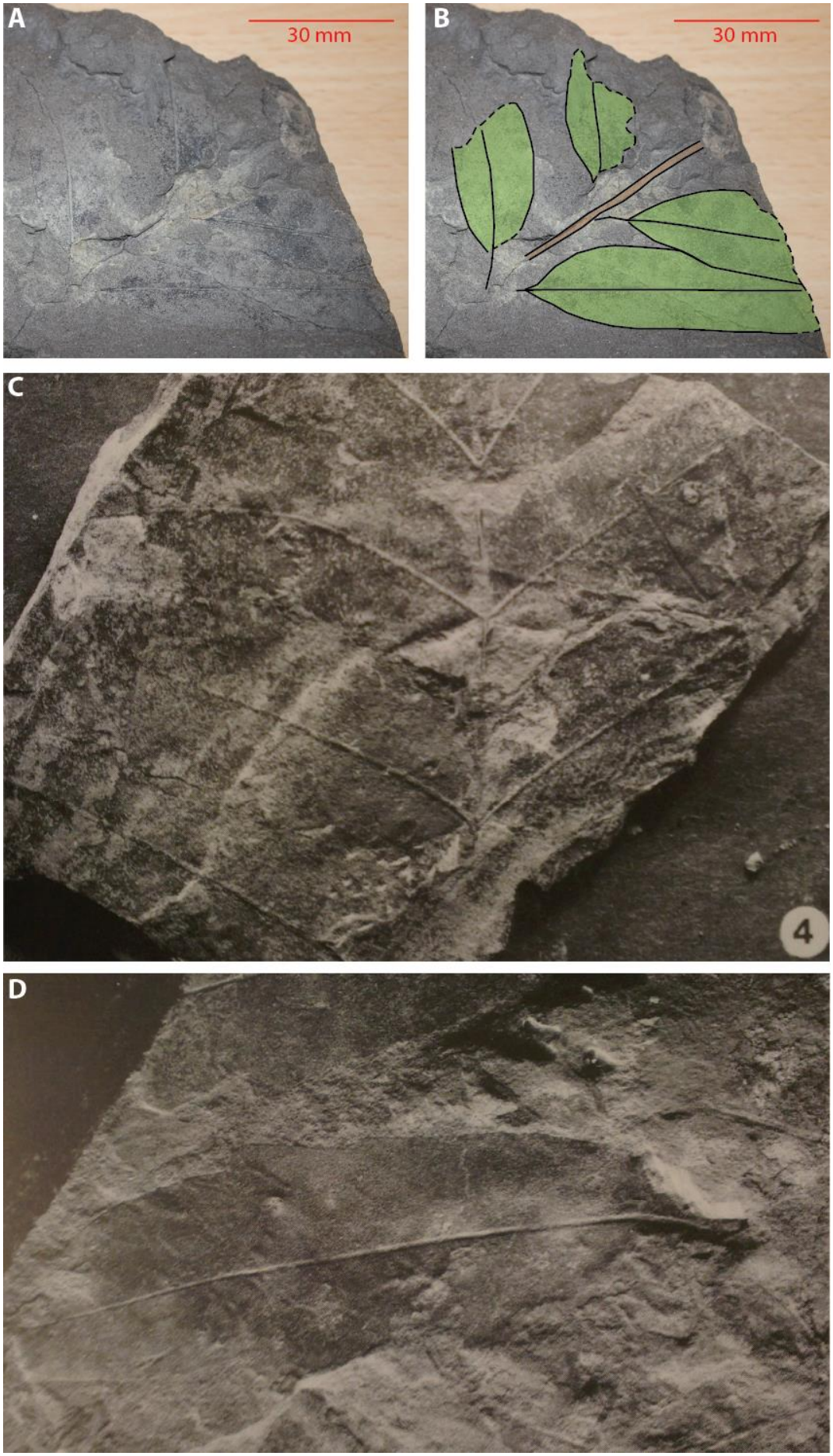
A
30 mm
B
30 mm
C
4
D

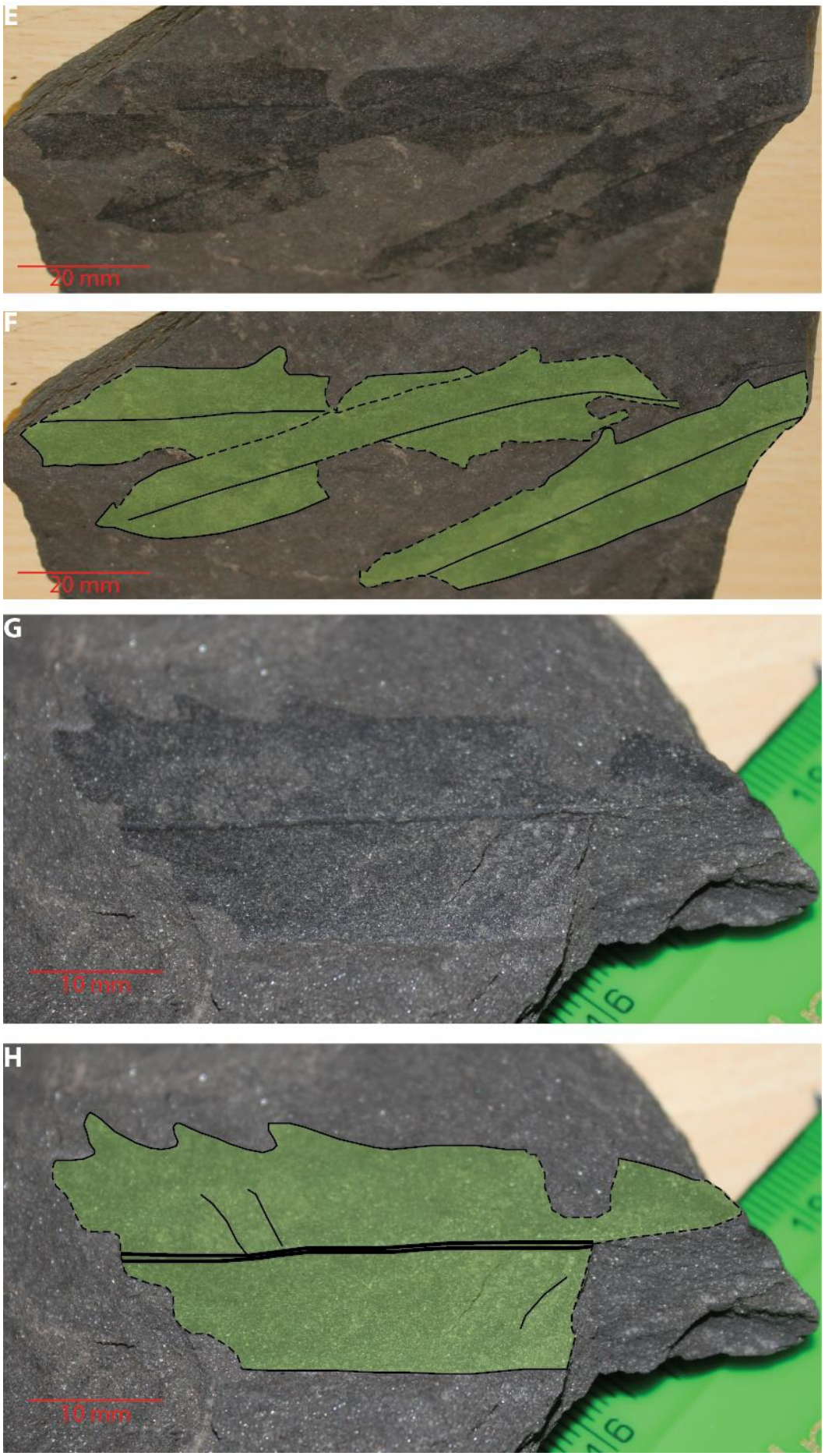
E
20 mm
F
20 mm
G
10 mm
H
10 mm

specimens collected (Figure ii G, H), which are upturned towards the leaf tip but lacked additional detail and otherwise higher order venation was not preserved. However, the better preserved specimens of Boyd (1998c) present eucamptodromous second order venation (see Ash *et al.*, 1999), and the second order venation identified in specimens from the present study are consistent with this venation pattern. Boyd (1998c) was not able to examine any cuticle for this species.

Figure iii

Figure iv

Figure v

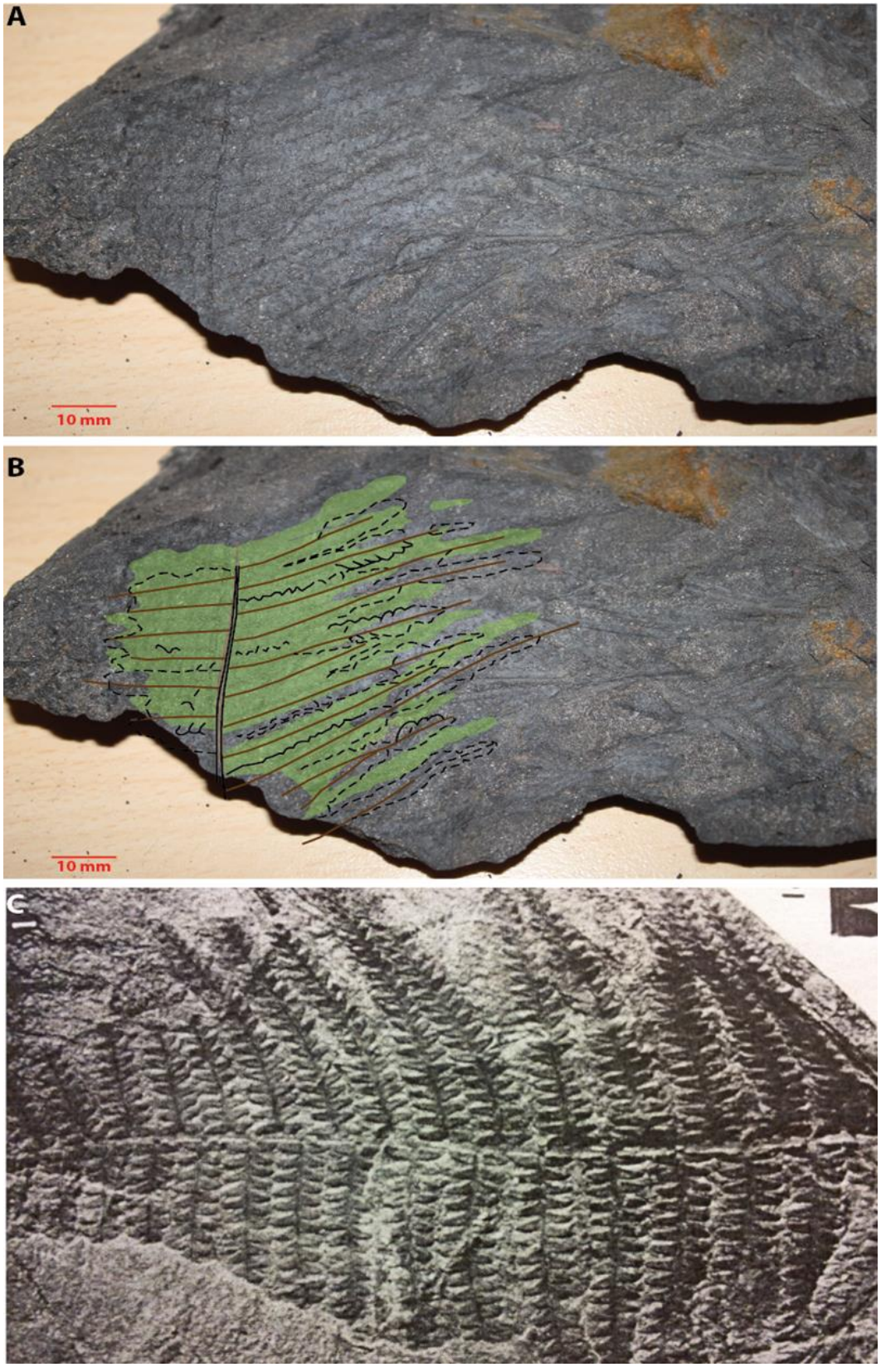

Figure vi

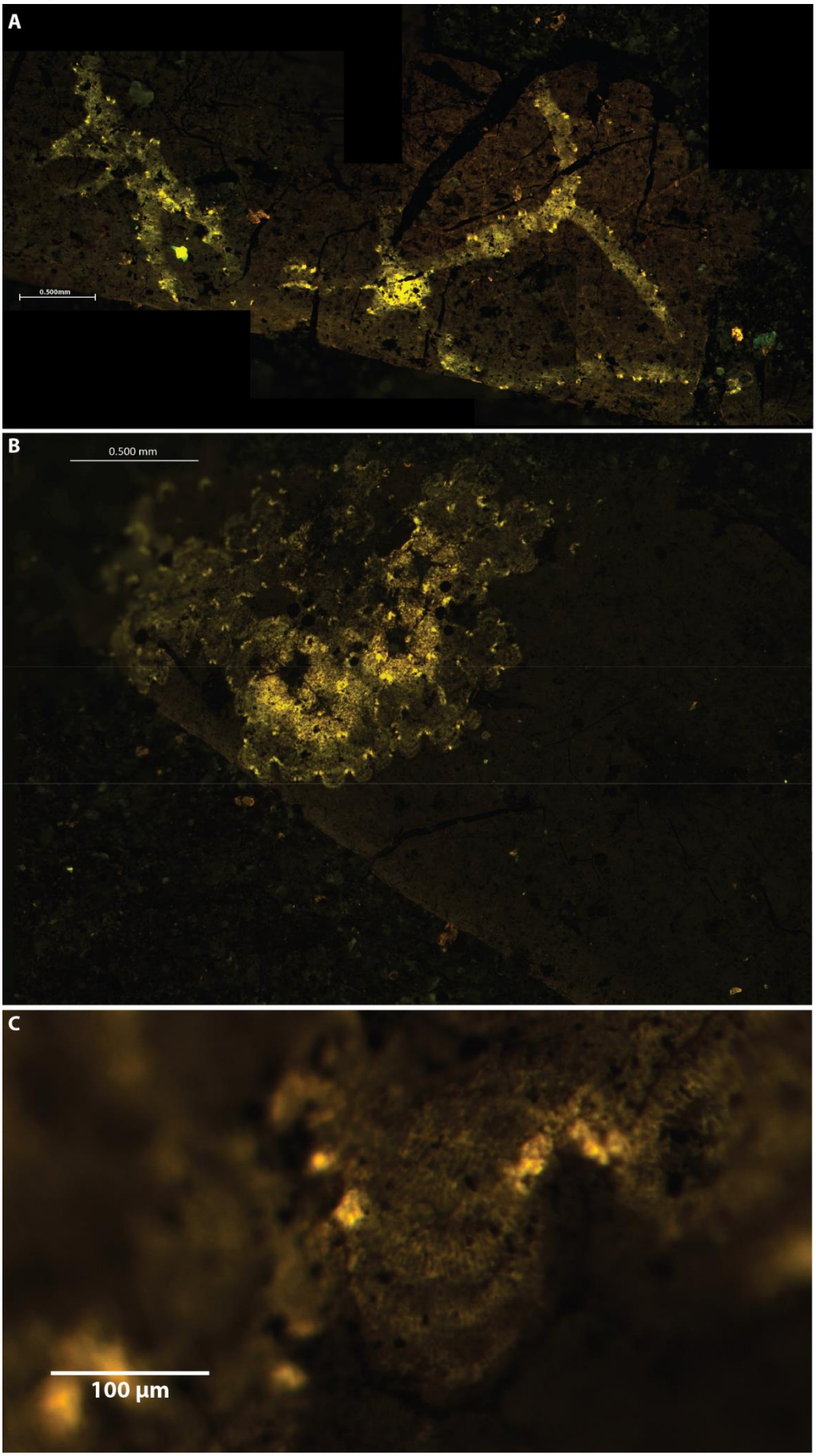

Appendix E: Stomatal data

- Table A: Stomatal density, index and frequency measurements (digital file).
- Table B: g_{wmax} and pore length data (digital file).
- Table C: pCO_2 reconstructions for morphotypes, data (digital file).
- Table D: pCO_2 reconstructions from Passalia (2009) compilation, both original and reassessed data (digital file).
- Table E: Change in pCO_2 based on stomatal ratio and g_{wmax} data (digital file).

Digital files – on disc